



CONTRIBUTION TO THE ASSESSMENT OF DAMAGE IN AGING CONCRETE INFRASTRUCTURES AFFECTED BY ALKALI-AGGREGATE REACTION

Thèse

LEANDRO SANCHEZ

Doctorat interuniversitaire en Sciences de la Terre
Philosophiae Doctor (PhD)

Québec, Canada
© Leandro Sanchez, 2014

Résumé

La réaction alcalis-granulat (RAG) fait partie des principaux processus affectant la durabilité des infrastructures en béton à travers le monde. Récemment, des chercheurs ont proposé un outil global de gestion (diagnostic et pronostic) de structures affectées par la RAG basé sur une série d'essais de laboratoire, incluant le Stiffness Damage Test (SDT) et le Damage Rating Index (DRI), des procédures micromécaniques d'évaluation de l'endommagement du béton. Quoique prometteurs, ces essais impliquent plusieurs paramètres dont l'impact n'est pas encore bien compris, ce qui réduit leur applicabilité à une vaste gamme de bétons (e.g. différentes formulations, types de mécanismes d'endommagement, variétés de granulats, etc.).

Ce projet de doctorat vise à mieux comprendre le mécanisme par lequel la RAG se développe et comment elle influence les propriétés physicomécaniques des bétons affectés, afin de pouvoir utiliser efficacement les outils mentionnés précédemment dans les contextes pratiques d'ingénierie. Pour atteindre cet objectif, des éprouvettes de béton de différentes résistances (25-45 MPa) et incorporant une variété de granulats réactifs et non réactifs (fins et grossiers) ont été fabriquées en laboratoire. Des essais mécaniques (SDT, traction, compression et module d'élasticité) et microscopiques (DRI) ont ensuite été effectués sur ces éprouvettes, à différents niveaux d'expansion, de façon à favoriser le caractère diagnostique optimal de chaque outil. Puis, le couplage micromécanique des résultats a été étudié en profondeur.

Les résultats démontrent que le SDT et le DRI permettent une évaluation diagnostique de l'endommagement associable à la RAG lorsqu'un certain nombre de paramètres critiques sont respectés. Les données optimales de sortie de ces essais sont ainsi basées sur des mesures « mécaniques » (énergie dissipée/déformation plastique, valeurs brutes ou indices relatifs) ou microstructurales (nombre/type de fissures) au sein des bétons affectés. En plus, un modèle microstructural qualitatif de l'endommagement de bétons en fonction de l'avancement de la RAG a été proposé. De même, le couplage micromécanique a permis d'expliquer efficacement l'influence de ce mécanisme sur les pertes de propriétés mécaniques de bétons affectés. Finalement, une charte permettant l'évaluation globale de l'endommagement de bétons affectés par la RAG est proposée.

Mots clés: Réaction alcalis-granulat (RAG), couplage microscopique/mécanique, évaluation de l'endommagement des infrastructures en béton vieillissantes.

Abstract

Alkali-aggregate reaction (AAR) is one of the main processes affecting the durability of concrete infrastructures worldwide. Recently, researchers proposed a comprehensive management tool for the diagnosis and prognosis of AAR affected structures based on a series of laboratory test procedures, including the Stiffness Damage Test (SDT) and the Damage Rating Index (DRI), micromechanical procedures for assessing damage in concrete. Although promising, these tests still have several parameters whose impact is not well understood, which reduces significantly their applicability for a wide range of distressed concretes (i.e. different concrete mix designs, damage mechanisms, variety of aggregate types, etc).

This PhD project aims at better understanding how AAR develops and influences the physicommechanical properties of affected concrete, in order to use more effectively the tools mentioned previously in practical engineering applications. To achieve this goal, concrete samples of different mix design strengths (25-45 MPa) incorporating a wide variety of both reactive and non-reactive aggregates (coarse and fine) were manufactured in the laboratory. Mechanical (SDT, tensile and compressive strengths and modulus of elasticity) and microscopic (DRI) tests were then performed on these samples at different expansion levels, in order to determine the optimal conditions enabling the effective diagnostic character through each tool. Then, the micromechanical coupling of the results was studied in depth.

The results show that both the SDT and the DRI are able to provide a diagnostic damage assessment of concrete distressed due to AAR when a number of critical parameters are adopted. The optimal output data from those procedures are thus based on either "mechanical" (dissipated energy/ plastic deformation, absolute values or indices) or microstructural (number /crack types) measurements on the affected material. Moreover, a qualitative microscopic damage model towards AAR development was proposed. Likewise, the above micromechanical coupling allowed to effectively explaining the impact of AAR on the reductions of the mechanical properties of affected concretes. Finally, a comprehensive chart enabling the overall damage assessment of concrete affected by AAR is proposed.

Keywords: alkali-aggregate reaction (AAR), microscopic/mechanical coupling, assessment of damage in aging concrete infrastructure.

Contents

RÉSUMÉ.....III

ABSTRACTV

LIST OF FIGURESIX

LIST OF TABLESXI

REMERCIEMENTSXV

FOREWORDSXXIII

1. INTRODUCTION..... 1

1.1 General context of the study..... 2

1.2 Scope of work and global structure of the PhD Thesis..... 5

2. LITTERATURE REVIEW..... 7

2.1 Introduction..... 7

2.2 ASR microscopic features and distress in concrete..... 8

2.3 ASR effects on the mechanical properties of affected concrete..... 14

2.4 Assessment of distress in concrete damaged by AAR..... 18

2.5 Predicting ASR expansion and damage..... 27

3. PROBLEM STATEMENT AND OBJECTIVES OF THE PHD STUDY..... 33

4. RESEARCH PROGRAM..... 35

4.1 Experimental procedures part I: laboratory-made specimens..... 35

4.2 Experimental procedures part II: extracted concrete cores..... 39

5. CORE OF THE PHD THESIS – THE SCIENTIFIC PAPERS..... 41

5.1 General overview..... 41

5.2 Scope and objectives of the scientific papers..... 43

**6. PAPER I: EVALUATION OF THE STIFFNESS DAMAGE TEST (SDT) AS A
TOOL FOR ASSESSING DAMAGE IN CONCRETE DUE TO ASR: TEST
LOADING AND OUTPUT RESPONSES FOR CONCRETES INCORPORATING
FINE AND COARSE AGGREGATES.....47**

**7. PAPER II: EVALUATION OF THE STIFFNESS DAMAGE TEST (SDT) AS A
TOOL FOR ASSESSING DAMAGE IN CONCRETE DUE TO ASR: INPUT
PARAMETERS AND TEST PROCEDURE.....109**

8. PAPER III: USE OF THE DAMAGE RATING INDEX (DRI) TO QUANTIFY DAMAGE DUE TO ALKALI-SILICA REACTION IN CONCRETE INCORPORATING REACTIVE FINE AND COARSE AGGREGATES.....	161
9. PAPER IV: ASSESSMENT OF MICROSCOPIC DAMAGE FEATURES OF ALKALI-AGGREGATE REACTION (AAR) THROUGH THE DAMAGE RATING INDEX (DRI).....	203
10. PAPER V: OVERALL ASSESSMENT OF ALKALI-AGGREGATE REACTION (AAR) IN CONCRETES PRESENTING DIFFERENT STRENGTHS AND INCORPORATING A WIDE RANGE OF REACTIVE AGGREGATE TYPES AND NATURES.....	244
11. PAPER VI: COMPARATIVE STUDY OF A CHEMO-MECHANICAL MODELING FOR ALKALI SILICA REACTION WITH EXPERIMENTAL EVIDENCES.....	303
12. SCIENTIFIC CONTRIBUTIONS OF THE PHD THESIS.....	343
13. CONCLUSIONS AND RECOMMENDATIONS.....	344
13.1 Summary of the experimental program.....	345
13.2 Development of AAR expansion and distress features in concrete.....	346
13.3 Proposal of a qualitative microscopic model of distress for ASR-affected concretes....	348
13.4 Tools for the condition assessment of ASR-affected concrete.....	349
13.5 Coupling between the development of the physical features of AAR and the mechanical behavior of the affected concretes.....	356
13.6 Quantitative damage chart/plot based on AAR micro-mechanical coupling.....	365
13.7 Validation of an ASR physico-chemical model for ASR.....	367
13.8 Comprehensive management approach for assessing aging concrete infrastructure affected by AAR – a brief discussion.....	368
13.9 Recommendations for future work.....	370
14. REFERENCES.....	373

List of Figures

Figure 1.1: Global flow chart proposed by Fournier et al. (2010) for the evaluation and management of concrete structures affected by AAR.....	3
Figure 1.2: Overall management approach proposed by Bérubé et al. (2005a) for the diagnosis and prognosis assessment of AAR in concrete structure	4
Figure 2.1: Crack pattern in concrete caused by different deleterious mechanisms (BCA, 1992). A. Freezing and thawing. B. Delayed ettringite formation (DEF). C. ASR from reactive sand. D. ASR from reactive coarse aggregate	9
Figure 2.2: AAR types of damage (described by Bérard & Roux 1986)	12
Figure 2.3: Signatures of concrete damage due to alkali-silica reaction (ASR) (Golterman, 1995)	13
Figure 2.4: Maximum stress range supported by an aggregate (quartz porphyry) before cracking vs. time of exposure (up to 560 days) in an alkaline medium (Reinhard & Mielich 2011)	14
Figure 2.5. Graphs from Kubo and Nakata (2012). A. Modulus of elasticity loss as a function of ASR expansion levels. B. Compressive strength loss in function of ASR expansion	15
Figure 2.6: Fragility Index (SII/SI) proposed by Ozkan et al. (2002)	18
Figure 2.7: Global assessment of concrete distress	19
Figure 2.8: Stress-strain behavior for damaged (A) and sound (B) concretes	21
Figure 2.9: Petrographic features of ASR in concrete incorporating reactive coarse aggregates; the abbreviations are given in the Table 1. The distance between the vertical lines is 1 cm (from Villeneuve et al. 2012)	25
Figure 2.10: Example of DRI chart for damaged concretes with different levels of distress (Transtec Group 2009)	25
Figure 2.11: Definition of the Representative Elementary Volume (REV) for several reactive aggregate sizes (Multon et al. 2009)	29
Figure 2.12: Mechanical equilibrium of the damaged REV (Multon et al. 2009)	30
Figure 2.13: Major stress found in REV due to ASR expansion (Multon et al. 2009) ...	30
Figure 2.14: Models used to evaluate AAR-generated damage (from Dunant and Scrivener, 2009). A. Expansion of the aggregate particles. B. Expansion of the reaction rims. C. Expansion of the gel-filled pockets in the aggregate particles	32
Figure 4.1: Structure of the Part I of the PhD project: laboratory-made specimens.....	35

Figure 4.2: Structure of the Part 2 of the PhD project: Core specimens extracted from the Robert Bourassa – Charest Viaduct	39
Figure 5.1: Core of the PhD Thesis – link between the scientific papers	42
Figure 13.1: SDT envelops using as output parameters the indices proposed in this project: A) SDI and B) PDI.....	352
Figure 13.2: SDT standard and practical procedure.....	353
Figure 13.3: DRI envelopes using: A) DRI numbers (following the test procedure proposed by Villeneuve et al 2012) and B) Crack density (counts/cm ²).....	356
Figure 13.4: Mechanical properties reduction (i.e. compared to a sound concrete presenting the same maturity) as a function of concrete expansions: A) Modulus of elasticity B) Tensile Strength and C) Compressive strength.....	364
Figure 13.5: Global analysis charts for: A) 25 MPa mixtures. B) 45 MPa mixtures. C) 35 MPa mixture	366

List of Tables

Table 2.1: Petrographic features and weighing factors used for Damage Rating Index determination (Villeneuve et al. 2012).....	27
Table 13.1: Classification of the damage degree in concrete due to ASR.....	358

Ce travail est consacré aux deux femmes de ma vie :

« À Diana, mon amour... tu étais toujours là aux moments les plus importants de ma vie, depuis le moment où nous avons décidé de changer notre vie, sortir de notre zone de confort et la recommencer dès le début, ensemble, à la recherche d'un rêve... jusqu'au moment où tu m'as donné le plus beau cadeau de ma vie : Ian... sans toi, cela aurait été impossible. »

« À Salete, ma lumière, mère et première professeuse... j'aimerais bien que tu saches que tout ton effort n'a pas été en vain. La plupart des choses auxquelles je crois viennent de tes enseignements. Je te remercierai pour toute ma vie ».

Remerciements

Premièrement, je voulais mentionner que lorsque j'ai complété mon baccalauréat au Brésil, j'étais convaincu que je voulais poursuivre une carrière scientifique dans le vaste sujet de la « durabilité du béton ». Pourtant, je n'avais alors aucune idée sur les possibilités de recherche existantes. À l'Université de São Paulo, il y avait une opportunité de maîtrise dans le domaine de la « corrosion des armatures » et je l'ai acceptée tout de suite. Pour une raison hors de mon contrôle, ce projet a été annulé et mon directeur de recherche de l'époque (Prof. Paulo Helene) a complètement changé le thème du projet pour un autre problème affectant la durabilité du béton à l'échelle mondiale, soit la réaction alcalis-granulats (RAG). Lors de mon premier cours portant sur la RAG (je n'avais aucune connaissance du sujet, évidemment), la première photo que m'a été montrée d'un ouvrage en service visiblement endommagé par ce mécanisme a été celle de l'ancien viaduc « Du Vallon Charest », à Québec, Canada. Finalement, la vie a voulu que 5 ans plus tard, je me retrouve à Québec pour étudier l'endommagement associable à la RAG sur des échantillons prélevés au sein du viaduc « Du Vallon Charest » avant la première démolition de la structure sud en 2010.

Je tiens à remercier vivement mon ami et directeur de recherche, Prof. Benoit Fournier, premièrement d'avoir cru à mon potentiel pour réaliser ce projet et, deuxièmement, pour m'avoir formé comme professionnel et chercheur au cours des dernières quatre années et demi. De plus, son effort, sa disponibilité, sa vision et surtout sa passion et son enthousiasme m'ont beaucoup aidé puis accompagné pendant tout le chemin. Aujourd'hui, je constate que de « petites séries en petites séries », on a pu réaliser ce projet ensemble. Je lui en serai éternellement reconnaissant.

Je voudrais également remercier mon ami et codirecteur de recherche, Prof. Marc Jolin, pour son soutien ainsi que pour ses commentaires, suggestions et sa vision intéressante sur le

projet. Toutes ses recommandations ont été indispensables pour la réussite du travail. Merci beaucoup Marc !

Je tiens aussi à remercier vivement les autres professeurs de l'Université Laval qui m'ont aidé de façon directe ou indirecte dans ce projet : Josée Duchesne, Josée Bastien, Benoit Bissonnette et Marc-André Bérubé. L'échange de connaissances avec vous a toujours été très enrichissant. D'ailleurs, les premiers articles scientifiques que j'ai lus sur la RAG ont été ceux rédigés par le groupe de recherche de l'Université Laval. En plus, toute la connaissance développée au Canada a servi de base pour le développement de la première norme brésilienne sur la RAG en 2008. Merci pour l'inspiration!!

J'aimerais beaucoup remercier le Ministère de Transports de Québec (MTQ), en particulier les ingénieurs Alain Hovington et Nadia Pouliot, ainsi que les techniciens Pascale Larouche et Serge Lamontagne; premièrement, pour cette belle opportunité de collaboration à ce magnifique projet et, deuxièmement, pour m'avoir ouvert leur laboratoire pour que je puisse y réaliser plusieurs de mes travaux expérimentaux.

Je voudrais remercier les techniciens Martin Plante et René Malo, ainsi que les professionnels de recherche Mathieu Thomassin et Nicolas Rouleau pour toute leur patience et disponibilité, de même que pour la planification permettant la confection des « petites séries » du projet. Sans votre aide, tout cela aurait été impossible !

Un gros merci à tous mes amis et collègues de travail (auxiliaires de recherche, étudiants de maîtrise et doctorat) de notre équipe de recherche au département de génie géologique qui m'ont beaucoup aidé pendant mes années de travail, directement ou indirectement : Pierre-Luc Fecteau, Sean Beauchemin, Anthony Allard, Mathieu Turcotte-Robitaille, Charles Lafrenière, Julie Francoeur, Charles-Frédéric Amringer, Steve Goyette, Andrea Rodrigues, Patrick Salva, Maria Alejandra Bedoya Bustamante, Sofie Tremblay, Véronique Villeneuve, Mathieu Labarre, Celestin Fortier, Cédric Drolet, Hubert Michaud, Roxanne Tremblay et Youness Kaghad. Plus qu'une excellente et efficace équipe de travail,

nous sommes devenus de très bons amis au cours de ces années de collaboration. Merci tout le monde !

À l'Université Laval, pour m'avoir donné l'occasion de réaliser deux grands rêves : obtenir une expérience professionnelle à l'extérieur de mon pays d'origine et poursuivre mes études de doctorat.

Je voudrais remercier mes amis de l'INSA de Toulouse : les professeurs Stéphane Multon, Allan Sellier et Martin Cyr, pour les agréables échanges techniques pendant les 4 mois de stage de doctorat à Toulouse. Cette collaboration a déjà donné des fruits et en donnera encore plus, j'en suis sûr. Merci!

Aux collègues de l'Université McGill à Montréal : Julie-Ann Hartell, Andrew Komar et Charles Desjardins, de même que le professeur Andrew Boyd, pour l'opportunité de réaliser des essais de « gas pressure » et l'aide apportée lors de la réalisation de ces essais. Merci mes amis !

Aux professionnels de recherche du département de statistique de l'Université Laval, particulièrement M. David Emond, pour m'avoir enseigné comment utiliser la statistique pour mieux expliquer/analyser mes résultats expérimentaux.

Je tiens à remercier énormément l'organisme CRSNG pour m'avoir accordé la Bourse Vanier. L'obtention de cette bourse a changé complètement la planification et la façon dont on a travaillé sur ce projet, tout en me permettant de me concentrer totalement sur les objectifs du projet sans avoir à me soucier du soutien financier de ma petite famille. Je vous en serai toujours reconnaissant.

À mon ami, ex-patron et ex-codirecteur de recherche à la maîtrise, M. Selmo Kuperman, pour m'avoir formé comme ingénieur et pour toutes les opportunités professionnelles et personnelles offertes à moi lors de mes travaux antérieurs au Brésil. Je lui serai toujours reconnaissant.

À mon ami et ex-directeur de recherche à la maîtrise, Prof. Paulo Helene, pour m'avoir appris plusieurs aspects techniques de la technologie du béton ainsi que pour m'avoir mis dans le chemin de l'alcali-réaction. Je vous remercie beaucoup Prof. Paulo Helene !

Au Prof. M. José Roberto Cardoso, doyen de l'École Polytechnique de l'Université à São Paulo, pour m'avoir encouragé à choisir mon chemin, à l'époque où tout semblait encore trop confus dans mon esprit.

Au Collège Rio Branco, à l'Institut Mauá de Technologie et à l'École Polytechnique de l'Université de São Paulo, pour m'avoir formé comme étudiant et ingénieur, mais surtout pour avoir implanté en moi le « goût pour le savoir ».

Je voudrais remercier fortement les trois femmes de ma vie : Salete, Lizandra et Diana, respectivement mère, sœur et épouse. La première est mon exemple, ma lumière, mon refuge; la seconde est un exemple de lutte, de courage, de génie. La troisième est l'amour de ma vie, mon équilibre, mon rêve, ma famille. Sans vous, rien ne serait possible!

À mon fils Ian, qui à date ne semble rien comprendre de ce que fait son père, à part peut-être de jouer avec ma souris à l'ordinateur, mais qui par le simple fait d'exister, me donne un autre sens à ma vie et m'encourage à aller plus loin.

À mon père, pour tout l'encouragement, pour toujours croire en moi, mais surtout, pour tous les enseignements procurés au cours de ma vie. Il m'a toujours dit que normalement les personnes qui ne lâchent pas, ont tendance à réussir et j'avoue que je suis en accord avec lui. Je lui en serai toujours reconnaissant.

À mes grands-parents : M. Francisco Sanchez Pascoal/Mme. Nanielza Sanchez; M. Idalino Moretti/Mme Santana Moretti, à l'origine de notre famille au Brésil. Ils ne sont plus là, dans le « monde de la matière », quoique tout ce qu'ils m'ont appris, je le porte en moi. Vous me manquez énormément.

Aux deux principaux professeurs de ma vie : 1) ma professeure de physique du Collège Rio Branco, Mme Virginia Simões Cortez, car grâce à quelques mots, elle a redirigé mon

chemin, et 2) mon professeur de mathématique appliquée, M. Aguinaldo Prandini Ricieri, qui après nous avoir appris des « dérivées simples et partielles », il a su « intégrer » le goût pour la connaissance au cœur de tous ses élèves. Je manque beaucoup le temps où nous avions des cours théoriques au 596 de la rue Tamandaré.

À toute ma famille et mes amis, parce qu'ils sont indirectement à l'origine de ce projet. De même, je tiens à remercier particulièrement mes amis de Québec (Fabiana/David, Jérôme/Luciana, Maxime/Andreia, Juan/Alejandra) qui m'ont beaucoup entendu parler de ce projet pendant les derniers 4,5 ans. Merci mes amis !

Je voudrais remercier/féliciter la *Librairie Spirite de Québec* pour tout l'effort de divulgation et de présentation du spiritisme au Canada, ainsi que pour les leçons hebdomadaires inoubliables sur la réforme intime données au cœur du Vieux-Québec.

Finalement, j'aimerais bien remercier la maison « Brogotá » (et toutes les personnes qui travaillent encore là-bas), particulièrement son fondateur M. Claudio Sérgio Infanti, où de façon hebdomadaire, des maîtres et des docteurs sont formés dans l'art de l'amour et de la charité. Sans eux, je ne serais jamais la personne que je suis.

À mon ami Ramon qui m'accompagne toujours puis à Dieu, pour m'avoir donné l'opportunité de réaliser un rêve.

« ... parce que tout ce qu'on essaie est de comprendre ou bien de trouver un motif dans le langage aléatoire de la nature, ce que l'on appelle science ».

Leandro Sanchez

“In the end, I don't really know anymore whether this work belongs to me, although I'm pretty sure that I completely belong to it”.

Leandro Sanchez

Foreword

This PhD thesis presents and analyses the results of a comprehensive investigation carried out by the author on either laboratory-made specimens or cores extracted from an ASR-affected concrete structure. The main objective of this work is to perform an in-depth evaluation of the *Stiffness Damage Test (SDT)* and the *Damage Rating Index (DRI)*, 1) for determining their reliability for the condition assessment of aging concrete infrastructures affected by alkali-aggregate reaction (AAR), and 2) for improving our understanding of the mechanisms responsible for the development of “damage” in concrete affected by AAR.

This document is divided into a number of sections, with the core of the document corresponding to six scientific papers covering specific but complementary themes of the research. In order to make the content of this paper-based PhD thesis clearer to readers, section 1 is first presented which aim at efficiently introducing the global context and the structure of the study, and of the document. A brief literature review of the current state-of knowledge on the *diagnosis of AAR* is presented (section 2). A problem statement is then established and the objectives of the study presented (section 3). The following section (section 4) then gives a summary of the global experimental program proposed to achieve the above objectives, which is followed by a summary of the scope and technical content of the six scientific papers (section 5).

Through this PhD project, I first establish, in collaboration with my director, since the project was carried out as part of a contractual agreement with the Quebec Ministry of Transportation, the global and particular objectives of the study. Thus, I designed the experimental program, which was further optimized with the support and recommendations of my supervisors. Then, I personally carried out and/or participated to all experimental works carried out in the laboratory, with the help/support of undergraduate students and technicians of *Le Centre de recherche sur les infrastructures de béton (CRIB)* at Laval University and of the Quebec Ministry of transportation. Moreover, I have treated/analyzed all the data used in this work, after which I wrote the first draft of each of the six enclosed papers (sections 6 to 11). The manuscripts were then reviewed by my supervisors and papers’ co-authors who made suggestions for the revision/improvement of the manuscripts, as required. It is to be noted that the first paper has been peer reviewed and published (February 2014) in *Cement and Concrete research Journal* (Volume 56, pp. 213-229). At the time of the final deposit of this thesis, papers II, III, IV and VI had been submitted for publication in scientific journals, although paper V is expected to be submitted over the summer of 2014.

Finally, based on the results obtained in this study, a series of conclusions and recommendations were prepared and are presented in sections 12 and 13 of this document.

1. INTRODUCTION

1.1 General context of the study

Alkali- aggregate reaction (AAR) is one of the main processes affecting the durability of concrete infrastructure worldwide (Fournier & Bérubé 2000). Over the years, several approaches and recommendations, including a comprehensive variety of laboratory tests, have been developed around the world to assess the potential alkali reactivity of concrete aggregates and the effectiveness of preventive measures (e.g. control of the concrete alkali content, use of supplementary cementitious materials, etc.) before their use in the field. Despite some issues with some of these test procedures, the majority of experts agree that, in general, it is now possible to construct concrete infrastructures with minimum or calculated risk of AAR. However, there is currently no consensus about the most efficient method(s) (surface treatments for moisture control, chemical treatments, strengthening, stress relief (slot cutting), etc.) that should be implemented, and when, for the rehabilitation of concrete structures/ structural elements suffering from AAR. In that context, many engineers and scientists around the world have been trying to develop appraisal tools that are able to determine both the current damage state (*diagnosis*) and the potential of further distress (*prognosis*) of AAR-affected concretes, which are essential steps in selecting efficient rehabilitation methods and optimum application periods for distressed concrete infrastructures.

Bérubé et al. (2005a) and Fournier et al. (2010) recently developed comprehensive management tools for the *diagnosis* and *prognosis* of AAR-affected concrete structures (Figures 1.1 and 1.2). The authors proposed protocols with a series of comparative field and laboratory investigations to confirm that AAR is the main cause or a significant contributor to the deterioration observed, thus aiming at selecting appropriate remedial actions. Such investigations include one or several of the following steps (Fournier et al. 2010):

- the routine field inspection of the structure under study to identify the presence/ distribution and severity of the defects affecting the various structural elements (especially those features related to AAR), as well as the exposure conditions to which the structure is subjected;

- a preliminary in-situ monitoring program of deterioration (especially signs of expansion and deformation) to quantify the rate/progress of deterioration on selected structural elements; and
- when appropriate (depending on the nature of deterioration / criticality of the structure), implementation of a detailed investigation program including extensive in-situ activities and laboratory tests (including petrographic characterization, chemical, physical, and mechanical tests) on samples collected from one or several components of the affected concrete structure.

In this context, and as highlighted in Figures 1.1 and 1.2, this study focuses on the detailed laboratory investigations aiming at quantifying the condition of concrete affected by AAR, and especially on the use of two testing methods, i.e. the *Stiffness Damage Test (SDT)* and the *Damage Rating Index (DRI)*

The philosophy of the SDT is to quantify the degree of internal damage due to AAR based on the cyclic loading (under compression) of concrete samples (cylinders/cores). So far, stiffness damage testing was typically carried out through the use of a fixed loading of 5.5 or 10 MPa, and output parameters such as the modulus of elasticity, the hysteresis area (or the dissipated energy) and the plastic deformation over loading, as well as the index of non-linearity (NLI) of the distress curve shape were selected for evaluating the extent of internal concrete damage due to AAR.

The DRI consists in a microscopic analysis performed with the use of a stereomicroscope (about 15-16x magnifications) where damage petrographic features associated to alkali-silica reaction (ASR) are counted through a 1 cm² grid drawn on the surface of a polished concrete section. The number of counts corresponding to each type of petrographic features is then multiplied by a set of weighing factors, whose purpose is to balance their relative importance towards the mechanism of distress (for instance ASR). The final DRI value is normalized to a 100 cm² area; in general, the greater the DRI number is, the greater the deterioration in the concrete specimens due to ASR will be.

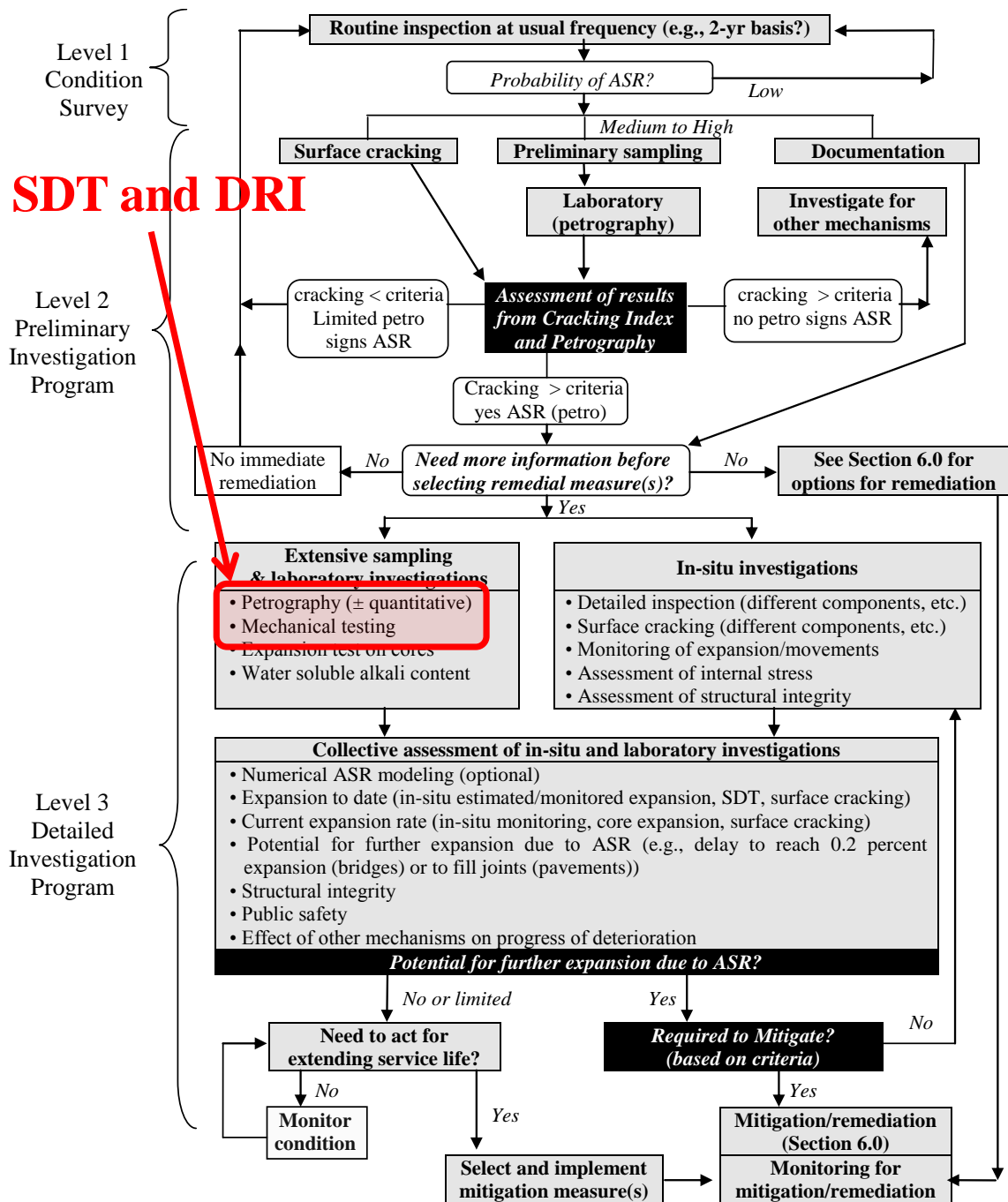


Figure 1.1: Global flow chart proposed by Fournier et al. (2010) for the evaluation and management of concrete structures affected by AAR.

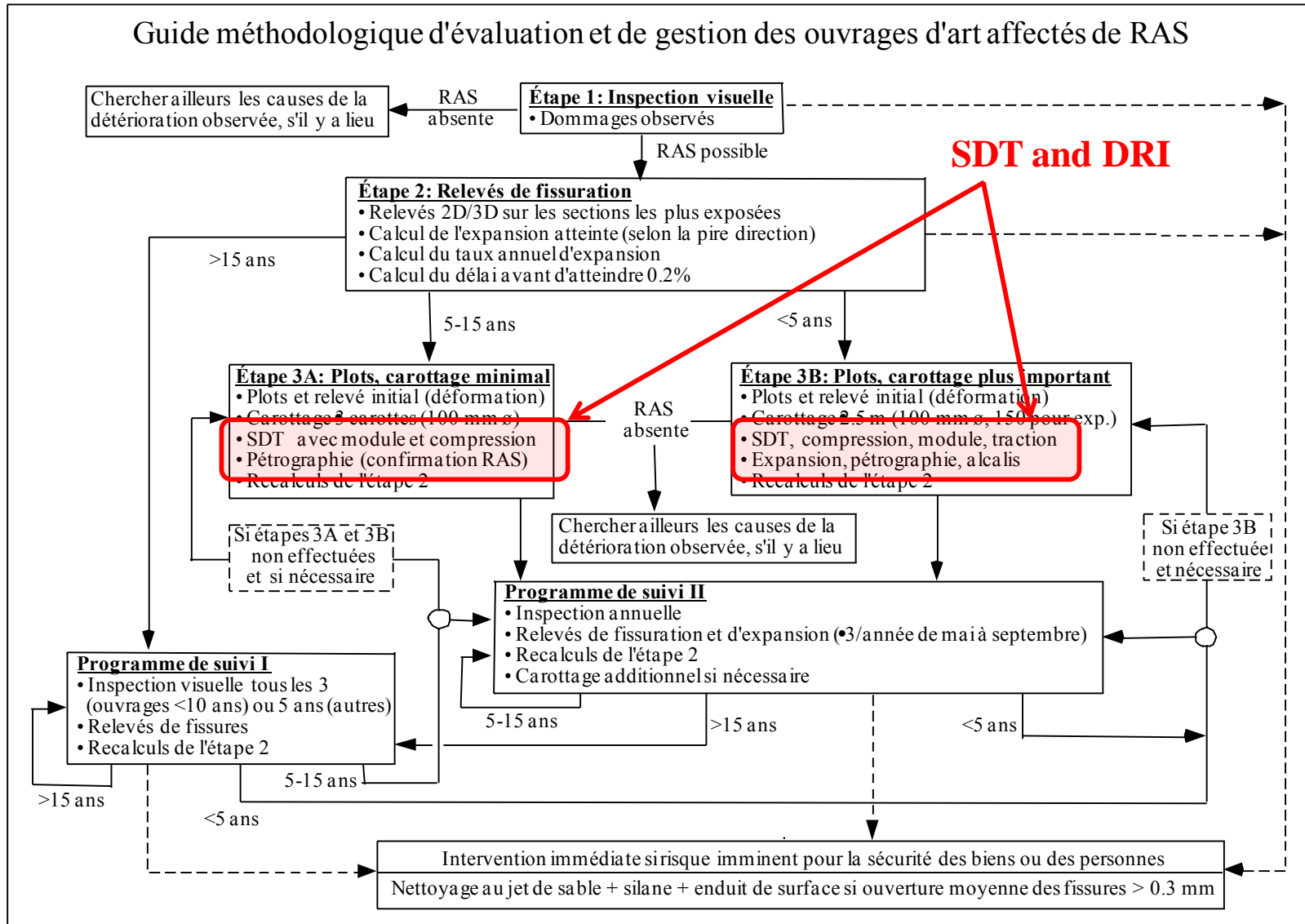


Figure 1.2: Overall management approach proposed by Bérubé et al. (2005a) for the diagnosis and prognosis assessment of AAR in concrete structure.

1.2 Scope of work and global structure of the PhD Thesis

The SDT and DRI are meant to evaluate the mechanical and microstructural properties of AAR-affected concrete, respectively. Although promising, these tests still have several parameters whose impact on their reliability and precision is not well understood, thus reducing their potential applicability for a wide range of distressed concretes (i.e. different concrete mix designs, variety of aggregate types and also different damage mechanisms). This work aims at improving the above assessment tools so they could be used to help engineers to better understand AAR distress development in concrete infrastructure and, in turn, select the most appropriate rehabilitation methods and optimum application periods for ASR-affected concrete infrastructures. In order to do so, an extensive investigation program was developed and implemented in the laboratory, which involve the manufacturing and testing (using the SDT, DRI and other appropriate methods) of a large number of concrete cylinders made from concrete mixtures of different strengths and incorporating a wide range of reactive aggregates, as well as cores extracted from structural elements of a reinforced concrete bridge affected by AAR.

This PhD thesis presents and analyses the results of the investigation program mentioned above. It is divided in a number of sections, with the core of the document corresponding to six scientific papers covering specific but complementary themes of the research. In order to make the content of this paper-based PhD thesis clearer to readers, section 1 aims at efficiently introducing the global context and the structure of the study, and of the document. A brief literature review of the current state-of knowledge on the *diagnosis of AAR* is then presented (section 2); this section is voluntarily meant to be brief to limit repetitions (since detailed references to the literature can be found in each of the scientific papers), but to be also informative. A problem statement is then established and the objectives of the study presented (section 3). The following section (section 4) then gives a summary of the global experimental program proposed to achieve the above objectives, which is followed by a summary of the scope and technical content of the six scientific papers (section 5); the latter section is meant to help the reader to better understand the scope and the link between the papers, which correspond to sections 6 to 11. Following the presentation of the scientific papers, conclusions and recommendations are given (sections 12 and 13).

2. LITTERATURE REVIEW

2.1 Introduction

Alkali-aggregate reaction (AAR), a chemical reaction between certain mineral phases from the aggregates and the alkali hydroxides from the concrete pore solution, is one of the main processes affecting the durability of concrete structures around the world (Fournier & Bérubé 2000).

Overall, AAR can be divided in two main reaction types: alkali-silica reaction (ASR) and alkali-carbonate reaction (ACR). ASR is by far the most common reaction type found worldwide, and its distress mechanism is already fairly well understood, at least in its major steps. It consists in a chemical reaction between “unstable” silica mineral forms within the fine and/or coarse aggregate materials and the alkali hydroxides (Na, K – OH) dissolved in the concrete pore solution. It generates a secondary *alkali-silica gel* that induces expansive pressures within the reacting aggregate material(s) and the adjacent cement paste upon moisture uptake from its surrounding environment, thus causing microcracking, loss of material’s integrity (mechanical/durability) and, in some cases, functionality in the affected structure. On the other hand, ACR is a much less common concrete distress whose mechanism is still mostly unknown, being considered as a form of ASR by some authors (Katayama 2010; Katayama & Grattan-Bellew 2012), while other researchers believe that ACR follows a “different” distress mechanism (Fecteau et al. 2012, CSA A23.1 – Appendix B). The period of time required to generate significant distress in concrete due to AAR may range from 2 to more than 25 years, depending on factors such as the alkali content in the concrete, the type of reactive mineral form present in the fine and/or coarse aggregate, and the availability of moisture.

One of the biggest challenges in dealing with aging/deteriorating concrete structures is to identify the cause of distress (e.g. AAR, freeze-thaw, Delayed Ettringite Formation), and to establish the correlation between the loss in mechanical properties, physical integrity, durability and performance of the affected *material*, and the *structural* implications. Therefore, any information on the nature of the deleterious mechanism(s) affecting the structures, the current condition and the potential for future deterioration of the affected

concrete is generally critical for engineers in charge of selecting appropriate remedial measures.

2.2 ASR microscopic features and distress in concrete

Different mechanisms can affect the long-term durability of concrete structures whose "patterns" were diagrammed by St-John et al. (1998) and BCA (1992) (Figure 2.1). For damage caused by freezing and thawing cycles, cracking develops mainly in the concrete matrix and often propagates through the interfacial transition zone (ITZ) between the aggregate particles and the cement paste, as those zones present a lower fracture toughness and are more porous than the bulk cement paste (Figure 2.1A). Delayed ettringite formation (DEF), a form of heat-induced sulfate attack, is characterized by expanding cement paste in the presence of moisture that becomes detached from the aggregate particles with the gaps thus created at the ITZ being progressively filled with large amounts of ettringite (Walker et al. 2006; PCA 2002) (Figure 2.1B). On the other hand, in the case of ASR, the cracks are generated at expansive sites where reactive forms of silica are present. Figures 2.1C and 2.1D present the cracking originating from the fine and coarse reactive aggregate particles, respectively. Normally, cracks generated by ASR propagate between or through the above particles, the ITZ and the bulk cement paste, with associated secondary reaction products, i.e. alkali-silica gel. Thus, it seems logical to think that the nature (i.e. hardness, stiffness, toughness, etc.) of the coarse aggregate play a significant role in the ASR crack propagation, as recently suggested by Reinhardt & Mielich (2011). Therefore, a detailed petrographic analysis of concrete specimens extracted from aging concrete structures, both on fractured surfaces and thin/polished concrete sections, is a powerful tool to help identifying the presence (or absence) of the main microscopic features of the above deleterious mechanisms, thus providing critical information on the potential origin and the extent of current damage of the distressed material (Rivard et al. 2002; Bérubé et al. 2005b; Wood et al. 1996; Grattan-Bellew & Mitchell 2006).

As previously stated, alkali-silica reaction (AAR) generates a gel containing alkalis (K and Na), silicium and calcium, which swells in the presence of water thus causing a significant amount of pressure and eventually cracking in the bulk concrete volume. As the swelling may vary between the various members of a given structure, because of variations in the exposure conditions and concrete compositions, differential movements may be observed, thus causing

important operational/safety issues, especially in the case of hydraulic dams and transportation structures such as concrete pavements. Although many researchers have worked on the AAR mechanism, there are still many uncertainties about the whole process of damage development and associated variations when different aggregate types/natures are used in concrete (Fournier & Bérubé 2000).

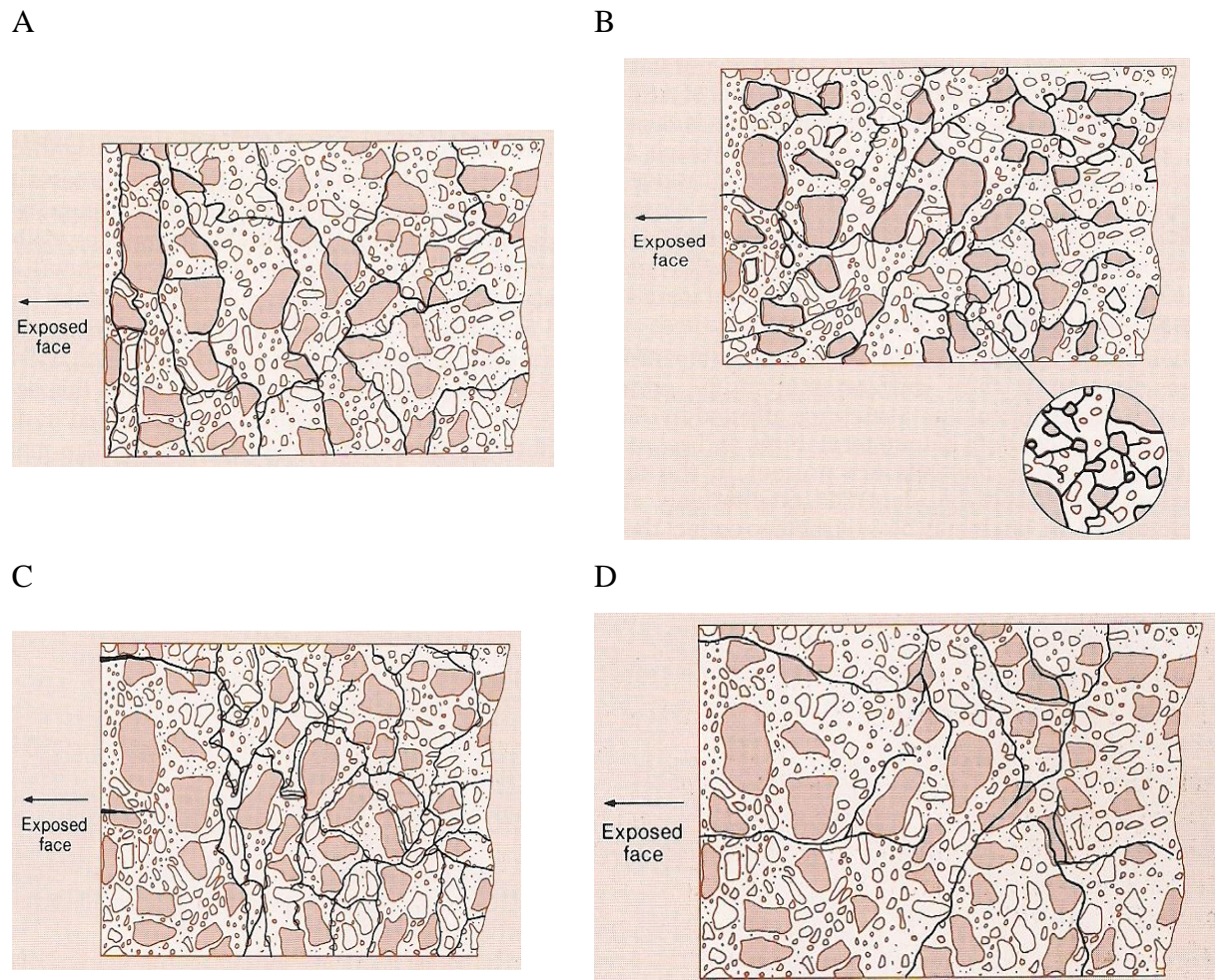


Figure 2.1: Crack pattern in concrete caused by different deleterious mechanisms (BCA, 1992). A. Freezing and thawing. B. Delayed ettringite formation (DEF). C. ASR from reactive sand. D. ASR from reactive coarse aggregate.

Back in 1955, Powers & Steinour introduced the concept of “safe” and “unsafe” gels. According to the authors, “safe” gels are those that produce limited swelling pressures upon water absorption and normally have high calcium contents. On the other hand, “unsafe” gels are osmotically active and contain high levels of sodium (Na) and/or potassium (K). More than just the gel characteristics, it has been found that the AAR process can vary significantly as a function of the aggregate types. The main differences are related to variations in the

expansion rate, the timing and length of the initiation period, the locations and sizes of the cracks formed within the concrete, the presence or not of gel in the cracks/voids of the aggregate particles and of the cement paste, and finally the development of reaction rims in the interfacial zone between the cement paste and the aggregate particles (ITZ) (Giaccio et al. 2008).

Considering the basic ASR distress mechanism, Dunant & Scrivener (2009) and Dunant & Bentz (2012) argued that the location of ASR gel formation and its morphology depend on the mineralogical nature of the aggregates. According to the authors, two large classes of aggregate types can be distinguished: the slowly-reactive aggregates and the rapidly-reactive aggregates. Distress caused by slowly-reactive aggregates (which are often used in ordinary concrete) is characterized by the formation of "gel pockets" within the aggregates particles. This phenomenon generates crack within the aggregate particles, which will extend into the bulk cement paste when the expansion levels increase. On the other hand, rapidly-reactive aggregates have more homogeneous microtextural and compositional characteristics than the previous group, and ASR is mainly produced on the surfaces of the particles. This more homogeneous reaction generates cracks in the outer part of the aggregate particles, thus resulting in the development of cracks in the bulk cement paste at lower reaction levels (i.e. leading to greater damage and a faster development of important expansions).

Bérard & Roux (1986) described three types of reaction processes within reactive rocks types from the province of Quebec (Canada), and consequently three different damage mechanisms/patterns due to ASR (Figure 2.2). According to the authors, these differences were directly related to the nature of the reactive aggregates used in concretes and, although the mechanisms differ from one aggregate type to another, the results, in terms of crack generation and growth, are quite similar. The three mechanisms are as follows (Bérard & Roux 1986):

- Peripheral reactions of non-porous aggregates;
- Diffuse reactions causing the swelling of the bulk reactive aggregate particles;
- Internal reactions causing the formation of veins of alkali-silica gel.

Peripheral reaction of non-porous aggregates

This type of reaction was identified in a number of concrete cores extracted from large hydraulic dams incorporating quartz-bearing rocks, such as granites, quartzitic diorites and

quartzo-feldspathic gneisses, as aggregate materials. The physical effects associated to this chemical reaction are slow to develop and the final expansions are of moderate levels. Although difficult to identify in the concrete specimens, the alkali-silica gel was typically observed around the reactive particles (i.e. interfacial transition zone - ITZ), thus lowering the bond between the aggregate particles and the cement paste (Bérard & Roux 1986).

Diffuse reactions causing swelling of the bulk reactive aggregate particles

In this ASR type, which typically involves quartzitic sandstones (or orthoquartzites) of the Potsdam Group in the greater Montreal area, the alkali ions diffuse into the reactive aggregate particles even if the latter do not present a high porosity. The above ions then rapidly attack the quartzitic cement between the well-rounded quartz grains, thus generating ASR gel causing a slight swelling of the aggregate particles. Among the main microscopic features of reaction, the authors reported the presence of 1), dark reaction rims, 2), “gel pockets” inside the aggregate particles or in the voids and cracks of the cement paste, 3), cracks radiating from the reactive particles into the cement paste and peripheral “onion skin” cracks within the aggregates, and 4), friable “reacted” aggregate particles affected by ASR (Bérard & Roux 1986).

Internal reactions causing the formation of veins of alkali-silica gel

In this third reaction type, the concrete swelling is occurring through the formation of whitish “silica gel” veinlets inside the reactive aggregate particles, which become thicker over the years. The aggregates responsible for this type of reaction are siliceous (“impure” – i.e. with high insoluble residue content including amorphous silica) limestones of Ordovician age exploited in several regions of the St. Lawrence Lowlands of Quebec. The authors reported the following characteristics of this type of reaction (Bérard & Roux 1986): 1), the white veinlets are generally aligned according to the original rock bedding; 2), these veinlets often form a complex and irregular network as if they had formed in microcracks generated during aggregate processing operations; 3), in certain cases, changes in the porosity, color and composition of the rock is observed on both sides of the silica gel veinlets; 4), the veinlets rarely extend into the cement paste; actually, they become thinner when approaching the periphery of the aggregate particles; and 5), sometimes, the finely cracked cement paste contains silica gel veinlets that connect a few adjacent aggregate particles. It is interesting to note that similar signs of reaction were also reported in concrete structures of the northeastern part of France incorporating a similar rock type exploited in a large quarry located in Belgium

(Guédon-Dubied et al. 2000); also, Villeneuve (2011) and Tremblay (2011) observed the presence of microcracks filled with secondary reaction products in the aggregate particles of concretes incorporating a wide range of reactive rock types, such as argillite/pélite, shale, greywacke, granite/gneiss, schist, quartzite, mixed volcanic rocks (e.g. rhyolite, andesite, tuff).

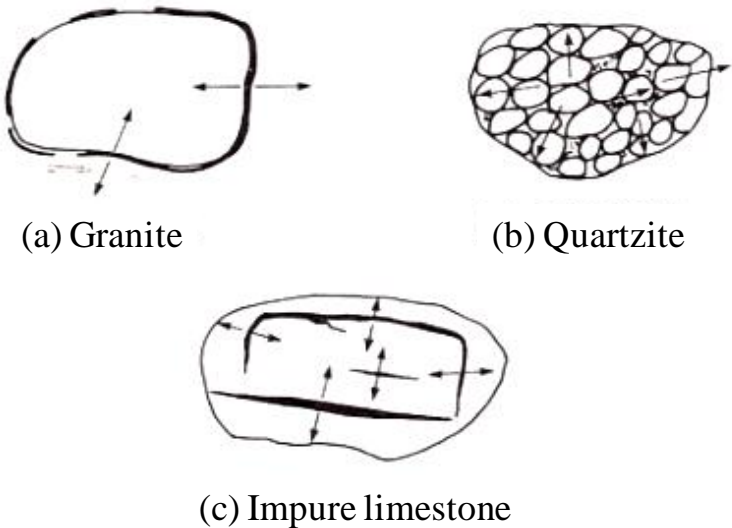


Figure 2.2: AAR types of damage (described by Bérard & Roux 1986).

Golterman (1995) stated that ASR damage and signs of distress are really complex to explain and they are not homogeneously distributed throughout the concrete material (Figure 2.3). According to the author, an heterogeneous deleterious mechanism generated by the reactive aggregates causes tensile stresses in the aggregate particles and compressive stresses on the aggregate surfaces (outer surface). Those stresses induce crack formation in the aggregate particles and, as these particles keep swelling, cracking is also formed in the bulk cement paste. The rate of cracking propagation for brittle materials (i.e. aggregate particles) is always faster than the rate of stress propagation. This effect induces cracks to form inside the aggregate particles (i.e. tension zones) and to run out radially through the outer part of the particles or even in the bulk cement paste areas (i.e. compression zones). The ITZ remains intact in most cases, except in the neighborhood of the radial cracks.

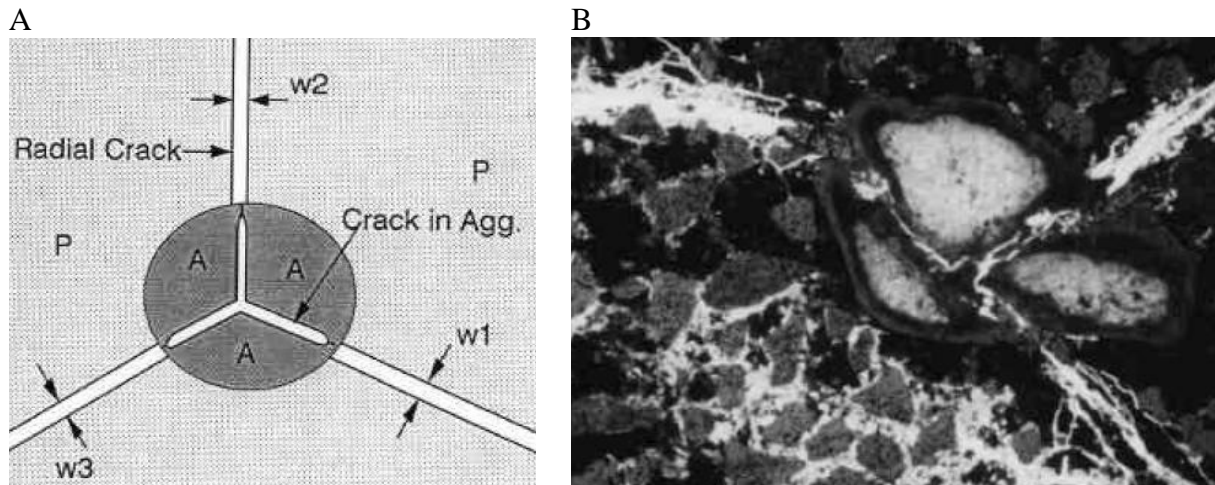


Figure 2.3: Signatures of concrete damage due to alkali-silica reaction (ASR) (Golterman, 1995).

According to Reinhard & Mielich (2011), there are two different distress mechanisms proposed for ASR. The first mechanism suggests that the dissolution process happens at the aggregate particles surfaces, thus ASR gel and cracks are formed at the ITZ and easily reach the bulk cement paste due to swelling pressures. The second approach states that cracks are formed within the aggregate particles as a result of gel pockets formation, reaching the cement paste when higher expansion levels are reached. This second theory assumes that the critical aggregate expansion must be achieved before cracks are generated. Critical distress due to ASR happens when the critical “crack length” is reached in the aggregate particle. The final aggregate fracture takes place because of pressure created by ASR gel swelling. Consequently, the aggregate’s toughness is considered a decisive parameter for the cracks extension. Indeed, the maximum stress supported by an aggregate varies as a function of ASR “time exposure” (i.e. period of time to which a reactive aggregate remains at ideal conditions for ASR development) (Figure 2.4). Yet, according to Reinhard & Mielich (2011), the fracture mechanism of reactive aggregates can be divided in two steps: 1) the alkali ions present in the concrete pore solution diffuse into the aggregate particles. They react within the grains with silica and calcium, thus producing ASR gel. This can occur due to the presence of “fast-tracks”, which correspond to pre-existing aggregate’s “defects or even cracks”; 2) ASR gel swells due to water absorption and exerts pressure on the grain “defects” inside the aggregate particles. This pressure can fracture the aggregate particle apart, depending on its intensity as well as the “maximum crack length” and the “critical stress intensity factor” of the rock type in question. Once the critical stress intensity factor is reached, the aggregate particle breaks down.

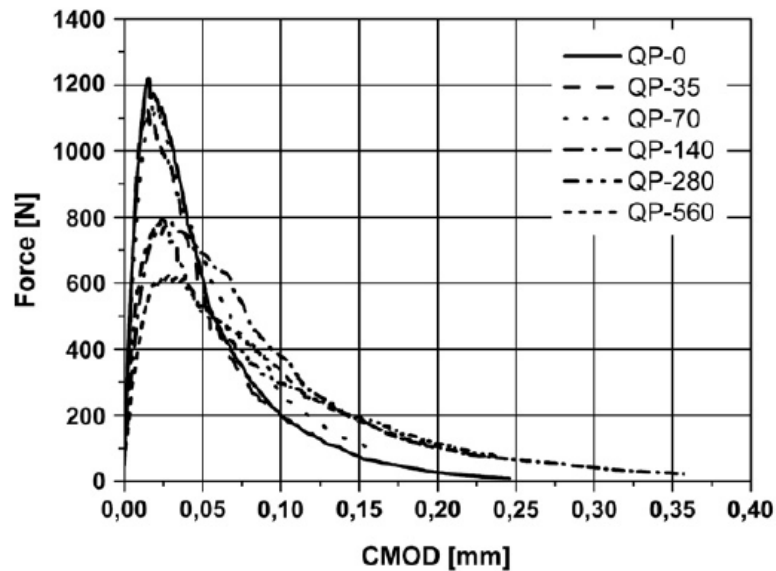


Figure 2.4: Maximum stress range supported by an aggregate (quartz porphyry) before cracking vs. time of exposure (up to 560 days) in an alkaline medium (Reinhard & Mielich 2011).

2.3 ASR effects on the mechanical properties of affected concrete

It is well established that conventional sound concrete presents a high compressive strength and modulus of elasticity, a low tensile strength, a brittle response under uniaxial loading (compression or tension) and an increase in both ductility and strength (compression and tension) in a confined environment. This sensitivity to the confinement state is linked to the presence of small defects, or even microcracks, which will ever exist in concrete. Thus, even for a non-distressed concrete under a triaxial compression state, there will always be local zones in tension within the bulk material volume due to its heterogeneous and defective nature. Moreover, the complexity of the concrete behavior is further increased when the material is already distressed due to a deleterious mechanism (Crouch & Wood 1990). Therefore, the knowledge of the mechanical properties (compressive and tensile strengths, modulus of elasticity and also the stress/strain behavior) of concrete affected by AAR or other deleterious mechanisms is very important and necessary when one designs a repair/reinforcement of distressed concrete elements or structures (Kubo & Nakata 2012).

Generally, AAR generates a very significant drop in terms of tensile strength and modulus of elasticity. These two properties are significantly more affected than the compressive strength, which begins to decrease significantly only at high levels of expansion (Nixon & Bollinghaus 1985; Smaoui et al. 2004a, Pleau et al. 1989) (Figures 2.5a and 2.5b).

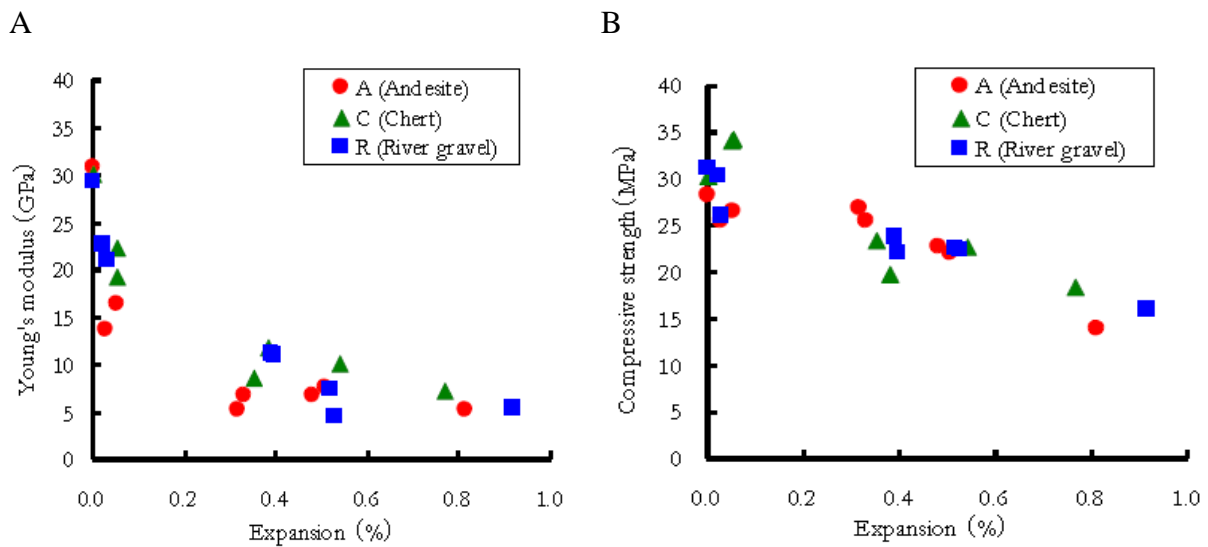


Figure 2.5. Graphs from Kubo and Nakata (2012). A. Modulus of elasticity loss as a function of ASR expansion levels. B. Compressive strength loss in function of ASR expansion.

The classical effect of AAR on the mechanical properties of concrete reported above suggests that microcracking caused by this deleterious mechanism can be identified even before the material reaches significant expansion and macrocracking and eventually significant compressive strength loss (Nixon & Bollinghaus 1985). According to ISE (1992), compressive strengths will normally increase in concrete structures exposed to natural environmental conditions to reach values beyond the design (28-day) values; thus, the compressive strength loss due to AAR is usually smaller than or similar to the gap between the design and the actual strength values measured at a given time. On the other hand, a significant compressive strength loss can be observed for concrete elements suffering from important expansions (i.e. 1 mm/m or 0.10%) (Wood & Johnson 1993; Wood et al. 1989). According to those authors, for expansions up to about 0.10%, it is very likely that the concrete element or even the structure will efficiently support its active stresses. However, after 0.30% of expansion, a structural appraisal should be carried out (Wood & Johnson 1993; Wood et al. 1989). Moreover, Kubo & Nakata (2012) reported the results of recent studies showing compressive strength losses for concretes with expansion levels higher than 0.30%. For expansion levels of 0.50%, the authors observed compressive strength losses of about 30%. In the same study, the authors found that neither the water-to-cement ratio of the concrete mixtures nor the aggregate types used influenced significantly the compressive strengths, at least up to expansion levels of 0.30%. On the other hand, the researchers found significant differences in the stress/strain behavior (especially for the modulus of elasticity) at similar expansion levels when different reactive aggregates were used. They associated those

differences to different patterns of cracking when different reactive aggregates are used in concrete (Kubo & Nakata 2012).

Naar (2010) suggested that the analyses of the mechanical properties reductions as a function of expansion due to AAR is complicated and many contradictory results are presented in the literature. In terms of compressive strength, some authors found losses just for very high expansion levels. On the other hand, others found either almost no change or even an increase in compressive strength with increasing expansion due to ASR. Considering the modulus of elasticity loss, the majority of the authors agree on a rapid loss even at low expansion levels (0.0% up to 0.05%); however, losses ranging from 20 to 80% of the modulus of elasticity of control non-reactive concretes of the same formulation were reported, which is considered a huge variation.

The mechanical response of concrete incorporating different types of reactive aggregate has been studied by several researchers. It was found that the reaction rate, the cracking patterns and also the mechanical properties reductions changed as a function of the type of coarse aggregate used in concrete (Giaccio et al. 2008). Reinhart & Mielich (2011) carried out a series of laboratory tests on concrete incorporating slowly reactive aggregates commonly used in concrete (greywacke, quartzite, granite, andesite, etc.), and which have already caused problems in real concrete structures after 10 to 20 years in service. The results showed that the dynamic modulus of elasticity, which can be measured through the ultrasonic pulse velocity procedure, is not a good parameter to determine concrete damage due to AAR. The compressive strength was found to vary as a function of the expansion level of the test specimens, but much less than the tensile strength. The modulus of elasticity appears to be the most affected parameter and, therefore, more effective for assessing the degree of damage in concrete due to AAR. Moreover, the reductions in the mechanical properties of the aggregates ranged as a function of the reactive aggregate types used (Reinhart & Mielich 2011).

Giaccio et al. (2008) verified that the compressive strength of concrete is clearly affected by AAR. Actually, several distinct periods characterizing the damaging process in concrete affected by AAR are affected by the progress of the chemical reaction, as follows: crack initiation, stable and unstable crack propagation. However, the period of crack initiation or the “critical compression load” (i.e. compression load needed to start cracking generation) cannot be easily linked to a “specific expansion level” in the test specimens because their behaviors

depend on several factors, such as the concrete design strength and the aggregate type (e.g. lithotype, aggregate size, reactivity level) used in the concrete. The authors also found that the period of stable crack propagation is less affected than the period of unstable crack propagation. This means that AAR affected concrete is not that efficient to control cracks spreading, thus allowing premature fracture. Moreover, Giaccio et al. (2008) also observed that the stress/strain behavior of concrete affected by AAR changed according to the coarse aggregate used. The authors concluded that those differences in behavior were related to the “competence” of the aggregate (i.e. ability of the aggregate particles to bond well to the cement paste, i.e. in the Interfacial Transition Zone - ITZ), as well as the presence of preexisting cracks which were created during aggregate’s processing operations.

Aitcin & Mehta (1990) found that the aggregate type changed not only the stress/strain behavior of concrete, but also the amount of energy dissipated during the loading cycle’s behavior. Therefore, the authors indicated that the hysteresis area (i.e. the amount of dissipated energy) of a concrete mixture was related to the ITZ strength of the material. Ozkan et al. (2002) proposed the definition of the “Fragility” Index of concrete, as the ratio between the elastic deformation energy (SII) and irreversible deformation energy of a material (SI) (Figure 2.6). According to them, when the SII/SI approaches zero, all the energy is irreversible. On the other hand, when the ratio approaches the infinity, the energy becomes reversible. Also, the greater is the ratio, the greater is the material’s fragility. Ozkan et al. (2002) verified that the Fragility Index changed with the strength (and also stiffness) of the concrete. According to the authors, the irreversible energy is lower with increasing strength, which indicates a more brittle material. The explanation for this phenomenon is that for ordinary concrete, the differences in the mechanical properties (strength, stiffness, etc.) between the concrete constituents (cement paste, aggregates and ITZ) results in cracks to develop in areas of lower strength over loading. However, in the case of high-performance concretes, those differences are less apparent. It would thus be of interest to determine the effect of AAR on the Fragility Index of concrete, as it could be an interesting parameter for damage evaluation.

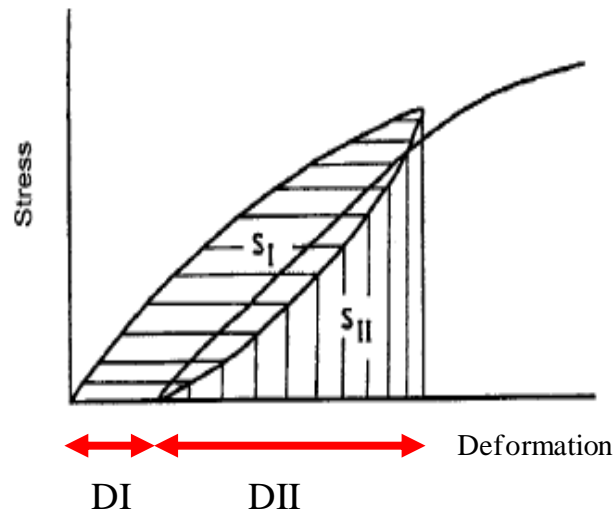


Figure 2.6: Fragility Index (S_{II}/S_I) proposed by Ozkan et al. (2002).

Alexander & Milne (1995) studied the influence of the cement type on the stress/strain concrete properties. The authors used loads of about 25% of the maximum material strength at 28 days. The results showed that not only the aggregates and the concrete strength, but also the type of binder plays a very important role in the stress/strain behavior of the concrete.

2.4 Assessment of distress in concrete damaged by AAR

A large number of concrete structures were built in North America and worldwide since the 1950's. Many of these structures have reached the end of their expected service life and/or are showing unexpected/important signs of deterioration that will require remedial actions in the near future to maintain their functionality. Selecting the most appropriate remedial actions for such structures requires that critical information be available not only on the mechanism(s) responsible for the observed damage and its extent, but also on the potential for further damage in various elements of the structure under study. Actually, the word "damage" is defined in this context as *the harmful consequences (measurable ones) of various phenomena (e.g. loadings, shrinkage, creep, alkali-silica reaction (ASR), sulphate attack, freezing and thawing, etc.) on the mechanical properties, physical integrity and durability of a concrete material/element*. In practical means, for the assessment of concrete distress due to some damage mechanism (i.e. for instance AAR in this work), the word "damage" can be divided into three main points of the following flowchart (Figure 2.7).

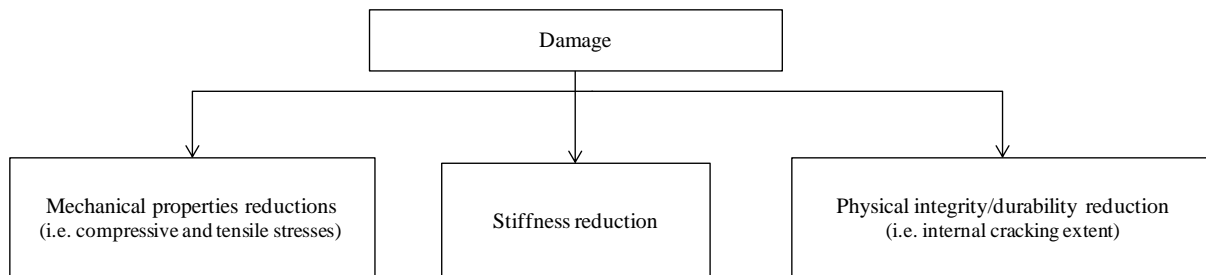


Figure 2.7: Global assessment of concrete distress.

As defined by BCA (1992) and St-John et al. (1998), it is well established that different deleterious mechanisms generate different patterns of internal damage. However, one of the biggest challenges in engineering is to establish the correlation between those patterns or microscopic "signatures" and the reduction in mechanical properties, durability and performance of the affected material or element, as well as their structural implications.

Over the years, petrographic methods were developed with the aim of identifying the presence and the extent of ASR in aging concrete structures. Grattan-Bellew and coworkers (Grattan-Bellew & Danay 1992; Dunbar & Grattan-Bellew 1995; Shrimmer 2000; Grattan-Bellew & Mitchell 2006) proposed the *Damage Rating Index* method (DRI), which consists in assessing the presence of petrographic features of deterioration on polished concrete sections. This method is increasingly being used, as well as other "parent" petrographic methods (Blight et al. 1981; Sims et al. 1992; Salomon & Panetier 1994; Clemena et al. 2000; Rivard et al. 2000, 2002; Broekmans 2002; Lindgård et al. 2004; Powers & Shrimmer 2007; Lindgard et al. 2012), but many of these analyses actually result in semi-quantitative assessment, at best, of the observed distress affecting the concrete. Also, the results are often heavily affected by the experience of the petrographer carrying out the examination. Therefore, petrographic analyses are often criticized by engineers who prefer a precise evaluation on the extent of damage of a concrete material or element.

Many studies carried out over the past few decades have shown that ASR affects the mechanical properties of the concrete "material". Moreover, studies dealing with the mechanical responses of damaged materials suggest that the "*Stiffness Damage Test (SDT)*" can provide a diagnostic evaluation of the "degree of damage" in concrete affected by ASR through cyclic loading (under compression) of the concrete test specimens. However, the SDT

does not have a standard test procedure yet, which limits its use for quantitative assessments when different concretes (i.e. \neq mix designs/strengths) and aggregate types are used.

2.4.1 Stiffness Damage Test (SDT)

From the mid 1980s, Crisp and coworkers used the SDT to quantify the degree of damage in concrete due to ASR (Crisp et al. 1989; 1993). Actually, Walsh (1965) had previously reported a good correlation between the crack density and the cycles of loading/unloading (stress/strain relationship) of rock specimens. Based on those results, Crouch (1987) then proposed a new test procedure (the SDT) based on cyclic loading (in compression) of concrete samples (cylinders or cores) with diameters greater than 70 mm (length / diameter of 2.0 – 2.75) (Crisp et al. 1989; 1993).

Initially, the SDT involved the application of a stress of up to 5.5 MPa at a rate of 0.10 MPa/s (Crisp et al. 1989; 1993); the authors wanted this testing procedure to be non-destructive, thus enabling the use of the test specimens for further testing. The loading was then controlled by a microprocessor and repeated five times. Crisp and coworkers carried out more than 1000 tests on cores extracted from damaged concrete structures; after analyzing the stress-strain response, they proposed the following as the diagnostic parameters for determining the extent of damage in a specimen (Crisp et al. 1989; 1993) (Figure 2.8):

- *Modulus of elasticity* (E): average modulus of elasticity value of the last four cycles, as concrete samples of damaged concretes presented lower secant modulus of elasticity than undamaged samples;
- *Hysteresis area* (HA, in J/m^3): area of the hysteresis loops averaged over the last four cycles, as damaged concrete samples showed greater energy loss (or hysteresis areas) than undamaged samples;
- *Non linearity index* (NLI): it represents the ratio of the slope of the stress response at half the maximum load over the secant E_c . This parameter provides information about either the extent of damage or the crack patterns of the samples.

Crisp et al. (1989; 1993) observed that the hysteresis area of the first cycle was much greater than that of the following four cycles (Figure 2.8) and attributed the above feature to a sliding effect across surfaces of the opened cracks in the early stage of the test. Therefore, the authors proposed to reject the results corresponding to the first cycle, as they wanted the SDT to be non-destructive. They also found that the modulus of elasticity is the most sensitive parameter

of the test, as significant reductions are often recorded even in slightly damaged concretes. However, for higher degrees of damage, the hysteresis area is the critical parameter for detecting deterioration. Also, the authors observed that the crack pattern could influence the results of the test. They found that samples with a main cracking pattern perpendicular to loading show a low modulus of elasticity, a high hysteresis area and a NLI greater than unity, while those with a main cracking pattern parallel to loading displayed a high modulus of elasticity, a low hysteresis area and a NLI lower than unity. It is important to mention that Crisp et al. (1989; 1993) did not provide any information about the aggregate types or the mix designs of the concretes tested in their work. However, Wood et al. (1996) presented the following results of the petrographic analysis of the aggregates in the concrete cores tested by Crisp et al. (1989; 1993): a) natural gravel (predominantly sandstones and metaquartzites, with presence of chert); b) reactive sand (with the presence of chert particles in the 3 to 8 mm size fraction); c) reactive sand (with presence of chert); and d) greywacke.

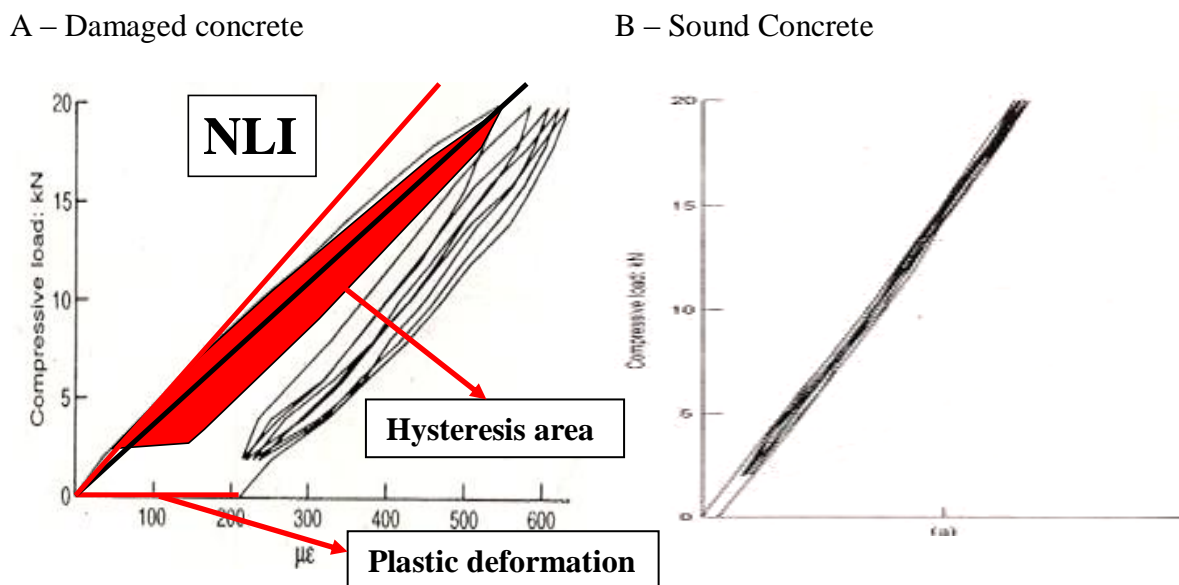


Figure 2.8: Stress-strain behavior for damaged (A) and sound (B) concretes (Crisp et al. 1993).

Smaoui et al. (2004b) further evaluated the reliability of the SDT on laboratory concrete samples incorporating a variety of reactive rock types that had reached different expansion levels (stored at 38°C at 100% R.H.). After carrying out many tests, the authors found that the best output response for the SDT was the hysteresis area of the first cycle for test specimens loaded up to a maximum of 10 MPa. They mentioned that the lowest stress level evaluated (5.5 MPa; same used by Crisp and coworkers) did not allow the ASR-induced microcracks to

stress (reclose) sufficiently, thus enabling to draw statistically reliable information on the level of ASR expansion reached by the concrete under investigation. The authors also found that the correlation between the expansion and the plastic deformation obtained after the five loading/unloading cycles was fairly satisfactory. However, they noted significant variations for either the hysteresis area or the plastic deformation for concrete specimens incorporating different types of reactive aggregates. These differences were possibly associated to the nature of the aggregates selected (fine or coarse) and differences in the internal pattern of damage, as they can generate their own reaction mode (i.e. pattern/density/orientation of cracking depending on whether the damage is generated in the fine or coarse aggregate, or by different rock types, etc.). It is also important to mention that the work carried out by Smaoui et al. (2004b) was based on one single concrete mix design (420 kg/m^3 , $w/c = 0.42$, 28-day compressive strength of about 35 MPa), and that the loading level of 10 MPa worked best with that particular type of concrete (they had also tested companion specimens up to a maximum load of 5.5 MPa, as proposed by Crisp et al (1989; 1993)).

It is logical to believe that using a single load of 10 MPa for concrete specimens extracted from different types of structural elements could result in different responses in the SDT, depending on the characteristics of the concrete analyzed (i.e. \neq mix designs, \neq types of fine / coarse aggregate, etc.). However, this hypothesis has not been studied in depth yet and, without it, the analysis of the data generated during the SDT for different mix designs could result in erroneous estimates of the actual degree of damage and of the expansion achieved to date.

Finally, although the SDT was originally developed for assessing the effects of ASR on concrete, the test certainly has the potential of evaluating the extent of damage in concrete affected by other deleterious mechanisms, such as freezing and thawing, action of fire, impact loads, DEF, etc. (Crisp et al. 1989; 1993). Smaoui et al. (2004b) also reported a good correlation between the expansion at the time of testing of concretes undergoing freezing-thawing cycles and the hysteresis area over the first cycle in the SDT. However, there is currently limited data available on the signature of specific damage mechanisms when concrete specimens are tested through the SDT (Bérubé et al. 2012).

Crisp et al. (1989; 1993) also thought that the SDT had the potential of being non-destructive, and since the number of samples taken within a structure under evaluation is often limited (for

economic or technical reasons), they considered interesting the possibility of using the same cores to perform other tests following the SDT, such as residual expansion, petrographic tests, compressive and tensile strengths, etc. Following mechanical testing, chemical tests (e.g. soluble alkalis, pore solution extraction, etc.) could also be performed on the same specimens (Bérubé et al. 2005b). The non-destructive character of the SDT is, however, yet to be confirmed, as it would likely depend on the loading level used. Moreover, the influence of some input parameters or test conditions on the various test responses, such as the concrete's conditioning history (storage conditions after coring), the type of specimens end preparation (end grinding vs. capping), the specimen's geometry and size, the specimen's environment (location and direction), as well as the choice of the sample's strength (critical for selecting the loading level in the test), as well as the basic precision of the test (e.g. variability of test results for specimens extracted very close to each other in a deteriorated concrete element) was not really studied in details, thus preventing the development of a standard test procedure.

2.4.2 Damage Rating Index (DRI)

The Damage Rating Index method (DRI) consists in a microscopic analysis, performed with the use of a stereomicroscope (about 16x magnification), where damage features generally associated to ASR are counted through a 1 cm² grid drawn on the surface of a polished concrete section (Figure 2.9). The number of counts corresponding to each type of petrographic features is then multiplied by a weighing factor, whose purpose is to balance their relative importance towards the mechanism of distress (for instance ASR). It is important to mention that the factors used in the method were chosen on a logical basis, but rather arbitrarily (Villeneuve et al. 2012). Ideally, a surface of at least 200 cm² should be used for DRI analysis, and it may be greater in the case of mass concrete incorporating larger size aggregate particles. However, for comparative purposes, the final DRI value is normalized to a 100 cm² area (Shrimer 2006). DRI results are often represented by charts enabling easy visualization of the different damage features in the specimen under study (Figure 2.10).

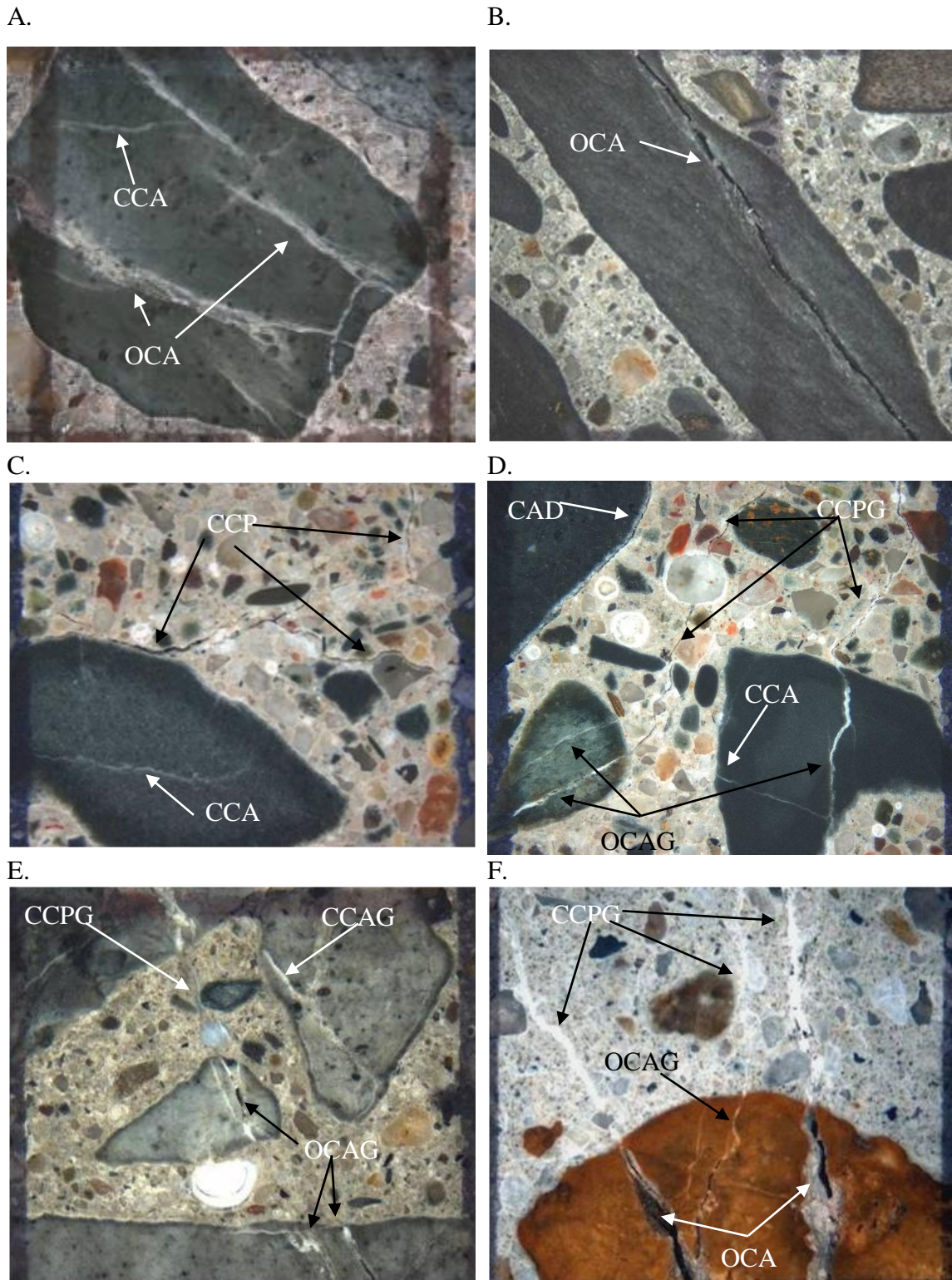
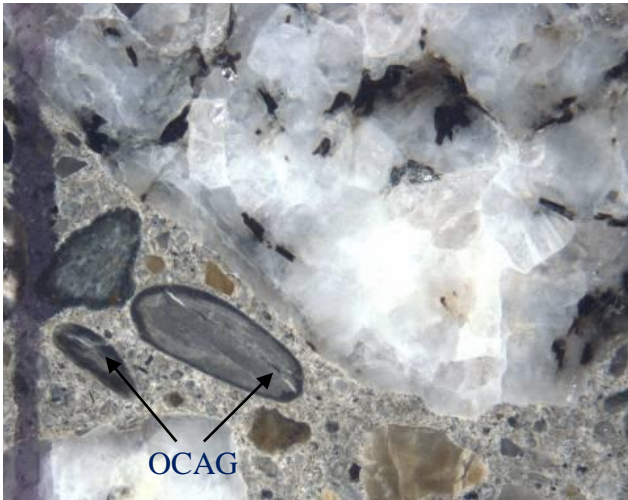


Figure 2.9a: Petrographic features of ASR in concrete incorporating reactive coarse aggregates; the abbreviations are given in the Table 1. The distance between the vertical lines is 1 cm (from Villeneuve et al. 2012). A. Closed (tight) cracks and network of cracks in the coarse aggregate particle. B. Opened crack in the coarse aggregate particle. C. Closed (tight) crack in the coarse aggregate particle; cracks in the cement paste. D. Cracks with reaction products in the coarse aggregate particles and in the cement paste; debonded coarse aggregate particle. E. Cracks with reaction products in the coarse aggregate particles and the cement paste. F. Cracks with reaction products in the cement paste; opened cracks and cracks with reaction products in the coarse aggregate particle. Other petrographic features or ASR present in the micrographs: reaction product in voids of the cement paste and reaction rims.

G



H

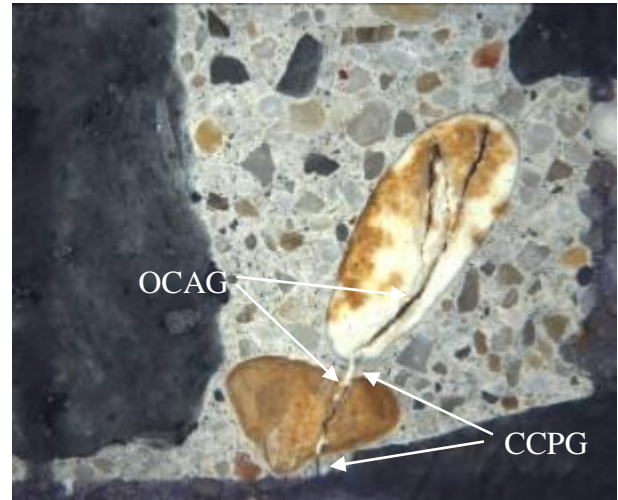


Figure 2.9b: Petrographic features of ASR in concrete incorporating reactive fine aggregates; the abbreviations are given in the Table 1. The distance between the vertical lines is 1 cm (from Villeneuve et al. 2012). G. Cracks with reaction products in fine aggregate particles and the cement paste. H. Cracks with reaction products in fine aggregate particles and in the cement paste (note: reaction products are still present in some portions of the cracks in the fine aggregate particles but some has disappeared through sample preparation).

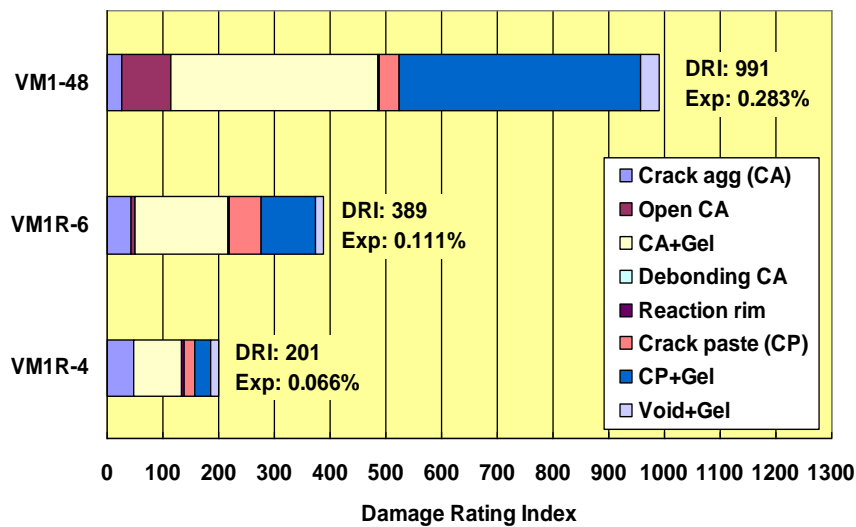


Figure 2.10: Example of DRI chart for damaged concretes with different levels of distress (Transtec Group 2009).

Recent studies dealing with the DRI indicated that the variability between the operators performing this test could be significantly reduced by improving the definition/description of the different damage features, modifying some weighing factors (Table 2.1), as well as by appropriate training of the petrographers using reference sections (Villeneuve et al. 2012). The authors proposed to use of identical factors for the two categories of opened cracks in the aggregate particles (factor of 2) or cracks in the cement paste (factor of 3), with or without

reaction products; this was done to reduce the variability associated to the difficulty in positively recognizing the presence of reaction products in cracks of the polished sections. Consequently, the two types of cracks could be grouped together (having the same weighing factors!), if one considers that a crack is an indication of damage, either with or without reaction products. Also, greater weighing factors for cracks in the cement paste, compared to that in the aggregate particles (i.e. factor of 3 vs. 2), were selected to indicate that a relatively greater importance is attributed to cracking in the cement paste, regarding the durability of the affected concrete element. Finally, it was found that eliminating the counts of the number of voids with reaction products in the cement paste and reaction rims at the periphery of reactive aggregate particles from the calculation of the DRI values also contributes at reducing the variability between the operators in the DRI determination. This is acceptable considering that the above, despite being generally associated to ASR (when the nature/origin of the reaction products and of the reaction rim can be positively confirmed), are not really direct indications of “damage” in concrete.

Since the process of damage generation varies with the type of reactive aggregate used (fine vs. coarse aggregate, lithotype, etc.), the DRI should ideally assess the nature and degree of distress signs and correlate them with either the expansion attained by the distressed concrete or the reductions in mechanical properties. Such information is, however, currently very limited. Moreover, although the differences between highly and mildly distressed concrete specimens are very clear under the microscope (Grattan-Bellew & Mitchell 2006; Transtec Group 2009), there is currently no classification established to separate low, moderate or high damage levels in the DRI.

Table 2.1: Petrographic features and weighing factors used for Damage Rating Index determination (Villeneuve et al. 2012).

Petrographic features	Abbreviation	Factors	Comments/Description
Closed/tight cracks in coarse aggregate particle	CCA	0.25	<ul style="list-style-type: none"> • Tight/fine cracks showing no gap at about 15x magnification; • Sometimes “appear” to contain whitish secondary products, as the crack forms an angle with the cutting plane thus causing such an optical effect simulating the presence of ASR products (Figures 2.9A & 2.9C); • A low factor is given as such cracks are likely/often produced by aggregate processing operations (quarried aggregate) or weathering (gravel).
Opened cracks or network of cracks in coarse aggregate particle	OCA	2.0	<ul style="list-style-type: none"> • Crack showing a gap at about 15x magnification (Figure 2.9B); • A “network” of cracks is also classified in this category, as it is likely caused by expansive reactions within the aggregate particles (Figure 2.9A).
Opened cracks or network cracks with reaction product in coarse aggregate particle	OCAG	2.0	<ul style="list-style-type: none"> • Cracks containing secondary reaction products (whitish; glassy or chalky in texture) (Figures 2.9D, 2.9E); • Secondary products often do not fill all the cracks (material likely lost during polished section preparation process) (Figure 2.9H).
Coarse aggregate debonded	CAD	3.0	<ul style="list-style-type: none"> • Crack showing a <u>significant</u> gap in the interfacial zone between the aggregate particle and the cement paste (Figure 2.9D); • Would likely cause debonding of the particle when fracturing the concrete, as it appears around a significant portion of the coarse aggregate particle.
Disaggregated/corroded aggregate particle	DAP	2.0	<ul style="list-style-type: none"> • Aggregate particle that shows signs of disintegration “corrosion” or disaggregation (ex: reacting opaline shale and chert/flint particles).
Cracks in cement paste	CCP	3.0	<ul style="list-style-type: none"> • Crack visible at about 15x magnification, but with no evidence of reaction products (Figure 2.9C).
Cracks with reaction product in cement paste	CCPG	3.0	<ul style="list-style-type: none"> • Cracks containing secondary reaction products (whitish; glassy or chalky in texture) (Figure 2.9D-2.9F, 2.9H); • Secondary products often do not fill all the cracks (material likely lost during polished section preparation process).

2.5 Predicting ASR expansion and damage

It was found over the years that the modeling of ASR and of the resulting expansion can be very useful to obtain relevant prediction of the structural response of distressed concrete

elements. Thus, in order to be efficient and reliable, models should take into account both the chemical and physical aspects of ASR (Multon et al. 2009).

Several ASR models were developed over the years to predict expansion and damage on both ASR affected materials (microscopic models) (Bazant & Steffens 2000; Comby-Pérot et al. 2009; Dunant & Scrivener 2009; Nielsen et al. 1993; Furusawa et al. 1994; Poyet et al. 2007; Suwito et al. 2002; Charpin & Ehrlicher 2012) and ASR affected structures/structural elements (macroscopic models) (Ulm et al. 2000; Li & Coussy 2002; Saouma & Perotti 2006; Grimal et al. 2008; Comi et al. 2009). The first group aims at modeling both the chemical reactions and the mechanical distresses caused by ASR, or even the coupling of both phenomena. The second group aims at understanding the process of distress generation in structures/structural concrete elements in a real context, thus simulating their likely in situ behavior (Naar 2010).

Multon et al. (2009) developed a micro chemo-mechanical ASR model at the Laboratoire des Matériaux et Durabilité des Constructions (LMDC), INSA, Toulouse (France), based on the works of Furusawa et al. (1994); Nielsen et al. (1993); Suwito et al. (2002) and Poyet et al. (2007), whose final objective is to predict the expansion of concrete in real damaged structures. The main input parameters of the above model are the alkali and reactive silica contents, the grading of the aggregate and the mechanical properties of the considered materials (aggregates, mortar/concrete). The model output results are the determination of concrete expansion and damage due to ASR, taking into account the physicochemical reaction mechanisms (chemo-mechanical modeling) (Multon et al. 2009). The LMDC micro-model approach for assessing damage/expansion of concretes is based on the definition of a representative elemental volume of concrete (REV – Figure 2.11) that contains both a mixture of aggregate particles (reactive or not, and of different sizes) and a cement paste enveloping those particles. The REV is considered to represent the behavior of the bulk concrete volume (Multon et al. 2009).

In the LMDC micromodel, the following chemical mechanisms are considered: 1) the alkali diffusion into the aggregate particles; 2) the production of ASR gel with the increase of alkali concentration in the aggregate particles; 3) the decrease of the alkali concentration in the cement paste as a function of their consumption by the ASR gel; 4) the displacement of a part of the ASR gels into the cement paste porous zone surrounding the reactive aggregate

particles. When that porous zone of thickness t_c is filled by ASR gel, the continuous gel generation provides significant pressure on the surrounding cement paste, leading to the material swelling (Multon et al. 2009).

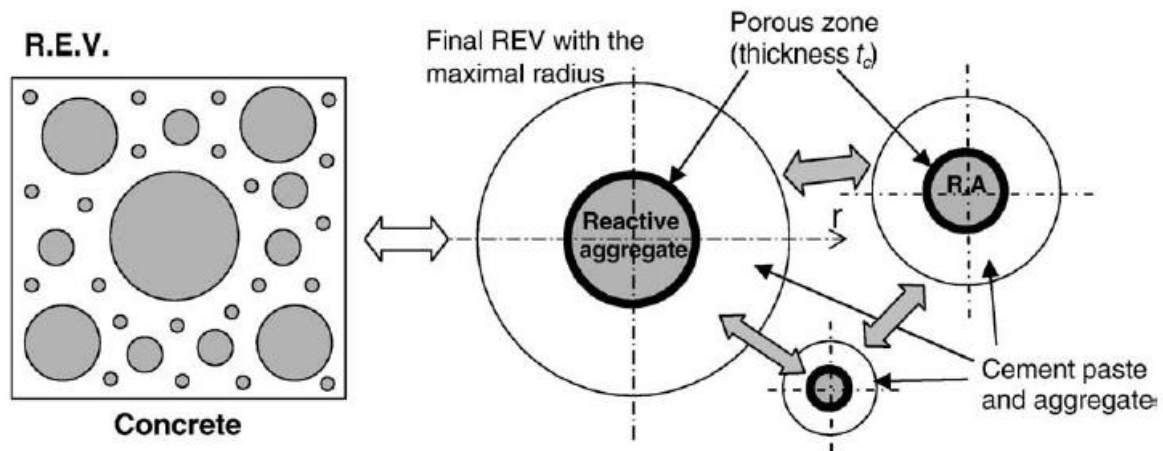


Figure 2.11: Definition of the Representative Elementary Volume (REV) for several reactive aggregate sizes (Multon et al. 2009).

In terms of mechanical effects, it is known that ASR expansions occur over long time periods. During this process, ASR-affected concretes are not subject to instantaneous loadings/stresses, but actually to progressive stresses that are very likely to cause creep on the distressed materials. Since the LMDC model takes into account creep effects on ASR expansion/distress, the modulus of elasticity of the concretes is adopted as one third of their instantaneous modulus at 28 days. This assumption is the typical approach used in the French design code for reinforced concrete structures. If the stresses provided by ASR gel, once all the cement paste porosity is filled, become greater than the tensile strength of the concrete material represented by the REV, cracks and damage are generated in the surrounding cement paste “ring” (Multon et al. 2009). If ASR progresses, which depends on the amount of silica available in the reactive aggregates, the thickness of the distressed concrete “ring” increases up to a point that “all the REV” is affected/damaged by the deleterious chemical reaction (Figure 2.12).

The models proposed by Furusawa et al. (1994), Nielsen et al. (1993), Suwito et al. (2002) and Poyet et al. (2007), as well as the LMDC model proposed by Multon et al. (2009), consider that the main cause of distress due to ASR is a consequence of ASR gel pressure generated once it fills a porous zone surrounding reactive aggregate particles, thus applying stresses on the cement paste (Figure 2.13). However, the above authors did not consider, at

least in their model calculus, the development/consequences of cracking in the aggregate particles, although Multon et al. (2009) mentioned that some cracks “are likely to be found in the aggregates” as part of ASR development.

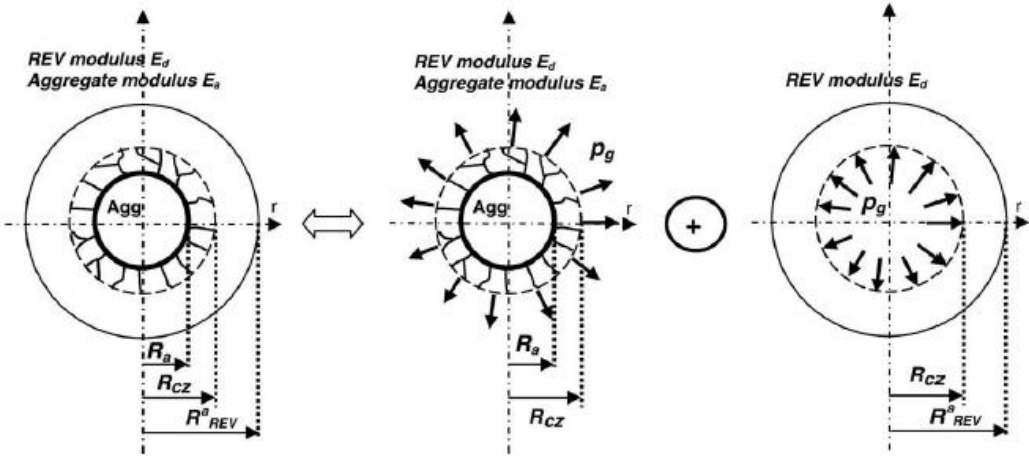


Figure 2.12: Mechanical equilibrium of the damaged REV (Multon et al. 2009).

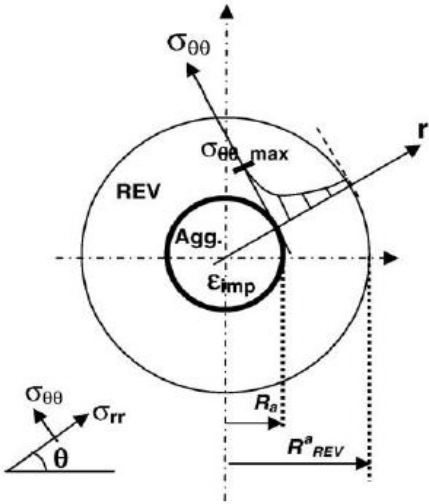


Figure 2.13: Major stress found in REV due to ASR expansion (Multon et al. 2009).

On the other hand, Dunant & Scrivener (2009) and Ben Haha et al. (2007) observed the presence of a huge amount of cracks inside the aggregates particles according to microscopic and macroscopic observations. They support the hypothesis that damage begins with a gel pocket formation inside the aggregates, before causing cement paste cracking. This statement confronts the LMDC model assumption. Pleau et al. (1989) found that either the macroscopic expansion or the “damage” in concrete affected by ASR are strongly related to the microstructural location of cracks. Thus, predicting the expansion and progress of this harmful chemical reaction is only possible for models which describe more accurately the

deterioration process at microstructural levels (Dunant and Scrivener, 2009; Ben Haha et al. 2007).

Figure 2.14 illustrates three damage mechanisms already adopted in the literature to characterize ASR distress. The first and simplest model (Figure 2.14A) applies a pseudo-thermal expansion in the aggregates as a source for ASR expansion. Although it has been found possible to calibrate such model type to fit the early part of the ASR curves, it does not capture distress in the aggregates, and thus their reduction in physical properties. Therefore, the predictive potential of such a model is low, since the expansion of the aggregate must be computed as an empirical function of the degree of reaction (Dunant & Scrivener, 2009). The second simplified model for ASR which has been proposed implies that the gel is formed as a “rim” around the aggregate (Figure 2.14 B). This is notably consistent with observations made on aggregates formed by just one mineral type. However, it is not representative for the vast majority of the aggregates used in concrete, which are made by a composition of several minerals. This model is different from the previous one in that it explicitly affects the bond properties between the reactive aggregate particles and the cement paste (i.e. Interfacial transition zone - ITZ). The fracture patterns obtained in such a setup show this model is not a good candidate neither to explain the ASR damage, mostly in the case of composite aggregates, because the *“cracks are located in the cement paste, while the aggregates remain largely intact”* for all ASR expansion levels (Dunant & Scrivener, 2009). Finally, the third and more complete model (Figure 2.14C) shows the presence of pocket gels formation in the aggregate particles which enables the full damage characterization of the composite affected material (aggregates and cement paste).

Preliminary researches show that ASR macroscopic expansion and damage are strongly linked to the microstructural location of the reaction. Thus, the prediction of expansion from the progress of the reaction is only possible in models that simulated the direct consequences of ASR at the microstructure level, which opposes to LMDC model (Dunant & Scrivener, 2009). Moreover, although the LMDC has already been effectively used for the assessment/prediction of mortars behavior containing highly reactive aggregates, it has never been applied so far to concrete specimens cast and cured in the laboratory, which makes its validation difficult since differences between the behavior of ASR-affected mortar and concrete specimens have been widely reported (Lu et al. 2006; Fournier et al. 2006; Sanchez

et al. 2008; Gao et al. 2013; Multon et al. 2008). Moreover, ASR prediction for concrete with different strengths was never studied using this model.

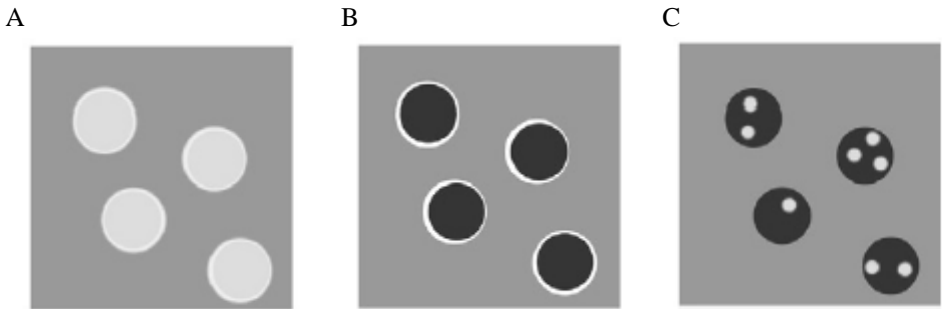


Figure 2.14: Models used to evaluate AAR-generated damage (from Dunant & Scrivener 2009). A. Expansion of the aggregate particles. B. Expansion of the reaction rims. C. Expansion of the gel-filled pockets in the aggregate particles.

3. PROBLEM STATEMENT AND OBJECTIVES OF THE PhD STUDY

As discussed in the literature review, the *Stiffness Damage Test (SDT)* is probably one of the most promising/diagnostic test procedures to quantify damage in concrete affected by AAR. Although Smaoui et al. (2004b) improved the test procedure originally proposed by Crisp et al. (1989; 1993), i.e. by performing the cyclic test at a fixed load of 10 MPa since the lower loading of 5.5 MPa was unable to distinguish the different expansion levels of expansion studied, the former authors noticed significant differences in the behavior of concretes incorporating different aggregate types. These differences were likely function of the aggregates nature (fine or coarse aggregate) and the differences in the “internal damage” generated by the different lithotypes used. However, this issue was not studied in details. Also, the analyses performed by Smaoui et al. (2004b) dealt with a unique concrete mix design (ASTM C 1293 or CSA A.23 14A). Consequently, the SDT procedure as it stands at the moment, presents many unknowns regarding the effect of some input parameters on the results of the test (i.e. on its main output parameters – Hysteresis area, plastic deformation and modulus of elasticity), which may lead to misleading interpretation when different concrete materials (i.e. different concrete strengths, mix designs and materials contents, types (fine or coarse) and nature (lithotype) of reactive aggregates are used.

The other promising test proposed by Bérubé et al. (2005a) for quantifying damage in concrete due to AAR was the *Damage Rating Index (DRI)*. The work by Smaoui and coworkers showed that a good correlation can be obtained between the DRI and the expansion of ASR-affected concrete specimens. However, the DRI should ideally assess the nature and the extent of the damage features of deterioration against reductions in mechanical properties of the damaged concrete. Such information is currently very limited. Moreover, although the differences between highly and mildly distressed concrete specimens are clear under the microscope (Grattan-Bellew & Mitchell 2006; Transtec Group 2009), there is currently no classification established to separate low, moderate or high damage levels in the DRI. It is also important to mention that even if the DRI has been used by several researchers, there is currently no standard test procedure. However, before one could think of developing a standard procedure for the DRI, it appears that the following questions should be answered (Rivard et al. 2002; Shrimmer 2006; Bérubé et al. 2012).

- Should the DRI provide an absolute output value representing a damage degree associated to a distress mechanism, such as AAR ?

- Does the type of the reactive aggregate (fine vs. coarse aggregate, lithotype, etc.) influence the output results of the DRI for the same level of expansion achieved ?
- Does the mechanical characteristics (for instance the stiffness) of the non-reactive coarse aggregate (in the case of ASR coming from a reactive sand) influence the crack's propagation process, and to what extent ?

Globally, there is currently very limited information about the relationship between the development of the micromechanical features of ASR and the loss in the mechanical properties of ASR-affected concrete incorporating different reactive rock types. Such shortcomings limit the applicability of the DRI and SDT for determining either the current damage degree or the potential for further ASR distress of concrete infrastructures.

Based on the gaps in the information available in the literature, as described above, this PhD study has been designed to meet the following objectives:

- Improve our understanding of the development of distress features of AAR in concretes incorporating a range of reactive rock types and concrete mix designs;
- Propose (a) qualitative distress microscopic model(s) for AAR-affected concretes incorporating a range of reactive rock types;
- Improve our understanding on how the development of the physical features of AAR (e.g. cracking in the aggregate particles and in the cement paste) influence the mechanical behavior of the affected concretes;
- Develop/improve and optimize the most promising microscopic (DRI) and mechanical (SDT) laboratory test procedures used for quantifying damage in concrete due to AAR, in order to develop an efficient management protocol for aging concrete infrastructures;
- Propose a global quantitative damage chart/plot based on AAR micro-mechanical coupling;
- Validate and/or discuss on the limitations of an ASR physico-chemical model developed by the LMDC (Laboratory of Materials and Durability of Constructions Toulouse – INSA Toulouse) research group, through the use of experimental data (i.e. chemical, microscopic and mechanical) obtained in the laboratory for a wide range of concretes (i.e. \neq concrete strengths, mix designs, etc.) and aggregate's nature (i.e. \neq lithotypes) and types (i.e. fine vs. coarse aggregate).

4. RESEARCH PROGRAM

The global experimental program carried out in this research can be divided into two main parts: 1) testing carried out on laboratory-made specimens and; 2) testing carried out on field cores extracted from an ASR-affected concrete structure (Robert-Bourassa/Charest viaduct, in Quebec City, Canada) (Figures 4.1 and 4.2, respectively).

4.1 Experimental procedures part I: laboratory-made specimens

For the first part of this PhD project, three non air entrained concrete mixtures (25, 35 and 45 MPa mix design strengths) and ten moderately to highly-reactive aggregates (fine and coarse) were selected. The coarse aggregates ranged from 5 to 20 mm in size, while the non-reactive and reactive sands were largely composed of particles < 5 mm. Non-reactive fine and coarse aggregates were used in combination with the above reactive aggregate materials for concrete manufacturing.

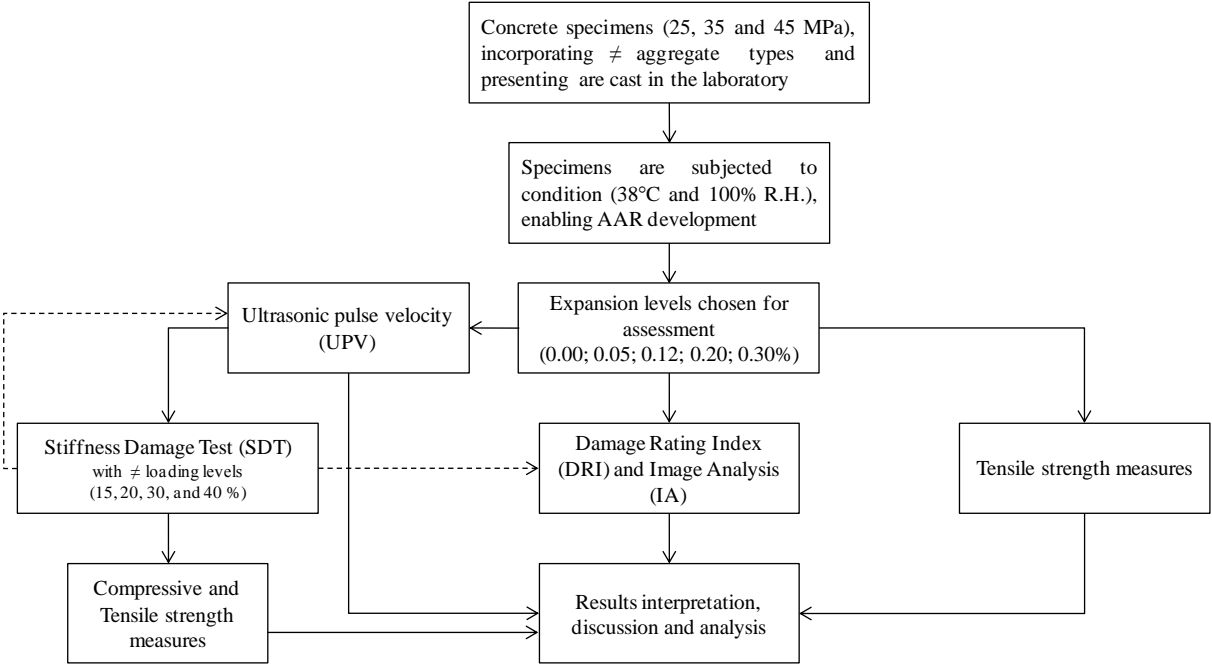


Figure 4.1: Structure of the Part I of the PhD project: laboratory-made specimens.

All the concrete mixtures were designed to contain the same volume of paste and aggregates (i.e. from one mix to another), in order to allow comparison between similar systems. All concretes were made with the same conventional (CSA Type GU) high-alkali (0.88% Na₂O_{eq}) Portland cement. Reagent grade NaOH was used to raise the total alkali content of

the mixtures to 1.25% Na₂O_{eq}, by cement mass, for accelerating the expansion process due to ASR. The concrete mixtures were divided in the following two series: *base series* and *complementary series*. The mixtures of the *base series* (incorporating the following two highly reactive aggregates: Texas sand (Tx) and New Mexico gravel (NM)) were chosen to provide initial/base results/data to serve as the background for further analysis throughout the testing of the mixtures of the *complementary series*. These base mixtures were the subject of three scientific articles (Papers I, III, and VI of this PhD thesis). The results of testing carried out on the test specimens of the *complementary series* were discussed in the other three scientific papers of this PhD thesis (Paper II, IV and V).

A total of 68 cylinders for each mixture of the *base series* and 35 cylinders for each of the *complementary series* (100 by 200 mm in size) were made in the laboratory. After casting, all the specimens were placed for 48h in the moist curing room (i.e. after the first 24h in the moist curing room, the specimens were demolded and left in this room for an additional 24h). Small holes, 5 mm in diameter by 15 mm long, were then drilled in both ends of each test cylinders and stainless steel gauge studs were glued in place, with fast-setting cement slurry, for longitudinal expansion measurements. After completion of the first 48 h at 23°C, the “0” length reading was performed and the specimens were placed in sealed plastic (22 liters) containers lined with damp cloth (4 cylinders per bucket). All buckets were then stored at 38°C and 100% R.H., and all the test cylinders were monitored regularly for length variations. Moreover, as per ASTM C 1293, all containers were cooled to 23 °C for 16 ± 4 h prior to periodic axial expansion measurements. Then, test cylinders were removed from the high-temperature storage conditions for SDT testing when they reached the expansion levels chosen for this research, i.e. 0.05% ± 0.01%, 0.12% ± 0.01%, 0.20% ± 0.01% and 0.30% ± 0.01%. Overall, ASR expansions among the test cylinders of a same batch were only slightly variable, as the entire test set was cast at the same time and from the same large concrete batch. *Note: All characteristics of the aggregates and concrete mixtures used in the PhD work are presented in the six scientific papers of the Thesis.*

Once the above mentioned expansion levels were reached, the specimens were wrapped in plastic films and stored at 12°C until testing (because of testing capacity issues). Prior to mechanical testing, both ends of each cylinder were carefully mechanically ground (to avoid any interference from the stainless steel gauge studs used for expansion measurements) and then non destructive testing (ultrasonic pulse velocity) was performed over all concrete

specimens. Also, even though they were wrapped in plastic film prior to testing, the specimens were restored for 48h in the moist curing room at 23°C, protected from running water, before the mechanical procedures. This approach was used in order to allow appropriate saturation of the test specimens, in accordance with the procedure proposed for concrete cores extracted from concrete structures (CSA A23.2-14C). Length and mass readings were also performed on a number of test specimens prior and upon unwrapping to make sure that they had not suffered from significant shrinkage or expansion over the storage period at 12°C. The monitoring of the test specimens showed that the 12°C storage resulted in slight shrinkage ($-0.02 \pm 0.01\%$) and mass loss ($0.7 \pm 0.2\%$) of the test specimens, which was recovered through the 48-hour re-saturation period prior to running stiffness damage testing. In the case of the petrographic assessment, the concrete cylinders that were stored at 12°C were cut, polished, rewrapped (i.e. plastic film) and restored at 23 ± 2 °C.

The investigation program carried out on the concrete cylinders at different expansion levels included mechanical testing (SDT, modulus of elasticity, compressive and tensile strength determination), semi-quantitative petrographic analysis (DRI) and non-destructive evaluation through the use of ultrasonic pulse velocity (UPV).

4.1.1 Stiffness Damage Test (SDT)

The SDT was carried out over five loading/unloading cycles at a controlled loading rate of 0.10 MPa/s. For the specimens from the *base series*, four different loading levels, i.e. 15%, 20%, 30% and 40% of the design (28-day) concrete strength were used. For the specimens of the *complementary series*, only 40% of their 28-day strength was adopted for loading. For the SDT, one test result corresponds to the average obtained on three cylinders.

4.1.2 Damage Rating Index (DRI)

A semi-quantitative petrographic analysis, using the DRI, was performed on concrete specimens. The examination was carried out in two ways. First, the DRI was performed on control and ASR-affected specimens to determine the microscopic degree of damage at each of the selected expansion levels, and for each concrete mix designs. Second, some specimens of the *base series* were cut and polished for microscopic examination, after completion of the SDT (40% load - 25 MPa concrete), thus allowing to verify the non-destructive character of the test.

4.1.3 Ultrasonic pulse velocity (UPV)

Ultrasonic pulse velocity measurements (UPV) were carried out on the specimens of the *base series*, before and after the completion of the SDT, for all the loading levels selected for the study. The goals of performing this test, as in the case of the microscopic analysis, were to assess the degree of damage in the concrete specimens due to AAR and to verify the non-destructive character of the SDT once different loading levels had been applied.

4.1.4 Compressive strength test

Compressive strength was determined in two ways throughout this project. First, tests were carried out on two cylinders cast from all concrete mixtures to determine their 28, 60, 90 and 180-day strength. For this project, as the specimens contained moderately to highly-reactive aggregates, it was considered that the conventional ASTM C 39 test procedure could not be followed as some specimens could likely develop ASR during the first 28 days in the moist room, thus potentially affecting their strength development. Therefore, the specimens were wrapped and placed at 12°C for 47, 100, 150 and 300-day periods, which are equivalent to the 28, 60, 90 and 180-day periods, respectively, according to the maturity concept presented by ASTM C 1074. Second, compressive strength was determined on two of the three cylinders of each concrete set subjected to stiffness damage testing, with the aim of verifying the compressive strength loss as a function of AAR expansion levels. Moreover, these analyses allowed the assessment of SDT's "destructive" character.

4.1.5 Tensile strength test

The tensile strength was determined on two or three specimens of all concrete mixtures, at each expansion level, using the pressure tension test. This testing procedure uses a specially designed chamber where compressed gas is used to apply a uniformly distributed pressure to the curved surface of standard 100 mm by 200 mm concrete cylinders or cores. Gas pressure is monotonically increased until the test cylinder fails in a plane transverse to the axis of the testing chamber, likely due to a strong tension force which is created over testing. This is actually the primary reason why the pressure tension method is thought to be well suited for detecting durability issues which affect the integrity of the cementitious microstructures.

4.2 Experimental procedures part II: extracted concrete cores

For the second part of the experimental program, a number of concrete cores were extracted from different zones (i.e. exposed, not exposed) of two structural elements (foundation blocks and bridge deck) of the Robert-Bourassa/Charest viaduct in Quebec City, Canada (an aging concrete structure, constructed in the middle of the 1960’s and suffering from significant damage due to ASR). Upon extraction, the cores were wrapped in plastic sheets and placed in the laboratory at 12°C to stop further ASR distress. Then, these cores were subjected to different conditions of preparation prior to testing, enabling the study of many different input parameters over SDT responses. Those test conditions are illustrated in Figure 4.2. Once these conditions were reached, as in the case of the Part I study, the test procedures described hereafter were performed.

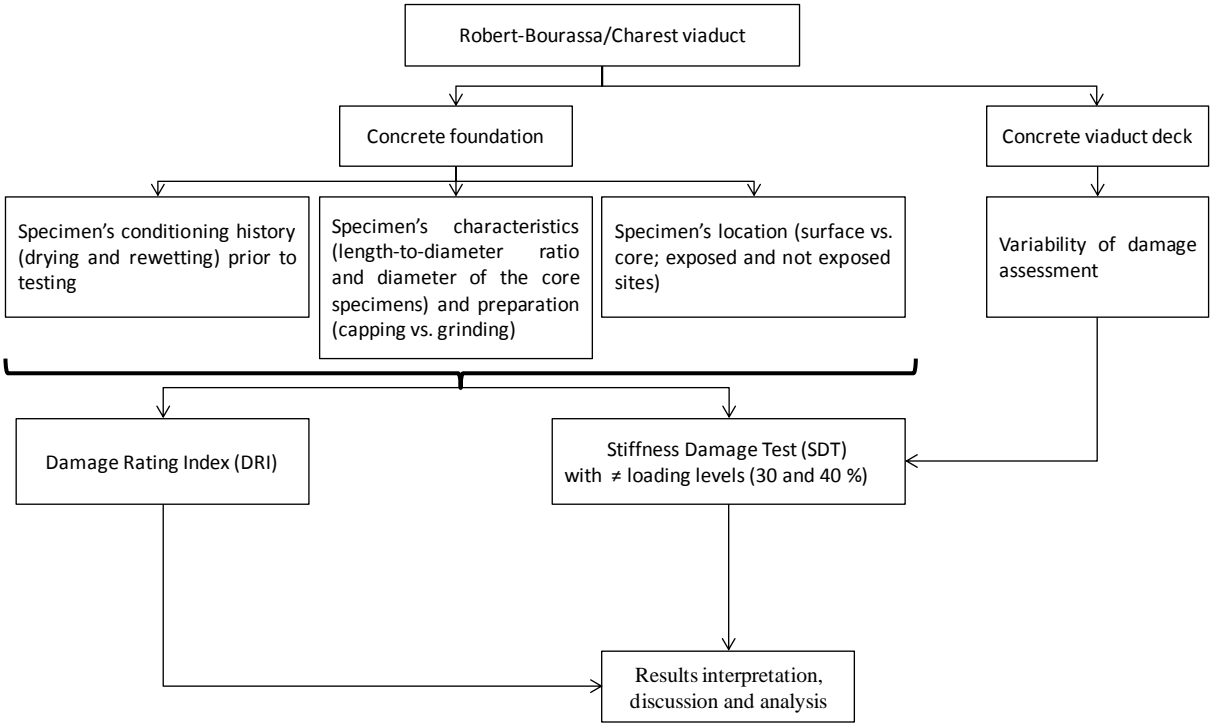


Figure 4.2: Structure of the Part 2 of the PhD project: Core specimens extracted from the Robert Bourassa – Charest Viaduct.

4.2.1 Stiffness Damage Test (SDT)

The SDT was carried out over five loading/unloading cycles at a controlled loading rate of 0.10 MPa/s. For the extracted cores, two different loading levels were chosen, i.e. 30% and 40% of the design (28-day) concrete strength, depending on the study scope.

4.2.2 Damage Rating Index (DRI)

A semi-quantitative petrographic analysis, using the DRI, was also performed on concrete cores. The goal of this part of the study was to confirm the condition of the concrete from the different zones of the structure (exposed, not exposed, surface or core of the structural element, etc.), thus enabling further correlations with the results of stiffness damage testing.

5. CORE OF THE THESIS – SCIENTIFIC PAPERS

5.1 General overview

In order to report and analyse the results obtained as part of the experimental program implemented in this PhD project, six scientific papers were strategically prepared. They cover all the major themes of the research, thus enabling to fully meet the various objectives of the PhD project. Figure 5.1 illustrates the links between the papers.

Overall, in the scientific papers I and II, the diagnostic character of the *Stiffness Damage Test (SDT)* for detecting/quantifying damage in concrete due to ASR is treated and discussed. Therefore, the most important input parameters and their influence on the output responses of the SDT are evaluated. Similarly, scientific papers III and IV deal with the evaluation of the diagnostic character of the semi-quantitative petrographic tool, the *Damage Rating Index (DRI)*, for evaluating the damage development as a function of expansion of ASR-affected concrete specimens.

Paper V presents a global appraisal (i.e. through a microscopic/mechanical coupling) of distress in concrete due to AAR, through the study of a wide range of concrete mixtures (25 concrete mixtures) and aggregate types and natures (ten different reactive aggregates). At this time of the PhD project development, the diagnostic character of both laboratory test procedures (SDT and DRI) has already been demonstrated (i.e. after the four first scientific papers) so that a full understanding of the coupling between “micro features of damage and macro mechanical behavior” of concretes affected by AAR is possible (which represents the main goal of paper V). Finally, paper VI deals with the prediction of ASR damage using a chemo-mechanical model proposed by LMDC (INSA-Toulouse). The model takes into account, as input parameters, all characteristics of the concrete mix designs used in this PhD project and compares its predictions with the results obtained in the laboratory (presented over the scientific papers 1 to 5).

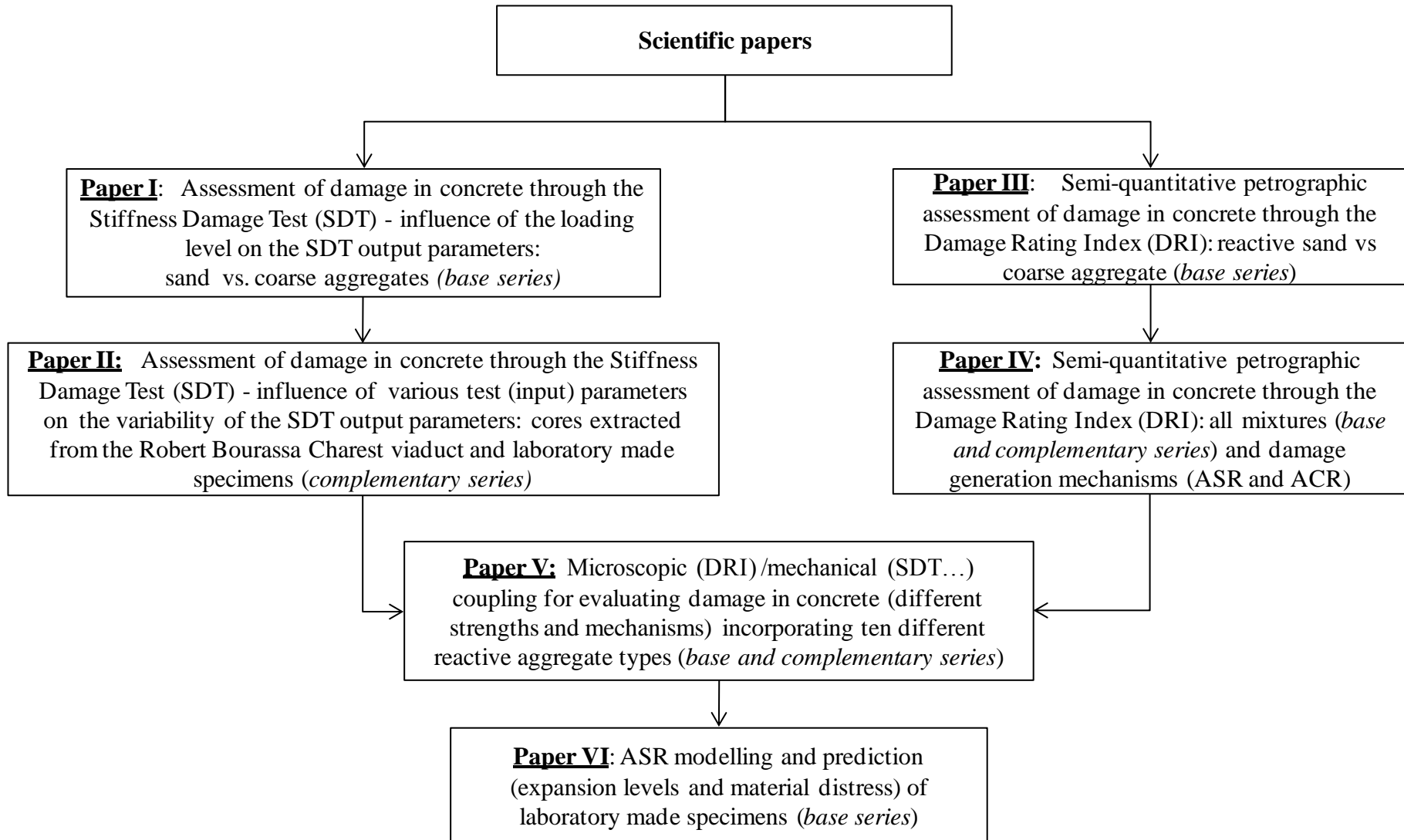


Figure 5.1: Core of the PhD Thesis – links between the scientific papers.

5.2 Scope and objectives of the scientific papers

A summary description of the content of each paper, as well as their specific objectives, is given hereafter.

5.2.1 Paper I (Section 6): *Evaluation of the Stiffness Damage Test (SDT) as a tool for assessing damage in concrete due to ASR: effect of test loading on the output responses for concretes incorporating fine or coarse reactive aggregates.*

This paper first presents a brief literature review on the use of the *Stiffness Damage Test (SDT)* for the *diagnosis* of ASR. Then, it focuses on the analysis of the results of stiffness damage testing of a series of laboratory-made concrete specimens, stored under highly controlled conditions, and incorporating two highly reactive aggregates (Tx sand and NM gravel - *base series*).

Three concrete types were used in this study (25, 35 and 45 MPa), from which a number of concrete cylinders (100 by 200 in size) were cast and then stored under conditions enabling ASR development. When the specimens reached the four expansion levels chosen for this work (i.e. 0.05%, 0.12%, 0.20% and 0.30%; $\pm 0.01\%$), they were submitted to stiffness damage test, by sets of three, using loading levels ranging from 15% up to 40% of their 28-day compressive strength. The diagnostic character of various output parameters (Hysteresis area - HA, Plastic deformation - PD and Modulus of elasticity - ME) was thus evaluated. The *Damage Rating Index (DRI)* was also performed on companion concrete specimens in two ways; first, concrete specimens were examined petrographically at the same expansion levels presented above, with the aim of determining the degree of physical damage in the test specimens; second, the DRI was also performed on specimens that were submitted to the SDT and the results “before SDT vs. after SDT” compared, enabling the evaluation of the destructive character of the test (i.e. the maximum loading level that can reliably detect the damage degree of ASR affected concrete without introducing significant “new” damage to the specimens evaluated). In addition, a statistical analysis (i.e. multivariable and two-variable ANOVA) was also performed in order to determine whether the conclusions drawn through the analysis of the data could be considered statistically significant.

5.2.2 Paper II (Section 7): Evaluation of the Stiffness Damage Test (SDT) as a tool for assessing damage in concrete due to ASR: input parameters and test procedure.

This paper, which also deals with the SDT, aims at verifying the impact of some “practical” input parameters on the SDT results, thus providing a more complete database for selecting the best parameters/conditions/approach to perform the SDT. Moreover, the impact of the above input parameters on the variability of the test results is assessed. To perform this work, several concrete cores were extracted from the foundation blocks and the bridge-deck of the Robert-Bourassa/Charest viaduct, affected by ASR. The influence of the following conditions on the SDT output responses (HA, PD and ME) was then assessed:

- Specimen’s conditioning history (effect of drying and rewetting before testing);
- Specimen’s shape characteristics (length-to-diameter ratio and different core diameters);
- Specimen’s end surface preparation (sulfur capping vs. surface grinding);
- Specimens location (surface vs. core of the concrete element; exposed vs. not exposed sites);
- Variability of the overall test results, considering field core specimens.

In addition, a series of specimens was cast from 35 and 45 MPa concrete mixtures made in the laboratory and incorporating four moderately/highly reactive aggregates (Tx sand, NM gravel, Wyo gravel and Pots sandstone). The cylinders were stored under conditions conducive to the development of ASR. When the specimens reached the expansion levels chosen for this work (i.e. 0.05%, 0.12%, 0.20% and 0.30%), they were submitted to stiffness damage test, by sets of three, at stress levels representing 40% of their 28-day compressive strength. The diagnostic character and variability of various output parameters (HA, PD and ME) were then assessed to verify the effect of the test loading on the output responses of the cyclic procedure. In addition, new output indices (*Stiffness Damage Index* - SDI and *Plastic Deformation Index* - PDI) were introduced so that the SDT could be even more diagnostic, being less impacted by the loading level’s choice. Finally, a statistical analysis (i.e. two-variable ANOVA) was performed in order to determine whether the conclusions drawn from the data analysis could be considered statistically significant.

5.2.3 Paper III (Section 8): *Use of the Damage Rating Index (DRI) to quantify damage due to alkali-silica reaction in concrete incorporating reactive fine and coarse aggregates.*

This paper first presents a brief literature review on the use of the *Damage Rating Index (DRI)* for the *diagnosis* of ASR. Then, it focuses on the analysis of the semi-quantitative petrographic results of a series of laboratory-made concrete specimens, stored under highly controlled conditions, and incorporating two highly reactive aggregates (Tx sand and NM gravel - *base series*).

The specimens used for this work were obtained from the same test series used for stiffness damage testing, i.e. three concrete strengths, four expansion levels - see description of Paper I), thus allowing direct comparison of the mechanical and petrographic test results. When the specimens reached the four expansion levels chosen for this work, they were cut, polished and the DRI was performed. The diagnostic character of the method was then critically evaluated through either its semi-quantitative “standard” results (i.e. DRI numbers using the weighing factors proposed in the original method) or its qualitative/quantitative values (i.e. total counts of each petrographic features of deterioration) for all the concrete mixtures. The development of the petrographic features of ASR distress was then analysed as a function of specimens’ expansions, for concretes where ASR is coming either from reactive sands or reactive coarse aggregates.

5.2.4 Paper IV (Section 9): *Assessment of microscopic damage features of alkali-aggregate reaction (AAR) through the Damage Rating Index (DRI).*

This paper also deals with the use of the *Damage Rating Index (DRI)* for assessing damage in concrete affected by AAR (i.e. ASR and ACR). It focuses on the analysis of the semi-quantitative petrographic observations obtained on laboratory-made concrete specimens incorporating ten moderately/highly reactive aggregates. This paper actually results of the semi-quantitative petrographic examination obtained for the *base series* specimens (presented in details in Paper III) and the specimens cast from 35 MPa concrete mixtures incorporating a wide range of reactive rock types (*complementary series*). The observations are then used to propose a qualitative model of damage generation in concrete due to AAR (ASR and ACR).

5.2.5 Paper V (Section 10): *Overall assessment of alkali-aggregate reaction (AAR) in concretes incorporating different reactive aggregate types.*

This paper presents a global critical/comparative analysis of the results obtained in the PhD research through the coupling of the microscopic features of deterioration (DRI observations) against the mechanical responses obtained on companion specimens tested through SDT, modulus of elasticity, compressive and tensile strength determination. Finally, a comprehensive quantitative AAR damage chart is proposed.

5.2.6 Paper VI (Section 11): *Comparative study of a chemo-mechanical modeling for alkali silica reaction with experimental evidences*

This paper compares the predictions provided by the chemo-mechanical model developed by the LMDC (INSA-Toulouse) and the experimental data obtained in the PhD project (scientific paper V). The results used for this comparison are those obtained from the concrete test specimens of the *base series*, i.e. results obtained from SDT, modulus of elasticity and tensile strength testing of test specimens incorporating the highly-reactive Tx and NM aggregates at the various expansion levels chosen (i.e. 0.05%, 0.12%, 0.20% and 0.30%) (i.e. Paper I). In addition, two “new concrete mixtures” were cast using the NM aggregate as a manufactured sand, and in combination with either a non-reactive coarse aggregate or with the reactive NM coarse aggregate. The aim of these mixtures was to analyse the model’s effectiveness in dealing with ASR kinetics’ changes due to the use of different aggregate size fractions presenting the same amount of reactive silica.

The main model variables were “set” as a function of the expansion behavior of the concrete specimens (i.e. ASR kinetics and amplitude) observed through laboratory readings over time. A full discussion of the result’s validation and reliability of the model is provided.

6. PAPER I: EVALUATION OF THE STIFFNESS DAMAGE TEST (SDT) AS A TOOL FOR ASSESSING DAMAGE IN CONCRETE DUE TO ASR: TEST LOADING AND OUTPUT RESPONSES FOR CONCRETES INCORPORATING FINE AND COARSE AGGREGATES

Sanchez. L. F. M.^a; Fournier. B.^b; Jolin. M.^c, Bastien, J.^d

(a) MSc. – Laval University – PhD candidate.

1065, avenue de la Médecine, Pavillon Adrien-Pouliot, local 3755 Tel.: 1 (418) 704-2435

leandrofms@gmail.com / le.sanchez@uol.com.br

(b) Prof. Dr. – Laval University. Quebec. QC. Canada

benoit.fournier@ggl.ulaval.ca

(c) Prof. Dr. – Laval University. Quebec. QC. Canada

marc.jolin@gci.ulaval.ca

(d) Prof. Dr. – Laval University. Quebec. QC. Canada

josee.bastien@gci.ulaval.ca

ABSTRACT

The Stiffness Damage Test (SDT) is a powerful tool developed for the evaluation of the damage's degree of concrete affected by ASR. This paper presents the assessment of some parameters (test loading and output responses) on the efficiency of the method. The analyses were carried out with three types of concrete (25, 35 and 45 MPa) and two highly-reactive aggregates (New Mexico gravel and Texas sand). The diagnostic character of various output parameters was analyzed and the results showed that the SDT should be carried out with a percentage of the design strength (ideally 40%) instead of working with a fixed load. Parameters such as the hysteresis area and the plastic deformation over the five cycles of loading/unloading as well as the average modulus of elasticity of the second and the third cycles seem to give quite good correlations with the amount of expansion reached by the concrete.

Keywords: stiffness damage test (SDT), assessment of damage's degree, alkali-silica reaction (ASR).

RÉSUMÉ

Le Stiffness Damage Test (SDT) est un outil puissant qui a été développé pour l'évaluation du degré d'endommagement de bétons affectés par la RAG. Cet article évalue l'influence de certains paramètres (effet du chargement et paramètres de sortie) sur l'efficacité de la méthode. Les analyses ont été effectuées avec trois types de béton (25, 35 et 45 MPa) et deux granulats réactifs (gravier du Nouveau-Mexique et sable du Texas). Le caractère diagnostique de plusieurs paramètres de sortie a été évalué en profondeur et les résultats montrent que le SDT doit être effectué avec un pourcentage de la résistance de conception du béton en question (idéalement 40%) au lieu de l'utilisation d'un chargement fixe. Des paramètres tels que l'aire d'hystérésis et la déformation plastique au cours des cinq cycles de chargement/déchargement ainsi que le module d'élasticité (comme la valeur moyenne du deuxième et troisième cycles) semblent donner de très bonnes corrélations avec l'expansion atteinte par les échantillons de béton affectés.

Mots clés: stiffness damage test (SDT), évaluation du degré d'endommagement, réaction alcali-silice (RAS).

6.1 ASSESSMENT OF DISTRESS IN CONCRETE DAMAGED BY ASR

A large number of concrete structures were built in North America and worldwide since the 1900's. Many of these structures have reached the end of their expected service life or are showing unexpected/important signs of deterioration that will require remedial actions in the near future to maintain their functionality. Selecting the most appropriate remedial actions for such structures requires that critical information be available not only on the mechanism(s) responsible for the observed damage and its extent, but also on the potential for further damage in various elements of the structure under study. Here, the word "damage" is defined in this context as the harmful consequences (measurable ones) of various phenomena (e.g. loadings, shrinkage, creep, alkali-silica reaction (ASR), sulphate attack, freezing and thawing, etc.) on the mechanical properties, physical integrity and durability of a concrete material/element.

It is well-established that different deleterious mechanisms affecting the long-term durability of concrete generate different patterns of internal damage whose "signatures" were defined by BCA [1] and St-John et al. [2]. However, one of the biggest challenges in engineering is to

establish the correlation between the above "signatures" and the loss in mechanical properties, durability and performance of the affected material or element, as well as their structural implications. Alkali-silica reaction (ASR), one of those common deleterious mechanisms, consists in a chemical reaction between "unstable" silica mineral forms within the aggregate materials and the alkali hydroxides (Na, K – OH) dissolved in the concrete pore solution. It generates a secondary alkali-silica gel that induces expansive pressures within the reacting aggregate material(s) and the adjacent cement paste upon moisture uptake from its surrounding environment, thus causing microcracking, loss of material's integrity (mechanical/durability) and, in some cases, functionality in the affected structure. Over the years, petrographic methods were developed with the aim of identifying the presence and the extent of ASR in aging concrete structures. Grattan-Bellew and coworkers [3-5] proposed the Damage Rating Index method (DRI), which consists in assessing the presence of petrographic features of deterioration on polished concrete sections. This method is increasingly being used, as well as other "parent" petrographic methods [6-15], but many of these analyses actually result in semi-quantitative assessment, at best, of the observed distress affecting the concrete. Also, the results are often heavily affected by the experience of the petrographer carrying out the examination. Therefore, petrographic analyses, although showing some promises, are often criticized by engineers who prefer a precise evaluation on the extent of damage of a concrete material or element.

Many studies carried out over the past few decades have shown that ASR can affect the mechanical properties of concrete as a "material". Usually, ASR generates a significant reduction in tensile strength and modulus of elasticity of concrete. These two properties are much more affected than compressive strength, which begins to decrease significantly only at high levels of expansion [1, 16, 17, 18]. Results suggest that compressive strength losses due to ASR are apparent at expansion degrees greater than 1 mm/m or 0.10%; particular attention is required for concrete with expansions greater than 0.30%; for structures incorporating such expansive concretes, a full structural assessment should be carried out to evaluate the impact on the structure behavior and ultimate capacity [19, 20, 21]. Moreover, the Institution of Structural Engineers in the UK [22] suggests that the structural assessment becomes appropriate at 0.6mm/m expansion when the concrete is not well constrained in 3 dimensions by reinforcement and at about 1.0mm/m for typically reinforced elements.

Studies dealing with the mechanical responses of damaged materials suggest that the "Stiffness Damage Test (SDT)" can provide a diagnostic evaluation of the "degree of damage" in concrete affected by ASR. Nevertheless, the SDT does not have a standard test

procedure yet, which limits its use for quantitative assessments when different concretes (i.e. \neq mix designs/strengths) and aggregate types are used. Thus, an in-depth evaluation on some input and output parameters of the test are required to optimize its applicability/reliability and precision.

6.2 STIFFNESS DAMAGE TEST (SDT)

From the mid 1980s, Crisp and coworkers used the SDT to quantify the degree of damage in concrete due to ASR [23, 24]. Actually, Walsh [25] had previously reported a good correlation between the crack density and the cycles of loading/unloading (stress/strain relationship) of rock specimens. Based on those results, Crouch [26] then proposed a new test procedure (Stiffness Damage Test - SDT) based on cyclic loading (in compression) of concrete samples (cylinders or cores) with diameters greater than 70 mm (length / diameter of 2.0 – 2.75) [23, 24].

Initially, the SDT involved the application of a stress of up to 5.5 MPa at a rate of 0.10 MPa/s [23, 24]; the authors wanted this testing procedure to be non-destructive, thus enabling the use of the test specimens for further testing. The loading was then controlled by a microprocessor and repeated five times [23, 24]. Crisp and coworkers carried out more than 1000 tests on cores extracted from damaged concrete structures; after analyzing the stress-strain response, they proposed the following as the diagnostic parameters for determining the extent of damage in a specimen [23, 24]:

- Modulus of elasticity (E_c): average modulus of elasticity value of the last four cycles, as concrete samples of damaged concretes presented lower secant modulus of elasticity than undamaged samples;
- Hysteresis area (H , in J/m^3): area of the hysteresis loops averaged over the last four cycles, as damaged concrete samples showed greater energy loss (or hysteresis areas) than undamaged samples;
- Non linearity index (NLI): it represents the ratio of the slope of the stress response at half the maximum load over the secant E_c . This parameter provided information about either the extent of damage or the crack patterns of the samples.

Crisp et al. [23, 24] observed that the hysteresis area of the first cycle was much greater than that of the following four cycles and attributed the behavior to a sliding effect across surfaces of the opened cracks in the early stage of the test. Therefore, the authors proposed to reject the results corresponding to the first cycle, as they wanted the SDT to be non destructive. They

also found that the modulus of elasticity is the most sensitive parameter of the test for slightly damaged concretes. However, for higher degrees of damage, the hysteresis area is the critical parameter for detecting deterioration. Also, the authors observed that the crack pattern could influence the results of the test. They found that samples with a main cracking pattern perpendicular to loading show a low modulus of elasticity, a high hysteresis area and a NLI greater than unity, while those with a main cracking pattern parallel to loading displayed a high modulus of elasticity, a low hysteresis area and a NLI lower than unity. It is important to mention that Crisp et al. [23, 24] did not provide any information about the aggregate types or the mix designs of the concretes tested in their work. However, Wood et al. [27] presented the following results of the petrographic analysis of the aggregates in the concrete cores tested by Crisp et al [23, 24]: a) natural gravel (predominantly sandstones and metaquartzites, with presence of chert); b) reactive sand (with the presence of chert particles in the 3 to 8 mm size fraction); c) reactive sand (with presence of chert) and; d) greywacke;

Smaoui et al. [18] further evaluated the reliability of the SDT on laboratory concrete samples incorporating a variety of reactive rock types that had reached different expansion levels (stored at 38°C at 100% R.H.). After carrying out many tests, the authors found that the best output response for the SDT was the hysteresis area of the first cycle for test specimens loaded up to a maximum of 10 MPa. They mentioned that the lower stress level evaluated (5.5 MPa) did not allow the ASR-induced microcracks to stress (reclose) sufficiently to enable drawing statistically reliable information on the level of ASR expansion reached by the tested concrete. The authors also found that the correlation between the expansion and the plastic deformation obtained after the five loading/unloading cycles was fairly satisfactory. However, they noted significant variations for either the hysteresis area or the plastic deformation for concrete specimens incorporating different types of reactive aggregates. These differences were possibly associated to the nature of the aggregates selected (fine or coarse) and differences in the internal pattern of damage, as they can generate their own reaction mode (i.e. pattern/density/orientation of cracking depending on whether the damage is generated in the fine or coarse aggregate, or by different rock types, etc.).

It is important to mention that the work carried out by Smaoui et al. [18] was based on one single concrete mix design (420 kg/m³, w/c = 0.42, 28-day strength of about 35 MPa), and that the loading level of 10MPa worked best with that particular type of concrete (they had also tested companion specimens up to a maximum load of 5.5 MPa, as proposed by Crisp et al.).

It is logical to believe that applying a single load of 10 MPa could result in different responses in the SDT, depending on the characteristics of the concrete analyzed (i.e. \neq mix designs. \neq types of fine / coarse aggregate, etc.). However, this hypothesis has not been studied in depth yet and, without it, the analysis of the data generated during the SDT for different mix designs could result into erroneous estimates of the actual degree of damage and the expansion achieved to date.

Finally, although the SDT was originally developed for assessing the effects of ASR on concrete, the test certainly has the potential of evaluating the extent of damage in concrete affected by other deleterious mechanisms, such as freezing and thawing, action of fire, impact loads, DEF, etc. (Crisp et al. [23, 24]). Smaoui et al. [18] also reported a good correlation between the expansion to date of a concrete undergoing freezing-thawing cycles and the hysteresis area over the first cycle in the SDT. However, there is currently limited data available on the signature of a damage mechanism over another one when concrete specimens are tested through the SDT [28]. In addition, the SDT has the potential of being non-destructive so, since the number of samples taken within a structure under evaluation is often limited (for economic or technical reasons), one could consider using the same cores to perform other tests following the SDT, such as residual expansion, petrographic tests, compressive and tensile strengths, etc [23, 24, 29]. Following mechanical testing, chemical tests (e.g. soluble alkalis, pore solution extraction, etc.) could also be performed on the same specimens [29]. The non-destructive character of the SDT is, however, yet to be confirmed, as it would likely depend on the loading level used.

6.3 OBJECTIVE AND SCOPE OF WORK

The results presented in this paper were obtained as part of an extensive field and laboratory investigation to develop reliable tools for assessing/quantifying the extent of damage in concrete affected by various deleterious mechanisms, including alkali-silica (ASR) and alkali-carbonate reactions (ACR), freezing and thawing cycles and delayed ettringite formation (DEF). The study combined several types of mechanical and petrographic investigations carried out on laboratory-made specimens and cores extracted from a concrete structure affected by ASR.

This paper specifically presents and discusses the results of the basic evaluation of the applicability of the Stiffness Damage Test (SDT) to detect/quantify damage in concrete when deleterious expansion due to ASR is generated either in the coarse or in the fine aggregate

material. In order to best achieve this objective, extensive testing was performed on (well-controlled) laboratory-made and cured concrete specimens of different mix designs (25 to 45 MPa) and incorporating coarse or fine reactive aggregates.

As indicated in the previous sections, the lack of a thorough study on the input/output parameters of the SDT (i.e. with a range of concrete mix designs) could lead to an erroneous interpretation of the test results, for instance the degree of damage in the concrete under study. Based on the literature review presented before, the most important parameters of the test, listed below, were included in the evaluation program carried out in this study and are reported in this paper:

- Input parameters: loading level (versus concrete mixture designs), reactive rock types (fine vs. coarse aggregate), ASR-expansion level;
- Output parameters: hysteresis area (first cycle, average of the last four cycles and over the five cycles), modulus of elasticity (first cycle, average value of the second and third cycles and average of the last four cycles) and plastic deformation (first cycle, value over the last four cycles and over the five cycles) of the damaged concretes.

Other test parameters, such as the specimen geometry (length-to-diameter ratio, diameter, etc.), the humidity condition of the test specimen (drying and rewetting effects), the specimen environment/location (core vs. surface of a structural element, exposed vs. not exposed structural elements, concrete element type, etc.), were also found to influence the test responses (output parameters) of the SDT, which is the topic of another paper [30].

6.4 MATERIALS AND METHODS

6.4.1 Materials and mixture proportions

Three types of non air entrained concrete mixtures (25 MPa, 35 MPa and 45 MPa mix design strengths) and two highly-reactive aggregates (New Mexico gravel-NM and Texas sand-Tx) were selected for the study. The coarse aggregates ranged from 5 to 20 mm in size. Non-reactive fine and coarse aggregates were used in combination with the above reactive aggregate materials for concrete manufacturing. Table 1 provides information on the different aggregates used in this study.

The three concrete types were designed to contain the same volume of paste and aggregates (i.e. from one mix to another), so one can compare similar systems. All concretes were made with the same conventional (CSA Type GU, ASTM type I) high-alkali (0.88% Na₂O_{eq}) Portland cement. Reagent grade NaOH was used to raise the total alkali content of the

mixtures to 1.25% Na₂O_{eq}, by cement mass, for accelerating the expansion process due to ASR. Table 2 gives the detailed concrete mixture proportions. A total of 64 cylinders, 100 by 200 mm in size, were cast from each of the six concrete mixtures manufactured in the laboratory.

Table 1: Aggregates used in the study.

Aggregate Identification				Rock Type [31] Reactive rock types are in bold	Specific gravity	Absorption (%)	AMBT ¹ 14d exp,%
Type	Reactivity	Designation (location)					
Coarse	Reactive	New Mexico (USA)	NM	Polymictic gravel (mixed volcanics, quartzite, chert)	2.53	1.59	1.114
	Non-reactive	Newfoundland (Canada)	HP	High purity limestone	2.68	0.44	0.001
	Non-reactive	Quebec (Canada)	Dia	Diabase (plutonic rock)	3.00	0.51	0.065
Fine	Reactive	Texas (USA)	Tx	Polymictic sand (granitic, mixed volcanics, quartzite, chert, quartz)	2.60	0.55	0.995
	Non-reactive	Quebec (Canada)	Lav	Natural derived from granite	2.71	0.54	0.032

¹ Accelerated Mortar bar expansion at 14 days [31].

After casting, the specimens were placed for 48h in the moist curing room (i.e. after the first 24h in the moist curing room, the specimens were demolded and left in this room for a further 24h). Small holes, 5 mm in diameter by 15 mm long, were then drilled in both ends of each test cylinders and stainless steel gauge studs were glued in place, with fast-setting cement slurry, for longitudinal expansion measurements. After completion of the first 48 h at 23°C, the “0” length reading was performed and the specimens were placed in sealed plastic (22 liters) containers lined with damp cloth (4 cylinders per bucket). All buckets were then stored at 38°C and 100% R.H., and all the test cylinders were monitored regularly for length variations. Moreover, as per ASTM C 1293 [32], all containers were cooled to 23 °C for 16 ± 4 h prior to periodic axial expansion measurements. Then, test cylinders were removed from the high-temperature storage conditions for SDT testing when they reached the expansion levels chosen for this research, i.e. 0.05% ± 0.01%, 0.12% ± 0.01%, 0.20% ± 0.01% and 0.30% ± 0.01%. Overall, ASR expansions amongst the test cylinders of a same batch were only slightly variable, as the entire test set was cast at the same time and from the same large concrete batch. Figure 1 illustrates the average expansion curves for the test specimens cast from the mixtures incorporating the reactive Texas sand or NM gravel.

Once the above expansion levels were reached, the specimens were wrapped in plastic film and stored at 12°C until testing (because of testing capacity issues). Prior to testing, both ends of each cylinder were carefully mechanically ground to avoid any interference from the

stainless steel gauge studs used for expansion measurements. Also, even though they were wrapped in plastic film prior to testing, the specimens were restored for 48h in the moist curing room, protected from running water, before stiffness damage testing, in order to allow appropriate saturation of the test specimens, following the procedure proposed for concrete cores extracted from real concrete structures (CSA A23.2-14C) [33]. Length and mass readings were also performed on a number of test specimens prior and upon unwrapping to make sure that they had not suffered from significant shrinkage or expansion over the storage period prior to testing. The monitoring of the test specimens showed that the 12°C storage resulted in slight shrinkage ($- 0.02 \pm 0.01\%$) and mass loss ($0.7 \pm 0.2\%$) of the test specimens, which was recovered through the 48-hour re-saturation period prior to running stiffness damage testing.

Table 2: Concrete mixture proportions.

Concrete Mix designs	Ingredients	Materials (kg/m ³)		Materials (L/m ³)	
		Mixtures Tx sand	Mixtures NM gravel	Mixtures Tx sand	Mixtures NM gravel
25 MPa	Cement	314	314	101	101
	Sand	790	714	304	264
	Coarse aggregate	1029	1073	384	424
	Water	192	192	192	192
	Air (%)	-	-	20	20
	Alkalis	3.93	3.93	-	-
	w/c	0.61	0.61	-	-
35MPa	Cement	370	370	118	118
	Sand	790	714	304	264
	Coarse aggregate	1029	1073	384	424
	Water	174	174	174	174
	Air (%)	-	-	20.0	20.0
	Alkalis	4.63	4.63	-	-
	w/c	0.47	0.47		
45 MPa	Cement	424	424	136	136
	Sand	790	714	304	264
	Coarse aggregate	1029	1073	384	424
	Water	157	157	157	157
	Air (%)	-	-	20	20
	Alkalis	5.30	5.30	-	-
	w/c	0.37	0.37		

Note: the non-reactive HP limestone was used in the concrete mixtures incorporating the Tx reactive sand. The non-reactive Lav sand was used in the concrete mixtures incorporating the reactive NM gravel.

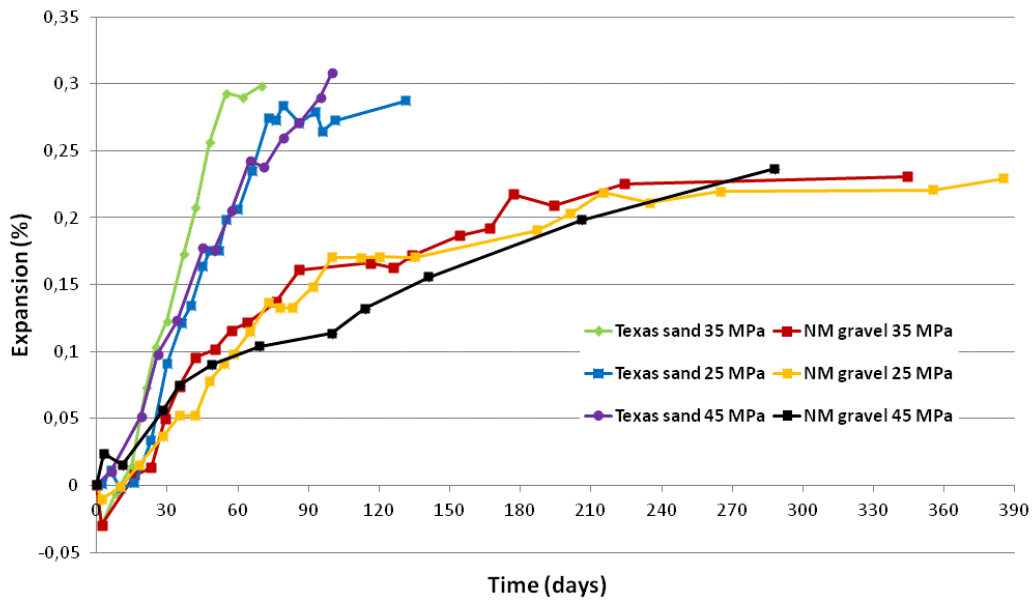


Figure 1: Average expansions for all mixtures used in this project. The data points on the above curves correspond to the average of a minimum of 12 specimens, and up to 17 specimens at each expansion level studied.

6.4.2 Methods for assessment and analysis

Table 3 presents the testing matrix developed for this study. The investigation program carried out on concrete cylinders of various expansion levels includes mechanical testing (SDT, elastic modulus, compressive and tensile strengths evaluation), semi-quantitative petrographic analysis (DRI) and non-destructive evaluation (ultrasonic pulse velocity (UPV) – Pundit).

Table 3: Testing matrix.

Mix design tested	Tests	Load level of SDT test (% of 28d - f_c)	Number of specimens for each expansion level				Sub-set no.
			0.05%	0.12%	0.20%	0.30%	
25, 35 and 45 MPa	<ul style="list-style-type: none"> • Stiffness Damage Test (% of the concrete mix design strength); • Compressive strength; • UPV before and after SDT. 	15%	3	3	3	3	1
		20%	3	3	3	3	2
		30%	3	3	3	3	3
		40%	3	3	3	3	4
25 MPa	Damage Rating Index		2	2	2	2	5
25, 35 and 45 MPa	Tensile strength		2	2	2	2	6
Total number of samples per series (i.e. for each mix design) : 64							

6.4.2.1 Stiffness damage test (SDT)

Test cylinders were subjected to five loading/unloading cycles at a controlled loading rate of 0.10 MPa/s. Each set of specimens was divided into 4 sub-sets of three cylinders (no. 1 to 4 in Table 3), in order to evaluate four different loading levels through the test, i.e. 15%, 20%, 30% and 40% of the design (28-day) concrete strength. All the results presented in this paper correspond to the average values obtained on three specimens (sub-sets).

6.4.2.2 Damage Rating Index (DRI)

A semi-quantitative petrographic analysis, using the Damage Rating Index method proposed by Grattan-Bellew & Danay [3] and recently modified by researchers from Laval University [34], was carried out on the concrete specimens. The method consists in a count, under the stereomicroscope ($\approx 16\times$ magnification), of the number of petrographic features of deterioration (commonly associated to ASR) on polished concrete sections on which a grid is first drawn (minimum 200 grid squares to be examined, 1 by 1 cm in size). The DRI thus represents the normalized value (to 100 cm^2) of the frequency of these features after the count of their occurrence, over the surface examined, has been multiplied by weighing factors representing their relative importance in the overall deterioration process (Figures 2A and 2B).

The examination was carried out in two ways. First, the DRI was performed on two polished sections of each set that were not subjected to SDT (sub-set no. 5 in Table 3), for verifying the microscopic degree of damage in the samples (i.e. for both reactive aggregates) at each of the selected expansion levels. Second, a sample of the sub-set 4 was cut and polished for microscopic examination (i.e. at each selected expansion level), after completion of the SDT (40% load - 25 MPa concrete), thus allowing to verify the non-destructive character of the test.

Numerous publications have shown that one of the main petrographic features of ASR is the progressive development of cracking within reactive aggregate particles, with cracking extending into the cement paste with increasing expansion of the concrete. The DRI had originally been developed to evaluate the degree of deterioration due to ASR in concrete incorporating reactive coarse aggregates. The DRI practice applied in this research consists in counting the number of cracks in every coarse aggregate particle greater than 1 mm in each of the 1 cm^2 examined. In the case of the Tx sand, since the main reactive constituents can be

found in the coarser fractions of the sand, cracking counts were also made in the fine aggregate particles down to 1 mm in size.

A

Petrographic features		Weighing factor
Cracks in coarse aggregate	CCA	0.25
Opened cracks in coarse aggregates	OCA	2
Crack with reaction product in coarse aggregate	OCAG	2
Coarse aggregate debonded	CAD	3
Disaggregate/corroded aggregate particle	DAP	2
Cracks in cement paste	CCP	3
Cracks with reaction product in cement paste	CCPG	3

B

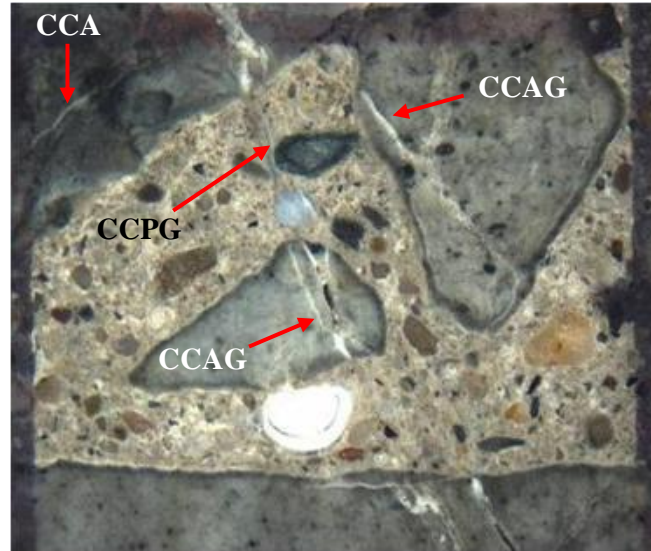


Figure 2: Damage Rating Index method. Micrograph D shows a 1cm² section where most of the petrographic features to be noted in the DRI (as listed in C) can be observed and identified (the distance between the vertical lines on both sides is 1 cm).

6.4.2.3 Ultrasonic pulse velocity (UPV)

Ultrasonic pulse velocity measurements (UPV) were carried out before and after the completion of the SDT, for all the loading levels selected for the study. The goal of performing this test (as well as the microscopic analysis) was to verify the non-destructive character of the cyclic test through the different loading level used.

6.4.2.4 Compressive strength test

Compressive strength was measured in two ways. First, tests were carried out on two cylinders cast from each mix to determine the 28-day strength of each concrete mixture. For this project, as the samples contained highly-reactive aggregates, they could not follow the ASTM C 39 [35] procedure (as they could develop ASR during the first 28 days in the moist room, which could affect their strength). Therefore, the samples were wrapped and placed at 12°C for a 47-day period (which represents the same 28-day period according to the maturity concept presented by ASTM C 1074 [36]).

Second, compressive strength test was evaluated on two of the three cylinders of each sub-set subjected to the SDT, with the aim of verifying, once again, its non-destructive character as well as the reliability of the test results after the cyclic test.

6.4.2.5 Tensile strength test

The tensile strength of two samples of each concrete mixture, and at each expansion level, was measured according to the pressure tension test (sub-set no. 6 in Table 3). The pressure tension test, also known as the indirect tension test, was first developed by The Building Research Establishment of Watford, UK, as a means of investigating anisotropic behavior in materials [37]. The pressure tension test uses compressed gas to apply a uniformly distributed pressure to the curved surface of standard 100 mm by 200 mm concrete test cylinders or cores. The apparatus consists of a hollow cylindrical test chamber that envelops the curved surface of the test cylinder. At either end of the testing chamber, rubbers “O-rings” are used to seal the compressed gas so that it only acts upon the curved surface of the specimen. Both ends are left open to atmospheric pressure, resulting in a biaxial loading configuration. Gas pressure is monotonically increased until the test cylinder fails in a plane transverse to the axis of the testing chamber [37]. The gas pressure applied to the curved surface is a biaxial loading condition but the reaction forces within the diphasic model differ. In particular, the pore water reacts hydrostatically whereas the solid phase reacts biaxially, resulting in a net internal tensile force driven by the pore fluid. The resultant internal tension force is the primary reason why the pressure tension method is well suited for detecting durability issues which affect the integrity of the cementitious microstructure [37].

6.5 TEST RESULTS

6.5.1 Stiffness Damage Test (SDT)

Typical results of the Strain-Stress relationship obtained for test specimens cast from the 35 MPa concrete incorporating the NM gravel, at the 0.05, 0.12 and 0.20% expansion levels are presented in Figure 3. The graphs show the increase in the hysteresis area, plastic deformation and reduction in modulus of elasticity of the test specimens over the five cycles as a function of increasing expansion.

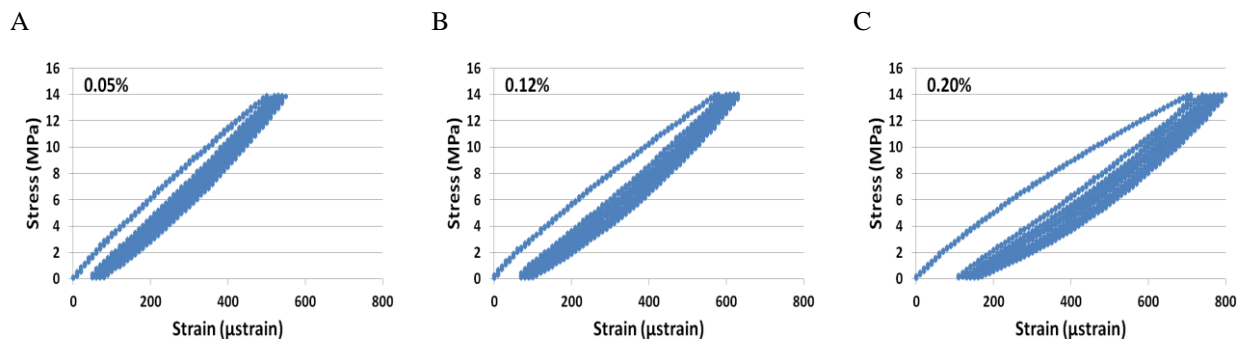
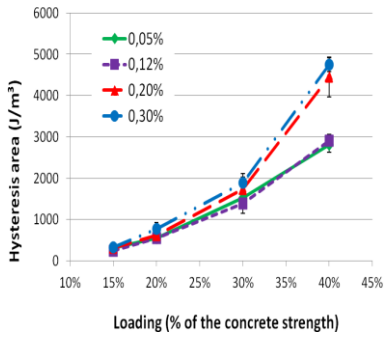


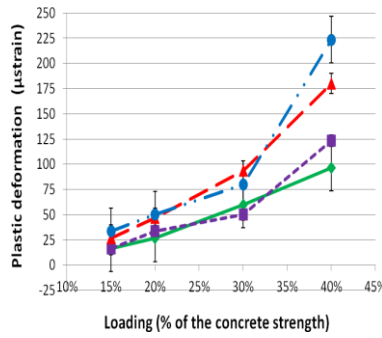
Figure 3: Typical stress-strain behavior curves obtained for test specimens cast from the 35 MPa concrete incorporating the NM gravel and tested at 40% of the 28-day concrete mix-design strength. A. Results at 0.05% expansion. B. Results at 0.12% expansion. C. Results at 0.20% expansion.

The results of the most critical output parameters (hysteresis area (HA), modulus of elasticity (ME), plastic deformation (PD)) are presented in Figure 4, for stiffness damage tests carried out at the four different loading levels (15 to 40% of the 28-day/design strength) and four expansion levels (up to 0.30%) in the 25 MPa concretes incorporating the reactive Texas sand. The same parameters are also illustrated in Figure 5 for three expansion levels (up to 0.20%) in the 25 MPa concretes incorporating the reactive New Mexico gravel. Each data point on the graph represents the average obtained on three cylinders tested at the specified expansion level (e.g. $0.05 \pm 0.01\%$, $0.12 \pm 0.01\%$, etc.). Variations bars are included in the plots which represent one standard deviation on each side of the average value. Figures 4 and 5 present data for the SDT responses over the five cycles for the HA and PD parameters and the average value of the second and third cycles for the ME parameter. Similar trends as those illustrated in Figures 4 and 5 were also obtained for testing carried out at different expansion levels in the 35 and 45 MPa concrete mixtures. The full database for the additional output parameters (i.e. first cycle, average of the last four cycles and five cycles) and for all the concrete mixtures can be found in the Annex (Supplementary material) of the electronic version of this paper.

A – HA - 5 loading-unloading cycles



B – PD - 5 loading-unloading cycles



C – ME- avg of the 2nd and 3rd cycles

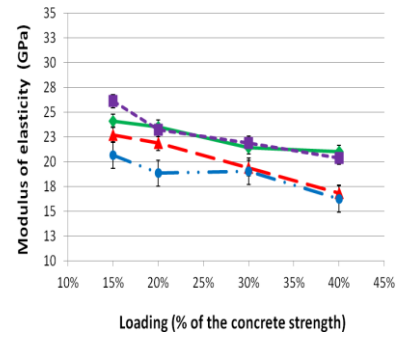
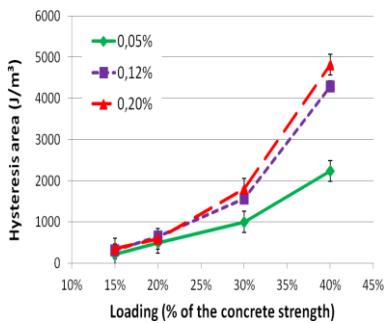
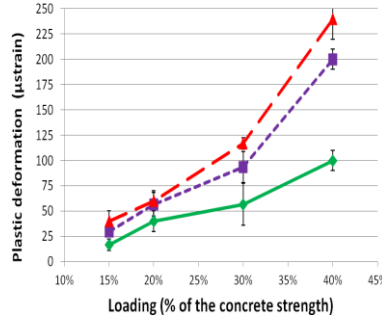


Figure 4: Responses of selected SDT output parameters as a function of the loading applied (% of the concrete strength) for 25 MPa concrete mixtures incorporating the reactive Tx sand and affected to various degrees by ASR. A: Hysteresis area (HA). B: Plastic deformation (PD). C: Modulus of elasticity (ME). The common legend for all the curves appears in (A).

A – HA - 5 loading-unloading cycles



B – PD - 5 loading-unloading cycles



C – ME- avg of the 2nd and 3rd cycles

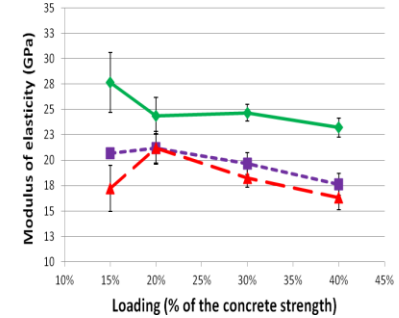


Figure 5: Responses of selected SDT output parameters versus the loading applied (% of the concrete strength) for 25 MPa concrete mixtures incorporating a reactive NM coarse aggregate and affected to various degrees by ASR. A: Hysteresis area (HA). B: Plastic deformation (PD). C: Modulus of elasticity (ME). C :. The common legend for all the curves appears in (A).

For concrete mixtures incorporating the Tx and NM reactive aggregates, clear differences in the HA and PD responses with increasing expansion in the test specimens can be observed only at loading levels corresponding to 30% and even better at 40% of the 28-day strength design, thus suggesting that the above parameters of the test were unable to distinguish the internal concrete damage corresponding to the selected expansion levels up to those loading levels (Figures 4A and 4B; 5A and 5B). For both concrete mixtures, the modulus of elasticity (ME) decreased as a function of the expansion level, relatively similar slopes being observed for each of the expansion levels as a function of the loading level used in the test. For all SDT parameters, at loading levels corresponding to 30 and 40% of the 28-day strength design, similar behaviors were generally obtained at the 0.05/0.12% and 0.20/0.30% expansion levels

for the concretes incorporating the Tx sand, and at the 0.05% and 0.12/0.20% expansion levels for the concretes incorporating the NM gravel (figures 4 and 5).

Despite a large number of samples for the whole testing matrix, the results presented before are based on the average value obtained for three samples per expansion level (i.e. 0.05% to 0.30%) and per level of test loading (i.e. 15% to 40%), which limits the statistical analysis of data. However, ANOVA was carried out (with two and multi-variables) in order to determine whether the differences between the different series of test results (i.e. at the various loading levels and expansion levels selected) were statistically significant. This topic is further discussed in the section 6.6.2.

6.5.2 Damage Rating Index (DRI)

Examples of the detailed DRI results obtained on polished concrete sections of the 25 MPa concretes incorporating the Tx sand or the NM gravel, before and after the SDT test (40% load level) are presented in Figure 6. The results indicate that the main features of deterioration in the concrete specimens consist in cracks in the aggregate particles and in the cement paste, with and without reaction products. The number of opened cracks in the aggregate particles (with or without reaction products) and cracks in the cement paste (with or without reaction products), which are thought to be diagnostic features of internal damage due to ASR in the test specimens, increases significantly with increasing expansion levels. The legend refers to the observed damage as presented in Figure 2(A).

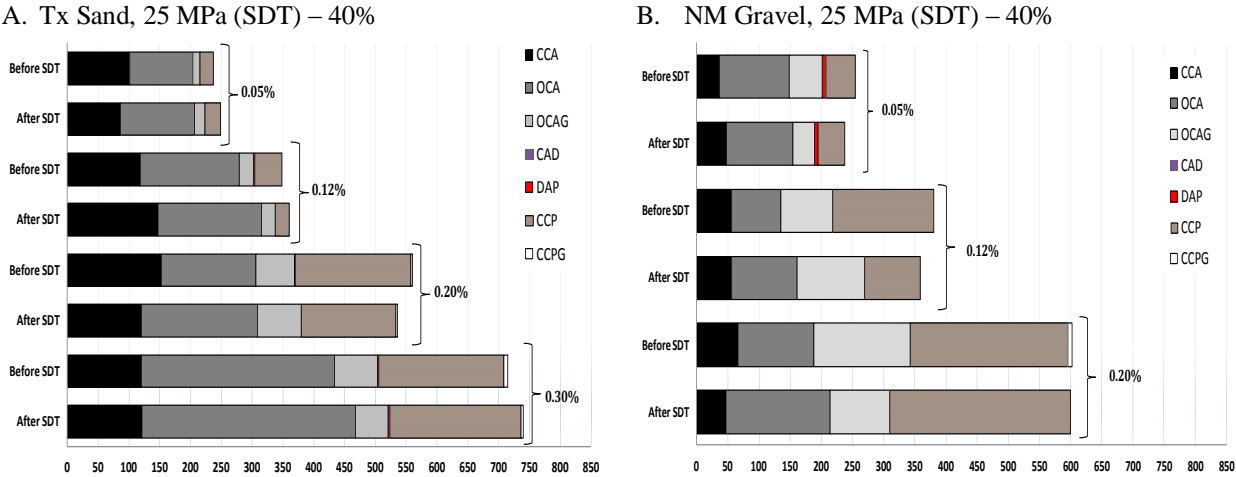


Figure 6: DRI values of 25 MPa concrete samples tested before and after SDT with A) Texas sand; and B) New Mexico gravel.

Table 4 further summarizes the results of the petrographic analysis, using the Damage Rating Index, performed on the 25 MPa specimens incorporating the Tx sand or the NM gravel. One can see that the DRI values, and the breakdown in the various petrographic features (Figure 6), are very similar before and after the SDT test (40%). The fairly low values of either the Deviation (i.e. difference between DRI values after and before SDT) or the Variation (i.e. the absolute value of Deviation divided by the DRI value before SDT), suggest that performing the SDT up to a load corresponding to 40% of the concrete design strength does not introduce additional damage into the sample analyzed, at least visible at the magnification used in the DRI analysis (16X). This is true for both aggregates investigated and further testing (not reported here but available in [30]) confirmed that this trend also applied to the 35 and 45 MPa mixtures studied. For DRI analyzes, the concepts of “standard deviation” and “coefficient of variation” were not used because of the small sample size (two, for each expansion degree) adopted.

Table 4: Microscopic analysis (using the DRI) of the 25 MPa mixtures incorporating the Texas sand and the New Mexico gravel for different degrees of expansion.

Tests		Expansion degrees for all the 25 MPa mixtures						
		0.05% Tx sand	0.05% NM gravel	0.12% Tx sand	0.12% NM gravel	0.20% Tx sand	0.20% NM gravel	0.30% Tx sand
Damage Rating Index Values and statistics	Standard SDT analysis (before SDT)	226	270	369	396	554	598	724
	After SDT analysis (40% loading level)	249	237	360	358	536	599	739
	Deviation (after – before values)	23	-33	-36	-38	-18	1	15
	Variation (%)	10.2	12.2	9.8	9.6	3.2	1.6	2.1

6.5.3 Ultrasonic pulse velocity (UPV) testing

Figure 7 shows the UPV test results performed on the 25 MPa concrete specimens incorporating the Tx sand and the NM gravel, before and after the SDT (40%). The results before the SDT are the average values obtained on 16 specimens at each expansion level (Table 3). The “SD” values correspond to the standard deviation calculated over those 16 specimens; on the other hand, the results of UPV after the SDT at 40% load level are the average of 3 specimens tested at each expansion level (Table 3).

First, one can see that, in the case of the concretes incorporating the highly-reactive Tx sand, for the before SDT series, there is almost no loss in UPV values (i.e. ranging from 4.28 to 4.17 km/s – about 2.5% of loss) for expansions ranging from 0.05 to 0.30%, despite significant microcracking in the concrete (Figure 7). In the case of the NM gravel, a drop of about 7 to 8.5% in UPV values was observed between the 0.05% expansion (4.50 km/s) and the 0.20% expansion (4.12 – 4.18 km/s). The relatively small drops in UPV and differences between the two test series possibly lie in the fact that the deterioration is induced in the fine aggregate (Tx sand) versus the coarse aggregate (NM gravel), as well as the presence of increasing amounts of alkali-silica gel in the microcracks with increasing expansion levels. Other studies reported that UPV was not that sensitive to deterioration due to ASR [38].

One can also see that for the majority of the expansion levels, the UPV values obtained after the SDT (i.e. carried out at 40% of the design strength), were lower than the values before SDT, thus suggesting that the SDT is somewhat inducing further damage to the concrete specimens. However, the difference (gap) between the values before and after the SDT is generally similar or lower than the standard deviation (SD) obtained from 16 test specimens (at each damage level) that were not subjected to the cyclic test (except for Tx sand with 0.30% of expansion). Therefore, one cannot conclude that the SDT is really “destructive”, or inducing significant additional damage to the test specimens, on the basis of the UPV results, at least for expansions up to 0.20% for both mixtures (with the two highly-reactive aggregates) tested. On the other hand, one could see that, generally, the greater the expansion, the greater is the gap between the values before and after the SDT. Although the gap is still relatively limited, these results were quite expected since one could think that the greater the sample’s damage level, the more susceptible is the concrete specimen to suffer additional damage at a specified load in the SDT (for instance 40% of the design strength in this case).

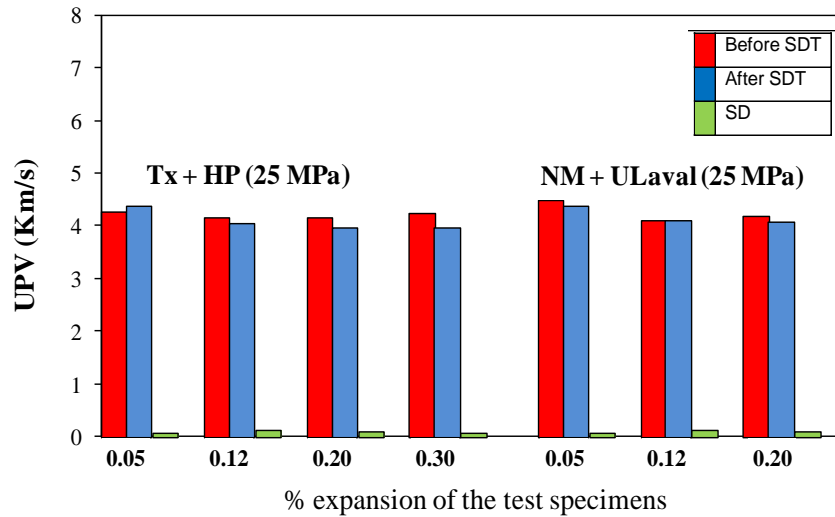


Figure 7: UPV values of 25 MPa concrete samples tested before and after SDT (at 40% of the 28-day strength) with Texas sand and New Mexico gravel. The SD values correspond to the standard deviation of the samples results at each expansion level.

6.5.4 Compressive and tensile strength tests

The 28-day compressive strength results (47-day period at 12°C according to ASTM C 1074, as discussed in section 6.4.2.4) for all the mixtures studied in this research are given in Table 5. The reason for keeping the specimens at 12°C was to avoid the development of ASR expansion/cracking in the test specimens. These results indicate that the target mix design strength was reached in most cases.

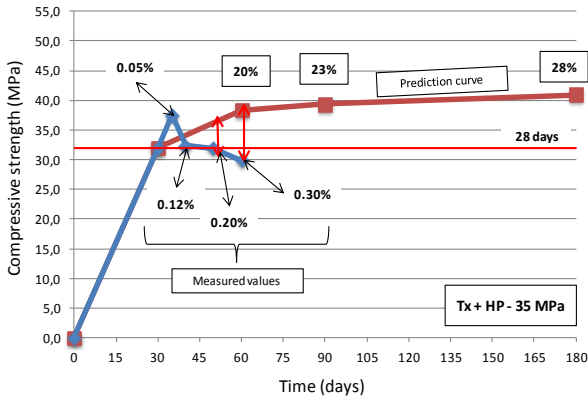
In order to evaluate the non-destructive character of the SDT, the development of compressive strength (C.S.) was determined on 35 MPa concrete specimens incorporating the Tx sand and NM gravel, before (Figure 8A and 8B) and after (Figure 8C and 8D) they were subjected to the SDT. In the first case (i.e. compressive strength determination before SDT), reactive concrete specimens from both 35 MPa concrete mixes were tested in compression after they reached the expansions selected in the research for analysis (0.05%, 0.12%, 0.20% and 0.30%). In addition, concrete specimens from non-reactive 35 MPa concrete mixtures presenting the same concrete mix design (water cement ratio, materials contents, etc.), but incorporating non-reactive coarse (diabase) and fine (granite) aggregates, were stored at 38°C and 100% R.H. and their compressive strength determined at 30, 60, 90 and 180 days. In the second case (C.S. after SDT), the concrete specimens were first subjected to stiffness damage testing at the four loading levels studied (from 15% to 40% of the 28-day design strength) for each expansion level studied, and their compressive strength then determined.

In both cases, each value presented in the graphs of Figure 8 corresponds to the average obtained on three specimens.

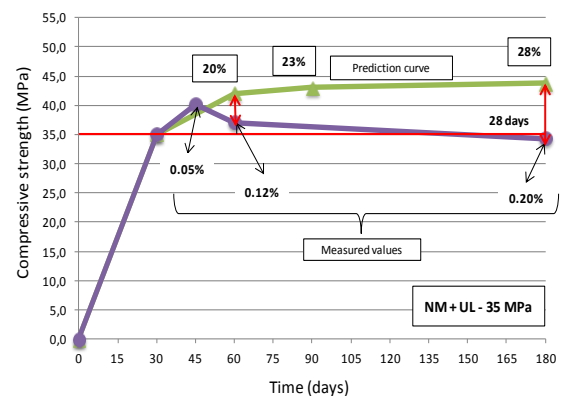
Table 5: Equivalent 28-day compressive strength results for all mixtures tested.

Compressive strength results	25 MPa		25 MPa		35 MPa		35 MPa		45 MPa		45 MPa	
	Tx sand		NM gravel		Tx sand		NM gravel		Tx sand		NM gravel	
Specimens' values	25.7	27.5	26.8	27.8	31.7	32.3	32.0	37.5	41.0	42.5	42.1	47.6
Average (MPa)	27		27		32		35		42		45	

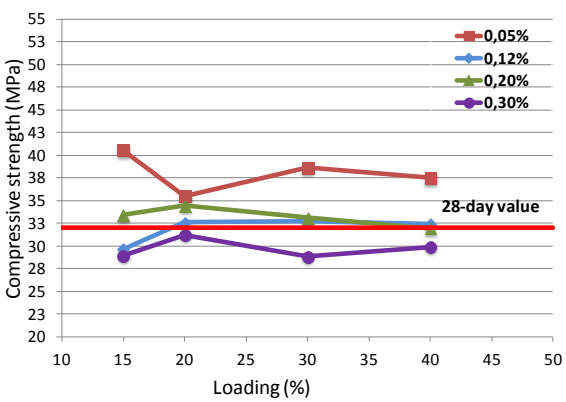
A: Compressive strength vs time – Tx + Dia 35 MPa



B: Compressive strength vs time – NM + UL 35 MPa



C: Tx sand - 35 MPa



D: NM gravel - 35 MPa

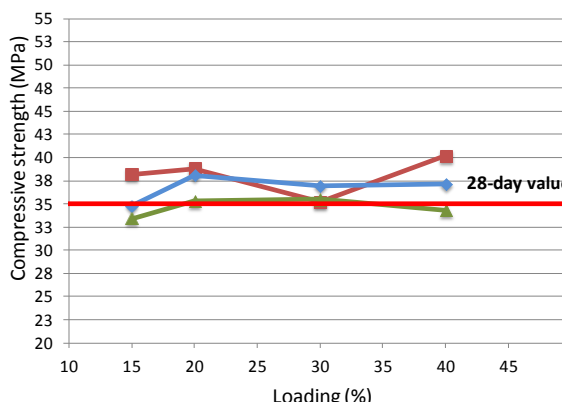


Figure 8: Compressive strength results obtained before (A, B) and after (C and D) the SDT versus time and the loading applied respectively for both aggregates (Tx sand and NM gravel).

The results obtained on the non-reactive concretes show a non negligible compressive strength increase (versus the 28-day value) at 60 days (20%), 90 days (23%) and 180 days (28%). This increasing trend, illustrated as the “prediction curves“ in Figures 8A and B), was adopted as “standard” compressive strength behavior over time for the concrete specimens stored under these temperature and humidity conditions. At the same time, compressive

strength was measured on the ASR affected samples and the values were plotted on the same graphs for comparison purposes (Tx mixes - 8A and NM mixes - 8B mixes).

Looking at the results, it is interesting to note that both concrete series presented progressive losses in compressive strength due to ASR. These losses were however quite comparable for both mixtures, and ranged from -7% (actually a gain in compressive strength at the 0.05% expansion level) up to 13% at 0.20% expansion (22% at 0.30% expansion) in the case of 35 MPa Tx mixtures, and from -4% (also a gain at the 0.05% expansion level) up to 23% (at 0.20% expansion) in the case of 35 MPa NM mixes. The above differences in compressive strength losses at similar expansion levels are related to the different reaction kinetics of the concretes incorporating the reactive Tx sand and the NM gravel, and the consequent contrasts in concrete maturity at the different testing times.

In the case of concrete strength determinations after stiffness damage testing of test specimens affected to different degrees by ASR (Figures 8C and 8D), one can see from that there is no obvious/constant/steady increasing or decreasing pattern that distinguishes the variation in compressive strength as a function of the loading level applied during the SDT. The greatest gap found for a specific concrete mixture, at a given expansion level, was about 5.0 MPa, which cannot be considered as a significant difference considering that the above analyses are sometimes carried out on fairly damaged materials. Thus, the variability in the test results observed (i.e. at the different loading levels) could likely just be related to the heterogeneous character of the damaged material.

The tensile strength results determined on concrete specimens after the SDT carried out at different loading levels, and for different expansion levels, are presented in Table 6. Albeit more limited in the number of results available compared to those of the compressive strength study, one can see that 1) there is no clear trend of decreasing tensile strength (as measured using the gas pressure test) with increasing expansion due to ASR, and 2) there is no trend of increasing or decreasing tensile strength values as a function of the loading percentage (up to 40% of the 28-day value) for all the mixtures analyzed and expansion levels studied.

Table 6: Tensile strength results obtained after the SDT versus the loading applied over the test for both aggregates (Texas sand: A, B and C; New Mexico gravel: D, E and F) and all the concrete mixtures.

SDT loading (%) of concrete strength	Tx sand mixtures								NM gravel mixtures				
	25 MPa			35 MPa					25 MPa		45 MPa		
	0.0%	0.20%	0.30%	0.0%	0.05%	0.12%	0.20%	0.30%	0.0%	0.12%	0.0%	0.20%	
28d value	3.8	-		4.6	-					3.1	-	5.1	-
15%	-	1.9	1.7	-	1.9	2.0	2.0	2.2	-	1.5	-	2.2	
20%		1.7	1.5		1.4	2.2	2.5	2.4		-		2.4	
30%		-	1.9		-	2.0	2.1	-		1.3		2.0	
40%		1.8	-		1.6	-	-	2.4		1.9		-	

6.6 DISCUSSION

6.6.1 SDT parameters

6.6.1.1 Testing (input) parameters

In this study, stiffness damage testing was carried out on concrete specimens cast from different mix designs (25, 35 and 45 MPa), incorporating fine or coarse reactive aggregates and having reached different expansions levels, as well as using loading levels ranging from 15 to 40% of the 28-day concrete mix design strength. The maximum value of 40% was chosen as higher loading levels are considered at risk of introducing new cracks/further damage in the specimens tested in compression [39]. At this stage, almost all the data reported in the literature for SDT carried out on ASR-affected concrete specimens were obtained through the use of fixed loading values of either 5.5 MPa [21, 22] or 10 MPa [18]. Testing carried out in this study confirmed that when fixed loading levels are used in the SDT, one could easily misinterpret the response of the test; this can be seen in Table 7 for the hysteresis area output parameter. For example, for concrete specimens loaded to a value of about 10 MPa (± 1 MPa), as proposed by Smaoui et al. [18] (lines highlighted in Table 7), the hysteresis areas for concrete incorporating the reactive Tx sand ranged from 278 to 1152 J/m³ (0.12% expansion) and from 396 to 1802 J/m³ (0.20% expansion) depending on the class of concrete (25 to 45 MPa design strength); similar ranges in results were also obtained with the reactive NM gravel. This confirms the critical importance of selecting the appropriate loading level to properly evaluate the damage level in concrete, and this loading level is a function of the nature (i.e. compressive strength in this case) of the concrete to be characterized.

Table 7: Comparison between fixed and percentages of mix designs loadings on the output parameter of the SDT.

Concrete mix design strength (MPa)	Loading level		Hysteresis area for the first cycle (J/m ³)			
	(% of the 28-day design strength)	MPa	0.12% expansion		0.20% expansion	
			Tx sand	NM gravel	Tx sand	NM gravel
25	20%	5.0	187	245	228	236
	30%	7.5	517	671	669	787
	40%	10.0	1152	1883	1802	2213
35	15%	5.3	75	116	100	135
	20%	7.0	253	192	281	291
	30%	10.5	692	623	897	913
	40%	14.0	1495	1456	2017	2263
45	15%	6.8	149	158	192	182
	20%	9.0	278	263	396	358
	30%	13.5	745	875	923	1131

It is clear that the use of a load corresponding to a proportion of the mix design strength, instead of a fixed load, is required to obtain a reliable evaluation of damage in ASR-affected concrete specimens through the SDT, 40% of the 28-day mix design strength providing the most effective diagnostic value of the loading levels used for the various concrete mixtures investigated in this study.

6.6.1.2 Output parameters

The test data obtained in this study confirmed the results reported previously by Crisp et al. [23, 24] and Smaoui et al. [18], i.e. that the Hysteresis area (HA), the Modulus of elasticity (ME) and the Plastic deformation (PD) are critical responses of ASR-affected concrete materials under cyclic loading in compression. Figure 9 (Tx sand and NM gravel) compares the trends between the above parameters (over 5 cycles for HA and PD; average of 2nd and 3rd cycles for ME) obtained at 40% of the 28-day mix design strength (25, 35 and 45 MPa concretes) and the expansion of the test specimens at the time of testing. Although not a direct measure of damage in concrete, expansion remains the most commonly used indicator of the extent of ASR in concrete specimens (in laboratory investigations) and DRI data confirmed that both parameters are largely correlated (e.g. Figure 6).

Globally, very similar trends between the SDT output parameters and concrete expansion were obtained whether those parameters were measured over the first loading/unloading

cycle, the last four cycles or the full five cycles of the test; the supporting data are presented in the Annex (Supplementary material) of the electronic version of the paper (Tables 12 to 21). However, it appears necessary to select the approach that best evaluates the overall degree of damage in the ASR-affected concretes. Therefore, each output parameter needs to be further assessed separately.

The *Hysteresis area* obtained upon compression testing corresponds to the energy used to close the macro and microcracks disseminated throughout the concrete specimens. The results obtained in this study indicate that, at the 40% loading level, the hysteresis area values for the first cycle are typically about 2 to 3 times larger than the average values obtained over the last four cycles; however, considering the trends of the curves, it appears that both parameters correlate similarly well with the expansion level reached by the concrete, and could thus be used almost interchangeably for evaluating the expansion/damage level in concrete affected by ASR (at the 40% load level). On the other hand, eliminating the response obtained during the first cycle (as proposed by Crisp et al. [23, 24]) likely results in losing important information about the extent of cracking in the test specimens. Moreover, when comparing the use of the hysteresis areas of the first cycle and of the entire testing process (i.e. all five cycles), it appears that for the majority of mixtures, the correlation against expansion is equally good or slightly better when using the data from the five cycles of the SDT (Figure 9). The results of statistical data analysis (ANOVA), discussed in section 6.6.4, further support this observation. This is likely attributed to the more complete closure of the macro- and microcracks during the full duration of the test (i.e. 5 cycles), the use of cycles 2 to 5 helping to further complete this process at the microlevel. Moreover, the use of the hysteresis area over the five cycles could also decrease or even mitigate the relative influence of the cage's setting (i.e. displacements of the testing set-up upon loading) that may occur during the early stages in the test. Therefore, based on the data obtained in this study for a range of concrete mixtures incorporating reactive siliceous materials both in the fine or coarse aggregates, it is recommended that the hysteresis area (J/m³) calculated over the 5 loading/unloading cycles be selected as the first SDT output parameter.

The *plastic deformation* occurring during the cyclic test corresponds to the permanent strain suffered by the ASR-affected concrete specimens under compressive stresses. This phenomenon, as discussed before, exists because the ASR-affected concrete will not fully recover its original state/condition upon unloading as the crack surfaces are rough/irregular and some sliding across those surfaces occurs during the test; also, the presence of alkali-silica reaction products moving into cracks with progressing ASR expansion likely contribute

at inducing permanent deformations in the test specimens through a sort of “edge/fill effect” that prevents full closure of cracks upon loading, which is not the case, for example, for “clean” cracks generated through freezing and thawing cycles. As this output parameter is linked to the hysteresis area and the crack’s closure process, it is logical to choose the same number of cycles previously selected for the hysteresis area (the five cycles). Similarly to the HA parameter, the trend/shape of the curves correlating the plastic deformation and the degree of expansion of the test specimens suggest that the reliability of the latter is generally improved when the five cycles are taken into account.

As mentioned previously, several studies have shown that the *modulus of elasticity* of concrete is rapidly and extensively affected by ASR. The results of our study support the above observations and confirm that it is a very important parameter for characterizing damage in concrete affected by ASR. Since the results of our experiments are very similar from one series to another (i.e. modulus values for the first cycle, the average of last 4 cycles and the average of 2nd and 3rd cycles), it is suggested that the same procedure commonly used for the ordinary modulus of elasticity determination should be maintained since we suggest that the SDT procedure be also carried out at 40% of the concrete mix design strength. Thus, the average value of the 2nd and 3rd cycles could be used as the third output parameter of SDT.

Finally, the *non linearity index* (NLI), a parameter proposed by Crisp et al. [23, 24] to assess the damage degree by the study of the curve shapes (representing the ratio of the slope of the stress response to half the maximum load over the secant modulus of elasticity) was also evaluated when the SDT was carried out at 40% of the 28-day concrete design strengths. This parameter is quite interesting for assessing concrete damage because it has been found that damaged concrete specimens present upward (concave) curve shapes over the first stress-strain cycle, while undamaged specimens are characterized by straight line curves [39]. This behavior can also be seen quite clearly in Figure 3. This phenomenon, as increased hysteresis area and plastic deformation values are related to the cracks’ closure over compression cycles, suggests that distressed concretes (with important internal cracking) are likely to present an elastoplastic behavior while undamaged samples are likely to behave much more in an elastic way. Therefore, the NLI parameter may indeed help to evaluate damage in concrete through stress-strain curve shape analysis, as it can vary from 1 (in the case of undamaged concretes presenting straight line curves) to 1.5 or even 2.0 (in the case of damaged concrete presenting a strong concave curve shape). Indeed, the evidences obtained for all the data assessed in this work were as good as the majority of data obtained from either the hysteresis area or the

plastic deformation parameters (Figure 17 – Supplementary Material). This means that the NLI could potentially be used as a fourth SDT output parameter as the interpretation of the first stress-strain cycle behavior is mostly linked to the physical integrity of the concrete specimens.

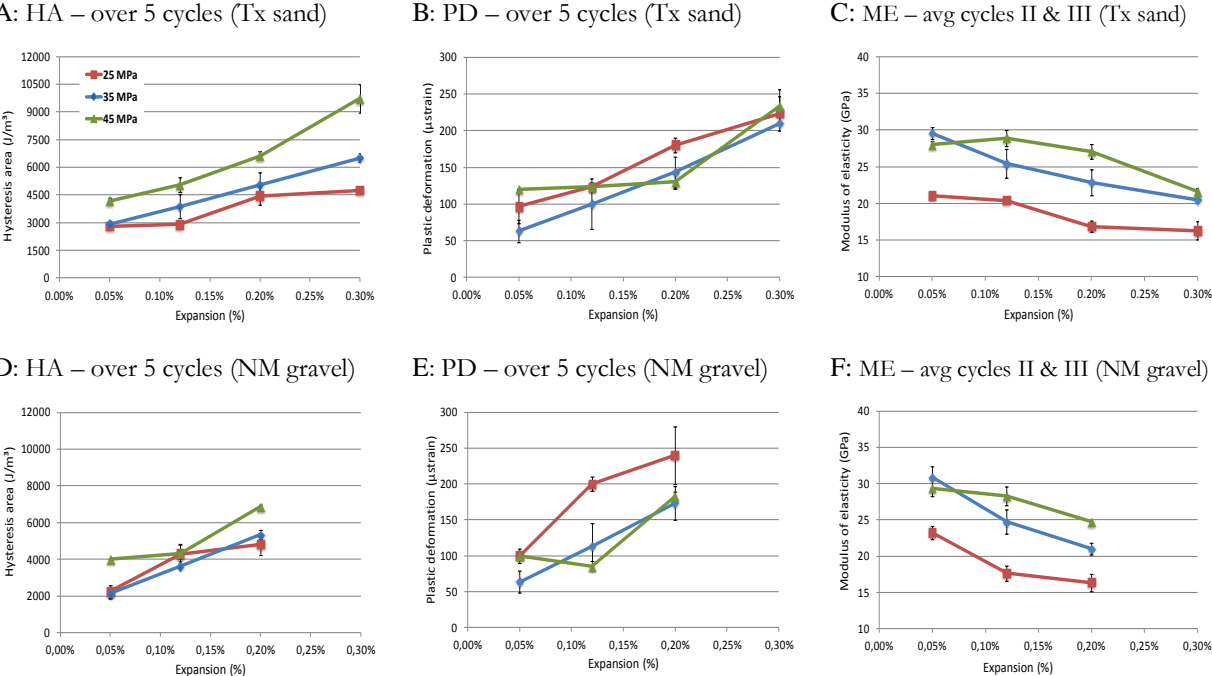


Figure 9: Analysis of the SDT output parameters when 40% of the mix design strength is used over the test for the 25. 35 and 45 MPa concrete mixtures with Tx sand (A, B and C) and NM gravel (D, E, F). The vertical bars correspond to variability data, i.e. one standard deviation on each side of the average value obtained at different expansion levels. The variability between the results obtained from the specimens of a set is often so small that the vertical bars are contained within the symbols.

Finally, it is important to look at the data obtained for each of the SDT output parameters for control concrete specimens, i.e. before any significant ASR expansion (i.e. $\leq 0.01\%$) has occurred (Table 8). It is possible to see that, as the modulus of elasticity is increasing from the 25 to the 45 MPa concrete mixtures, as expected, non negligible and increasing base values of dissipated energy (or Hysteresis area (HA)) and plastic deformation (PD) are also obtained for each set of specimens cast from the above mixtures. In proportion, however, a significantly higher increase in the HA values is observed from one mix to another compared to the PD parameter, which suggests that the former parameter is relatively more sensitive to differences in concrete mix design or microstructural characteristics / properties. These base values might be attributed to either the aggregate “competence” (i.e. quality of the aggregate/cement paste bonding which is related to several parameters such as w/c ratio, shape and roughness of the

aggregate, etc., [40]) or other problems than ASR such as increased self desiccation in concretes with lower w/c [41] potentially causing internal microcracking/shrinkage, etc. Moreover, differences from aggregate to aggregate need to be further investigated with the aim of verifying the possibility of having the quantitative results from SDT output parameters used for concretes incorporating different reactive aggregates, sizes, as well as other mechanisms of distress.

Table 8: Data obtained for SDT output parameters on control samples (with no expansion).

Concrete mixtures / Output parameters	Tx sand			NM gravel		
	25 MPa	35 MPa	45MPa	25 MPa	35 MPa	45 MPa
Hysteresis area first cycle (J/m³)	220	397	738	477	550	1225
Hysteresis area average value of last four cycles (J/m³)	127	217	369	205	312	390
Hysteresis are over the five cycles (J/m³)	758	1287	2211	1290	1800	2500
Plastic deformation first cycle (µstrain)	20	25	30	20	30	35
Plastic deformation value over the last four cycles (µstrain)	5	5	5	18	10	10
Plastic deformation over the five cycles (µstrain)	25	30	35	38	40	45
Non linearity index (NLI) first cycle	1.05	1.05	1.05	1.1	1.06	1.1
Modulus of elasticity (GPa) average value of the cycles II and III	34	37	39	28	31	32

6.6.2 Effect of the concrete mixture design

The data presented in the Figure 9 indicate that the behavior of the 25 and 35 MPa concretes is generally similar for the various SDT output parameters as a function of expansion. Indeed, despite some inherent variability in the test results, fairly linear increasing trends in the

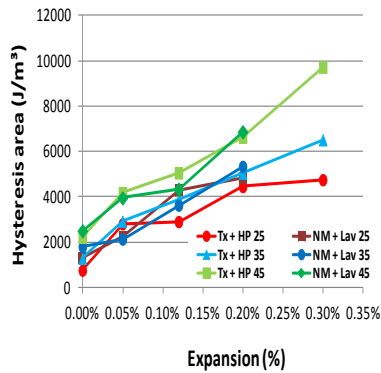
Hysteresis area and Plastic deformation values can be observed, which suggests a somewhat uniform progress of damage in the above types of concrete as a function of expansion. The progress of expansion/damage seems, however, to affect slightly more rapidly the modulus of elasticity of the above concretes. Such a rapid decrease in modulus of elasticity, as a function of increasing expansion (or internal distress!) due to ASR, has also been reported in the literature for ordinary concretes [16, 22].

On the other hand, the SDT results suggest a non linear progress of internal damage due to ASR in the 45 MPa concrete. The relatively higher values for both the Hysteresis area and the Plastic deformation, and relatively lower modulus of elasticity values (\leq that of the 35 MPa concrete), at low expansion levels (0.05%), suggest that internal damage/microcracking due to ASR or other mechanisms (e.g. self desiccation due to lower W/C) develops somewhat early in this concrete type. However, as the expansion level increases, the development/progress of distress seems to stagnate (or increase more slowly than the more ductile 25 and 35 MPa mixtures), at least up until a certain level (between 0.12% and 0.20%), after which the damage seems to accelerate (Figure 9). This difference in behavior could likely be explained by the more refined pore structure and higher stiffness of the 45 MPa concretes, which contribute at “tolerating” a somewhat higher degree of expansive stresses (due to ASR) before significant microcracking develops that will result in higher HA and PD values, and significant reduction in the ME.

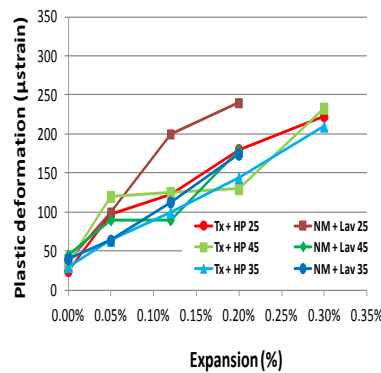
6.6.3 Effect of the type of reaction - fine vs. coarse reactive aggregates

The SDT output parameters for the different concrete mixtures incorporating reactive coarse (NM) and fine aggregates (Tx) are compared in Figure 10. Despite some inherent variability in the test results, the data globally show similar increasing trends for the Hysteresis area and Plastic deformation parameters as a function of expansion, for concretes incorporating a reactive fine or coarse aggregate, as the test results are generally grouped together for similar mix designs. On the other hand, the modulus of elasticity seems to be affected slightly more slowly, as a function of expansion, for the 35 and 45 MPa concretes incorporating the reactive NM coarse aggregate; however, similar losses in ME seem to be induced towards higher expansion/damage levels in the different concretes. Further analysis is in progress to verify whether the above conclusion applies to a larger selection of reactive aggregate materials (i.e. different rock types and sands) [30].

A: HA (40%) – over 5 cycles



B: PD (40%) – over 5 cycles



C: ME loss (40%) – avg cycles II & III

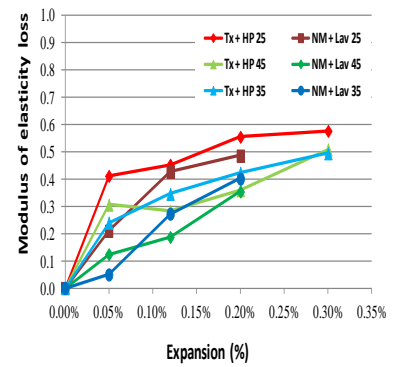


Figure 10: Analysis of the effect of the aggregate type (fine vs. coarse reactive aggregate) on the SDT output parameters when 40% of the mix design strength is used as the loading level over the test for the 25, 35 and 45 MPa concrete mixtures with either Tx sand or NM gravel. A) Hysteresis area (HA); B) Plastic deformation (PD) and C) Modulus of elasticity (ME) loss (calculated in % as a function of the value obtained at 0.0% of expansion at each expansion level).

6.6.4 Statistical treatment of test results

6.6.4.1 Variability of the test results

In this study, the SDT procedure was tested on laboratory-made concrete specimens of well-controlled expansion levels in order to perform a thorough evaluation of the best output parameters for the test. However, the validity/acceptability of a test largely remains a function of the variability of the results within the set of specimens used for that test (the between-laboratory variability of the test being outside of the scope of this study). Table 9 presents the variability information for the output responses of the SDT when carried out at 40% of the 28-day mix design strength. For each output parameter, concrete mix design and reactive aggregate, the average test value obtained for the three specimens is given, along with the *coefficient of variation* (CV- in percent), which was calculated by dividing the standard deviation values by the average of the test results within that set (three) of specimens.

Table 9: Average and CV(%) results for the SDT output parameters when the test is carried out at 40% of the concrete mix design strength.

Concrete mix design	SDT output parameters CV (%) for 40% of the 28-day concrete mix design strength		Tx sand mixtures				NM gravel mixtures		
			0.05%	0.12%	0.20%	0.30%	0.05%	0.12%	0.20%
25 MPa	Hysteresis area (J/m ³) – 5 cycles	Avg.	2808	2903	4449	4752	2238	4293	4819
		CV	5.2	5.2	10.9	3.5	11.4	3.1	5.2
	Plastic deformation (µε) – 5 cycles	Avg.	97	123	180	223	100	200	240
		CV	23.9	4.7	5.6	10.3	10.0	5.0	16.7
	Modulus of elasticity (GPa) – average of 2 nd and 3 rd cycles	Avg.	21	20.4	16.8	16.3	23.2	17.3	16.3
		CV	3.1	3.2	4.8	8.1	4.1	6.1	7.4
Concrete mix design	SDT output parameters CV (%) for 40% of the 28-day concrete mix design strength		Tx sand mixtures				NM gravel mixtures		
			0.05%	0.12%	0.20%	0.30%	0.05%	0.12%	0.20%
35 MPa	Hysteresis area (J/m ³) – 5 cycles	Avg.	2916	3882	5045	6508	2130	3627	5340
		CV	5.1	16.9	13.0	3.4	16.8	15.1	11.3
	Plastic deformation (µε) – 5 cycles	Avg.	63	100	143	210	63	113	173
		CV	24.1	34.6	14.5	4.8	24.1	28.4	13.3
	Modulus of elasticity (GPa) – average of 2 nd and 3 rd cycles	Avg.	29.5	25.4	22.9	20.5	30.9	24.7	21.0
		CV	2.2	7.4	7.7	0.8	4.8	6.8	3.9
Concrete mix design	SDT output parameters CV (%) for 40% of the 28-day concrete mix design strength		Tx sand mixtures				NM gravel mixtures		
			0.05%	0.12%	0.20%	0.30%	0.05%	0.12%	0.20%
45 MPa	Hysteresis area (J/m ³) – 5 cycles	Avg.	4177	5055	6628	9728	3996	4333	6869
		CV	4.1	8.0	3.4	7.9	0.2	10.6	1.2
	Plastic deformation (µε) – 5 cycles	Avg.	120	123	130	233	100	85	183
		CV	0.0	4.7	7.7	9.9	0.0	8.3	3.1
	Modulus of elasticity (GPa) – average of 2 nd and 3 rd cycles	Avg.	28.0	28.9	27.1	21.6	29.3	28.3	24.7
		CV	1.5	4.3	4.3	2.3	3.9	4.4	0.1

The *modulus of elasticity* (ME) parameter showed the lowest variability among the test parameters, with CVs ranging from 0.1% up to 8.1%. The hysteresis area (HA) parameter presented CVs ranging from 0.22% up to 16.9%, with about 60% of those CVs being < 10%. On the other hand, the plastic deformation (PD) parameter presented the highest CVs, ranging from 0.0% to 34.6%.

It is important to note that an increase in the expansion levels generally resulted in a decrease in the variability factor of the results within a set of specimens, which in case of the HA and PD parameters is partly related to a significant increase in the absolute values of the test results measured with increasing expansion (higher J/m³ for HA and µε for the PD).

Moreover, the analysis of the whole database including variability parameters, which is presented as an annex in the electronic version of this paper, indicates that reductions in variability are generally obtained with an increase in the maximum loading level in the test, i.e. from 15 to 40% of the 28-day mix design strength. This is likely attributable, once again, to a significant increase in the absolute values of the test results measured with increasing loading level, but also to a more complete “stressing” of the test specimens (closure of macro/microcracks) at higher load levels, thus contributing at reducing the differences between the test specimens of a same set (i.e. expansion levels). However, considering the inherent variability in the development of damage due to ASR (or other deleterious mechanisms) within a concrete member (due to differences in exposure to moisture, concentrations of alkalis, etc.), one must accept that the variability in the SDT test results will invariably be higher between a set of specimens extracted from "damaged" concrete than that obtained for sound concrete specimens.

6.6.4.2 Analysis of variance (ANOVA)

SDT approach and output responses' validity assessment

In order to assess the statistical validity of the database generated as part of this study, multi-variable and two-variable analyses of variance (ANOVA) were carried out. First, a multi-variable ANOVA was performed (R software) over all the data generated (i.e. all the specimens and expansions for all the concrete strengths, aggregate types, and output responses) in order to verify whether all the parameters tested in this study were statistically significant (with a significant level of 5%). The results of the above analysis indicated that all the parameters were statistically different from each other, as all the “F values” were greater than the “F_{critic}” and the “p values” were less than 0.05 for each case. Therefore, an analysis of the homogeneity of the results was performed, which confirmed the previous statement (Figure 18). Examples of the results of the multi-variable analysis are given in the Annex of the electronic paper (Supplementary information) (Tables 22 and 23).

The multi-variable ANOVA showed that all the parameters (i.e. different strengths, aggregate types, expansion levels, etc.) were different but influence each other, which suggests that there are no specific scenario or testing approach that could provide the most significant and reliable results. However, thinking about the SDT as a diagnostic engineering tool for damage evaluation in aging concrete, the best scenario would be to adopt one single testing regime that would provide the most reliable results while requiring minimal local/individual decision upon testing conditions that could result in misleading results. The testing carried out in this

study showed that the loading level is one of the most critical parameter for stiffness damage testing. The multi-variable ANOVA showed that the most statistically reliable scenarios for testing regime involve testing at 40% of the 28-day design strength, while 30% was also found to work in some instances (see Table 24 in the Annex of the electronic paper (*Supplementary information*)). This can also be seen in Table 10, which presents a two-variable ANOVA while fixing the loading levels and analyzing the results as a function of the expansion levels, concrete strengths and aggregate types.

It is quite clear from the results presented in Table 10 that the only loading levels capable of performing SDT in a “diagnostic manner” (i.e. being able to differentiate the degree of damage as a function of increasing expansion through SDT HA and PD output parameters) are 30% and 40% of the 28-day design concrete strength (as suggested in section 6.5.1) (i.e. highlighted lines where $F > F_{critic}$ and $P < 0.05$). In fact, one can see that the 40% loading level is statistically reliable in all cases. The 30% loading level is reliable in 50% of the cases, and even for the scenarios where it could well classify the differences in the physical integrities; the 40% approach still presented better results (i.e. higher “F values” at 40% than at 30%). Moreover, through the multi-variable ANOVA, the 40% load showed both the lowest variability and the highest average values, which yet confirms the superior statistical reliability of this testing regime.

Table 10: Two-variable ANOVA performed for the HA (five cycles) and PD (five cycles) parameters for all loading levels/concrete strengths and aggregate types used.

ANOVA analysis				Hysteresis area (HA) - 5 cycles (J/m ³)						Plastic deformation (PD) - 5 cycles (μstrain)					
Aggregate type	Strength (MPa)	Load (%)	Expansion (%)	HA_F	HA_Fcritic	F>Fcritic	HA_P value	α	P<α	PD_F	PD_Fcritic	F>Fcritic	PD_P value	α	P<α
Tx	25	15	0.05% - 0.30%	1.28	4.75	-	0.36000	0	-	2.37	4.75	-	0.17000	0.05	-
		20	0.05% - 0.30%	3.00	4.75	-	0.12000	0.05	-	1.92	4.75	-	0.22000	0.05	-
		30	0.05% - 0.30%	1.80	4.75	-	0.25000	0.05	-	3.70	4.75	-	0.08000	0.05	-
		40	0.05% - 0.30%	55.30	4.75	X	0.00009	0.05	X	23.70	4.75	X	0.00100	0.05	X
	35	15	0.05% - 0.30%	30.67	4.75	X	0.00040	0.05	X	3.18	4.75	-	0.10000	0.05	-
		20	0.05% - 0.30%	15.40	4.75	X	0.00310	0.05	X	2.86	4.75	-	0.12000	0.05	-
		30	0.05% - 0.30%	36.80	4.75	X	0.00029	0.05	X	22.22	4.75	X	0.00112	0.05	X
		40	0.05% - 0.30%	37.00	4.75	X	0.00031	0.05	X	23.33	4.75	X	0.00009	0.05	X
	45	15	0.05% - 0.30%	4.14	4.75	-	0.07000	0.05	-	7.37	4.75	X	0.02000	0.05	X
		20	0.05% - 0.30%	18.00	4.75	X	0.02000	0.05	X	1.33	4.75	-	0.348	0.05	-
		30	0.05% - 0.30%	12.90	4.75	X	0.00500	0.05	X	10.98	4.75	X	0.00750	0.05	X
		40	0.05% - 0.30%	90.54	4.75	X	0.00002	0.05	X	58.55	4.75	X	0.00007	0.05	X
NM	24	15	0.05% - 0.30%	5.51	6.94	-	0.07000	0	-	49.00	6.94	X	0.00150	0.05	X
		20	0.05% - 0.30%	6.20	6.94	-	0.06000	0.05	-	2.69	6.94	-	0.18000	0.05	-
		30	0.05% - 0.30%	18.83	6.94	X	0.00900	0.05	X	14.11	6.94	X	0.01500	0.05	X
		40	0.05% - 0.30%	134.76	6.94	X	0.00020	0.05	X	36.00	6.94	X	0.00200	0.05	X
	35	15	0.05% - 0.30%	1.30	6.94	-	0.37000	0.05	-	1.75	6.94	-	0.28440	0.05	-
		20	0.05% - 0.30%	1.60	6.94	-	0.31000	0.05	-	12.13	6.94	X	0.02000	0.05	X
		30	0.05% - 0.30%	10.70	6.94	X	0.02500	0.05	X	1.3	6.94	-	0.37000	0.05	-
		40	0.05% - 0.30%	20.72	6.94	X	0.00800	0.05	X	10.30	6.94	X	0.02500	0.05	X
	45	15	0.05% - 0.30%	0.16	6.94	-	0.85000	0.05	-	4.26	6.94	-	1.00000	0.05	-
		20	0.05% - 0.30%	2.89	6.94	-	0.16000	0.05	-	1.75	6.94	-	0.28400	0.05	-
		30	0.05% - 0.30%	4.14	6.94	-	0.10000	0.05	-	3.74	6.94	-	0.12250	0.05	-
		40	0.05% - 0.30%	135.90	6.94	X	0.00020	0.05	X	247.00	6.94	-	0.00010	0.05	-

Another two-variable ANOVA was carried out to verify the differences of using the first cycle versus the five cycles during the SDT procedure. The results showed that both approaches are significant and could be used as SDT output parameters (Table 11); however, the greater the numbers of cycles, better are the responses obtained through stiffness damage testing (higher F values and lower p values), which confirms the conclusions presented in Section 6.6.1 (full results presented in *Supplementary information*).

Table 11: Statistical evaluation (ANOVA) of the SDT diagnostic character: First cycle vs. five cycles. Example for the Hysteresis area parameter for the Tx sand concrete mixtures.

ANOVA analysis			Hysteresis area (HA) - 1 cycle (J/m ³)						Hysteresis area (HA) - 5 cycles (J/m ³)					
Load (%)	Strength (MPa)	Expansion (%)	HA_F	HA_Fcritic	F>Fcritic	HA_P value	α	P< α	HA_F	HA_Fcritic	F>Fcritic	HA_P value	α	P< α
40	25	0.05%	48	4.75	X	0.00010	0.05	X	55	4.75	X	0.00009	0.05	X
		0.12%												
		0.20%												
		0.30%												
	35	0.05%	30	4.75	X	0.00052	0.05	X	36	4.75	X	0.00029	0.05	X
		0.12%												
45	0.05%	63	4.75	X	0.00006	0.05	X	90	4.75	X	0.00002	0.05	X	
	0.12%													
		0.20%												
		0.30%												

In summary, the ANOVA carried out on the test results obtained in this study confirmed that a statistically reliable assessment of the degree of damage in 25, 35 and 45 MPa concretes incorporating reactive fine or coarse aggregates was obtained by carrying out stiffness damage testing at 40% of the 28-day design strength, through the use of the Hysteresis area (5 cycles), Plastic deformation (5 cycles) and Modulus of elasticity (average of 2nd and 3rd cycles) output parameters.

Compression and tensile strengths validity after SDT

A two-variable ANOVA was performed to verify whether the compressive and tensile stresses responses were significantly different when different loading levels were used through the SDT, for each of the expansion levels studied. The results of this investigation are presented in the Annex of the electronic paper (*Supplementary information*) (Tables 25 and 26). All the values obtained over this analysis (“F value”< “F critic” and “p values” > 0.05) indicated that there are no differences in the test results when different loadings are used over SDT, thus suggesting that performing the SDT up to 40% of the 28-day design strength does not deleteriously impact on the compressive or tensile strengths of the test specimens (25 to 45 MPa concrete) affected to various degrees by ASR.

6.6.5 Assessment of damage in the ASR-affected concrete specimens by petrographic examination

The Stiffness Damage Test (SDT), as well as other tools developed for assessing damage in concrete, such as the Damage Rating Index (DRI), are proposed to “measure and quantify” the micro/macroscale features of damage in concretes due to a given distress mechanism. The detailed results of the petrographic examination of the test specimens are presented and analyzed in [30]; however, Figure 11 presents a summary of these results, which correspond to the counts of the following features of deterioration in the test specimens, averaged over a 100 cm² surface:

- Group I corresponds to closed cracks in the aggregate particles (CCA) (considered to be, in many cases, pre-existing cracks in the aggregate particles due to aggregate processing operations);
- Group II corresponds to opened cracks in the aggregate particles, with or without reaction products (OCA + OCAG); and
- Group III corresponds to cracks in the cement paste, with or without reaction products (CCP + CCPG).

Cracks of Groups II and III are considered to be linked to the development and progress of ASR in the concrete specimens.

In the case of the 25 MPa (Figure 11A) and 35 MPa (Figure 11B) concretes, a progressive increase in the number of cracks in the reactive fine (Tx) or coarse (NM) aggregate particles (Groups I and II) and in the cement paste (Group III) was measured as a function of increasing expansion of the concrete specimens, which correlates with the progressive (\approx linear) increase in the Hysteresis area and Plastic deformation parameters measured through stiffness damage testing (Figure 9). Moreover, as reported in the literature, the above increase in cracking results in a slightly more rapid decrease in modulus of elasticity, as this parameter is more sensitive to the early development of cracking in the test specimens.

On the other hand, the development of the petrographic features of deterioration is different for the 45 MPa concretes. The total counts of cracking in the aggregate particles and in the cement paste (sum of Groups I to III counts) are generally higher at early expansion level than in the 25 and 35 MPa concretes. In the case of the concrete incorporating the Tx reactive fine aggregate (left portion of Figure 11C), the counts for Group I cracks are significantly higher

than for the 25 and 35 MPa concretes, which is associated to a significant increase in cracking in the non-reactive limestone coarse aggregate particles.

This phenomenon is thought to happen due to the finer pore structure and higher mechanical properties of the cement paste and ITZ (interfacial transition zone) of the 45 MPa concrete mixture (that present a quite low water-to-cement ratio - 0.37), compared to the less “stiff” limestone coarse aggregate particles. Therefore, the expansive ASR stresses generated by the reactive Tx sand particles would choose a “path of least energy release”, thus causing the crack increase in the limestone particles. This hypothesis is supported by the fact that no significant differences in Group I cracks is measured between the 25, 35 and 45 MPa concretes incorporating the reactive NM coarse aggregate, the latter being mainly composed of harder and stiffer rock types (mixed volcanics, quartzite, chert). Also, for both 45 MPa concretes incorporating the Tx and NM reactive aggregates, the amount of Group II and III cracks remain relatively stable up to about 0.12% expansion, being however slightly higher for the concrete incorporating the NM aggregate (right portion of Figure 11C), before increasing significantly (Figure 11C). All of the above petrographic observations correlate well with the behavior observed for the 45 MPa concretes through stiffness damage testing, i.e. 1) somewhat higher HA and PD values (and ME values lower than that of the 35 MPa concrete) at early expansion level (0.05%) related to rapid formation of microcracking in the 45 MPa concrete, followed 2) by a slow increase/progress in microcracking up to about 0.12% expansion resulting in stable HA, PD and ME values during that period, with and then 3) a significant increase in microcracking causing significant increase in HA and PD (and decrease in ME) towards higher expansion levels (Figure 9).

A: 25 MPa Mixtures

B: 35 MPa mixtures

C: 45 MPa mixtures

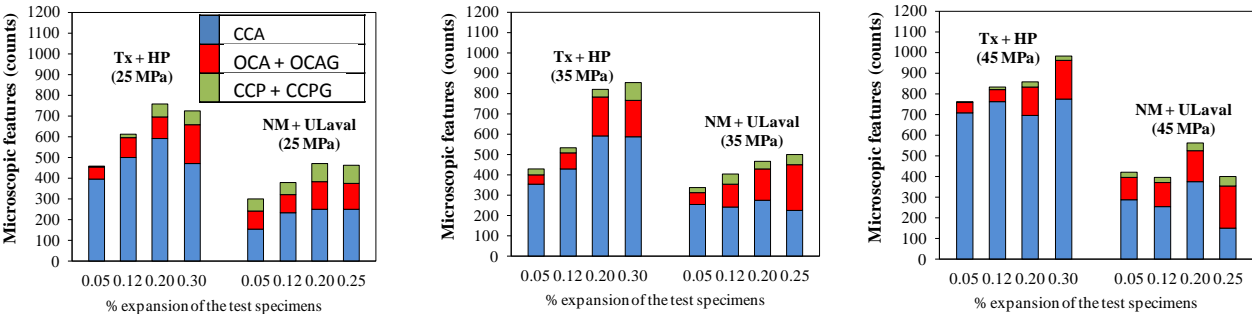


Figure 11: Development of ASR cracks: 1) closed cracks in the aggregates (OCA); 2) opened cracks in the aggregates with and without gel (OCA + OCAG) and; 3) opened cracks in the cement paste with and without gel (CCP + CCPG) in function of the expansion levels for the 25 MPa (A), 35 MPa (B) and 45 MPa (C) concrete mixtures containing both Tx sand and NM gravel as reactive aggregates

In order to be a diagnostic tool, the SDT should be capable of assessing or “measure”, through its output parameters, the physical changes in the concrete specimens as ASR expansion progresses. It has been found through previous work and during this study that the SDT presents three main but somewhat different “measures” of damage in the concrete material [18, 23 and 24]: 1) Hysteresis area (HA); 2) Plastic deformation (PD) and; 3) Modulus of elasticity (ME). As discussed in 6.1.2, the HA represents the energy used for closing microcracks under compression cycles. The PD is linked to the HA but it measures a different physical property, i.e. the sliding across crack surfaces over closure under compression. Finally, the ME represents the stiffness of the concrete, which varies as a function of concrete mixture proportions but decreases as a function of microcracking development due to ASR. The results presented in Figure 11 and discussed in the previous paragraphs provide a very interesting link between cracking development in a variety of concretes (25 to 45 MPa) and the response measured through stiffness damage testing. However, the results presented and discussed in Section 6.5 showed that a significant loading level is required for obtaining diagnostic evaluation of internal damage due to ASR; in other words, the greater is the loading used for stiffness damage testing, within a reasonable range, the more reliable is the distinction between the different ASR expansion levels/damage degrees in the test specimens. In fact, despite the presence of significant microcracking in the test specimens at all the expansion levels investigated (Figure 11), loading levels of less than 30% of the 28-day concrete strength were not capable of distinguishing between the different “physical integrities” reached for different ASR expansions levels. The test data and their statistical analysis through ANOVA indicated that the 30% loading level was sometimes but not always (i.e. for some concrete strengths, aggregate types and output parameters) able to reliably distinguish the different expansion/damage levels. On the other hand, the 40% loading level largely provided the expected response. Those results demonstrated that in order to obtain diagnostic results over the SDT, one really needs to “load/stress” the material analyzed, which means taking the material up to a “threshold” of performance thus allowing to reliably measure its current condition/physical integrity.

6.6.6 The non-destructive character of the SDT

One of the arguments used by [18, 23 and 24] to support the use of a fairly low and fixed loading level in the SDT (e.g. 5.5 MPa) was that the test needs to be non destructive if one wants to use the same cores to perform additional testing, such as compressive strength,

residual expansion and petrographic examination. Although the above argument may have some economical sense in practical applications, the selection of the loading level should primarily be such that a reliable evaluation of the current condition of the concrete be obtained from the test without introducing additional damage through the evaluation process. Within the parameters selected for this study, i.e. mixture designs and ASR-related expansion levels, it appears that testing concrete specimens in the SDT up to a load corresponding to 40% of the 28-day mix design strength allows to reach the above objective in a diagnostic manner. That loading level is known not to generate any deleterious effects upon testing of sound concrete since it is the recommended level used in the determination of a concrete's modulus of elasticity (ASTM C 469).

It is possible, however, that testing ASR-affected concrete specimens in the SDT at a loading level corresponding to 40% of the 28-day compressive strength may contribute at increasing internal damage in the concrete. The magnitude of that damaging effect will depend not only on the level/extent of reaction/expansion reached by the concrete (higher risk of damaging effect at higher expansion level), but also on the tools used to evaluate the impact in question. For instance, the petrographic examination under the SEM of polished sections after completion of the SDT would very likely indicate the progression of some microcracks after SDT in those ASR-affected concrete specimens having reaching higher expansion levels. This is perhaps suggested by the ultrasonic pulse velocity measurements that seem to highlight slight damaging effects of the test, especially for specimens having reached the highest expansion levels studied (i.e. 0.30% - Figure 7), despite the fact that UPV has already demonstrated to be somewhat unreliable for the assessment of damage due to ASR [16, 38]. On the other hand, the results of semi-quantitative petrographic analyses (DRI), compressive strength and tensile strength evaluations carried out in this study, suggest that running the SDT at a loading level corresponding to 40% of the 28-day mix design strength does not induce additional damage in the ASR-affected concrete specimens tested. Compressive strength is generally not recognized as a diagnostic test for ASR until high expansion levels were reached [42]. The Institution of Structural Engineers [22] indicates that the tensile strength of concrete is generally rapidly affected by ASR; however, the results vary largely according to the method used for evaluation. In this project, a gas pressure test was used, which had shown some promises in previous work [37]; however, the results obtained in this study did not highlight significant differences between the various test specimens investigated. The petrographic examination of polished concrete sections using the Damage Rating Index did not reveal any significant differences between test specimens before and

after the SDT, at least visible on polished sections examined at 16 x magnification under a stereomicroscope.

The overall results of this study reveal that the SDT can meet the objective of being a diagnostic tool for evaluating the current condition of ASR-affected concretes when performed at the appropriate loading level, i.e. at a threshold level that will somewhat “challenge” the material to reveal its current condition without generating additional damage.

6.7 CONCLUSIONS

The main objective of the test program carried out in this study was to develop basic information on the effectiveness/reliability of the *Stiffness Damage Test* for assessing the degree of damage in ASR-affected concretes. Input and output parameters of the SDT were evaluated for tests carried out on laboratory-made and cured specimens (100 x 200 mm cylinders) cast from 25, 35 and 45 MPa concrete mixtures incorporating two types of reactive aggregates (Texas sand and New Mexico gravel) and that had reached various expansion levels (0.05 to 0.30%) due to ASR. The main conclusions of the above investigations are:

- The *Stiffness Damage Test* can provide a reliable assessment of the effects of ASR expansion on damage generation in different types of concretes. In order to do so, the maximum load used for the loading/unloading cycles in the SDT should be selected on the basis of a percentage of the mix design strength instead of a fixed loading value, as previously proposed in the literature;
- Carrying out the SDT with percentages of loading of less than 30% and preferably 40% of the concrete mix design strength does not make the SDT a diagnostic tool for assessing the degree of expansion attained by ASR-affected concretes, as the results evidences showed that the test cannot distinguish different expansion levels/damage degrees of concretes through its output responses. Loadings at 30% of the concrete mix design strength could sometimes distinguish well ASR damage and development but not for all the cases. However, the 40% loading level was a preferable scenario for all the scenarios studied. ANOVA analyzes confirmed those results;
- The hysteresis area and the plastic deformation over the complete five cycles, as well as the average value of the modulus of elasticity obtained in the second and third cycles, were found to be the best parameters to use as output responses when the test is carried out up to a load corresponding to 40% of the mix design (28-day) strength. The non

linearity index (NLI) parameter proposed by Crisp et al [22, 23] was found to have the potential of providing complementary information for damage assessment in concrete affected by ASR;

- Even when using 40% of the concrete mix design strength, the SDT seems to maintain its “non-destructive” character, as one could see from the results of the microscopic examination of the test specimens carried out through the Damage Rating Index (DRI), as well as from the results of either compressive or tensile strength. Ultrasonic pulse velocity measurements, however, suggest slight increased damage in test specimens after stiffness damage testing, especially at higher expansion levels. Therefore, although examination under the SEM of polished sections after completion of the SDT would likely indicate the progression of some microcracks after SDT in those ASR-affected concrete specimens having reaching higher expansion levels, it is believed that performing SDT at the 40% loading level provides a reliable assessment of the current condition of concrete affected by ASR without inducing significant additional damage that could jeopardize the reliability of the assessment. Also, concrete specimens could thus be used for mechanical assessment (compressive and tensile strengths) determination, petrographic examination or even chemical assessment after completion of the SDT without jeopardizing the quality/reliability of the test results. ANOVA analyzes confirmed this statement. This is true for the range of expansion values obtained in this study;
- The behavior of the 25 and 35 MPa concretes is generally similar for the various SDT output parameters as a function of expansion, showing a uniform progress of damage (i.e. fairly linear with a \sim constant rate) in the above types of concrete as a function of expansion. On the other hand, slightly different behavior of the SDT output parameters suggest that internal damage/ microcracking due to ASR progresses more slowly as a function of increasing expansion in the 45 MPa concrete, at least up until a certain level after which damage seems to accelerate. The results of the petrographic examination (i.e. counts of cracks in the aggregate particles and in the cement paste) confirm the behavior observed from stiffness damage testing. The results obtained for the different mixtures, in terms of either *hysteresis area* or the *plastic deformation* over the five cycles, were quite similar for damage generated in the fine aggregate (Tx sand) and the coarse aggregate (NM gravel) portion of the concrete;

- In general, the greater is the concrete mix design strength, the greater is the hysteresis area obtained through the SDT for the same aggregate type. However, it does not seem that the plastic deformation output value is significantly affected by the concrete strength;
- Despite a large number of specimens for the whole testing matrix, this study presented a small number of samples per scenario studied (i.e. three specimens per concrete mixture, per expansion level and per level of test loading). However, trends in the test results, plots and statistical analysis of data (ANOVA, two and multi-variables) confirmed that the results obtained in this work are statistically significant (for a significant level of 5%);
- Work is currently in progress to compare the result of stiffness damage testing (i.e. the hysteresis area and modulus of elasticity) to the microstructural characteristics of the concretes investigated (using the *Damage Rating Index – DRI*, and image analysis on UV-epoxy-impregnated concrete specimens) for establishing a quantitative assessment/model of “damage” generation in the concrete samples; one could indeed argue that the “expansion degree” due to ASR, which was the basic comparative parameter used to differentiate concrete specimens affected by ASR in this study, is actually not a good/appropriate indicator of “damage” in concrete due to ASR [30];
- The above-mentioned SDT output parameters are also being evaluated for determining their potential in quantifying the extent of damage/expansion in concretes affected by other deleterious mechanisms, such as Delayed Etringite Formation (DEF) and freezing and thawing [30].

6.8 ACKNOWLEDGEMENTS

The funding of this project was provided by a grant from the Quebec Department of Transportation, under the supervision of Mr. Alain Hovington and Mrs. Nadia Pouliot. The authors would like to thank Mr. René Malo and Mr. Mathieu Thomassin from “le Centre de recherche sur les infrastructures en béton (CRIB)” at Laval University, as well as the undergraduate research assistants who helped with the manufacturing and testing of the test specimens used in this project. L. Sanchez benefits from a Vanier scholarship financed by NSERC (Natural Sciences and Engineering Research Council of Canada).

6.9 REFERENCES

- [1] British Cement Association. The diagnosis of alkali silica reaction – report of a working party. England. 1992. 36p.
- [2] St-John. D.A.; Poole. A.W.; Sims. I. 1998. Concrete Petrography: A handbook of investigative techniques. Arnold. London. 474 p.
- [3] Grattan-Bellew, P.E., Danay, A. 1992. Comparison of laboratory and field evaluation of AAR in large dams, Proc. of the Int. Conf. on Concrete AAR in Hydroelectric Plants and Dams, Canadian Electrical Association & Canadian National Committee of the Int. Commission on Large Dams, 23p.
- [4] Dunbar, P.A., Grattan-Bellew, P.E. 1995. Results of damage rating evaluation of condition of concrete from a number of structures affected by ASR. CANMET/ACI International Workshop on Alkali-Aggregate Reactions in Concrete, Darmouth, Canada, 257-266.
- [5] Grattan-Bellew, P.E., Mitchell, L.D. 2006. Quantitative petrographic analysis of concrete –The Damage Rating Index (DRI) method, a review. Proc. Marc-André Bérubé symposium on AAR in concrete, CANMET/ACI Advances in concrete technology seminar, Montréal, Canada, 321-334.
- [6] Blight, G.E., McIver, J.R., Schutte, W.K., Rimmer, R. 1981. The effects of alkali-aggregate reaction on reinforced concrete structures made with Witwatersrand quartzite aggregate. Proc. 5th Int. Conf. on AAR in Concrete, Cape Town, South Africa, 13 p.
- [7] Sims, I., Hunt, B., Miglio, B. 1992. Quantifying microscopical examinations of concrete for AAR and other durability aspects. American Concrete Institute, SP 131-114, 267-287.
- [8] Salomon, M., Panetier, J.L. 1994. Quantification du degré d'avancement de l'alcali-réaction dans les bétons et de la néofissuration associée. Proc. 3rd CANMET/ACI Int. Conf. on Durability of Concrete, Nice, France, 383-401.
- [9] Clemena, G.G., Lane, S., Freeman, T., Lozev, M. 2000. Evaluation of nondestructive evaluation methods for application in early detection of deterioration in concrete pavements. VTRC 00-R13. Virginia Transportation Research Council, Charlottesville, USA, 26p.
- [10] Rivard, P., Fournier, B., Ballivy, G. 2000. Quantitative petrographic Technique for Concrete Damage Due to ASR: Experimental and Application. Cement, Concrete and Aggregates, 22 (1): 63-72.
- [11] Broekmans, M.A.T.M. 2002. The alkali-silica reaction: mineralogical and geochemical aspects of some Dutch concretes and Norwegian mylonites, PhD. Thesis, Utrecht University, 144 p.
- [12] Lindgaard, J., Skjolsvold, O., Haugen, M., Hagelia, P., Wigum, B.J. 2004. Experience from evaluation of degree of damage in fluorescent impregnated plan polished sections of half-cores based on the “Crack Index Method”. Proc. 12th Int. Conf. on AAR in Concrete, Beijing, China, 939-947.
- [13] Powers. L.; Shrimmer. F. H. Quantification of ASR in Concrete: An Introduction to the Damage-Rating Index Method. Paper. January. 2008.
- [14] Villeneuve, V., Fournier, B. & Duchesne, J. 2012. Determination of the damage in concrete affected by ASR – the Damage rating Index (DRI). Proceedings of the 14th International Conference on Alkali-Aggregate Reaction in Concrete, May 20-25th 2012, Austin (Texas), electronic.
- [15] Lindgård, J., Haugen, M., Castro, N. and Thomas, M.D.A. Advantages of using plane polished analysis as part of microstructural analyses to describe internal cracking due to Alkali-Silica Reaction. Proceedings of the 14th International Conference on Alkali-Aggregate Reaction in Concrete, May 20-25th 2012, Austin (Texas), electronic.
- [16] Pleau, R.; Bérubé, M. A.; Pigeon, M.; Fournier, B.; Raphael, S. Mechanical Behavior of Concrete Affected by AAR. 8th ICAAR - International Conference on Alkali-Aggregate Reaction in Concrete. Kyoto, Japan, 1989.
- [17] Nixon, P.J.; Bollinghaus, R. The effect of alkali aggregate reaction on the tensile strength of concrete. Durability of Building Materials pp. 243-248, 1985.

- [18] Smaoui. N.; Bérubé. M.A.; Fournier. B.; Bissonnette. B. & Durand. B. Evaluation of the Expansion Attained to Date by Concrete Affected by ASR - Part I: Experimental Study. *Canadian Journal of Civil Engineering*. 2004, 31: 826-845.
- [19] Wood, G. M.; JOHNSON, R. A. An engineer's perspective on UK. Experience with alkali-aggregate reaction. 8th ICAAR - International Conference on Alkali-Aggregate Reaction in Concrete. Kyoto, Japan, 1989.
- [20] Wood, G. M.; Johnson, R. A. The appraisal and maintenance of structures with alkali-silica reaction. Paper, Institution of Structural Engineers, February 1993.
- [21] Wood, G. M.; Norris, P.; Leek, D. Physical Behavior of AAR Damaged Concrete in Structures and in Test Conditions. 8th ICAAR - International Conference on Alkali-Aggregate Reaction in Concrete. Kyoto, Japan, 1989.
- [22] Institution of Structural Engineers. Structural effects of alkali-silica reaction. Technical guidance on the appraisal of existing structures. Report of an IStructE task group. London, SETO Ltd, 1992. 48 pp.
- [23] Crisp, T. M.; Waldron. P.; Wood. J. G. M. Development of a non destructive test to quantify damage in deteriorated concrete. *Magazine of Concrete Research*. 45. n° 165. 1989.
- [24] Crisp, T. M.; Wood, J. G. M.; Norris, P. Towards Quantification of Microstructural Damage in AAR Deteriorated Concrete. International Conference on Recent Developments on the Fracture of Concrete and Rock. September. 1993.
- [25] Walsh. J. B. The effects of cracks on the uniaxial elastic compression of rocks. *J. Geophys. Res.*. vol. 70. p.339 - 411. 1965.
- [26] Crouch. R. S. Specification for the determination of stiffness damage parameters from the low cyclic uniaxial compression of plain concrete cores. Revision A. Mott. Hay & Anderson. Special services division. Internal technical note. 1987.
- [27] J. G. M. Wood; P. J. Nixon; and P. Livesey. "Relating ASR structural damage to concrete composition and environment". Ed. A Shayan, pp 450 - 457. Proc. 10th Int Conf Alkali-Alkali Reaction in Concrete, Melbourne, 1996.
- [28] Bérubé, M. A.; Fournier, B.; Côté, T. Using the damage rating index for assessing the expansion of concrete affected by freeze-thaw, sulphate attack, or ASR. 14th ICAAR - International Conference on Alkali-Aggregate Reaction in Concrete. Texas, USA, 2012.
- [29] Giannini, E.; Folliard, K. Stiffness damage and mechanical testing of core specimens for the evaluation of structures affected by ASR Proceedings of the 14th International Conference on Alkali-Aggregate Reaction in Concrete, May 20-25th 2012, Austin (Texas), electronic.
- [30] Sanchez, L. F. M. Contribution to the assessment of damage in aging concrete infrastructures affected by alkali-aggregate reaction and other distress mechanisms, PhD thesis, Laval University, department of geology and geological engineering (to be published in 2014).
- [31] Fournier, B.; Ideker, J.H.; Folliard, K.J.; Thomas, M.D.A.; Nkinamubanzi, P.C.; Chevrier, R. 2010. Effect of environmental conditions on expansion in concrete due to alkali-silica reaction (ASR). *Materials Characterization Journal*, 60, 669-679.
- [32] ASTM C 1293. 2008. Standard Test Method for Determination of Length Change of Concrete due to Alkali-Silica Reaction.
- [33] CSA A23. 2-14C. 2009. Obtaining and Testing Drilled Cores for Compressive Strength Testing.
- [34] Villeneuve, V; Fournier, B. Détermination de l'endommagement du béton par méthode pétrographique quantitative. ACI Québec. November. 2009.
- [35] ASTM C 39. 2012. Standard Test Method for Compressive Strength of Cylindrical Concrete Specimens.
- [36] ASTM C 1074. 2011. Standard Practice for Estimating Concrete Strength by the Maturity Method.
- [37] Komar, A., J. Hartell and A. J. Boyd 2013. Pressure tension test: reliability for assessing concrete deterioration. Proceedings of the Seventh International Conference on Concrete under Severe Conditions - Environment and Loading. Nanjing, China, September 2013.
- [38] Saint-Pierre, F., Rivard, P., Sauriol, B., Ballivy, G. 2004. Étude de l'évolution de la réaction alcalis-silice par méthodes ultrasoniques. 11e Colloque sur la progression de la recherche québécoise portant sur les ouvrages d'art, Université Laval, Québec, 12 p.

- [39] Mindess, S.; Young, J. F.; Darwin, D. 2003. Concrete. Book. Pearson Education Ltda. second edition.
- [40] Alexander, M.; Mindess, S. Aggregates in concrete. 2005. Book. Modern concrete technology series. Taylor & Francis. London.
- [41] Lindgard, J; Sellevold, E.; Thomas, M. D. A.; Pedersen, B.; Justnes, H.; Ronning, T. F. 2013. Alkali-silica reaction (ASR) – performance testing: Influence of specimen pre-treatment, exposure conditions and prism size on concrete porosity, moisture state and transport properties. Cement and concrete research, vo. 53, p.145-167.
- [42] Kubo, Y.; Nakata, M. 2012. Effect of reactive aggregate on mechanical properties of concrete affected by alkali-silica reaction. 14th International conference on alkali-aggregate reaction (ICAAR). Texas, USA.

ANNEX – Supplementary information

Table 12: Responses of selected SDT output parameters versus the loading applied (15 to 40% of the concrete strength) for the 35 MPa concrete mixture incorporating a reactive fine aggregate (Tx sand) and affected to various degrees (i.e. different expansion levels) by ASR.

Concrete Mix design	Output Parameters		0.05% expansion				0.12% expansion			
			15%	20%	30%	40%	15%	20%	30%	40%
35 MPa	Hysteresis area (J/m ³)	First cycle	76	156	470	1056	114	253	691	1495
		Average of last four cycles	45	94	230	465	63	128	300	597
		Five cycles	257	531	1391	2916	367	764	1889	3882
	Plastic deformation (μ ϵ)	First cycle	10	10	27	50	13	23	43	70
		Over the last four cycles	3	3	13	13	10	7	20	30
		Five cycles	13	13	40	63	23	30	63	100
	Modulus of elasticity (GPa)	First cycle	34.2	32.9	30.3	28.1	30.7	27.2	25.7	24.2
		Average of last four cycles	35.4	31.6	28.9	26.5	31.0	28.4	26.1	24.9
		Average of cycles II and III	36.2	32.9	31.3	29.5	30.8	28.8	26.6	25.4
	Output Parameters		0.20% expansion				0.30% expansion			
			15%	20%	30%	40%	15%	20%	30%	40%
	Hysteresis area (J/m ³)	First cycle	110	281	897	2017	130	345	1265	2647
		Average of last four cycles	69	132	364	757	66	157	480	965
		Five cycles	386	810	2353	5045	396	974	3184	6508
	Plastic deformation (μ ϵ)	First cycle	10	23	57	93	20	33	77	130
		Over the last four cycles	10	17	30	50	7	7	57	80
		Five cycles	20	40	87	143	27	40	133	210
	Modulus of elasticity (GPa)	First cycle	29.7	25.3	23.2	21.6	26.7	23.2	19.3	19.0
		Average of last four cycles	29.8	25.2	23.8	22.3	27.8	24.1	19.5	19.8
		Average of cycles II and III	30.2	25.6	24.3	22.9	28.3	24.5	20.2	20.5

Table 13: Responses of selected SDT output parameters versus the loading applied (15 to 40% of the concrete strength) for the 45 MPa concrete mixture incorporating a reactive fine aggregate (Tx sand) and affected to various degrees (i.e. different expansion levels) by ASR.

Concrete Mix design	Output Parameters		0.05% expansion				0.12% expansion			
			15%	20%	30%	40%	15%	20%	30%	40%
45 MPa	Hysteresis area (J/m ³)	First cycle	276	558	1336	1714	149	278	754	1922
		Average of last four cycles	139	253	551	616	88	148	339	783
		Five cycles	833	1572	3540	4177	500	870	2110	5055
	Plastic deformation (μ ϵ)	First cycle	25	40	70	75	10	17	30	77
		Over the last four cycles	10	20	40	45	7	10	20	47
		Five cycles	35	60	110	120	17	27	50	123
	Modulus of elasticity (GPa)	First cycle	24.6	23.0	24.0	26.4	33.8	31.4	30.5	27.1
		Average of last four cycles	24.7	24.2	25.2	27.6	33.9	31.4	30.7	28.2
		Average of cycles II and III	25.2	24.6	25.5	28.0	33.9	31.6	31.1	28.9
	Output Parameters		0.20% expansion				0.30% expansion			
			15%	20%	30%	40%	15%	20%	30%	40%
	Hysteresis area (J/m ³)	First cycle	192	396	923	2524	164	311	1026	4042
		Average of last four cycles	103	192	376	1026	90	163	460	1421
		Five cycles	603	1163	2425	6628	526	962	2867	9728
	Plastic deformation (μ ϵ)	First cycle	20	27	43	87	17	20	47	167
		Over the last four cycles	13	7	17	43	3	13	27	67
		Five cycles	33	33	47	130	20	33	73	233
	Modulus of elasticity (GPa)	First cycle	30.2	27.6	27.1	25.6	31.7	30.3	27.4	19.5
		Average of last four cycles	30.7	28.2	28.2	26.5	33.2	30.4	27.9	21.0
		Average of cycles II and III	31.1	28.4	28.6	27.1	33.5	30.8	28.3	21.6

Table 14: Responses of selected SDT output parameters versus the loading applied (15 to 40% of the concrete strength) for the 35 MPa concrete mixture incorporating a reactive coarse aggregate (NM gravel) and affected to various degrees (i.e. different expansion levels) by ASR.

Concrete Mix design	Output Parameters		0.05% expansion				0.12% expansion			
			15%	20%	30%	40%	15%	20%	30%	40%
35 MPa	Hysteresis area (J/m ³)	First cycle	97	209	748	743	110	192	623	1456
		Average of last four cycles	58	107	303	347	59	99	266	543
		Five cycles	329	637	1960	2130	344	589	1687	3627
	Plastic deformation (μ ϵ)	First cycle	13	17	53	43	20	20	43	77
		Over the last four cycles	7	16	27	20	7	7	20	37
		Five cycles	20	32	80	63	27	27	63	113
	Modulus of elasticity (GPa)	First cycle	30.9	27.8	24.0	28.6	27.6	27.6	25.2	23.1
		Average of last four cycles	31.9	28.2	25.0	30.5	28.7	29.0	26.2	24.3
		Average of cycles II and III	32.1	28.2	25.4	30.9	28.7	29.1	26.6	24.7
	Output Parameters		0.20% expansion							
			15%	20%	30%	40%				
	Hysteresis area (J/m ³)	First cycle	132	291	913	2263				
		Average of last four cycles	69	122	361	769				
		Five cycles	406	778	2355	5340				
	Plastic deformation (μ ϵ)	First cycle	20	30	63	123				
		Over the last four cycles	10	23	27	50				
		Five cycles	30	47	90	173				
	Modulus of elasticity (GPa)	First cycle	25.4	23.0	21.6	18.9				
Average of last four cycles		26.7	25.1	22.8	20.5					
Average of cycles II and III		27.2	25.5	23.3	21.0					

Table 15: Responses of selected SDT output parameters versus the loading applied (15 to 40% of the concrete strength) for the 45 MPa concrete mixture incorporating a reactive coarse aggregate (NM gravel) and affected to various degrees (i.e. different expansion levels) by ASR.

Concrete Mix design	Output Parameters		0.05% expansion				0.12% expansion			
			15%	20%	30%	40%	15%	20%	30%	40%
45 MPa	Hysteresis area (J/m ³)	First cycle	167	336	841	1650	158	263	875	1582
		Average of last four cycles	85	176	342	594	79	125	368	688
		Five cycles	507	1039	2211	3996	473	762	2346	4333
	Plastic deformation (μ ϵ)	First cycle	13	27	43	75	20	17	43	55
		Over the last four cycles	10	7	13	25	3	3	20	30
		Five cycles	23	33	57	100	23	20	63	85
	Modulus of elasticity (GPa)	First cycle	30.2	29.1	26.5	26.6	29.9	29.1	27.1	27.1
		Average of last four cycles	30.2	29.5	27.6	29.1	31.5	29.5	27.8	27.9
		Average of cycles II and III	30.4	29.8	27.8	29.3	31.8	29.6	28.1	28.3
	Output Parameters		0.20% expansion							
			15%	20%	30%	40%				
	Hysteresis area (J/m ³)	First cycle	182	358	1131	2484				
		Average of last four cycles	88	173	459	1096				
		Five cycles	533	1049	2968	6869				
	Plastic deformation (μ ϵ)	First cycle	17	23	53	93				
		Over the last four cycles	7	17	27	90				
		Five cycles	23	40	80	183				
	Modulus of elasticity (GPa)	First cycle	26.7	26.1	24.5	22.0				
		Average of last four cycles	26.9	26.6	25.5	24.3				
		Average of cycles II and III	27.1	27.0	25.9	24.7				

Table 16: Variability (CV%, measured as the standard deviation of three samples divided by the average value among them) of SDT output parameters for the 25 MPa concrete mixture incorporating a reactive sand (Tx sand).

Concrete Mix design	CV(%) of the SDT output Parameters		0.05% expansion				0.12% expansion			
			15%	20%	30%	40%	15%	20%	30%	40%
25 MPa	Hysteresis area (J/m ³)	First cycle	22.8	16.2	15.9	8	15.2	7.7	21.7	8
		Average of last four cycles	9.3	10.1	13.9	3.5	8.4	3.5	14.6	3.5
		Five cycles	14.8	12.4	14.4	5.2	10.2	4.9	17.1	5.2
	Plastic deformation (μ ϵ)	First cycle	0.0	33.0	16.7	11.1	34.6	0.0	25.0	0.0
		Over the last four cycles	50.0	40	26.0	23.3	0.0	43.3	35.0	13.3
		Five cycles	34.6	43.3	16.7	23.9	34.6	17.3	40.0	4.7
	Modulus of elasticity (GPa)	First cycle	5.0	7.2	11.4	4.3	5.0	3.7	11.3	4
		Average of last four cycles	9.3	6.8	2.4	2.8	6.3	7.4	3.1	2.3
		Average of cycles II and III	8.6	5.8	9.4	3.1	6.4	7.3	10.7	3.2
	CV(%) of the SDT output Parameters		0.20% expansion				0.30% expansion			
			15%	20%	30%	40%	15%	20%	30%	40%
	Hysteresis area (J/m ³)	First cycle	17.5	14.4	22.6	10.3	29.2	15.0	11.0	5.1
		Average of last four cycles	21.4	22.6	21.6	11.3	20.2	25.1	6.1	3.0
		Five cycles	18.0	19.1	22.0	10.9	24.8	21.2	7.8	3.5
	Plastic deformation (μ ϵ)	First cycle	0.0	17.2	28.9	4.7	50.0	25.0	21.3	10.0
		Over the last four cycles	86.7	43.3	17.7	10.2	43.3	50	24.3	14.3
		Five cycles	21.6	24.7	16.4	5.6	45.8	52.9	21.7	10.3
	Modulus of elasticity (GPa)	First cycle	2.9	6.9	5.6	3.3	6.7	5.2	7.8	8.4
		Average of last four cycles	3.1	4.5	2.6	4.6	2.3	5.4	2.6	8.0
		Average of cycles II and III	4.1	4.3	5.2	4.8	2.6	3.1	10.1	8.1

Table 17: Variability (CV%, measured as the standard deviation of three samples divided by the average value among them) of SDT output parameters for the 35 MPa concrete mixture incorporating a reactive sand (Tx sand).

Concrete Mix design	CV(%) of the SDT output Parameters		0.05% expansion				0.12% expansion			
			15%	20%	30%	40%	15%	20%	30%	40%
35 MPa	Hysteresis area (J/m ³)	First cycle	3.4	7.8	12.6	4.6	10.0	5.5	19.7	20.8
		Average of last four cycles	4.5	3.8	14.0	5.6	6.6	8.9	15.5	14.5
		Five cycles	2.6	0.7	13.5	5.1	7.3	7.8	17.0	17.0
	Plastic deformation (μ ϵ)	First cycle	0.0	100.0	43.3	20.0	43.3	24.7	13.3	24.7
		Over the last four cycles	90.0	80.0	43.3	43.3	0.0	86.6	50.0	57.7
		Five cycles	43.3	90.0	25.0	24.1	24.7	33.3	24.1	34.6
	Modulus of elasticity (GPa)	First cycle	3.1	5.8	6.0	2.7	6.0	2.0	6.6	9.2
		Average of last four cycles	4.6	5.8	5.6	3.2	3.1	3.8	6.5	7.9
		Average of cycles II and III	3.4	0.5	3.2	2.2	1.3	3.2	6.1	7.4
	CV(%) of the SDT output Parameters		0.20% expansion				0.30% expansion			
			15%	20%	30%	40%	15%	20%	30%	40%
	Hysteresis area (J/m ³)	First cycle	6.5	5.3	5.0	16.0	4.4	18.5	16.5	3.2
		Average of last four cycles	9.6	5.0	0.4	10.9	0.8	13.1	7.7	3.5
		Five cycles	6.7	5.0	1.7	13.0	1.9	14.1	11.2	3.4
	Plastic deformation (μ ϵ)	First cycle	43.3	24.7	10.2	12.4	0.0	17.3	27.1	7.7
		Over the last four cycles	0.0	34.6	0.0	20.0	86.7	86.6	10.2	0.0
		Five cycles	0.0	0.0	6.7	14.5	21.7	25.0	17.3	4.8
	Modulus of elasticity (GPa)	First cycle	3.3	2.15	4.7	8.4	2.2	7.4	9.3	0.7
		Average of last four cycles	3.8	1.8	3.2	7.9	0.4	6.4	7.3	0.6
		Average of cycles II and III	4.5	1.8	3.3	7.7	0.9	6.4	7.3	0.8

Table 18: Variability (CV%, measured as the standard deviation of three samples divided by the average value among them) of SDT output parameters for the 45 MPa concrete mixture incorporating a reactive sand (Tx sand).

Concrete Mix design	CV(%) of the SDT output Parameters		0.05% expansion				0.12% expansion			
			15%	20%	30%	40%	15%	20%	30%	40%
45 MPa	Hysteresis area (J/m ³)	First cycle	8.7	5.4	18.7	2.0	30.0	12.7	19.5	8.3
		Average of last four cycles	4.7	6.2	12.7	5.6	42.4	18.4	14.9	7.9
		Five cycles	6.0	5.9	15.0	4.1	38.7	16.1	16.4	7.9
	Plastic deformation (μ ϵ)	First cycle	28.3	0.0	20.2	0.3	0.0	34.6	33.3	4.4
		Over the last four cycles	0.0	0.0	0.0	15.7	86.6	0.0	50.0	12.4
		Five cycles	20.2	0.0	12.9	0.0	34.6	21.7	40.0	4.7
	Modulus of elasticity (GPa)	First cycle	2.0	0.2	9.0	0.3	4.5	7.1	4.2	4.4
		Average of last four cycles	0.7	1.8	7.9	1.7	2.5	7.4	4.7	3.8
		Average of cycles II and III	0.6	2.8	7.6	1.5	2.5	7.7	3.9	4.3
	CV(%) of the SDT output Parameters		0.20% expansion				0.30% expansion			
			15%	20%	30%	40%	15%	20%	30%	40%
	Hysteresis area (J/m ³)	First cycle	13.1	12.0	8.2	6.0	17.0	9.1	11.3	10.2
		Average of last four cycles	25.7	10.0	5.0	2.3	17.6	11.1	2.7	6.2
		Five cycles	21.5	10.7	6.2	3.4	17.4	10.5	5.6	7.8
	Plastic deformation (μ ϵ)	First cycle	0.0	21.7	13.3	3.8	34.6	0.0	12.4	2.2
		Over the last four cycles	43.4	86.6	34.6	13.3	90.0	43.3	21.7	8.7
		Five cycles	17.3	17.3	49.5	7.7	50.0	17.3	15.7	9.9
	Modulus of elasticity (GPa)	First cycle	5.7	4.7	2.8	4.8	2.5	2.1	4.9	4.1
Average of last four cycles		6.7	3.0	1.9	4.3	2.9	2.2	6.0	2.3	
Average of cycles II and III		6.7	3.1	2.1	4.3	2.9	1.8	6.1	2.3	

Table 19: Variability (CV%, measured as the standard deviation of three samples divided by the average value among them) of SDT output parameters for the 25 MPa concrete mixture incorporating a reactive coarse aggregate (NM gravel).

Concrete Mix design	CV(%) of the SDT output Parameters		0.05% expansion				0.12% expansion			
			15%	20%	30%	40%	15%	20%	30%	40%
25 MPa	Hysteresis area (J/m ³)	First cycle	31.9	22.4	15.2	12.5	9.6	10.7	14.0	1.7
		Average of last four cycles	32.9	16.2	8.3	10.3	6.2	11.2	11.5	6.3
		Five cycles	33.0	18.0	11.1	11.4	8.1	5.4	12.6	3.1
	Plastic deformation (μ ϵ)	First cycle	100.0	21.7	25.0	7.5	0.0	31.5	17.3	10.4
		Over the last four cycles	86.7	87.0	69.3	24.7	0.0	30.0	21.7	10.8
		Five cycles	34.6	25.0	36.7	10.0	0.0	20.0	16.4	5.0
	Modulus of elasticity (GPa)	First cycle	2.0	9.3	3.9	3.6	2.2	10.6	6.2	5.1
		Average of last four cycles	9.7	7.1	3.4	4.2	1.6	8.1	5.7	5.9
		Average of cycles II and III	10.2	7.4	3.4	4.0	1.6	7.6	5.6	6.1
	CV(%) of the SDT output Parameters		0.20% expansion							
			15%	20%	30%	40%				
	Hysteresis area (J/m ³)	First cycle	19.1	24.8	9.7	8.5				
		Average of last four cycles	20.8	18.7	4.3	3.5				
		Five cycles	18.0	21.1	6.6	5.2				
	Plastic deformation (μ ϵ)	First cycle	21.7	25.0	7.5	17.3				
		Over the last four cycles	43.3	0.0	0.0	18.2				
		Five cycles	25.0	16.7	4.9	16.7				
	Modulus of elasticity (GPa)	First cycle	11.5	8.9	5.7	9.3				
		Average of last four cycles	17.1	7.1	5.4	7.4				
		Average of cycles II and III	11.6	6.8	5.0	7.4				

Table 20: Variability (CV%, measured as the standard deviation of three samples divided by the average value among them) of SDT output parameters for the 35 MPa concrete mixture incorporating a reactive coarse aggregate (NM gravel).

Concrete Mix design	CV(%) of the SDT output Parameters		0.05% expansion				0.12% expansion			
			15%	20%	30%	40%	15%	20%	30%	40%
35 MPa	Hysteresis area (J/m ³)	First cycle	5.1	22.1	13.1	17.7	16.7	9.4	15.3	21.3
		Average of last four cycles	8.0	15.5	8.3	16.6	26.9	13.3	11.1	11.1
		Five cycles	5.7	17.4	9.5	16.8	23.6	11.0	12.6	15.2
	Plastic deformation (μ ϵ)	First cycle	43.3	34.6	21.7	3.3	0.0	0.0	26.7	27.1
		Over the last four cycles	86.8	32.7	21.7	50.0	86.6	86.6	50.0	31.5
		Five cycles	50.0	21.5	21.7	24.1	21.6	21.7	33.0	28.4
	Modulus of elasticity (GPa)	First cycle	6.1	9.6	8.2	4.7	0.6	2.1	3.2	8.0
		Average of last four cycles	4.1	8.0	5.8	5.2	0.5	6.3	2.8	7.0
		Average of cycles II and III	4.8	8.0	5.9	4.8	0.5	3.2	2.5	6.8
	CV(%) of the SDT output Parameters		0.20% expansion							
			15%	20%	30%	40%				
	Hysteresis area (J/m ³)	First cycle	4.4	20.0	3.8	14.2				
		Average of last four cycles	12.3	18.2	5.2	9.2				
		Five cycles	9.6	18.9	4.6	11.3				
	Plastic deformation (μ ϵ)	First cycle	0.0	33.3	9.1	18.7				
		Over the last four cycles	0.0	24.7	21.7	0.0				
		Five cycles	0.0	32.7	11.1	13.3				
	Modulus of elasticity (GPa)	First cycle	3.7	8.2	2.7	6.1				
		Average of last four cycles	3.8	13.6	1.9	3.6				
		Average of cycles II and III	3.2	12.9	2.0	3.9				

Table 21: Variability (CV%, measured as the standard deviation of three samples divided by the average value among them) of SDT output parameters for the 45 MPa concrete mixture incorporating a reactive coarse aggregate (NM gravel).

Concrete Mix design	Output Parameters		0.05% expansion				0.12% expansion			
			15%	20%	30%	40%	15%	20%	30%	40%
45 MPa	Hysteresis area (J/m ³)	First cycle	20.2	8.1	26.3	3.4	27.4	20.7	1.3	6.1
		Average of last four cycles	25.0	12.4	23.2	3.9	36.5	13.2	1.0	13.1
		Five cycles	23.3	8.3	24.3	0.2	33.4	15.8	1.0	10.6
	Plastic deformation (μ ϵ)	First cycle	43.3	21.7	26.7	9.4	0.0	34.5	13.3	12.9
		Over the last four cycles	0.0	86.7	43.3	28.3	86.6	90.0	0.0	0.0
		Five cycles	24.7	34.5	27.0	0.0	24.7	0.0	9.1	8.3
	Modulus of elasticity (GPa)	First cycle	2.0	4.7	5.9	6.0	8.9	5.8	0.6	3.1
		Average of last four cycles	2.6	0.9	4.4	3.9	9.3	3.1	1.4	3.8
		Average of cycles II and III	3.1	0.5	4.7	3.9	9.0	3.6	1.8	4.4
	CV(%) of the SDT output Parameters		0.20% expansion							
			15%	20%	30%	40%				
	Hysteresis area (J/m ³)	First cycle	6.7	18.0	11.6	3.4				
		Average of last four cycles	23.2	18.0	12.6	0.1				
		Five cycles	17.4	17.9	12.2	1.2				
	Plastic deformation (μ ϵ)	First cycle	34.6	49.5	28.6	6.2				
		Over the last four cycles	86.6	34.6	21.7	11.1				
		Five cycles	24.7	43.3	12.5	3.1				
	Modulus of elasticity (GPa)	First cycle	6.0	3.2	1.73	0.9				
		Average of last four cycles	6.1	3.1	0.7	0.1				
		Average of cycles II and III	6.0	2.9	1.2	0.1				

Table 22: Multi-variable ANOVA results for the HA and PD over the five cycles.

ANOVA (HA5 and PD5)	Sum Sq	Mean Sq	F value	Pr(>F)
Loading	213.76	71.25	3622.021	< 2e-16
Strength	13.21	6.61	335.803	< 2e-16
Aggregates vs. Expansion	6.44	1.07	54.532	< 2e-16
Loading vs. Strength	0.58	0.10	4.883	0.000126
Loading: Aggregates vs. Expansion	2.40	0.13	6.788	1.22e-12
Strength: Aggregates vs. Expansion	2.88	0.24	12.186	< 2e-16
Loading :Resistance:Aggregates vs. Expansion	1.50	0.04	2.117	0.000787
Residuals	3.30	0.02	0.02	0.02

Table 23: Multi-variable ANOVA results for the Modulus of elasticity parameter as an average value of the cycles II and III.

ANOVA (E23)	Sum Sq	Mean Sq	F value	Pr(>F)
Loading	1.163	0.3877	134.935	< 2e-16
Strength	4.365	2.1823	759.463	< 2e-16
Aggregates vs. Expansion	1.328	0.2214	77.041	< 2e-16
Loading vs. Strength	0.113	0.0188	6.549	3.12e-06
Loading: Aggregates vs. Expansion	0.322	0.0179	6.221	1.65e-11
Strength: Aggregates vs. Expansion	0.900	0.0750	26.092	< 2e-16
Loading :Resistance:Aggregates vs. Expansion	0.295	0.0082	2.849	3.33e-06
Residuals	0.483	0.0029	0.0029	0.0029

Table 24: Average values found for the HA parameter (five cycles) using a multi-variable ANOVA.

Loading (%)	Strength (MPa)	Aggregate type	Expansion (%)	Average value	SE	df	lower	upper
40	45	Tx	0.3	8301	0.085	168	8133	8469
40	35	Tx	0.3	7881	0.085	168	7713	8048
40	45	Tx	0.2	7833	0.085	168	7665	8000
40	45	NM	0.2	7817	0.085	168	7650	7985
40	35	NM	0.2	7718	0.085	168	7550	7886
40	25	NM	0.2	7700	0.085	168	7532	7867
40	25	Tx	0.3	7622	0.085	168	7455	7790
40	35	Tx	0.2	7600	0.085	168	7433	7768
40	45	Tx	0.12	7559	0.085	168	7391	7727
40	25	NM	0.12	7541	0.085	168	7373	7708
40	25	Tx	0.2	7493	0.085	168	7325	7660
40	45	Tx	0.05	7451	0.085	168	7284	7619
40	45	NM	0.05	7400	0.085	168	7233	7568
40	45	NM	0.12	7380	0.085	168	721	7548
40	35	Tx	0.12	7296	0.085	168	7128	7463
40	35	NM	0.12	7269	0.085	168	7102	7437
30	45	Tx	0.05	7233	0.085	168	7066	7401
30	35	Tx	0.3	7135	0.085	168	6967	7302
40	25	Tx	0.12	7047	0.085	168	6880	7215
40	25	Tx	0.05	7029	0.085	168	6862	7197
30	45	NM	0.2	7027	0.085	168	6859	7194
40	35	Tx	0.05	6961	0.085	168	6794	713
30	45	Tx	0.3	6929	0.085	168	6762	7097
40	25	NM	0.05	6835	0.085	168	6668	70
30	45	Tx	0.2	6825	0.085	168	6658	6993
30	35	NM	0.2	6816	0.085	168	6648	6984
30	35	Tx	0.2	6798	0.085	168	663	6966
30	45	NM	0.12	6774	0.085	168	6606	6941
30	45	NM	0.05	6708	0.085	168	6540	6876
30	25	NM	0.2	6665	0.085	168	6497	6833
30	45	Tx	0.12	6613	0.085	168	645	6781
30	35	NM	0.05	6612	0.085	168	6444	6779
40	35	NM	0.05	6601	0.085	168	6433	68
30	25	Tx	0.3	6581	0.085	168	6413	6749
30	35	Tx	0.12	6526	0.085	168	6358	6694
30	25	NM	0.12	650	0.085	168	6334	6670
30	25	Tx	0.2	6491	0.085	168	6323	6658
30	35	NM	0.12	6427	0.085	168	6260	660
30	25	Tx	0.05	6417	0.085	168	6249	6584
20	45	Tx	0.05	6312	0.085	168	6144	6479
30	25	Tx	0.12	6233	0.085	168	6066	6401
30	35	Tx	0.05	6147	0.085	168	598	6315
20	45	Tx	0.2	598	0.085	168	5807	6143
30	25	NM	0.05	5971	0.085	168	5803	6138
20	45	NM	0.2	5869	0.085	168	5701	6037
20	35	Tx	0.3	5831	0.085	168	566	5999
20	45	NM	0.05	5814	0.085	168	5646	5982
20	45	Tx	0.3	5737	0.085	168	5569	5905
20	25	Tx	0.3	5689	0.085	168	5521	5856
20	35	NM	0.2	5658	0.085	168	5491	5826
15	45	Tx	0.05	5639	0.085	168	5471	5807
20	35	Tx	0.2	5637	0.085	168	5470	5805
20	45	Tx	0.12	5622	0.085	168	5454	5790
20	45	NM	0.12	5557	0.085	168	5389	5724
20	35	Tx	0.12	5532	0.085	168	5365	5700
20	25	NM	0.12	5499	0.085	168	5331	5666
20	25	NM	0.2	5443	0.085	168	5275	5611
20	25	Tx	0.2	5422	0.085	168	5255	5590
20	35	NM	0.05	5329	0.085	168	5161	5496
20	25	Tx	0.05	5323	0.085	168	52	5490
20	35	NM	0.12	525	0.085	168	5087	5422
15	45	Tx	0.2	5250	0.085	168	5082	5418
20	25	Tx	0.12	5231	0.085	168	5063	5399
15	45	NM	0.2	5201	0.085	168	5033	5368
20	25	NM	0.05	5139	0.085	168	4971	5307
15	45	NM	0.05	5103	0.085	168	4936	5271
15	45	Tx	0.3	5090	0.085	168	4923	5258
20	35	Tx	0.05	5048	0.085	168	4880	5215
15	45	NM	0.12	5039	0.085	168	487	5207
15	45	Tx	0.12	4979	0.085	168	4811	515
15	25	NM	0.2	4893	0.085	168	4725	5060
15	35	NM	0.2	4880	0.085	168	4712	5047
15	35	Tx	0.3	4867	0.085	168	4699	5034
15	25	NM	0.12	4750	0.085	168	4583	4918
15	35	Tx	0.12	4730	0.085	168	4562	4898
15	25	Tx	0.05	4715	0.085	168	4547	4883
15	25	Tx	0.3	4715	0.085	168	4547	488
15	35	NM	0.12	4698	0.085	168	4530	4865
15	35	Tx	0.2	4696	0.085	168	4529	4864
15	25	Tx	0.2	4594	0.085	168	4426	4762
15	35	NM	0.05	4574	0.085	168	4406	4741
15	35	Tx	0.05	4326	0.085	168	4158	449
15	25	Tx	0.12	4318	0.085	168	4151	4486
15	25	NM	0.05	4179	0.085	168	4011	4346

Table 25: Assessment of the non destructive character (as well as results validity) of the SDT for the compressive strength (Cs) results through a two-variable ANOVA.

Load (%)	Expansion (%)	Strength (MPa)	Aggregate type	Cs_F	Cs_Fcritic	F>Fcritic	Cs_P value	α	P < α
15% to 40%	0.05%	25	Tx	2.69	3.86	-	0,10800	0.05	-
	0.12%	25	Tx						
	0.20%	25	Tx						
	0.30%	25	Tx						
15% to 40%	0.05%	35	Tx	0.07	3.86	-	0.98000	0.05	-
	0.12%	35	Tx						
	0.20%	35	Tx						
	0.30%	35	Tx						
15% to 40%	0.05%	45	Tx	1,02	3.86	-	0.42000	0.05	-
	0.12%	45	Tx						
	0.20%	45	Tx						
	0.30%	45	Tx						
15% to 40%	0.05%	25	NM	1.32	4.75	-	0.35000	0.05	-
	0.12%	25	NM						
	0.20%	25	NM						
15% to 40%	0.05%	35	NM	1.28	4.75	-	0.36000	0.05	-
	0.12%	35	NM						
	0.20%	35	NM						
15% to 40%	0.05%	45	NM	1.59	4.75	-	0.28670	0.05	-
	0.12%	45	NM						
	0.20%	45	NM						

Table 26: Assessment of the non destructive character (as well as results validity) of the SDT for the tensile strength (Ts) results through a two-variable ANOVA.

Load (%)	Expansion (%)	Strength (MPa)	Aggregate type	Ts_F	Ts_Fcritic	F>Fcritic	Ts_P value	α	P < α
15% to 40%	0.05%	25	Tx	1.60	9.27	-	0.34500	0.05	-
	0.12%	25	Tx						
15% to 40%	0.05%	35	Tx	1.86	3.86	-	0.20640	0.05	-
	0.12%	35	Tx						
	0.20%	35	Tx						
	0.30%	35	Tx						

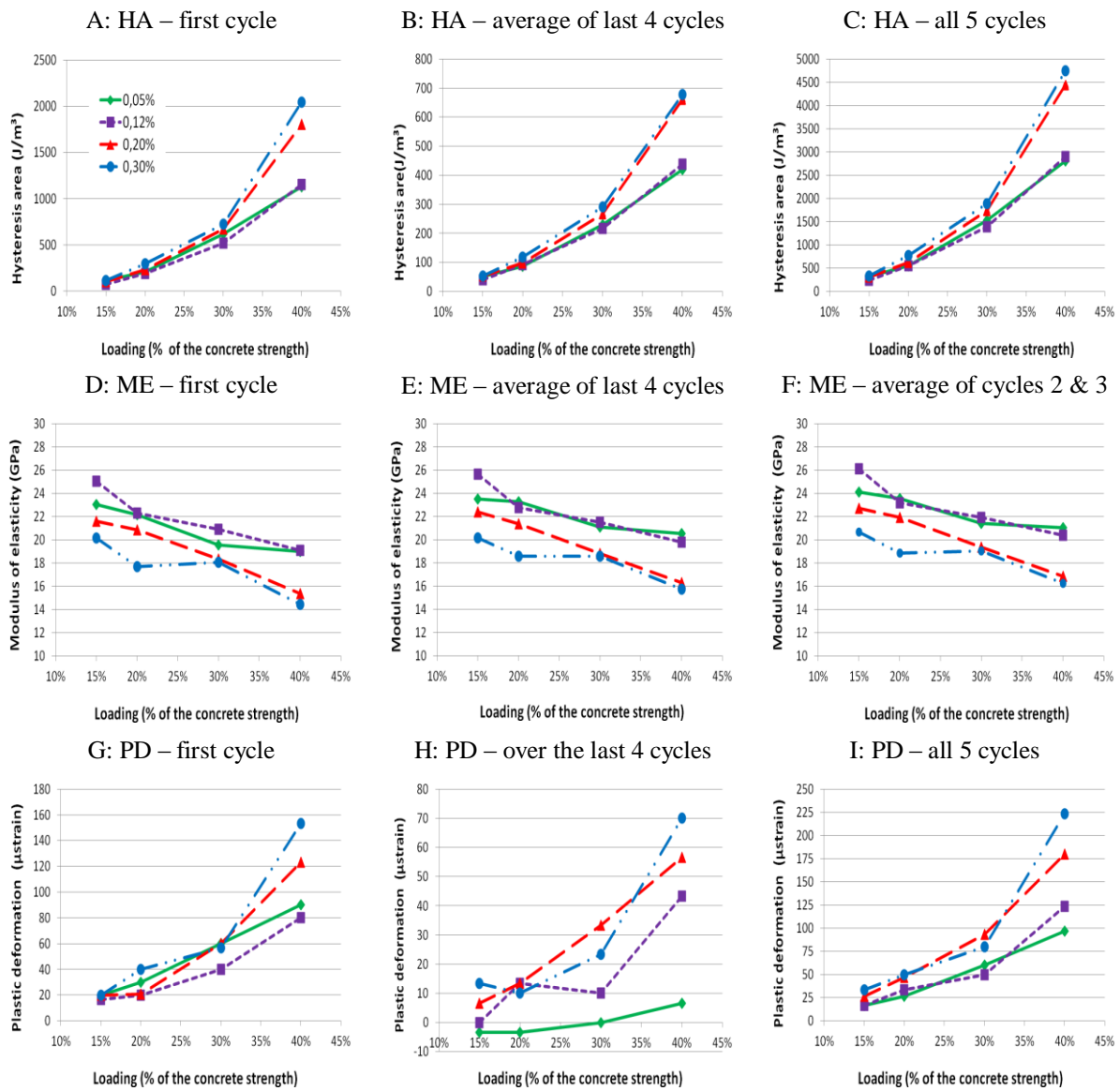
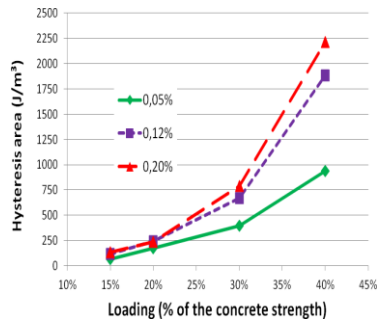
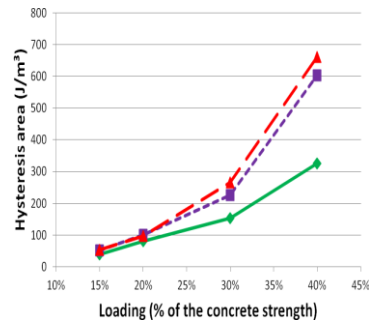


Figure 12: Responses of selected SDT output parameters as a function of the loading applied (% of the concrete strength) for 25 MPa concrete mixtures incorporating the reactive Tx sand and affected to various degrees by ASR. A to C: Hysteresis area (HA). D to F: Modulus of elasticity (ME). G to I: Plastic deformation (PD). The common legend for all the curves appears in (A).

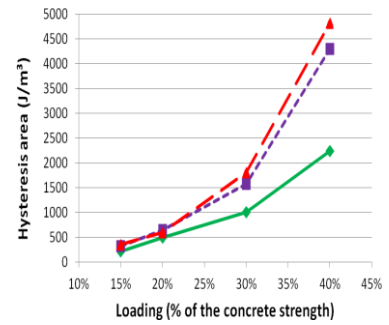
A: HA – first cycle



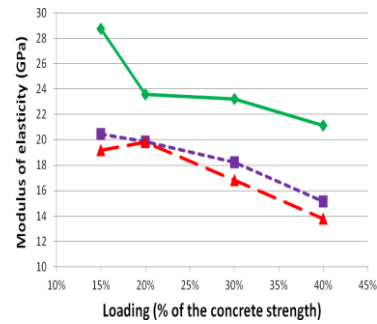
B: HA – average of last 4 cycles



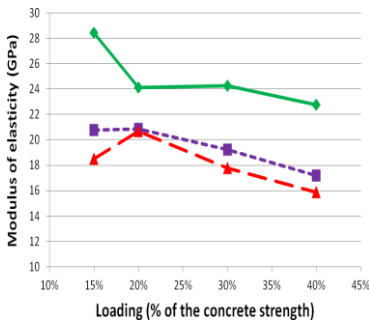
C: HA – all 5 cycles



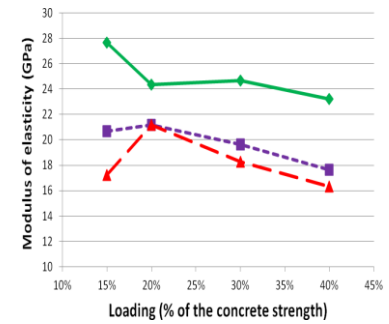
D: ME – first cycle



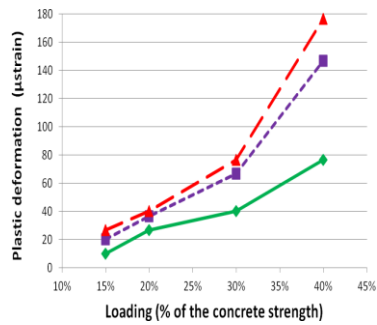
E: ME – average of last 4 cycles



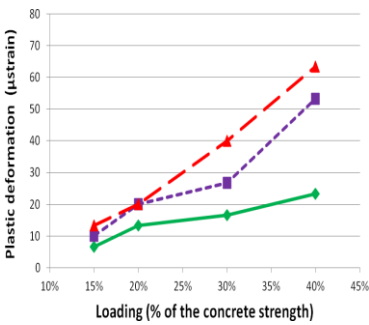
F: ME – average of cycles 2 & 3



G: PD – first cycle



H: PD – over the last 4 cycles



I: PD – all 5 cycles

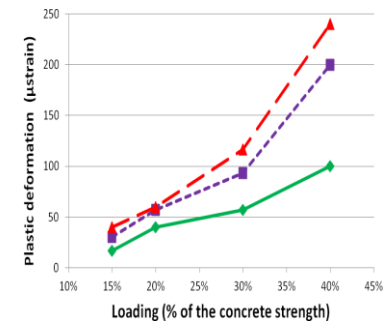
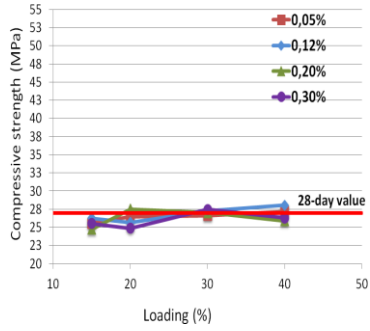
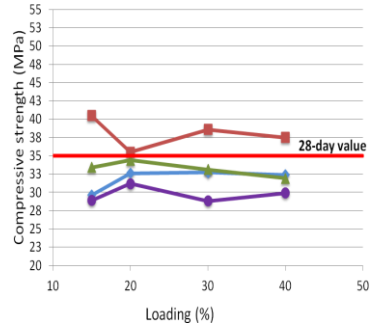


Figure 13: Responses of selected SDT output parameters versus the loading applied (% of the concrete strength) for 25 MPa concrete mixtures incorporating a reactive NM coarse aggregate and affected to various degrees by ASR. A to C: Hysteresis area (HA). D to F: Modulus of elasticity (ME). G to I : Plastic deformation (PD). The common legend for all the curves appears in (A).

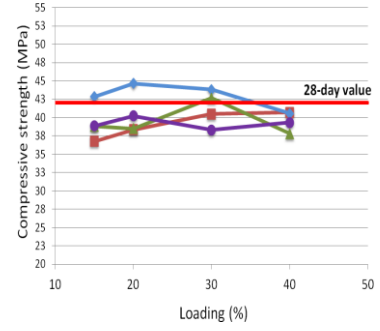
A: Tx sand – 25 MPa



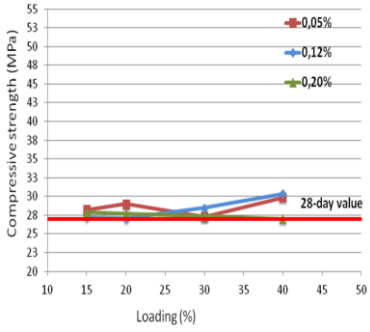
B: Tx sand – 35 MPa



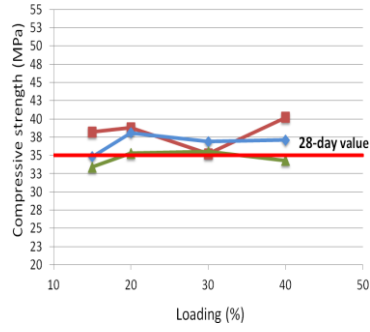
C: Tx sand – 45 MPa



D: NM gravel – 25 MPa



E: NM gravel – 35 MPa



F: NM gravel – 45 MPa

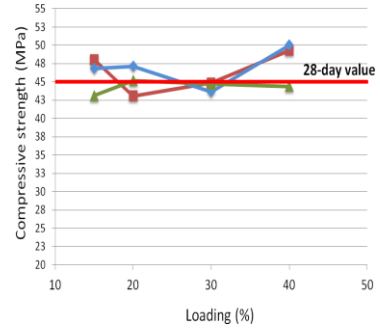
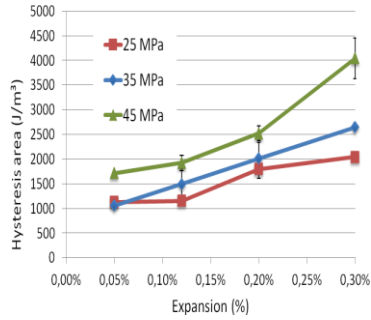
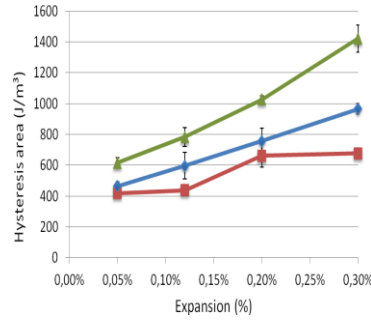


Figure 14: Compressive strength results obtained after the SDT versus the loading applied over the test for both aggregates (Tx sand: A, B and C; NM gravel: D, E and F) and all the concrete mixtures.

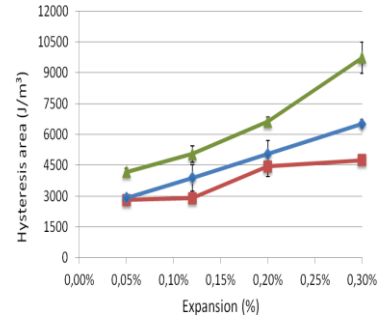
A: HA – first cycle



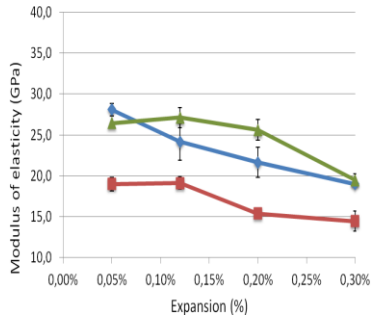
B: HA – average of last 4 cycles



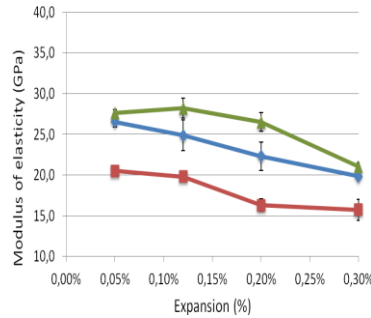
C: HA – over 5 cycles



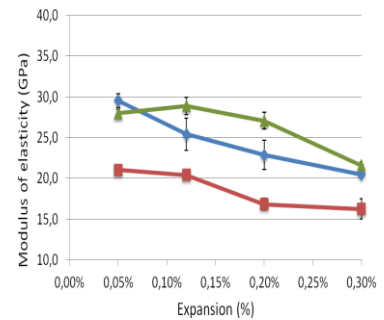
D: ME – first cycle



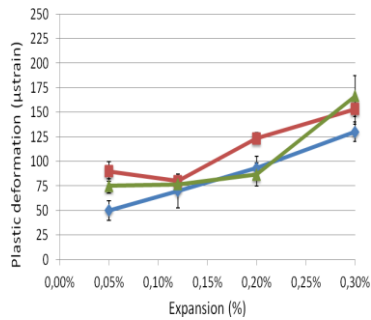
E: ME – average of last 4 cycles



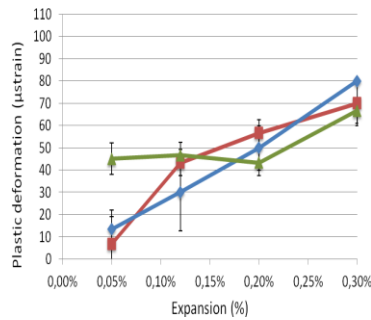
F: ME – average value (cycles II and III)



G: PD – first cycle



H: PD – over the last 4 cycles



I: PD – over 5 cycles

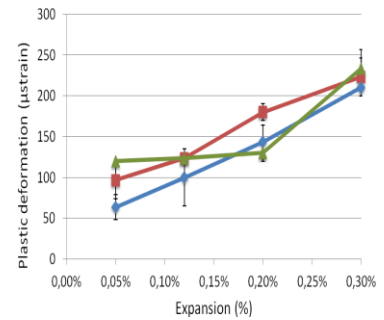
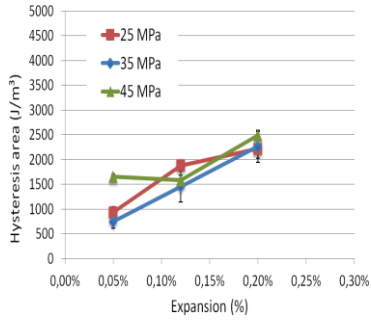
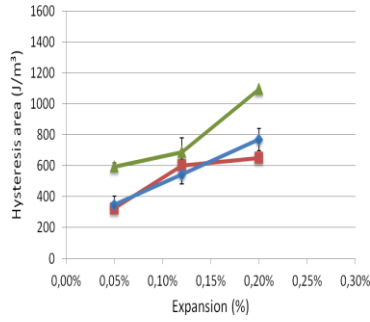


Figure 15: Analysis of the SDT output parameters when 40% of the mix design strength is used over the test for the 25. 35 and 45 MPa concrete mixtures with Tx sand. The vertical bars correspond to variability data, i.e. one standard deviation on each side of the average value obtained at different expansion levels. The variability between the results obtained from the specimens of a set is often so small that the vertical bars are contained within the symbols.

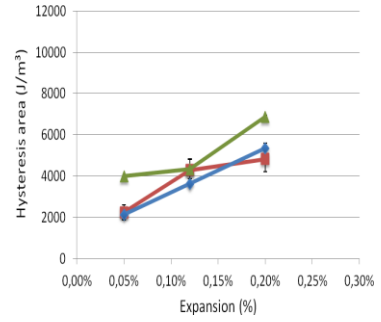
A: HA – first cycle



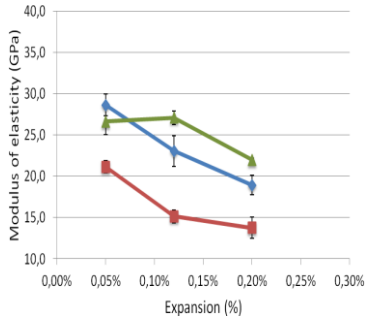
B: HA – average of last 4 cycles



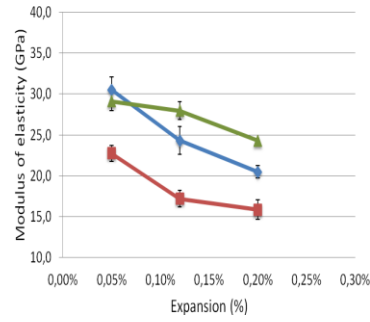
C: HA – over 5 cycles



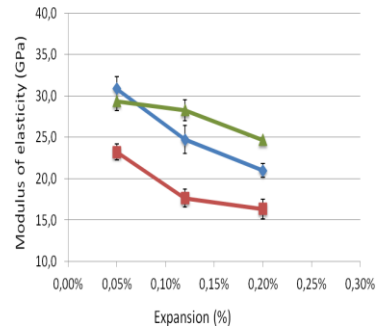
D: ME – first cycle



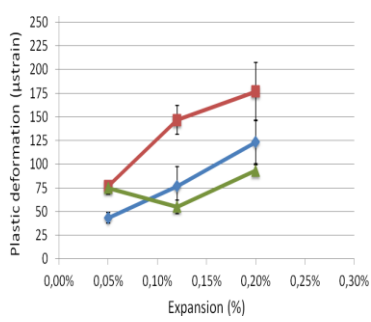
E: ME – average of last 4 cycles



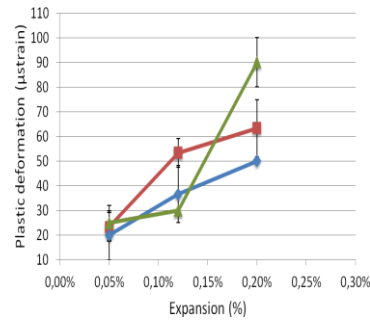
F: ME – average value (cycles II and III)



G: PD – first cycle



H: PD – over the last 4 cycles



I: PD – over 5 cycles

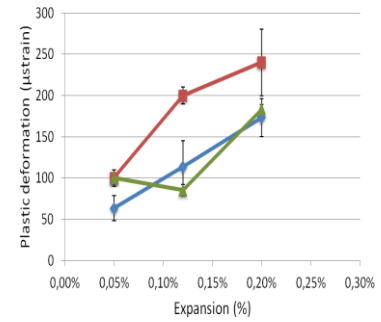
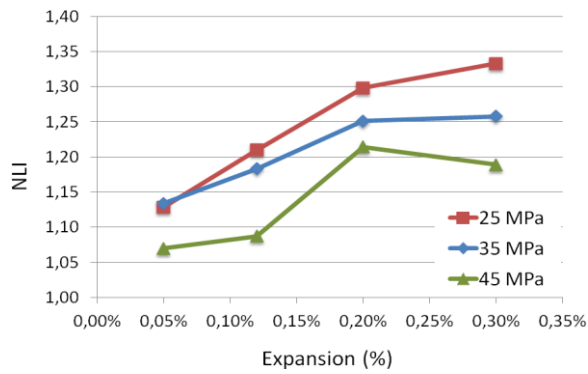


Figure 16: Analysis of the SDT output parameters when 40% of the mix design strength is used over the test for the 25, 35 and 45 MPa concrete mixtures with NM Gravel. The vertical bars correspond to variability data, i.e. one standard deviation on each side of the average value obtained at different expansion levels. The variability between the results obtained from the specimens of a set is often so small that the vertical bars are contained within the symbols

A: NLI – first cycle – Tx sand



B: NLI – first cycle – NM gravel

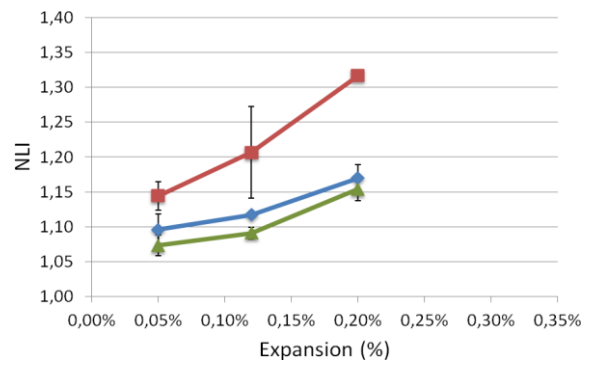
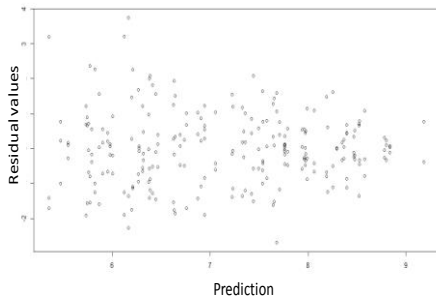
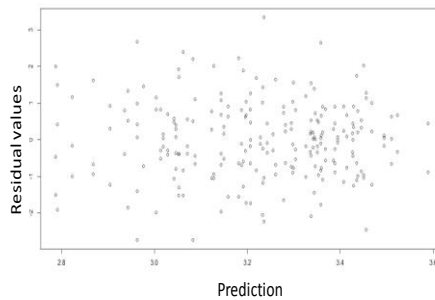


Figure 17: Analysis of the NLI parameter proposed by Crisp et al. [23, 24] when 40% of the mix design strength is used over the test for the 25, 35 and 45 MPa concrete mixtures with either Tx sand or NM Gravel.

A: HA homogeneity – over 5 cycles



B: ME homogeneity (cycles II and III)



C: PD homogeneity – over 5 cycles

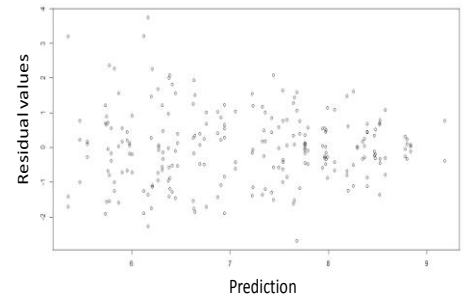


Figure 18: Study of the variance homogeneity of the multi-variable ANOVA results.

7. PAPER II: EVALUATION OF THE STIFFNESS DAMAGE TEST (SDT) AS A TOOL FOR ASSESSING DAMAGE IN CONCRETE DUE TO ALKALI-SILICA REACTION (ASR): INPUT PARAMETERS AND TEST PROCEDURE

Sanchez. L F.M.^a; Fournier. B.^b; Jolin. M.^c, Bastien, J.^d

(a) MSc. – Laval University – PhD candidate.

1065, avenue de la Médecine, Pavillon Adrien-Pouliot, local 3755 Tel.: 1 (418) 704-2435

leandrofms@gmail.com / le.sanchez@uol.com.br

(b) Prof. Dr. – Laval University. Quebec. QC. Canada

benoit.fournier@ggl.ulaval.ca

(c) Prof. Dr. – Laval University. Quebec. QC. Canada

marc.jolin@gci.ulaval.ca

(d) Prof. Dr. – Laval University. Quebec. QC. Canada

josee.bastien@gci.ulaval.ca

ABSTRACT

The Stiffness Damage Test (SDT) is an interesting tool for assessing damage in concrete affected by alkali-silica reaction (ASR). It has been found that the use of a fixed loading over the test limits its ability to reliably appraise the distress level of concrete samples, mainly when different concrete strengths and aggregate types are used. Moreover, the test output parameters should be properly used/interpreted so that the SDT becomes a powerful diagnostic procedure. However, there is currently very limited data on the influence of various input parameters on the test responses. This paper presents thus a critical evaluation of several input parameters of the SDT. Parameters such as the load's level, the core's environmental conditions as well as the samples' characteristics and conditioning history seem to influence significantly the SDT output results. Otherwise, different types of surface preparation and the specimens' size did not seem to affect the test results.

Keywords: stiffness damage test (SDT), assessment of damage degree, alkali-silica reaction (ASR).

RÉSUMÉ

Le Stiffness Damage Test (SDT) est un outil intéressant pour l'évaluation de l'endommagement de bétons affectés par la réaction alcalis-silice (RAS). Récemment, il a été constaté que l'utilisation de cette méthode, sur la base d'un chargement fixe, limite beaucoup sa capacité à évaluer de façon fiable le niveau d'endommagement d'échantillons de béton, principalement lorsque des matériaux avec différentes résistances et incorporant une grande variété de granulats sont évalués. De plus, les paramètres de sortie de l'essai doivent être bien utilisés/interprétés de sorte que le SDT soit une procédure de diagnostic efficace. Toutefois, il existe actuellement très peu de données concernant l'influence de divers paramètres d'entrée sur les réponses de l'essai. Ainsi, cet article présente une évaluation critique de plusieurs paramètres d'entrée de la méthode SDT. Des paramètres, tels que le choix de la charge de l'essai, les conditions environnementales des éléments de béton, les caractéristiques des échantillons et leur histoire de conditionnement, semblent influencer de manière significative les réponses du SDT. Cependant, les différents types de préparation de surface et la taille des éprouvettes ne semblent pas modifier les résultats de l'essai.

Mots clés: stiffness damage test (SDT), évaluation du degré d'endommagement, réaction alcali-silice (RAS).

7.1 INTRODUCTION

Alkali-silica reaction (ASR), one of the most common deleterious mechanisms identified in concrete structures worldwide, consists in a chemical reaction between “unstable” silica mineral forms within the aggregate materials and the alkali hydroxides (Na, K – OH) dissolved in the concrete pore solution. It generates a secondary alkali-silica gel that induces expansive pressures within the reacting aggregate material(s) and the adjacent cement paste upon moisture uptake from its surrounding environment, thus causing microcracking, reduction of material's properties (mechanical/durability) and, in some cases, functionality in the affected structure.

One of the biggest challenges in dealing with aging/deteriorating concrete structures is to establish the correlation between the distress "signatures" caused by a damage mechanism (i.e. ASR, for instance), and the loss in mechanical properties, physical integrity, durability and performance of the affected material or element, as well as their structural implications.

Studies dealing with the evaluation of the mechanical performance of aging concrete suggest that the “Stiffness Damage Test (SDT)” can provide a diagnostic evaluation of the “degree of damage” in concrete affected by ASR. Although very promising, the SDT does not have a standard test procedure yet, which limits its use for quantitative assessments in engineering applications. Thus, an in-depth evaluation of some input and output parameters of the test is required to optimize its applicability/reliability and precision.

7.2 THE STIFFNESS DAMAGE TEST (SDT)

The Stiffness Damage Test (SDT) has been proposed as a tool to quantify the degree of physical damage in concrete due to ASR [1, 2]. The test method was first developed by Walsh et al. (1965) for rock specimens [3] and then Crouch (1987) [4] adapted the method for concrete. The method is based on a cyclic loading (in compression) of concrete specimens (cylinders/cores), and was initially carried out using a fixed load of 5.5 MPa, at a loading rate of 0.10 MPa/s [1]. After further research and testing, Smaoui et al. [5] proposed to increase the load to 10 MPa to better quantify damage in concrete due to ASR. Although their work involved a range of reactive aggregates, it was based on just one type of concrete mix design (Concrete Prism Test mix design, in accordance with CSA A23.2-14A or ASTM C 1293). Recently, after an in depth study performed on different reactive aggregates (coarse vs. fine) and concrete mix designs (25 MPa, 35 MPa and 45 MPa), the procedure was further modified to be carried out with a percentage of the 28-day concrete strength instead of using a fixed load. Moreover, a percentage of 40% of the concrete design strength seemed to reliably distinguish ASR-affected concretes as a function of their expansion levels [6]. Parameters such as the Hysteresis Area (HA) and the Plastic Deformation (PD) over the five loading-unloading cycles, as well as the Modulus of Elasticity (ME) (as the average value of the second and third cycles), were chosen as the best output parameters of the test [6]. However, the influence of some input parameters or test conditions on the various test responses, such as the concrete’s conditioning history (storage conditions after coring), the type of specimen’s end preparation (grinding vs. capping), the specimen’s geometry and size, the specimen’s environment (location and direction of coring in the structural element), as well as the choice of the specimen’s strength (critical for selecting the loading level in the test) was not really studied in details, thus preventing the development of a standard test procedure.

Considering that the SDT is a mechanical test in compression, the development of a standard test procedure needs to focus on the parameters that normally impact on the results of this

type of test. Amongst those, the parameters described hereafter are seen as potential sources of variations on either the responses of the test or on its analyses.

7.2.1 Specimen's conditioning history prior to testing

It is well established that the specimens conditioning history (e.g. wetting/drying conditions) prior to testing changes the response of either compressive strength or modulus of elasticity of the concrete [7]. It has been found that concretes subjected to drying prior to testing show an increase in their compressive strength, while an opposite behavior is often observed in the case of the modulus of elasticity [7]. The real reason for this phenomenon is not well understood yet, but it seems that the changes in the microstructural characteristics of CSH upon drying could lead to enhanced internal cohesion and friction at the microscale, thus increasing the concrete strength. On the other hand, the lower strength obtained for saturated concretes could be generated by hydraulic pressures created within the saturated concrete pores over a compression test. Those changes in the specimen's behavior appear to be reversible when re-drying or re-saturation of the concrete is carried out [7], as least in the case of sound (undamaged) concrete.

When the SDT is carried out on concrete cylinders cast in the laboratory, the control of the specimen's moisture condition before testing can be readily applied/selected, e.g. storage in the moist curing room at a controlled temperature; however, when cores are extracted from structures in service, variations in the moisture condition of the test specimens from coring to testing can be observed, depending on the storage procedure selected, that can significantly affect the test results. According to ASTM C 42, one must test the cores "in the same moisture condition than that they were in the field". However, it must be remembered that the moisture content in concrete structures in contact or not with water or an external source of moisture varies from their core up to the surface, thus causing a moisture gradient and possible variations in the test results. For this reason, it is recommended to wrap and store the cores for at least five days before testing [8]. Still according to ASTM C 42, one should adopt the storage procedure depending on the structure conditions (elements in contact or not with water - e.g. 100% RH) [8]. Canadian Standards (CSA23.2-14C) suggest that the cores extracted from structures be rewetted for 48 hours in a moist curing room prior to testing for ordinary tests (compressive strength and modulus of elasticity), thus allowing to evaluate the samples with the same moisture's condition [9].

A common situation in testing laboratories is to extract cores from concrete structures or elements under investigation and then wrapping and storing them for a couple of days or even a few weeks, in extreme cases, prior to testing (depending on the laboratory's test facilities and capacity). Therefore, the moisture content of the specimens could vary significantly from the field's conditions; actually even when wrapped, the cores may lose some moisture, the extent of which is not necessarily known or measured. As there is currently no data regarding the influence of the conditioning history (drying effect) of test specimens over the SDT, more research on this becomes necessary.

7.2.2 Specimen's shape characteristics

It is well known that specimen's geometry, size or length-to-diameter ratio may influence the response of compressive strength tests [7]. Usually, a cylindrical specimen (laboratory specimen or core) with a length-to-diameter ratio of 2:1 is used to perform standard compressive tests. However, when another geometry or length-to-diameter ratio is used, corrections should be applied on the test results [7]. Considering that the SDT is a compressive strength test, it is logical to think that the same procedure should be adopted through this test, although there is no data showing whether the correction factors regularly used readily apply to the SDT procedure.

7.2.3 Specimens' end preparation

Concrete cylinders cast in the laboratory or concrete cores extracted from concrete structures generally possess rough/uneven end surfaces. If the specimens are tested without a smooth/plane end surface, one may obtain compressive strength values lower than that expected, as this roughness increases the stress concentrations over loading. Moreover, it has been shown that specimens with convex end surfaces have lower compressive strength values than those with concave end surfaces [7]. One can achieve flatness on the specimen's extremities using procedures such as "capping" with sulfur mortar or by grinding using a rectifier. Both procedures are acceptable and produce almost similar results when ordinary concrete (e.g. up to approximately 50 MPa) is tested. On the other hand, for high strength concrete, grinding is always the best choice [7]. As the SDT is a compressive test and since it is carried out at relatively low loading levels, it is fair to believe that the use of both "capping" and grinding would not introduce significant differences in the test results. However, there is

currently no data showing the effects of different specimen's rectification techniques over the SDT.

7.2.4 Loading rate

Generally, in a concrete compression test, the greater is the loading rate, the greater is the material's strength. The reason for this phenomenon is not well known, but it seems that a lower loading rate allows the cracks to open/progress more easily, thus leading to lower strengths [7]. The effect of this parameter on SDT results was evaluated by Crisp et al. [1, 2] and based on their results, the authors suggested the use of 0.10MPa/s. The same loading rate was then adopted by Smaoui et al [5]. Therefore, in order to reduce variability, it was decided to keep performing the cyclic test at the same loading rate in this study, although this value is lower than that suggested by ASTM standards for evaluating the modulus of elasticity of concretes (0.241 ± 0.034 MPa/s) [10], which is most of the times carried out on "sound" concrete specimens.

7.2.5 Specimens' location and direction of the cores

Many mechanisms of distress (such as ASR) are extremely dependent on the location of sampling in the structure (e.g. exposed/not exposed zones of structural elements, core/surface portions of a structural component, etc.), as well as the direction of the extracted cores [11, 12]. It means that in order to properly characterize the real state of distress of a zone/element or even of a structure, one should be careful in choosing sampling location(s) that represent exactly what is being assessed or planned to be assessed. Many studies have highlighted those dependencies in the past (in a qualitative way), especially in relation to the effect of restraint against expansion, but there is currently no quantitative data comparing those differences, at least with reference to stiffness damage testing.

7.2.6 Output parameters: effect of the choice of the loading level and variability of the test results

Sanchez et al. [6] demonstrated that the SDT provides a more diagnostic evaluation of the damage in ASR-affected concrete when carried out with a percentage of the concrete mix design strength instead of a fixed loading level. Moreover, the authors found that the test

distinguishes satisfactorily the concrete conditions at different expansion levels due to AAR when carried out to a maximum load corresponding to 40% of the 28-day concrete strength. Parameters such the Hysteresis Area (HA) (in J/m^3) and the Plastic Deformation (PD) (in μstr) over the five cycles of the test, as well as the Modulus of Elasticity (ME), as the average value of the second and third cycles (GPa), seem to be the best output responses through the SDT.

Working with laboratory-made specimens makes the choice of the test loading level somewhat easier as the strength characteristics of the concretes under test are either well known or controlled. However, when aging/deteriorated concrete structures are assessed, in most of the cases, the 28-day design/actual strength value is not known precisely, which leads to uncertainties over to use the procedure proposed by [6]. The common procedure carried out in this case, which is often used for the modulus of elasticity assessment of concrete structures, would be to choose an area/element of the structure that is not (or less) distressed due to the deleterious mechanism under investigation (like ASR, etc.), extract a couple of cores from that zone/element and to determine their compressive strength. Thus, this value would be attributed as the reference strength of the material, especially knowing that concrete strength increases over time and this value could be nearly 20 or even 30% higher than the actual 28-day design strength, at least for concretes incorporating ordinary Portland cements [13]. Therefore, the quantitative impact of working with different strengths (28-day design strength value vs. the value obtained from a compression test at a specific age) is not currently known but is likely to have a significant impact on the output responses proposed by [6].

7.3 SCOPE OF WORK

As indicated in the previous sections, a thorough study is needed on the impact of some practical input parameters on either the results or the analyses of stiffness damage testing, thus providing a more complete database for selecting the best parameters/conditions in the possible standardization process of the SDT. This paper presents the analyses of the following parameters, based on testing that was carried out on laboratory specimens and cores extracted from different components of an ASR-affected concrete structure:

- Variability in the test results
 - *Specimen's conditioning history (effect of drying and rewetting before testing);*
 - *Specimen's shape characteristics (length-to-diameter ratio and different diameters);*
 - *Specimen's end surface preparation (sulfur capping vs. surface grinding);*

- *Variability of the test results for laboratory test specimens;*
- *Variability of the test results for field core specimens.*
- Variability in the test analyses
 - *Specimens location (surface vs. core of concrete element; exposed vs. not exposed sites/structural elements);*
 - *Effect of the specimen's loading level.*

7.4 MATERIALS AND METHODS

As mentioned before, the effect of different input parameters on the SDT results was evaluated by a combination of field (cores) and laboratory-made specimens. The data thus generated were found to provide very complementary information as laboratory specimens were obtained after having been subjected to well-controlled laboratory conditions conducive to the development of ASR and were representing known expansion levels due to ASR; on the other hand, the field specimens were used to account for the typical variability (in internal damage) observed within ASR-affected concrete members.

7.4.1 Specimens from different components of an ASR-affected field structure

The analyses of the effect of the parameters listed hereafter on the results of the SDT, i.e.: specimen's location, specimen's conditioning history, specimen's coring direction, specimen's shape characteristics (length/diameter ratio and size) and the study of the variability of the test results, were carried out on cores extracted from both the foundation blocks and the bridge deck of the ASR-affected Robert-Bourassa/Charest viaduct located in Quebec City, Canada. The structure was built in 1966 and several studies previously concluded on its advanced stage of deterioration due to ASR (Figure 1). Technical reports stated that the concrete of the foundation blocks was designed to reach 24 MPa at 28 days, while the columns and decks were made of 28 MPa concrete. The concrete incorporated a dark-grey, fine-grained Ordovician limestone which was later recognized as alkali-silica reactive in several studies [14, 15] (Figures 1C and 1D).

Several cores, 100mm in diameter, were extracted, adjacent to each other to reduce variability, from both the exposed (end portions) and protected portions (i.e. under the bridge deck) of the foundation blocks supporting the Y-shaped columns of the structure (Figures 1 and 2A to 2D). Three large (1m in diameter) cores were extracted vertically within the bridge

deck prior to its demolition (Figures 2E and 2F); 100 and 150mm diameter cores were further extracted in the vertical direction from those large cores. After extraction, the cores from the foundation blocks were all wrapped in plastic film and taken to the laboratory. They were then subjected to different storage conditions, according to the type of tests to be performed (or parameters to be evaluated):

- Condition A: cores wrapped in plastic film and then placed at 12°C until testing (to stop the progress of damage, due to testing capacity issues); prior to testing, 48 hours “resaturation” in the moist curing room (protected from running water) – “control cores”;
- Condition B: cores wrapped in plastic film and then left on a stand in the laboratory for 5 weeks (at $23 \pm 2^\circ\text{C}$) – “drw cores”;
- Condition C: cores unwrapped and left on a stand for 5 weeks or 9 months prior to testing (at $23 \pm 2^\circ\text{C}$) – “dr cores”;
- Condition D: cores unwrapped and left on a stand for 5 weeks (at $23 \pm 2^\circ\text{C}$). Then, the cores were rewetted for 48 hours in the moist curing room, protected from running water, prior to testing – “rw cores”;

After extraction from the bridge deck, the large concrete cores were taken to the Quebec Ministry of Transportation Central Laboratory and remained unprotected in their laboratory at $23 \pm 2^\circ\text{C}$ for several weeks. Then, several cores were extracted and subjected to the storage Condition A prior to testing.

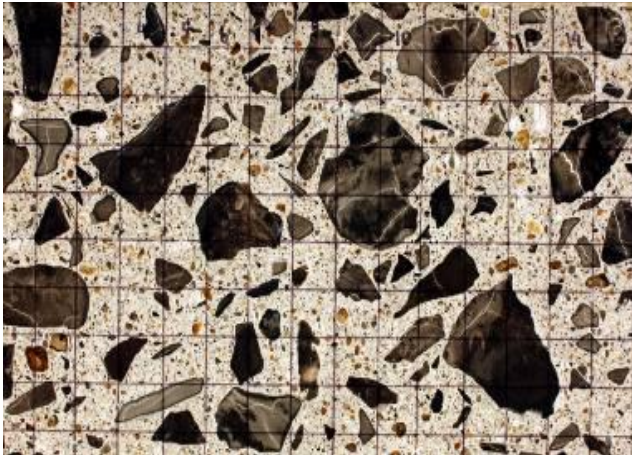
A



B



C



D



Figure 1: Robert-Bourassa/Charest concrete viaduct. A & B. General views of the structure showing the foundation blocks supporting the “Y-shaped” columns, as well as the bridge deck. C & D. Polished section of a concrete core extracted from the foundation block and showing extensive signs of ASR: cracking in the aggregate particles filled with alkali-silica reaction products and extending into the cement paste where gel is found filling voids (scale: each square is 1cm^2).

A



B



C



D



E



F



Figure 2: Robert-Bourassa/Charest concrete elements: A. Very severe cracking in the end (or exposed) portion of a foundation block and Y-shaped columns. B. Extensive cracking and reinforcement corrosion in the exposed portion of the foundation block. Severe longitudinal cracking is also observed in the Y-shaped columns. C & D. Extraction of cores from the foundation blocks after the demolition of the columns and bridge deck. E & F. Extraction of large cores (~1 m in diameter) across the bridge deck.

The testing matrix for the cores extracted from the two elements of the Robert Bourassa-Charest structure is given in Table 1. Prior to testing, the end surfaces of the core specimens were prepared (e.g. cut and ground) and, according to the characteristics of the study carried out (Table 1), they were either subjected to a 48-hour preconditioning period in the moist curing room (according to CSA A23.2-14C; all cores except those specifically used for the conditioning study), or wrapped/unwrapped and left on a stand in the laboratory.

Table 1: Stiffness damage testing matrix for the studies carried out on Robert-Bourassa/Charest concrete cores.

Concrete element ¹		Number of samples by type of study									
		Effect of core location and shape ²				Effect of core conditioning ³				Effect of core shape ⁴	
		Surface layer; L/D 2.0	Core of the elements; L/D			A Core Wrapping "Control"	B Core Drying "drw"	C Core Drying "dr"	D Core Drying + Rewetting "rw"	Samples diameter (surface samples)	
2.0	1.8		1.6	Vertical (100 x 200 mm)	Vertical (150 x 300 mm)						
Foundation blocks	Exposed portions	3	3	3	3	6	2	4	3	-	-
	Non exposed portions ¹	3	3	-	-	-	-	-	-	-	-
Bridge deck	-	-	-	-	-	-	-	-	-	7	3

- The sections of the foundation block that were sampled were either exposed or protected (under the bridge deck) from direct exposure to rain/snow.
- All cores tested were 100 mm in diameter. Cores were taken either from the 50 to 250 mm portion of the concrete element ("surface layer") or from the 250 to 450 mm portion of the element sampled ("core of the element")
- Upon extraction from the concrete structure, the core specimens were wrapped in plastic film and taken to the laboratory. They were then subjected to the following conditions :
Condition A: placed at 12°C until testing; prior to testing, 48 hours "resaturation" of unwrapped cores in the moist curing room (protected from running water) – "control cores";
Condition B: left on a stand in the laboratory for 5 weeks (at 23 ± 2°C), no rewetting – "drw cores";
Condition C: unwrapped and left on a stand for 5 weeks or 9 months prior to testing (at 23±2°C), no rewetting – "dr cores";
Condition D: unwrapped and left on a stand for 5 weeks (at 23 ± 2°C). Then, the cores were rewetted for 48 hours in the moist curing room (protected from running water) prior to testing – "rw cores";
The SDT for these sets of cores was carried out at both 30% and 40% of the 28-day design compressive strength value, depending on the test.
- Cores, either 100 or 150mm in diameter, were taken from the 1 m cylindrical blocs (vertical direction) extracted from the bridge deck.

7.4.2 Laboratory-made specimens

The other four sub-studies (effect of specimen's end surface preparation type, effect of specimen's loading level, effect of the specimen's shape (L/D) and the variability of the SDT) were carried out on concrete cylinders, 100 x 200 mm in size (except for the sub-study of the specimen's shape whose specimen's lengths varied to cover different L/D), cast in the laboratory and stored in an environment to accelerate ASR (38°C and 100% R.H.). Table 2 describes the various aggregates used in the laboratory investigations; Table 3 gives the

concrete mixtures used in these sub-studies; finally, Table 4 presents the testing matrix implemented.

For the sub-study of the effect of the specimen's end surface preparation type, concrete specimens of 28-day, 45 MPa mix design strength, and containing the highly-reactive NM gravel, were used [6]. When these specimens reached $0.10 \pm 0.01\%$ of expansion, they were wrapped in plastic film and stored at 12°C (largely stopping further chemical reaction). Prior to testing, the end surfaces of the specimens were rectified with either sulfur capping compound or through surface grinding and then stored in a moist curing room for 48h (following the A23.2-14C procedure).

Table 2: Aggregates used in the study.

Aggregate		Location	Rock Type	Specific gravity	Absorption (%)	AMBT 14d exp,%
Coarse	NM	New Mexico (USA)	Polymictic Gravel (mixed volcanics, quartzite, chert)	2.53	1.59	1.114
	Wyo	Wyoming (USA)	Polymictic Gravel (granite, amphibolite, rhyolite)	2.64	0.87	0.296
	HP	Newfoundland (Canada)	High-purity limestone	2.68	0.44	0.001
	Pot	Montreal (Canada)	Siliceous sandstone	2.57	1.15	0.093 ¹
	Dia	Quebec (Canada)	Diabase (plutonic rock)	3.00	0.51	0.065
Fine	Tx	Corpus Christi (USA)	Polymictic sand (granitic, mixed volcanics, quartzite, chert, quartz)	2.60	0.55	0.995
	Lav	Quebec (Canada)	Natural derived from granite	2.71	0.54	0.032

¹The Potsdam sandstone typically does not expand significantly in the AMBT, while being reactive in field structures.

Table 3: Concrete mix designs used for the laboratory-made specimens.

Ingredients	Materials (kg/m ³)				
	35 MPa mixtures			45 MPa mixture	
	Tx sand + Dia	Laval + Wyo	Lav + Pot	Lav + NM	Tx sand + HP
Cement	370	370	370	424	424
Sand	896	770	737	714	790
Coarse aggregate	1029	1065	1068	1073	1029
Water	174	174	174	157	157

Table 4: Stiffness damage testing matrix for the sub-studies carried out on laboratory-made concrete specimens.

Mixtures (reactive aggregate)	Study	Testing matrix						
		Effect of the surface end preparation type		Effect of the specimen's loading level			Effect of the core shape: L/D	
		40% of the 28-day design strength value					40% of the 28- day design strength value	
		Sulfur capping	Mechanical grinding (according to the standards)	Loading corresponding to 40% of the 28-day design strength value	Loading corresponding to 40% of the design strength measured from a non-reactive concrete with the same age	1.4	1.6	2.0
45 MPa (NM)	Surface end preparation Expansion – 0.10%	3	3	-	-	-	-	-
35 MPa (Tx)	Loading level Expansions - 0.05%, 0.12%, 0.20%, 0.30%	-	-	8 (2 at each expansion level)	12 (3 at each expansion level)	-	-	-
35 MPa (Wyo, Pot)	Variability in the laboratory Expansions – 0.05%, 0.15%	-	-	7 (Wyo at 0.05%) and 7 (Pot at 0.15%)	-	-	-	-
45 MPa (Tx)	Sample's shape –0.12%	-	-	-	-	2	2	2

Regarding the sub-study of the effect of specimen's loading level for SDT testing, and in order to simulate a real field situation, i.e. where the original mix design strength is often unknown, two 35 MPa (reactive and non-reactive) concrete mixtures were designed. In the case of the reactive mixture, concrete cylinders, 100 x 200 mm in size, containing the highly-reactive Tx sand were cast, stored at 38°C and 100% R.H, and their length change measured regularly. Once the specimens (by sets of three) reached the following expansions (0.05%, 0.12%, 0.20% and 0.30%; $\pm 0.01\%$), they were wrapped in plastic films and placed at 12°C prior to testing, because of testing capacity limitations. Specimens from the non-reactive concrete mixture, i.e. incorporating the non-reactive Dia coarse aggregate and the non-reactive Lav sand, were cast and stored in the same conditions, and tested in compression at the age corresponding to the expansion levels reached by the reactive samples. Thus, it was possible to compare the following loading levels in the SDT: 1) 40% of the 28-day value obtained from the reactive mixture and; 2) 40% of the value measured at a given age (same age the distressed concrete reached at the selected expansion levels), which represented the evolution of the compressive strength of the concrete material over time.

For the sub-study on the effect of the specimen's shape, 45 MPa concrete specimens containing the highly-reactive Tx sand and with different L/D values (1.4, 1.6 and 2.0) were used. When these samples reached $0.12 \pm 0.01\%$ expansion, they were wrapped in plastic films and stored at 12°C. Prior to testing, the specimen's end surfaces were ground and then the unwrapped specimens stored in a moist curing room for 48h (following the A23.2-14C procedure).

The fourth sub-study (i.e. variability of the SDT) was carried out on concrete cylinders, 100 x 200 mm in size, cast from 35 MPa concrete mixtures containing two types of reactive aggregates (Wyo and Pot) and two expansion levels (0.05% and 0.15%). The procedure carried out was basically the same to that described before, i.e. samples cast, placed at 38°C and 100% R.H up to the expansion levels selected, wrapped in plastic film and placed at 12°C, for stopping further ASR until testing was possible. The specimens were then subjected to the SDT in order to determine the variability between a number of test specimens showing very similar expansion levels.

7.4.3 Methods for damage assessment and analysis

7.4.3.1 Stiffness Damage Test (SDT)

All the specimens (cores or laboratory-made cylinders) were subjected to five cycles of loading/unloading at a controlled loading rate of 0.10 MPa/s. Most of the specimens were tested at a strength level corresponding to 40% of the 28-day concrete mix design strength, according to [6]. When a different loading level was used, for any reason, it was indicated accordingly. The results presented in this paper are the average values obtained on the number of specimens presented in Tables 1 and 4.

7.4.3.2 Compressive strength

Compressive strength was measured on the laboratory specimens to determine either the 28-day strength of each concrete mixture assessed or the increase in the concrete strength over time, e.g. in the case of the effect on the loading level sub-study. For the 28-day strength assessment, as the specimens contained highly-reactive aggregates, one could not follow the ASTM C 39[16] procedure, as the specimens could develop ASR during the first 28 days in the moist room. Therefore, upon demoulding, the specimens were wrapped in plastic film and

placed at 12°C for a 47-day period, which represents the same 28-day curing period according to the maturity concept presented by ASTM C 1074) [17]. Expansion measurements confirmed that the 12°C storage resulted in only a slight shrinkage ($- 0.02 \pm 0.01\%$) and mass loss ($0.7 \pm 0.2\%$) of the test specimens, which was recovered through the 48-hour re-saturation period prior to running stiffness damage testing.

7.4.3.3 Damage Rating Index

A semi-quantitative petrographic method, the *Damage Rating Index*, originally proposed by Grattan-Bellew & Danay [18] and recently modified by researchers from Laval University [19], was carried out on selected concrete specimens to determine their microtextural characteristics and validate the damage responses found over the stiffness damage testing. The method consists in a count, under the stereomicroscope ($\approx 16\times$ magnification), of the number of petrographic features of deterioration (commonly associated to ASR) on polished concrete sections on which a grid is first drawn (minimum 200 grid squares to be examined, 1 by 1 cm in size). The *DRI* thus represents the normalized value (to 100 cm^2) of the frequency of these features after the count of their occurrence, over the surface examined, has been multiplied by weighing factors representing their relative importance in the overall deterioration process (Figures 3A and 3B). Studies carried out by the authors have shown the good correlation between the DRI values and the expansion of laboratory test specimens affected by ASR [20].

A

Petrographic features		Weighing factor
Closed crack in coarse aggregate	CCA	0.25
Opened crack in coarse aggregates	OCA	2
Opened crack with reaction product in coarse aggregate	OCAG	2
Coarse aggregate debonded	CAD	3
Disaggregated/corroded aggregate particle	DAP	2
Crack in cement paste	CCP	3
Crack with reaction product in cement paste	CCPG	3

B

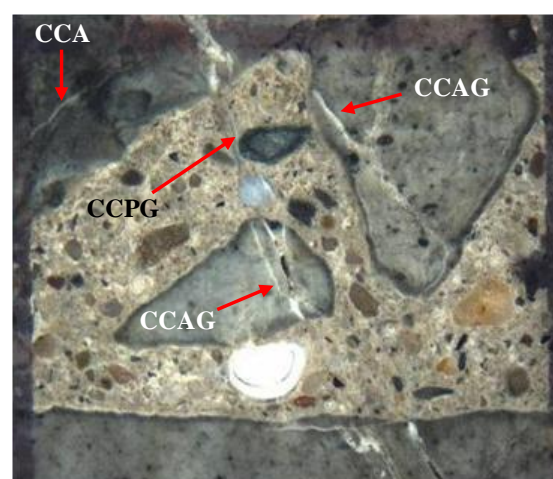


Figure 3: Damage Rating Index method. Micrograph B shows a 1cm^2 section where most of the petrographic features to be noted in the DRI (as listed in A) can be observed and identified [19] (the distance between the vertical lines on both sides of the micrograph is 1 cm).

7.5 RESULTS OF DAMAGE EVALUATION TESTING

The following sections presents the results of testing carried out to evaluate the effect of various input parameters on the SDT output responses. These results are often based on the average value obtained for a limited number of specimens, which limits the full statistical analysis of data. The results should thus be taken as indicative only. However, two-variable ANOVA was carried out on a number of those results in order to determine whether the differences between the different series of test results are statistically significant. This topic is further discussed in the section 7.6.1.

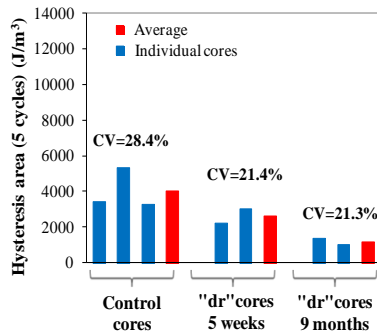
7.5.1 Specimen's conditioning history (drying and rewetting) prior to testing

The influence of the specimen's conditioning history on the SDT responses is illustrated in Figure 4. The results are compared for control samples (*Condition A* in Table 1; 3 cores) and samples that were unwrapped and left for drying in the laboratory ("dr" cores) for 5 weeks (2 cores) and 9 months (2 cores) (no rewetting) (*Condition C* in Table 1).

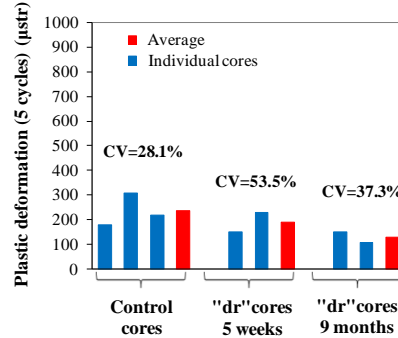
Although Sanchez et al. [6] demonstrated that loading the test specimens up to 40% of the 28-day concrete mix design strength in the SDT provides the best diagnostic evaluation of the condition of ASR-affected concrete, the cores for this series of testing were tested at 30% of their concrete mix design strength (i.e. 7.2 MPa), which still allowed a comparative evaluation of the effect of drying on the SDT results.

It is apparent from the results in Figure 4 that the longer was the drying period, the more dramatic was the impact on the SDT output responses, i.e. for both the *Hysteresis Area* (HA) and the *Plastic Deformation* (PD) parameters. For 5 weeks and 9 months of drying (no rewetting), the values obtained from the test specimens were respectively 50% and 70% lower than the control for the HA parameter, and 20% and 45% lower for the PD parameter. Likewise, the specimens' behavior in terms of *Modulus of Elasticity* (ME) was strongly influenced by the drying effect. The dried samples presented an increase of 37% and 12% for 5 weeks and 9 months of drying, respectively. A distortion was however found for drying effects between the 5-week and 9-month periods, which remains unexplained at this stage.

A – HA – all five cycles



B – PD – all five cycles



C – ME – av. of 2nd and 3rd cycle

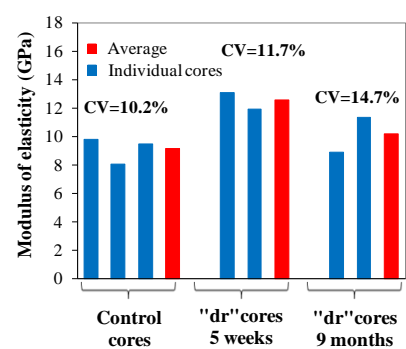
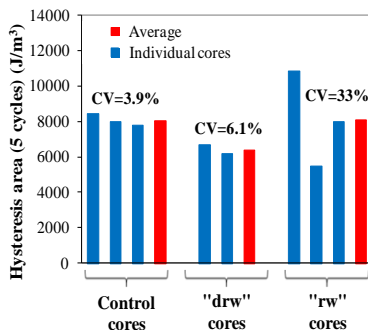


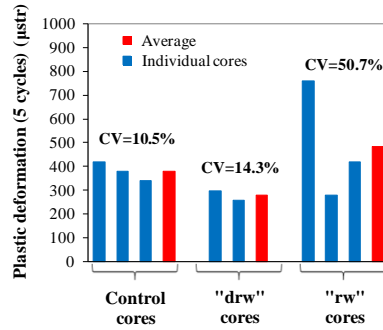
Figure 4: SDT results for concrete cores extracted from the Robert-Bourassa/Charest foundation block : sub-study on the effect of preconditioning on the SDT output responses. A, Hysteresis area (HA) over the five cycles. B. Plastic deformation (PD) over the five cycles. C. Average modulus of elasticity (ME) of the 2nd and 3rd cycles.

Figure 5 compares the effect of core conditioning on the SDT results for 1) control specimens – *Condition A*; 2) specimens that were wrapped in plastic film and left for 5 weeks in the laboratory (“drw” cores) before testing (no rewetting) – *Condition B*; and, 3) specimens that were left unwrapped in the laboratory, also for 5 weeks, but that were rewetted (48 hours in moist curing room) prior to testing (“rw” cores) – *Condition D*.

A – HA- five cycles



B – PD - five cycles



C – ME – avg of 2nd and 3rd cycles

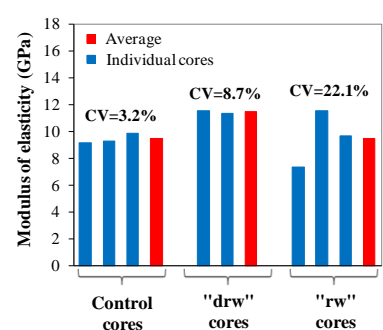


Figure 5: SDT results for concrete cores extracted from the Robert-Bourassa/Charest foundation block : sub-study on the influence of the pre-conditioning on the SDT output responses – drying versus rewetting effects. A. Hysteresis area (HA) (J/m³) (5 cycles). B. Plastic deformation (PD) (µstrain) (5 cycles). C. Modulus of elasticity (ME) (GPa) (average of the 2nd and 3rd cycles). (CV = coefficient of variation).

It is possible to notice from the results in Figure 5 that even though the “drw” cores were well wrapped, they presented lower average *Hysteresis Area* or *Plastic Deformation* values in the SDT than the control specimens, similar to the behavior showed in Figure 4. However, the difference with the control samples, for the HA parameter, was lower when the samples were wrapped (20% reduction, Condition B, Figure 5A) compared to left unwrapped (34%

reduction, Condition C, Figure 4A) in the laboratory, thus confirming that wrapping with plastic film helped to decrease the effect of drying on the test results, for a given time of analysis (five weeks). For the *Plastic Deformation* parameter, the losses were somewhat similar for both scenarios (wrapped and not, respectively 27% and 20%, compare Figures 5B and 4B). Finally, the *Modulus of Elasticity* presented, once again, the opposite behavior than the two other parameters and, like the Hysteresis Area, wrapping decreased the difference with the control cores (21% reduction instead of 37%, compare Figures 5C and 4C).

Rewetting (“rw” samples) seemed to somewhat reset the initial conditions of the cores, as the average HA and ME values of both the control and rewetted set of samples were almost equal; however, rewetting following an extended drying period seemed to increase the variability of the test results (significantly higher CV’s in Figure 5).

7.5.2 Specimen’s characteristics (length-to-diameter ratio and diameter of the core specimens)

The influence of the length-to-diameter ratio on the SDT responses for core samples extracted from the foundation blocks of the Robert-Bourassa/Charest viaduct (all from the 200 to 400 mm portion under the surface) is illustrated in Figure 6. For the *Hysteresis Area* parameter, the average test values were respectively 20% (L/D=1.6) and 38% (L/D=1.8) greater than those obtained for the conventional core dimension (L/D=2.0). Similarly, for the plastic deformation, they were 22% (L/D=1.6) and 58% (L/D=1.8) greater. On the other hand, the *Modulus of Elasticity* values were not that influenced, on an average, by the different ratios.

The results also suggest that the use of specimens with lower length-to-diameter ratios (either 1.6 or 1.8) largely increased the variability of the test results (e.g. CV ranging from 4% to about 40% for the hysteresis area parameter, see figure 6A). Also, for the lower length-to-diameter ratio tested, the average values of the output responses (i.e., *Hysteresis Area* and *Plastic Deformation*), were greater than those obtained for a length/diameter of 2.0. This can be partly attributed to the platen restraint created over the test, which is used to conceal loss in compressive strength from ASR-affected specimens and, maybe, it could also have an important effect on the SDT procedure [21].

The influence of the length-to-diameter ratio on the SDT responses was also evaluated on test cylinders cast from a 45 MPa concrete mixture manufactured in the laboratory and presenting $0.12 \pm 0.01\%$ of expansion. Despite the limited number of specimens tested, but as for the field cores, the use of specimens with lower length-to-diameter ratio (both 1.4 and 1.6)

changed significantly the test results for all the SDT output parameter compared to the values obtained on “standard” size specimens (i.e. $L/D = 2.0$) (Figure 7). Those differences can be once again partly attributed to the platen restraint created over the test [21]. For the *Hysteresis Area* parameter, the average values were respectively 42% ($L/D=1.4$) and 51% ($L/D=1.6$) greater than those obtained for the conventional core dimension ($L/D=2.0$). Similarly, for the plastic deformation, they were 4% ($L/D=1.4$) and 24% ($L/D=1.6$) greater. Finally, for the modulus of Elasticity parameter, they were 10% lower (for both $L/D=1.4$ and $L/D=1.6$) than the values obtained for longer test specimens ($L/D = 2.0$) (Figure 7).

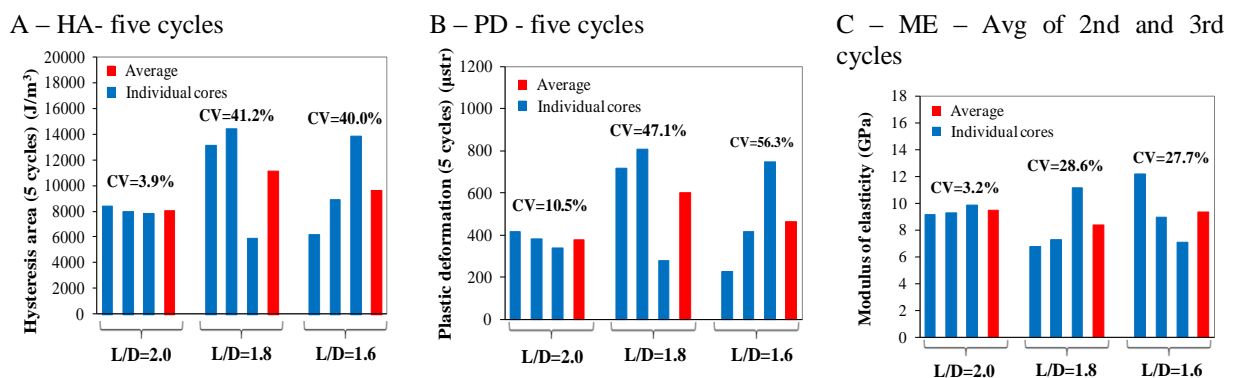


Figure 6: SDT results for concrete cores extracted from the Robert-Bourassa/Charest foundation block : sub-study on the influence of specimens’ characteristics (L/D ; exposed portions of block foundation) on the SDT output responses. A. Hysteresis area (HA) (J/m^3) (5 cycles). B. Plastic deformation (PD) (μ strains) (5 cycles). C. Modulus of elasticity (ME) (GPa) (average of the 2nd and 3rd cycles). (CV = coefficient of variation).

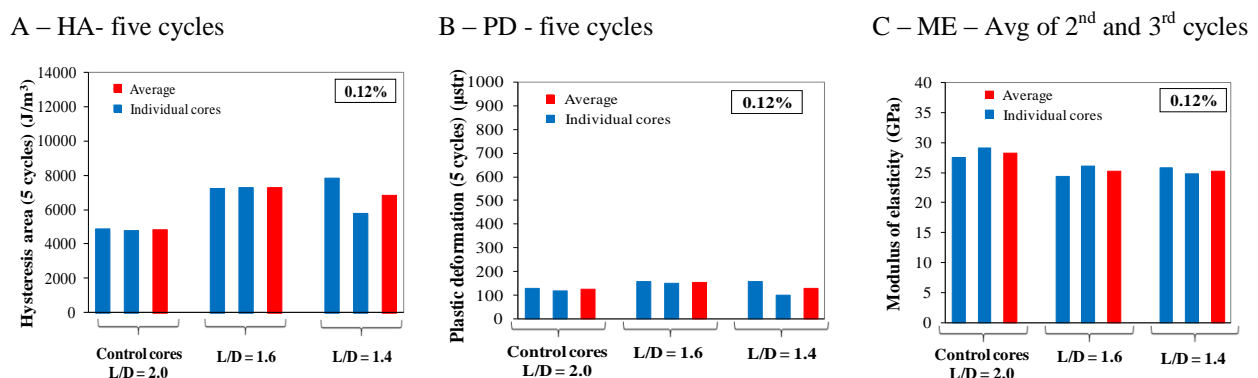


Figure 7: SDT results for the 45 MPa concrete samples cast in the laboratory and incorporating the reactive Tx sand : sub-study on the influence of sample’s shape (L/D) on the SDT output responses. A. Hysteresis area (HA) (J/m^3) (5 cycles). B. Plastic deformation (PD) (μ strains) (5 cycles). C. Modulus of elasticity (ME) (GPa) (average of the 2nd and 3rd cycles).

The effect of the core diameter on the SDT results was evaluated on core specimens extracted in the vertical direction from the concrete deck of the Robert-Bourassa/Charest viaduct; the results are illustrated in Figure 8. The results obtained on seven cores, 100 by 200 mm in size, 128

are compared to those obtained on three cores of 150 by 300 mm in size. Although a direct comparison cannot be done considering the difference in the number of specimens tested, the results in Figure 8 suggest that, on an average, the use of larger core samples may result in slightly lower *Hysteresis Area* and *Plastic Deformation* values, as well as higher modulus of elasticity values compared to the smaller core specimens. However, considering the variability (CV) in the test results obtained within each size groups, it appears that the difference in the output responses obtained between the 100 by 200 mm and 150 by 300 mm specimens is likely not that significant and could actually be attributed, to some extent, to the inherent variability of the test or the variability in the condition of the concrete in adjacent core specimens extracted from the ASR-affected structural element.

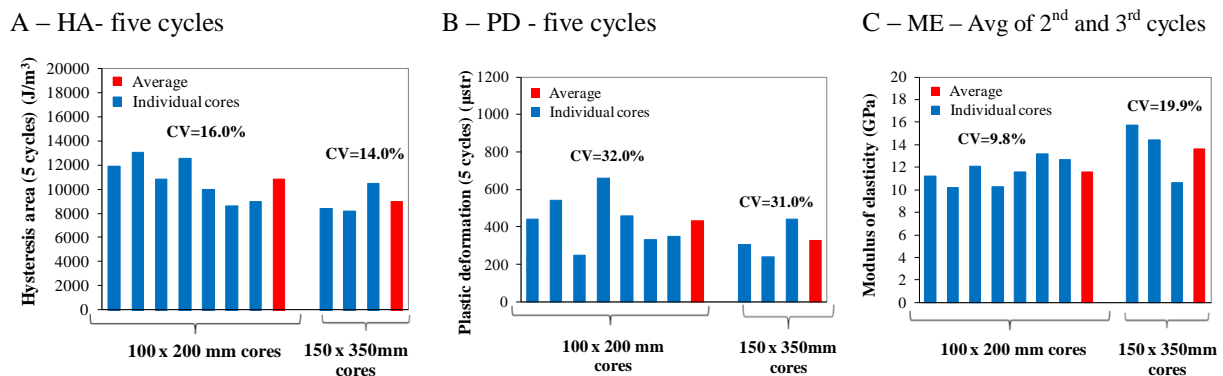


Figure 8: SDT results for concrete cores extracted from the Robert-Bourassa/Charest bridge deck (vertical direction) : sub-study on the influence of sample’s geometry (diameter size) on the SDT output responses. A. Hysteresis area (HA) (J/m³) (5 cycles). B. Plastic deformation (PD) (µstrains) (5 cycles). C. Modulus of elasticity (ME) (GPa) (average of the 2nd and 3rd cycles). (CV = coefficient of variation).

7.5.3 Specimens end surface preparation (sulfur capping vs. surface grinding)

The influence of the specimen’s end surface preparation procedure on the SDT output parameters was evaluated through the testing of test cylinders cast from 45 MPa concrete mixtures incorporating the highly reactive NM gravel. For this study, similar to the evaluation of the effects of the conditioning history of the test specimens (see section 7.5.1), a loading level of 30% (i.e. 13.5 MPa) was chosen. Therefore, according to [6], one needs to interpret the results in relative and qualitative means. The results presented in the Figure 9 indicates that it is possible to use both end surface preparation procedures (sulfur capping or grinding) without impacting significantly on the SDT output parameters. Moreover, almost all data obtained with the above two procedures presented similar coefficients of variation for the output parameters (only the grinding procedure for *Plastic Deformation* parameter was

slightly greater than the others), which confirms that the different types of surfaces preparation procedures used in this study resulted in similar test results.

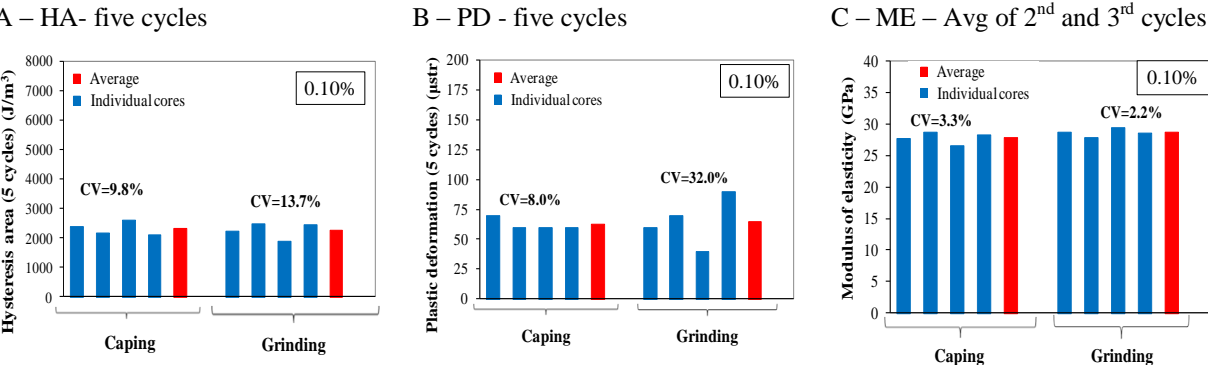


Figure 9: SDT results for 45 MPa laboratory concrete specimens incorporating the reactive NM gravel: sub-study on the influence of the sample’s end surface preparation on the SDT output responses – sulfur capping vs. grinding. A. Hysteresis area (HA). B. Plastic deformation (PD). C. Modulus of elasticity (ME). (CV = coefficient of variation).

7.5.4 Specimen’s location (surface x core; exposed and not exposed sites)

This section compares the results obtained from stiffness damage testing of concrete cores extracted from exposed and non-exposed (under the bridge deck) portions of the foundation blocks of the Robert-Bourassa/Charest viaduct (Table 1). The test results for the SDT output parameters obtained for cores corresponding to the surface portion of the foundation blocks, i.e. 50 to 250 mm portion, are presented in Figure 10. As expected, the data show that the cores extracted from the exposed sites present a greater amount of damage than the cores from the non-exposed sites. Both the *Hysteresis Area* and the *Plastic Deformation* values for the non-exposed sites were significantly lower, about 40% on an average, than those obtained for the exposed sites. In addition, the cores from the non-exposed site presented *Modulus of Elasticity* values that were about 53% times greater than those obtained from the exposed zones.

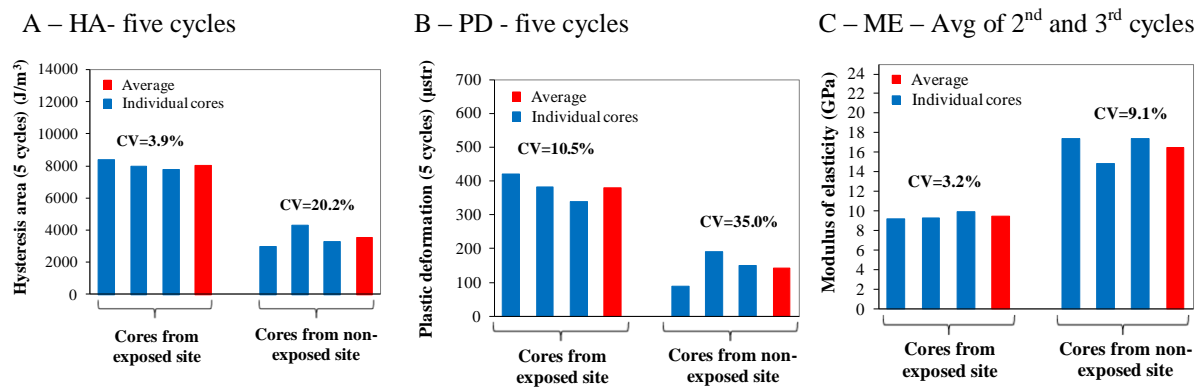


Figure 10: SDT results for concrete cores extracted from the Robert-Bourassa/Charest viaduct: sub-study on the influence of specimens' environment (exposed vs. non-exposed portions of the foundation blocks; superficial portion (50-250mm) of the blocks) on the SDT output responses. A. Hysteresis area (HA) (J/m³) (5 cycles). B. Plastic deformation (PD) (µstrains) (5 cycles). C. Modulus of elasticity (ME) (GPa) (average of the 2nd and 3rd cycles). (CV = coefficient of variation).

Figure 11 compares the SDT output response for cores corresponding to the superficial (50 to 250mm) and the “core” (250 to 450mm) portions of exposed and non-exposed sections of the block foundations. The results suggest a higher degree of damage in the superficial portion of the structural element, and this for both (exposed and non-exposed) zones. The difference between the surface and the core values, in terms of damage, was greater for the exposed site (compare Figures 11A to 11C against Figures 11D to 11F). Actually, for both the *Hysteresis Area* and the *Plastic Deformation* parameters, the values for the “core” samples represented about 60% (exposed area) and 75% (non-exposed area) of the values obtained for the surface samples.

Regarding the *Modulus of Elasticity* parameter, the behavior obtained was the same (but "opposite": higher damage = higher HA and PD values, but lower ME values!) than that obtained for the other two output parameters. Once again, the influence was greater for the exposed zone; the values of the “superficial concrete” samples represented 73% and 87% of that obtained for the "core" concrete for exposed and non-exposed zones, respectively. Therefore, it seems that the higher the exposure to moisture, the greater is the difference in damage from the “core” up to the surface of concrete elements.

The above results are very interesting. Courtier [22] proposed that macrocracking develops in a direction perpendicular to the surface in ASR-affected concrete member resulting from reduced ASR expansion in the skin portion of the structural element due to alkali leaching, moisture variations due to the effect of wetting-drying cycles and higher porosity, while expansion and microcracking increases towards the central zone of the member influenced by

applied loads, pre-stress or reinforcement. The results in the Figure 11 suggest that, in the case of exposed portions of the foundation block, the *damage* is actually relatively higher in the outer (superficial) part of the concrete foundation block (i.e. 50-250 mm vs. 250-450 mm), while the overall damage and the difference in damage between the outer and inner part of the concrete member is not as developed in the case of the protected part of the foundation block. It is likely that wetting/drying and freezing/thawing cycles have contributed significantly to the increased damage observed in the external portion of the exposed foundation blocks. It is important to mention that, in both cases (exposed and non-exposed sections), the first 50 mm of the cores extracted from the massive foundations had been eliminated from the test samples to minimize the effect of surface macrocracks (opened cracks) on the results of mechanical testing. Finally, all the CVs can be considered quite satisfactory, mainly considering the assessment of field cores.

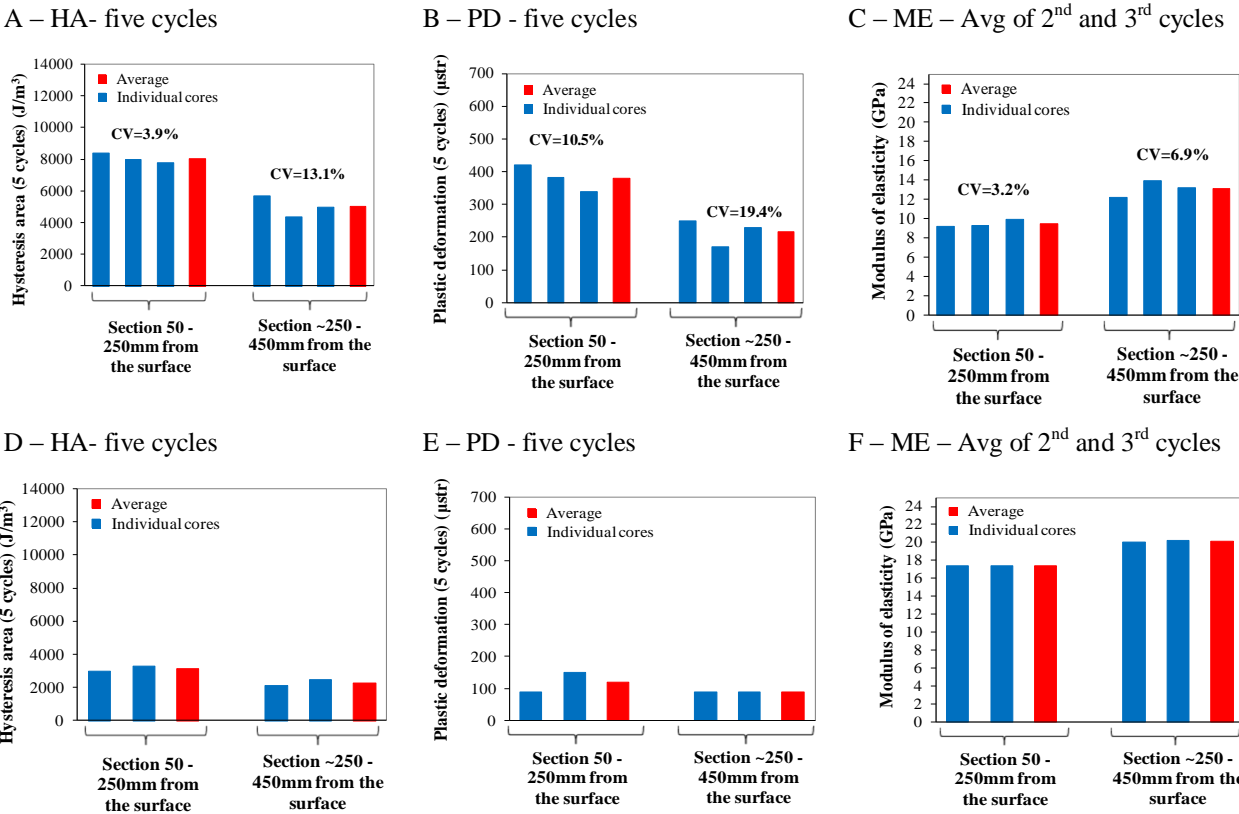


Figure 11: SDT results for concrete cores extracted from the Robert-Bourassa/Charest viaduct: study on the influence of sample’s environment (superficial vs. core portions of exposed vs. non-exposed foundation blocks) on the SDT output responses. A,B,C. Output parameters for cores extracted from the exposed portion of the foundation block. D,E,F. Output parameters for cores extracted from the non-exposed portion of the foundation block.

In order to verify and validate the results obtained from stiffness damage testing, semi-quantitative petrographic analysis was carried out on companion core specimens following the Damage Rating Index Method; the results are illustrated in the Figure 12. The DRI charts confirmed that the cores extracted from exposed zones presented greater degree of damage than that obtained for the cores extracted from non exposed zones. Moreover, the "surface" cores (50-250 mm) of both zones (exposed and non exposed) showed greater damage than the "core" specimens (250-450mm). In both cases, it is very interesting to note that higher numbers of *Opened Cracks in the aggregate particles (OCA)* as well as *Cracks in the Cement Paste (without (CCP) and with (CCPG) gel)* are generally observed in the surface portions of the cores compared to the core (or internal) portion of the specimens. The above features are definitely indicative of the extent of ASR in the core specimens.

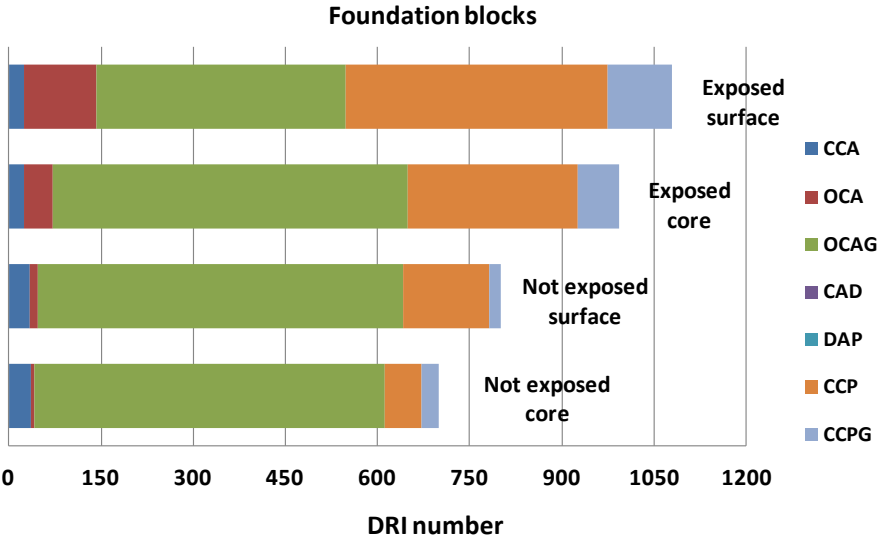
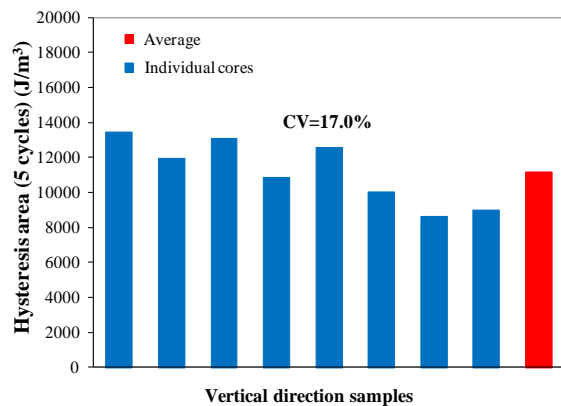


Figure 12: DRI results for concrete cores extracted from the Robert-Bourassa/Charest viaduct - study on the influence of sample’s environment (superficial vs. core portions from both exposed and non-exposed portions of the foundation blocks).

7.5.5 Variability over SDT responses

The results of stiffness damage testing on cores extracted in the vertical direction from the concrete deck of the Robert-Bourassa/Charest viaduct are illustrated in Figure 13. These results are reported for cores extracted from the upper portion (i.e. ≈50-250 mm deep) of the bridge deck. The variability of the test results differs according to the output parameter studied. In a general way, the *Modulus of Elasticity* seems the least variable output parameter (9%), followed by the *Hysteresis Area* (17%) and the *Plastic Deformation* (30%) parameters.

A – HA (five cycles)



B - PD (five cycles)

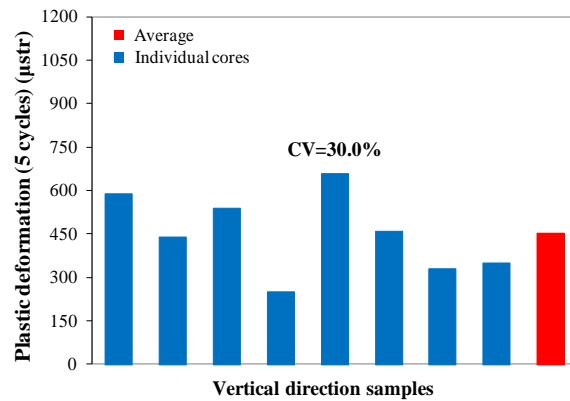
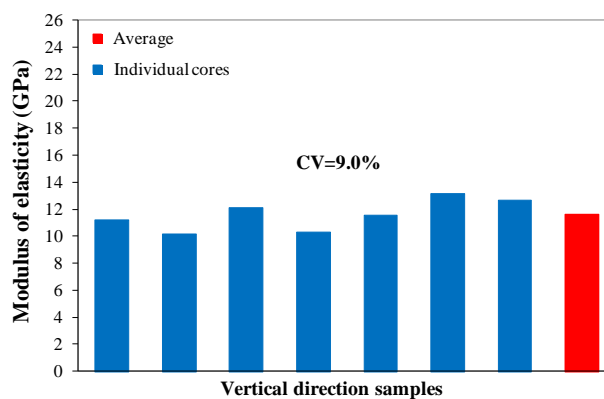
C - ME (avg of 2nd and 3rd cycles)

Figure 13: SDT results obtained on cores extracted in the vertical direction from the Robert-Bourassa/Charest bridge deck: study on the variability of the SDT output responses. A. Hysteresis area (HA) (J/m^3) (5 cycles). B. Plastic deformation (PD) (μstr) (5 cycles). C. Modulus of elasticity (ME) (GPa) (average of the 2nd and 3rd cycles). (CV = coefficient of variation).

The variability of the SDT output parameters was also evaluated on two sets of seven concrete cylinders, 100 by 200 mm in size, cast from for mixtures incorporating two different reactive aggregates (Wyo and Pot) and having reached expansion levels of 0.05 and 0.15%, respectively (Figure 14). The lowest coefficients of variations were obtained for the *Modulus of Elasticity* parameter (4 and 5%) (Figure 14C), which were somewhat similar to that obtained for the *Hysteresis Area* (8%) and *Plastic Deformation* (6%) parameters of the Pot specimens (0.15% expansion) (Figures 14A and 14B). On the other hand, the highest CVs% were found for the lowest expansion levels (i.e. 0.05%; Wyo aggregate), i.e. for the *Hysteresis Area* (15%) and *Plastic Deformation* (28%) output parameters. It is interesting to compare the above data to the C.V. obtained for a set of eight cores extracted from the Robert-Bourassa/Charest bridge deck: 17% for the *Hysteresis Area*, 30% for the *Plastic Deformation* and 9% for the *Modulus of Elasticity* parameters (Figure 13). The above results confirmed that

the lowest and highest variability is obtained for the *Modulus of Elasticity* and *Plastic Deformation* parameters, respectively. Also, the variability seems somewhat higher for core specimens extracted from structures compared to laboratory specimens, which is understandable considering that the latter are maintained under well-controlled conditions and subjected to a tight control (i.e. ± 0.01) on the expansion level at which the specimens were tested.

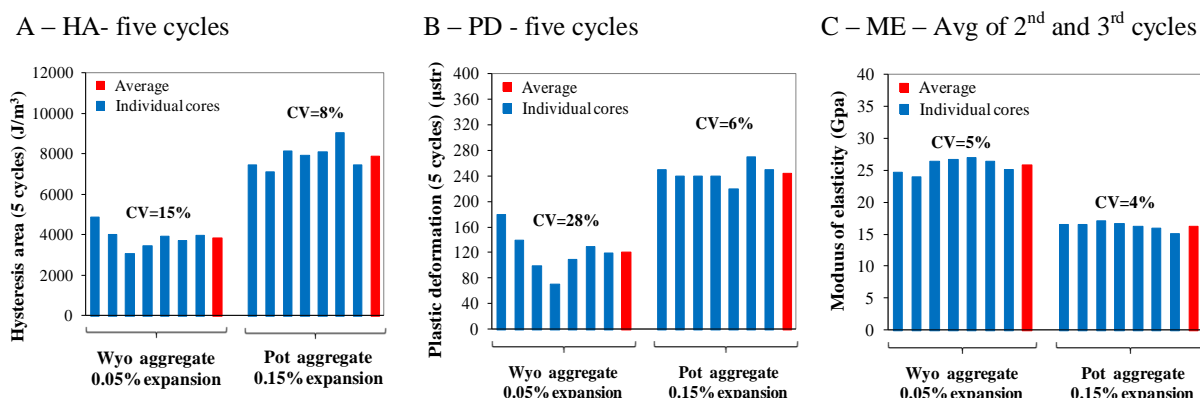


Figure 14: SDT results for 35 MPa laboratory made concrete specimens incorporating the reactive Wyo and Pot aggregates: sub-study on the variability of SDT output parameters. A. Hysteresis area (HA) (J/m³) (5 cycles). B. Plastic deformation (PD) (μstrains) (5 cycles). C. Modulus of elasticity (ME) (GPa) (average of the 2nd and 3rd cycles). (CV = coefficient of variation).

7.6 DISCUSSION

7.6.1 Statistical analysis of the data

Based on an extensive series of tests carried out on laboratory-made samples, including ANOVA analyzes of the test results, Sanchez et al. [6] showed that the 40% loading level was a preferable scenario for condition assessment of ASR-affected concretes using the SDT. Even though there were many evidences that the different input parameters tested through the SDT and discussed in the previous sections do influence the SDT output responses, a two-variable ANOVA (confidence interval of 5%) was performed for each of the different parameters evaluated to confirm those assumptions. Table 5 presents the data (“p values) obtained through the variance analysis for the *Hysteresis Area* (HA) and *Plastic Deformation* (PD) parameters obtained under the various conditions evaluated.

Table 5: Two-variable ANOVA analysis over the test hypothesis tested on the SDT.

Load (%)	Study type	p values		p critic	p < p critic HA	p < p critic PD
		HA (J/m ³)	PD (μstrain)			
30%	Drying effect (Condition C)	0.0100	0.040	0.05	ok	ok
40%	Drying effect (Condition B)	0.0007	0.030	0.05	ok	ok
40%	Drying effect (Condition D)	0.9800	0.490	0.05	no	no
40%	L/D (2.0 vs 1.8 vs 1.6)	0.0018	0.400	0.05	ok	no
40%	Exposed vs. Non exposed	0.0130	0.0350	0.05	ok	ok
40%	Exposed (surf) vs. Exposed (core)	0.0077	0.0320	0.05	ok	ok
40%	Non exposed (surf) vs. Non exposed (core)	0.0500	0.210	0.05	ok	no

Three interesting phenomena can be observed from this analysis; 1) first, as expected, the parameters that were assumed to influence SDT results according to [6] were again considered significant over ANOVA analysis (i.e. those cases where the “p-values” are lower than the “p critic - 0.05), which means that the difference in the input parameters also made the responses over the tests different; 2) in the drying effect study (condition D), the values found were not considered significant through ANOVA analysis, which means that this condition does not affect SDT responses. Condition D involves rewetting the specimens for 48 hours after they were stored for 5 weeks (wrapped) in the laboratory, which confirms that this practical approach could be used without jeopardizing SDT responses, and; 3) the *Hysteresis Area* parameter is more influenced than the *Plastic Deformation* by differences in the input parameters (what can be found through p values analyses). However, in two situations (“p values” greater than 0.05 in Table 5), the *Plastic Deformation* did not show responses that were considered different through ANOVA analyses (i.e. exposed vs. non exposed zones and non exposed (surface) vs. non exposed (core)). This result can be explained by the more variable character of this parameter (plastic deformation), which was illustrated over the whole study.

7.6.2 The quest for the most diagnostic and reliable SDT procedure

The results presented by Sanchez et al. [6] and in the first part of this paper showed that the SDT has the potential of being an efficient tool for quantifying the degree of damage in concrete due to ASR. However, engineers intending to use that tool need to be well aware of its limitations, and especially of the various factors that will critically influence the results (or output parameters) of the test. Sanchez and coworkers [6] indeed showed the critical effect of the loading level used for stiffness damage testing on the results of SDT’s output parameters and their diagnostic character for quantifying the degree of damage in concrete affected by

ASR. Through this study, the impact of additional practical input parameters on the responses of the SDT or in the test analyses, and that can easily occur in daily activities in concrete laboratories, was investigated. Indeed, the knowledge of the impact of those parameters on the SDT test results is essential to the development of a standard procedure/approach for practical purposes. Because of the somewhat limited number of samples used in some of the sub-studies carried out in this research, it may not be possible to provide a fully appropriate quantitative assessment, in terms of variability, of the impact of the various parameters on the SDT test results (which would allow the development and proposal of correction factors). However, the qualitative analysis carried out in this study provides a good indication of the influence of each parameter tested, showing that some of them have a strong impact on the SDT output responses, while others could be neglected. Parameters such as the specimens' location (depth and coring direction in the structural element sampled), specimen's characteristics (length-to-diameter ratio), specimen's conditioning history, and choice of the loading level, had a significant impact on SDT's output parameters (as absolute values). On the other hand, the size of the core (core diameter as far as a length/diameter of 2.0 is used) and the end surface preparation technique (sulfur capping vs. grinding) did not seem to induce significant differences in the test results.

7.6.2.1 Practical implications - effect of the specimens' loading level on SDT responses

General considerations

As mentioned before, Sanchez et al. [6] showed that the selection of the loading level has a critical impact on the results of stiffness damage testing. The authors tested laboratory manufactured concrete specimens at selected expansion levels (0.05 to 0.30%) under loadings ranging from 15% to 40% of the 28-day concrete design strength of a range of concrete mixtures (25, 35 and 45 MPa) incorporating reactive fine or coarse aggregates. The results of the above investigations showed that SDT does not highlight any significant difference between the various expansion levels in the test specimens (an indirect measure of ASR-related damage) when both fixed loadings (e.g. 10MPa proposed by [5]) and loading levels lower than 30% of the 28-day mix design strength are used. Sanchez et al. [6] suggested that, in order to obtain diagnostic results over the SDT, one really needs to "load/stress" the material analyzed, which means taking the material up to a "threshold" of performance thus allowing to reliably measure its current condition/physical integrity without creating significant additional damage within the test specimens. Moreover, loading the damaged

concrete specimens up to 40% of the 28-day mix design strength was statistically and petrographically identified as the best approach (i.e. more diagnostic approach) for ASR diagnosis through stiffness damage testing for the sets of test specimens used in that study. That loading level is known not to generate any deleterious effects upon testing of sound concrete since it is the recommended level used in the determination of a concrete's modulus of elasticity (ASTM C 469).

Now, how can the above information apply for the condition survey of an aging/deteriorated concrete structure/structural element in service? For example, how can the damage in a bridge structural element, such as the abutment/wing wall of the bridge structure illustrated in Figure 15, be assessed using the SDT? It is interesting to note that cracking is typically well developed in the exposed portions of the structure (wing/abutment walls) (Figures 15A, 15C and 15D), while no or limited signs of cracking are observed in the non-exposed portion of the structure (e.g. zone of the abutment wall under the bridge deck) (Figure 15B).

Based on the results obtained in this study, the options that would likely be available to engineers for selecting the loading level for stiffness damage testing as follows: 1) 40% of the original 28-day mix design compressive strength (as per [6]; however, past experience has revealed that precise information on the original concrete mix design is rarely available for older (i.e. 20 years +) concrete structures); 2) 40% of the compressive strength determined from a non deteriorated portion of the same structural element (e.g. Figure 15B); it is generally accepted that the mechanical properties of sound concrete under field conditions improve over time and are likely significantly higher at the time of a condition assessment than the 28-day design strength [7]; 3) fixed loading of 10 MPa; this has been proposed by Smaoui et al. [5]; and 4) 40% of the compressive strength of the distressed concrete itself (Figures 15C and 15D).

A



B



C



D



Figure 15: Pictures illustrating the variations in ASR-related damage in a bridge structure. A. General view of the structure. B. portion of the abutment wall protected from direct moisture under the bridge deck. B. Portion of the abutment wall exposed to moisture. C. Portion of the wing wall exposed to moisture [23].

In order to evaluate and illustrate the effect of the various testing parameters/options mentioned above for concrete condition assessment using the SDT, the results of three test series are presented in the next subsections. These are represented by different scenarios for concrete condition assessment using the SDT illustrated in Figure 16. The Line 1 represents the “typical” compressive strength development of a sound (or less distressed) conventional concrete over time. In that case, the concrete strength keeps improving over time up to the point it reaches a plateau (i.e. point X% - about 25 to 30% increase from the 28-day value). The Line 2 (dotted line) illustrates the behavior of an aging concrete structure affected by a slowly-developing deleterious mechanism. In that case, the compressive strength of the concrete improves for a certain period until the deleterious mechanism starts developing, thus

compromising the progress in compressive strength (Y% of loss). This is often the case for structures affected by ASR considering that ASR is known not to affect the compressive strength of concrete until a very high expansion level is reached. The Line 3 (dashed line) presents a concrete undergoing relatively rapid/extensive distress, which resulted in a sharp decrease in compressive strength over time (Z% of loss).

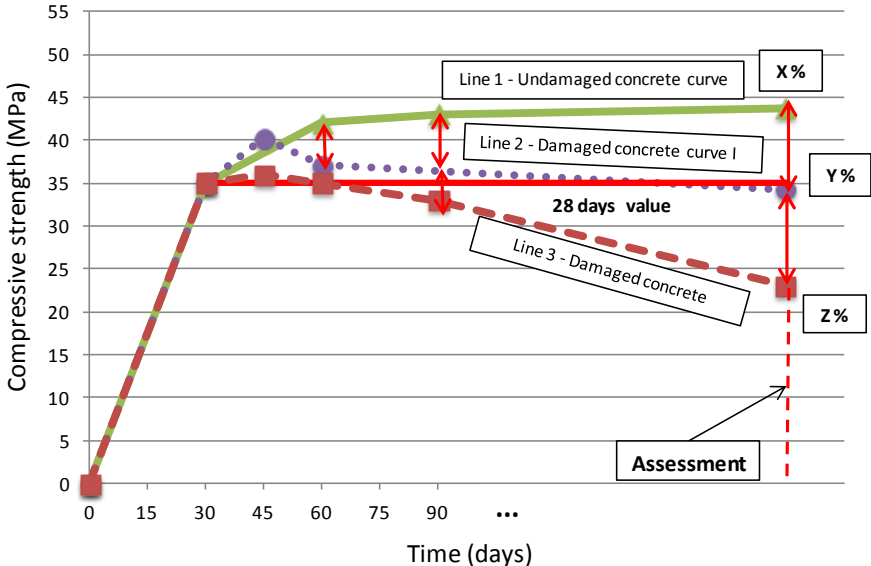


Figure 16: Qualitative plot representing ASR (or other damage mechanisms) damage over time.

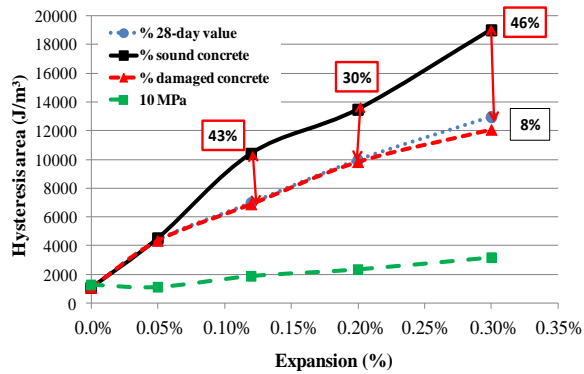
Test Series no. 1

In this first test series, a number of cylinders, 100 x 200 mm in size, were cast from two 35 MPa concrete mix designs manufactured in the laboratory. The first mix incorporates the highly-reactive Tx sand and the non-reactive Dia coarse aggregate, while the second one is made with a non-reactive granitic sand and the same non-reactive coarse aggregate (Dia); the characteristics of the above aggregates are given in Table 2. Both mixes presented the same materials contents (in volume) and the same water cement ratio; details on the mix designs are given in [6]. For this study, four ASR expansion levels were chosen for analysis (0.05%, 0.12%, 0.20% and 0.30%) and when the ASR distressed samples reached each of the above expansions level, three specimens (per mix) were tested in compression, thus enabling the determination of the compressive strength of both sound and damaged concrete at the time of the “assessment”. Figure 16 illustrates the typical compressive strength development obtained for both mixtures as a function of time (i.e. Undamaged concrete curve (Line 1) and Damaged concrete curve 1 (Line 2), while Figure 17 presents the differences in the SDT output responses for the following options of loading levels: 1) 40% of the 28-day design

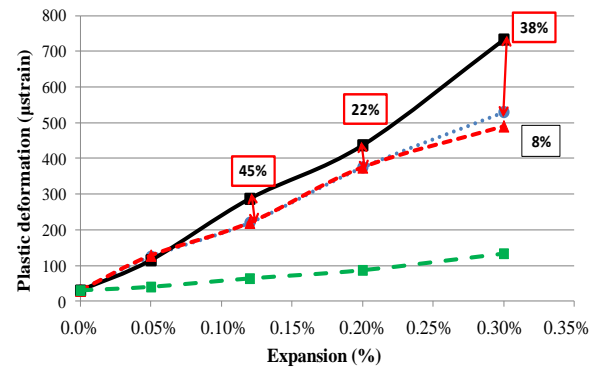
compressive strength; 2) 40% of the compressive strength determined from the sound (non-reactive) concrete specimens of the same age as the reactive concrete; 3) use of a fixed loading of 10 MPa; and 4) 40% of the compressive strength of the damaged concrete mixture. It is good to mention that the test results for the 10 MPa loading level were obtained through the assessment of a 35 MPa concrete mixture made with the Tx sand and a non-reactive limestone (HP) (Table 2). Even though both concrete mixtures (Tx sand + HP and Tx sand + Dia) presented the same mix design and the same material contents in volume, one could consider that as the mixes presented different non-reactive coarse aggregates, they could show different responses over the SDT for the same ASR distress. However, as presented in [6], these differences are not considered significant for the *Hysteresis Area* and *Plastic Deformation* parameters. On the other hand, a more significant change is found for the *Modulus of Elasticity* values.

One can see in Figures 16 that the variation in compressive strengths between the reactive (Line 2, Figure 16) and the non-reactive (Line 1, Figure 16) concretes over the 60-day testing period required to reach the 0.30% expansion in the reactive concrete ranged from +3% to -18%. The differences in the loading level used for the different scenarios of stiffness damage testing for the four sets of cylinders at the selected expansion levels are given in Table 6. These changes induced differences for the *Hysteresis Area* (HA) parameter ranging from 30 to 46% (Figure 17A), and from 22 to 38% for the *Plastic Deformation* (PD) parameter (Figure 17B) for scenarios using a loading level based on a percentage basis. Moreover, the graphs clearly show that the use of a fixed load of 10 MPa, as proposed by [5], would not indicate significant differences in damage between the concrete specimens tested (i.e. affected by expansions ranging from 0.05 to 0.30%) when considering the HA and PD parameters. On the other hand, the use of loading levels corresponding to 40% of 28-day design strength values and 40% of damaged concrete strengths resulted in very similar HA and PD values for all expansion levels. This is due to the fact that the compressive strength in the test specimens subjected to accelerated curing for ASR testing was still improving for a while despite the development of ASR; this resulted in similar loading levels being applied for stiffness damage testing (Testing options 2 (28 days line in Figure 16) vs. 4 (Line 2 in Figure 16); Table 5). Also, one can see on Figures 17A and 17B that after the 0.12% expansion level, similar rates of increasing HA and PD values were obtained as a function of expansion (i.e. parallel lines), no matter which option of loading level (i.e. 40% of either 28-day strength, 40% of non-reactive concrete or 40% of the strength of the ASR-affected concrete) is selected for stiffness damage testing.

A – HA (five cycles)



B – PD (five cycles)



C – ME (Avg of 2nd and 3rd cycles)

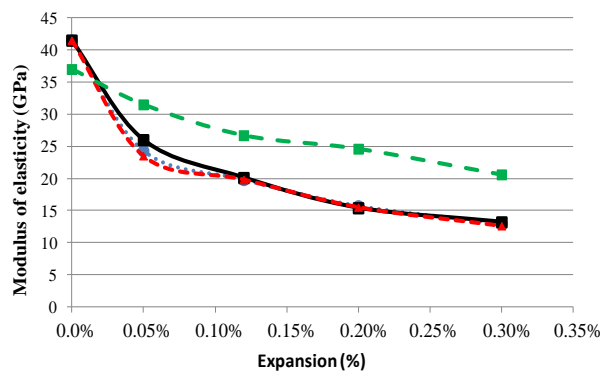


Figure 17: Effect of the specimen's loading level on SDT output parameters for test specimens cast from a reactive and a non-reactive 35 MPa concrete mixtures. A) Hysteresis area (HA) - J/m³ (5 cycles); B. Plastic deformation (PD) – μstrain (5 cycles) and; C) Modulus of elasticity (ME) – GPa (average value of the second and third cycles). Each data points on the graphs represent the average of the results obtained on three test specimens.

Interestingly, no significant impact on the "diagnostic character" of the *Modulus of Elasticity* (ME) parameter resulted from the use of the different loading levels in % (Figure 17C). Exception was seen for the 10 MPa fixed loading scenario. The increase in strength of about 18% over 2 months for the non-reactive concrete, i.e. from 35 MPa to 41.5 MPa, made that the use of 14 MPa loading level (which represents 40% of 35 MPa) represents 34% of 41.5 MPa. Therefore, it seems that the modulus of elasticity of the concretes is not largely affected when this test is performed between 30% and 40% of the concrete strength.

Table 6: Different loading levels used for the test series no. 1.

Expansion level	Loading level used for stiffness damage testing			
	Testing option 1	Testing option 2	Testing option 3	Testing option 4
	Fixed loading (MPa) (as per [5])	40% of 28-day design strength (MPa) (as per [6])	40% of sound concrete (same age) (MPa)	40% of damaged concrete (\neq expansion levels) (MPa)
0.05%	10	14	15.8	13.8
0.12%	10	14	15.8	13.9
0.20%	10	14	16.5	13.2
0.30%	10	14	17.3	12.9

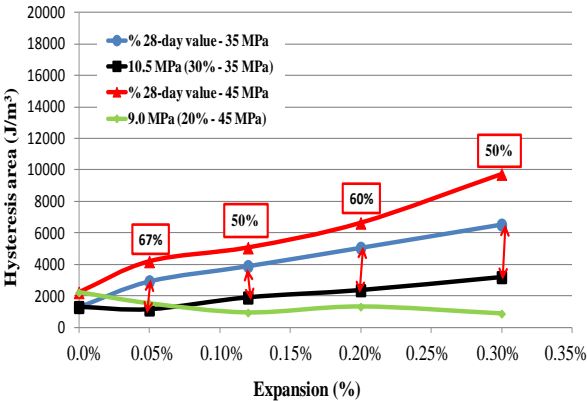
Test Series no. 2

This particular test series was carried out to further evaluate the impact of using a fixed loading level (as proposed by [5]) or loadings corresponding to a percentage of the design strength (as proposed by [6]) when carrying out stiffness damage testing on concrete mixtures of different design strengths. For this study, concrete cylinders, 100 by 200 mm in size, were made from 35 and 45 MPa concrete mixtures incorporating the reactive Tx sand and a non-reactive limestone (HP – Table 2); details on the mix designs are given in [6]. The specimens, by sets of three, were tested in the SDT at expansion levels ranging from 0.05 to 0.30% and using: a) 40% of the 28-day compressive strength, i.e. 14 and 18 MPa for the 35 and 45 MPa concretes, respectively; and b) a fixed loading at about 10 MPa, as proposed by [5] (i.e. 10 MPa \pm 1 MPa; representing either 30% of 35 MPa or 20% of 45 MPa, respectively).

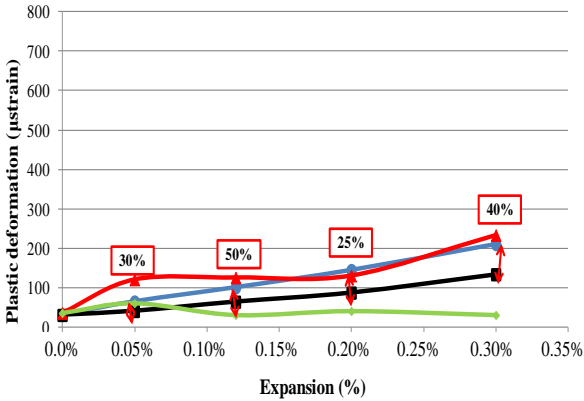
The results of this series of test, illustrated in Figure 18, clearly show, once again, the huge impact of the loading level on the results of stiffness damage testing. First, the use of a fixed loading level of about 10 MPa induced low and fairly similar *Hysteresis Area* and *Plastic Deformation* values for both 35 and 45 MPa concretes, thus suggesting a somewhat limited diagnostic capacity of that procedure for determining the expansion level (indirect measurement of internal damage) of the test specimens. Second, the gaps between the two testing scenarios, i.e. use of 40% of the 28-day design concrete strength versus fixed 10MPa fixed load, increases with increasing strength of the concrete. The differences when 10 MPa was used compared to the 28-day design strengths ranged from 50% to 67% for the *hysteresis area* (Figure 18A) and from 25% to 50% for the plastic deformation (Figure 18B) parameters depending on the different expansion levels for the 35 MPa concretes. The ranges between these two scenarios were actually much greater for the 45 MPa concretes. In other words, the use of a fixed loading level of 10 MPa will cause misleading evaluation/quantitative assessment of the internal damage in concrete that will be worst and worst with increasing

mix design strength of the concrete. Similarly to the Test Series no. 1, very similar reduction rates in modulus of elasticity were obtained as a function of the loadings level used (Figure 18C), with the exception of the use of the fixed load (10 ± 1 MPa) on the 45 MPa concrete mixture at the higher expansion levels.

A – HA (five cycles)



B – PD (five cycles)



C – ME (Avg of 2nd and 3rd cycles)

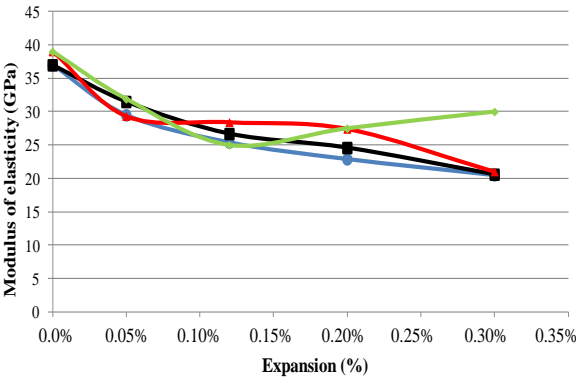


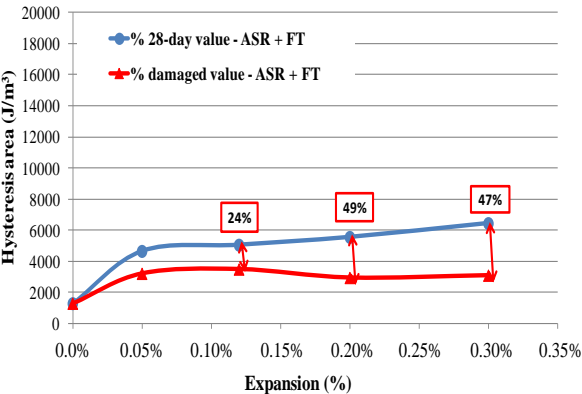
Figure 18: Effect of the specimen’s loading level on SDT output parameters for test specimens cast from reactive 35 and 45MPa concrete mixtures. A) Hysteresis area (HA) - J/m³ (5 cycles); B. Plastic deformation (PD) – μstrain (5 cycles) and; C) Modulus of elasticity (ME) – GPa (average value of the 2nd and 3rd cycles). Each data points on the graphs represent the average of the results obtained on three test specimens.

Test Series no. 3

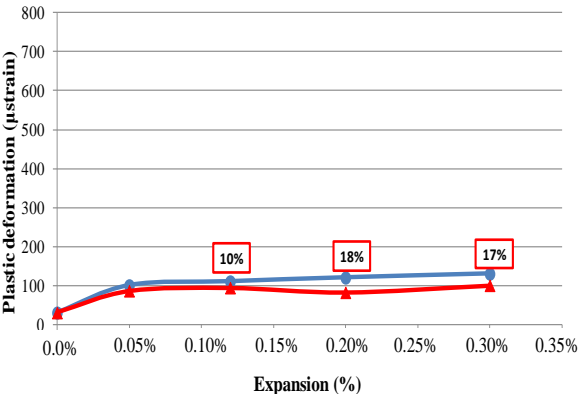
As mentioned before, ASR will often not contribute at decreasing significantly the compressive strength of concrete until very high expansions are reached, which means a small gap between the 28-day design strength value line and the Damage concrete curve I (dotted line) in Figure 17. However, other deleterious mechanisms can contribute at further reducing concrete strength in aging concrete structures. Therefore, a series of concrete cylinders, 100 x 200 mm in size, were made from a non air-entrained 35 MPa concrete mixture incorporating

the reactive Tx sand and a non-reactive limestone (HP). The specimens were first subjected to storage conditions in the laboratory conducive to ASR development (i.e. 38°C and 100% R.H.); however, when the specimens reached half of the targeted expansion levels (mentioned before), i.e. 0.025%; 0.06%; 0.10% and 0.15%, they were then subjected to freezing and thawing (FT) cycles following the ASTM C666 test condition A (freezing in air and thawing in water) to complete the other half of the desired expansion. Each test specimens, by sets of three, were stiffness damage tested using either 40% of the 28-day strength value (i.e. 14 MPa for the 35 MPa concrete) or 40% of the strength value obtained on companion specimens of the damaged specimens at each expansion level chosen for analysis (i.e. ranging from 14 to 11 MPa). The latter corresponds to the behavior illustrated by Line 3 – Damage concrete curve II in Figure 16. Figure 19 illustrates the differences in the SDT output responses obtained for the scenarios proposed.

A – HA (five cycles)



B – PD (five cycles)



C – ME (Avg of 2nd and 3rd cycles)

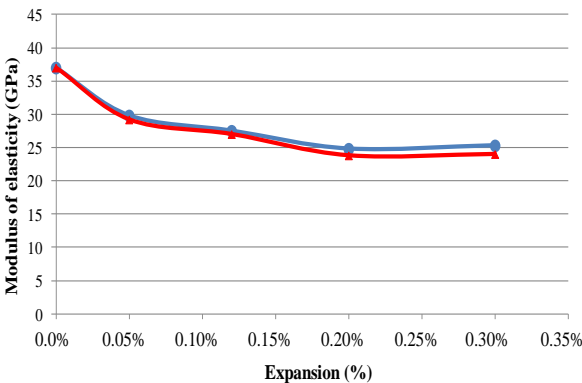


Figure 19: Effect of the specimen’s loading level on SDT output parameters for test specimens cast from reactive 35 MPa concrete mixtures and that were subjected to both ASR and freeze-thaw deterioration: A) Hysteresis area (HA) - J/m³ (5 cycles); B. Plastic deformation (PD) – µstrain (5 cycles) and; C) Modulus of elasticity (ME) – GPa (average value of the second and third cycles). Each data points on the graphs represent the average of the results obtained on three test specimens.

The results presented in Figure 19 show that both testing scenarios described above have somewhat different impacts on the various SDT output parameters (HA, PD and ME), which is likely related to the differences in the internal cracking patterns developed with increasing expansions when different deleterious mechanisms (or combinations thereof) are involved. The gaps found ranged from 24% to 49% for the Hysteresis Area parameter (Figure 19A) and from 10% to 18% for the Plastic Deformation parameter (Figure 19B), depending on the expansion level. On the other hand, very similar behaviors were obtained between the two testing scenarios for the Modulus of Elasticity parameter, as illustrated in Figure 19C; such a result had also been obtained in the case of test series no. 1 (Figure 17C). These results will be discussed further in the next section.

7.6.2.2 Comparative analysis of SDT results

The use of index parameters - Stiffness Damage Index (SDI) and Plastic deformation Index (PDI)

Based on the results of the various Test Series presented before, regarding the selection of an appropriate loading level for stiffness damage testing (illustrated in Figures 17, 18 and 19), it appears that the various scenarios analyzed provide similar global assessments of damage generation in concrete due to ASR as similar rates of increasing HA, PD or decreasing ME are obtained as a function of increasing expansion due to ASR, with the exception of the use of a fixed (10 MPa) loading level. However, these results confirm that considering absolute SDT output values (HA, PD or NE) may lead to misleading interpretations/conclusions when characterizing concrete damage due to ASR, as these values change significantly depending on numerous factors such as the concrete mix design strength and characteristics (i.e. aggregate's type, contents, etc). Moreover, in most cases, the 28-day design strength of concretes used in the construction of older structures/elements is largely unknown, which complicates the selection of the input parameters for stiffness damage testing and consequently the analysis of the output parameters for damage assessment in ASR-affected concrete. Besides that, the use of absolute threshold SDT values largely limits the understanding of what really happens in terms of damage generation in concrete as a function of ASR expansion, as its output parameters (*Hysteresis Area* and *Plastic Deformation*) are linked to the amount of energy provided to the system through compressive loading, which will always be greater for greater materials' strengths. Consequently, one could think that analyzing the SDT results in a relative manner, i.e. by using indices that take into account the

ratio of “elastic energy” (i.e. the energy recovered after loading/unloading cycles) over the “total energy” provided to the system through testing would better characterize damage generation for different materials and, moreover, would provide easier understanding of the impact of ASR (or other mechanisms) as the reaction/expansion develops.

Ozkan et al. [25], studying the stress-strain behavior of different concrete types, proposed the use of an index, which they called “*Fragility Index*”, and which represents the ratio between the elastic deformation energy (SII) and the irreversible deformation energy of a material (SI) (Figure 20).

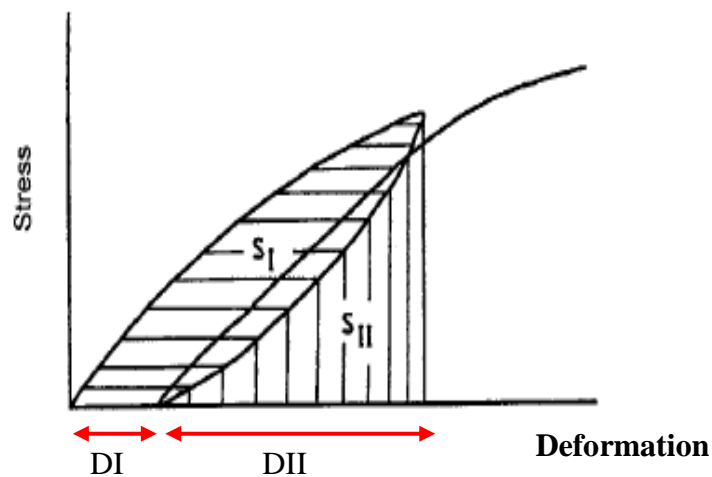


Figure 20: Fragility Index (S_{II}/S_I) proposed by [25].

According to [25], the greater is the ratio S_{II}/S_I , the more important is the material fragility. Moreover, it has been found that the *Fragility Index* changed with the material’s strength (and also stiffness). Yet, the author realized that the irreversible energy (SI) is lower with increasing concrete strength, which indicates a more brittle material. The explanation for this phenomenon is that for ordinary concrete, the differences in mechanical properties between the component/materials characteristics (cement paste, aggregates and ITZ) are more evident, thus favoring crack generation (over loading) in the zones or materials of lower strength. On the other hand, for high-performance concretes, those differences are less apparent.

The concept of “Fragility Index” makes sense for sound materials (mainly for high performance concretes) when a ductile behavior is sometimes targeted. However, in the case of damaged materials, the most practical index would likely be the following: $SI/(SI+S_{II})$, which gives the amount of energy (in %) that is consumed by the system over a cyclic loading in compression. Therefore, when the concrete material is sound, $SI/(SI+S_{II})$ is equal to zero (or a very small value). On the other hand, when the material is extremely damaged, and SI is very high, the above ratio tends to 1. The use of indices instead of the “bulk” values obtained

over SDT (i.e. HA, PD and ME parameters) still enables the comparison between different concrete strengths, as one verifies that different concrete mixtures (presenting different compressive strengths and elastic moduli) would show different SDT output values in terms of dissipated energy for the same cracking extent (i.e. the greater the concrete modulus of elasticity, the greater the amount of dissipated energy for the same extent of cracking). Therefore, the energy ratio approach described above for sound concretes could be used in the SDT assessment in two different/new parameters: a) *Stiffness Damage Index* (SDI), which would correspond to $SI/(SI+SII)$ and; b) *Plastic Deformation Index* (PDI) which would correspond to $DI/(DI+DII)$ (Figure 20).

In terms of modulus of elasticity and curve shape changes, Crisp and coworkers [1, 2] proposed the Non Linearity Index, (NLI) which represents the ratio of the slope of the stress response at half the maximum load (red/tangent straight line) over the secant modulus of elasticity (ME – dark/secant straight line) at 40% of the concrete strength. According to the authors, this index provides information about either the crack extent or the crack pattern (i.e. distribution, directions, etc.) of the distressed samples. They found that samples with a main cracking pattern perpendicular to loading show NLI greater than unity, while those with a main cracking pattern parallel to loading displayed a high modulus of elasticity, and a NLI lower than or even equal to unity. Therefore, NLI could also be used and an output SDT parameter to add information about distress on ASR affected specimens or cores.

A – Damaged concrete

B – Sound Concrete

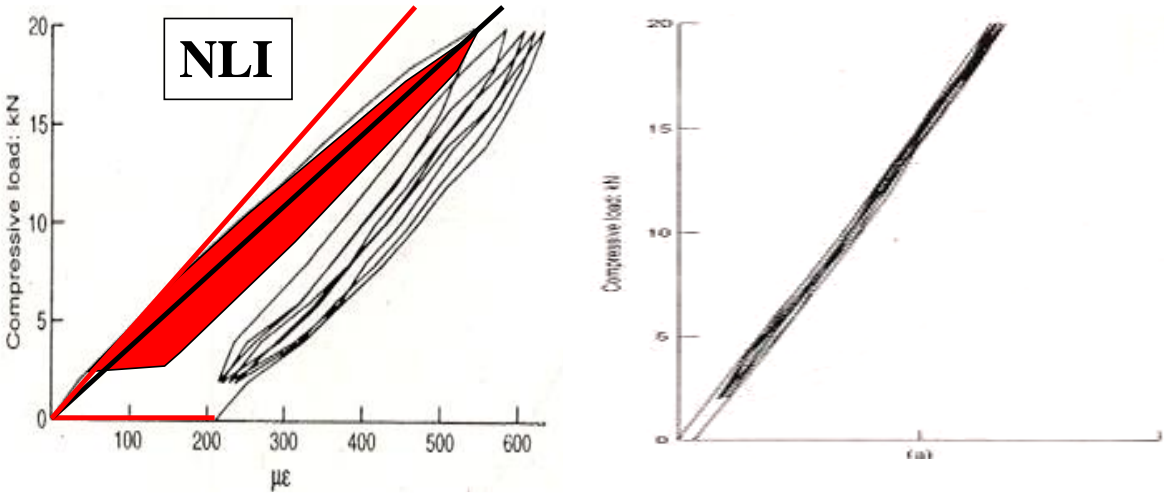
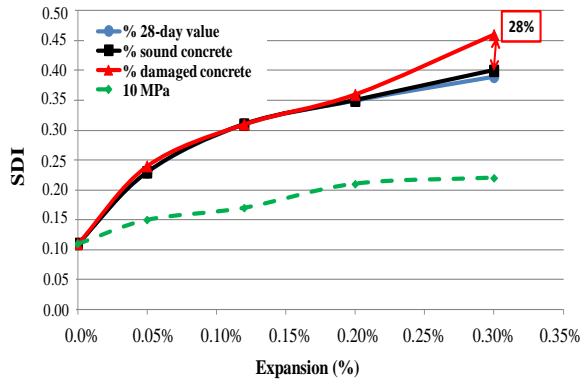


Figure 21: NLI values for a) damaged concrete (left) and b) sound concrete (right) [1, 2].

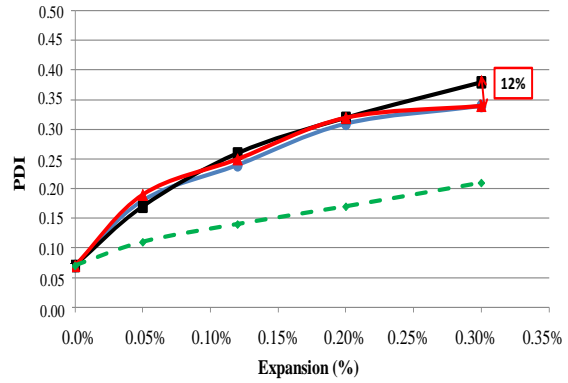
Impact on the results of Test Series 1 to 3

Figure 22 illustrates the results of stiffness damage testing reported previously in Figure 17 (Test Series no. 1), but this time calculated according to both indices mentioned above (SDI and PDI). Moreover, NLI index (which was proposed by [1, 2] and presented in [6]) was used as an indicator of the modulus of elasticity and curve shape changes against distress. The results in Figure 22 indicate that when the indices described above are used instead of the bulk HA or PD values (Figure 17), the gaps between the SDT output responses for the different testing scenarios involving a "%" approach decrease significantly and that interesting relationships can be observed between the indices and the expansion of the test specimens. Thus, the use of 40% of the 28-day mix design strength or 40% of the strength of sound (or less distressed) concrete measured at the time of the assessment provided almost the same responses (gaps lower than 5%). Likewise, the use of 40% of the strength measured at the time of the assessment on the damaged concrete under investigation showed similar responses, except for the expansion level of 0.30% where the gap between this approach and the 28-day and sound concrete approaches was about 28% for the SDI. The same considerations can be made for the PDI, as the most important gap was about 12%. Likewise, regarding the NLI, relatively similar values were obtained from the three "%" scenarios (Figure 22C). The results in Figure 22 also clearly show that even with the use of indices, fairly different responses are obtained when the SDT is performed with a fixed loading level (as proposed by [5]), which is characterized by lower increases in the Index values as a function of expansion.

A – SDI- five cycles



B – PDI - five cycles



C – NLI – first cycle

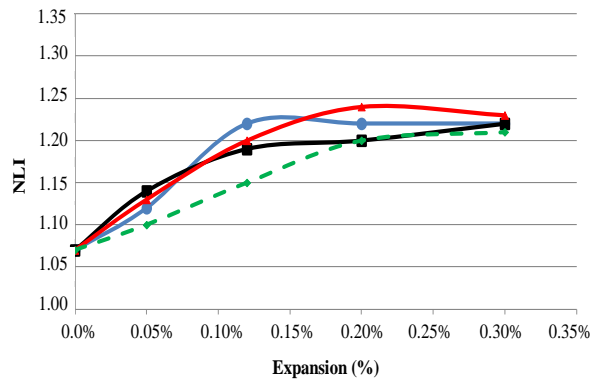
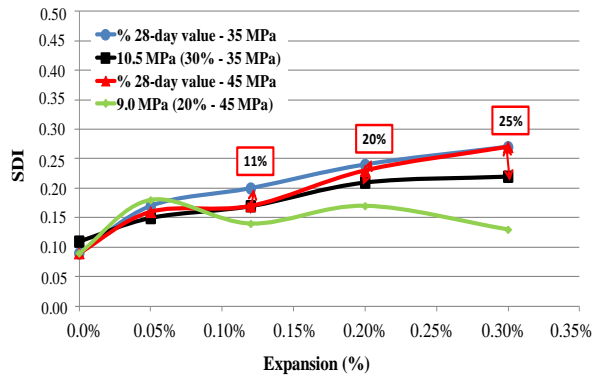


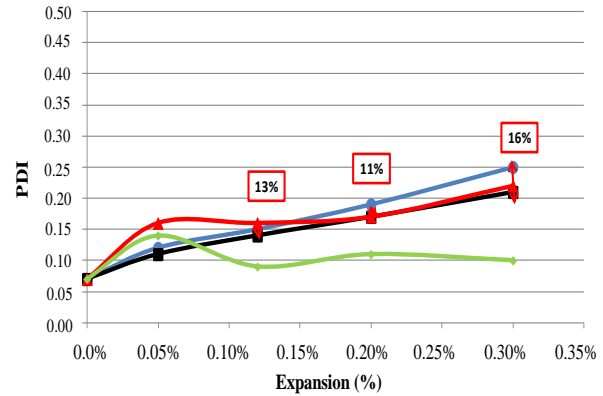
Figure 22: The use of Indices as SDT output parameters for the test series no 1 and for the parameters SDI (5 cycles), PDI (5 cycles) and NLI (first cycle).

Figure 23 illustrates the results of stiffness damage testing reported previously in Figure 18 (Test Series no. 2), but this time calculated according to both indices mentioned above (SDI and PDI). Once again, these results show that fairly similar responses for the SDI, PDI (and \approx NLI) parameters are obtained when the “40% of 28-day strength approach”, are used for stiffness damage testing; However, when the approach proposed by [5] is used (i.e. fixed 10 MPa load level) for both the 35 MPa and 45 MPa concrete mixtures, the results were not satisfactory, showing deviations which ranged from 11% to 25% for SDI and from 11% to 16% for PDI. Therefore, these results confirm the importance of using a % of the concrete strength instead of a fixed loading on the SDT procedure, even with the use of SDI, PDI and NLI indices.

A – SDI- five cycles



B – PDI - five cycles



C – NLI – first cycle

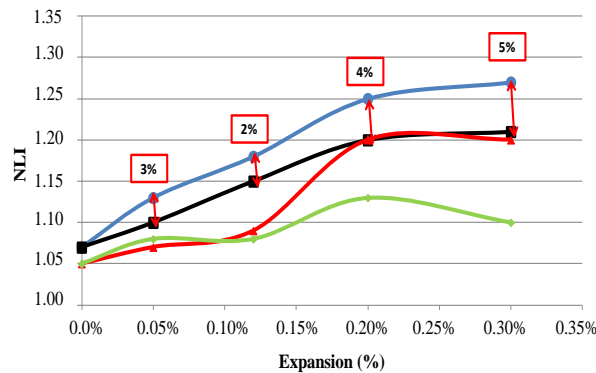
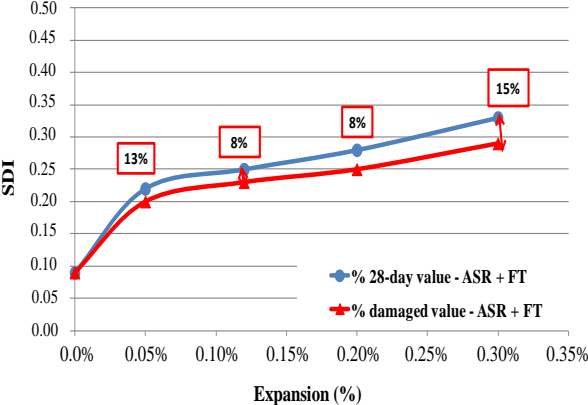


Figure 23: The use of Indices as SDT output parameters for the test series no. 2, and for the parameters SDI (5 cycles), PDI (5 cycles) and NLI (first cycle).

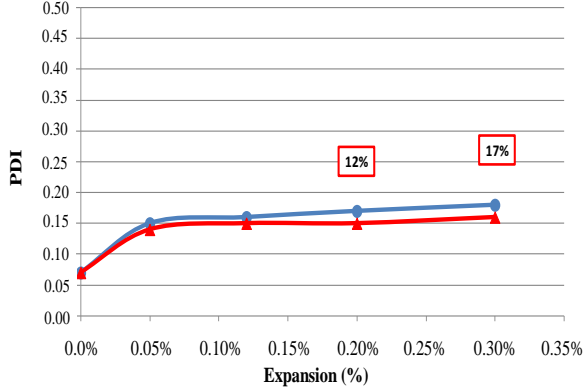
Finally, Figure 24 illustrates the results of stiffness damage testing reported previously in Figure 19 (Test Series no. 3), but this time calculated according to all indices mentioned above (SDI, PDI and NLI). The concrete affected by freeze-thaw cycles shows a higher loss in compressive strength with increasing expansion (similar to Line 3: Damaged concrete curve II in Figure 16), compared to test specimens affected by ASR only (see Line 2: Damaged concrete curve I in Figure 16); despite that, the results in Figure 19 show that fairly similar patterns are obtained for the SDI, PDI (and \approx NLI) parameters as a function of increasing expansion when the two scenarios investigated are used for stiffness damage testing (i.e. "40% of 28-day strength" vs. "40% of the damaged value"). However, slightly higher index values are obtained for the ASR + FT specimens, likely due to higher internal damage in those concretes with increasing expansion (see section 7.6.3.1) (Figure 24). Interestingly, these results conflict with those obtained over the Test Series 1 (see Figure 22),

i.e. when ASR only is affecting the concrete, where both loading scenarios gave about the same values of SDI and PDI (except at the highest expansion level); the difference is likely associated to the combined effect of ASR + FT that enhances internal damage in concrete and increases losses in strength with increasing expansion.

A – SDI- five cycles



B – PDI - five cycles



C – NLI – first cycle

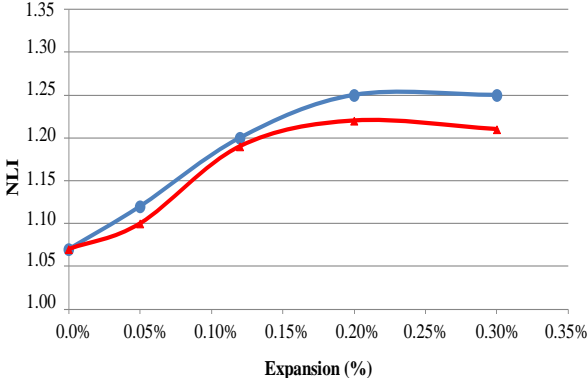


Figure 24: The use of Indices as SDT output parameters for the test series no. 3, and for the parameters SDI (5 cycles), PDI (5 cycles) and NLI (first cycle).

7.6.3 Validation of the SDT for assessing damage in concrete

The results of testing carried out in this study on laboratory-manufactured specimens and cores extracted from a structure in service showed that the results of damage assessments using the SDT generally correlated well with those obtained through semi-quantitative petrographic examination when the DRI procedure is carried out on companion specimens (cylinders from the same set or cores extracted from the same structural elements or zones (exposed – non exposed; surface/top or core/bottom portions)) [26]. Figure 25 presents the results of the petrographic examination (DRI) of laboratory-made concrete specimens affected

by ASR only and ASR + FT. In both cases, the greater is the expansion level, the greater is the DRI number, as expected. Sanchez et al. [26] showed that the most important damage feature in ASR-affected concrete is the presence/development of *Opened cracks (with and without gel) in the aggregate particles and cracks in the cement paste (with and without gel)*, which is highlighted in Figure 25A. In the case of concrete specimens affected by ASR + FT specimens, the critical features of deterioration also correspond to *Opened cracks in the aggregate particles* and *Cracks in the cement paste* (see Figure 25B). The bar charts of Figure 25 however suggest that larger amounts of secondary reaction products (e.g. ASR gel...) can be found in cracks (aggregate particles and cement paste) for the test specimens affected by ASR + FT (Figure 25B) than for those affected by ASR only (Figure 25A), which seems somewhat surprising. Actually, the identification of the presence and the nature of the above secondary products is difficult at the magnification used for the DRI, especially in the case of ASR generated in the sand fraction, and additional investigations (e.g. under SEM + EDXA) are required to confirm the exact nature of the above products. However, since identical factors were used for *opened cracks in the aggregate particles* (factor of 2) or *cracks in the cement paste* (factor of 3), with or without reaction products (according to [19]; Figure 3), the presence or not of secondary products in cracks of the aggregate particles and the cement paste has no incidence on the DRI numbers obtained. Overall, the difference in the DRI values of the two sets of specimens is related to the presence of extensive cracking in the cement paste of the (non air-entrained) concrete subjected to freeze-thaw attack.

A: 35 MPa ASR affected specimens

B: 35 MPa ASR + FT affected specimens

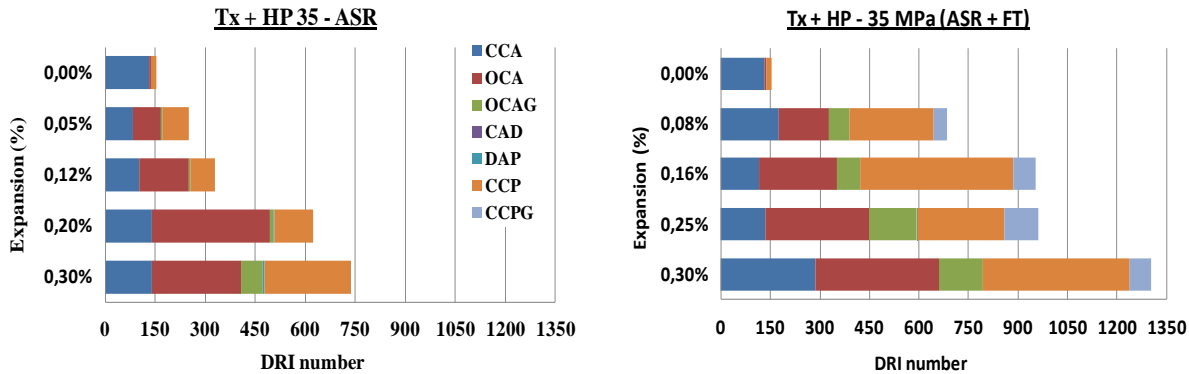


Figure 25: DRI numbers for ASR and ASR + FT mechanisms.

Figure 26 shows the correlation between the SDI, PDI and NLI parameters and the DRI numbers illustrated in Figure 25B, for both deleterious mechanisms combined. The data indicate that an evaluation of the extent and progress of internal distress with increasing

expansion in concrete due to deleterious mechanisms like ASR + FT can invariably be obtained from the use of the three main SDT output parameters described before (SDI, PDI and NLI), when either 40% of the 28-day design strength or 40% of the strength of the deteriorated concrete is used to select the loading level for stiffness damage testing.

The results presented in Figures 22, 23, 24 and 26 indicate that the use of the *Stiffness Damage Index* (SDI) and of the *Plastic Deformation Index* (PDI) reduces the risk of misleading interpretation based on an appropriate choice of SDT input parameters (i.e. selection of the loading level). Also, the use of the above indices validates the approach of using 40% of a measured strength value in situ (instead of a fixed loading level). However, the use of a loading level corresponding to 40% of the compressive strength of cores obtained from a sound (or even less damaged) concrete at the time of the assessment is a more logical choice for condition assessment using the SDT. If a concrete material had not suffered from significant damage due to any distress mechanism it would have reached higher strength levels due to a progress in cement hydration (which can be measured in the field through cores extracted in zones not or even less damaged). Therefore, the use of 40% of this “sound” value for loading damaged concrete samples involves stressing the material in the same way than a sound material would be stressed, which enables the comparison of sound vs. damaged responses, thus indicating the real physical integrity losses affecting the distressed concrete material.

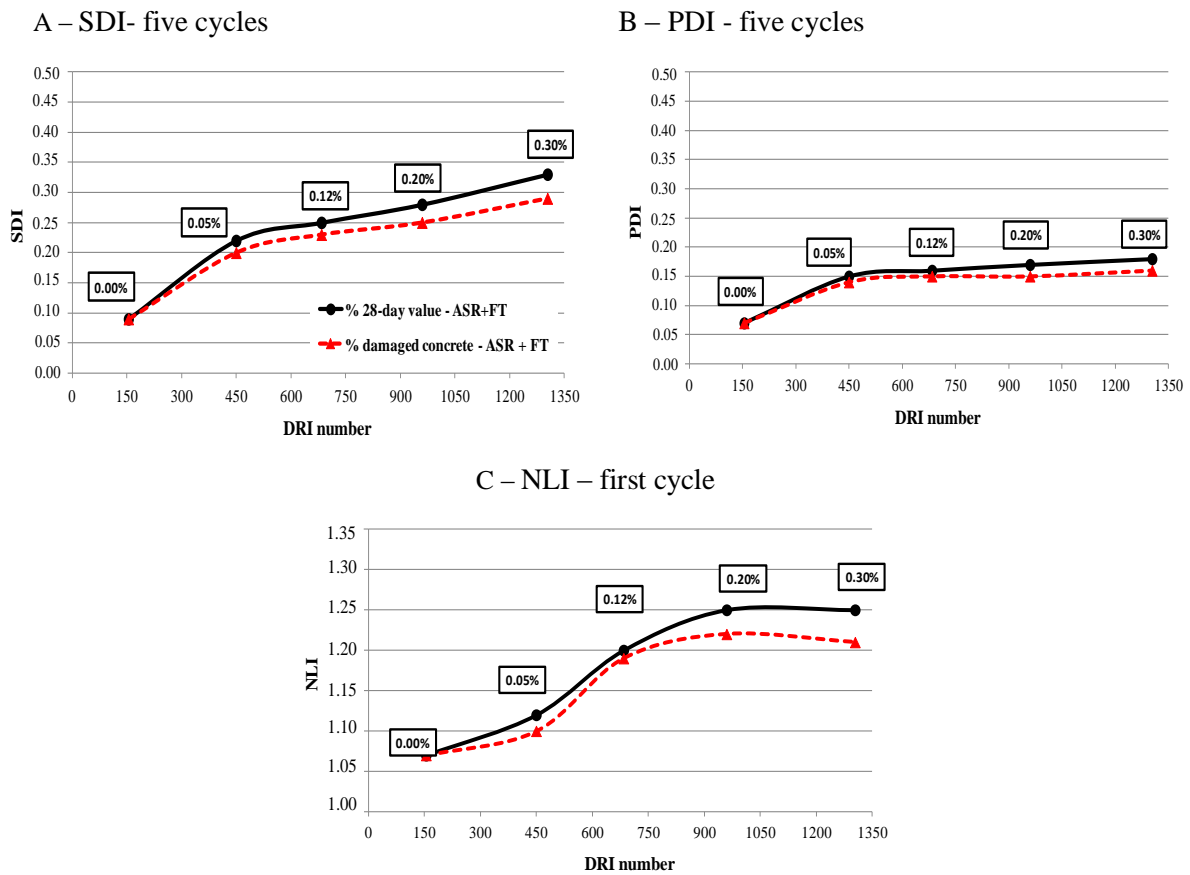


Figure 26: Correlation between the SDI, PDI and NLI parameters and the DRI numbers for ASR + FT mechanisms.

7.6.4 Stiffness damage test procedure

This study has shown that various SDT input parameters can impact significantly on the output responses of the procedure, e.g. the environment and zone of the specimens (exposed vs. not exposed element; core vs. surface zone, the conditioning history of the core (exposure to moisture condition prior to testing) and the length/diameter ratio. The selection of the loading level is certainly amongst the parameters that most largely influence SDT output responses. The use of the *Stiffness Damage Index* (SDI) and of the *Plastic Deformation Index* (PDI), instead of the absolute output parameter values (HA, PD and ME) suggests that quantitative damage assessment can be achieved through this mechanical and cyclic procedure, and yet this approach is less dependent of the 28-day strength knowledge.

Based on the various series of test results presented in this paper, a "preliminary" flow chart is proposed for the damage assessment in ASR-affected concrete structures using the SDT (Figure 27). This should be considered as "work in progress" as information such as *classes of damage* using the SDI, PDI and NLI have not yet be established and will require additional work with a wider range of reactive aggregates and concrete mix designs. However, it should

be considered as a basis allowing further comparisons and aims at minimizing potential distortions between different operators interested in using the SDT in practical engineering applications.

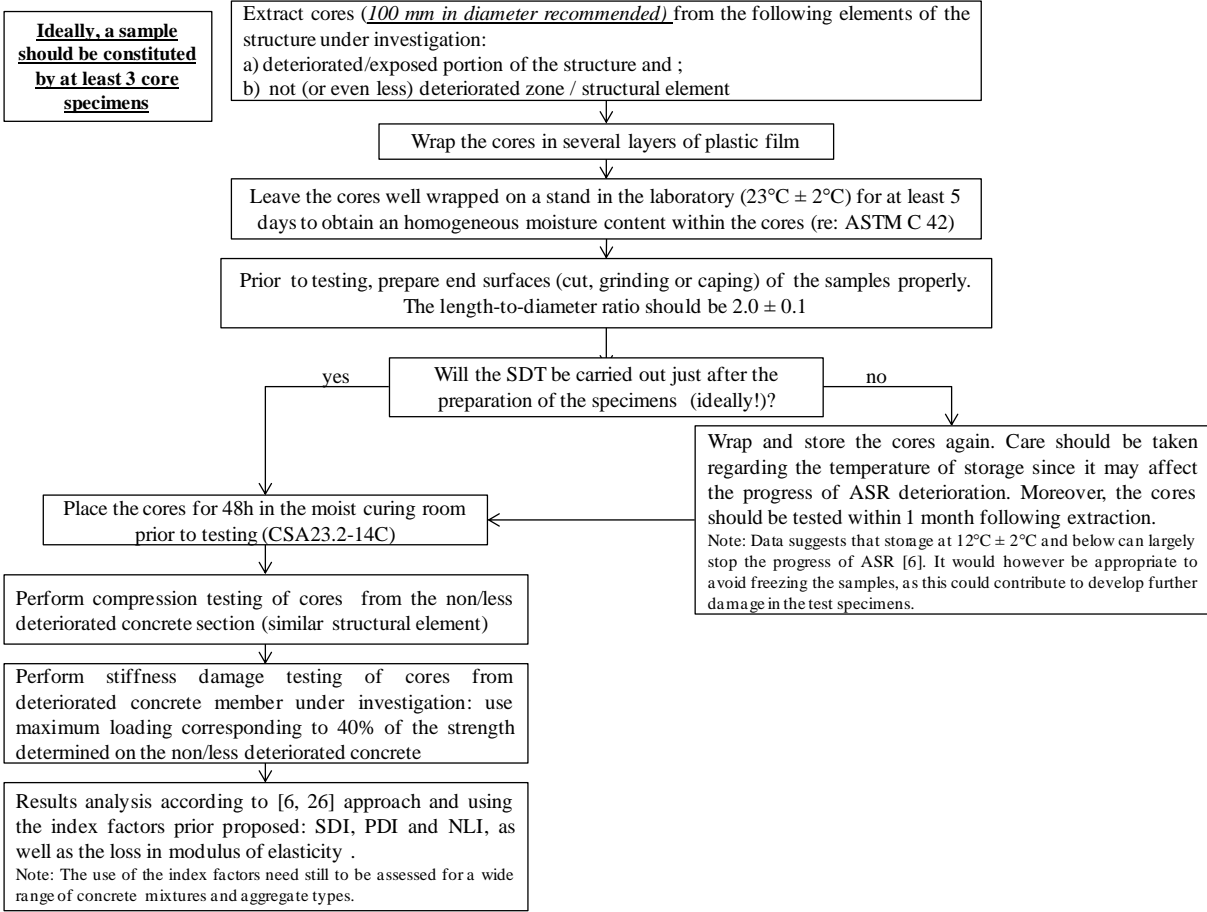


Figure 27: SDT standard and practical procedure.

7.7 CONCLUSIONS

In this work, several input parameters were tested through the SDT procedure with the aim of verifying their influence on the test responses. After analyzing the results, the main conclusions are as follows:

- When a damage assessment is carried out on an aging concrete structure/element potentially affected by ASR, one should take into account the environmental characteristics of the specimens (cores) extracted, such as the core depth from the surface, the exposure condition of the element investigated, etc. All of these parameters largely influence the SDT responses and thus the conclusions that can be drawn from the test results;

- It has been found that significantly different values for all the SDT output parameters are obtained for cores extracted from exposed and not exposed portions of the structure investigated, confirming a greater damage in the sections exposed to moisture. Likewise, SDT and DRI test results confirmed that the degree of damage can vary as a function of the depth in the exposed and non-exposed elements investigated;
- Length-to-diameter ratios smaller than 2.0 can significantly affect the results of stiffness damage testing, especially the *hysteresis area* and *plastic deformation* parameters. Thus, the results suggest that the core shape play a very important role in this procedure. Moreover, the closest the above ratio is to 2.0, the lower is the variability between the specimens, which means that the test is more accurate when a 2.0 length/diameter is used. In addition, the use of a greater sample size (e.g. cores of 150 mm by 300 mm in size) did not show important variations in the tests results (when a 2.0 length/diameter ratio is used);
- The moisture condition (conditioning history) of the specimens prior to testing can largely influence the responses over SDT. It seems that drying of the cores/test specimens increases their stiffness and elastic modulus, while decreasing both the *hysteresis area* and the *plastic deformation* values measured over stiffness damage testing. The drying effect was also found to affect specimens that were well wrapped in plastic sheets, but to a much lower degree. However, a 48-hour rewetting period was found to reduce the bias due to drying, restoring the initial conditions of the specimens and thus enabling reliable condition assessment. Meanwhile, it has been found that the standard deviation can increase when a rewetting period is applied, especially if the concrete specimens have been stored for a lengthy time period before stiffness damage testing.
- The different types of end surface preparation (capping vs. grinding) do not seem to influence significantly the SDT responses;
- The statistical evaluation of the results obtained in this study was performed following a two-variable variance analysis (ANOVA). This analysis confirmed the importance and impact of the various parameters presented and discussed before. The use of the absolute (bulk) SDT output values for characterizing concrete damage due to ASR can be misleading, as they are very sensitive to the concrete design strength and characteristics (i.e. aggregate's type, contents, etc). Moreover, in most of the cases, the 28-day strength of concretes used in the concrete structures/elements under evaluation is not known. Beyond that, the use of absolute SDT output values limits the understanding of what really happens in terms of damage generation, as the output parameters (*hysteresis area*

and *plastic deformation*) are linked to the amount of energy implemented in the system (which will be always greater for concretes of greater design strengths).

- The use of indices (SDI and PDI), which take into account the ratio “dissipated energy/total energy” implemented in the system, better represents damage for different materials and, moreover, provides easier understanding of what happens due to ASR as the expansion develops.
- Testing has shown that the greater the compressive strength reduction in concrete due to ASR or other mechanisms, the greater is the gap between the use of 40% of the sound concrete (or of the 28-day value) and the use of 40% of the damaged concrete strength as the test loading level; this means that for practical purposes, SDT should ideally be performed at 40% of a sound (or even less damaged) concrete at the time of the assessment to become a quantitative concrete damage assessment tool;
- The SDT seems to be a powerful tool for assessing damage in concrete structures/elements affected by ASR or even other distress mechanisms. However, more work is still needed (e.g. using a wide range of aggregates types and mechanisms of distress, like freezing and thawing, DEF, etc.) so that SDT could be implemented in practical engineering applications.
- A practical approach was proposed for damage assessment in concrete affected by ASR using the SDT, which should be considered prior to testing in order to generate reliable results.

7.8 ACKNOWLEDGEMENTS

The funding of this project was provided by a grant from the Quebec Department of Transportation, under the supervision of Mr. Alain Hovington and Mrs. Nadia Pouliot. The authors would like to thank Mr. René Malo and Mr. Mathieu Thomassin from “le Centre de recherche sur les infrastructures en béton (CRIB)” at Laval University, as well as the undergraduate research assistants who helped with the manufacturing and testing of the test specimens used in this project. L. Sanchez benefits from a Vanier scholarship financed by NSERC (Natural Sciences and Engineering Research Council of Canada).

7.9 REFERENCES

- [1] Crisp, T. M.; Waldron, P.; Wood, J. G. M. 1993. Development of a non destructive test to quantify damage in deteriorated concrete. *Magazine of Concrete Research*, 45, n° 165, 247-256.
- [2] Crisp, T. M.; Wood, J. G. M.; Norris, P. 1989. Towards quantification of microstructural damage in AAR deteriorated concrete. *International Conference on Recent Developments on the Fracture of Concrete and Rock*, The University of Wales, Cardiff, September 1989, 9p.
- [3] Walsh, J. B. 1965. The effects of cracks on the uniaxial elastic compression of rocks, *J. Geophys. Res.*, 70, 339 - 411.
- [4] Crouch, R. S. 1987. Specification for the determination of stiffness damage parameters from the low cyclic uniaxial compression of plain concrete cores. Revision A, Mott, Hay & Anderson, Special services division, internal technical note.
- [5] Smaoui, N.; Bérubé, M.A.; Fournier, B.; Bissonnette, B.; Durand, B. 2004. Evaluation of the expansion attained to date by concrete affected by ASR - Part I: Experimental Study. *Canadian Journal of Civil Engineering*, 31, 826-845.
- [6] Sanchez, L.; Fournier, B.; Jolin, M.; Bastien, J. Evaluation of the Stiffness Damage Test (SDT) as a tool for concrete's assessment damaged due to ASR – test loading and output responses for concretes incorporating fine or coarse reactive aggregates. *Cement and concrete research*, 56: 213-229.
- [7] Mindess, S.; Young, J. F.; Darwin, D. *Concrete*. 2003. Book. Pearson Education Ltda, second edition.
- [8] ASTM C42 / C42M. 2013. Standard Test Method for Obtaining and Testing Drilled Cores and Sawed Beams of Concrete. ASTM International, West Conshohocken (USA), 2013.
- [9] CSA23.2-14C. 2009. Obtaining and Testing Drilled Cores For Compressive Strength Testing. Canadian Standards Association, Mississauga, Ontario (Canada),
- [10] ASTM C469/469M. 2010. Standard Test Method for Static Modulus of Elasticity and Poisson's Ratio of Concrete in Compression. ASTM International, West Conshohocken (USA), 2013.
- [11] Smaoui, N.; Bérubé, M. A.; Fournier, B.; Bissonnette, B. 2004b. Influence of specimen geometry, orientation of casting plane, and mode of concrete consolidation on expansion due to ASR. *Cement, concrete and aggregates*, 26 (2), 58-70.
- [12] Bérubé, N.; Smaoui, N.; Fournier, B.; Bissonnette, B.; Durand, B. 2005. Evaluation of the expansion attained to date by concrete affected by alkali-silica reaction. Part III: Application to existing structures. *Canadian journal of civil engineering*, 32, 463-479.
- [13] EUROCODE 2 - COMMENTARY. 2008. European Concrete Platform ASBL.
- [14] Fournier, B.; Bérubé, M.A. 1991. Évaluation du potentiel de réactivité alcaline des granulats à béton produits dans les Basses-Terres du Saint-Laurent du Québec (Canada). *Revue canadienne de génie civil*, 18(2), 282-296.
- [15] Sanchez, L, Salva, P., Fournier, B, Jolin, M., Pouliot, N., Hovington, A. 2012. Evaluation of damage in the concrete elements of the viaduct “Du Vallon Charest” after nearly 60 years in service. *Proc 14th Int Conf on AAR*, May 20-25th 2012, Austin (Texas), electronic.
- [16] ASTM C 39. 2012. Standard Test Method for Compressive Strength of Cylindrical Concrete Specimens. ASTM International, West Conshohocken (USA), 2012.
- [17] ASTM C 1074. 2011. Standard Practice for Estimating Concrete Strength by the Maturity Method. ASTM International, West Conshohocken (USA), 2011.
- [18] Grattan-Bellew, P.E.; Danay, A. 1992. Comparison of laboratory and field evaluation of AAR in large dams, *Proc. of the Int. Conf. on Concrete AAR in Hydroelectric Plants and Dams*, Canadian Electrical Association & Canadian National Committee of the Int. Commission on Large Dams, September 28 – October 2 1992, Fredericton, New Brunswick, (Canada), 23p.
- [19] Villeneuve, V; Fournier, B. 2009. Détermination de l'endommagement du béton par méthode pétrographique quantitative. 2009 Annual Progress in Concrete Technology Conference, Québec and Eastern Ontario Chapter of ACI, Boucherville, Québec (Canada), November 2009.
- [20] Sanchez, L. F. M.; Fournier, B.; Jolin, M.; Bedoya, M. A. B. 2013. Evaluation of the microscopic ASR features through the Damage Rating Index (DRI) for different concrete strengths and aggregate types (fine vs. coarse aggregates). Extended abstract - 14th Euroseminar on Microscopy Applied on Building Materials (EMABM), 10-14 June 2013, Helsingør, Denmark.

- [21] Institution of Structural Engineers. 1992. Structural effects of alkali-silica reaction. Technical guidance on the appraisal of existing structures. Report of an IStructE task group. London, SETO Ltd, 1992. 48 pp.
- [22] Courtier 1990. The assessment of ASR-affected Structures. *Cement and Concrete Composites*, 12, 191-201.
- [23] Thomas, M.D.A.; Folliard, K.J.; Fournier, B.; Drimalas, T.; Rivard, P. 2012. Study of remedial actions on highway structures affected by ASR. Proc 14th Int Conf on AAR, May 20-25th 2012, Austin, Texas.
- [24] ASTM 666. 2008. Standard Test Method for Resistance of Concrete to Rapid Freezing and Thawing. ASTM International, West Conshohocken (USA), 2008.
- [25] Özkan, S.; Canan, T.; Mehmet Ali, T. 2002. Influence of Aggregate Type on Mechanical Behavior of Normal- and High-Strength Concretes. *ACI materials journal*, November, 99.
- [26] Sanchez, L. F. M. Contribution to the assessment of damage in aging concrete infrastructures affected by alkali-aggregate reaction, PhD thesis, Laval University, department of geology and geological engineering (to be published in 2014).

8. PAPER III: USE OF THE DAMAGE RATING INDEX (DRI) TO QUANTIFY DAMAGE DUE TO ALKALI-SILICA REACTION IN CONCRETE INCORPORATING REACTIVE FINE AND COARSE AGGREGATES

Sanchez, L. F. M.^a; Fournier, B.^b; Jolin, M.^c; Bedoya, M. A. B., Bastien, J.^e, Duchesne, J.^f

(a) PhD candidate, Laval University

**1065, ave de la Médecine, Pavillon Pouliot, Office 3755, Québec, Qc, Canada, G1V 0A6
Tel.: (1) (418) 6562131, ext. 12709**

leandrofms@gmail.com / le.sanchez@uol.com.br

(b) Prof. Dr. – Laval University, Quebec, QC, Canada

benoit.fournier@ggl.ulaval.ca

(c) Prof. Dr. – Laval University, Quebec, QC, Canada

marc.jolin@gci.ulaval.ca

(d) – MSc. Candidate, Laval University.

maria-alejandra.bustamante-bedoya.1@ulaval

(e) Prof. Dr. – Laval University, Quebec, QC, Canada

josee.bastien@gci.ulaval.ca

(e) Prof. Dr. – Laval University, Quebec, QC, Canada

josee.duchesne@ggl.ulaval.ca

ABSTRACT

The Damage Rating Index (DRI), a microscopic and semi-quantitative petrographic tool, is a method that has increasingly been used in North America because it can answer interesting questions regarding the nature and the degree of damage in concrete affected by deleterious mechanism such as alkali-aggregate reaction (AAR). This paper presents the results of the condition assessment, using the DRI, of concrete mixtures of different strengths and incorporating different reactive aggregate types (fine vs. coarse aggregate), with the aim of verifying how alkali-silica reaction (ASR) develops as well as how the DRI could be used to better quantify damage in concrete due to ASR.

Keywords: damage rating index (DRI), assessment microscopic damage features, alkali-silica reaction (ASR).

RÉSUMÉ

Le Damage Rating Index (DRI), un outil microscopique semi-quantitatif, est une méthode de plus en plus utilisée en Amérique du Nord, car il peut répondre aux questions intéressantes concernant la nature et l'ampleur de l'endommagement de bétons affectés par la réaction alcali-granulats (RAG). Cet article présente l'évaluation du degré d'endommagement microscopique par l'entremise du DRI, pour des bétons de différentes formulations et incorporants différents types de granulats réactifs (sable vs gros granulats), et ce dans le but de mieux comprendre le développement de la RAG ainsi que les possibilités d'utilisation de la méthode DRI pour mieux quantifier l'endommagement de bétons affectés par ce mécanisme délétère.

Mots clés: damage rating index (DRI), évaluation de l'endommagement microscopique, réaction alcali-silice (RAS).

8.1 INTRODUCTION

Alkali-silica reaction (ASR), a chemical reaction between certain siliceous mineral phases from the aggregates and the alkali hydroxides from the concrete pore solution, is one of the main processes affecting the durability of concrete structures around the world [1]. Nowadays, several test methods are available for evaluating the potential alkali-reactivity of concrete aggregates, and recommendations/practices for selecting efficient preventive measures against ASR have progressed to such a point that it is now generally possible to manufacture concrete risk-free of ASR. On the other hand, the management of existing concrete structures affected by ASR still remains a huge challenge for engineers. Therefore, any information on the nature of the deleterious mechanism(s) affecting the structures, their current condition and the potential for future deterioration is generally critical for engineers in charge of selecting appropriate remedial measures [2]. In that context, Grattan-Bellew and coworkers [3, 4] proposed the *Damage Rating Index method* (DRI), a semi-quantitative analysis of petrographic features of damage in polished concrete sections. The DRI is increasingly being used [5-10], as well as other petrographic methods [11-17], with the objective of quantifying the condition of concrete affected by ASR, thus avoiding criticism of being a qualitative and "narrative" condition assessment [2, 10].

8.2 ASR PETROGRAPHIC COMMON FEATURES AND THE DRI

Different mechanisms can affect the long-term durability of concrete structures whose "patterns" were diagrammed by St-John et al. and BCA [18, 19] (Figure 1). For damage caused by freezing and thawing cycles, cracking develops mainly in the concrete matrix and often propagates through the interfacial transition zone (ITZ) between the aggregate particles and the cement paste, as those zones present a lower fracture toughness and are more porous than the bulk cement paste (Figure 1A). Delayed ettringite formation (DEF), a form of heat-induced sulfate attack, is characterized by expanding cement paste in the presence of moisture that becomes detached from the aggregate particles with the gaps thus created at the ITZ being progressively filled with large amounts of ettringite [20] (Figure 1B). On the other hand, in the case of ASR, the cracks are generated at expansive sites where reactive forms of silica are present. Figures 1C and 1D present the cracking originating from the fine and coarse aggregate particles, respectively. Normally, cracks generated by ASR propagate between or through the above particles, the ITZ and the bulk cement paste, with associated secondary reaction products, i.e. alkali-silica gel. Thus, it seems logical to think that the nature (i.e. hardness, stiffness, toughness, etc.) of the coarse aggregate play a significant role in the ASR crack propagation, as recently suggested by Reinhardt and Mielich [21]. Therefore, a detailed petrographic analysis of concrete specimens extracted from aging concrete structures, both on fractured surfaces and thin/polished concrete sections, is a powerful tool to help identifying the presence (or absence) of the main microscopic features of the above deleterious mechanisms, thus providing critical information on either the potential origin or the extent of current damage of the distressed material [6, 8, 22-26].

The DRI is a microscopic analysis performed with the use of a stereomicroscope (about 15-16x magnification) where damage features generally associated with ASR are counted through a 1 cm² grid drawn on the surface of a polished concrete section (Figures 2 and 3). The number of counts corresponding to each type of petrographic features is then multiplied by weighing factors, whose purpose is to balance their relative importance towards the mechanism of distress (for instance ASR). It is important to mention that the factors used in the method were chosen on a logical basis, but relatively arbitrarily.

Ideally, a surface of at least 200 cm² should be used for DRI analysis, and it may be greater in the case of mass concrete incorporating larger size aggregate particles. However, for comparative purposes, the final DRI value is normalized to a 100 cm² area [9]. DRI results are often represented by charts enabling easy visualization of the different damage features in the

specimen under study (Figure 4). Recent studies dealing with the DRI indicated that the variability between the operators performing this test could be significantly reduced by improving the definition/description of the different damage features, modifying some weighing factors (Table 1), as well as by appropriate training of the petrographers using reference sections [2]. These authors proposed to use identical factors for the two categories of *opened cracks in the aggregate particles* (factor of 2) or *cracks in the cement paste* (factor of 3), with or without reaction products; this was done to reduce the variability associated to the difficulty in positively recognizing the presence of reaction products in cracks of the polished sections. Consequently, the two types of cracks could be grouped together having the same weighing factors if one considers that a crack is an indication of damage, either with or without reaction products. Also, larger weighing factors were selected for cracks in the cement paste, compared to that in the aggregate particles (i.e. factor of 3 vs. 2), to indicate a relatively greater importance regarding the durability of the affected concrete element. Finally, it was found that eliminating the counts of the number of *voids with reaction products in the cement paste* (RPAV in Figure 3) and *Reaction rims* (RR in Figure 3) from the calculation of the DRI values also contributes at reducing the variability between the operators and are not really direct indications of “damage” in concrete.

Since the process of damage generation vary through the type of reactive aggregate used (fine vs. coarse aggregate, lithotype, etc.), the DRI should ideally assess the nature and degree of distress features and correlate them with either the expansion attained by the distressed concrete or, ideally, with losses in mechanical properties [4, 6]. Such information is, however, currently very limited. Moreover, although the differences between highly and mildly distressed concrete specimens are generally clear under the microscope [27-29], there is currently no published classification based on DRI values that separates low, moderate or high damage levels in concrete affected by ASR. Finally, it is important to mention that even if the DRI has already been used by several researchers, there is currently no standard test procedure available to petrographers.

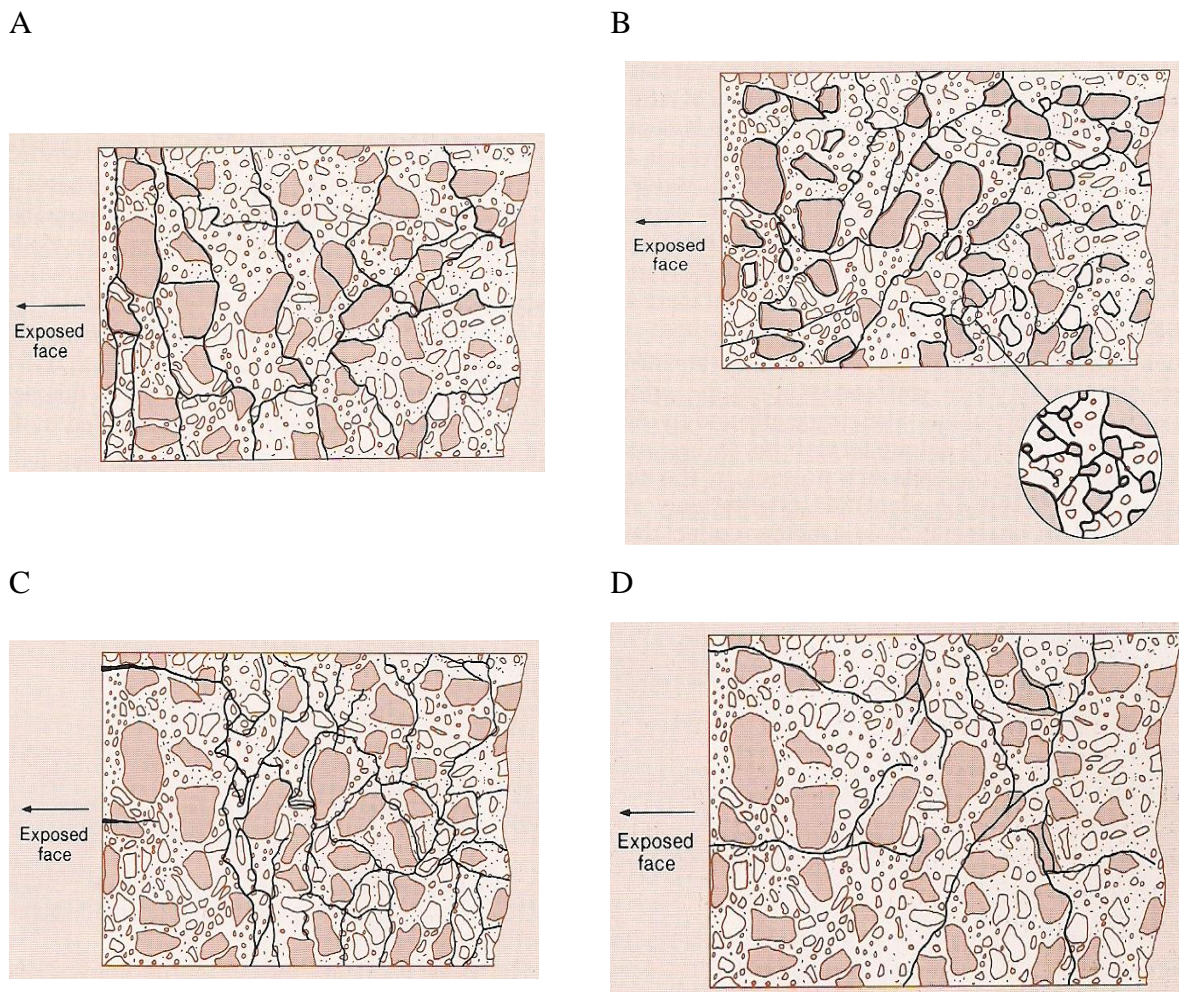


Figure 1: Crack pattern in concrete caused by different deleterious mechanisms [18]. A. Freezing and thawing. B. Delayed ettringite formation (DEF). C. ASR from reactive sand. D. ASR from coarse reactive aggregate.

In view of eventually developing a standard procedure for the DRI, it appears that the following questions should be answered [9]:

- Should/can the DRI provide an absolute output value representing a damage degree associated to a specific distress mechanism ?
- Does the type of the reactive aggregate (fine vs. coarse aggregate, lithotype, etc.) influence the output results of the DRI for the same level of expansion achieved ?
- Does the nature of the coarse aggregate (when ASR comes from a reactive sand) influence the crack's propagation process, and to what extent ?
- Could the DRI be a global analytical procedure allowing the assessment of damage mechanisms other than ASR, as recently suggested by Bérubé et al. [30] ?

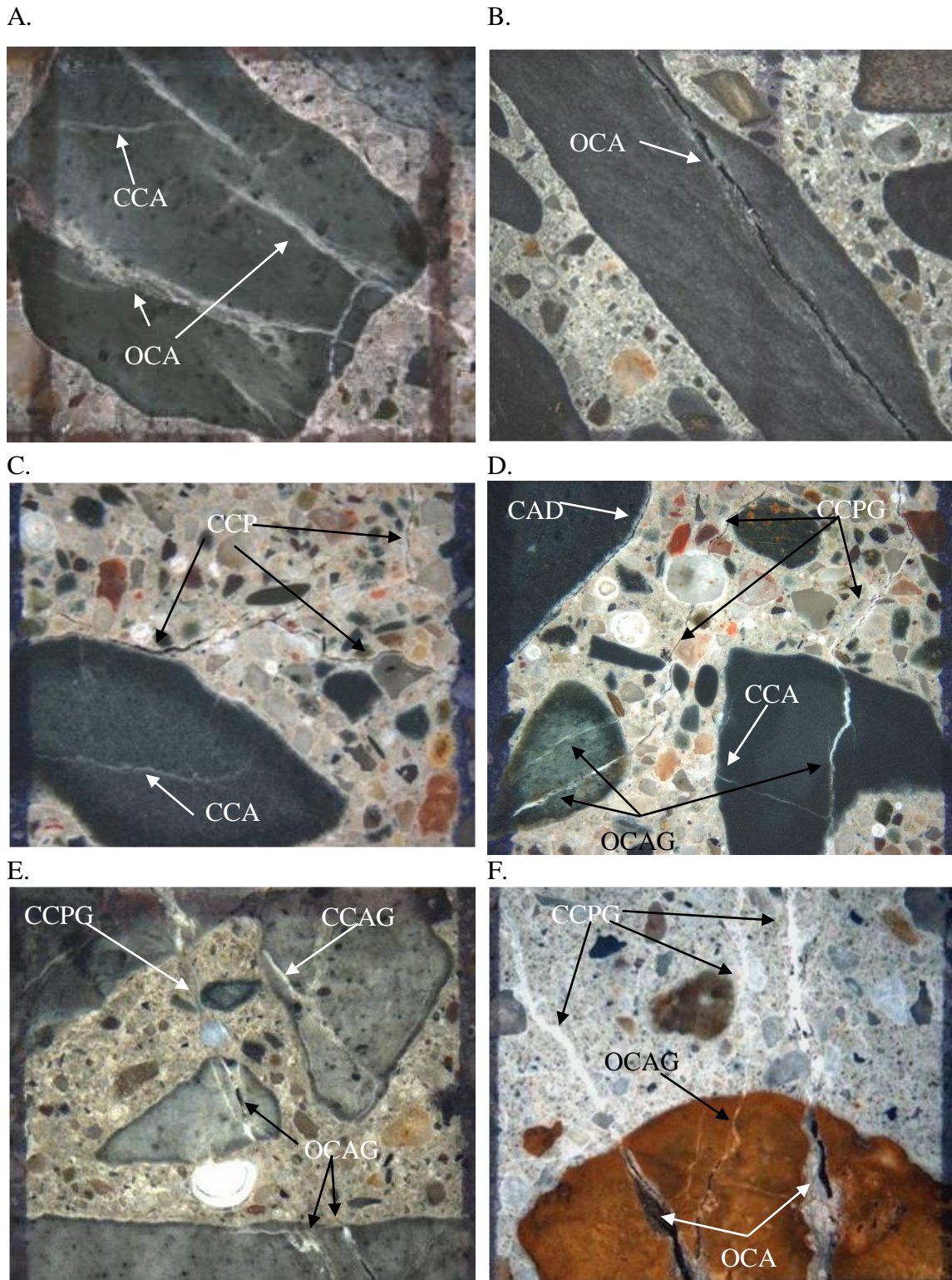
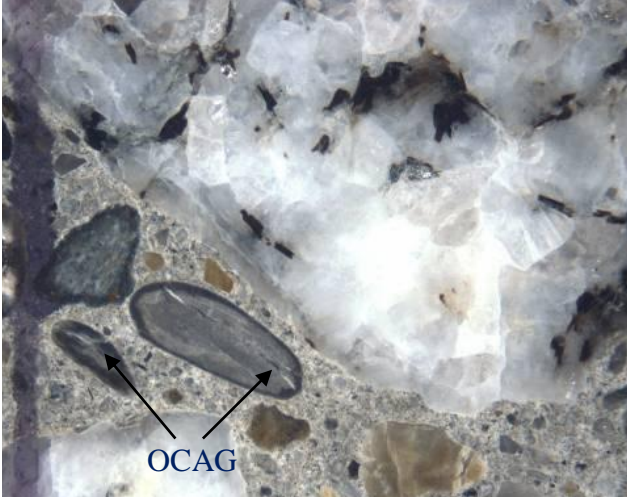


Figure 2a: Petrographic features of ASR in concrete incorporating reactive coarse aggregates; the abbreviations are given in the Table 1. The distance between the vertical lines is 1 cm (from Villeneuve et al. 2012). A. Closed (tight) cracks and network of cracks in the coarse aggregate particle. B. Opened crack in the coarse aggregate particle. C. Closed (tight) crack in the coarse aggregate particle; cracks in the cement paste. D. Cracks with reaction products in the coarse aggregate particles and in the cement paste; debonded coarse aggregate particle. E. Cracks with reaction products in the coarse aggregate particles and the cement paste. F. Cracks with reaction products in the cement paste; opened cracks and cracks with reaction products in the coarse aggregate particle. Other petrographic features or ASR present in the micrographs: reaction product in voids of the cement paste and reaction rims.

G



H

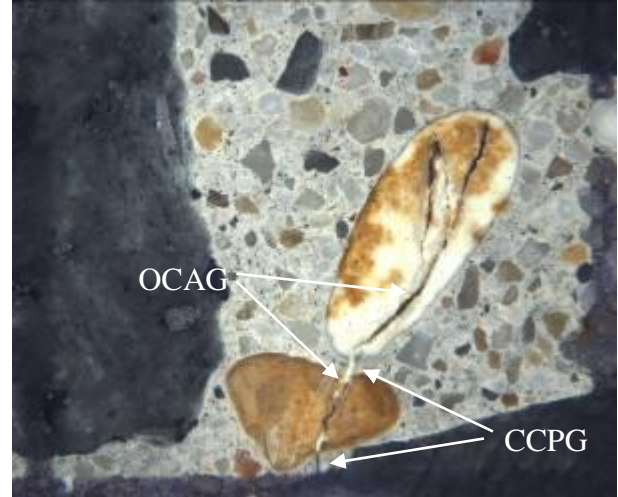


Figure 2b: Petrographic features of ASR in concrete incorporating reactive fine aggregates; the abbreviations are given in the Table 1. The distance between the vertical lines is 1 cm (from Villeneuve et al. 2012). G. Cracks with reaction products in fine aggregate particles and the cement paste. H. Cracks with reaction products in fine aggregate particles and in the cement paste (note: reaction products are still present in some portions of the cracks in the fine aggregate particles but some has disappeared through sample preparation).

A



B

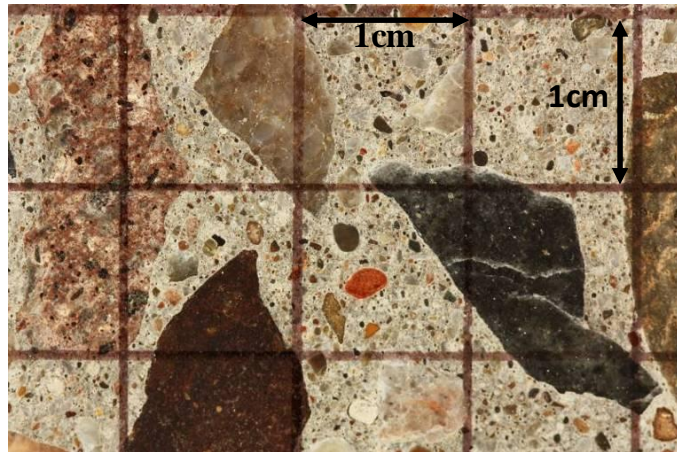


Figure 3: Damage Rating Index (DRI). A. Example of a stereomicroscope used for the microscopic analysis. B. 1cm² grid drawn at the surface of the polished section and used for damage feature's counting [2].

Table 1: Petrographic features and weighing factors used for Damage Rating Index determination [2].

Petrographic features	Abbreviation	Factors	Comments/Description
Closed/tight cracks in coarse aggregate particle	CCA	0.25	<ul style="list-style-type: none"> • Tight/fine cracks showing no gap at about 15x magnification; • Sometimes “appear” to contain whitish secondary products, as the crack forms an angle with the cutting plane thus causing such an optical effect (Figures 3A & 3C); • A low factor is given as such cracks are likely/often produced by aggregate processing operations (quarried aggregate) or weathering (gravel).
Opened cracks or network of cracks in coarse aggregate particle	OCA	2.0	<ul style="list-style-type: none"> • Crack showing a gap at about 15x magnification (Figure 3B); • A “network” of cracks is also classified in this category, as it is likely caused by expansive reactions within the aggregate particles (Figure 3A).
Opened cracks or network cracks with reaction product in coarse aggregate particle	OCAG	2.0	<ul style="list-style-type: none"> • Cracks containing secondary reaction products (whitish; glassy or chalky in texture) (Figure 3D-3F); • Secondary products often do not fill all the cracks (material likely lost during polished section preparation process) (Figure 3E).
Coarse aggregate debonded	CAD	3.0	<ul style="list-style-type: none"> • Crack showing a <u>significant</u> gap in the interfacial zone between the aggregate particle and the cement paste (Figure 3D); • Would likely cause debonding of the particle when fracturing the concrete as it appears around a significant portion of the coarse aggregate particle.
Disaggregated/corroded aggregate particle	DAP	2.0	<ul style="list-style-type: none"> • Aggregate particle that shows signs of disintegration “corrosion” or disaggregation (ex: reacting opaline shale and chert/flint particles).
Cracks in cement paste	CCP	3.0	<ul style="list-style-type: none"> • Crack visible at about 15x magnification, but with no evidence of reaction products (Figure 3C).
Cracks with reaction product in cement paste	CCPG	3.0	<ul style="list-style-type: none"> • Cracks containing secondary reaction products (whitish; glassy or chalky in texture) (Figure 3D-3F); • Secondary products often do not fill all the cracks (material likely lost during polished section preparation process).

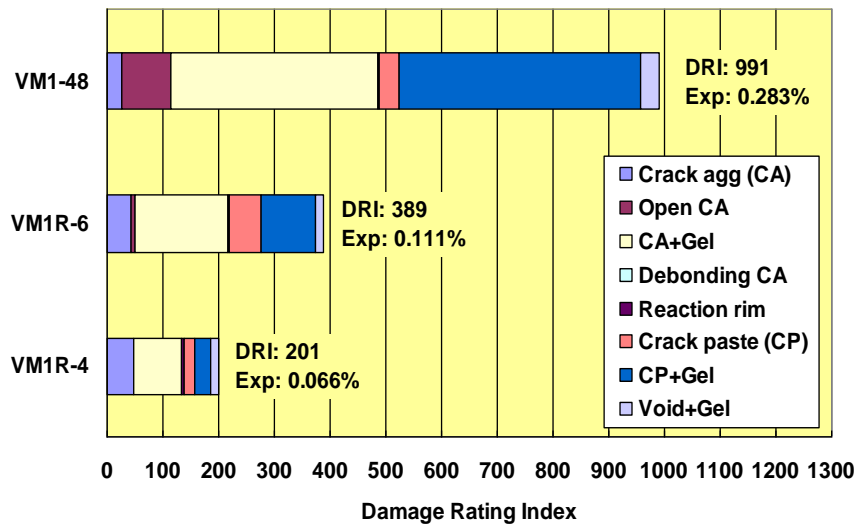


Figure 4: Example of DRI chart for damaged concretes with different levels of distress [29].

8.3 SCOPE AND OBJECTIVES OF THE WORK

As indicated in the previous section, there are still some questions that should be answered so that the DRI could be widely considered as a diagnostic tool for quantitatively assessing concrete distress due to ASR or different damage mechanisms. Thus, a study of some DRI features was carried out for assessing its diagnostic character. The main features of this study consisted of the following:

- Assessment of both the DRI output values and distress chart for evaluating damage in concrete specimens of different design strengths, affected to various degrees by ASR, and incorporating reactive fine and coarse aggregates;
- Assessment of crack's pattern change for mixtures made with different non-reactive coarse aggregates when ASR expansion originates from a reactive sand;
- Determining whether additional information, i.e. more than just the output final DRI number, could be extracted from the DRI determination that could help for quantitatively/qualitatively assessing concrete distress.

8.4 MATERIALS AND METHODS

8.4.1 Materials and mixture proportions

The damage assessment analyses were carried out on test cylinders, 100 by 200 mm in size, cast from three types of concrete (25 MPa, 35 MPa and 45 MPa) incorporating two highly-reactive aggregates (NM gravel and Tx sand) and having reached various degrees of expansion due to ASR (from 0.05 to 0.30%). The main reactive material in the Tx sand is chert present in the coarser fractions of the aggregate material (~ 1.25 – 5 mm fractions), while it is chert and volcanic rock (rhyolite/andesite) particles in the case of the NM gravel. The reactive sand and gravel were used in combination with non-reactive coarse and fine aggregates, respectively. In the case of the mixtures containing the reactive Tx sand, two non-reactive coarse aggregates (a high-purity limestone (HP) and a magmatic rock (Dia)) were used for each of the concrete strengths tested. Table 2 gives the main characteristics of the aggregates selected.

The three types of non air-entrained concrete mixtures were designed to contain the same amount of paste and aggregates in volume (i.e. from one mix to another), so one can compare similar systems (Table 3). All concretes were made with the same conventional CSA Type GU high-alkali (0.90% Na₂O_{eq}) Portland cement. Reagent grade NaOH was used to raise the total alkali content of the mixtures to 1.25% Na₂O_{eq}, by cement mass, for accelerating the ASR expansion process.

Table 2: Characteristics of aggregates.

Aggregate		Location	Rock Type	Bulk relative density	Absorption (%)	AMBT ¹ 14d exp,%
Coarse	NM	New Mexico (USA)	Polymictic gravel (mixed volcanics, quartzite, chert)	2.53	1.59	1.114
	HP	Newfoundland (Canada)	High-purity limestone	2.68	0.44	0.001
	Dia	Quebec (Canada)	Diabase (plutonic rock)	3.00	0.51	0.065
Fine	Tx	Corpus Christi (USA)	Polymictic sand (granitic, mixed volcanics, quartzite, chert, quartz)	2.60	0.55	0.995
	Lav	Quebec (Canada)	Natural derived from granite	2.71	0.54	0.032

¹ Accelerated Mortar Bar Test (ASTM C 1260)

Table 3: Description of concrete mix designs.

Ingredients	25 MPa - Materials (kg/m ³)		35 MPa - Materials (kg/m ³)		45 MPa - Materials (kg/m ³)	
	Tx sand	NM gravel	Tx sand	NM gravel	Tx sand	NM gravel
Cement	314 (101) ¹	314 (101)	370 (118)	370 (118)	424 (136)	424 (136)
Sand	790 (304)	714 (264)	790 (304)	714 (264)	790 (304)	714 (264)
Coarse aggregate	1029 (384)	1073 (424)	1029 (384)	1073 (424)	1029 (384)	1073 (424)
Water	192 (192)	192 (192)	174 (174)	174 (174)	157 (157)	157 (157)

¹The number in brackets correspond to the volume occupied by the materials (in L/m³)

8.4.2 Fabrication and curing of test specimens

A total of 64 cylinders, 100 by 200 mm in size, were cast from each of the nine concrete mixtures manufactured in the laboratory (Tx + HP, Tx + Dia, NM + Lav – 25, 35 and 45 MPa). After 24 hours in their mould, the specimens were demolded and then placed for 24h in the moist curing room. Small holes, 5 mm in diameter by 15 mm long, were then drilled in both ends of each test cylinders and stainless steel gauge studs were glued in place, with a fast-setting cement slurry, for longitudinal expansion measurements. The cylinders were left to harden for 48 h in the moist room at 23°C prior to performing the “0” length reading, after what they were placed in sealed plastic (22 liters) buckets lined with damp cloth (4 cylinders per bucket). All buckets were then stored at 38°C and 100% R.H. and the test cylinders monitored for length changes regularly until they reached the expansion levels chosen for this research, i.e. 0.05%, 0.12%, 0.20% and 0.30%. As per ASTM C 1293, the buckets were cooled to 23 °C for 16 ± 4 h prior to periodic axial expansion measurements. When the above expansion levels were reached, the specimens were wrapped in plastic film and stored at 12°C until testing (because of testing capacity issues). Prior to testing, after rewetting in the moist room at 23° C, the specimens were measured and weighed in order to confirm that they had not suffered from significant length or mass changes.

In order to perform the DRI, the concrete cylinders were first cut in two axially and then one of the flat surfaces thus obtained was polished. A portable hand-polishing device, which uses diamond-impregnated rubber disks (no. 50 (coarse), 100, 400, 800, 1500 à 3000 (very fine)), was found most suitable as it does not use loose abrasive powders that can fill up cracks/voids in the concrete and quality polishing is obtained with minimal water supply [2].

8.4.3 Methods for assessment and analysis

The DRI was performed on specimens cast from all concrete mixtures and for all expansion levels selected for this work. It is important to mention that the DRI was originally developed for evaluating damage in concrete specimens incorporating reactive coarse aggregate particles. In this study, concrete mixtures made with either coarse or fine reactive aggregates were tested. Counts of cracking in the aggregate particles were made in particles down to 1 mm in size, instead of 2 mm normally used in the original method [2]. The latest weighing factors proposed by Villeneuve et al. [2] were used for the calculation of the DRI output values.

As recommended in the original method, analyses were carried out on 200 cm² (or 100 cm² on each of two 100 by 200 mm specimens) for each of the three 25 MPa concrete mixtures (i.e. Tx + HP, Tx + Dia, NM + Lav). Since the variation (%) (i.e. deviation/average value; where deviation is the difference between two samples) between two specimens (Specimens A and B - polished surfaces of cylinders) of 100 cm² each was really low (i.e. < 10%, Figure 5) for all the expansion/damage levels investigated in the 25 MPa concretes, it was decided, for practical reasons, that it would be sufficient to use only one polished section (i.e. 100 cm²) for the 35 and 45 MPa specimen's analyses. The main reason for such a low variability in the DRI values is the tight control in the expansion levels between two companion cylinders of a same set, i.e. 0.05 ± 0.01%, 0.12 ± 0.01%, etc. Also, in order to reduce the potential impact of alkali leaching on the development of ASR cracking and consequently on the DRI values, as highlighted by Lindgard et al. [31], only the central portion of the test cylinders was used for DRI determinations.

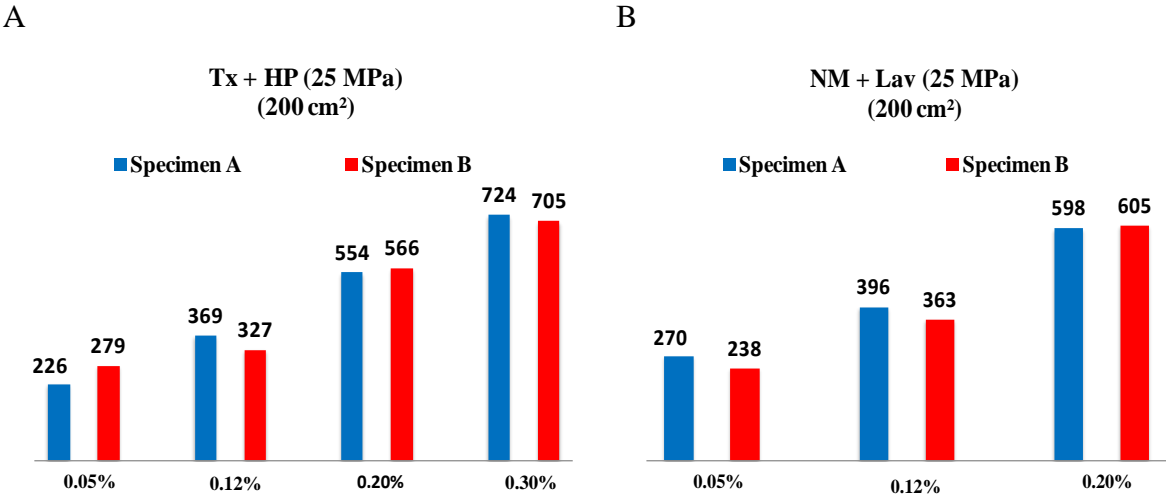


Figure 5: Variation between DRI's calculated on two 100 cm² samples (total of 200 cm²) for all levels of expansion for the 25 MPa mixtures incorporating: A. Tx + HP. B. NM + Lav.

Several "sub-studies" were carried out for the global analysis of the petrographic features of deterioration identified in the test specimens. This was done to complete the information obtained from conventional DRI calculations, possibly about the chemical or the physical distress mechanism of ASR. The "sub-studies" are the following:

- Assessment of petrographic features of damage, in relative (%) and absolute (counts) ways, and as a function of the expansion of the test samples without the use of weighing factors;

- Evaluation of the development/progress of cracking in the aggregate particles as a function of expansion. This part of the study was carried out by counting the number of cracks in each individual aggregate particle without considering the 1 cm² grid used in the conventional DRI procedure;
- Assessment of the development/progress of cracking in the concrete specimens as a function of expansion. In this part of the work, the measurements of crack's length and widths were made at a global scale, once again without taking into account the 1 cm² grid used for DRI determinations;
- Assessment of the crack density at the surface of the sample as a function of expansion by measurement of the total length of cracking over the surface area examined.

8.5 RESULTS

The results of the petrographic examination of the test specimens are presented by considering first the basic counts of the various petrographic features of deterioration as a function of expansion. The results are then evaluated through the use of weighing factors recently proposed by Villeneuve et al. [2] to determine whether a quantitative assessment of the deterioration could be proposed by the use of the *Damage Rating Index*.

8.5.1 Microscopic features of deterioration in the test specimens as a function of expansion.

The analysis of the petrographic features of deterioration, as described in the Table 1, was carried out in absolute counts (Figure 6) and in a relative way (% of main damage features) (Figure 7). Special attention was given to identify the most common microscopic features at each step of the reaction/expansion. As this study was carried out without focusing on the kinetics of the reaction, it is considered that each level of expansion actually represents an interesting comparative base for determining the degree of distress generated within the concrete as ASR is progressing.

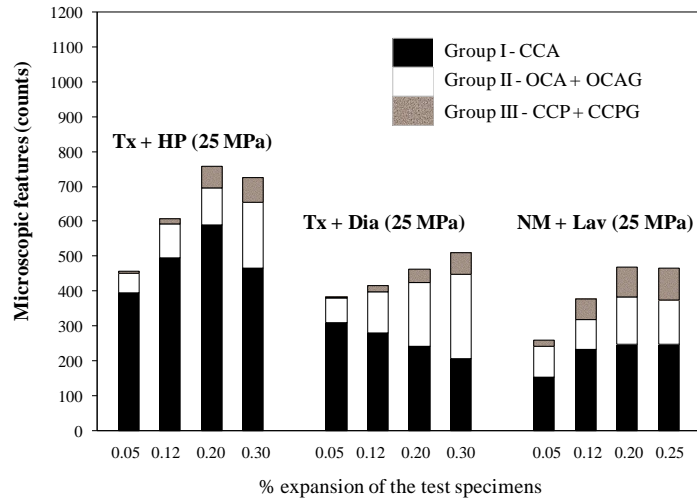
The data illustrated in Figure 6 correspond to the counts of the following features of deterioration in the test specimens, averaged over a 100 cm² surface and regrouped as follows:

- Group I: closed cracks within the coarse aggregate particles or the coarse fraction of the sand particles (1 to 5 mm) (CCA);

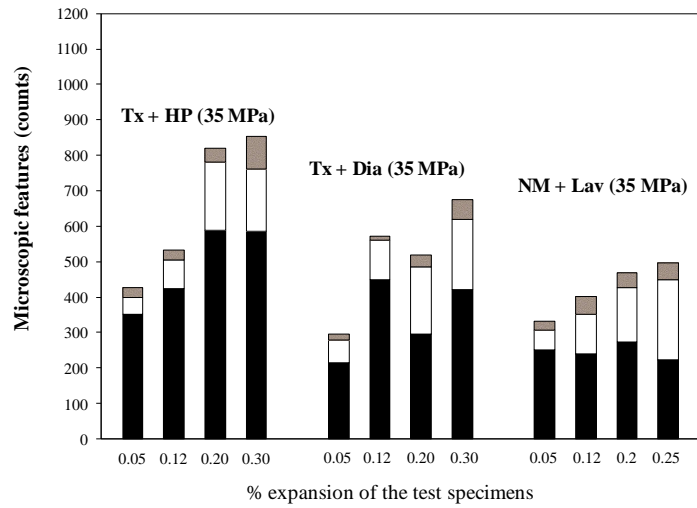
- Group II: opened cracks within the coarse aggregate particles or the coarse fraction of the sand particles (1 to 5 mm), with or without reaction products (OCCA + CCAG); and
- Group III: cracks in the cement paste, with or without reaction products (CCP + CCPG).

At first glance, the following general trends can be observed from the graphs in Figure 6: 1) the most common feature of “deterioration” in all polished sections corresponds to *Closed cracks within the aggregate particles* (Group I; CCA); 2) a progressive increase in the total number of Group I to III cracks is found as a function of increasing expansion for the large majority of the concrete specimens examined (different aggregate combinations and mix designs); 3) at similar expansion levels within each set of concrete mix design specimens (i.e. 25, 35 or 45 MPa), the total number of counts for Group I to III cracks is always higher in the Tx + HP specimens; this is related to higher counts of Group I cracks in the non-reactive HP limestone particles; 4) at similar expansion levels within each set of concrete mix design specimens (i.e. 25, 35 or 45 MPa), the total number of counts of Group I to III cracks is always the lowest in the NM + Lav mixtures; this is partly related to the lower number of reactive coarse aggregate particles, or “sites of expansive reactions”, in the above concretes compared to the number of reactive fine aggregate particles in Tx + HP and Tx + Dia samples and; 5) the counts of Group II and Group III cracks definitely increased with increasing expansion; they are considered as more indicative of the progress of ASR in the test specimens evaluated.

A: 25 MPa mixtures



B: 35 MPa mixtures



C: 45 MPa mixtures

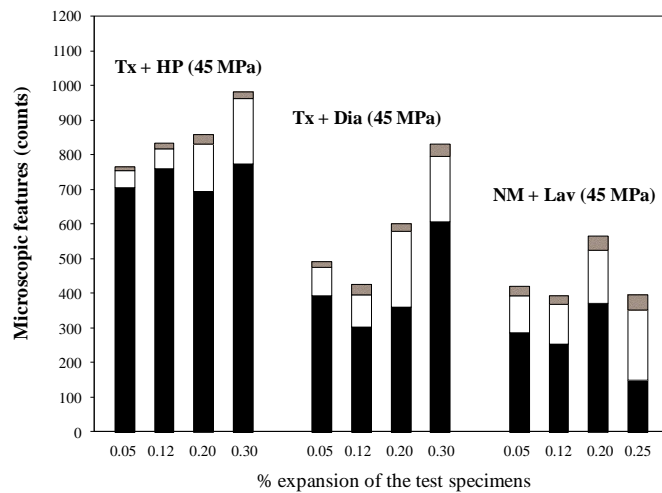
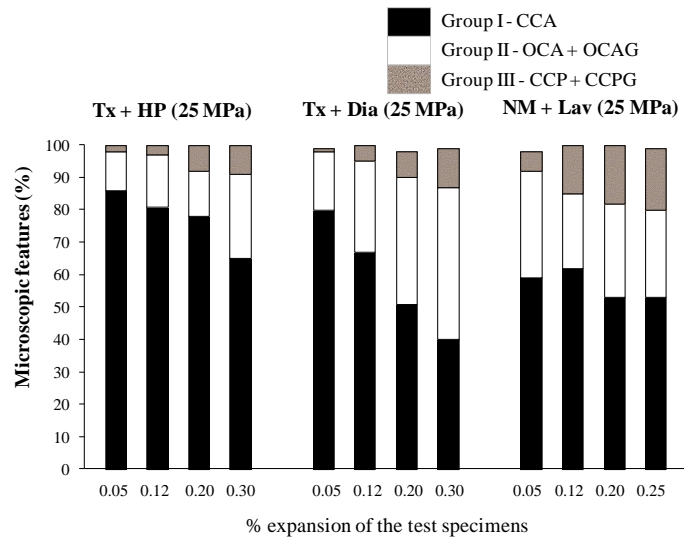


Figure 6: Counts of microscopic features of deterioration normalized for 100 cm² specimens: A. 25 MPa concretes. B. 35 MPa concretes. C. 45 MPa concretes.

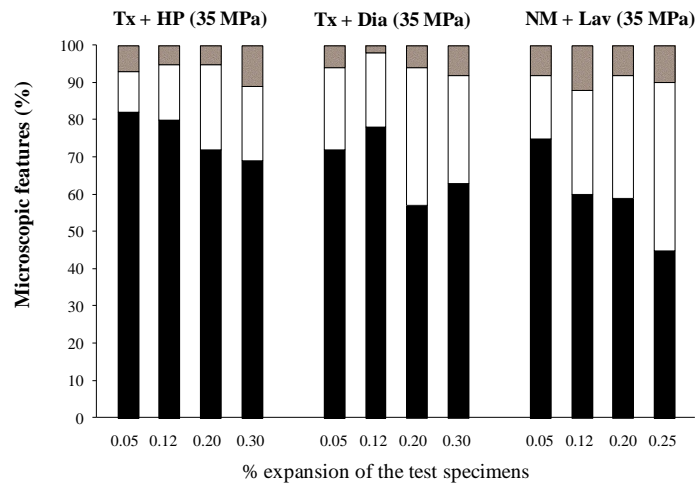
More specifically, the counts for *Closed cracks within the aggregate particles* (Group I; CCA) were found to increase with increasing expansion up to about 0.20% in the 25 and 35 MPa concretes incorporating the Tx + HP aggregates (left portion of Figures 6A and 6B), while remaining fairly stable in the 45 MPa concrete mixture made with the same aggregates (left portion of Figure 6C). The Group I cracks is also the largest single feature of “deterioration” in the concrete mixtures incorporating the other aggregate combinations (i.e. Tx + Dia and NM + Lav); however, significant variations in their counts was observed for the concrete mixtures Tx + Dia, while they remained somewhat similar with increasing expansion in the test specimens NM + Lav. The above observations suggest that a significant proportion of the closed cracks in the aggregate particles were actually generated through aggregate processing operations and/or weathering, and were consequently already present within the particles before their incorporation into concrete. However, the increasing expansion due to ASR resulted in an increase in the number of closed cracks in the HP (limestone) coarse aggregate particles (or lower toughness), despite being non-reactive, but not in the “tougher” Dia and NM coarse aggregate particles.

The relationships between the different petrographic features of deterioration can actually be more readily observed on Figure 7, which plots the relative proportion (%) of the *Group I to III cracks* as a function of the expansion of the test specimens. At the early stage of the reaction (i.e. 0.05% expansion level), *Group I cracks* (CCA) represent between 60 and 90% of the petrographic features of deterioration in the test specimens. At that expansion level, *Group II cracks* (OCA, OCAG) count for 7 to 28% and from 17 to 33% of the petrographic features of deterioration for concretes incorporating a reactive sand (Tx) and a reactive coarse aggregate (NM), respectively; the proportion of *Group III cracks* (CCP, CCPG) remains quite low for all concretes at that stage ($\leq 7\%$). As the expansion in the test specimens increases, the proportion of *Group I cracks* generally shows a decreasing trend, as the relative importance of Group II and Group III cracks increases due to the progress of ASR.

A: 25 MPa mixtures



B: 35 MPa mixtures



C: 45 MPa mixtures

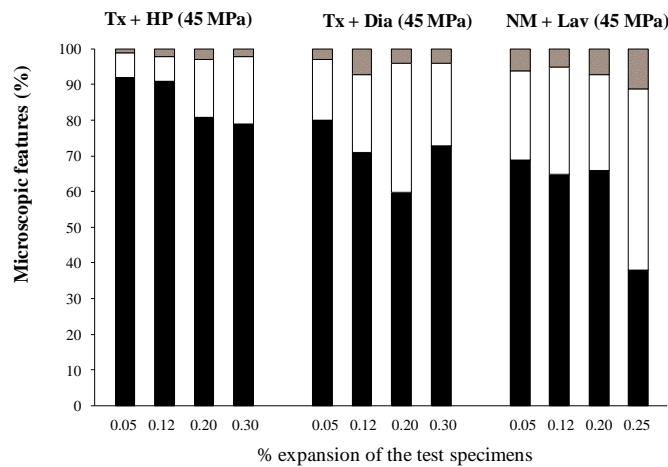


Figure 7: Microscopic features of deterioration expressed in % of cracks: A. 25 MPa concretes. B. 35 MPa concretes. C. 45 MPa concretes.

8.5.2 Progress of cracking in the aggregate particles as a function of expansion level.

When the petrographic features of ASR are counted through the DRI method, the number of aggregate particles in the test samples is not taken into account. In this study, similar paste and aggregates volumes were used for each series of mixes, so it is expected that variations in the total number of aggregate particles from one specimen to another will be somewhat minimized. Despite that, it might be interesting to look more specifically at the development of cracking within individual aggregate particles as a function of expansion, since this has been proposed as a critical parameter in the progress of ASR [32].

So, polished sections from three concrete mixtures (Lav + NM 25 and 35 MPa; Tx + HP 25 MPa) were examined by counting the number of coarse and fine (1 – 5 mm) aggregate particles and the number of cracks in each of the above individual particle. For this exercise, the number of cracks is obtained by determining the number of crack segments and nodes, as per the method proposed by Sims et al. [12] and described in Villeneuve et al. [2]. Table 4 gives the counts for all the test specimens examined. Figure 8 illustrates those counts divided by the total number of aggregate particles (from 1 mm up to 20 mm) examined in the respective specimens, and as a function of increasing expansion in those specimens.

Table 4: Aggregate features counted.

Mixture	Expansion	Number of aggregate particles counted			Counts of cracks in the coarse aggregate particles		Counts of cracks in the sand particles	
		Coarse aggr. particles	Sand particles (1mm to 5 mm)	Total	CCA	OCA + OCAG	CCA	OCA + OCAG
Tx + HP 25 MPa	0.05%	77	428	505	202	-	91	43
	0.12%	82	386	468	212	-	56	78
	0.20%	86	192	278	246	-	28	54
	0.30%	81	278	359	378	-	66	74
Lav + NM 25 MPa	0.05%	95	-	95	129	60		-
	0.12%	91	-	91	130	70		-
	0.20%	84	-	84	114	72		-
	0.25%	85	-	85	109	75		-
Lav + NM 35 MPa	0.05%	82	-	82	157	48		-
	0.12%	76	-	76	85	66		-
	0.20%	84	-	84	102	79		-

In the case of the concretes incorporating the reactive sand (Tx + HP - 25 MPa mix), the number of closed (CCA) and opened cracks (with or without gel) were counted in the coarse fraction of the sand particles (1-5 mm particles) as well as in the coarse (non-reactive)

aggregate particles. In the case of the concretes incorporating the reactive coarse aggregate NM (Lav + NM - 25 and 35 MPa mixes), the number of closed and opened cracks (with or without gel) was determined in the reactive coarse aggregate particles only (NM), as the counts of the closed cracks in the non-reactive sand (Lav) were found to be negligible. Figure 9 shows more specifically the results obtained for the mixture Tx + HP 25 MPa, looking at the data separately for cracking observed in either the reactive sand (Tx) or the non-reactive coarse aggregate (HP) particles; Figure 9A shows the values of either the opened or the closed cracks in the reactive sand particles (as a ratio basis, i.e. counts divided by the number of particles), while Figure 9B illustrates the number of closed cracks in the non-reactive limestone (ratio basis). The opened cracks in these non-reactive limestone particles were found to be negligible.

The results confirm that, generally, the larger is the expansion, the larger is the number of opened cracks (with or without gel) in the aggregate particles when ASR comes either from a reactive sand or a reactive coarse aggregate (i.e. increased ratios for OCA + OCAG in Figure 8). Such cracks are indeed considered to be linked to the development and progress of ASR in the concrete specimens. However, the presence and development of closed cracks that are often associated to weathering or even aggregates processing operations according to the progression of expansion is somewhat different. When the reaction is generated in the sand fraction (Tx + HP 25 MPa mixture) an increasing trend in the proportion of closed cracks in the aggregate particles (CCA) is observed as a function of expansion (Figure 8). The results illustrated in Figure 9 confirm that this is mainly related to a significant increase in the proportion of closed cracks in the non-reactive coarse aggregate particles at higher expansion levels (Figure 9B).

On the other hand, when the reaction is generated in the coarse aggregate (Lav + NM mixtures), the proportion of closed cracks in the reactive coarse aggregate particles does not change significantly or is decreasing slightly as a function of expansion (despite a high value of 1.91 obtained in the 35 MPa sample at 0.05% expansion, perhaps an anomaly which is unexplained at this stage). This was expected as the proportion of "active" ASR cracks (i.e. opened cracks, with or without reaction products) is increasing with the progress of expansion in the reactive coarse aggregate particles.

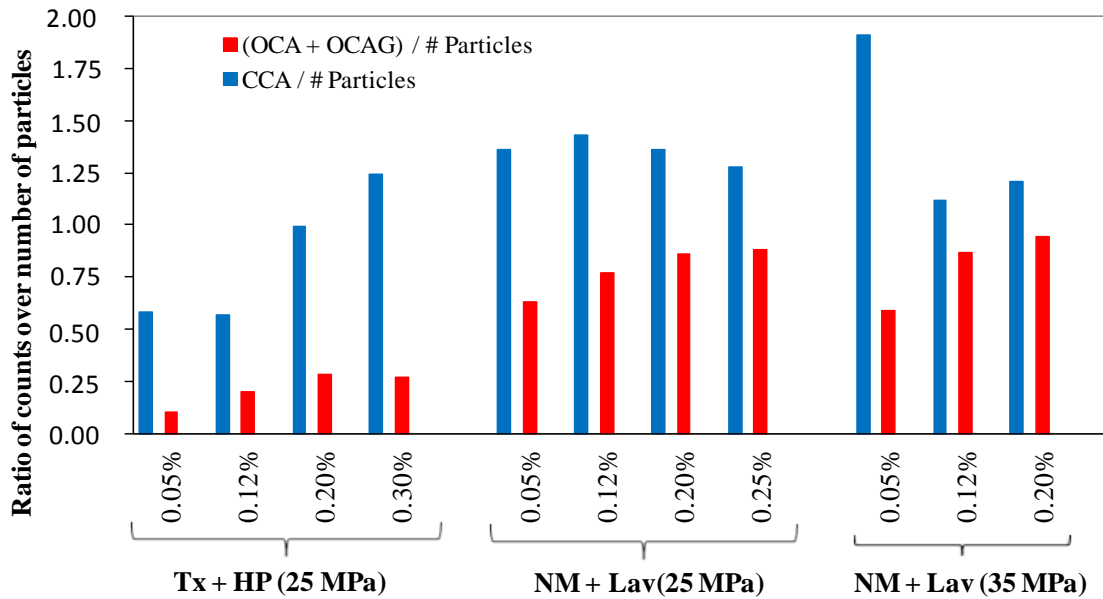


Figure 8: Cracks development in the aggregate particles as a function of expansion.

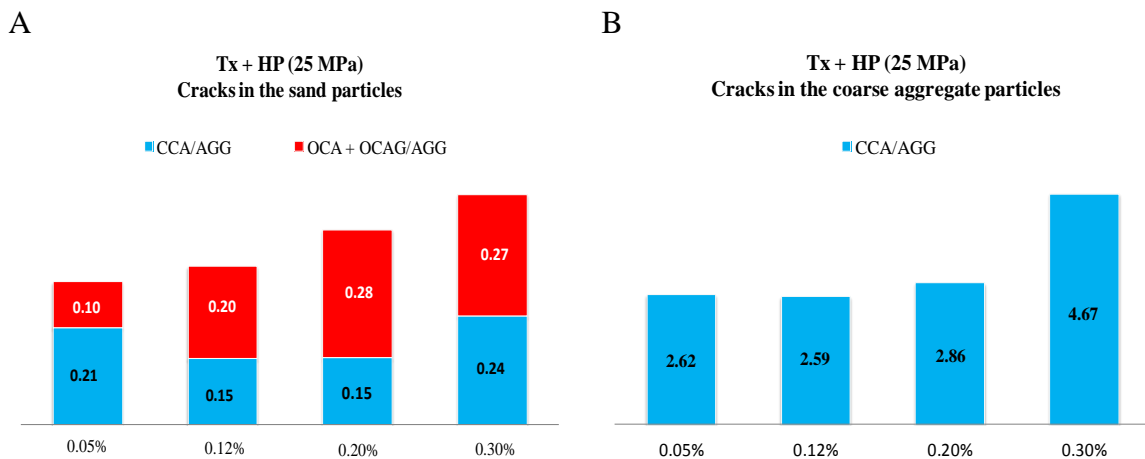


Figure 9: Crack development in the aggregate particles as a function of expansion due to ASR. A. Microscopic features in the reactive sand particles (Tx) expressed as counts for the closed and opened cracks divided by the total number of particles examined. B. Microscopic features in the non-reactive limestone particles (HP), expressed as counts of closed cracks divided by the total number of particles examined.

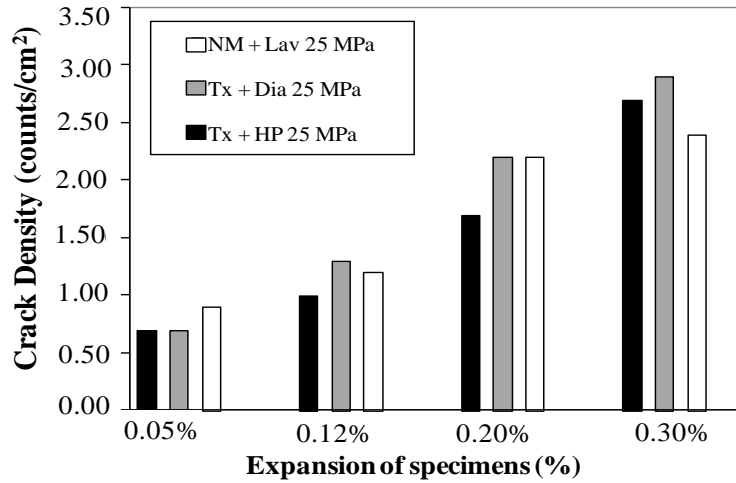
8.5.3 Crack density as a function of expansion/damage.

The crack density was determined, as part of the DRI analysis, to further verify if there was any difference in the damage generated in the reactive sand or the reactive coarse aggregate fraction in terms of "amount" of cracking with increasing expansion due to ASR. Figure 10

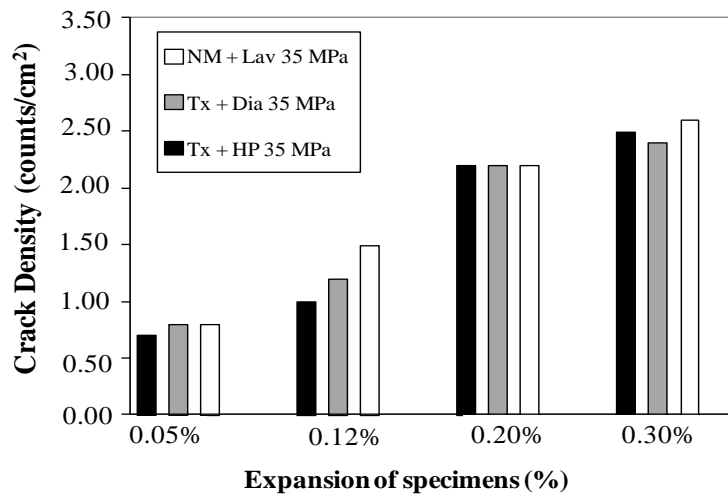
shows the “2D crack density” as a function of the expansion of the test specimens. The crack density was calculated from DRI observations as the sum of the counts of opened cracks in the aggregate particles and cracks in the cement paste, with or without reaction products, divided by the overall area examined and was expressed in cm². As mentioned before, such cracks are considered to be linked to the development and progress of ASR in the concrete specimens. In the case of the concretes incorporating the reactive sand (Tx; with HP or Dia as coarse aggregates), the number of opened cracks in the aggregate particles were counted in the coarse fraction of the sand particles (1-5 mm particles), while in the case of the concretes incorporating the reactive coarse aggregate (NM; Lav as fine aggregate), the number of opened cracks was determined in the reactive coarse aggregate particles NM.

As expected, the data show that the crack density increases with increasing expansion for all the concrete mixtures studied. Moreover, there are no significant or systematic differences, in terms of crack density, between different concrete mix designs or different reactive aggregates within a concrete mix design. However, an exception was observed for the 45 MPa mixtures, for which the highest values of crack density were generally observed for the concrete incorporating the reactive coarse aggregate NM (Figure 10C).

A: 25 MPa mixtures



B: 35 MPa mixtures



C: 45 MPa mixtures

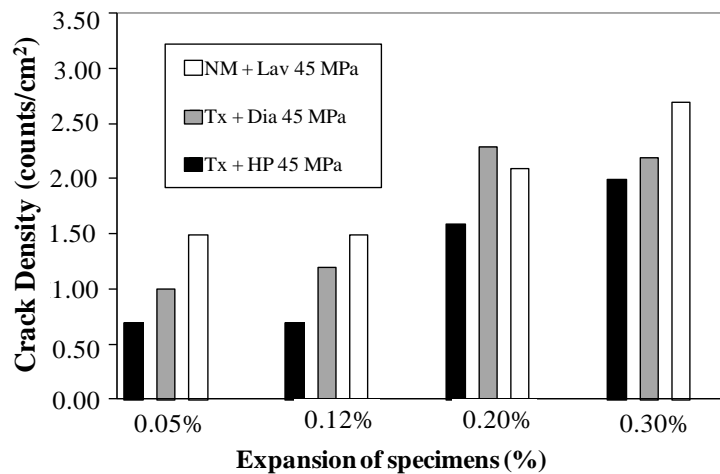


Figure 10: Crack density (sum of opened cracks in the aggregate particles and cracks in the cement paste, with and without reaction products) (counts/cm²) as a function of expansion: A. 25 MPa mixes. B. 35 MPa mixes. C. 45 MPa mixes.

8.5.4 Crack widths/lengths versus degree of expansion/damage

The petrographic examination of the polished sections revealed interesting differences in the distress characteristics caused by either the reactive sand or the coarse aggregates. For example, the cracking can be localized or sparsely distributed through the sample, cracks may be thinner or wider (in average), etc. However, additional information/trends can be obtained when the petrographic examination is performed by also measuring the main lengths and widths of cracks, as a function of expansion (Figure 11). The maximum length of cracking (L_{max}) was measured at a 15x magnification for cracks running either in the cement paste only or running into the cement paste through aggregate particles. The maximum crack width (W_{max}) was determined for cracks within the aggregate particles only, as this was more readily/reliably measurable than in the case of cracks in the cement paste.

In the specimens examined, it was found that the L_{max} generally increases with increasing expansion/damage for all the concrete mixtures, which was expected (Figures 11A to 11C); however, in the case of the 45 MPa concretes, L_{max} seems to remain relatively stable or progress more slowly until higher expansions were reached. The W_{max} values measured in the reactive aggregate particles were also found to generally increase with increasing degree of expansion/damage for all the concrete mixtures, despite more scattering in the data (Figures 11D to 11F). It does appear that both parameters are interesting features of the presence and progress of ASR deterioration in the test specimens.

If one works with zones of crack lengths (envelopes from the minimum up to the maximum values) instead of fixed/absolute values, one can see that, on average, reactive coarse aggregates tend to create slightly longer cracks than reactive sands in the ASR-affected.

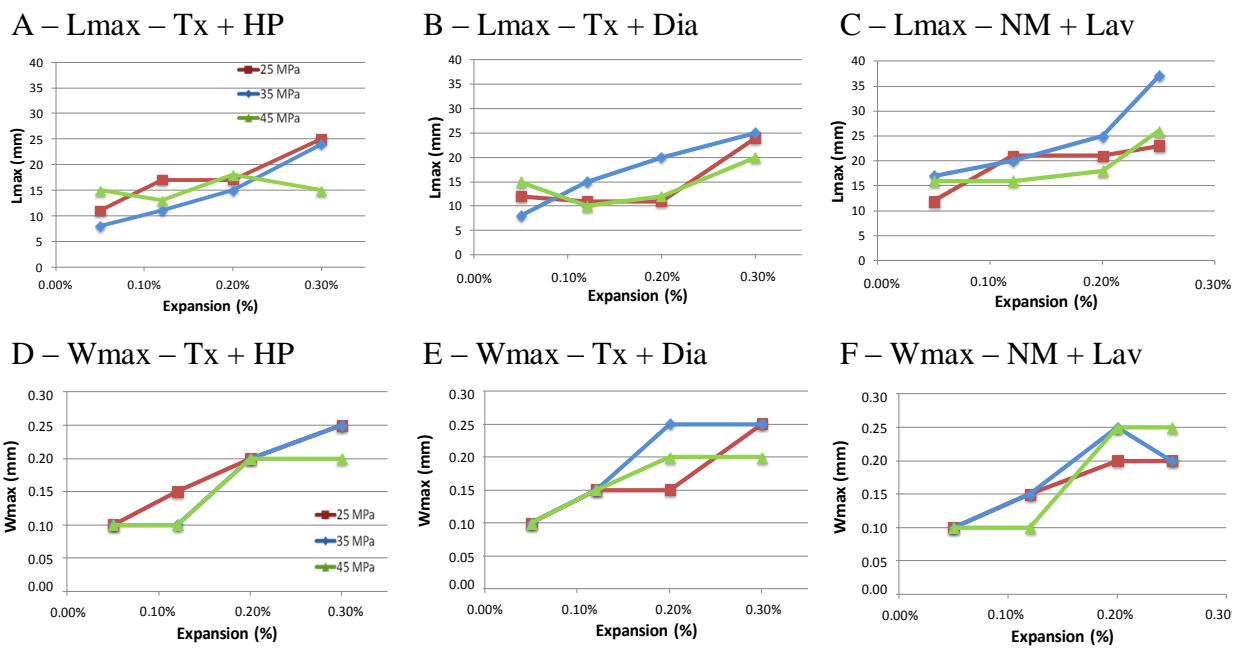


Figure 11: Additional information provided through petrographic examination. Maximum length (A-C.) or width (D-F) of cracking for all the mixtures, as a function of the expansion degree.

8.5.5 Quantitative assessments of damage obtained through DRI

The detailed results of the DRI determinations, i.e. in terms of the relative importance of each of the various petrographic features of deterioration (see Table 1), are illustrated in Figure 12. As mentioned before, the DRI results were obtained using the latest weighing factors proposed after the investigations carried out at Laval University [2] (Table 1). Figure 13 gives a plot of the DRI values as a function of the expansion of the concrete specimens, and this for all the mixtures (strengths and aggregates) used in this study.

As previously mentioned, it is clear from the data illustrated in Figure 12 that, for all concrete mixture designs and aggregate combinations, the relative importance of opened cracking within the aggregate particles as well as cracks in the cement paste, with and without gel, increases with increasing expansion of the test specimens. It is important to note in Figure 12 that the DRI was measured in control polished sections of the 35 MPa concrete mixtures incorporating the various aggregate combinations selected. The control samples were fabricated, wrapped and stored at 12°C for 150 days (which would represent 90 days at 20°C according to ASTM C 1074 [33]). Then, they were prepared and the DRI was performed.

The data indicate that a certain degree of damage already exists in the test specimens (DRI ranging between 100 and 160, from some cracking in the aggregate particles and in the cement paste) for concrete specimens showing no significant expansion (indicated 0% in Figures 12B, 12E and 12H) expansion level.

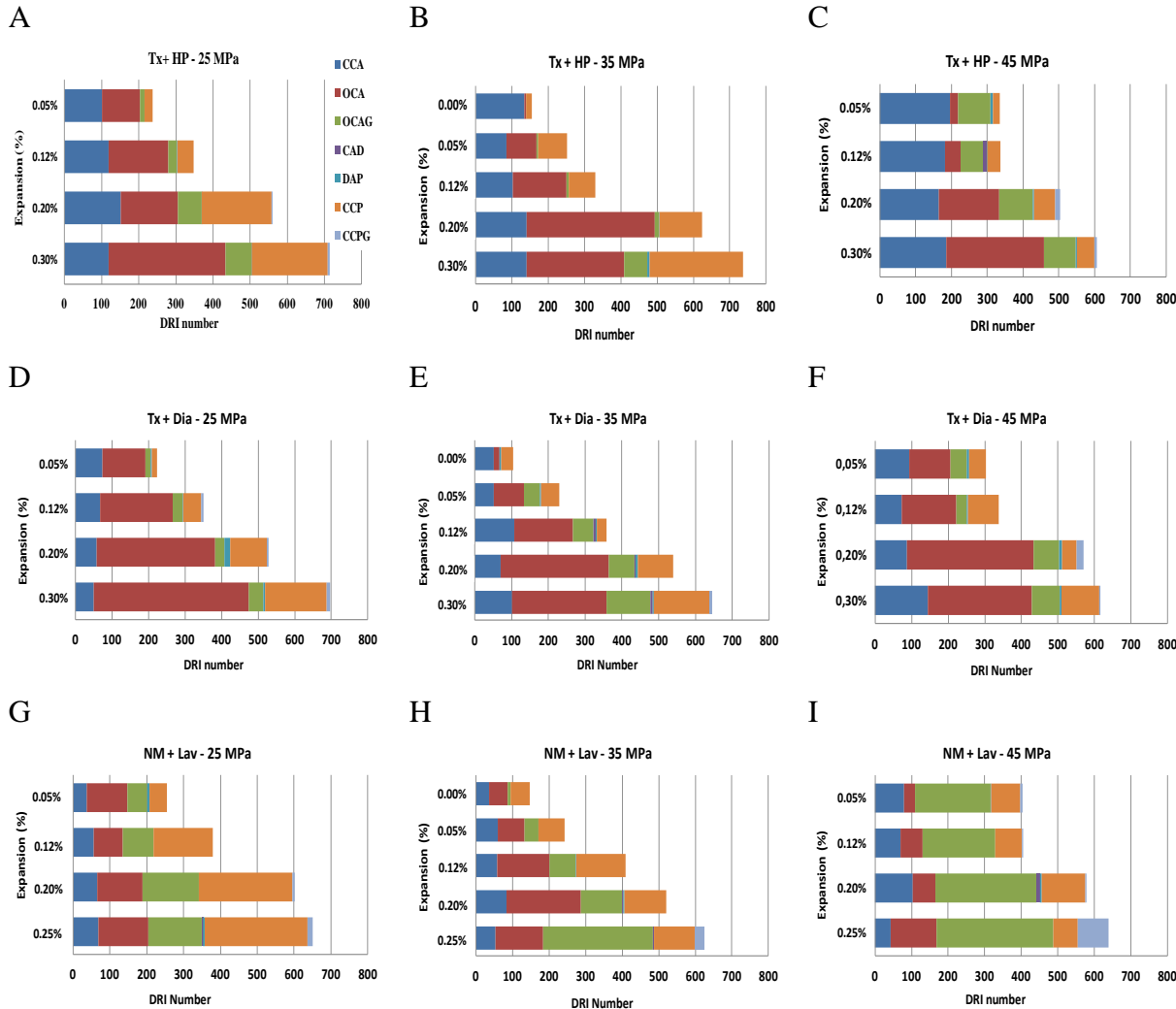


Figure 12: DRI charts for all the mixtures analyzed over the study: A, B, C. Tx sand + HP D, E, F. Tx sand + Dia. G, F, H. NM gravel + Lav. The common legend for all graphs is given in Figure A; Table 1 provides the definition of the various petrographic features.

The DRI values correlate well with the expansion levels measured for all the mixtures and aggregates selected for the study (Figure 13). Moreover, it appears that the DRI values do not change significantly as a function of the concrete strength as all the mixtures presented quite similar results for all the expansion levels studied. Also, the DRI values seem to be not affected by the deleterious expansion process whether it originates from the fine (Tx) or the

coarse (NM) aggregate (Figure 13). It is important to mention that the original method proposed by Grattan-Bellew and coworkers had been developed for ASR generated in the coarse aggregate fraction. Consequently, in order to use it with reactive sands, the original method was modified by determining the cracking characteristics of aggregates for particles down to 1 mm in size, thus allowing to include particles of the coarse portion of the Tx sand, the main source of the reaction in that case. It is also important to mention that the identification of ASR products in cracks of the aggregate particles and of the cement paste is often a challenge, especially at low expansion levels. This was indeed found to be an important source of variability between petrographers involved in a DRI precision study carried out at Laval University [2]. The use of chemical treatments, such as uranyl acetate solution [34], or of coloration techniques [35] can help in confirming the presence and distribution of ASR products; however, their use/ availability is not necessarily generalized for various reasons. In order to minimize the negative impact on the DRI calculations resulting from the difficulties in identifying ASR products, Villeneuve et al. [2] proposed to use similar weighing factors for cracks, with or without reaction products (see Table 1). This is indeed logical considering that the identification of ASR gel for ASR diagnosis purposes can be done through formal petrographic examination of the concrete specimens using advanced petrographic tools like scanning electron microscopy (SEM) with energy dispersive X-ray analysis (EDXA). The DRI is really a complementary tool whose objective is to quantify damage through crack counting. Consequently, the potential impact on the DRI values resulting from differences in the amount of gel that could have been generated from one aggregate type to another, or from one mix design to another, as a function of increasing expansion due to ASR, was minimized since the examinations primarily focused on crack counting.

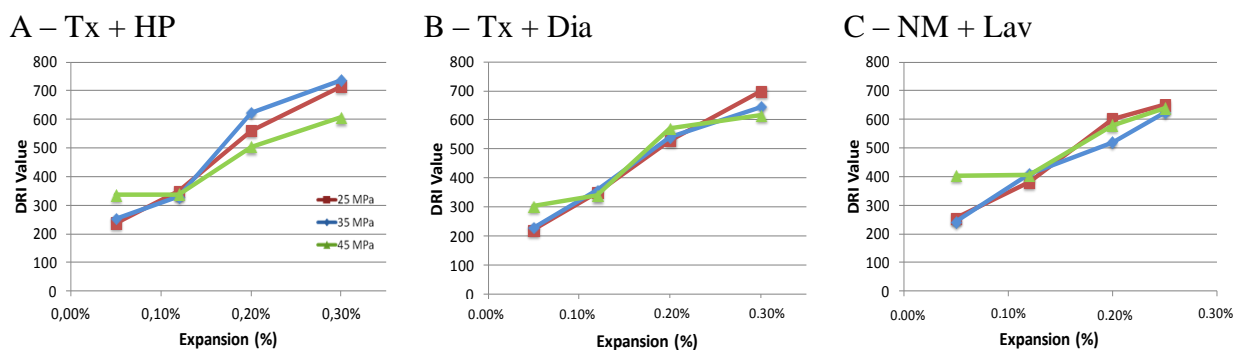


Figure 13: Comparison between the DRI values and the expansion of the test specimens: A) Tx sand + HP, B) Tx sand + Dia. C) NM gravel + Lav.

An interesting behavior could be noticed for all 45 MPa concrete mixtures. There is almost no noticeable difference between the damage degrees highlighted by the DRI values obtained for expansion levels of 0.05% and 0.12%, at least at the magnification used for the test, which is about 15-16x. It thus seems that for such cases, a significant degree of damage due to ASR has developed at relatively low expansion (i.e. 0.05%) in 45 MPa concretes. The above deterioration is, on one hand, higher than that obtained for the 25 and 35 MPa concretes at low expansion, but, on the other hand, remains stable up to 0.12% for 45 MPa mixtures, while increasing almost linearly and similarly to the other mixtures from about 0.12% up to the highest expansion levels tested in this study (0.30%).

8.6 DISCUSSION

This section provides more detailed analysis and discussion of the results obtained in this study. Four different items for further discussion can be identified from the data presented in Section 6 and illustrated in Figure 12, i.e. a) the development of damage in concrete as a function of increasing ASR-induced expansion; b) the effect of the concrete strength on damage generation with increasing expansion levels; c) the effect of fine vs. coarse reactive aggregates on the generation of expansion and damage and; d) the effect of the nature of the non-reactive coarse aggregate used in combination with the reactive sand.

8.6.1 Review of the development of damage in concrete with increasing expansion due to ASR

Figures 14 and 15 illustrate the above typical features of deterioration observed at 15x magnification as a function of increasing expansion for ASR generated either in the fine (Tx) or coarse (NM) aggregates. Based on the petrographic observations made on the polished sections selected for this study, it appears quite clearly that *opened cracks* (Group II – see section 5.1) generally appear inside the reactive aggregate particles in the early stages, visible at 0.05% expansion, as a result of the chemical reaction process (Figures 12, 14A, 15A). For low expansion degrees (0.05%), only few cracks are visible in the cement paste and they are generally very thin (≤ 0.05 mm); it is unusual to observe *opened cracks* in the cement paste at that level of expansion, at least, once again, at the magnification used for the DRI. When such cracks are present, it is not clear that they necessarily resulted from ASR. These cracks might

have perfectly been created by other mechanisms of distress such as early shrinkage, creep, etc.

With the progress of reaction/expansion process, some of the opened cracks that were formed inside the aggregate particles increase in length and width, some of them extending slightly into the cement paste; this is readily visible at the 0.12% expansion level (Figures 14B and 15B). At that point, only a small amount of silica gel can undoubtedly be identified in the cracks in either the aggregate particles or in the concrete matrix.

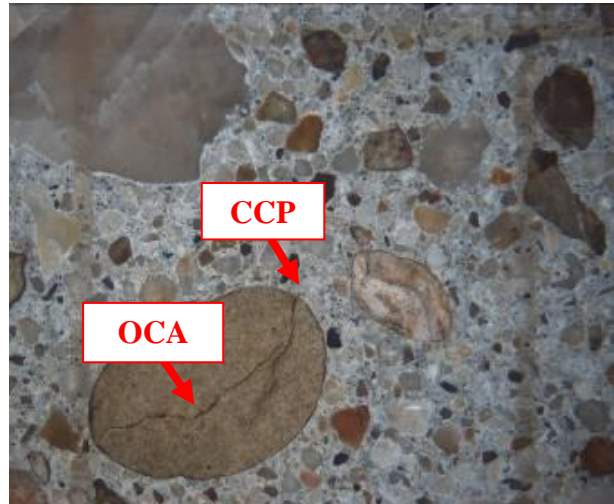
For higher expansion levels (e.g. 0.20%), most of the *opened cracks* formed inside the aggregate particles due to ASR extend into the cement paste. At this point, the crack density values calculated by the sum of opened cracks in the reactive aggregate particles and cracks in the cement paste given in units/cm² (Figure 10) are noticeably larger than before. Likewise, gel can be easily found at that level, mainly inside the aggregate particles (Figures 14C and 15C).

Finally, at a very high expansion degree (0.25-0.30%), *cracks* in the cement paste are often found linked to opened cracks (with or without reaction products) formed inside other aggregate particles, which results in an extended network formation (highest L_{max} values – Figure 11; Figures 14D and 15D).

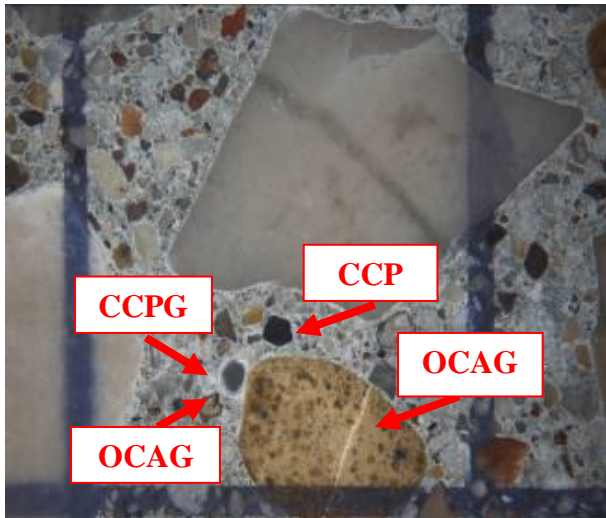
A – 0.05% - Tx + HP



B – 0.12% - Tx + HP



C – 0.20% - Tx + HP



D – 0.30% - Tx + HP

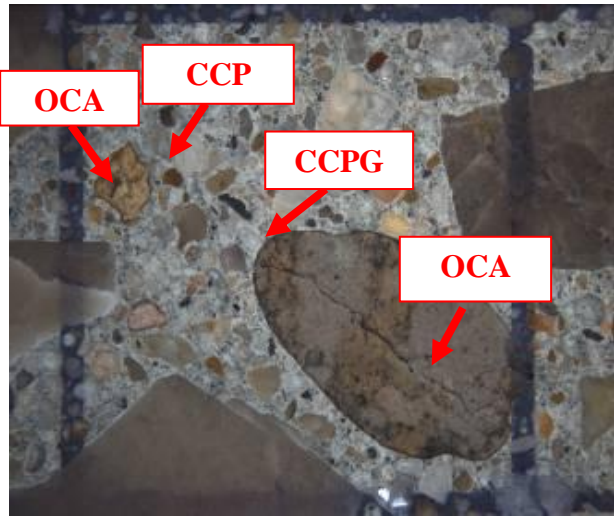
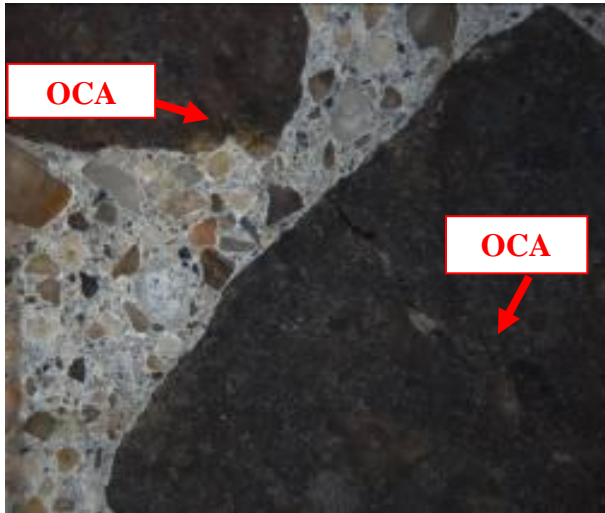
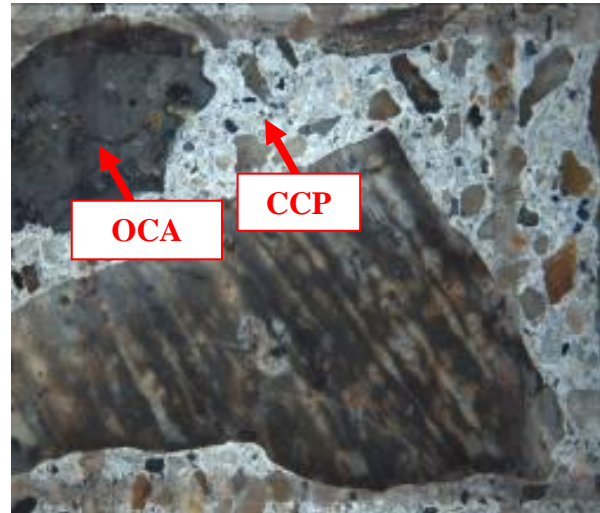


Figure 14: Micrographs from polished sections made with reactive Tx sand mixtures for all the expansion levels assessed: A. 0.05% - few microcracks limited to the reactive aggregate particles. B. 0.12% - opened cracks in the reactive aggregate particles (coarse sand particles) extending into the cement paste. C. 0.20% - cracks formed in three different fine aggregate particles which already reached the cement paste but are not connected; closed cracks are also observed in non-reactive HP limestone particles. D. cracks formed in reactive Tx sand particles linked to each other.

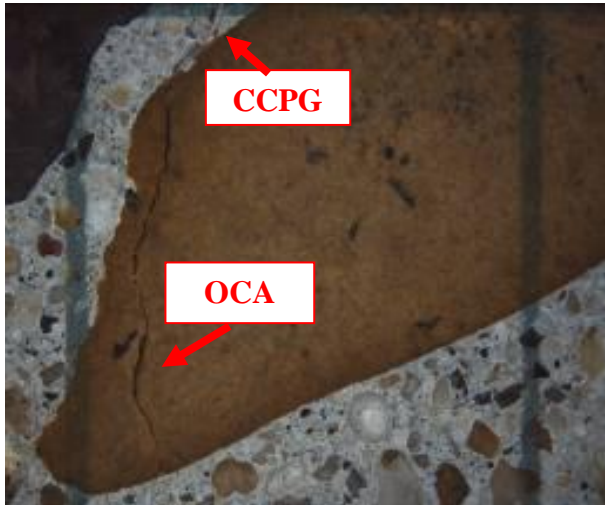
A – 0.05% - NM + Lav



B – 0.12% - NM + Lav



C – 0.20% - NM + Lav



D – 0.25% - NM + Lav

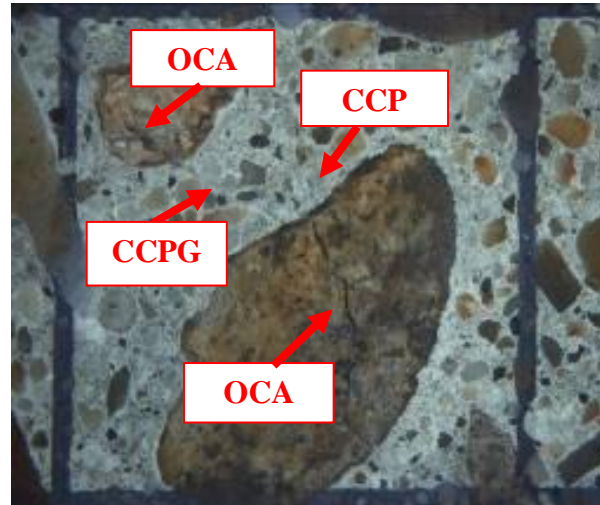


Figure 15: Micrographs from polished sections made with reactive NM gravel mixtures for all the expansion levels assessed: A. 0.05% - opened cracks in the reactive aggregate particles. B. 0.12% - opened cracks in the aggregate particles extending into the cement paste. C. 0.20% - opened cracks formed in two different aggregate particles which already reached the cement paste but are not connected. D. 0.25% - cracks formed in a reactive gravel particle extending into the cement paste - formation of a dense cracking pattern.

8.6.2 Effect of the concrete strength on damage generation at increasing expansion levels

Regarding the effect of the concrete mix design strength on damage generation/expansion, petrographic data suggest that, for each aggregate combination tested, there is no major difference between the 25 and the 35 concrete mixtures, in terms of development of microscopic features of damage as a function of expansion due to ASR (see Figures 12 and 13). Therefore, this suggests that a similar pattern of distress develops within both concrete mixtures and the slight differences could likely be linked to the heterogeneity of either the concrete studied or the ASR damage process.

Petrographic observations suggest, however, that the development of the features of deterioration is somewhat different for the 45 MPa concretes. First, for similar expansion levels, cracking in the 45MPa polished sections was significantly more difficult to identify because cracks were much finer in the cement paste than for the 25 and 35MPa concretes, at the magnification used for the DRI (15-16x); this was particularly true for the polished sections incorporating the reactive Tx sand. In the early stages of the reaction/expansion process (i.e. at 0.05% expansion), a higher degree of damage was observed in the 45 MPa concrete specimens than in the 25 and 35 MPa concrete; this was mainly related to a greater number of opened and closed microcracking inside the aggregate particles, but also to a greater presence of the reaction product (Figure 12), thus resulting in higher DRI values in the above concretes (Figure 13). This was found for all 45 MPa concretes, i.e. incorporating the various aggregate combinations (reactive fine and coarse aggregates) investigated. Between 0.05 and 0.12% expansion levels, however, no significant differences/increase in the counts of features of deterioration was noticed within the 45 MPa mixtures. This can be seen from Figure 6C with relatively small changes in the proportions of the different features of deterioration, in Figures 11A to 11C with similar L_{max} values, and in Figures 12 and 13 with similar DRI values, in that range of expansions for the 45 MPa concretes. Petrographic symptoms of distress would then start increasing again in the 45 MPa concretes following very similar trends as the other mix designs for higher expansion levels (0.20% and 0.30%) (Figure 13). Moreover, the presence of gel in cracks of the aggregate particles and of the cement paste is significantly larger or much more readily visible in the 45 MPa concrete specimens than in the 25 and 35 MPa specimens, at similar expansion levels (Figures 12G, 12H and 12I).

8.6.3 Effect of fine vs. coarse reactive aggregates on the generation of damage and expansion

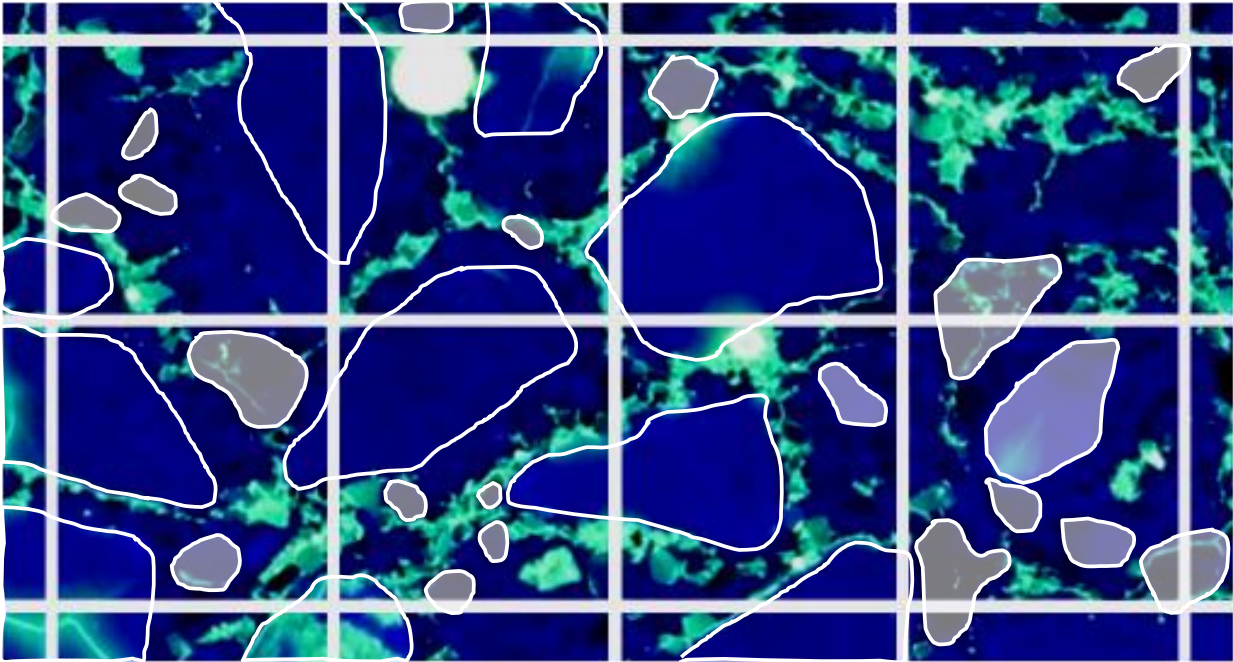
As mentioned before, the DRI method was modified from the original procedure proposed by Grattan-Bellew and coworkers [3,4] in order to evaluate the effect of the type of reactive material (i.e. reactive sand versus reactive coarse aggregate) on damage generation in concrete. It was indeed necessary to count distress features down to particles of 1 mm in size to account for reactive sand particles, instead of 2 mm as proposed for reactive coarse aggregates. In general, the examination of polished sections under the stereomicroscope at 15-

16x magnification for DRI determination was found to be adequate for measuring crack development in aggregate particles down to 1mm in size as well as in the cement paste around such reactive particles. It is important to note that most of the reactive particles in the Tx sand are concentrated in the 1 to 5 mm size fraction.

Considering the results in a quantitative way, no significant differences in the DRI values were obtained for ASR generated within the sand or the coarse aggregate fraction as the results were very similar for all the concrete mixtures (Figures 13A, 13B and 13C). However, regarding the petrographic observations in a more qualitative way in terms of global cracking patterns, one could notice, as illustrated in Figure 16, that the cracking pattern for ASR coming from a reactive sand is somewhat more sparsely distributed within the concrete matrix (Figures 16A), compared to when ASR is generated in the coarse aggregate fraction (Figures 16B) (see also Figures 1C et 1D).

Other interesting petrographic features of deterioration were identified in the test specimens, especially regarding the presence and progress of closed cracks within the aggregate particles of the different types of concrete mixtures. In the case of ASR generated in the sand fraction, the proportion of closed cracks in the “reactive” sand particles (i.e. mainly concentrated in the 1 to 5 mm size fraction) was found to decrease as a function of the expansion up to about 0.20%, while the proportion of opened cracks increases (Figure 9A); this suggests that the concrete pore solution “uses” at least some of these “fast tracks” channels to penetrate into the reactive fine aggregate particles and access siliceous minerals to form alkali-silica gel, which will in turn induce internal expansion within the above fine aggregate particles that will extend into the cement paste with increasing expansion. For higher expansion values (e.g. 0.30%), an increase in the proportion of closed cracks seems to occur in the above particles (Figure 9A), which could be linked to the development of expansive stresses and associated extensive microcracking that is progressing into the cement paste due to ASR. Petrographic observations also confirmed that the proportion of closed cracks within the non-reactive coarse limestone aggregate particles (HP) increases with increasing expansion, especially at the higher levels (Figure 9B). It does appear that the expansive ASR stresses generated by the large number of reactive Tx sand particles in the concrete matrix would choose a “path of least energy release”, thus causing cracking to increase also in some sand particles as well as in non-reactive coarse aggregate particles. Actually, at higher expansion levels (0.25%, 0.30% and further), some of those closed cracks found in non-reactive coarse aggregate particles actually became opened through the progress of the expansion in the test specimens.

A: Tx + HP, 25 MPa – 0.20% expansion



B. NM + Lav, 25 MPa, 0.20% expansion

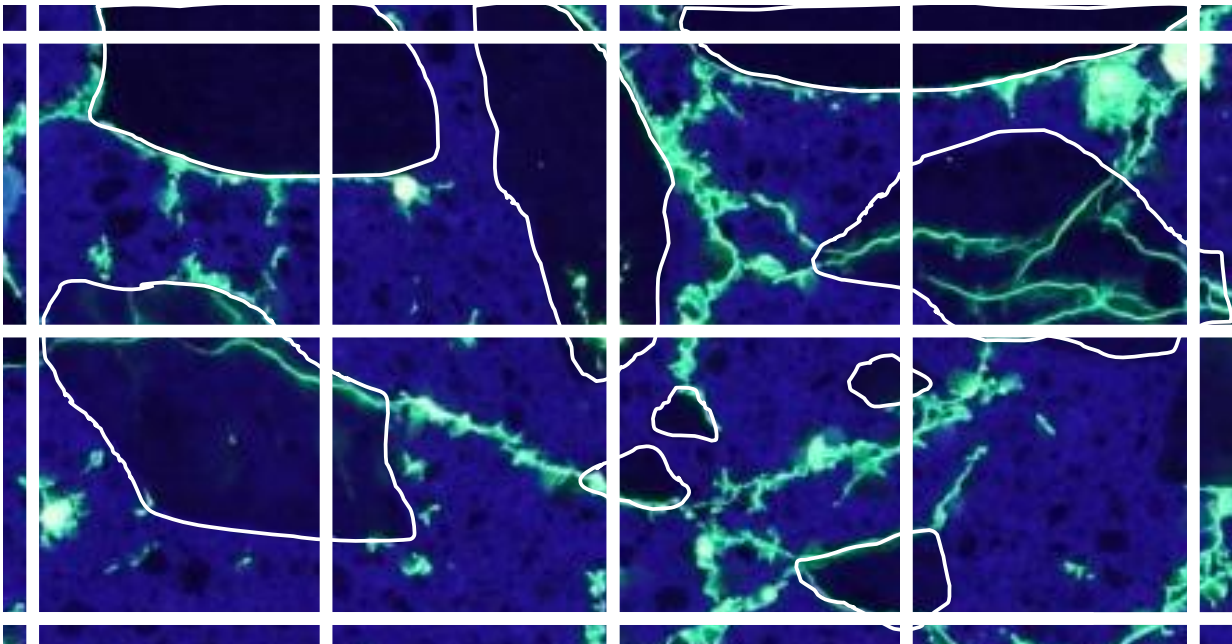


Figure 16: Series of eight 1cm² sections on polished concrete slabs impregnated with a fluorescent epoxy under UV illumination; A. 25 MPa concrete incorporating the reactive Tx sand at 0.20% expansion. The reactive fine aggregate particles (Tx) are of grey color (or shaded), while the perimeter of the non-reactive coarse aggregate particles are highlighted. B. 25 MPa concrete incorporating the reactive NM gravel at 0.20% expansion. The perimeter of the reactive coarse aggregate particles (NM) are highlighted; some particles (volcanic) show internal cracking that extends into the cement paste.

In the case of ASR generated in reactive coarse aggregate particles, the proportion of closed cracks in the reactive coarse aggregate particles remains stable or decreases slightly with

increasing expansion (Figures 6 to 8); on the other hand, the Group II cracks (opened cracks in the aggregate particles, with and without gel) and Group III cracks (cracks in the cement paste, with and without gel) increase, especially in the 25 and 35 MPa concretes (Figure 7). This is related to the progress of ASR in the coarse aggregate particles.

8.6.4 Effect of the nature of the non-reactive coarse aggregate used in combination with the reactive sand

As suggested in the data presented in the Figures 6 and 7, the extent of cracking in the non-reactive coarse aggregate particles, when expansion is generated in the fine aggregate fraction, seems to depend, to some extent, on the nature of that coarse aggregate. The data suggest that the tougher/stiffer the coarse aggregate (e.g. Diabase (Dia) - theoretical average toughness (K_c) – 3.49 MN/m^{1.5}) versus limestone (HP) - theoretical average toughness (K_c) – 2.23 MN/m^{1.5}) [36], the higher the expansion, or actually the stress level generated in the concrete matrix, required to induce cracking within the coarse aggregate particles. The petrographic observations indeed showed that the non-reactive coarse limestone aggregate particles in the mixtures Tx + HP presented at all levels of expansion a much larger number of closed cracks compared to that obtained in the diabase particles of the Tx + Dia mixtures. This might be explained by either the crushing process (or weathering of the aggregates) or even by the differences of mechanical characteristics of those aggregates. However, since the final DRI values for both series of mixtures (i.e. Tx + HP and Tx + Dia), were comparable at similar expansion levels, it means that the differences in the closed crack features were offset by other different distress features (opened cracks in the aggregates or in the paste, for example), which made the final values of these analysis almost similar.

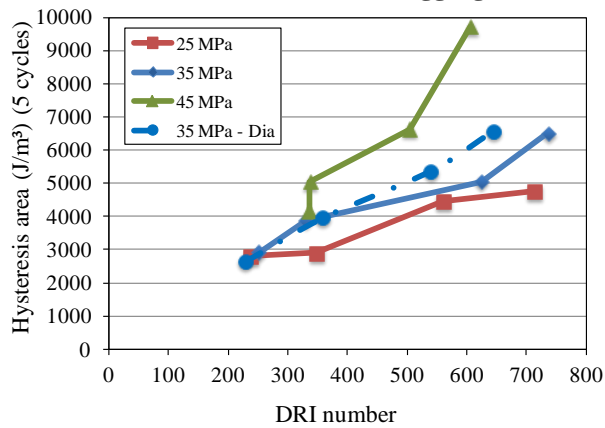
8.6.5 Correlation between petrographic features of deterioration and mechanical properties of ASR-affected concrete

The evaluation of the current condition of aging concrete structures, especially those affected by deleterious mechanisms such as ASR, often takes part of the process of evaluating options for extending their service life and/or establishing mitigation strategies. The DRI is certainly interesting as it provides a semi-quantitative assessment of the severity of damage in the concrete element under investigation. Data presented in the previous sections have shown that

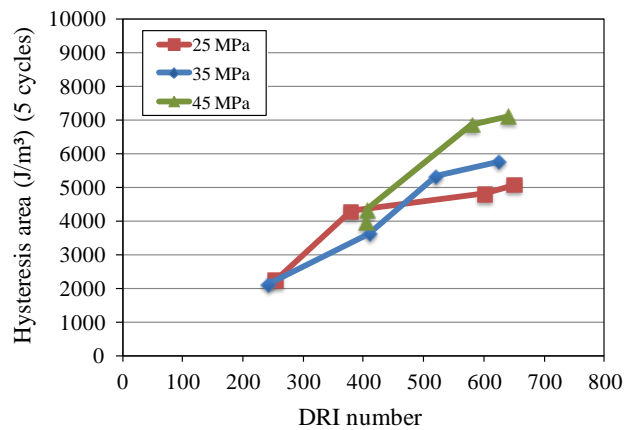
the DRI correlates well with the amount of expansion induced in concrete specimens where ASR is generated through deleterious reactions either in the coarse or the fine aggregate. Even if expansion is often considered an indirect indication of the extent of ASR in concrete specimens in laboratory investigations, it would appear necessary to validate the diagnostic character of the DRI for evaluating the condition and progress of damage in concrete. Many studies carried out over the past few decades have shown that ASR can affect the mechanical properties of concrete as a “material”. Usually, ASR generates a significant reduction in tensile strength and modulus of elasticity of concrete. These two properties are much more affected than compressive strength, which begins to decrease significantly only at high levels of expansion [25, 37-40]. Studies dealing with the mechanical responses of damaged materials suggest that the *Stiffness Damage Test* (SDT) can provide a diagnostic evaluation of the “degree of damage” in concrete affected by ASR [41-42]. The SDT consists in subjecting a set of concrete specimens, for example 100 by 200 mm cores extracted from an aging concrete member, to five cycles of uniaxial loading/unloading up to a selected loading level. As part of this study, Sanchez et al. [43] applied the SDT to companion concrete cylinders cast from the same mixtures as those described in this study. The analyses of the test data carried out with the three types of concrete (25, 35 and 45 MPa) and the two highly-reactive aggregates (NM gravel and Tx sand) selected showed that the SDT should be carried out with a percentage of the 28-day design strength (ideally 40%) to optimize its diagnostic value as a tool for damage evaluation. Also, SDT output parameters such as the *hysteresis area* (especially) and the *plastic deformation* over the five cycles of loading/unloading as well as the average *modulus of elasticity* of the second and the third cycles, were found to provide a good indication of the amount of expansion reached by the concrete.

The graphs in Figure 17 compare the results of the *Hysteresis Area* (HA) and loss in *Modulus of Elasticity* (ME) parameters and the main results of the petrographic examination of the test specimens (i.e. DRI numbers). Results are reported for test specimens of the 25, 35 and 45 MPa concrete mixtures incorporating reactive fine (Tx sand) and coarse (NM gravel) aggregates and tested at each of the expansion levels selected for this study. Good correlations are generally obtained between the HA and ME parameters and the DRI values for ASR expansion/damage being generated either in the fine aggregate (Figures 17A and 17C) or the coarse aggregate (Figures 17B and 17D) particles.

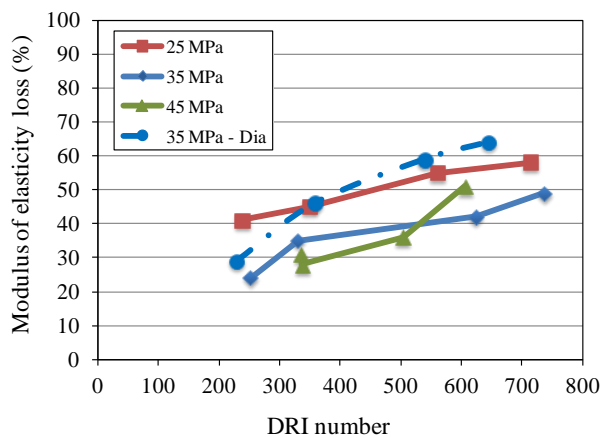
A – Tx sand + HP coarse aggregate



B – Lav sand + NM coarse aggregate



C – Tx sand + HP coarse aggregate



D – Lav sand + NM coarse aggregate

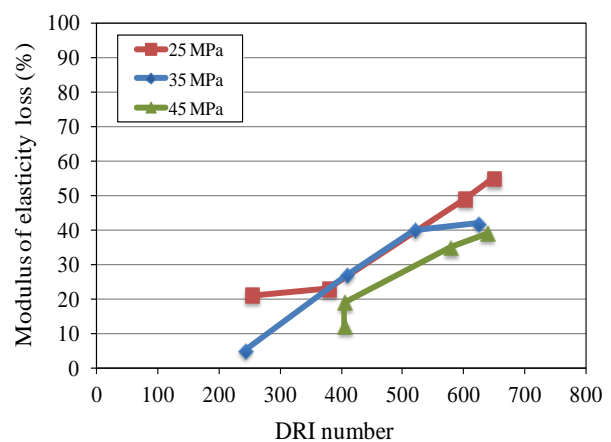


Figure 17: Correlation between the results of the petrographic examination (DRI values) of polished sections cast from 25, 35 and 45 MPa concrete specimens incorporating reactive coarse (NM) or fine (Tx) aggregates and the results of stiffness damage testing of companion specimens at the same expansion levels (0.05, 0.12, 0.20 and 0.25 for NM gravel; 0.05, 0.12, 0.20 and 0.30% for Tx sand). A & B. Hysteresis area (HA); C & D. Loss in elasticity modulus (calculated in % as a function of the value obtained at 0.0% of expansion at each expansion level).

In the case of the 25 MPa and 35 MPa concretes, a progressive increase in the DRI values, mainly related to an increase in the number of cracks in the reactive fine (Tx) or coarse (NM) aggregate particles (Groups I and II) and in the cement paste (Group III) (Figure 6), was measured as a function of increasing expansion of the concrete specimens (Figures 12 and 13); this correlates well with the progressive increase in the *Hysteresis area* (HA) and loss in *Modulus of elasticity* (ME) parameters measured through stiffness damage testing (Figure 17). On the other hand, the 45 MPa concrete specimens showed a somewhat different behavior. First, higher HA values are generally obtained for the 45 MPa specimens since more energy is required to close microcracks disseminated throughout the concrete specimens under compression testing in 45 MPa concretes. Also, petrographic observations indicated that the total number of counts of cracking in the aggregate particles and in the cement paste (sum of

Groups I to III counts) (Figure 6), and consequently the DRI values, are generally higher at early expansion level in the 45 MPa concretes than in the 25 and 35 MPa concretes, with only a small increase in microcracking (or DRI values) being observed between the 0.05 and 0.12% expansion levels (Figure 6C). This resulted in higher HA values for the 45 MPa concrete at 0.05% expansion than for the 25 and 35 MPa concretes, but a small increase in the HA values (Figures 17A and 17B) and limited loss in ME values (Figures 17C and 17D) between 0.05 and 0.12% expansion levels. Starting with the 0.12% expansion level, the correlations between the DRI and the HA and ME parameters were found to change at fairly similar rates (i.e. increase in HA values and in ME losses) as a function of increasing expansion, as for the 25 and 35 MPa concretes.

8.7 CONCLUSION

Concrete specimens cast from a series of concrete mixtures of different strengths (25, 35 and 45 MPa) and incorporating reactive coarse or fine aggregates were examined at expansion levels ranging from 0.05 to 0.30% in order to determine their internal damage through the use of the *Damage Rating Index*. The following conclusions can be drawn from the results obtained in this study:

- The DRI output final value (using the latest procedure proposed by Villeneuve et al. [2]) was found to correlate well with the different ASR expansion levels studied in this work, when the deleterious reaction comes from either a reactive sand or a reactive coarse aggregate;
- Interesting and important information can also be obtained through the evaluation of the detailed DRI results/charts, as well as through the study of the cracking development in the aggregate particles as a function of the expansion level of the affected concrete specimens. A trend for increasing counts of *opened cracks* (with and without gel) was observed with increasing expansion of the test specimens. Those cracks generally appear inside the reactive aggregate particles (sand or coarse aggregate) and when the expansion increases, the cracks increase in length and width. For higher levels of distress (expansion levels $\geq 0.20\%$), most of the cracks formed inside the aggregate particles extend into the cement paste, increasing significantly the crack density (units/cm²) in the concrete matrix. On the other hand, the behavior of the closed cracks (within either the reactive or non-reactive aggregate particles) is not so simple and linear vs. the expansion level. To explain this behavior, one needs to analyze the following two scenarios:

- for ASR coming from the sand, the number of closed cracks within the reactive fine aggregate particles tend to decrease as a function of the expansion up to about 0.20%, which means that the pore solution “uses” at least some of these “fast track” channels to access the inner parts of the particles, generate alkali-silica gel and induce excessive expansion forces that will in turn cause cracking to extend into the cement paste with increasing expansion. For higher expansion values (0.25%, 0.30% and further), an increase in the number of closed cracks in the sand particles is observed, which could be linked to the development of ASR (i.e. indirect effects due to the pressure generation in the mortar fraction of the concrete). On the other hand, the number of closed cracks within the non-reactive coarse aggregate particles increases with increasing expansion, which means that ASR pressure influences the development of new cracks in those aggregate particles (more or less depending on the mechanical characteristics of the coarse aggregates). At higher expansion levels (0.25%, 0.30% and further), some of the closed cracks generally found in the non-reactive coarse aggregate particles can actually become opened by the progress of the expansion;
- for ASR coming from the coarse aggregate, the same trend was generally found (decreasing of the closed cracks vs. increasing expansion level). However, the mixture NM + Lav 25 presented just a slight decreasing trend for this parameter;
- For each of the different expansion levels selected in this study (0.05 to 0.30%), no significant differences in the DRI values were obtained between the 25 and 35 MPa concrete mixtures incorporating reactive material in the fine or coarse aggregate fraction. However, cracking seems to develop faster but remain stable up to 0.12% expansion in the 45 MPa mixtures, after what similar DRI values were found for all concretes investigated with increasing expansion. Moreover, the presence of gel was found to be greater in cracks of the 45 MPa concrete mixtures than with the other mixtures;
- The crack density (counts/cm²), as well as the measurement of the maximum cracks length and width, are interesting parameters to complement DRI determinations;
- The analyses of the basic counts of petrographic features of deterioration indicate that the number of either opened cracks within the aggregate particles or cracks in the cement paste increases with increasing expansion in the test specimens; the features are consequently considered as indicative of the progress of ASR in the test specimens examined;
- Studies carried out by the authors on the mechanical response of ASR-affected concretes showed that the “Stiffness Damage Test (SDT)” can provide a diagnostic evaluation of the “degree of damage” in the above concrete. Running the SDT at 40% of the mix design

strength was found to provide a good indication of the amount of expansion reached by the concrete through the use of parameters such as the *Hysteresis Area* (especially) and the *Plastic Deformation* over the five cycles of loading/unloading, as well as the average *Modulus of Elasticity* of the second and the third cycles;

- Coupling the results of the petrographic examination (DRI) and of the mechanical testing (SDT) of the ASR-affected concretes, it was found that:

- in the case of the 25 MPa and 35 MPa concretes, the progressive increase in the DRI values correlated very well with the progressive increase in the *Hysteresis Area* (HA) and loss in the *Modulus of Elasticity* (ME) parameters;

- Higher HA values are found for the 45 MPa specimens since more energy is required to close microcracks disseminated throughout the concrete specimens under compression testing in 45 MPa concretes. The total number of counts of cracking in the aggregate particles and in the cement paste, and consequently the DRI values, are generally higher and remain fairly stable up to about 0.12% expansion in the above concrete, which resulted in a small increase in the HA values and limited loss in ME values. After the 0.12% expansion level, the DRI and the HA and ME values were found to change at fairly similar rates (i.e. increase in HA values and in ME losses) as a function of increasing expansion for all concrete mixtures (25 to 45 MPa);

- Finally, the *Damage Rating Index* (DRI) was found to be a powerful tool for evaluating damage in concrete specimens affected by ASR incorporating reactive fine or coarse aggregates. However, this procedure still needs to prove its efficiency for a larger variety of aggregate types or for evaluating concretes affected by other distress mechanisms (e.g. delayed ettringite formation (DEF), freezing and thawing (FT)). Moreover, a careful analysis and assessment of the weighing factors would give even more impact on the DRI final results. Ideally, this study would be carried out comparing the microscopic features and the mechanical properties of the damaged concretes (*Stiffness Damage Test*, tensile and compressive strength). The above comparison could possibly help identifying DRI ranges corresponding to various degrees of internal damage in the aging concretes.

8.8 ACKNOWLEDGEMENTS

The funding of this project was provided by a grant from the Quebec Department of Transportation, under the supervision of Mr. Alain Hovington and Mrs. Nadia Pouliot. The authors would like to thank Mr. René Malo and Mr. Mathieu Thomassin from “le Centre de

recherche sur les infrastructures en béton (CRIB)” at Laval University, as well as the undergraduate research assistants who helped with the manufacturing and testing of the test specimens used in this project. L. Sanchez benefits from a Vanier scholarship financed by NSERC (Natural Sciences and Engineering Research Council of Canada).

8.9 REFERENCES

- [1] Fournier, B.; Bérubé, A. 2000. Alkali-aggregate reaction in concrete: a review of basic concepts and engineering implications. *Canadian journal of civil engineering*, 27 (2): 167-191.
- [2] Villeneuve, V.; Fournier, B.; Duchesne, J. 2012. Determination of the damage in concrete affected by ASR – The damage rating index (DRI). 14th International conference on alkali-aggregate reaction (ICAAR). Austin, Texas (USA). May 2012.
- [3] Dunbar, P.A.; Grattan-Bellew, P.E. 1995. Results of damage rating evaluation of condition of concrete from a number of structures affected by ASR. CANMET/ACI International Workshop on Alkali-Aggregate Reactions in Concrete, Dartmouth, Canada, October 1995.
- [4] Grattan-Bellew, P.E.; Mitchell, L.D. 2006. Quantitative petrographic analysis of concrete –The Damage Rating Index (DRI) method, a review. Proc. Marc-André Bérubé symposium on AAR in concrete, CANMET/ACI Advances in concrete technology seminar, Montréal, Canada, May 31 & June 1, 2006.
- [5] Shrimmer, F.H. 2000. Application and use of Damage Rating Index in assessment of AAR-affected concrete-selected case studies. 11th International conference on alkali-aggregate reaction (ICAAR). Québec, Canada, June 2000, 899-907.
- [6] Rivard, P.; Fournier, B.; Ballivy, G. 2002. The DRI method for ASR affected concrete - A Critical review of petrographic features of deterioration and Evaluation Criteria. *Cement, concrete and aggregates*, 24(2): 1-10.
- [7] Rivard, P.; Ballivy, G. 2005. Assessment of the expansion related to alkali-silica reaction by the Damage Rating Index method. *Construction and Building Materials*, 19: 83-90.
- [8] Bérubé, M.A.; Smaoui, N.; Fournier, B.; Bissonnette, B.; Durand, B. 2005. Evaluation of the expansion attained to date by concrete affected by ASR - Part III: Application to existing structures. *Canadian Journal of Civil Engineering*, 32: 463-479.
- [9] Shrimmer, F.H. 2006. Development of the Damage Rating Index Method as a tool in the assessment of alkali-aggregate reaction in concrete: a critical review. Proc. Marc-André Bérubé symposium on AAR in concrete, CANMET/ACI Advances in concrete technology seminar, Montréal, Canada, May 31 & June 1 2006, 391-411.
- [10] Powers, L.; Shrimmer, F. H. 2009. Quantification of ASR in concrete: an introduction to the Damage Rating Index. ICMA conference. International Cement Microscopy Association / Society of Concrete Petrographers joint meeting, Quebec City, Canada, May 2009.
- [11] Blight, G.E.; McIver, J.R.; Schutte, W.K.; Rimmer, R. 1981. The effects of alkali-aggregate reaction on reinforced concrete structures made with Witwatersrand quartzite aggregate. 5th International conference on AAR in Concrete (ICAAR). Cape Town, South Africa, 1981.
- [12] Sims, I.; Hunt, B.; Miglio, B. 1992. Quantifying microscopical examinations of concrete for AAR and other durability aspects. American Concrete Institute, SP 131-114, 267-287.
- [13] Salomon, M.; Panetier, J.L. 1994. Quantification du degré d'avancement de l'alcali-réaction dans les bétons et de la néofissuration associée. 3rd CANMET/ACI International conference on durability of concrete. Nice, France, 1994, 383-401.
- [14] Clemena, G.G.; Lane, S.; Freeman, T.; Lozev, M. 2000. Evaluation of nondestructive evaluation methods for application in early detection of deterioration in concrete pavements. Report VTRC 00-R13. Virginia Transportation Research Council, Charlottesville, USA, 26p.
- [15] Rivard, P.; Fournier, B.; Ballivy, G. 2000. Quantitative petrographic technique for concrete damage due to ASR: Experimental and Application. *Cement, concrete and aggregates*, 22 (1): 63-72.

- [16] Broekmans, M.A.T.M. 2002. The alkali-silica reaction: mineralogical and geochemical aspects of some Dutch concretes and Norwegian mylonites. PhD Thesis, Utrecht University, 144 p.
- [17] Lindgaard, J.; Skjolsvold, O.; Haugen, M.; Hagelia, P.; Wigum, B.J. 2004. Experience from evaluation of degree of damage in fluorescent impregnated plan polished sections of half-cores based on the "Crack Index Method". 12th International conference on AAR in Concrete. Beijing, China, 939-947.
- [18] British Cement Association. 1992. The diagnosis of alkali silica reaction – report of a working party. England.
- [19] St-John, D.A.; Poole, A.W.; Sims, I. 1998. Concrete Petrography: A handbook of investigative techniques, Arnold, London, 1998.
- [20] Detwiler, R.J.; Taylor, P.C. 2005. Specifier's guide to durable concrete. Engineering Bulletin 221, Portland Cement Association, Skokie (Illinois).
- [21] Reinhard, H. W.; Mielich, O. 2011. A fracture mechanics approach to the crack formation in alkali sensitive grains. *Cement and concrete research*. 2011, 41: 255- 262.
- [22] Wood, G. M.; Johnson, R. A. 1993. The appraisal and maintenance of structures with alkali-silica reaction. Paper, Institution of Structural Engineers.
- [23] Wood, G. M.; Norris, P.; Leek, D. 1989. Physical Behavior of AAR Damaged Concrete in Structures and in Test Conditions. 8th ICAAR - International Conference on Alkali-Aggregate Reaction in Concrete. Kyoto, Japan, 1989.
- [24] Wood, G. M.; Johnson, R. A. 1989. An engineer's perspective on UK. Experience with alkali-aggregate reaction. 8th ICAAR - International Conference on Alkali-Aggregate Reaction in Concrete. Kyoto, Japan, 1989.
- [25] Smaoui, N.; Bérubé, M.A.; Fournier, B.; Bissonnette, B.; Durand, B. 2004b. Evaluation of the Expansion Attained to Date by Concrete Affected by ASR - Part I: Experimental Study. *Canadian Journal of Civil Engineering*, 31, 826-845
- [26] Walker, H. N.; Lane, D. S.; Stutzman, P. E. 2006. Petrographic Methods of Examining Hardened Concrete: A Petrographic Manual, FHWA-HRT-04-150, Federal Highway Administration, McLean, VA (USA).
- [27] Grattan-Bellew, P. E.; Mitchell, L. D. 2002. Quantitative Petrographic Analysis for Concrete. 8th Symposium on Alkali-Aggregate Reactivity in Concrete. Montréal, Canada, 2002.
- [28] Grattan-Bellew, P.E.; Danay, A. 1992. Comparison of laboratory and field evaluation of AAR in large dams. Proc. of the International Conference on Concrete AAR in Hydroelectric Plants and Dams, Canadian Electrical Association & Canadian National Committee of the Int. Commission on Large Dams, September 28 – October 2 1992, Fredericton, New Brunswick, (Canada),.
- [29] Transtec Group. Field Site and Petrographic Evaluation - ASR Development and Deployment Program - Field Trials and Demonstration Projects. September 2009.
- [30] Bérubé, M. A.; Fournier, B.; Côté, T. 2012. Using the damage rating index for assessing the expansion of concrete affected by freeze-thaw, sulphate attack, or ASR. 14th ICAAR - International Conference on Alkali-Aggregate Reaction in Concrete. Texas, USA, May 2012.
- [31] Lindgard, J. 2013. Alkali-silica reaction (ASR) – Performance testing. PhD Thesis. NTNU (Norwegian University of Science and Technology), Norway.
- [32] Fournier, B.; Bérubé, M.A.; Folliard, K.J.; Thomas, M.D.A. 2010. Report on the diagnosis, prognosis and mitigation of ASR in transportation structures. Publication FHWA-HIF-09-004, Federal Highway Administration, McLean, VA (USA).
- [33] ASTM C 1074. 2011. Standard Practice for Estimating Concrete Strength by the Maturity Method.
- [34] Natesaiyer, K.; Hover, K.C. 1988. In situ identification of ASR products in concrete, *Cement and Concrete Research*, 18, 455-463.
- [35] Guthrie, G.D.; Carey, J.W. 1997. A simple environmentally friendly and chemical specific method for the identification and evaluation of the alkali-silica reaction, *Cement and Concrete Research*, 27, 1407-1417
- [36] Alexander, M.; Mindess, S. Aggregates in concrete. 2005. Book. Modern concrete technology series. Taylor & Francis. London.

- [37] Mindess, S.; Young, J. F.; Darwin, D. 2003. Concrete. Book. Pearson Education Ltda. second edition 2003.
- [38] British Cement Association. The diagnosis of alkali silica reaction – report of a working party. England. 1992. 36p.
- [39] Pleau, R.; Bérubé, M. A.; Pigeon, M.; Fournier, B.; Raphael, S. 1989. Mechanical Behavior of Concrete Affected by AAR. 8th ICAAR - International Conference on Alkali-Aggregate Reaction in Concrete. Kyoto, Japan, 1989.
- [40] Nixon, P.J.; Bollinghaus, R. The effect of alkali aggregate reaction on the tensile strength of concrete. *Durability of Building Materials* pp. 243-248, 1985.
- [41] Crisp, T. M.; Waldron. P.; Wood. J. G. M. 1993. Development of a non destructive test to quantity damage in deteriorated concrete. *Magazine of Concrete Research*. 45 (165), 247-256.
- [42] Crisp, T. M.; Wood, J. G. M.; Norris, P. 1989. Towards Quantification of Microstructural Damage in AAR Deteriorated Concrete. International Conference on Recent Developments on the Fracture of Concrete and Rock. , The University of Wales, Cardiff, September 1989, 9p.
- [43] Sanchez, L.; Fournier, B.; Jolin, M.; Bastien, J. Evaluation of the Stiffness Damage Test (SDT) as a tool for concrete's assessment damaged due to ASR – test loading and output responses for concretes incorporating fine or coarse reactive aggregates. *Cement and concrete research*, 56: 213-229.

9. PAPER IV: ASSESSMENT OF MICROSCOPIC DAMAGE FEATURES OF ALKALI-AGGREGATE REACTION (AAR) THROUGH THE DAMAGE RATING INDEX (DRI)

Sanchez. L.F.M.^a; Fournier. B.^b; Jolin. M.^c, Josée Duchesne^d

(a) MSc. – Laval University – PhD candidate.

1065, avenue de la Médecine, Pavillon Adrien-Pouliot, local 3755 Tel.: 1 (418) 704-2435

leandrofms@gmail.com / le.sanchez@uol.com.br

leandrofms@gmail.com / le.sanchez@uol.com.br

(b) Prof. Dr. – Laval University. Quebec. QC. Canada

benoit.fournier@ggl.ulaval.ca

(c) Prof. Dr. – Laval University. Quebec. QC. Canada

marc.jolin@gci.ulaval.ca

(d) Prof. Dr. – Laval University, Quebec, QC, Canada

josee.duchesne@ggl.ulaval.ca

ABSTRACT

This work presents the assessment of twenty concrete mixtures incorporating ten different reactive aggregates through the Damage Rating Index (DRI), a microscopic and semi-quantitative petrographic tool, with the aim of verifying the AAR distress development as a function of the specimen's expansion as well as the likely differences of the microscopic distress features resulting from different aggregate types/natures. The DRI was found to provide a reliable assessment of the damage degree in concretes incorporating reactive fine or coarse aggregates. An envelope of damage results against the expansion level of the affected materials is proposed. For all alkali-silica reactive aggregates investigated, the progress of counts and proportions of opened cracks in the aggregate particles and in the cement paste, with and without gel, as well as the crack density parameter, were found to be diagnostic petrographic features for quantifying ASR progress. Moreover, a qualitative ASR distress model in concrete was defined.

Keywords: damage rating index (DRI), assessment of damage, microscopic damage features, alkali-silica reaction, alkali-carbonate reaction

RÉSUMÉ

Ce travail présente l'évaluation de vingt mélanges de béton incorporant dix granulats réactifs différents par l'entremise du Damage Rating Index (DRI), un outil pétrographique semi-quantitatif. Cette étude vise à vérifier le développement de l'endommagement du à la RAG en fonction de l'expansion des échantillons affectés, ainsi que les probables différences provenant des caractéristiques microscopiques distinctes des différents types/natures de granulats étudiés. Le DRI a permis d'obtenir une évaluation fiable du degré d'endommagement des bétons incorporant une large variété de granulats réactifs. En plus, une enveloppe de résultats a été établie en fonction du niveau d'expansion des éprouvettes analysées. Pour les granulats susceptibles de la réaction alcalis-silice (RAS), l'évaluation du nombre de fissures dans les particules de granulats ou la pâte de ciment (avec ou sans gel), en nombre ou en proportion, ainsi que la densité de fissures (sur la surface examinée) ont été jugées fiables et diagnostiques pour quantifier l'avancement de la RAS. De plus, un modèle qualitatif du développement de la RAS en fonction de l'expansion est proposé.

Mots clés: damage rating index (DRI), évaluation de l'endommagement microscopique, réaction alcalis-silice (RAS), réaction alcalis-carbonate (RAC)

9.1 INTRODUCTION

Alkali-silica reaction (AAR), a harmful chemical reaction between certain mineral phases of the aggregates and the alkali hydroxides of the concrete pore solution is one of the main deleterious processes affecting the durability of concrete infrastructure worldwide [1]. Over the past decades, engineers and researchers have been trying to develop tools and procedures to assess the current condition (diagnosis) and the potential for further expansion/distress (prognosis) of concrete damaged due to ASR, essential steps for selecting efficient methods to treat (protect, repair and/or reinforce) a structural concrete element suffering from ASR. In this context, Grattan-Bellew and coworkers [2, 3] proposed the *Damage Rating Index method* (DRI), a semi-quantitative petrographic method that is increasingly being used around the world [4-9], as well as other petrographic methods [10-16], for assessing damage in polished concrete sections.

9.2 AAR DISTRESS MECHANISMS IN CONCRETE

Overall, AAR can be divided in two main reaction types: alkali-silica reaction (ASR) and alkali-carbonate reaction (ACR). ASR is by far the most common reaction type found worldwide, and its distress mechanism is already fairly well understood, at least in its major steps. It consists in a distressful chemical reaction between “unstable” silica mineral forms within the fine and/or coarse aggregate materials and the alkali hydroxides (Na, K – OH) dissolved in the concrete pore solution. It generates a secondary *alkali-silica gel* that induces expansive pressures within the reacting aggregate material(s) and the adjacent cement paste upon moisture uptake from its surrounding environment, thus causing microcracking, loss of material’s integrity (mechanical/durability) and, in some cases, functionality in the affected structure [1, 17]. On the other hand, ACR is a much less common concrete distress whose mechanism is still mostly unknown, being considered as a form of ASR by some authors [18-19], while other researchers believe that ACR follows a “different” distress mechanism [20, 21]. The period of time required to generate significant distress in concrete due to AAR may range from 2 to more than 25 years, depending on factors such as the alkali content in the concrete, the type of reactive mineral form present in the fine and/or coarse aggregate, and the availability of moisture.

Although many researchers have worked on the ASR mechanism, there are still many uncertainties about the process of damage generation in concrete involving different aggregate/rock types [17]. Back in 1955, Powers introduced the concept of “safe” and “unsafe” gels [22]. The author proposed that “safe” gels normally have high calcium contents and produce little swelling upon water absorption. On the other hand, “unsafe” gels possess high levels of sodium (Na) and/or potassium (K) and are osmotically active. More than just the gel characterization, it was found that ASR changes as a function of the reactive aggregate/rock types. The main differences are the expansion rate, the length of the initiation period, the location and sizes of the cracks formed due to ASR, the presence/abundance of gel in the cracks or pores of the aggregate particles and of the cement paste, and finally the development of reaction rims at the outer part of the aggregates [17].

Dunant & Scrivener and Dunant & Bentz [23, 24] argued that ASR gel location and morphology depend on the mineralogical nature of the aggregates. According to the authors, two large classes of aggregate types can be distinguished: the slowly reactive aggregates and the rapidly reactive aggregates. Distress caused by slowly reactive aggregates, which are often used in ordinary concrete, is characterized by the formation of “gel pockets” within the

aggregates particles. This phenomenon generates the formation of crack patterns inside the aggregate particles, which can reach the bulk cement paste when the expansion levels increase. On the other hand, rapidly reactive aggregates are more homogeneous in composition than the slowly reactive aggregates so that ASR is mainly produced on the surfaces of the particles; this results in cracks developing in the outer part of the aggregate particles, which leads to the appearance of cracks in the bulk cement paste at early reaction levels and leading to greater damage and a faster development of important expansions [17]. Bérard and Roux [25] suggested the following three types of damage mechanisms due to ASR in different reactive rock types from Quebec, Canada (Figure 1):

- Peripheral reactions of non-porous aggregates (Figure 1a);
- Diffuse reactions causing the swelling of the bulk reactive aggregate particles (figure 1b);
- Internal reactions causing the formation of veins of alkali-silica gel (figure 1c).

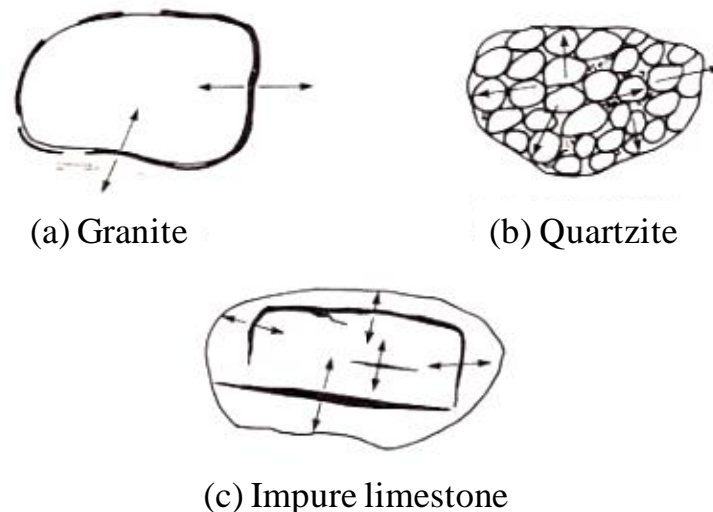


Figure 1: AAR types of damage described by [25].

Peripheral reaction of non-porous aggregates

This type of reaction was identified in a number of concrete cores extracted from large hydraulic dams incorporating quartz-bearing rocks, such as granites, quartzitic diorites and quartzo-feldspathic gneisses, as aggregate materials. The physical effects associated to this chemical reaction are slow to develop and the final expansions are of moderate levels. Although difficult to identify in the concrete specimens, the alkali-silica gel was typically observed in the interfacial transition zone (ITZ) around the reactive particles, thus lowering the bond between the aggregate particles and the cement paste [25].

Diffuse reactions causing swelling of the bulk reactive aggregate particle

In this ASR type, which typically involves quartzitic sandstones (or *orthoquartzites*) of the Potsdam Group in the greater Montreal area, the alkali ions diffuse into the reactive aggregate particles, even if the latter do not present a high porosity. The above ions then rapidly attack the quartzitic cement between the well-rounded quartz grains, thus generating ASR gel causing a slight swelling of the aggregate particles. Among the main microscopic features of reaction, the authors reported the presence of 1), dark reaction rims, 2), “gel pockets” inside the aggregate particles or in voids and cracks of the cement paste, 3), cracks radiating from the reactive particles into the cement paste and peripheral “onion skin” cracks within the aggregates, and 4), friable “reacted” aggregate particles affected by ASR [25].

Internal reactions causing the formation of veins of alkali-silica gel

In this third reaction type, the concrete swelling is occurring through the formation of whitish “silica gel” veinlets inside the reactive aggregate particles, which become thicker over the years. Typical aggregates responsible for this type of reaction are siliceous limestones of Ordovician age exploited in several regions of the St. Lawrence Lowlands of Quebec. These “impure” limestones typically contain an insoluble residue content that can reach up to about 16% [26], including amorphous silica, the reactive material in the above rocks. The authors reported the following characteristics of this type of reaction [25]: 1), the white veinlets are generally aligned according to the original rock bedding; 2), these veinlets often form a complex and irregular network as if they had formed in microcracks generated during aggregate processing operations; 3), in certain cases, changes in the porosity, color and composition of the rock is observed on both sides of the silica gel veinlets; 4), the veinlets rarely extend into the cement paste; actually, they become thinner when approaching the periphery of the aggregate particles; and 5), sometimes, the finely cracked cement paste contains silica gel veinlets that connect a few adjacent aggregate particles. It is interesting to note that similar signs of reaction were also reported in concrete structures of the northeastern part of France incorporating a similar rock type exploited in a large quarry located in Belgium [27]. Villeneuve [28] and Tremblay [29] also observed the presence of microcracks filled with secondary reaction products in the aggregate particles of concretes incorporating a wide range of reactive rock types, such as argillite/siltstone, shale, greywacke, granite/gneiss, schist, quartzite, mixed volcanic rocks (e.g. rhyolite, andesite, tuff).

Golterman [30] stated that ASR damage and signs of distress are really complex to explain and they are not homogeneously distributed throughout the concrete material. According to

the author, an heterogeneous deleterious mechanism generated by the reactive aggregates causes tensile stresses in the aggregate particles and compressive stresses on the aggregate surfaces (outer surface). Those stresses induce crack formation in the aggregate particles and, as they keep swelling, a cracking network is also formed in the bulk cement paste. The rate of cracking propagation for brittle materials (i.e. aggregate particles) is always faster than the rate of stress propagation. This effect induces cracks to form inside the aggregate particles (i.e. tension zones) and to run out radially through the outer part of the particles or even in the bulk cement paste areas (i.e. compression zones) (Figure 2). The ITZ remains intact in most cases, except in the neighborhood of the radial cracks.

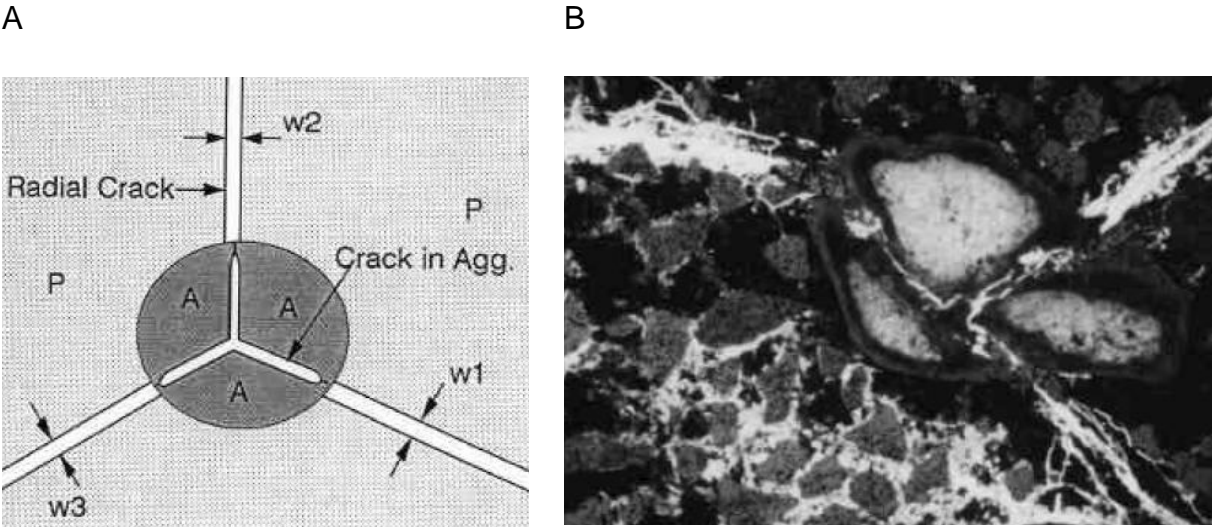


Figure 2: Signatures of concrete damage due to alkali-silica reaction (ASR) [30].

According to Reinhard & Mielich [31], there are two different distress mechanisms proposed for ASR. The first mechanism suggests that the dissolution process happens at the aggregate particles surfaces, thus ASR gel and cracks are formed at the ITZ and easily reach the bulk cement paste due to swelling pressures. The second approach states that cracks are formed within the aggregate particles as a result of gel pockets formation, reaching the cement paste when higher expansion levels are reached. This second theory assumes that the critical aggregate expansion must be achieved before cracks are generated. Critical distress due to ASR happens when the critical “crack length” is reached in the aggregate particle. The final aggregate fracture takes place because of pressures created by ASR gel swelling. Consequently, the aggregate’s toughness is considered a decisive parameter for the cracks extension (Figure 3). Indeed, the maximum stress supported by an aggregate varies as a function of ASR “time exposure”, i.e. the period of time for which a reactive rock remains

exposed to an environment conducive to ASR development. Yet, according to Reinhard & Mielich [31], the fracture mechanism of reactive aggregates can be divided in two steps: 1) the alkali ions present in the concrete pore solution diffuse into the aggregate particles. They then react within the aggregate particles with silica and calcium, thus producing ASR gel. This can occur due to the presence of “fast-track” channels, which correspond to pre-existing aggregate’s “defects or even cracks”; 2) ASR gel swells due to water absorption and exerts pressure on the grain “defects” inside the aggregate particles. This pressure can fracture the aggregate particle apart, depending on its intensity as well as the “maximum crack length” and the “critical stress intensity factor” of the rock type in question. Once the critical stress intensity factor is reached, the aggregate particle breaks down.

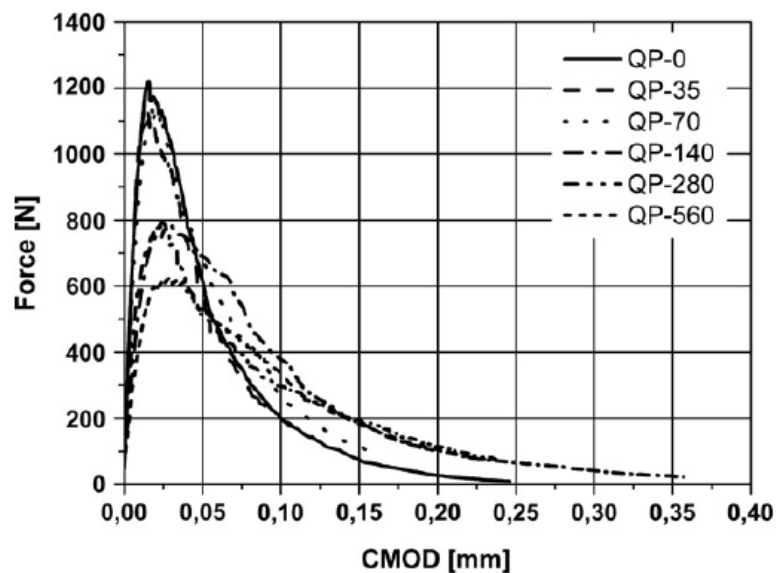


Figure 3: Maximum stress range supported by aggregates before cracking vs. time of exposure (alkaline medium) [31].

9.3 THE USE OF THE DRI FOR ASSESSING DAMAGE IN CONCRETE DUE TO ASR

9.3.1 General comments on the DRI

The DRI is a microscopic analysis performed with the use of a stereomicroscope (about 15x magnification) where damage features generally associated with ASR are counted through a 1 cm² grid drawn on the surface of a polished concrete section. The number of counts corresponding to each type of petrographic features is then multiplied by a weighing factor, whose purpose is to balance their relative importance towards the mechanism of distress, for

instance ASR. It is important to mention that the factors used in the method were chosen on a logical basis, but relatively arbitrarily; they were recently modified in order to reduce the variability between the petrographers performing the test [32]. Ideally, a surface of at least 200 cm² should be used for DRI analysis, and it may be greater in the case of mass concrete incorporating larger size aggregate particles. However, for comparative purposes, the final DRI value is normalized to a 100 cm² area [3].

Although the differences between highly and mildly distressed concrete specimens are generally clear under the microscope [33-35], there is currently no classification established to separate low, moderate or high damage levels in the DRI. It is also important to mention that even if the DRI has been used by several researchers, there is not currently a standard test procedure.

The main goal of the DRI is not to “replace” the conventional petrographic procedures of concrete (i.e. ASTM C 856, for example) whose main goal is to determine the “distress causes”. These approaches may involve the use of either special techniques (i.e. colorimetry) or tools such as the Scanning electron microscopy (SEM) with energy dispersive X-ray analysis (EDXA), X-Ray diffraction (XRD), etc. Actually, the DRI is not really a tool for the diagnosis of AAR in concrete, although it has the potential to do so, but rather a complementary microscopic/petrographic tool with the aim of quantifying the “damage degree” in concrete due to AAR. Likewise, the DRI can be very useful for engineers that are responsible for the management of aging concrete structures as it enables quantifying the degree of distress between the different concrete elements of the structure. Moreover, if the DRI is performed over the years, it allows determining the progress of damage within individual structural elements.

9.3.2 Preliminary results of damage assessment in ASR-affected concrete obtained through the DRI

Sanchez [36] used semi-quantitative petrographic examination, including the new version of the DRI test procedure proposed by [32], to quantify the petrographic features of damage in polished sections of ASR-affected concrete incorporating highly-reactive fine (Tx sand) and coarse (NM gravel) aggregates (*base series*). The author used concrete specimens cast from mixtures of different strengths (25 to 45 MPa) and of different expansion levels (0.05% up to 0.30%). The following main conclusions were drawn from that study:

- The DRI output values can clearly distinguish different ASR expansion levels in concretes incorporating either a fine or a coarse reactive aggregate. Moreover, the DRI was found to

increase almost linearly with increasing expansion in the selected test specimens and no significant differences in DRI numbers were noticed between the concretes made with the fine or coarse reactive aggregates, at each of the different expansion levels selected;

- There are only small differences in the nature and progress of the microscopic features of deterioration due to ASR between the 25 and 35 MPa concrete mixtures. However, for the 45 MPa mixes, the distress pattern seems to be slightly different. A higher degree of damage (i.e. DRI value) was observed at low expansion levels (i.e. 0.05%), and those distress values remained stable up to moderate levels (i.e. 0.12%); at higher expansion levels (0.20% and 0.30%), petrographic features of distress were then found to increase with increasing expansion in the 45 MPa concretes, actually following similar trends to those obtained for 25 and 35 MPa concretes. Finally, the presence of gel was greater in the 45 MPa concrete mixtures, at all expansion levels assessed;
- The analysis of the DRI results clearly indicated that the counts of *opened cracks* in the aggregate particles, as well as cracks in the cement paste, with and without gel, increased with increasing expansion in the concrete specimens. These petrographic features of deterioration are thus highly indicative of ASR expansion. On the other hand, the behavior of the *closed cracks*, present either in the reactive or non-reactive aggregate particles, was not so simple and linear with increasing expansion level; such cracks are thought to be related, in good part, to weathering or aggregates processing operations prior to their use in concrete. To explain this behavior, the following two scenarios were analyzed.
- In the case of ASR coming from the sand, the number of closed cracks within individual reactive fine aggregate particles was found to decrease as a function of the expansion up to about 0.20%, as the alkali hydroxides from the pore solution “uses” at least some of these “fast track” channels to access the inner parts of the particles, generate alkali-silica gel and induce excessive expansion forces that will in turn cause cracking to extend into the cement paste with increasing expansion. For higher expansion values (0.25%, 0.30% and further), an increase in the number of closed cracks in the sand particles was observed, which could be linked to the development of ASR (i.e. indirect effects due to the pressure generation in the mortar fraction of the concrete). On the other hand, the number of closed cracks within individual non-reactive coarse aggregate particles increased with increasing expansion, suggesting that ASR pressure influences the development of new cracks in those aggregate particles (more or less depending on the mechanical characteristics of the coarse aggregates). At higher expansion levels (0.25%, 0.30% and further), some of the closed cracks generally found in the non-reactive

coarse aggregate particles actually became opened through the progress of the expansion.

- In the case of ASR coming from the coarse aggregate, a decrease in the counts of closed cracks in individual reactive coarse aggregate particles was observed with increasing expansion level, for most cases. This was in line with an increase in the counts for opened cracks resulting from alkali-silica reaction/expansion developing in the above particles.
- At the 15-16x magnification level used in the DRI, one could notice that ASR coming from reactive sands induced a very thin and sparsely distributed cracking pattern while, for ASR coming from the coarse aggregate, the cracking is more localized.

9.4 SCOPE AND OBJECTIVES OF WORK

As mentioned in the above sections, Sanchez [36] used the DRI for assessing the progress of damage in concretes incorporating an alkali-silica reactive fine aggregate from Texas and a reactive coarse aggregate from New Mexico. However, according to the information available in the literature, the use of different reactive aggregate types in concrete can generate different reaction kinetics and physical features of deterioration as a function of the expansion levels in the affected concrete, which could produce different damage responses of the AAR affected materials. Therefore, a study incorporating a wider range of different reactive aggregates was necessary to further understand the mechanisms of damage generation in concrete due to AAR, and to confirm the efficiency of the DRI as a tool to quantify this damage.

A correlation was thus established between the development of internal (petrographic) distress features as a function of AAR expansions induced in test specimens cast from concretes of different design strengths (25, 35 and 45 MPa) and incorporating aggregates of different types/natures. Expansion is certainly not a “direct” indicator of *damage* in concrete; however, it is a feature commonly used in the laboratory worldwide to evaluate/classify the potential alkali-reactivity of concrete aggregates. Also, it can allow comparing, at specific/selected levels, the presence/development of different distress features in concretes incorporating a wide range of reactive aggregates and presenting different strengths. This information will then be used to analyze further the changes in the physical and mechanical properties of the above concretes as a function of expansion/development of internal distress due to AAR [36].

9.5 MATERIALS AND METHODS

9.5.1 Materials and mixture proportions

Twenty concrete mixtures of different strengths (i.e. 25, 35 and 45 MPa) and incorporating ten different reactive aggregates were selected for this study. The coarse aggregates ranged from 5 to 20 mm in size. Non-reactive fine (Lav) and coarse (HP or Dia) aggregates were used in combination with the reactive aggregate materials for concrete manufacturing. Table 1 provides information on the different aggregates used in this study. All the 20 concrete mixtures were designed to contain the same volume of paste and aggregates, i.e. from one mix to another, regardless of the mixture strength, so one could compare similar systems (Table 2) with different aggregates and strengths.

Table 1: Aggregates used in the study.

Aggregate	Reactivity	Location	Rock Type	Specific gravity	Absorption (%)	AMBT ¹ 14d exp,%	
Coarse	NM	R	New Mexico (USA)	Polymictic Gravel (mixed volcanics, quartzite, chert)	2.53	1.59	1.056 [37]
	QC	R	Quebec (CAN)	Siliceous and argillaceous limestone	2.50	1.16	0.302
	Wyo	R	Wyoming (USA)	Granite, amphibolite, mixed volcanics	2.64	0.87	0.296 [37]
	Conr	R	Halifax (CAN)	Metagreywacke, shale, siltstone	2.72	0.37	0.365 [29]
	King ²	R (ACR)	Kingston (CAN)	Dolomitic argillaceous limestone	2.69	0.55	0.110 [38]
	Virg	R	Virginia (USA)	Metagranite	2.78	0.45	0.090 [37]
	Rec	R	Recife (Brazil)	Granite, gneiss, mylonite	2.64	0.59	0.230 [39]
	Pots	R	Montreal (CAN)	Siliceous sandstone (orthoquartzite)	2.57	1.15	0.093 [40]
	Dia	NR	Quebec (CAN)	Diabase (plutonic rock)	3.00	0.51	0.065
HP	NR	Newfoundland (CAN)	High-purity fine-grained limestone	2.68	0.44	0.001	
Fine	Tx	R	Corpus Christi (USA)	Polymictic sand (granitic, mixed volcanics, quartzite, chert, quartz)	2.60	0.55	0.755 [29]
	Wt	R	Texas (USA)	Polymictic sand (chert, quartz, feldspar)	2.602	0.4	0.335 [37]
	Lav	NR	Quebec (CAN)	Natural derived from granite	2.71	0.54	0.068

¹Typical results of accelerated mortar bar testing (ASTM C 1260) carried out on the aggregates selected. The number in brackets indicates the source of the information, when testing was not carried out as part of this study.

² This aggregate is supposed to generate the so-called alkali carbonate reaction (ACR).

Table 2: Concrete mixtures cast with different aggregates using the same quantity (in volume) of aggregates and paste.

Type of concrete	Concrete Mix designs: Ingredients and strengths		25 MPa		35 MPa		45 MPa		
			kg/m ³	L/m ³	kg/m ³	L/m ³	kg/m ³	L/m ³	
Equivalent volumes (paste and aggregates) (<i>Base series</i>)	Common to all mixtures of this series	Cement	314	101	370	118	424	151	
		Water	192	192	174	174	157	142	
		Air (%)	-	20	-	20	-	20	
	Tx + HP ¹	Sand	790	304	790	304	790	304	
		Coarse aggregate	1029	384	1029	384	1029	384	
	Tx + Dia ¹	Sand	896	344	896	344	896	344	
		Coarse aggregate	1029	343	1029	343	1029	343	
	Lav + NM ¹	Sand	714	264	714	264	714	264	
		Coarse aggregate	1073	424	1073	424	1073	424	
	Lav + QC	Sand	705	260	705	260	705	260	
		Coarse aggregate	1068	427	1068	427	1068	427	
	Equivalent volumes (paste and aggregates) (<i>Complementary series</i>)	Common to all mixtures of this series	Cement			370	118		
			Water			174	174		
			Air (%)			-	20		
Lav + Wyo		Sand			770	286			
		Coarse aggregate			1065	403			
Lav + Pots		Sand			737	272			
		Coarse aggregate			1068	416			
Lav + Conr		Sand			807	298			
		Coarse aggregate			1060	390			
Lav + King		Sand			794	293			
		Coarse aggregate			1062	395			
Lav + Virg		Sand			829	306			
		Coarse aggregate			1061	382			
Lav + Rec I		Sand			773	285			
	Coarse aggregate			1062	402				
Wt + HP	Sand			790	304				
	Coarse aggregate			1029	384				
Tx + NM	Sand			719	276				
	Coarse aggregate			1040	411				

¹ Detailed DRI results presented in Sanchez [36].

9.5.2 Fabrication and curing of test specimens

A total of 35 cylinders, 100 by 200 mm in size, were cast from each of the twenty concrete mixtures manufactured in the laboratory. After 24 hours in their mould, the specimens were demolded and then placed for 24h in the moist curing room. Small holes, 5 mm in diameter by 15 mm long, were then drilled in both ends of each test cylinders and stainless steel gauge studs were glued in place, with a fast-setting cement slurry, for longitudinal expansion measurements. The cylinders were left to harden for 48 h in the moist curing room at 23°C prior to performing the “0” length reading, after what they were placed in sealed plastic (22 liters) buckets lined with damp cloth (4 cylinders per bucket). All buckets were then stored at 38°C and 100% R.H. and the test cylinders monitored for length changes regularly until they reached the expansion levels chosen for this research, i.e. $0.05 \pm 0.01\%$, $0.12 \pm 0.01\%$, $0.20 \pm 0.01\%$ and $0.30 \pm 0.01\%$. As per ASTM C 1293, the buckets were cooled to 23 °C for 16 ± 4 h prior to periodic axial expansion measurements. When the above expansion levels were reached, the specimens were wrapped in plastic film and stored at 12°C until testing (because

of testing capacity issues). Prior to testing, the specimens were measured and weighed in order to confirm that they had not suffered from significant length or mass changes.

In order to perform the DRI, the concrete cylinders were first cut in two axially and then one of the flat surfaces thus obtained was polished. A portable hand-polishing device, which uses diamond-impregnated rubber disks (no. 50 (coarse), 100, 400, 800, 1500 à 3000 (very fine)), was found most suitable as it does not use loose abrasive powders that can fill up cracks/voids in the concrete and quality polishing is obtained with minimal water supply.

9.5.3 Methods for assessment and analysis

The Damage Rating Index was performed on specimens cast from all concrete mixtures at each of the expansion levels selected, according to the procedure proposed by Villeneuve and Fournier [32]. Actually, the DRI was originally developed for evaluating damage in concrete specimens incorporating reactive coarse aggregate particles. In this study, concrete specimens were made with reactive material in the coarse and fine aggregates. Counts of cracking in the aggregate particles were made in particles down to 1 mm in size, instead of 2 mm normally used in the original method [32]. The latest weighing factors proposed by [28] were used for the calculation of the DRI output values (Figure 4A). Examples of the petrographic features of deterioration used for the DRI are given in Figure 4B.

The semi-quantitative DRI numbers presented hereafter are the normalized value to 100 cm² obtained on one concrete polished section at each given expansion level. Moreover, two “sub-studies” were carried out in order to generate complementary information about the characteristic of AAR distress in each of the test specimens, as follows:

- Assessment of petrographic features of damage, in a relative way (%) and in counts (i.e. without the use of weighing factors), as a function of the expansion level of the test specimens;
- Assessment of the crack density (i.e. total number of cracks per area examined) as a function of the specimen’s expansion level.

A

Petrographic features	Abbreviation	Weighing factor
Closed cracks in coarse aggregate	CCA	0.25
Opened cracks in coarse aggregates	OCA	2
Opened crack with reaction product in coarse aggregate	OCAG	2
Coarse aggregate debonded	CAD	3
Disaggregate/corroded aggregate particle	DAP	2
Cracks in cement paste	CCP	3
Cracks with reaction product in cement paste	CCPG	3

B

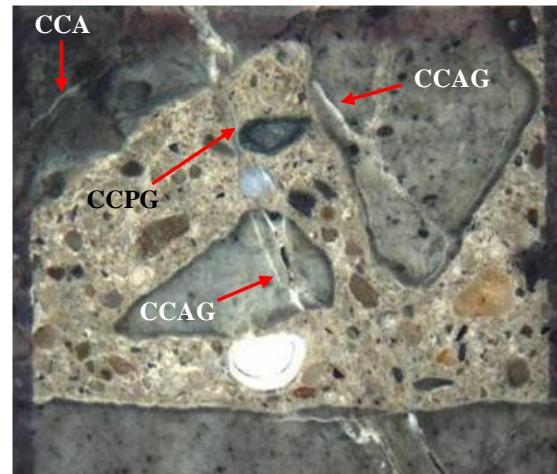


Figure 4: Damage Rating Index method. Micrograph B shows a 1cm² section where most of the petrographic features to be noted in the DRI (as listed in A) can be observed and identified [32]. The distance between the vertical lines on both sides of the micrograph is 1 cm.

9.6 RESULTS

The results of the petrographic examination of the test specimens are presented by considering first the basic counts of the various petrographic features of deterioration as a function of the expansion level of the specimens. The results are then evaluated through the use of weighing factors proposed in Figure 4A to determine whether a quantitative (or even semi-quantitative) assessment of the deterioration could be proposed throughout the use of the DRI, for different concrete strengths and aggregate types/lithologies.

9.6.1 Microscopic features of deterioration in the test specimens as a function of expansion

The petrographic features of deterioration for all concrete mixtures are presented in absolute counts in Figures 5 and 6, while they are given in a relative way (% of each different feature) in Figures 7 and 8. As this study was carried out without focusing on the kinetics of the reaction, it is considered that each level of expansion actually represents an interesting comparative base for determining the degree of distress generated within the concrete with the progress of ASR. The data correspond to the counts of the following features of deterioration in the test specimens regrouped as follows: 1), Group I: closed cracks within the coarse aggregate particles or the coarse fraction of the sand particles (1 to 5 mm) (CCA); 2), Group

II: opened cracks within the coarse aggregate particles or the coarse fraction of the sand particles (1 to 5 mm), with or without reaction products (OCA + OCAG); and 3), Group III: cracks in the cement paste, with or without reaction products (CCP + CCPG).

Special attention was given to establish the most common microscopic features at each step of the reaction/expansion level of the affected concrete samples. The detailed results and analysis of the petrographic examination of the concrete mixtures Tx + HP, Tx + Dia and NM + Lav, for the three concrete strengths 25, 35 and 45 MPa, are presented in Sanchez [36].

At first glance, the following general trends can be observed from Figures 5 and 6: 1) the most common feature of “deterioration” in the polished sections corresponds to *Closed cracks within the aggregate particles* (Group I; CCA), at least at the lower expansion levels; 2), a progressive increase in the total number of Group I to III cracks is observed with increasing expansion for the large majority of the concrete specimens examined (different aggregate combinations and mix designs), with perhaps the exception of the 45 MPa concretes incorporating the reactive coarse aggregates NM and QC that do not show such a clear trend in the beginning of the expansion; 3), at similar expansion levels within the 35 MPa concrete mix design (Figure 6), the total number of counts for Group I to III cracks is the highest in the Tx + HP specimens; this is related to higher counts of Group I cracks in the non-reactive HP limestone particles used in combination with the reactive Tx sand; 4), in the case of the alkali-carbonate reactive King aggregate (Figure 6C), the counts for cracks in the cement paste (Group III) is significantly higher at all expansion levels than for any of the other alkali-silica reactive aggregates investigated; also, those counts remain fairly stable with increasing expansion; and 5), the counts of Group II and Group III cracks generally increase with increasing expansion for all aggregate combinations; they are considered as features more indicative of the progress of ASR in the test specimens.

It is interesting to note that, similar to the mixture NM + Lav, similar total counts of Group I to III cracks were observed at the 0.05 and 0.12% expansion levels in the 45 MPa concrete QC + Lav, with a significant increase in counts being obtained at higher expansion levels (0.20% and 0.25%) (Figure 5). This suggests that the difference in the progress of damage due to ASR in the 45 MPa concrete is not related to the aggregate type (siliceous gravel NM vs. limestone QC; Table 1) but rather to differences in the mechanical characteristics of that type of concrete.

Coming back to the counts for *Closed cracks within the aggregate particles* (Group I; CCA), significant variations in their counts were observed from one mixture to another, showing clear increasing trends in counts with increasing expansion for some aggregates combinations

(e.g. Tx + HP (Figure 6A), Wyo + Lav (Figure 6B), King + Lav (Figure 6C) and Virg + Lav and Rec + Lav (Figure 6C), or a stable or decreasing trend with increasing expansion (e.g. QC + Lav (Figure 5), Wt + HP (Figure 6A), NM + Lav and Tx + NM (Figure 6B)). Sanchez [36] suggested that a significant proportion of the closed cracks within the aggregate particles were actually generated through aggregate processing operations and/or weathering, and were consequently already present within the particles before their incorporation into concrete.

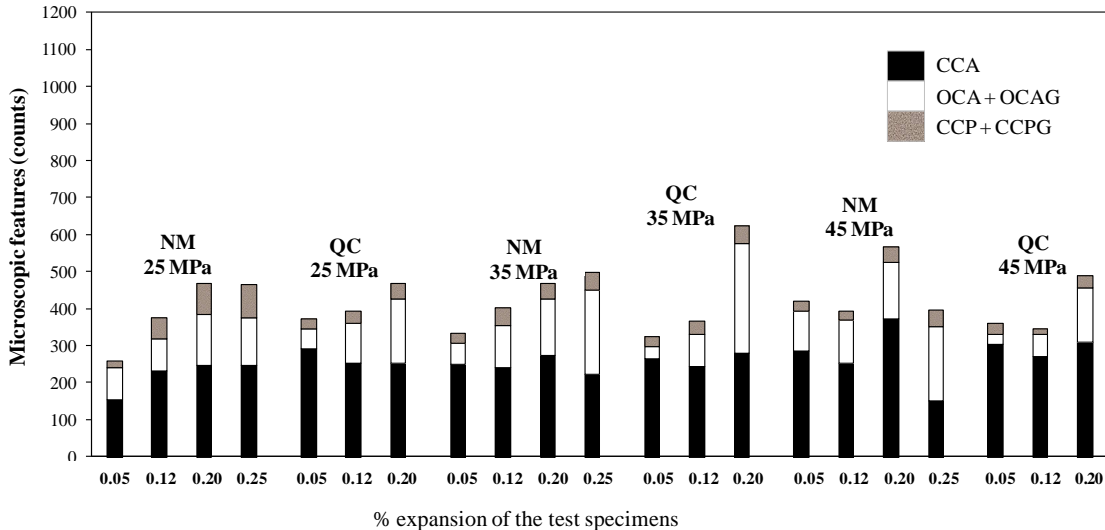


Figure 5: Microscopic features of deterioration (in counts without using the weighing factors) normalized for 100 cm² surface area. 25 to 45 MPa concrete mixtures incorporating two types of reactive coarse aggregates: NM and QC mixtures.

The relationships between the different petrographic features of deterioration can actually be more readily observed on Figures 7 and 8, which plots the relative proportion (%) of the *Group I to III cracks* as a function of the expansion of the test specimens. At the early stages of the chemical reaction and for low expansion levels (i.e. 0.05%), the “*Closed cracks in the aggregate particles (CCA)*” represent between about 55 and 92% of the petrographic features of deterioration in the test specimens. At that low expansion level, the “*Opened cracks in the aggregate particles (with and without reaction products – OCA + OCAG)*” count for 7 to 33% of the petrographic features of deterioration; the proportion of “*Cracks in the cement paste (with or without reaction products – CCP and CCPG)*” remains quite low for all concretes at that stage ($\leq 10\%$), except for the alkali-carbonate reactive King + Lav mixture (35%). In general, as the expansion level in the concrete specimens increases, the proportion of “*Closed cracks in the aggregate particles (CCA)*” presents a decreasing trend (in proportion) due to the increasing proportions of both the “*Opened cracks within the aggregate*

particles (OCA + OCAG)” and “Cracks in the cement paste (CCP + CCPG)”, with or without secondary products; the amplitude and the evidence of that decreasing trend however varies from one aggregate combination to another.

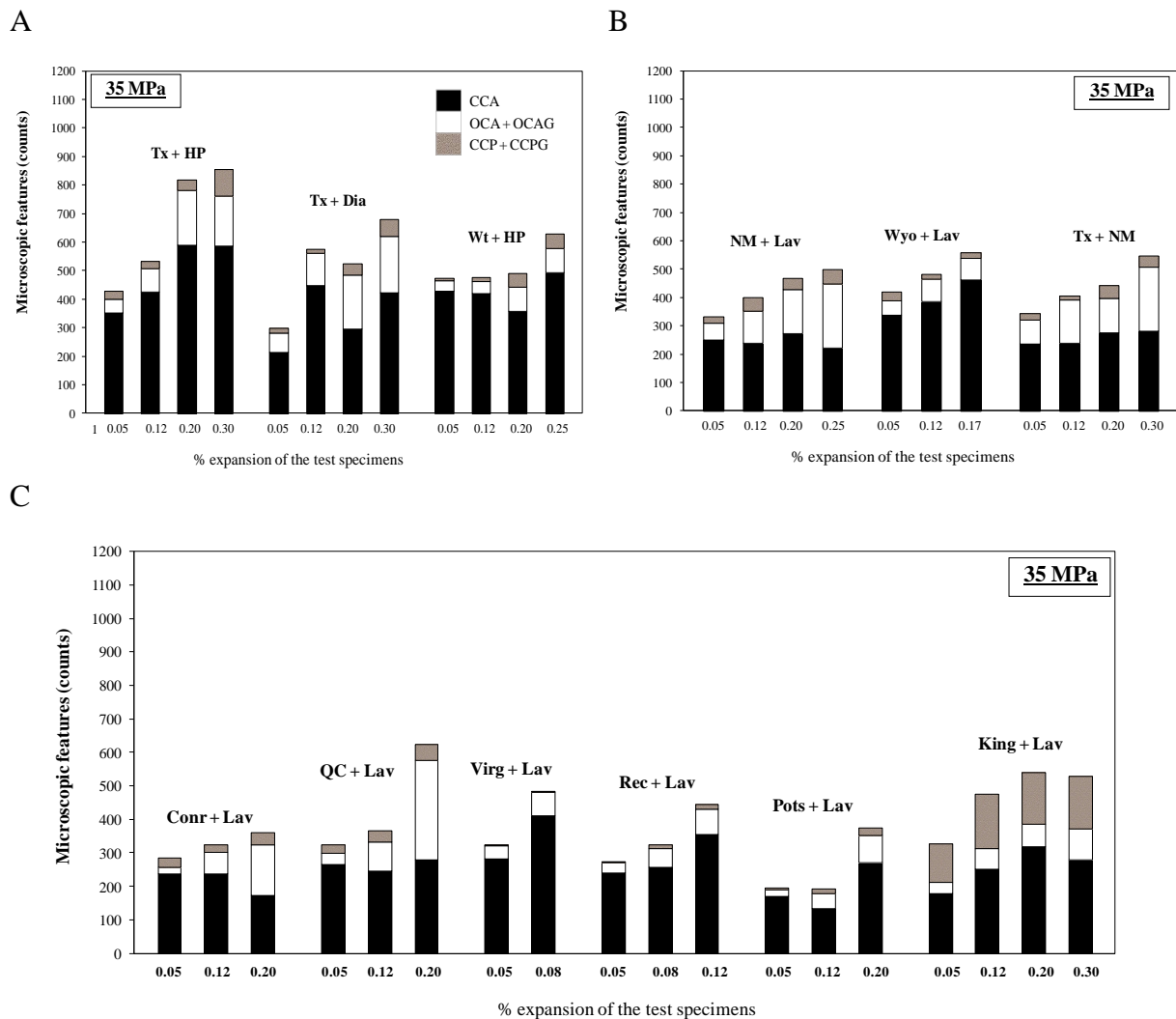


Figure 6: Microscopic features of deterioration (in counts without using the weighing factors) normalized for 100 cm² surface area. All 35 MPa mixtures contained different aggregate/rock types but with the same contents, in volume, of both aggregates and cement paste. A. Reactive sands (Tx and Wt) with non-reactive coarse aggregates (HP or Dia). B. Reactive coarse gravel aggregates (NM and Wyo) with non-reactive (Lav) or reactive (Tx) sand. C. Reactive coarse aggregates with non-reactive sand (Lav); the last coarse aggregate corresponds to the alkali-carbonate reactive King.

For higher expansion levels and extents of the chemical reaction (i.e. $\geq 0.20\%$), the “Closed cracks in the aggregate particles (CCA)” represent between about 48 and 81% of the petrographic features of deterioration in the test specimens. At those expansion levels, the “Opened cracks in the aggregate particles (with and without reaction products – OCA +

OCAG)” account for 19 to 51% of the petrographic features of deterioration; the proportion of “Cracks in the cement paste (with or without reaction products – CCP and CCPG)” remains somewhat fairly low for all concretes, even at that stage, i.e. ≤ 19% - being less than 10% for the majority of the concrete mixtures. Once again, an exception was found for the King + Lav mixture which presented 30% of this type of distress feature.

Finally, it is important to mention that, in general, cracking in the cement paste (and sometimes in the aggregate particles) was significantly more difficult to identify for the 45MPa polished sections than for the 25 and 35MPa concretes, at the magnification used for the DRI procedure (≈15x to 16x).

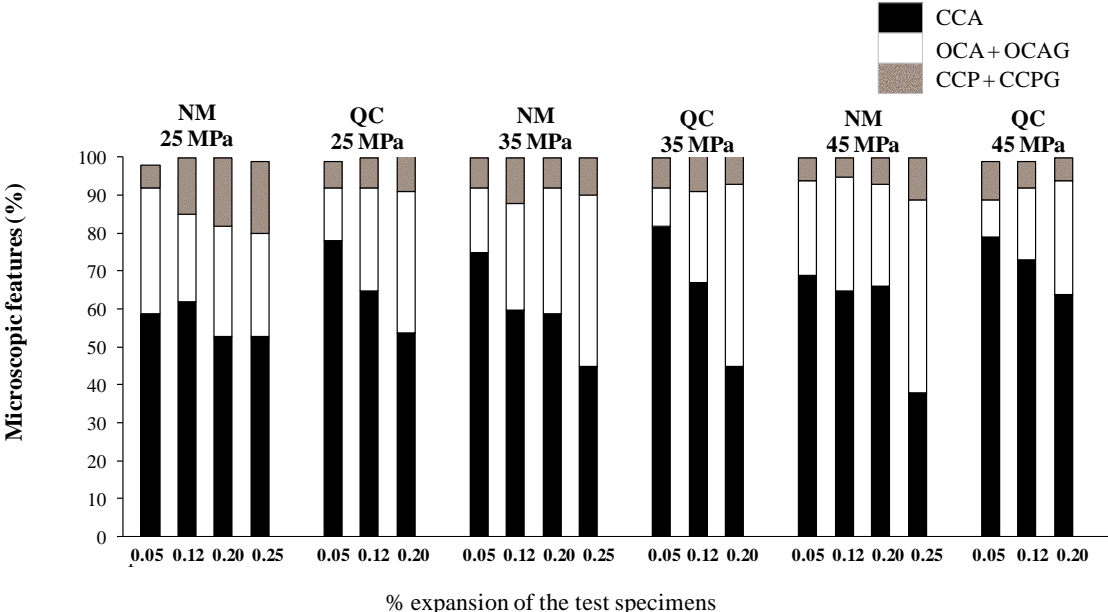
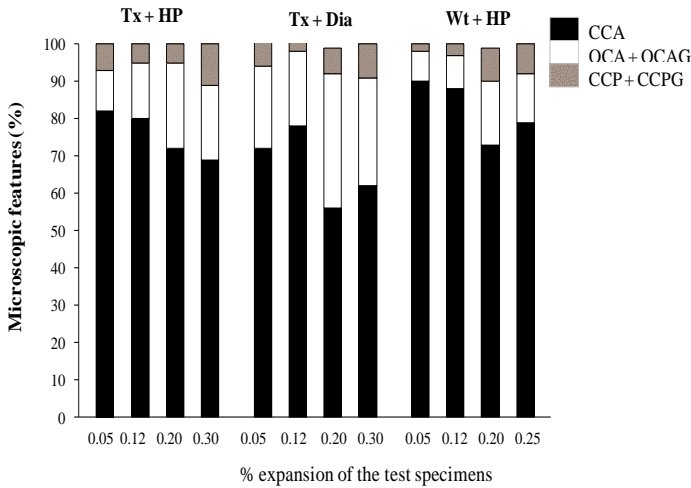
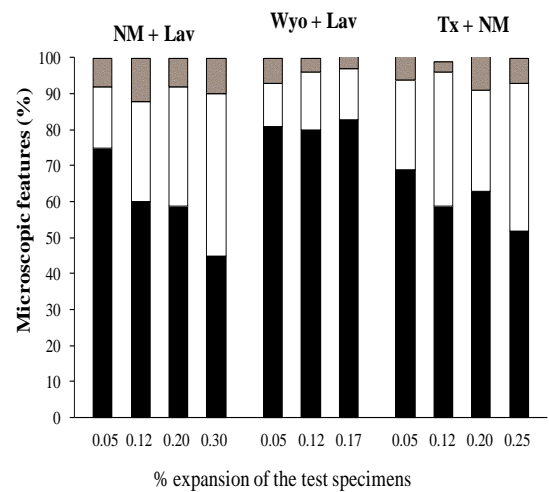


Figure 7: Microscopic features of deterioration (in % without using the weighing factors) normalized for 100 cm² surface area. 25 to 45 MPa concrete mixtures incorporating two types of reactive coarse aggregates: A. NM mixtures; B. QC mixtures.

A – 35 MPa



B – 35 MPa



C – 35 MPa

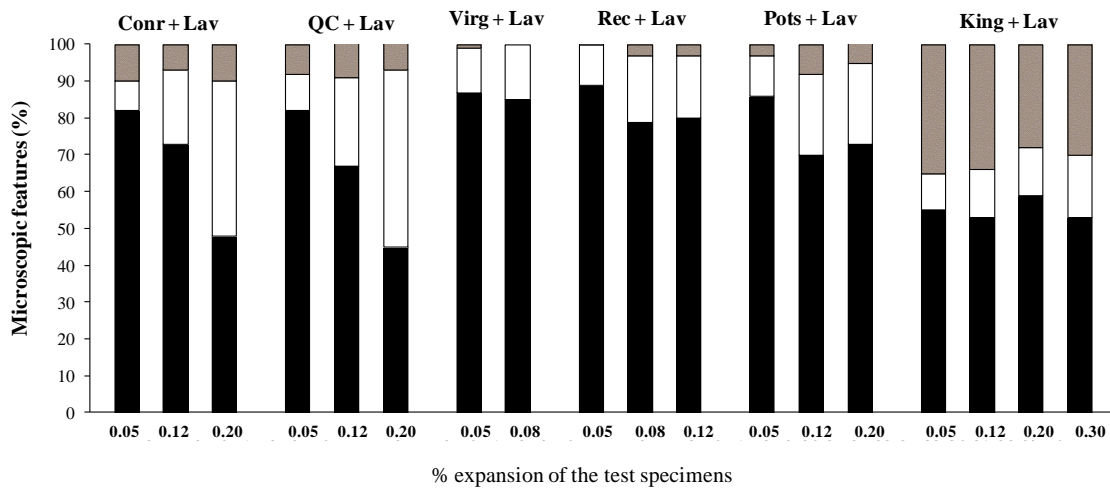


Figure 8: Microscopic features of deterioration (in % without using the weight factors) normalized for 100 cm² surface area. All 35 MPa mixtures contained different aggregate/rock types but with the same contents, in volume, of both aggregates and cement paste. A. Reactive sands (Tx and Wt) with non-reactive coarse aggregates (HP or Dia). B. Reactive coarse gravel aggregates (NM and Wyo) with non-reactive (Lav) or reactive (Tx) sand. C. Reactive coarse aggregates with non-reactive sand (Lav); the last coarse aggregate corresponds to the alkali-carbonate reactive King.

9.6.2 Crack density (CD) as a function of expansion/damage.

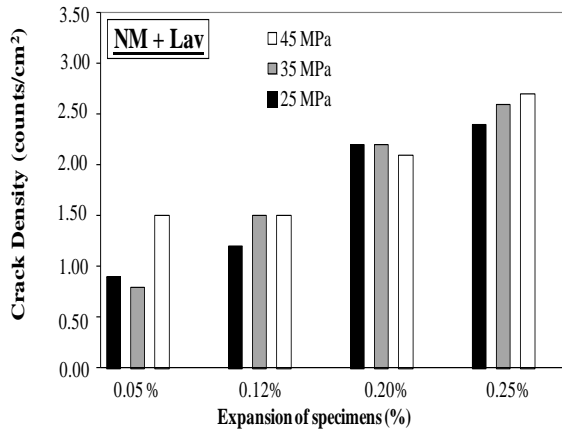
Sanchez [36] found that the crack density (CD) for 25 to 45 MPa ASR-affected concretes incorporating the reactive Tx sand and NM gravel increases as function of the specimen's expansion level. Moreover, this trend did not seem to be influenced by the concrete mix design strength (Figures 9A and B).

The CD (units/cm²) was once again analyzed as part of the DRI analysis, but this time to further evaluate damage generated from different reactive aggregate/rock types. Figure 9 shows the crack density, calculated by the sum of the counts of both opened cracks in the aggregate particles and in the cement paste (with or without reaction products) divided by the overall area examined (in cm²), as a function of the expansion level of the test specimens. Figures 9A and 9B compare the results obtained from two types of reactive coarse aggregates, for concrete mix design strengths ranging from 25 to 45 MPa. On the other hand, Figure 9C compares the crack densities measured in 35 MPa concretes incorporating various reactive coarse and fine aggregates. In the case of the concretes incorporating the reactive sand Tx and Wt, the number of opened cracks in the aggregate particles was counted in the coarse fraction of the sand particles (i.e. from 1mm up to 5 mm particles), as the presence in the coarse non-reactive particles was negligible, while in the case of the concretes incorporating the reactive coarse aggregates (with Lav as a non-reactive fine aggregate), the number of opened cracks in the aggregate particles was determined in the reactive coarse aggregate particles only, as the presence of opened cracks in the non-reactive Lav particles was also negligible.

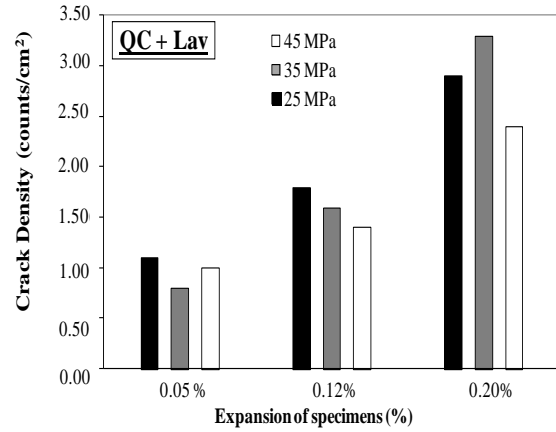
It is quite clear from the data in Figure 9 that the majority of the aggregates tested follow a similar pattern, despite differences in extents from one aggregate to another. The CD was indeed generally found to increase with increasing expansion in the concrete specimens, actually ranging between 0.4 to about 1.9 cracks/cm² at low expansion levels (i.e. 0.05%), and about 2.2 to 3.5 cracks/cm² at higher expansion levels (i.e. $\geq 0.20\%$). The alkali-carbonate mixture King + Lav mixture showed, once again, a different behavior than the other mixtures, mainly for low and moderate expansion levels (i.e. 0.05% and 0.12%), where much larger crack densities were obtained.

Regarding the effect of concrete strength, a slight difference was observed between the two reactive coarse aggregates investigated, lower CD values being observed in the 45 MPa concrete in the case of the QC + Lav mixture (Figure 9B). Once again, cracks in the cement paste (and sometimes in the aggregate particles) were much more difficult to identify in the 45MPa polished sections than in the 25 and 35MPa concretes at the magnification used for the DRI procedure ($\approx 15-16x$).

A – NM + Lav, all mixtures



B - QC + Lav, all mixtures



C – 35 MPa, all mixtures

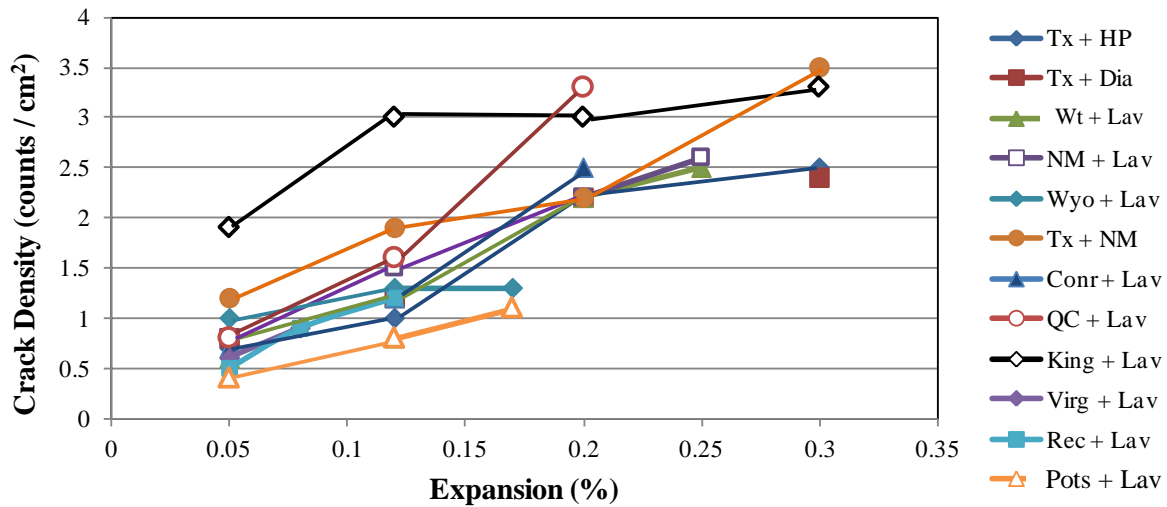


Figure 9: Crack density (sum of *Opened cracks in the aggregate particles and cracks in the cement paste*, with and without reaction products) (counts/cm²) as a function of expansion.

9.6.3 Quantitative assessments of damage obtained through DRI

Figures 10 to 12 illustrate the detailed results of the semi-quantitative petrographic investigations carried out in this study, i.e. taking into account the weighing factors proposed by Villeneuve and Fournier [28] for the calculation of the final DRI numbers. They illustrate the correlation between the DRI numbers and the expansion, ranging from 0.00 (control specimens) to 0.30%, in the 25 to 45 MPa test specimens examined as part of this study.

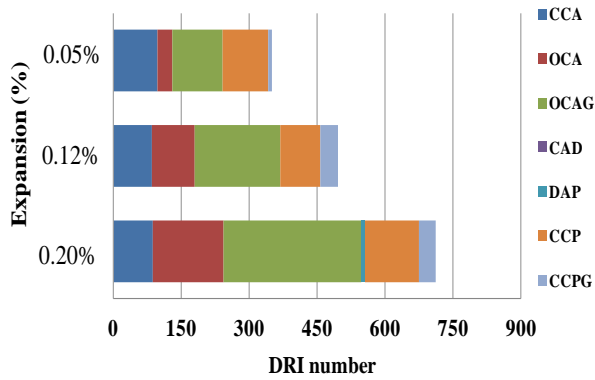
The bar charts in Figures 10 and 11 provide interesting detailed information on the development of the various petrographic features of damage within the sets of test specimens of each series (i.e. evolution as a function of expansion), which can in turn be compared from one reactive aggregate/rock type to another. For instance, *Closed cracks within the aggregate particles (CCA)* are present for all concrete specimens examined; however, although this

petrographic feature was often the most important in terms of counts (Figures 5 and 6) and proportions (Figures 7 and 8), their related importance in the DRI is significantly reduced because of the use of the 0.25 weighing factor proposed for DRI calculation (Figure 4A). On the other hand, the relative importance of *Opened cracks within the aggregate particles* (OCA) and *Cracks in the cement paste* is enhanced through the use of weighing factors of 2 and 3, respectively.

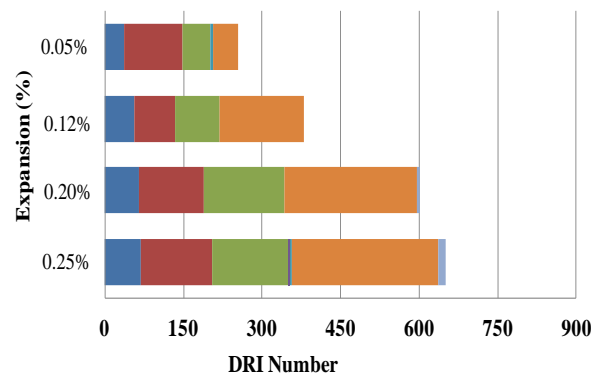
The examination of the various series of bar charts confirm that, in general, the relative importance (in the DRI values) of *Opened cracks within the aggregate particles* (OCA, OCAG) and *Cracks in the cement paste* (CCP, CCPG), without or with gel, increases with increasing expansion for all test specimens, irrespective of the rock type involved. These petrographic features are definitely more indicative of the development/progress of AAR in the test specimens.

Regarding the production of alkali-silica reaction products, it is important to mention that the identification of alkali-silica gel in cracks of the aggregate particles, and especially in cracks of the cement paste, is often a challenge at the magnification used for the DRI, particularly at low expansion levels. This was indeed found to be an important source of variability between petrographers involved in a DRI precision study carried out at Laval University [28]. In order to minimize the negative impact on the DRI calculations resulting from the difficulties in identifying ASR products, Villeneuve and Fournier [28] proposed to use similar weighing factors for cracks, with or without reaction products (see Figure 4A). Amongst the various aggregates combinations investigated, the results in Figures 10 and 11 indicate that the reactive coarse aggregates NM, QC, Wyo and Conr, and fine aggregates Tx and Wt, indeed produced noticeable amounts of gel with increasing expansion, which could be more readily be observed filling cracks in the aggregate particles (OCAG feature). It is also interesting to mention that secondary reaction products were identified in cracks of the reactive alkali-carbonate reactive King aggregate.

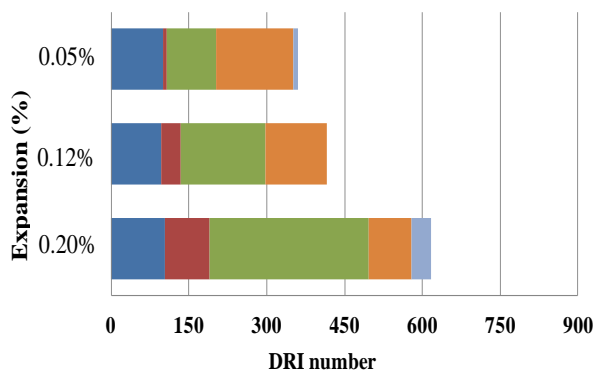
A – 25 MPa, QC + Lav



B – 25 MPa, NM + Lav



C – 45 MPa, QC + Lav



D – 45 MPa, NM + Lav

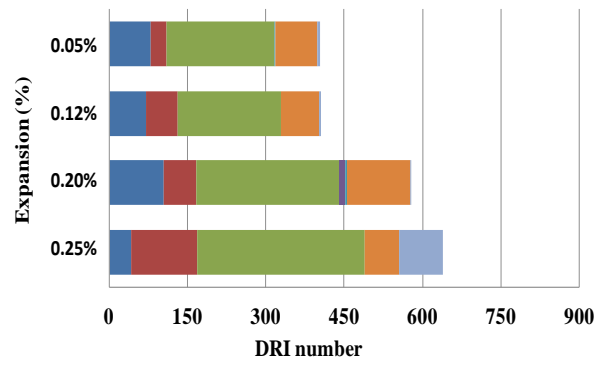


Figure 10: DRI charts for the different concrete strengths analyzed over the study: A, B. 25 MPa mixtures. C, D. 45 MPa mixtures.

Figure 12 presents the correlation between the DRI values and the expansion in the test specimens cast from the 25 to 45 MPa concretes incorporating the variety of aggregates selected for this research. These results indicate that the DRI method can efficiently distinguish the different expansion levels in the above concrete mixtures. A fairly linear correlation was generally observed, in the case of the 25 (Figure 12A) and 35 MPa (Figure 12C) mixtures, between the DRI numbers and the expansion of the test specimens. A different behavior was however noticed for the 45 MPa concrete mixtures (Figure 12B). There is almost no noticeable difference between the damage degrees highlighted by the DRI values obtained for expansion levels of 0.05% and 0.12%, at least at the magnification used for the test. It thus seems that a significant degree of damage due to ASR has developed at relatively low expansion (i.e. 0.05%) in the 45 MPa concretes. The above deterioration is, on one hand, higher than that obtained for the 25 and 35 MPa concretes at low expansion, but, on the other hand, remains stable up to 0.12% for 45 MPa mixtures, while increasing almost linearly and similarly to the other mixtures from about 0.12% up to the highest expansion levels tested in this study (0.30%).

Figure 12C illustrates the DRI results obtained for all 35 MPa concrete mixtures assessed. Once again, fairly linear and similar relationships/rates were obtained as a function of the expansive behavior of the different aggregate/rock types.

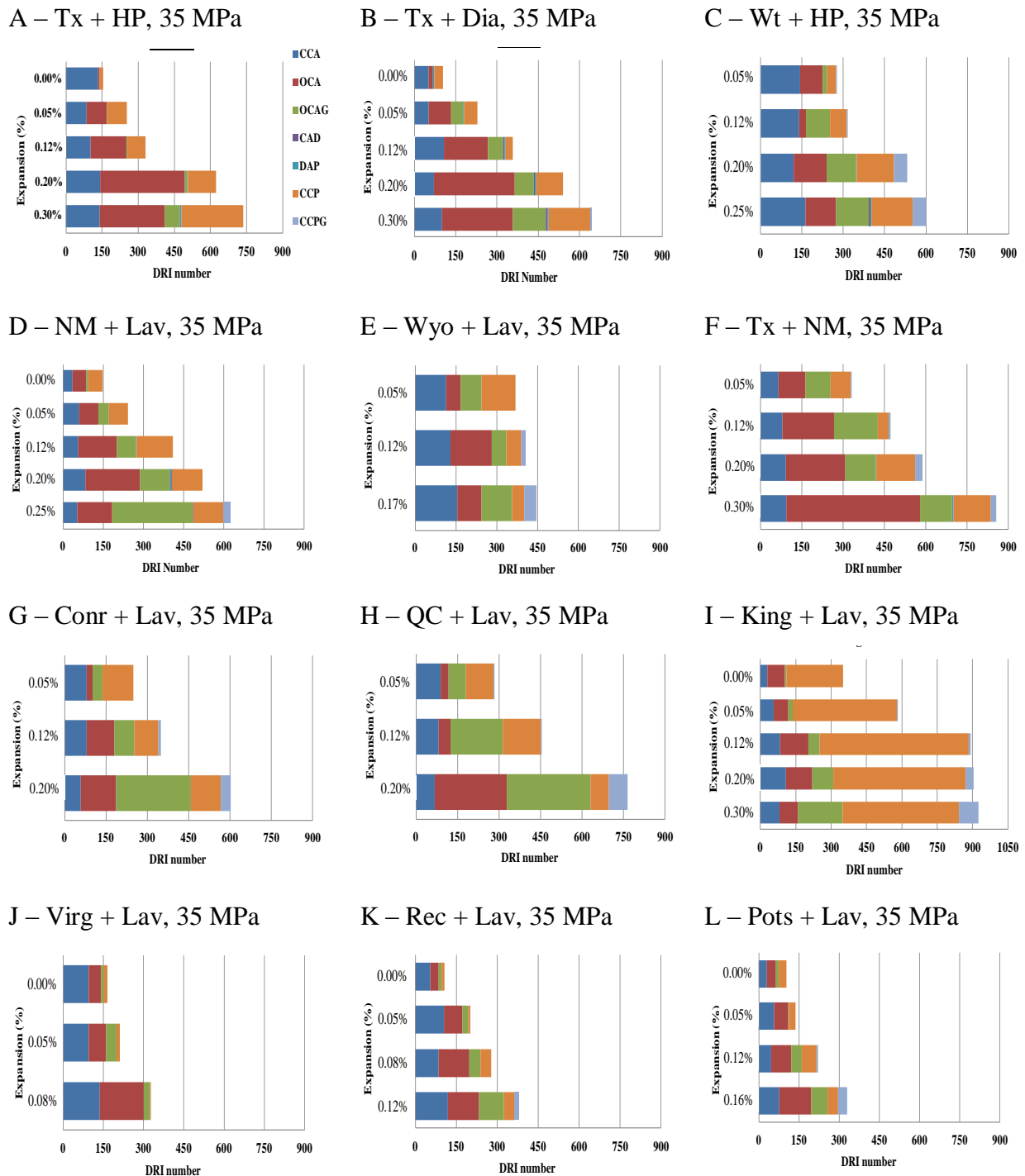
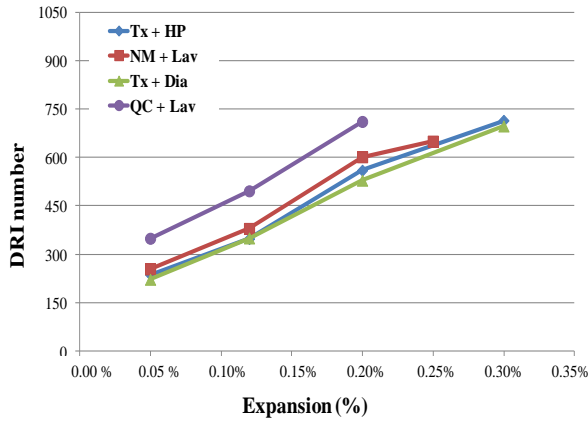
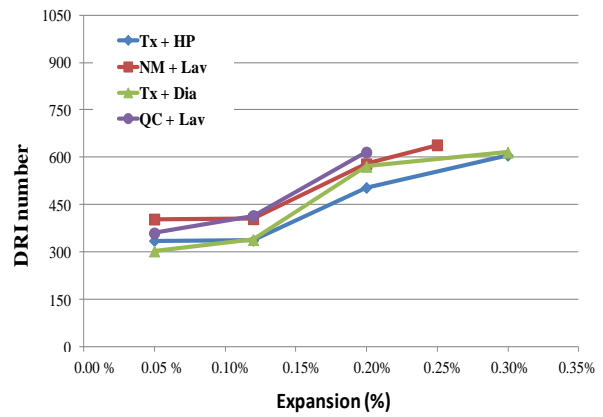


Figure 11: DRI charts for 35 MPa concrete specimens incorporating different aggregate types.

A – 25 MPa mixtures



B – 45 MPa mixtures



C – 35 MPa, all mixtures

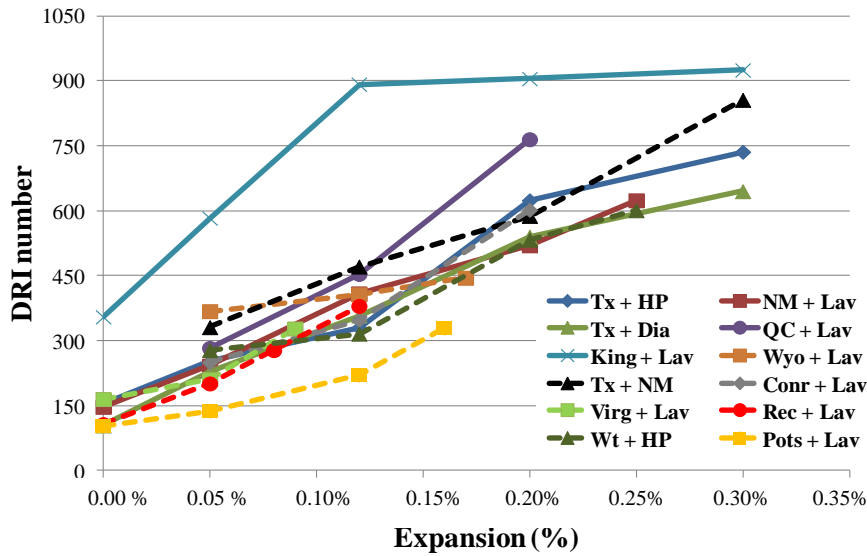


Figure 12: DRI values for all the mixtures analyzed as part of this study: A) 25 MPa mixtures, B) 45 MPa mixtures and C) all 35 MPa concrete mixtures.

9.7 DISCUSSION AND OVERALL DAMAGE ASSESSMENT IN AAR-AFFECTED CONCRETE USING THE DRI

9.7.1 AAR damage vs. DRI measurements: what are we really measuring?

First of all, to properly evaluate the DRI as a tool to detect and ideally quantify damage in concrete due to AAR, the word *damage* needs to be defined. In this work, *damage* is defined as the harmful consequences (measurable ones) of various types of mechanisms (e.g. loadings, shrinkage, creep, AAR, DEF, freezing and thawing, etc.) on the mechanical properties, physical integrity and durability of a concrete element/material. Thus, in practical terms, *damage* is considered here as: 1) the stiffness loss of the concrete material – measured

by the modulus of elasticity (ME); 2) the mechanical properties losses (tensile and compressive strength) of the concrete material and; 3) the durability and physical integrity loss (linked to the materials' cracking extent/crack density) of the affected concretes. Therefore, to be a reliable tool of damage detection, the DRI needs ideally to correlate well with those three damage "elements" [36]. In this paper, a correlation has been established among the internal cracking development due to AAR as a function of the expansion induced in various AAR-affected concrete specimens. Although not a direct/full indicator of *damage*, expansion was selected here as the basis for comparing the development of physical distress in the above concretes through the use of the DRI, before further comparison be established with changes in the mechanical properties of the concrete be carried out by [36].

The results confirm that a semi-quantitative petrographic analysis using the *Damage Rating Index* (DRI) and complementary tools (e.g. measurements of crack density, features analysis – in counts or %, crack lengths) can reliably assess the development of distress in concrete due to AAR. Moreover, this tool confirmed its efficiency for analyzing the condition in concretes of different strengths (25, 35 and 45 MPa) and incorporating various aggregate types (i.e. fine vs. coarse aggregates) and nature (i.e. ≠lithotypes). However, to perform the DRI, since a grid composed of 1 cm² squares is drawn on the polished concrete specimens in order to enable the distress features counting, the features measured through this petrographic investigation take into consideration not only the counts of cracks, but also indirectly their length, as the same cracks present in adjacent squares would be counted twice or several times instead of once depending on their extent. Therefore, the DRI measurement of the concrete's "damage degree" contains, in an implicit way, both the number of cracks and the importance of those cracks, represented by either the crack's lengths and the weighing factors proposed by the method, which is a very important characteristic of this petrographic procedure.

On the other hand, this type of analysis limits the understanding of how AAR really develops as a function of the concrete expansion. This phenomenon is actually better assessed through the analysis of the development of distress in the individual aggregates particles, as stated by Sanchez et al. [36] for the *base series* specimens (Table 1; Figure 13). Figure 13A compares the counts of closed cracks (CCA) and opened cracks (OCA+OCAG) in reactive sand particles divided by the total number of sand particles in 25 MPa concrete specimens of different expansion levels. On the other hand, Figure 13B compares the counts of opened cracks (OCA) in reactive coarse aggregate particles divided by the total number of coarse aggregate particles in 25 and 35 MPa concrete specimens of different expansion levels.

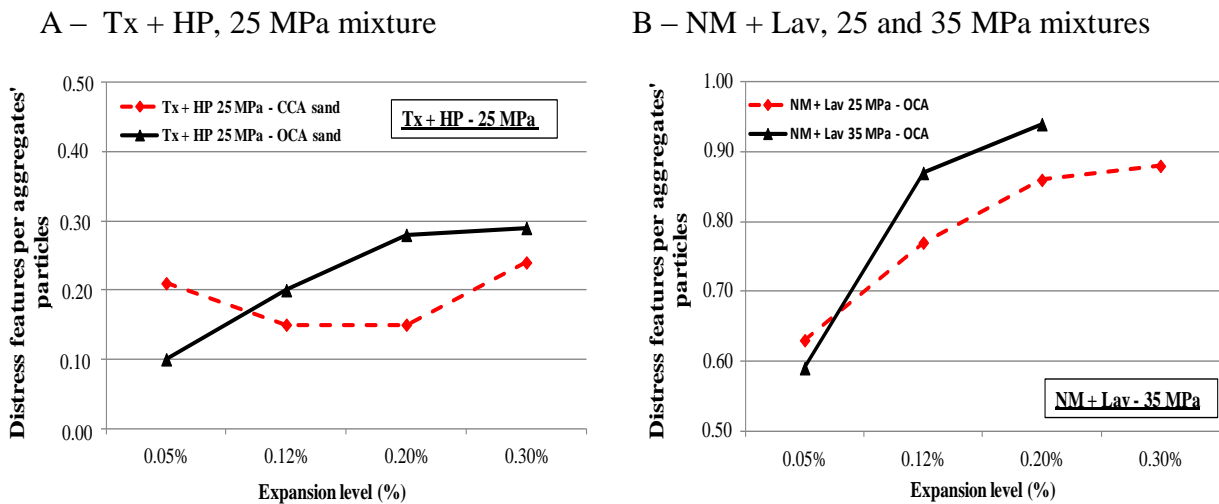


Figure 13: Evolution of AAR-generated cracks in individual reactive aggregate particles as a function of the concrete expansion [36].

The graphs in Figure 13 suggest that the development of distress features within reactive aggregate particles is actually not linear as a function of concrete expansion due to AAR, the relationship showing a concave shape, closer to a logarithmic function. This phenomenon can likely be explained by the following two-step process: a), the formation of new cracks in the early stages of the chemical reaction, and b), since all mechanisms are governed by the minimum energy law, once the cracks formed in the early stages of the reaction reach a given critical length and width, they become very important to the fracture process. At this point, it is easier for the expanding system to propagate those cracks instead of creating new ones. Thus, the rate of cracks' generation decreases or keeps increasing but at a lower rate. In other words, as observed during the petrographic analysis of the test specimens described before, new cracks will always be generated as the alkali reaction keeps developing, but the amount of “new” cracks will be overcome by the increase in length and width of the cracks already formed, thus making the counts of distress features to keep increasing but at a lower rate. Otherwise, the behavior of the closed cracks towards the expansion levels of affected concrete was quite different (Figure 13A). Looking just at the reactive particles behavior, it seems that for low/average expansion levels (i.e. $\leq 0.12\%$), the closed cracks decrease as a function of ASR expansion. This phenomenon likely means that some closed cracks in the reactive aggregate particles are used for the development of ASR opened cracks, due to the fragile character of those zones. This trend keeps happening up to a point at which new closed cracks are likely to be formed in the reactive particles, which possibly demonstrates the action of ASR pressure on the aggregate particles.

As illustrated in Figure 12, with a couple of exceptions, including the 45 MPa concretes and the alkali-carbonate reactive system (King), a fairly linear relationship is observed between the DRI values and expansion in concretes incorporating a variety of reactive rock types. This relationship is however different from the data illustrated in Figure 13, which covers the development of cracking due to ASR within the reactive aggregate particles only. Actually, the DRI covers the development of distress in the overall concrete specimens and not only in the aggregate particles, which constitutes an overall condition assessment of the concrete specimens but may not reliably measure the mechanism/process of crack generation within the reactive aggregate particles. It will thus be interesting to validate the damage assessment obtained from DRI investigations against the losses in the mechanical properties of the AAR-affected concrete, which is discussed in details in Sanchez [36].

9.7.2 Effect of the reactive aggregate type/nature and the development of AAR damage features

The results obtained in this study can be grouped together to produce a *DRI damage assessment envelope* representing the condition of 25 to 45 MPa concretes incorporating a wide range of reactive coarse and fine aggregates, i.e. from the control specimens “0.0%” expansion to the highest expansion level studied in this work (0.30%) (Figure 14). Exceptions to the above are found for two concrete mixes, i.e. King + Lav and Pots + Lav (Figure 12C), which present somewhat different kinetics/mechanisms of damage generation in concrete due to AAR.

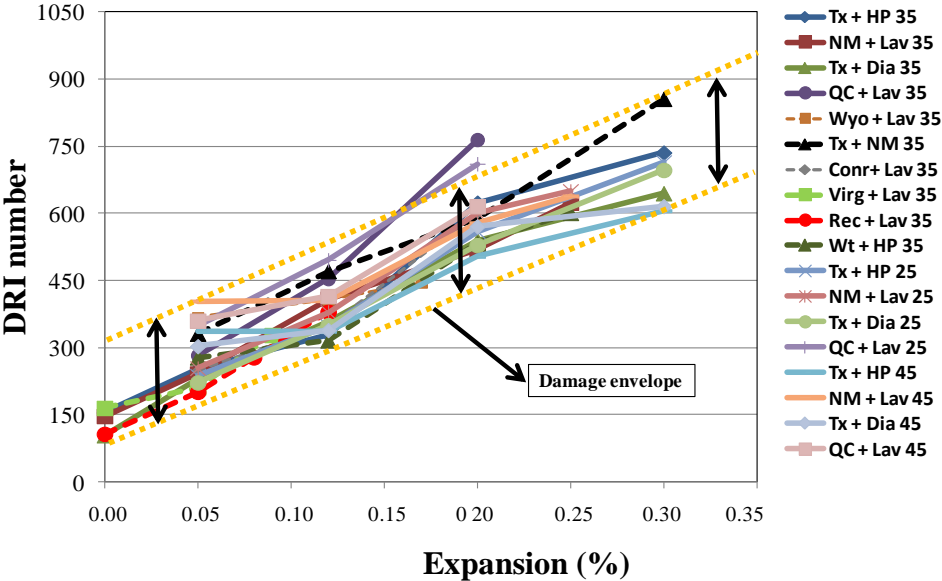


Figure 14: DRI damage assessment envelope.

Looking at the mixes inside the envelope and getting further in the analysis of the results, it seems that “control” concretes already present some measurable “damage”, which mainly consist in closed (and some opened) cracks within the aggregate particles and limited microcracking sparsely distributed within the cement paste. The control samples were fabricated, wrapped and stored at 12°C for 150 days (which would represent 90 days at 20°C according to ASTM C 1074 [41]). Based on the results obtained in this study, the following DRI ranges were obtained for the various aggregate combinations included in the envelope illustrated in Figure 14: Control specimens: DRI values between about 100 and 165; expansion of 0.05%: DRI values between 200 and 350; expansion of 0.12%: DRI values between 300 and 500; expansion of 0.20%: DRI values between 500 and 700; expansion of 0.30%: DRI values between 600 and 850.

For the King + Lav concrete, a different kinetic/mechanism of reaction/expansion was obtained compared to the other typical alkali-silica reactive aggregates, and this already from the early stages of testing. Several cracks were indeed identified in the cement paste already for low and moderate expansion levels (0.05% - 0.12%), which resulted in significantly higher DRI results outside of the envelope obtained for ASR aggregates (Figures 12C vs 14). This so called *alkali-carbonate reaction (ACR)*, which still causes many conflicts and debates in the scientific community, showed in this work to be completely different from the other common ASR mechanisms in terms of development of distress features at each expansion levels analyzed (see Figures 11I and 12C).

The opposite behavior was however obtained in the case of the Pots + Lav concrete. It was indeed extremely difficult to identify cracks both in the aggregate particles and in the cement paste of those ASR-affected specimens. Therefore, the total counts of petrographic features of deterioration were much lower than those found for the other concrete mixtures at similar expansion levels, which explains the significantly lower DRI values thus obtained (under the envelope; Figures 11L and 12C). Interestingly, despite lower values, the progress of DRI values as a function of expansion remained similar to that obtained with the other alkali-silica reactive aggregates (curve somewhat parallel to the envelope).

In the same way, it is quite clear that the crack density (CD) increases when increasing expansion in the test specimens and, once again, an envelope of CD values could be drawn from the results obtained in this study (Figure 15). Therefore, for low expansion levels (i.e. 0.05%), it is likely to find between 0.5 and ≈ 1.5 cracks/cm², depending on the concrete strength and aggregate types. For higher expansion levels (i.e. $\geq 0.20\%$), one should expect a crack density ranging from about 1.5 to about 3.25 cracks/cm². Those differences were more

related to the characteristics of the reactive aggregates than to the concrete mix designs. As for the DRI values, the crack density values obtained for the King + Lav concrete were quite different from the others, showing much greater CD values that however peaked at about 3 cracks/cm² after the 0.12% expansion level (Figure 9). This suggest that after that expansion level, a limited number of new cracks were observed in the King + Lav concrete but the existing cracks became actually wider/longer with increasing expansion in the test specimens.

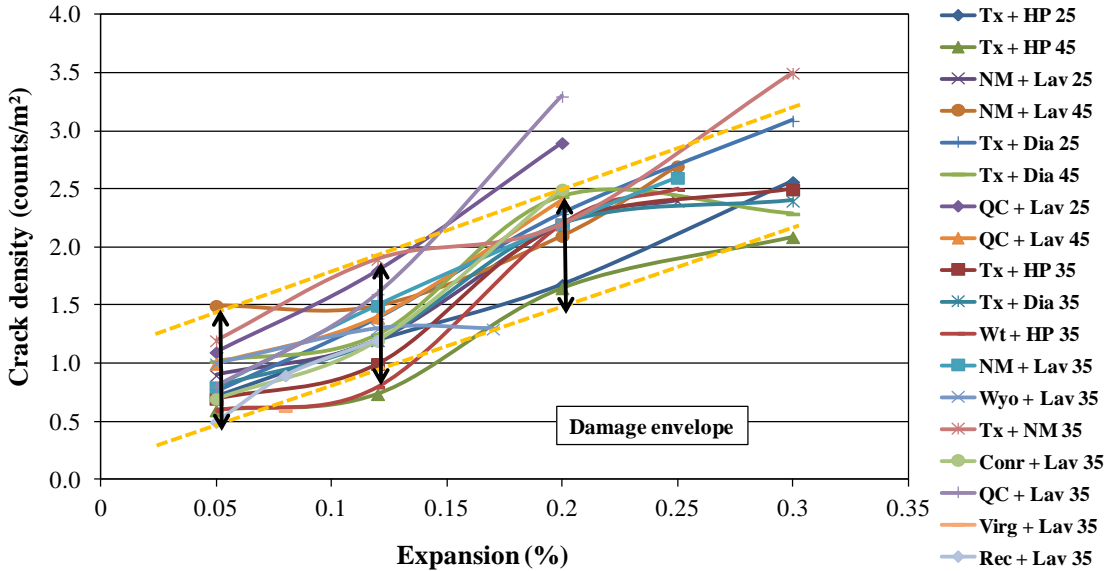


Figure 15: Crack density (CD) assessment envelope.

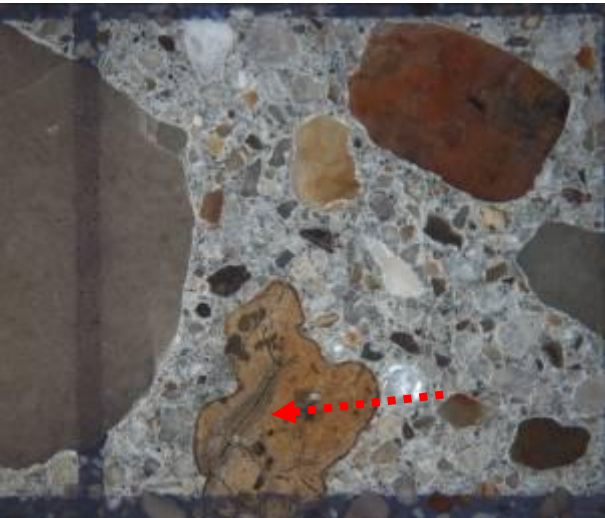
9.7.3 Models of damage generation due to AAR

The microscopic analysis carried out in this study on 25 to 45 MPa concretes incorporating a wide variety of reactive rock/aggregate types supports the development of “damage” features due to ASR corresponding to two of the three types proposed by Bérard and Roux [25] described in Section 2. These correspond to “diffuse reactions causing swelling of the bulk reactive aggregate particle”, which induce peripheral “onion skin” cracks in the reactive aggregate particles causing radial/tangential cracks in the cement paste, and the “Internal reactions causing or not the formation of veins of alkali-silica gel” in the aggregate particles, which induce sharp cracks in the aggregate particles and thus radial cracks in the cement paste. However, the peripheral reactions of non-porous aggregates proposed by [25] was not considered/identified in this work as a direct effect of ASR, even for the non porous aggregates selected, which presented also extensive cracking inside their particles. Therefore, this type of distress feature, sometimes identified in the specimens analyzed, but not in a large

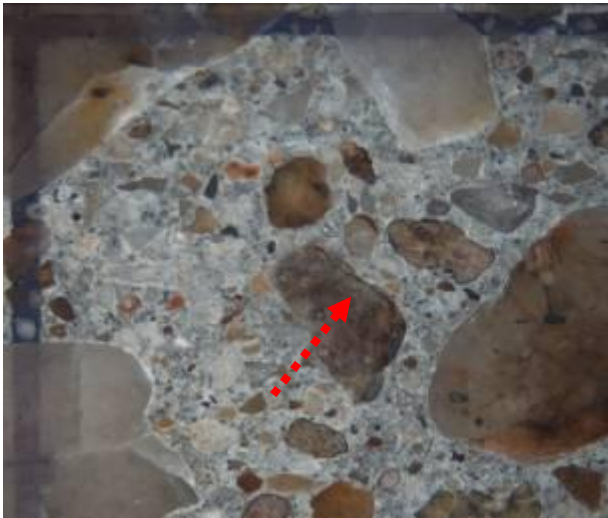
amount, was considered to be an indirect effect of ASR pressure during silica gel formation. Likewise, the presence of few cracks found near some concrete pores was associated to the same mechanism.

Figure 16 illustrates typical crack features identified in the concretes incorporating the different aggregate types used in this work, for the highest expansion levels measured in each concrete mixture. It is good to mention that King + Lav mix, which presented a completely different distress pattern, is not covered through the above conclusions and will be discussed separately afterwards.

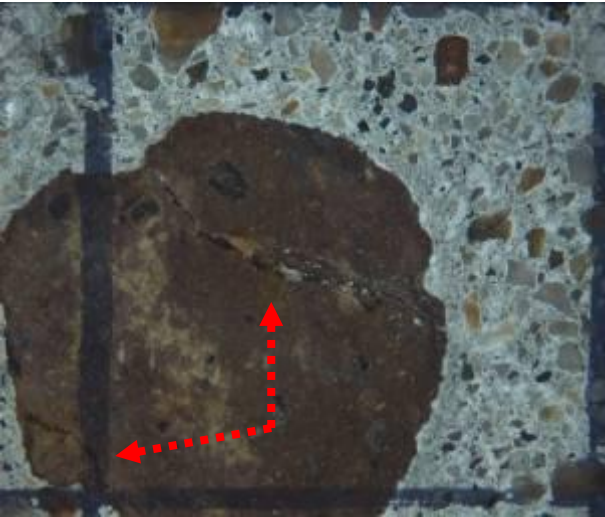
A - Tx + HP, 35 MPa (0.30%) – *sharp crack* type



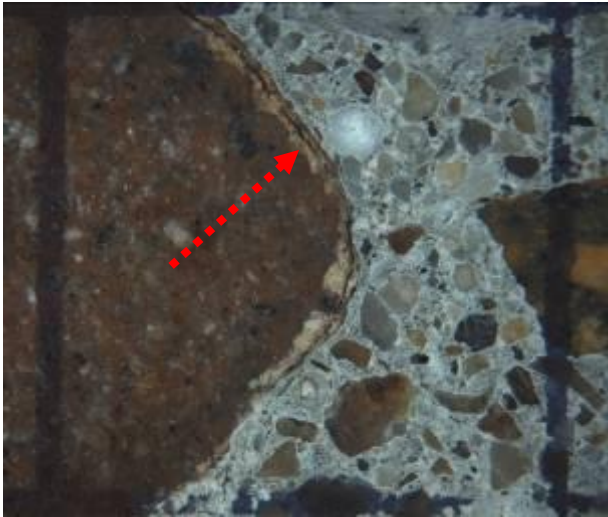
B - Tx + HP, 35 MPa (0.30%) – *onion skin* crack type



C - Lav + NM, 35 MPa (0.25%) – *sharp crack* type



D - Lav + NM, 35 MPa (0.25%) – *onion skin* crack type



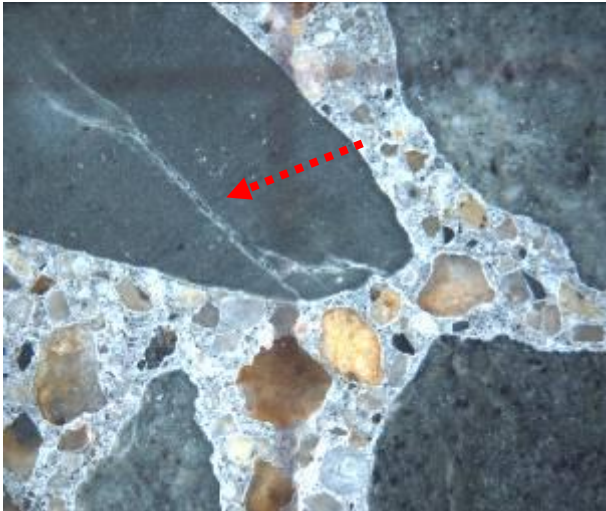
E - Lav + Wyo, 35 MPa (0.17%) – *sharp crack* type



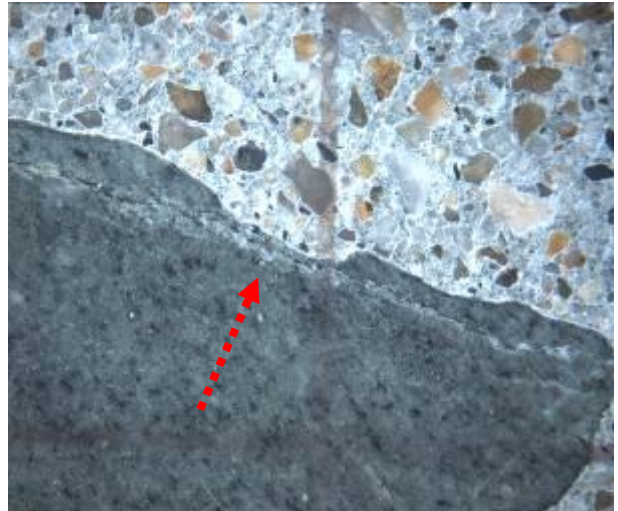
F - Lav + Wyo, 35 MPa (0.17%) – *onion skin* crack type



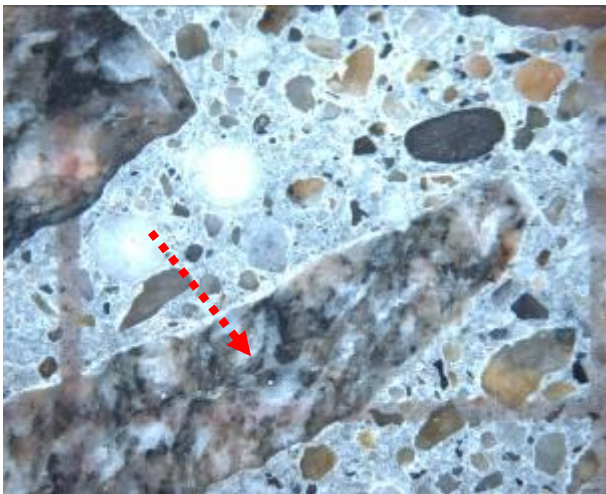
G - Lav + Conr, 35 MPa (0.20%) – *sharp crack* type



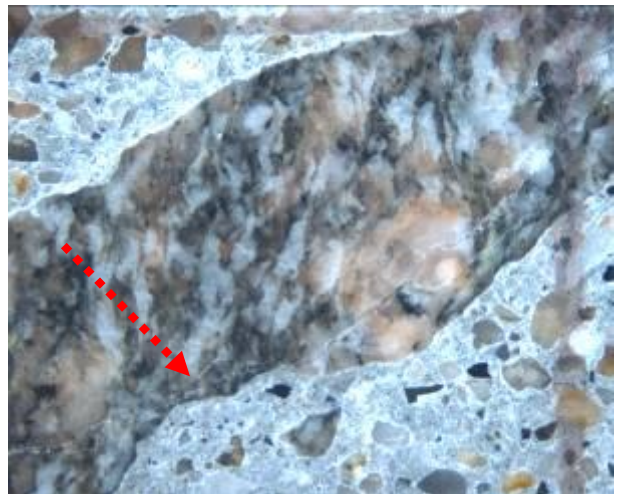
H - Lav + Conr, 35 MPa (0.20%) – *onion skin* crack type



I - Lav + Rec, 35 MPa (0.12%) – *sharp crack* type



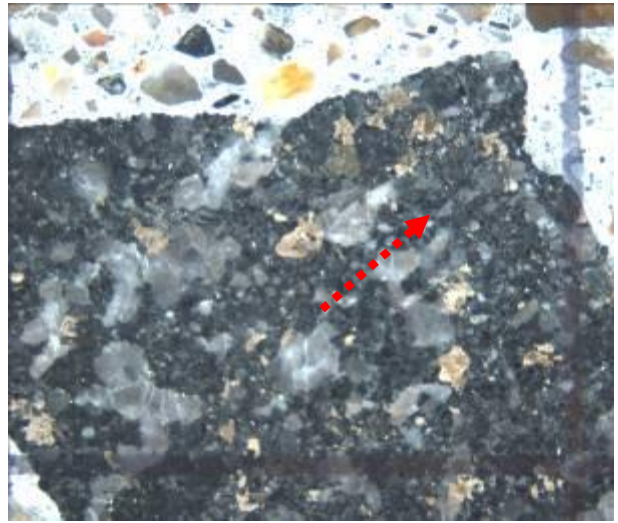
J - Lav + Rec, 35 MPa (0.12%) – *onion skin* crack type



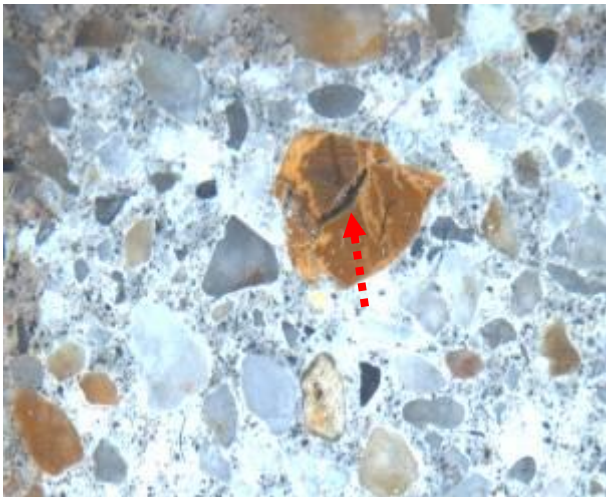
K- Lav + Virg, 35 MPa (0.09%) – *sharp crack* type



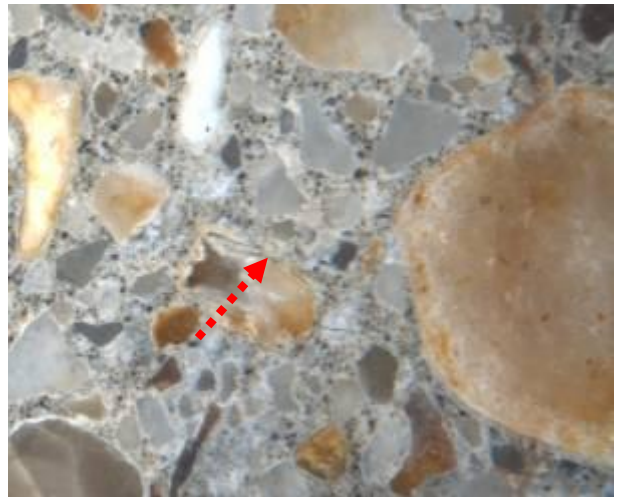
L- Lav + Virg, 35 MPa (0.09%) – *sharp crack* type



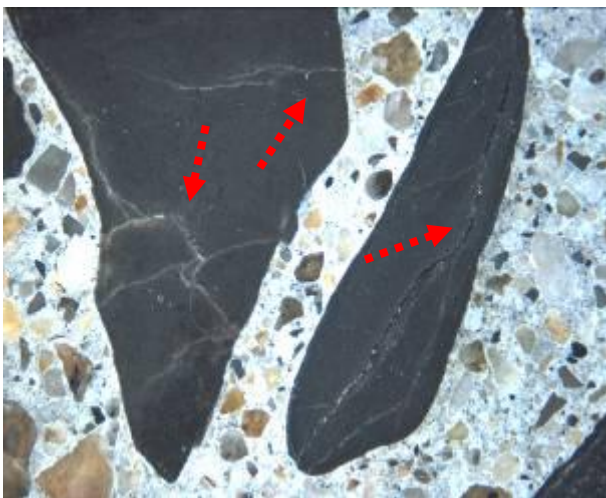
M- Wright + HP, 35 MPa (0.25%) – *sharp crack* type



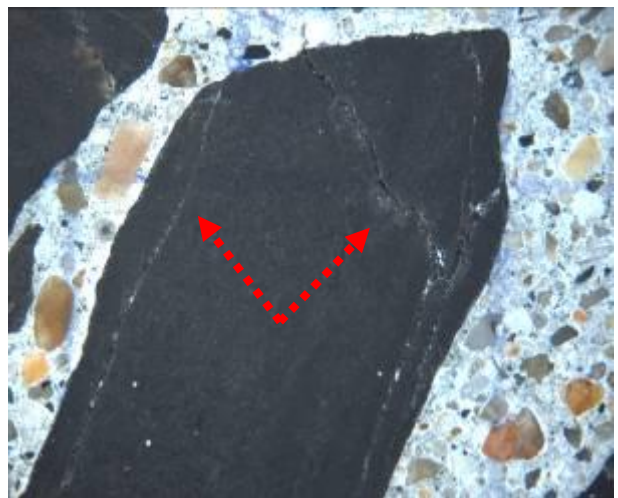
N- Wright + HP, 35 MPa (0.25%) – *onion skin* crack type



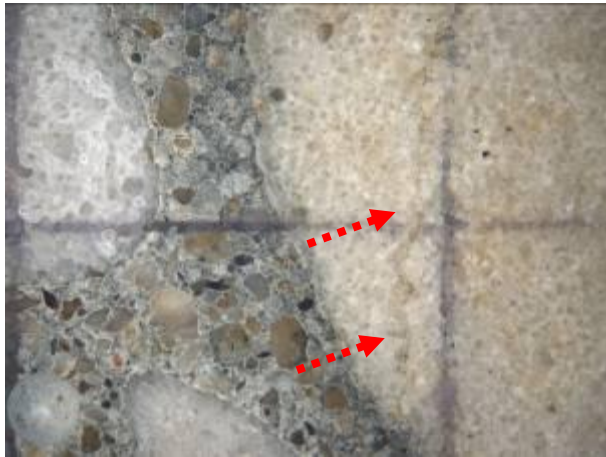
O- Lav + QC, 35 MPa (0.20%) – *sharp crack* type (white veinlets)



P- Lav + QC, 35 MPa (0.20%) – *sharp crack* type (white veinlets)



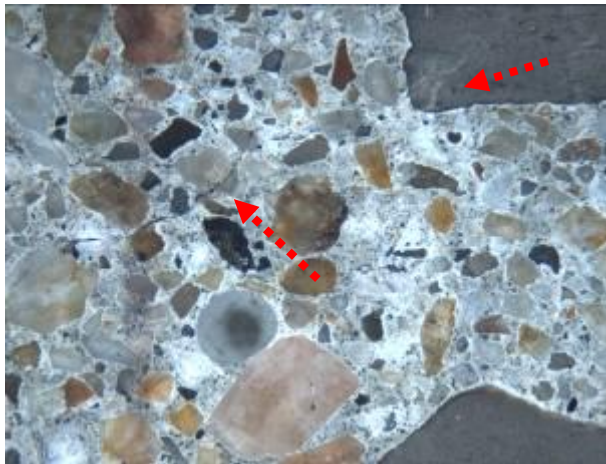
Q- Lav + Pots, 35 MPa (0.16%) – *sharp crack* type



R- Lav + Pots, 35 MPa (0.16%) – *sharp crack* type



S- Lav + King, 35 MPa (0.30%) – *sharp crack* type



T - Lav + King, 35 MPa (0.30%) – ITZ crack type

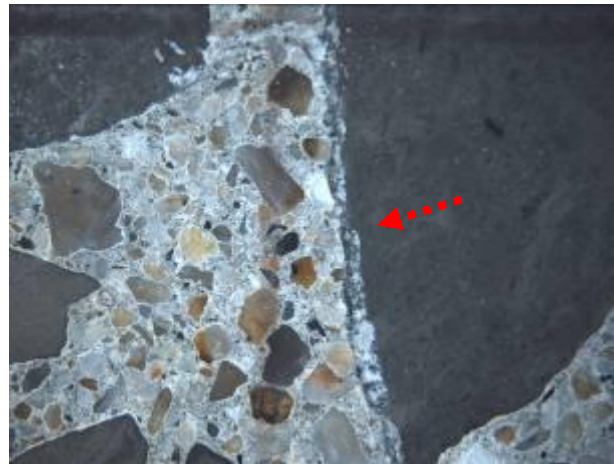


Figure 16: Typical cracking features in the concretes incorporating a variety of reactive rock/aggregates types, and for the highest expansion levels observed in the concrete specimens. The distance between vertical lines equals 1cm.

Therefore, based on the analyses of the petrographic data discussed previously, i.e. qualitative descriptions and quantitative DRI values, the following qualitative damage model of ASR development against expansion in concretes incorporating alkali-reactive quartz-bearing rocks (category 2 of reactive rock types according to the Appendix B of CSA A23.1-2009) [42] is proposed (Figure 17). Note that the expansion levels mentioned in the various steps of the proposed model are not absolute values but rather used as indicative only.

- Figure 17A: At low expansion levels (i.e. around 0.05%), Types A and B cracks can be observed in the aggregate particles. Type A cracks are sharp cracks that could correspond to closed cracks produced through aggregate processing operations or weathering, or more

porous zones in the aggregate particles. Such zones would facilitate the penetration of the alkali hydroxide solution, and thus a faster reaction process happens compared to other areas of the bulk aggregate particle. This crack type is often formed according to the aggregate's characteristics, being generated either in the bulk aggregate volume or in the aggregate's periphery, as illustrated by Figure 17A. In addition, in sedimentary or metamorphic rocks, microcracks of the A Type could form preferentially along the bedding or metamorphic layering through aggregate processing operations. On the other hand, Type B cracks (onion skin type) could be formed in the aggregate particles that do not present a preexisting closed cracked/porous zone, which facilitates the ionic movements from the concrete pore solution. The alkali hydroxide solution penetration is thus quite homogeneous and the crack's feature would be almost parallel (peripheral) to the aggregate's boundary. At this level, both crack types are found inside the aggregate particles and it is quite unlikely to find cracks in the cement paste extending from aggregate's cracking. Moreover, it is quite unusual to notice the presence of gel at this expansion level (at least at the magnification used over this project - $\approx 15-16x$).

- Figure 17B: At moderate expansion levels (from 0.10 - 0.12%), the cracks described above start growing and some Type A cracks extend to a point that they will reach and extend into the cement paste. However, the type B cracks continue their development inside the aggregate's boundary. At this expansion level, the presence of ASR gel is noticed (mainly in the opened cracks in the aggregate particles).
- Figure 17C: At high expansion level (e.g. 0.20%), Type A cracks typically extend into the cement paste and are likely to reach the cement paste on both sides of the aggregate particle. Type B cracks are likely to have enveloped more than a half of the aggregate particles at this point. In addition, the presence of ASR gel is generally found in both the aggregate particles and the cement paste of affected specimens, and its amount depends on the aggregate's nature and concrete characteristics.
- Figure 17D: At very high expansion levels (e.g. $> 0.30\%$), type A cracks link to other cracks formed at other location in the concrete, either due to ASR within adjacent reactive aggregate particle or non-reactive aggregate particles or the cement paste resulting from ASR pressure developing in the concrete matrix, as described in the previous section. A more or less extensive network of cracking will then link several aggregate particles to each other. On the other hand, type B cracks can extend into the cement paste at a specific location. These cracks either extend into the interfacial transition zone (ITZ), which may cause the debonding of the aggregate particle, or into the cement paste to link to cracking

network. Moreover, the amount of ASR gel found in either the cement paste or the aggregate particles is greater than that observed at the 0.20% expansion level.

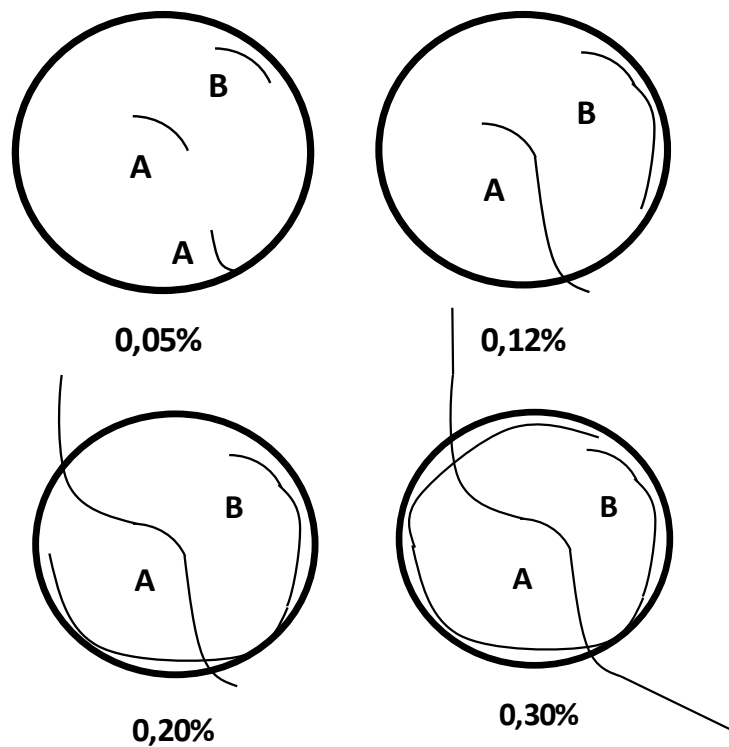


Figure 17: Qualitative microscopic AAR damage model vs. levels of expansion: 0.05% (A), 0.12% (B), 0.20% (C), 0.30% (D).

It is important to mention that both Type A and B cracks will not necessarily be present simultaneously in all reactive aggregate particles, and that a particular crack type may be forming preferentially in some rock types, depending on their nature. Crushed aggregates may be more prone to the formation of crack A Type considering the processing operations that can induce additional internal cracking prior to their use in concrete. The presence of layering in sedimentary/metamorphic rocks may also significantly control cracking shape in the aggregate particles (e.g. Figures 16O and 16P). In the case of gravel aggregates, both types of cracking could be observed depending on the extent of the processing operations and of the rock composition.

In the specific case of the King + Lav aggregate combination, where a somewhat different chemical reaction is involved (i.e. so called alkali-carbonate reaction – ACR), the distress pattern was indeed largely different. In the early stages of the chemical reaction and for low expansion levels (i.e. 0.05%), some closed cracks along with minor opened cracking in the aggregate particles were observed. However, significant cracking without gel is already present in the cement paste, mainly at the ITZ. Actually, this ITZ type cracking could be caused by two different phenomena: expansion of the cement paste (which is likely not the

case) or shrinkage of the aggregate particles, as stated by [26]. For moderate expansion levels (i.e. 0.12%), the network of cracking keep increasing in the cement paste up to a point where a very important crack density is observed in the concrete specimens. Likewise, some opened cracks are also generated in the aggregate particles. For higher expansion levels (i.e. 0.20% or more), the features already found for 0.12% level keep progressing, increasing their lengths and widths and some debonding of the aggregate particles is seen.

9.8 CONCLUSIONS

The main objective of this study was to assess the condition, as a function of expansion, of different types of concretes (25 to 45 MPa) incorporating a wide range of reactive aggregate types using semi-quantitative petrographic methods, including the *Damage Rating Index (DRI)*. Such investigations were also used to better understand AAR-related damage generation and development as a function of expansion in the concrete specimens. The main conclusions from the above investigations are as follows:

- The DRI output final value can provide a reliable assessment of the degree of expansion in AAR-affected specimens when the deleterious reaction comes either from a reactive sand or a reactive coarse aggregate. However, the use of just the DRI number does not give further information about the nature of the specimen's damage;
- For the vast majority of the mixes investigated, the DRI values did not change significantly for concretes of different strengths or incorporating different rock/aggregates types. Therefore, it seems possible to obtain, through the DRI, an envelope of damage results against the expansion level of the concrete specimens. However, exceptions could be seen for an alkali-carbonate reactive rock (King) and a siliceous sandstone (Pots), which displayed somewhat different reaction mechanisms than that observed for most other reactive quartz-bearing rocks investigated;
- For the aggregates investigated, no significant differences in the development of petrographic features of deterioration were observed between 25 and 35 MPa concretes at similar expansion levels. However, for the 45 MPa mixtures, the cracking pattern was more difficult to identify and also seemed slightly different, especially in the early stages of the chemical reaction where damage degrees higher than that observed in the 25 and 35 MPa concretes were obtained. Moreover, the amount of gel was found to be greater for 45 MPa concrete mixtures for all expansion levels;

- For all aggregates investigated, the counts and proportions of opened cracks in the aggregate particles, as well as cracks in the cement paste, with and without gel, increased with increasing expansion in the test specimens. They were found to be more indicative petrographic features of the development of AAR in the concrete specimens. Opened cracks are likely to appear inside the reactive aggregate particles in the early stages as a result of the chemical reaction process. With the progress of ASR, the number and importance (i.e. length and width) of those cracks increase and those cracks formed inside the aggregate particles extend into the cement paste for higher expansion levels ($\approx 0.12\%$). Exceptions were seen for the mixture King + Lav where a largely different damage pattern was found for all the expansion levels studied;
- The crack density (CD) (counts of opened cracks in the aggregate particles and cracks in the cement paste/surface area examined (cm^2)) was confirmed as an useful supplementary information of the DRI procedure. CD was typically found to increase almost linearly as a function of increasing expansion in the test specimens. All CD data obtained for the various concretes investigated were used to trace an envelope of CD values that could be used for estimating the AAR expansion in the test specimens. Once again, the King and Pots aggregates were excluded from the above relationship because of their somewhat different reaction mechanism/kinetics;
- The analyses of the basic data from the petrographic examination of the test specimens, for instance the counts of the different petrographic features of deterioration in absolute and relative ways, help to better understand the development of ASR distress in the concrete specimens and also how this chemical reaction progresses as a function of the expansion level of the samples;
- A model for the development of ASR damage in concrete as a function of expansion in concrete was defined, mainly based on two cracking types commonly found in the concrete specimens. Sharp (Type A) and/or Onion skin (Type B) cracks were found to form in the aggregates particles in the early stages of the reaction, then extending into the cement paste with increasing expansion to eventually connect reactive aggregate particles in an extensive cracking network. Type A and Type B cracks are not necessarily present at the same time in the affected aggregate particles. Their presence seems to be a function of rock type characteristics;
- A different pattern of damage generation is observed with the alkali-carbonate reactive aggregate King. In this case, extensive cracking in the cement paste develops in the early stages of the reaction/expansion process, with cracking also developing, but to a lesser

extent, within the aggregate particle. Alkali-silica gel was also found in cracks of the aggregate particles and of the cement paste in such concretes, thus suggesting that ASR is also playing a role in the deterioration process;

- The petrographic investigations carried out in this study suggest that the development of cracking within individual alkali-silica reactive aggregate particles does not follow a linear pattern as a function of expansion in concrete. It is proposed that a significant number of new cracks will form in the early stages of the chemical reaction until some of them reach given critical length and width. Following the minimum energy law, it will then be easier for the expanding system to propagate those “critical” cracks instead of creating new ones. Thus, the rate of crack generation within the aggregate particles will start slowing down.

9.9 ACKNOWLEDGEMENTS

The funding of this project was provided by a grant from the Quebec Department of Transportation, under the supervision of Mr. Alain Hovington and Mrs. Nadia Pouliot. The authors would like to thank Mr. René Malo and Mr. Mathieu Thomassin from “le Centre de recherche sur les infrastructures en béton (CRIB)” at Laval University, as well as the undergraduate research assistants who helped with the manufacturing and testing of the test specimens used in this project. L. Sanchez benefits from a Vanier scholarship financed by NSERC (Natural Sciences and Engineering Research Council of Canada).

9.10 REFERENCES

- [1] Fournier, B.; Bérubé, M. A. 2000. Alkali–aggregate reaction in concrete: a review of basic concepts and engineering implications. *Canadian Journal of Civil Engineering*, 27 (2): 167-191.
- [2] Dunbar, P.A.; Grattan-Bellew, P.E. 1995. Results of damage rating evaluation of condition of concrete from a number of structures affected by ASR. CANMET/ACI International Workshop on Alkali-Aggregate Reactions in Concrete, Darmouth, Canada, October 1995.
- [3] Grattan-Bellew, P.E.; Mitchell, L.D. 2006. Quantitative petrographic analysis of concrete –The Damage Rating Index (DRI) method, a review. Proc. Marc-André Bérubé symposium on AAR in concrete, CANMET/ACI Advances in concrete technology seminar, Montréal, Canada, May 31 & June 1 2006.
- [4] Shrimmer, F.H. 2000. Application and use of Damage Rating Index in assessment of AAR-affected concrete-selected case studies. 11th ICAAR - International conference on alkali-aggregate reaction (ICAAR). June 11 – 16th, Quebec, Quebec (Canada), 899-907.
- [5] Rivard, P.; Fournier, B.; Ballivy, G. 2002. The DRI method for ASR affected concrete - A Critical review of petrographic features of deterioration and Evaluation Criteria. *Cement, Concrete and Aggregates*, 24(2): 1-10.
- [6] Rivard, P.; Ballivy, G. 2005. Assessment of the expansion related to alkali-silica reaction by the Damage Rating Index method. *Construction and Building Materials*, 19: 83-90.

- [7] Bérubé, M.A.; Smaoui, N.; Fournier, B.; Bissonnette, B.; Durand, B. 2005. Evaluation of the expansion attained to date by concrete affected by ASR - Part III: Application to existing structures. *Canadian Journal of Civil Engineering*, 32: 463-479.
- [8] Shrimmer, F.H. 2006. Development of the Damage Rating Index Method as a tool in the assessment of alkali-aggregate reaction in concrete: a critical review. Proc. Marc-André Bérubé symposium on AAR in concrete, CANMET/ACI Advances in concrete technology seminar, Montréal, Canada, 391-411, May 31 & June 1 2006.
- [9] Powers, L.; Shrimmer, F. H. 2009. Quantification of ASR in concrete: an introduction to the Damage Rating Index. 29th International Conference on Cement Microscopy, 20-24 May 2007, Québec, Canada, 527p..
- [10] Blight, G.E.; McIver, J.R.; Schulte, W.K.; Rimmer, R. 1981. The effects of alkali-aggregate reaction on reinforced concrete structures made with Witwatersrand quartzite aggregate. 5th ICAAR - International Conference on Alkali-Aggregate Reaction in Concrete, Cape Town, South Africa, 1981.
- [11] Sims, I.; Hunt, B.; Miglio, B. 1992. Quantifying microscopical examinations of concrete for AAR and other durability aspects. *American Concrete Institute*, SP 131-114, 267-287.
- [12] Salomon, M.; Panetier, J.L. 1994. Quantification du degré d'avancement de l'alcali-réaction dans les bétons et de la néofissuration associée. 3rd CANMET/ACI International conference on durability of concrete. Nice, France, 383-401, 1994.
- [13] Clemena, G.G.; Lane, S.; Freeman, T.; Lozev, M. 2000. Evaluation of nondestructive evaluation methods for application in early detection of deterioration in concrete pavements. VTRC 00-R13. Virginia Transportation Research Council, Charlottesville, USA, 26p.
- [14] Rivard, P.; Fournier, B.; Ballivy, G. 2000. Quantitative petrographic technique for concrete damage due to ASR: Experimental and Application. *Cement, Concrete and Aggregates*, 22 (1): 63-72.
- [15] Broekmans, M.A.T.M. 2002. The alkali-silica reaction: mineralogical and geochemical aspects of some Dutch concretes and Norwegian mylonites. PhD Thesis, Utrecht University (The Netherlands), 144 p.
- [16] Lindgaard, J.; Skjolsvold, O.; Haugen, M.; Hagelia, P.; Wigum, B.J. 2004. Experience from evaluation of degree of damage in fluorescent impregnated plan polished sections of half-cores based on the "Crack Index Method". 12th ICAAR - International Conference on Alkali-Aggregate Reaction in Concrete. Beijing, China, 939-947.
- [17] Giaccio G.; Zerbino, R.; Ponce, J. M.; Batic, R. 2008. Mechanical behavior of concretes damage due to ASR. *Cement and Concrete Research*. 38: 993-1004.
- [18] Katayama, T. 2010. The so-called alkali-carbonate reaction (ACR) — Its mineralogical and geochemical details, with special reference to ASR. *Cement and Concrete Research*, 40: 643-675.
- [19] Katayama, T.; Grattan-Bellew, P. E. 2012. Petrography of Kingston experimental sidewalk at age 22 years. ASR as the cause of deleteriously expansive, so-called alkali-carbonate reaction. 14th ICAAR - International Conference on Alkali-Aggregate Reaction in Concrete. May 20-25th, Austin (Texas), electronic.
- [20] Fecteau, P. L.; Fournier, B.; Choquette, M.; Duchesne, J. 2012. Contribution to the understanding of the so-called alkali-carbonate reaction (ACR). 14th ICAAR - International Conference on Alkali-Aggregate Reaction in Concrete. May 20-25th, Austin (Texas), electronic.
- [21] CSA A864. Guide to the Evaluation and Management of Concrete Structures Affected by Alkali-Aggregate Reaction. Canadian Standards Association, Mississauga, Ontario (Canada),
- [22] Diamond, S. 1975. A review of alkali-silica reaction and expansion mechanisms. *Cement and concrete research*, 5:329-346.
- [23] Dunant, C. F.; Scrivener, K. L. 2009. Micro mechanical modeling of alkali-silica reaction induced degradation using the AMIE framework. *Cement and Concrete Research*, 40: 517-525.
- [24] Dunant, C.; Bentz, E. 2012. The effect of multi-axial restraint on ASR-affected concrete. 14th ICAAR - International Conference on Alkali-Aggregate Reaction in Concrete, May 20-25th 2012, Austin (Texas), electronic.

- [25] Bérard, J; Roux, R. 1986. La viabilité des bétons du Québec : le rôle des granulats. *Canadian Journal of Civil Engineering*, 13 (1): 12-24.
- [26] Fournier, B. 1993. Contribution à l'étude de la durabilité des structures de béton construites avec des granulats carbonatés produits dans les Basses-Terres du Saint-Laurent du Québec : les réactions alcalis granulats. Thèse de doctorat, Département de géologie et de génie géologique, Université Laval, Québec (Canada), novembre 1993.
- [27] Guédon-Dubied, J.S.; Cadoret, G; Durieux, V.; Martineau, F.; Fasseu, P.; Van Overbecke, V., 2000. Study on Tournai limestone in Antoing Cimescaut quarry – petrological, chemical and alkali-reactivity approach. 11th ICAAR - International Conference on Alkali-Aggregate Reaction in Concrete, June 11 – 16th, Quebec, Quebec (Canada), 335-344.
- [28] Villeneuve, V. 2011. Détermination de l'endommagement du béton par méthode pétrographique quantitative. Mémoire de maîtrise, *Géologie et Génie Géologique*. Université Laval, Québec.
- [29] Tremblay, S. 2011. Étude de l'efficacité d'adjuvants à base de lithium afin de contrôler la réaction alcalis-silice dans le béton frais et dans les structures existantes incorporant cet adjuvant. Mémoire de maîtrise, *Géologie et Génie Géologique*. Université Laval, Québec.
- [30] Golterman, P. 1995. Mechanical predictions on concrete deterioration – Part 2: classification on crack patterns. *ACI Materials Journal*, 92: 01-06.
- [31] Reinhard, H. W.; Mielich, O. 2011. A fracture mechanics approach to the crack formation in alkali sensitive grains. *Cement and Concrete Research*, 41: 255- 262.
- [32] Villeneuve, V., Fournier, B. 2012. Determination of the damage in concrete affected by ASR – the damage rating index (DRI). 14th ICAAR - International Conference on Alkali-Aggregate Reaction in Concrete, May 20-25th 2012, Austin (Texas), electronic.
- [33] Shrimmer, F.H. 2006. Development of the Damage Rating Index Method as a tool in the assessment of alkali-aggregate reaction in concrete: a critical review. Proc. Marc-André Bérubé symposium on AAR in concrete, CANMET/ACI Advances in concrete technology seminar, Montréal, Canada, 391-411.
- [34] Grattan -Bellew, P.E.; Danay, A. 1992. Comparison of laboratory and field evaluation of AAR in large dams. Proc. of the International Conference on Concrete AAR in Hydroelectric Plants and Dams, Canadian Electrical Association & Canadian National Committee of the Int. Commission on Large Dams, September 28 – October 2 1992, Fredericton, New Brunswick, (Canada), 23p.
- [35] Transtec Group. 2009. Field Site and Petrographic Evaluation - ASR Development and Deployment Program - Field Trials and Demonstration Projects.
- [36] Sanchez, L. F. M. Contribution to the assessment of damage in aging concrete infrastructures affected by alkali-aggregate reaction, PhD thesis, Laval University, department of geology and geological engineering (to be published- 2014).
- [37] Fournier, B. Bilodeau, A., Thomas, M.D.A. and Folliard, K. (2007). Uses of Class C fly ash in Ternary Blends for Mitigation of Alkali-Silica Reactivity. EPRI, Palo Alto, Ca: 2007, 1014271.
- [38] Lu, D., Fournier, B., Grattan-Bellew, P.E., Lu, Y., Xu, Z. & Tang, M. 2008. Expansion behaviour of Spratt and Pittsburg limestones in different test procedures. 13th Int. Conf. of Alkali-Aggregate Reaction in Concrete, Trondheim, Norway, June 16-20.
- [39] Sanchez, L. F. M.; Kuperman, S, C; Helene, P; Kihara, Y. 2008. Trials to correlate the accelerated mortar bar test, the standard and the accelerated concrete prism tests. 13th ICAAR - International Conference on Alkali-Aggregate Reaction in Concrete. June 16-20, Trondheim, Norway.
- [40] Lu, D., Fournier, B. & Grattan-Bellew, P.E. (2006). Effect of Aggregate Particle Size on Determining Alkali-Silica Reactivity by Accelerated Tests. *Journal of ASTM International*, 3 (9).
- [41] ASTM C 1074. 2011. Standard Practice for Estimating Concrete Strength by the Maturity Method. ASTM International, West Conshohocken (USA), 2011.
- [42] CSA A23.1. Concrete Materials and Methods of Concrete Construction - APPENDIX B. Canadian Standards Association, Mississauga, Ontario (Canada).

10. PAPER V: OVERALL ASSESSMENT OF ALKALI-AGGREGATE REACTION (AAR) IN CONCRETES PRESENTING DIFFERENT STRENGTHS AND INCORPORATING A WIDE RANGE OF REACTIVE AGGREGATE TYPES AND NATURES

Sanchez. L.^a; Fournier. B.^b; Jolin. M.^c

(a) MSc. – Laval University – PhD candidate.

1065, avenue de la Médecine, Pavillon Adrien-Pouliot, local 3755 Tel.: 1 (418) 704-2435

leandrofms@gmail.com / le.sanchez@uol.com.br

(b) Prof. Dr. – Laval University. Quebec. QC. Canada

benoit.fournier@ggl.ulaval.ca

(c) Prof. Dr. – Laval University. Quebec. QC. Canada

marc.jolin@gci.ulaval.ca

ABSTRACT

Recent works suggest that the *Stiffness Damage Test* and the *Damage Rating Index* can reliably assess the condition of concrete affected by ASR. However, the full correlation of the data obtained from the above tools for condition assessment of AAR has not been discussed in details so far. This paper presents the global assessment of twenty concrete mixtures presenting different strengths and incorporating a wide range of aggregate types/natures. Evaluations of both AAR crack development and its influence on the mechanical properties of affected concrete materials is performed over a micro mechanical point of view. The results show that strong data envelopes are obtained that correlate various critical output parameters of the SDT and the DRI with the expansion in the test specimens due to AAR. In addition, such assessments at the micro level allow a better understanding/prediction of the material's properties changes as a function of AAR expansion levels. Moreover, the micromechanical analyses of the data obtained on the different concretes enabled the comprehensive classification of different damage degrees, which seems to demonstrate that ASR, as a function of its development, might induce serviceability/durability issues and even possibly some structural capacity concerns.

Keywords: stiffness damage test (SDT), damage rating index (DRI), overall assessment of damage, alkali-aggregate reaction.

RÉSUMÉ

Des travaux récents suggèrent les essais du *Stiffness Damage Test* (SDT) et du *Damage Rating Index* (DRI) peuvent évaluer de façon fiable le degré d'endommagement de bétons affectés par la RAG. Cependant, la corrélation entre les données obtenues à partir de ces outils d'évaluation n'a jamais été évaluée en détail à ce jour. Cet article présente l'évaluation globale de vingt mélanges de béton impliquant différentes formulations et une large variété de types/natures de granulats. Des évaluations du développement de la fissuration associable à la RAG et son influence sur les propriétés mécaniques des matériaux affectés sont effectuées d'un point de vue micromécanique. Les résultats montrent que des enveloppes de données sont obtenues lorsque des paramètres critiques des deux méthodes sont corrélés, ainsi que lorsque les résultats sont comparés avec l'expansion des échantillons affectés. En plus, les évaluations micromécaniques permettent une meilleure compréhension/prédiction des changements des propriétés des matériaux en fonction des niveaux d'expansion de la RAG. Ainsi, l'analyse micromécanique des données obtenues sur ce projet a permis la classification globale de différents degrés d'endommagement, ce qui semble démontrer que RAG, en fonction de son développement, peut engendrer des problèmes de service/durabilité et même possiblement de capacité portante.

Keywords: stiffness damage test (SDT), damage rating index (DRI), overall assessment of damage, alkali-aggregate reaction.

10.1 INTRODUCTION

Alkali-aggregate reaction (AAR), a chemical reaction between certain mineral phases from the aggregates and the alkali hydroxides from the concrete pore solution is one of the most harmful distress mechanisms affecting the durability of concrete infrastructures worldwide [1]. Bérubé et al. [2] and Fournier et al. [3] recently developed comprehensive management programs for the diagnosis and prognosis of ASR in aging concrete structures based on a series of laboratory test procedures. Although promising, these lab-procedures still present several parameters whose impact is not completely understood, which reduce significantly their applicability for the appraisal of concrete structures/structural elements in service. Sanchez et al. [4, 5, 6 and 7] showed that both the *Stiffness Damage Test* (SDT) and the *Damage Rating Index* (DRI), mechanical and microscopic tools respectively, can reliably assess the damage degree of ASR affected concretes by the adjustment of some of their input

and output parameters. However, an overall distress evaluation, which would encompass the full characterization of the damaged concrete through a micro-mechanical coupling (i.e. microscopic features vs. mechanical behavior), was almost never performed before and very few data are available.

Smaoui et al. [8, 9] and Bérubé et al. [10] recently proposed an overall distress evaluation involving the characterization of damage in concrete through micro-mechanical coupling (i.e. microscopic features using the DRI and mechanical behaviour using the SDT). Their work opened the doors to a comprehensive investigation involving a larger range of concrete mixtures and aggregate materials, as described in this paper.

10.2 AAR INFLUENCE ON THE MECHANICAL PROPERTIES OF AFFECTED CONCRETE

Well-designed concrete generally presents good strength and modulus of elasticity, reasonable tensile strength, a brittle response under uniaxial loading (compression or tension) and an increase in both ductility and strength (in compression and tension) in a confined environment [11]. This sensitivity to the confinement state is linked to the presence of small defects or microcracks that are always present in this *composite* material. Thus, even for a sound concrete under a triaxial compression state, there will always be local zones in tension within the bulk material volume due to its heterogeneous and “defective” nature [11]. Moreover, the complexity of concrete behavior under stresses is even greater when one deals with a damaged material [11]. Therefore, the understanding of the mechanical properties’ changes (i.e. compressive and tensile strengths, modulus of elasticity and also the stress/strain behavior) as a function of AAR development is a very important step for designing repair/reinforcement strategies for aging concrete elements/structures [12].

Generally, the development of AAR induces a very significant drop in tensile strength and modulus of elasticity of the affected concretes. These two properties are significantly more affected than the compressive strength, which begins to decrease significantly only at high levels of expansion (Figure 1 and Figure 2) [8, 12, 13,14].

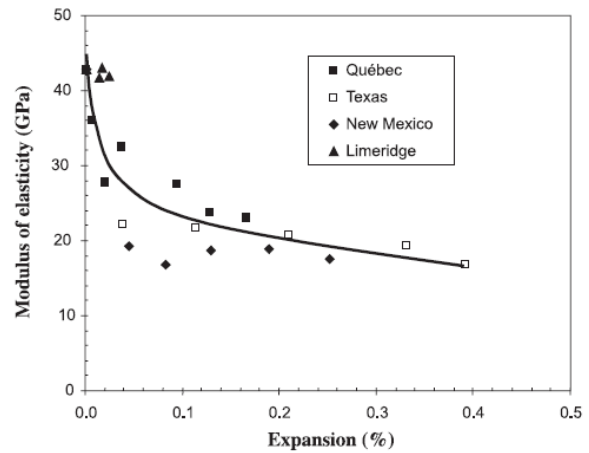
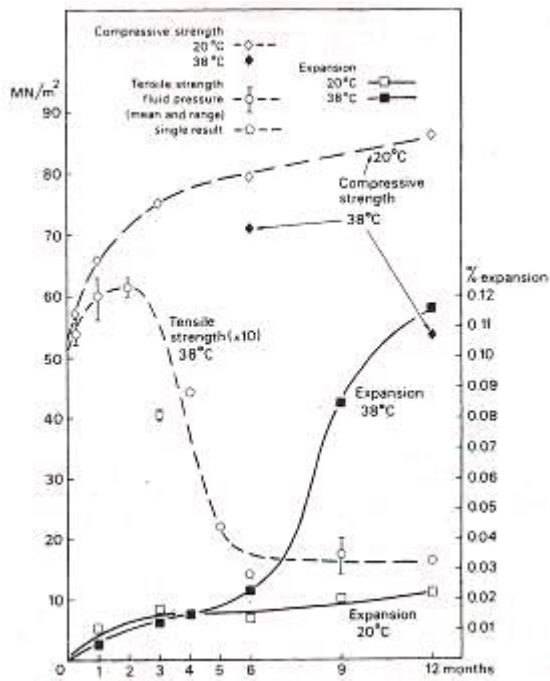


Figure 1: Expansion and strength development in tension and compression for concrete stored at 20 ° C and 38 ° C [13].

Figure 2: Modulus of elasticity loss as a function of ASR expansion [8].

This classic description of the AAR impact on the mechanical properties of concretes suggests that significant microcracking caused by this mechanism can be identified even before the material reaches significant expansion and mechanical distress, which might lead to significant compressive strength loss [13]. According to ISE [15], it is likely that concrete structures/structural elements in service develop compressive strengths greater than their design values, thus the compressive strength losses of AAR affected materials are often smaller than the “gap” between the design and the actual strength values measured at a given time. On the other hand, significant compressive strength losses were observed on affected concrete specimens presenting important “free” expansion levels (i.e. 1 mm/m or 0.10%) [16, 17]. According to these authors, it is very likely that AAR-affected concrete structures/structural elements still efficiently withstand the active stresses for expansion levels lower than 0.10%. However, after 0.30% of expansion, a complete structural appraisal should be carried out [15, 16, 17]. Moreover, Kubo et al. [12] have shown significant compressive strength losses for concretes with expansion levels higher than 0.30%, reaching up to 30% drop for expansion levels of 0.50% (those losses were obtained in comparison with the 28-day value obtained for the same mixtures). In the same study, the authors found that neither the water/cement ratio of the concrete mixtures nor the type of reactive aggregates used influenced significantly the responses in terms of compressive strength, at least up to

expansion levels of 0.30% (Figure 3). On the other hand, the researchers found significant differences in the stress/strain behavior (especially for the modulus of elasticity) at similar expansion levels when different aggregates are used (Figure 4). They considered those differences associated with the various cracking patterns generated when different reactive aggregates are used in concrete [12].

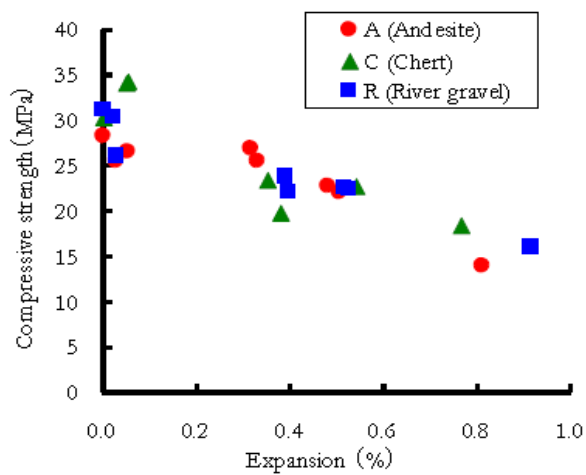


Figure 3: Compressive strength loss in function of ASR expansion levels [12].

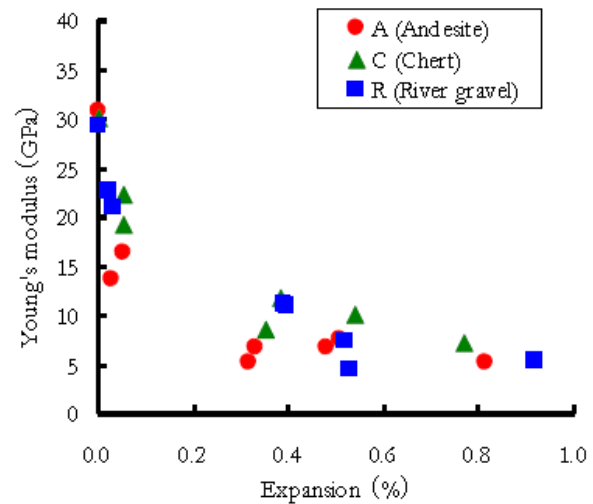


Figure 4: Modulus of elasticity loss in function of ASR expansion [12].

Naar [18] suggests that the global understanding of the mechanical properties losses, as a function of the progress of AAR expansions, is extremely difficult as several “contradictory” results are presented in the literature. In terms of compressive strength, some authors found losses just for very high expansion levels while others found either almost no change in this property or even an increase of the compressive strength with the expansion increase. The majority of the authors, however, agree on a rapid loss in modulus of elasticity already for low and moderate expansion levels (i.e. from 0.0% up to 0.12%), with values ranging from 20 to 80% of the modulus of elasticity of sound concretes for specimens presenting the same mix design (but different aggregate types/natures), which can be considered an important variation.

The mechanical response of concretes incorporating different reactive aggregate types/natures has been studied by several researchers. It was found that the reaction rate, the cracking patterns and also the mechanical properties losses changed for AAR affected concrete as a function of the type/nature of coarse aggregate used in the material [19]. Reinhart & Mielich

[20] carried out a series of laboratory tests on concretes cast with commonly-used slowly reactive aggregate types (i.e. greywacke, quartzite, granite, andesite, etc.), which have already caused problems in concrete structures after 10 to 20 years in service. Their test results showed that the dynamic modulus of elasticity, which can be measured through the ultrasonic pulse velocity procedure, is generally not a good indicator of concrete damage due to AAR. Moreover, the compressive strength was found to change as a function of the expansion level, but much less than the tensile strength. Finally, the modulus of elasticity appears to be the most sensitive parameter to AAR expansion/distress development, and therefore more effective for assessing the degree of damage of an affected material.

Giaccio et al. [19] verified that the compressive strength of concretes is clearly affected by AAR at all the steps of the physical distress process, i.e. crack's initiation, stable and unstable crack's propagation. However, the period necessary to initiate cracking or even "the critical compression load" (i.e. the compression load beyond which cracks are generated) cannot be easily linked to the expansion levels measured on the specimens since those behaviors depend on several factors, such as the concrete mix design and aggregate's characteristics (lithotype, aggregate size, kinetics and microscopic damage features of AAR) used in the concrete. The authors also found that the period of stable crack growth is less affected than the period of unstable crack growth, showing that an AAR affected concrete presents less ability to efficiently "control the cracks spreading", thus controlling its premature fracture [19]. Giaccio et al. [19], testing ASR-affected concrete ranging from 0.135 % to 0.145% of expansion, verified that the stress/strain behavior of the affected materials changed according to the coarse aggregate used (Figure 5, where C1 is a non-reactive control mixture). The authors concluded that those differences were related to the "competence", i.e. the ability of the aggregates to provide a better bond with the cement paste (which depends on some aggregate's characteristics such as mineralogy, texture, toughness, hardness, soundness, etc.), as well as the presence of preexisting cracks that were created over crushing/weathering processes.

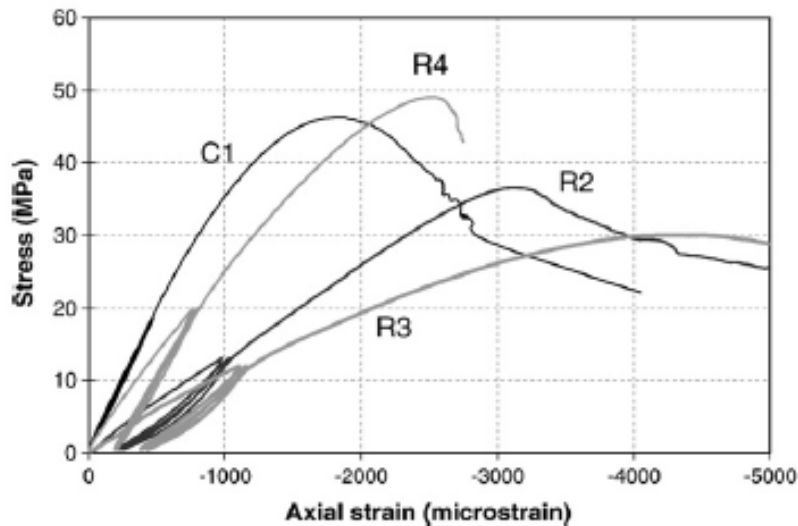


Figure 5: Stress/strain behavior of concrete damaged by AAR for concrete containing different reactive aggregates [19].

In the case of sound concretes, Aitcin et al. [21] found that the aggregate type/nature changed not only the stress/strain relationship of concrete under compression loading, but also the amount of dissipated energy during the loading cycles (Figure 6). Therefore, the authors indicated that the hysteresis area (i.e. the amount of dissipated energy) of a concrete mixture was directly related to the Interfacial Transition Zone (ITZ) strength of the material. Ozkan et al. [22] proposed the “Fragility Index” of concrete, which is the ratio between the elastic deformation energy (SII) and the irreversible deformation energy of a material (SI) obtained under compressive loading (Figure 7). When the SII/SI approaches zero, all the energy is dissipated. On the other hand, when the ratio approaches the infinity, the energy becomes reversible. Therefore, the greater is the ratio, the higher is the material fragility. The authors verified that the Fragility Index changed with the strength (and also the stiffness) of the concrete; the irreversible energy is lower with increasing strength, thus indicating a more brittle behavior. The explanation for this phenomenon is that for ordinary sound concrete, the differences in the mechanical properties (strength, stiffness, etc.) between the various component materials (especially cement paste vs. aggregates) induce cracks to propagate through the lowest strength areas/zones of the material upon loading (e.g. ITZ). However, for high-performance concretes, those differences are less apparent, leading to easier crack propagation.

Alexander and Milne [23] studied the influence of the cement type on the stress/strain concrete properties. The authors used loads of about 25% of the maximum material strength at

28 days. The results showed that not only the aggregate types/natures and the concrete strength (and maturity), but also the type of binder, plays a very important role on the stress/strain behavior of the concrete (Figure 8), again demonstrating the importance of the ITZ in the resulting behavior of concrete.

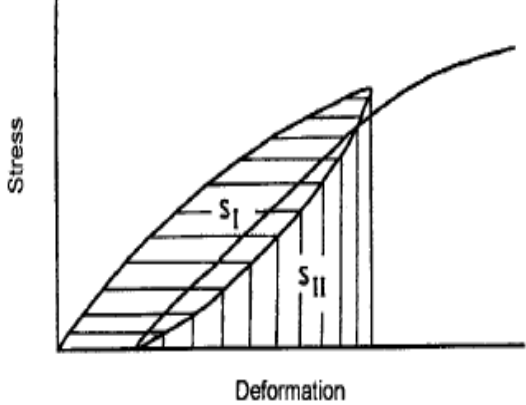
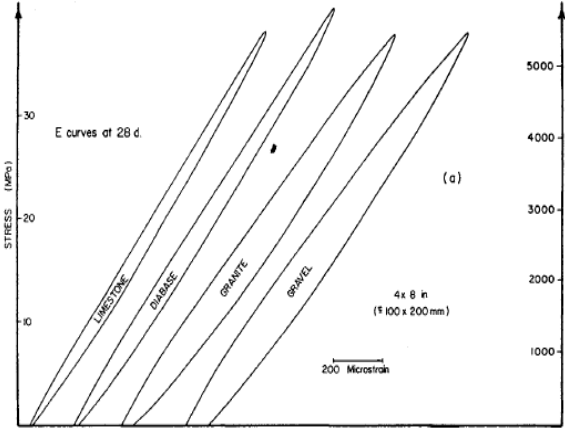


Figure 6: Hysteresis areas for different aggregate types used in concrete [21].

Figure 7: Fragility index (S_{II}/S_I) proposed by [22].

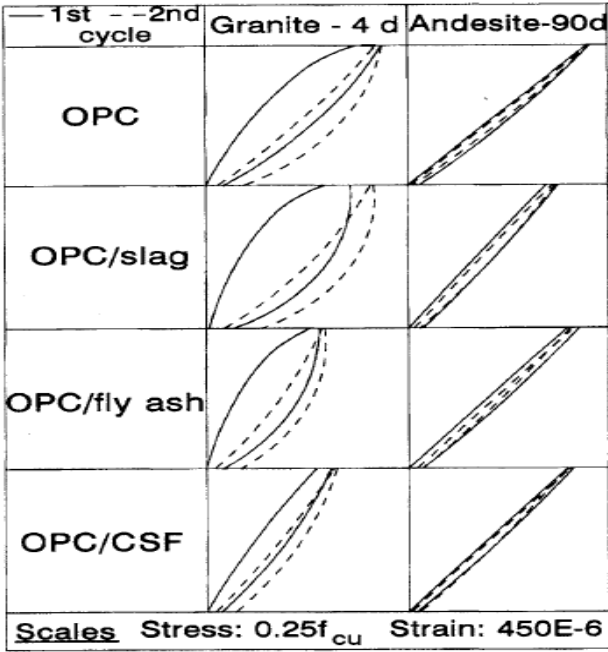


Figure 8: Stress-strain behavior of concrete incorporating different cement types [23].

10.3 TOOLS FOR ASSESSING CONCRETE DAMAGED BY ASR

“Damage” is defined in this work as the harmful consequences (measurable ones) of various types of mechanisms (e.g. loadings, shrinkage, creep, ASR, DEF, freezing and thawing, etc.) on the mechanical properties, physical integrity and durability of a concrete element/material. Therefore, in practical terms, the word *damage* is considered here as being part of: 1) the stiffness loss of the concrete; 2) the mechanical properties reductions of the material and; 3) the durability loss (related to the physical integrity or cracking extent) of the concrete (Figure 9).

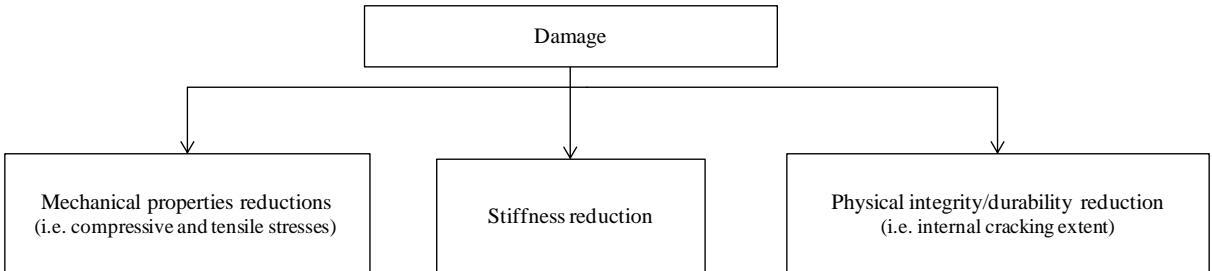


Figure 9: Global assessment of damage.

As discussed previously, AAR strongly influences some of the mechanical properties of the affected concrete material. This influence depends on several factors such as the cement type, the reactive (or non-reactive) aggregates types/natures, the material’s strength as well AAR type, kinetics and amplitude. Moreover, as stated by [19], both AAR kinetics and distress (in terms of cracks’ evolution) change as a function of the aggregate’s types/natures. Therefore, the development and use of laboratory/field procedures to evaluate the AAR damage degree in concrete (diagnosis) and also its development over time, thus enabling the prediction of further damage in the affected material (prognosis), would be extremely interesting, mainly for the selection of effective methods for repairing/reinforcing distressed concrete structures/structural elements. Over the years, several microscopic and mechanical tools were developed and used for assessing damage in concrete due to AAR, and among them, the procedures described in the following sections were found to be the most suitable.

10.3.1 Stiffness Damage Test (SDT)

In the early 1990's, Crisp and coworkers proposed to use the *Stiffness Damage Test* to quantify the degree of distress in concrete due to ASR [24, 25]. The test method was actually developed by Walsh [26] who observed a good correlation between the crack density and the cycles of loading/unloading (stress/strain relationship) of rock specimens. Crouch [27], following those results, proposed a new test procedure (*Stiffness Damage Test - SDT*) based on cyclic compression loading of concrete specimens (cylinders or cores). A review on the SDT development as a diagnostic tool for assessing ASR affected concrete is presented in [4]. Sanchez et al. [4, 5] actually pursued the work of Smaoui and coworkers [8, 9, 10], by applying the SDT procedure to specimens cast from concrete mixtures of various mix designs (25, 35 and 45 MPa) and incorporating a range of reactive aggregates (coarse vs. fine), as well as on concrete cores extracted from an extremely damaged concrete overpass in Quebec City (Canada). The goal of those studies was to verify the influence of either the *test loading level* or several *input parameters* (concrete environment, humidity, specimen size, etc.) on the output test analyses. Likewise, the evaluation of the output test responses against the expansion levels of the affected specimens was performed.

Based on an extensive investigation program and the statistical analysis of the test results, the authors presented the following main conclusions: 1) the SDT should be carried out with a percentage of the concrete strength instead of using a fixed load (as originally proposed by [8, 9, 24, 25]); 2) the use of 40% of the design concrete strength seems to be the best approach for distinguishing damaged concrete specimens with regard to their expansion levels; 3) the use of percentages up to 40% of the design concrete strength enables the use of the same specimen for supplementary analyses, such as compressive or tensile strength, since the test seems to keep its “non destructive” character up to that point; 4) the output parameters such as the hysteresis area (HA) and the plastic deformation (PD) over the five cycles, as well as the modulus of elasticity (ME) (as an average value of the second and third cycles), were chosen as the most diagnostic output results of the test; 5) the input parameters such as the concrete's cure history (i.e. the specimen moisture condition), the sample's geometry and size, the sample's location within the structural member (zone and direction), as well as the selection of the sample's strength level for stiffness damage testing, seems to strongly influence the output analyses of the SDT and; 6) the use of indices (*Stiffness Damage Index - SDI* and *Plastic Deformation Index - PDI*) instead of absolute HA or PD values, which take into account the ratio “dissipated energy/total energy” implemented in the system, better

represents the real “damage” of the affected materials; actually, this approach decreases the impact of a poor selection of maximum loading level for stiffness damage testing and provides easier understanding of AAR evolution as a function of its expansion [4, 5].

10.3.2 Damage Rating Index (DRI)

The *Damage Rating Index* method (DRI) is a semi-quantitative microscopic analysis performed with the use of a stereomicroscope (about 15x magnification) where damage features associated with ASR are counted through a 1 cm² grid drawn on the surface of a polished concrete section [28]. The number of counts corresponding to each type of petrographic features is then multiplied by weighing factors, whose purpose is to balance their relative importance towards the mechanism of distress considered (for instance ASR) [29-31]. Details on the test procedure and specific considerations on its application for the specimens examined as part of this study are given in Sanchez et al. [6, 7].

Sanchez et al. [6, 7] used the DRI, applying the new version proposed by [28], to evaluate ASR distress coming from different reactive aggregate types (Tx reactive sand and NM reactive coarse aggregate) and concrete strengths. The concrete specimens assessed by the authors presented different expansion levels (from 0.05% up to 0.30%) and the design compressive strength of the concretes ranged from 25 MPa to 45 MPa. The main results found were the following:

- DRI semi-quantitative output final value distinguished well the different expansion levels in ASR affected concretes incorporating either reactive sands or reactive coarse aggregates. However, for being an effective semi-quantitative tool, the analyses should be performed on the aggregate particles down to 1 mm in size, instead of 2 mm as proposed by [28]. Moreover, all the DRI semi quantitative data correlated well with the expansion level of the affected specimens;
- DRI semi-quantitative numbers were quite similar between the 25 and 35 MPa mixes at each expansion level. However, in the 45 MPa concretes, the behavior was found to be slightly different as greater numbers were found for low expansion levels (i.e. 0.05%), while the presence of gel was found to be greater at all expansion levels studied [6, 7]. Also, cracking in the cement paste (and sometimes in the aggregate particles) was significantly more difficult to identify in the 45MPa polished sections than in the 25 and

35MPa concretes, at least at the magnification used for the DRI procedure ($\approx 15x$ to $16x$); this was particularly true for the polished sections incorporating the reactive sands [6, 7];

- Considering the DRI results, a strong “envelope of damage results” (i.e. results found within well defined boundaries/limits) was found towards the expansion level of the affected samples. Exceptions were however noted for concretes incorporating the alkali-carbonate reactive Kingston limestone and the Potsdam orthoquartzite, which presented much more and much less damage at similar expansion levels, respectively, than the average range of the other mixes;
- The analysis of all data from petrographic features counting allows a better understanding of the damage mechanism in the ASR-affected specimens than just relying on the absolute DRI numbers. For instance, the number of opened cracks in the aggregate particles and their extension into the cement paste, with and without gel, was found to increase with increasing expansion, thus confirming those features as diagnostic of the progress of ASR in the test specimens examined. Similarly, the crack density (CD - counts/cm²), increases with increasing expansion in the AAR affected specimens for all the concrete mixtures studied. Moreover, as for the DRI number, a strong “envelope of crack density results” is observed towards the expansion level of the affected samples [7].

10.3.3 Ultrasonic Pulse Velocity (UPV)

Traditionally, the assessment of the AAR damage degree and its evolution in aging concrete structures is carried out by conventional destructive methods (mechanical testing, petrographic analysis of thin sections and qualitative/quantitative study on concrete cores). However, there are limited data available on the use of non-destructive test methods for assessing both AAR damage and its evolution over time, especially when considering the use of a wide range of reactive aggregate types/natures and concrete strengths [32].

The most widely used non destructive test procedure for assessing AAR damage is the ultrasonic pulse velocity (UPV), which deals with the propagation of compression waves within AAR affected samples. This procedure is performed using the Pundit® device and it is carried out according to ASTM C597 [33].

Saint Pierre et al. [32] tested the UPV for assessing concrete damage due to ASR and they found that the UPV sensitivity is not precise enough to establish “damage criteria” related to AAR distress. Likewise, Sanchez [4], working on ASR affected concretes of different strengths and incorporating different reactive aggregates (fine vs. coarse aggregates) verified

that the UPV was not capable of evaluating the expansion levels of the affected specimens. Therefore, further work is still necessary to develop a “new and reliable” non destructive test procedure which enables either AAR damage detection or development.

In this context, Morad-Marani et al. [34] recently developed a nonlinear acoustic technique of time shift for ASR evaluation in concrete structures. This test method showed to be much more sensitive to ASR expansion/development than the ordinary UPV procedure. However, although promising, there is currently very few data obtained through this new technique and further development/evaluation is still needed, using a wide range of concrete strength and aggregate types/natures in order to prove its efficiency for ASR assessment.

10.3.4 Compressive and tensile strengths

Compressive and tensile strengths are commonly used for design purposes as well as condition assessment of aging structural elements. However, since compressive strength is not much influenced by ASR unless large expansions are reached, compressive strength determinations on concrete cores taken from aging concrete structures should rather be used for determining the actual and residual strength of an affected material than for assessing ASR damage level and progress over time. On the other hand, tensile strength is a parameter which is not commonly used for designing reinforced concrete structures (other than pavements) and it is usually adopted (for sound materials!) as being about 10% of the compressive strength of concrete at a given age. Otherwise, it has been found that this parameter is much more influenced by ASR and thus its analysis could likely add interesting information about ASR distress degree and development [13, 35].

10.4 SCOPE OF WORK

As indicated in the previous sections, AAR affects differently the mechanical properties of concretes (stress/strain behavior, modulus of elasticity, tensile and compression strengths, etc.) which may impact on the performance of structures/structural elements in service. Moreover, according to several researches, the use of different reactive aggregate types/lithologies could also produce different “alkali-aggregate reaction patterns” in the affected concretes, such as reaction kinetics, distress features types and evolution against expansion, etc., which could require different remedial actions/solutions.

This paper presents the overall evaluation of the *progress of damage*, as a function of expansion, in concrete specimens cast in the laboratory from different concrete mixtures (25,

35 and 45 MPa) incorporating a wide range of reactive aggregate types/natures. The assessment of this global damage was performed through the microscopic and mechanical tools described in section 3, as well as from conventional mechanical test procedures to evaluate compressive and tensile strengths, and the modulus of elasticity. A statistical analysis of the test data is also presented to further support their reliability. Finally, a global testing scheme is presented for the condition assessment of AAR in aging concrete structures.

10.5 MATERIALS AND METHODS

10.5.1 Materials and mixture proportions

Twenty concrete mixtures of different strengths (i.e. 25, 35 and 45 MPa) and incorporating ten different reactive aggregate types/natures were selected for this study. The coarse aggregates ranged from 5 to 20 mm in size. Non-reactive fine (Lav) and coarse (HP or Dia) aggregates were used in combination with the reactive aggregate materials for concrete manufacturing. Table 1 provides information on the different aggregates used in this study. One important note, all the 20 concrete mixtures were designed to present the same volume of paste and aggregates, so one can compare similar systems (Table 2) with different aggregates and strengths.

Table 1: Aggregates used in the study.

Aggregate	Reactivity	Location	Rock Type	Specific gravity	Absorption (%)	AMBT ¹ 14d exp,%	
Coarse	NM	R	New Mexico (USA)	Polymictic Gravel (mixed volcanics, quartzite, chert)	2.53	1.59	1.056 [36]
	QC	R	Quebec (CAN)	Siliceous and argillaceous limestone	2.50	1.16	0.302
	Wyo	R	Wyoming (USA)	Granite, amphibolite, mixed volcanics	2.64	0.87	0.296 [36]
	Conr	R	Halifax (CAN)	Metagreywacke, shale, siltstone	2.72	0.37	0.365 [37]
	King ²	R (ACR)	Kingston (CAN)	Dolomitic argillaceous limestone	2.69	0.55	0.110 [38]
	Virg	R	Virginia (USA)	Metagranite	2.78	0.45	0.090 [36]
	Rec	R	Recife (Brazil)	Granite, gneiss, mylonite	2.64	0.59	0.230 [39]
	Pots	R	Montreal (CAN)	Siliceous sandstone (orthoquartzite)	2.57	1.15	0.093 [40]
	Dia	NR	Quebec (CAN)	Diabase (plutonic rock)	3.00	0.51	0.065
HP	NR	Newfoundland (CAN)	High-purity fine-grained limestone	2.68	0.44	0.001	
Fine	Tx	R	Corpus Christi (USA)	Polymictic sand (granitic, mixed volcanics, quartzite, chert, quartz)	2.60	0.55	0.755 [37]
	Wt	R	Texas (USA)	Polymictic sand (chert, quartz, feldspar)	2.60	0.40	0.335 [36]
	Lav	NR	Quebec (CAN)	Natural derived from granite	2.71	0.54	0.068

¹ Typical results of accelerated mortar bar testing (ASTM C 1260) carried out on the aggregates selected. The number in brackets indicates the source of the information, when testing was not carried out as part of this study.

² This aggregate is supposed to generate the so-called alkali carbonate reaction (ACR).

10.5.2 Fabrication and curing of test specimens

A minimum of 35 cylinders, 100 by 200 mm in size, were cast from each of the twenty concrete mixtures manufactured in the laboratory. After 24 hours in their mould, the specimens were demolded and then placed for 24h in the moist curing room. Small holes, 5 mm in diameter by 15 mm long, were then drilled in both ends of each test cylinders and stainless steel gauge studs were glued in place, with a fast-setting cement slurry, for longitudinal expansion measurements. The cylinders were left to harden for 48 h in the moist curing room at 23°C prior to performing the “0” length reading, after what they were placed in sealed plastic (22 liters) buckets lined with damp cloth (4 cylinders per bucket). All buckets were then stored at 38°C and 100% R.H. and the test cylinders monitored for length changes regularly until they reached the expansion levels chosen for this research, i.e. $0.05 \pm 0.01\%$, $0.12 \pm 0.01\%$, $0.20 \pm 0.01\%$ and $0.30 \pm 0.01\%$. As per ASTM C 1293 [41], the buckets were cooled to 23 °C for 16 ± 4 h prior to periodic axial expansion measurements. When the above expansion levels were reached, the specimens were wrapped in plastic film and stored at 12°C until testing (because of testing capacity issues).

Prior to mechanical testing, both ends of each cylinder were carefully mechanically ground to avoid any interference from the stainless steel gauge studs used for expansion measurements. Also, even though the specimens were wrapped in plastic film over storage at 12°C, they were restored for 48h in the moist curing room, protected from running water, before testing, in order to allow appropriate saturation of the test specimens, following the procedure proposed for concrete cores extracted from real concrete structures (A23.2-14C [42]). Length and mass readings were also performed on a number of test specimens prior and upon unwrapping to make sure that they had not suffered from significant shrinkage or expansion over the storage period. The monitoring of the test specimens showed that the 12 °C storage resulted in slight shrinkage ($-0.02 \pm 0.01\%$) and mass loss ($0.7 \pm 0.2\%$) of the test specimens, which was recovered through the 48-hour re-saturation period prior to running stiffness damage testing. It was thus found that the 12°C storage did not have any adverse effect on the test specimens. In order to perform the microscopic analyses, the concrete cylinders were, after the storage period, first cut in two axially and then one of the flat surfaces thus obtained was polished. A portable hand-polishing device, which uses diamond-impregnated rubber disks (no. 50 (coarse), 100, 400, 800, 1500 à 3000 (very fine)), was found most suitable as it does not use loose abrasive powders that can fill up cracks/voids in the concrete and quality polishing is obtained with minimal water supply.

Table 2: Concrete mixtures cast with different aggregates using the same quantity (in volume) of aggregates and paste.

Type of concrete	Concrete Mix designs: Ingredients and strengths	25 MPa		35 MPa		45 MPa		
		kg/m ³	L/m ³	kg/m ³	L/m ³	kg/m ³	L/m ³	
Equivalent volumes (paste and aggregates) (<i>Base series</i>)	Common to all mixtures of this series	Cement	314	101	370	118	424	151
		Water	192	192	174	174	157	142
		Air	-	20	-	20	-	20
	Tx + HP ¹	Sand	790	304	790	304	790	304
		Coarse aggregate	1029	384	1029	384	1029	384
	Tx + Dia ¹	Sand	896	344	896	344	896	344
		Coarse aggregate	1029	343	1029	343	1029	343
	Lav + NM ¹	Sand	714	264	714	264	714	264
		Coarse aggregate	1073	424	1073	424	1073	424
	Lav + QC	Sand	705	260	705	260	705	260
		Coarse aggregate	1068	427	1068	427	1068	427
	Equivalent volumes (paste and aggregates) (<i>Complementary series</i>)	Common to all mixtures of this series	Cement			370	118	
Water					174	174		
Air					-	20		
Lav + Wyo		Sand			770	286		
		Coarse aggregate			1065	403		
Lav + Pots		Sand			737	272		
		Coarse aggregate			1068	416		
Lav + Conr		Sand			807	298		
		Coarse aggregate			1060	390		
Lav + King		Sand			794	293		
		Coarse aggregate			1062	395		
Lav + Virg		Sand			829	306		
		Coarse aggregate			1061	382		
Lav + Rec I		Sand			773	285		
		Coarse aggregate			1062	402		
Wt + HP		Sand			790	304		
		Coarse aggregate			1029	384		
Tx + NM		Sand			719	276		
	Coarse aggregate			1040	411			

¹ Detailed DRI results presented in Sanchez et al [6, 7].

10.5.3 Methods for assessment and analysis

Table 3 presents the testing matrix developed for this study. The investigation program carried out on concrete cylinders of various expansion levels includes mechanical testing (SDT, elastic modulus, compressive and tensile strengths evaluation) and semi-quantitative petrographic analysis (DRI).

Table 3: Testing matrix.

Concrete mixtures	Tests methods	Number of samples for each expansion level				
		0.00% (control)	0.05%	0.12%	0.20%	0.30%
25, 35 and 45MPa	Stiffness Damage Test/compressive strength	2	3	3	3	3
	Tensile strength (pressure tension test)	2	2	2	2	2
	Damage Rating Index	1	1	1	1	1
	28, 90 and 180-day compressive strength (ASTM C1074) ¹	6	--	--	--	--
Minimum number of specimens tested for each concrete mixture = 35						

¹ See section 5.3.3

10.5.3.1 Stiffness damage test (SDT)

Three cylinders (two in the control's case) of each concrete mixture and at each expansion level chosen (0.00% (control); 0.05%; 0.12%; 0.20% and 0.30%) were subjected to five cycles of loading/unloading at a controlled loading rate of 0.10 MPa/s. The *Stiffness Damage Test* procedure was performed according to the procedure recommended in the first part of this study [4, 5], i.e. using a loading level corresponding to 40% of the 28-day concrete strength. In the case of the control specimens, the SDT was carried out on two cylinders cast and maintained at 12°C for a 47-day period, as described in 10.5.3.2. All the results presented hereafter are the average values obtained on three specimens at each expansion level tested.

10.5.3.2 Damage Rating Index (DRI)

A semi-quantitative petrographic analysis, using the DRI, was performed on one specimen from each concrete mixtures at the various expansion levels studied (Table 3), according to the method described by Sanchez et al. [6, 7]. Actually, the counts of cracks in the aggregate particles were performed on particles down to 1 mm in size, so that the distress coming from reactive sands might be well assessed. The DRI final number presented hereafter is the normalized 100 cm² value obtained over polished concrete specimens at each expansion level.

10.5.3.3 Compressive strength test

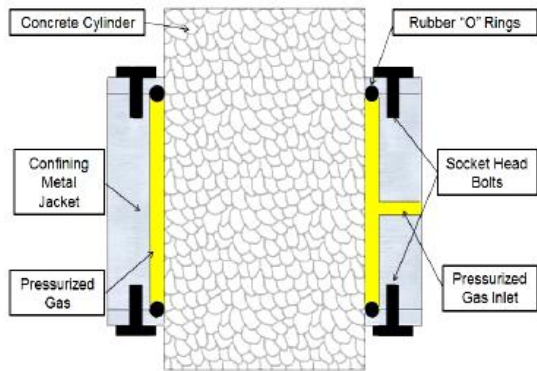
Compressive strength was measured in two ways. First, tests were carried out on sets of two cylinders to determine the 28, 90 and 180-day strength of each concrete mixture. For this first procedure, since some of the specimens contained highly-reactive aggregates, the Standard ASTM C 39 [43] procedure could not be followed as they could develop some ASR. Therefore, the samples were wrapped and placed at 12°C for a 47, 150 and 300-day period, which represents, respectively, the same 28, 90 and 180-day period according to the maturity concept presented by ASTM C 1074 [44]. The “equivalent” 28-day compressive strengths obtained from this procedure were actually used to determine the loading level (40%) to be used for stiffness damage testing.

Second, compressive strength test was determined on two of the three cylinders of each concrete mixture and at each expansion level, at the completion of stiffness damage testing, with the aim of verifying the compressive strength loss of the material as ASR develops. This procedure was adopted and considered valid after the results obtained by Sanchez et al. [4] confirmed the largely non destructive character of the SDT.

10.5.3.4 Tensile strength test

The tensile strength of two specimens of each concrete mixture, at each expansion level, was measured according to the pressure tension test. This method, also known as the indirect tension test, was first developed by The Building Research Council of Waterford, UK, as a means of investigating anisotropic behavior in materials [35]. The pressure tension test uses compressed gas to apply a uniformly distributed pressure to the curved surface of standard 100 mm by 200 mm concrete test cylinders or cores. The apparatus consists of a hollow cylindrical test chamber which envelops the curved surface of the test cylinder. At either end of the testing chamber, rubbers “O-rings” are used to seal the compressed gas so that it only acts upon the curved surface of the specimen (Figure 10). Both ends are left open to atmospheric pressure, resulting in a biaxial loading configuration. Gas pressure is monotonically increased until the test cylinder fails in a plane transverse to the axis of the testing chamber [35].

A



B



Figure 10: Cross section of pressure chamber used to perform tensile strength test on concrete specimens [35].

The gas pressure applied to the curved surface is a biaxial loading condition but the reaction forces within the diphasic model differ. In particular, the pore water reacts hydrostatically whereas the solid phase reacts biaxially, resulting in a net internal tensile force driven by the pore fluid. The resultant internal tension force is the primary reason why the pressure tension method is thought to be well suited for detecting durability issues which affect the integrity of the cementitious microstructure [35].

10.6 RESULTS

10.6.1 ASR kinetics

In this section, AAR kinetics (average expansion vs. time) and amplitude results are presented for all twenty mixtures cast in the laboratory.

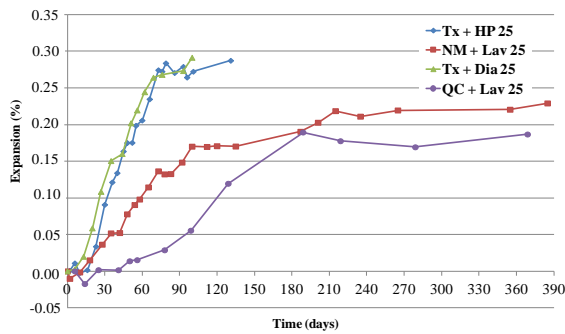
Figure 11A presents the average values from each 25 MPa concrete mixture (standard deviations of about 0.03% were found for all testing ages), while Figure 11B illustrates the average mass gain vs. time for the same concrete mixtures. Both mixtures with the Tx sand presented a much higher expansion rate than those containing reactive coarse aggregates NM or QC. The 0.30% expansion level for both mixtures with Tx sand was reached by 90 days at 38°C and 100% R.H. On the other hand, the maximum expansion levels reached by QC and NM coarse aggregates, i.e. 0.20% and 0.25%, respectively, were obtained after 180 days or 360 days of testing. Overall, the mass gain ranged from 0.6 to 1.6% at the maximum expansion level reached by the specimens. Concrete mixtures incorporating the Tx sand showed the greater and faster mass gain over time. Interestingly, a strong difference was

found between the Tx + HP (maximum 1.6% mass gain) and Tx + Dia mixtures (maximum 1.0 mass gain), despite very similar expansion behaviors over time were obtained.

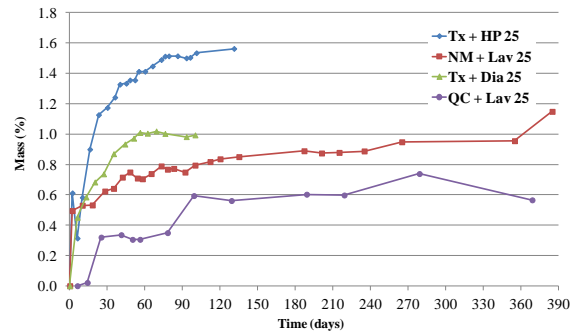
Figures 11C and 11D present the same plots for the twelve 35 MPa concrete mixtures analyzed. A large range of expansion kinetics and amplitudes was obtained as a function of the reactive aggregate tested. In general, the mixtures containing the reactive Tx sand (Tx + HP, Tx + Dia and Tx + NM) presented faster reactivity than those incorporating reactive coarse aggregates. Exception was for the Lav + King mixture, which involves an extremely reactive coarse limestone aggregate from Kingston (Canada) and is known to be susceptible to the so-called alkali-carbonate reaction (ACR). It presented the fastest expansion kinetics of all aggregates tested. An interesting behavior was also found for the Tx + NM mixture, which presented a slower expansion kinetics at early ages than both mixtures Tx + HP and Tx + Dia, although it contained both reactive aggregates together, i.e. Tx sand and NM gravel. Overall, the mass gain ranged from 0.6 to 1.4% at the maximum expansion levels. Differently from the 25 MPa mixtures, this time the mixtures showing the largest mass gain (NM and Pots aggregates - gaining about 1.4% of mass at their highest expansion levels) were not the mixes that presented the fastest expansion kinetics.

Figures 11E and 11F present the expansion and mass gain plots for the 45 MPa concrete mixtures. Once again, the test specimens incorporating the Tx sand presented a significantly higher expansion kinetics compared to those made with two reactive coarse aggregates NM and QC. The 0.30% expansion level for both mixtures with Tx sand was reached by 90 days at 38°C and 100% R.H, while the maximum expansion levels reached by QC (0.20%) and NM (0.25%) coarse aggregates were obtained after 240 days and 300 days, respectively. In terms of mass gain of the 45 MPa test specimens, a similar behaviour was observed than the 25 MPa mixtures; however, the mass gains at the highest expansion levels were less for the 45 MPa concrete mixtures.

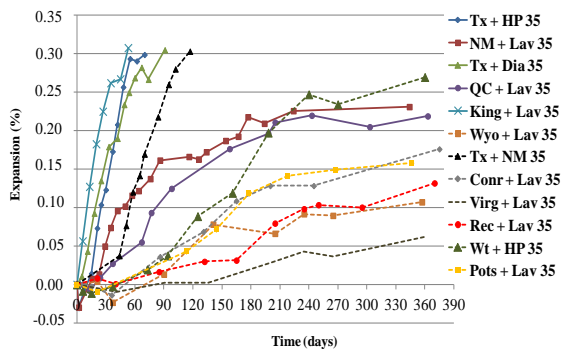
A – 25 MPa mixtures: expansion vs. time



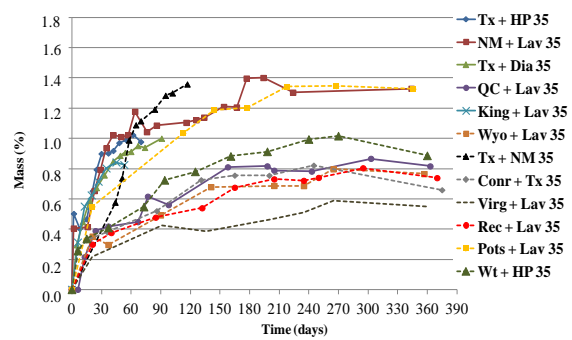
B – 25 MPa mixtures: mass gain vs. time



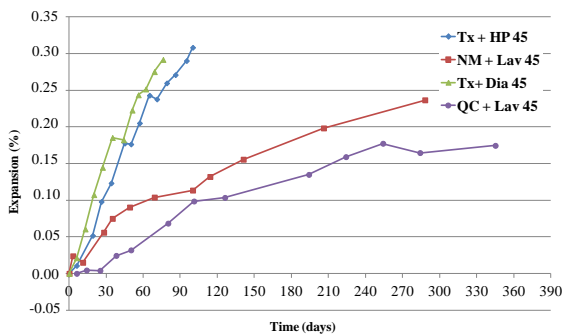
C – 35 MPa mixtures: expansion vs. time



D – 35 MPa mixtures: mass gain vs. time



E – 45 MPa mixtures: expansion vs. time



F – 45 MPa mixtures: mass gain vs. time

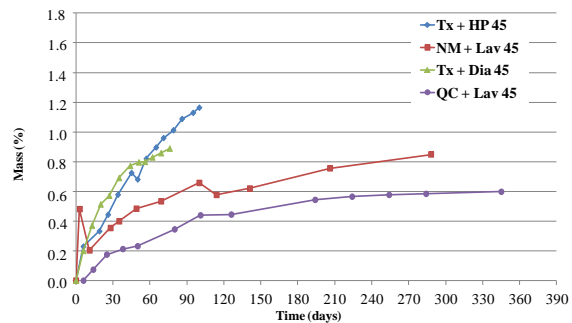


Figure 11: AAR kinetics (expansion vs. time – A, C, E) and mass gain (B, D, F) for the 25, 35 and 45 MPa concrete mixtures, respectively.

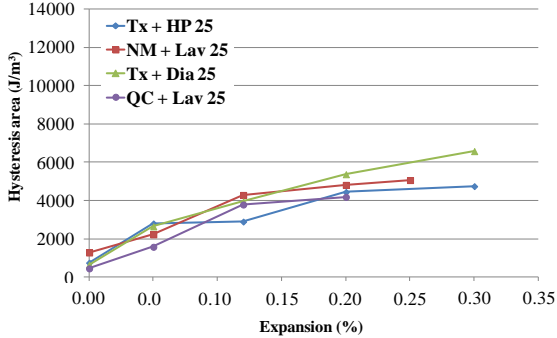
10.6.2 Stiffness Damage Test (SDT)

10.6.2.1 SDT output parameters: absolute values

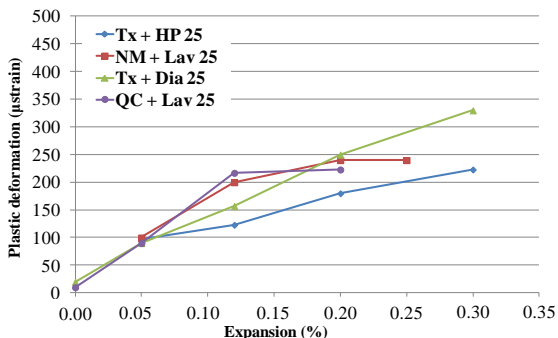
In this section, the SDT results are presented according to the procedure proposed by [4, 5], i.e. using a maximum loading level corresponding to 40% of the design (28-day) strengths. The latter are given in Table 8 of the supplementary materials section.

Figures 12A, C and E illustrate the SDT results in terms of hysteresis area (HA – J/m³) over the five cycles for all mixtures. Figures 12B, D and F present the results for the plastic deformation parameter (PD - μ strain) over the same cycles for the mixes studied.

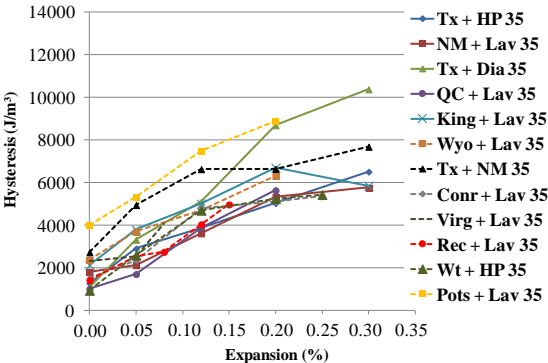
A – 25 MPa mixtures: HA (J/m³) vs. expansion



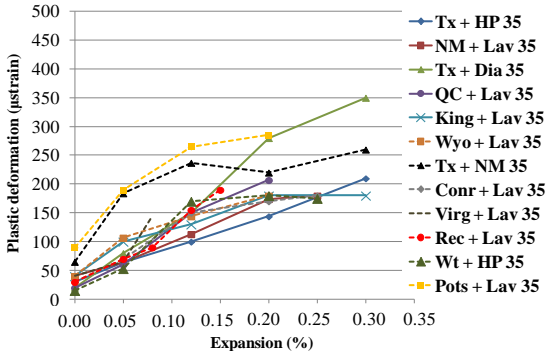
B – 25 MPa mixtures: PD (μ strain) vs. expansion



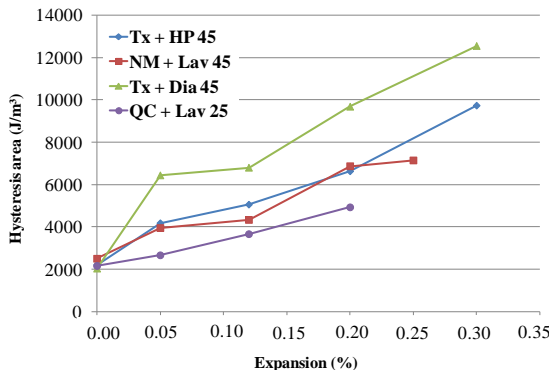
C – 35 MPa mixtures: HA (J/m³) vs. expansion



D – 35 MPa mixtures: PD (μ strain) vs. expansion



E – 45 MPa mixtures: HA (J/m³) vs. expansion



F – 45 MPa mixtures: PD (μ strain) vs. expansion

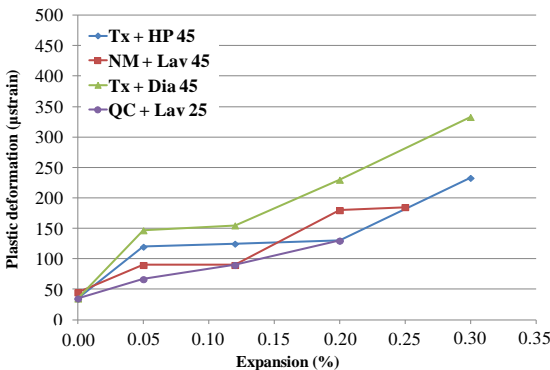


Figure 12: Hysteresis area (HA) and plastic deformation (PD) results, i.e. over the five cycles, for all the concrete mixtures used in this study: A, B) 25 MPa mixtures; C, D) 35 MPa mixtures; E, F) 45 MPa mixtures.

A strong increasing trend is observed for the HA parameter as a function of the expansion levels for all the concrete mixtures assessed, thus indicating that this parameter could well distinguish the different expansion levels chosen in this work. Moreover, the HA values were somewhat similar among the various concrete mixtures at the same expansion levels (ranging

from about 1000-2000 J/m³ for sound concretes up to 12000 J/m³ for 0.30% of expansion), although, for the majority of the mixes, increasing HA values were found with increasing concrete strengths for all expansion levels, as expected and discussed in [4].

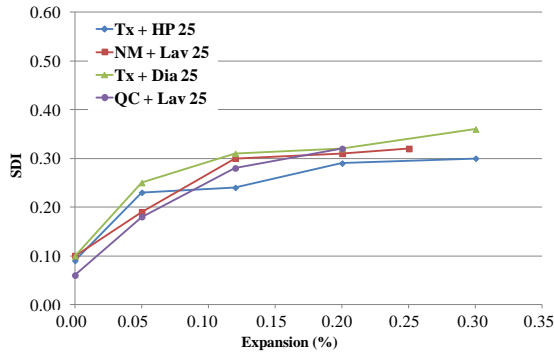
Once again, a strong increasing trend of PD values was observed against the expansion level of the concrete specimens, ranging from about 50 μ strains for sound concretes up to 350 μ strains for all the concrete types and different aggregates. Moreover, the PD values were also fairly similar between the various concrete mixtures at each expansion level. However, and differently from HA, the PD parameter does not seem to be affected by concrete strength.

10.6.2.2 SDT output values: indices

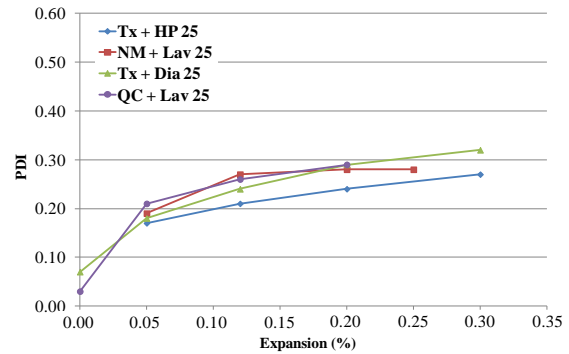
As mentioned before, Sanchez et al. [4] showed that the SDT needs to be carried out at 40% of the design (28-day) concrete strength to obtain diagnostic responses over the test. However, in most cases, when condition assessments are carried out on aging concrete structures, the 28-day strength of the concrete(s) used is unknown. Thus, the author suggested that the most practical approach would be to first determine the compressive strength on cores extracted from zones that are not/less damaged in the structural element under investigation. Then, stiffness damage testing could be carried out at 40% of that value for damage assessments. However, it has been found that this approach disables the use of both absolute HA and PD values because, depending on the loading level chosen for testing, a huge variability in the test responses can be obtained, thus leading to a misinterpretation of the damage degree in the concrete under investigation.

Based on the above discussion, Sanchez et al. [5] proposed to use the following two indices instead of absolute HA and PD values: SDI and PDI. The first index represents the dissipated energy (over the five compression cycles)/the total energy implemented in the system (area under the stress/strain curve), while the second corresponds to the plastic deformation (over the five compression cycles)/total deformation in the system. Figures 13A, 13C and 13E show that the SDI values distinguishes well the different expansion levels in the 25, 35 and 45 MPa mixtures, respectively.

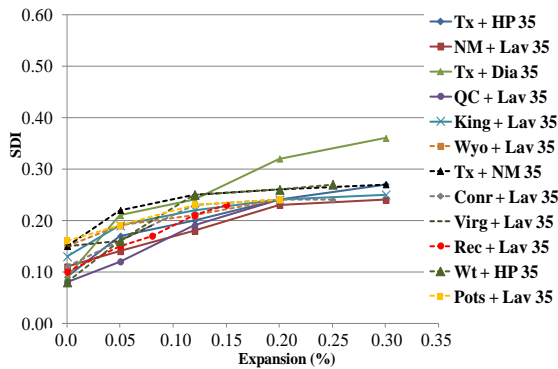
A – 25 MPa mixtures: SDI vs. expansion



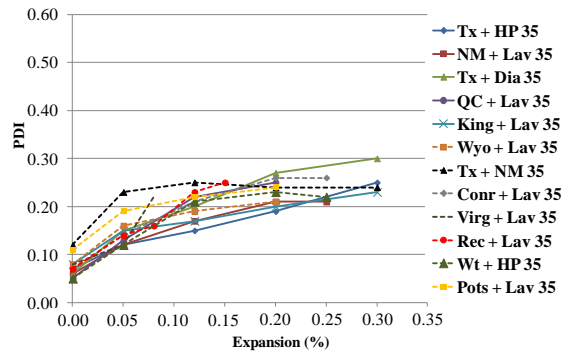
B – 25 MPa mixtures: PDI vs. expansion



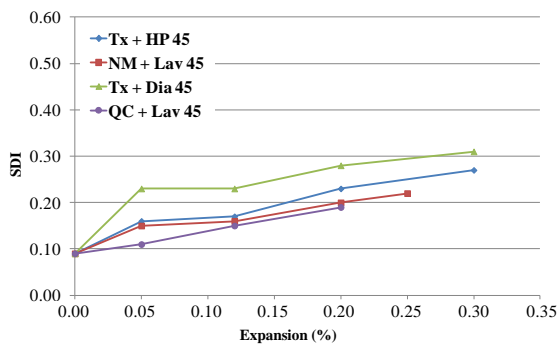
C – 35 MPa mixtures: SDI vs. expansion



D – 35 MPa mixtures: PDI vs. expansion



E – 45 MPa mixtures: SDI vs. expansion



F – 45 MPa mixtures: PDI vs. expansion

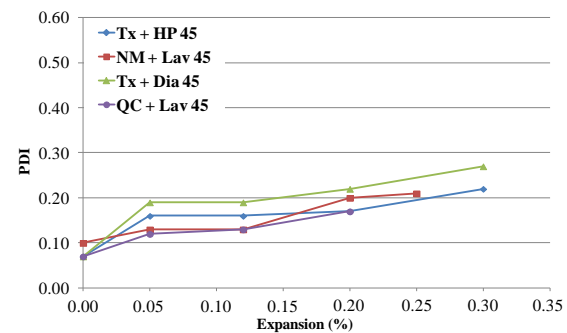


Figure 13: Stiffness damage indices for: A, B) 25 MPa mixtures; C, D) 35 MPa mixtures; E, F) 45 MPa mixtures.

In general, except for some 45 MPa mixtures, there is a concave trend of this index against the expansion level of the affected specimens, with values ranging from about 0.08 for sound concretes up to 0.35 for 0.30% of expansion. The PDI values distinguish similarly well the different expansion levels in all concrete mixtures investigated (Figures 13B, 13D and 13F, for the 25, 35 and 45 MPa mixtures, respectively), with values ranging from about 0.05 up to 0.30 for 0.30% of expansion. Again, except for some 45 MPa mixtures, the progress of this index is mostly characterized by a concave trend towards the expansion levels of the affected samples.

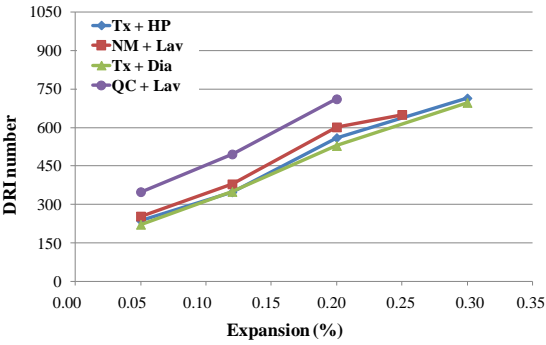
Further analyses of the SDT data were performed through the non linearity index (NLI - first cycle). The efficiency of this parameter for damage assessments in concretes affected by ASR had been highlighted by Crisp and coworkers [24, 25], and later confirmed by Sanchez et al. [4]; the NLI graphs are presented in Figure 22, in the supplementary materials' section of the paper. Similar to the SDI and PDI, the assessment of the ASR expansion level in concretes through the NLI parameter may be considered quite satisfactory, as this parameter was found to increase steadily with increasing expansion in all the concretes investigated. The NLI values ranged from about 1.05 for sound concretes up to 1.30 for 0.30% of expansion.

10.6.3 Damage Rating Index (DRI)

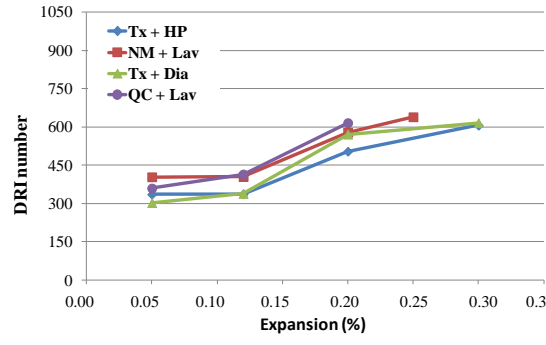
Figure 14 gives a plot of the DRI numbers as a function of the expansion levels of the concrete specimens. A full description of the development of microscopic AAR features of deterioration against the expansion level of the affected concrete specimens, both in a qualitative and a semi-quantitative way, is given in [6, 7].

The graphs in Figure 14 confirm that the DRI well distinguished the different AAR expansion levels in the 25, 35 and 45 MPa mixtures investigated. Actually, strong “envelopes of results” were generally observed, with the exception of the concrete mixtures incorporating the King alkali-carbonate reactive aggregate and Pots siliceous sandstone (35 MPa mixtures), which presented respectively much more and much less damage than the average range of the other mixes.

A – 25 MPa mixtures: DRI number vs. expansion



B – 45 MPa mixtures: DRI number vs. expansion



C – 35 MPa mixtures: DRI number vs. expansion

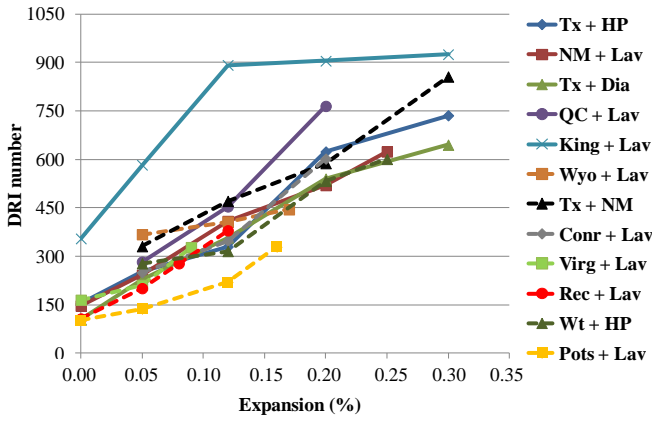


Figure 14: DRI number and crack density values for the different concrete strengths analyzed over the study: A) 25 MPa mixtures; B) 45 MPa mixtures; C) 35 MPa mixtures.

10.6.4 Mechanical properties reduction

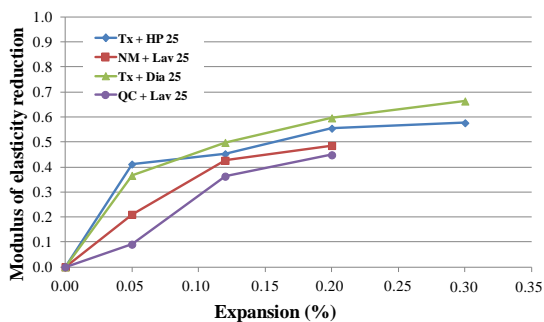
This section analyses the losses in modulus of elasticity, tensile strength and compressive strength of the various concretes investigated, as the ratio of values obtained at each selected expansion levels against the values obtained on concrete specimens of "equivalent maturity" but wrapped in plastic sheets at 12°C to prevent ASR expansion (see section 5.3.3). The modulus of elasticity corresponds to the average values obtained from the 2nd and 3rd cycles of stiffness damage testing, i.e. at each of the selected expansion levels and for the various mixtures used in this study. The compressive strengths were determined on the test specimens that were previously subjected to stiffness damage testing, while the tensile strengths were obtained on a separate set of test cylinders et each selected expansion levels.

10.6.4.1 Modulus of elasticity (ME)

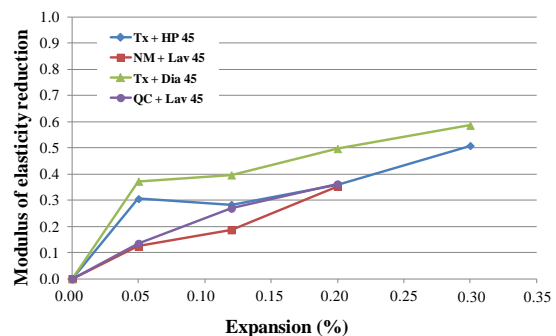
Figures 15A and 15B present the modulus of elasticity losses for the 25 MPa and 45 MPa mixes, respectively. Similar increasing trends of ME losses against expansion were found for both concrete types, although the 45 MPa concretes seem to present slightly lower losses than the 25 MPa mixtures for the same expansion level, mainly when ASR came from reactive coarse aggregates. Globally, for low expansion levels (i.e. 0.05%), a fairly wide range in ME losses (i.e. from 10% up to about 40%) was obtained between the different aggregate combinations tested. For higher expansion levels ($\geq 0.20\%$), the modulus of elasticity losses ranged from 40% up to $\approx 65\%$.

Similar trends can be observed for the 35 MPA concretes (Figure 15C), with ME losses ranging fairly widely both at low (5 – 30%) and high (40-65%) expansion levels. Moreover, even though the levels of modulus of elasticity losses varied from one aggregate to another, similar “reduction trends” were generally observed as a function of the expansion level of the various AAR-affected specimens.

A – 25 MPa mixtures: ME reduction vs. expansion



B – 45 MPa mixtures: ME reduction vs. expansion



C – 35 MPa mixtures: ME reduction vs. expansion

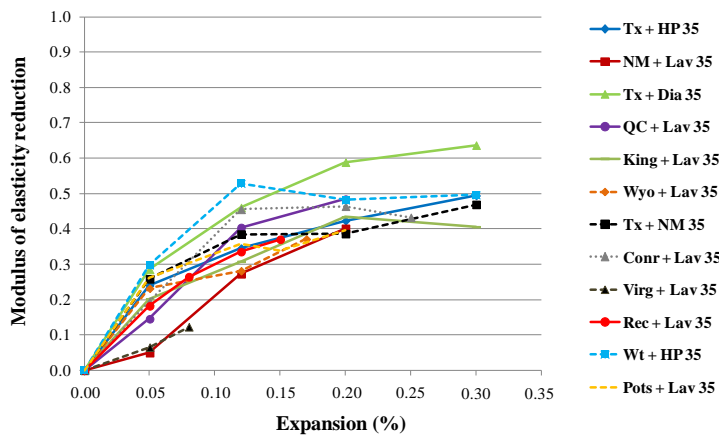


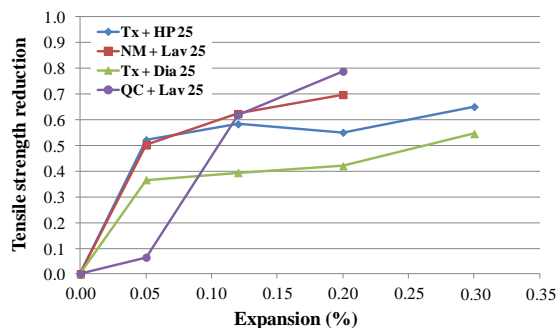
Figure 15: Modulus of elasticity (ME) reduction for: A) 25 MPa mixtures. B) 45 MPa mixtures. C) 35 MPa mixtures.

10.6.4.2 Tensile strength (TS)

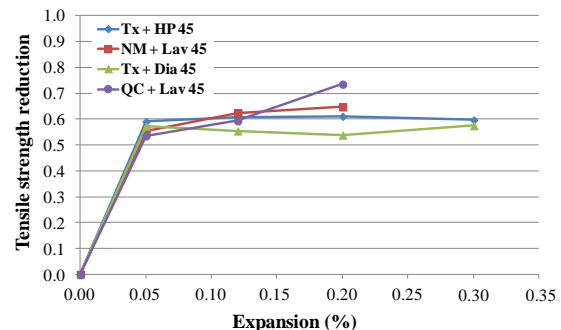
Figure 16 illustrates the tensile strength reductions for all the concrete mixtures investigated. In the case of the 25 MPa mixes, TS losses ranged from 5% to $\approx 55\%$ and from 40% to $\approx 80\%$ at low (i.e. 0.05%) and high expansion levels (0.20% and 0.30%), respectively (Figure 16A). The 45 MPa concretes however displayed a slightly different behavior (Figure 16B). All 45 MPa specimens indeed presented a similar and important loss in TS at the 0.05% expansion level, ranging from 55 up to 60%, without significant changes being obtained at higher levels of expansion (up to 0.30%).

The results for the 35 MPa concretes were most interesting, being intermediate between the behaviours of the 25 and the 45 MPa concretes. They were indeed characterized by a wide range in TS losses at the 0.05% expansion level (as for the 25 MPa mixtures). Furthermore, mixtures showing TS losses $\leq 30\%$ at 0.05% expansion actually showed continuing reductions at higher expansion levels (up to $\approx 70\%$). On the other hand, mixtures showing higher TS losses at low expansions (i.e. 40 to 70% TS reductions at 0.05%) generally did not result in significantly higher TS reductions with increasing expansion.

A – 25 MPa mixtures: TS reduction vs. expansion



B – 45 MPa mixtures: TS reduction vs. expansion



C – 35 MPa mixtures: TS reduction vs. expansion

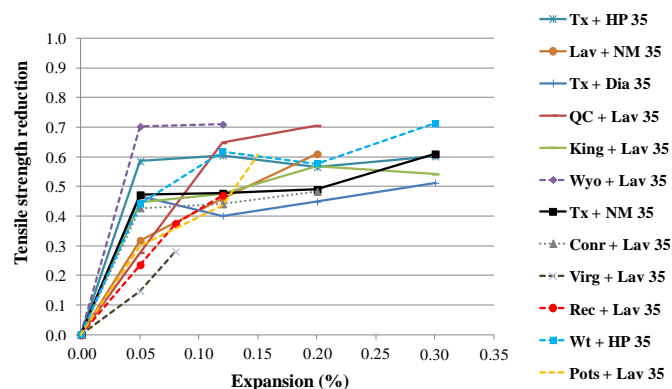
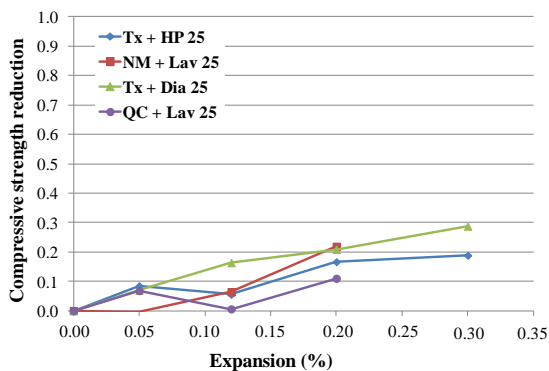


Figure 16: Tensile strength reduction for: A) 25 MPa mixtures; B) 45 MPa mixtures; C) 35 MPa mixtures.

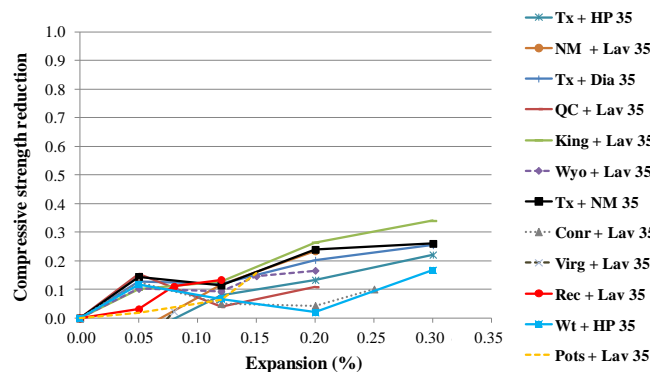
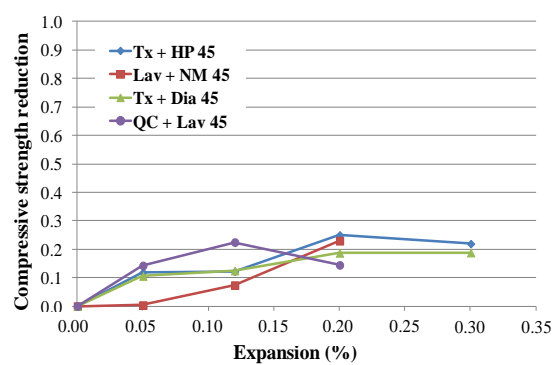
10.6.4.3 Compressive strength (CS)

Figure 17 illustrates the compressive strength reductions for all the concrete mixtures investigated. In general, CS was found to decrease in a somewhat modest way with increasing expansion. Despite some variations from one reactive aggregate combination to another, similar trends in CS reductions were obtained for the various mixtures investigated (25 to 45 MPa), with maximum CS losses reaching about 10% at 0.05% expansion, 10 to 20% at 0.12% expansion and 20 to 30% at expansions $\geq 0.20\%$ (Figures 17).

A – 25 MPa mixtures: CS reductions vs. expansion



B – 45 MPa mixtures: CS reductions vs. expansion



C – 35 MPa mixtures: CS reductions vs. expansion

Figure 17: Compressive strength reduction for: A) 25 MPa mixtures. B) 45 MPa mixtures. C) 35 MPa mixtures.

10.7 DISCUSSION AND OVERALL ASSESSMENT

The global data analysis presented in this section will be divided into four main topics. First of all, a discussion on the development of both AAR expansion and petrographic features of AAR distress is presented; second, coupling is made between the development of petrographic features of AAR distress and the mechanical properties losses of affected

materials; third, a damage global approach is discussed and proposed and; finally, a validation (statistical significance) of all the results obtained in this work is performed through an analysis of variance (ANOVA).

10.7.1 Development of AAR expansion and distress features in concrete

Interesting and singular behaviors are observed for the concrete mixtures incorporating just fine (Tx) or coarse (NM) highly reactive aggregates or even both reactive aggregates together (Figure 18), i.e. Tx sand + NM gravel and NM manufactured sand + NM gravel.

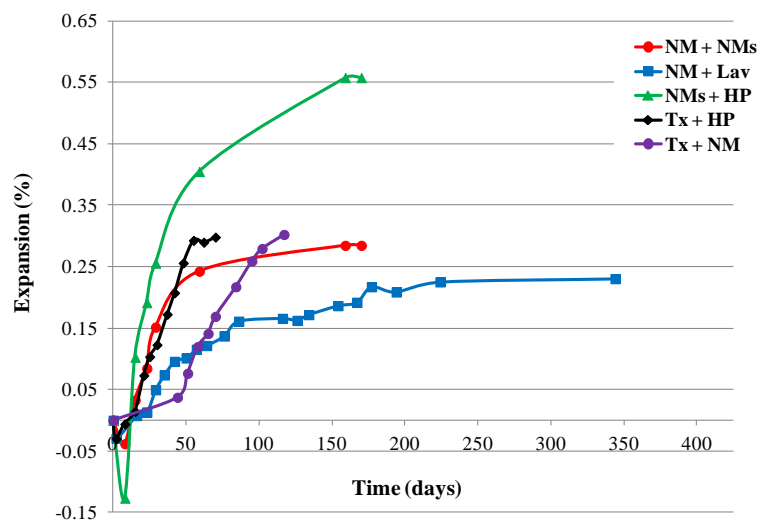


Figure 18: ASR kinetics for the 35 MPa concrete mixtures cast with either sand (Tx) or coarse (NM) reactive aggregates.

Regarding the above plot and considering Tx mixtures, one observes that the Tx + NM mix showed a slower reaction kinetics than the concrete mixture containing just Tx as reactive aggregate (i.e. Tx + HP). This suggests that a “competition” develops between both highly reactive aggregate (fine Tx vs. coarse NM) and, although the system presents a greater amount of available silica, this competition strongly impacts on AAR reaction kinetics for the same amount of available alkalis (or cement content), thus resulting in a “pessimun effect” of the expansion obtained in the test specimens.

Considering NM mixtures, one notices that the smaller the reactive aggregate particle size, the larger and faster was ASR expansion. Therefore, NMs + HP (i.e. NM as a manufactured sand) showed the fastest expansion kinetics and magnitude followed by NMs + NM and NM + Lav (NM as a coarse aggregate). Moreover, when NM was used as both coarse and fine aggregates, the results were in between those obtained when NM was used just as a manufactured sand or coarse aggregate, showing, as for Tx mixtures, the likely presence of a

“competition” between ASR coming from the fine and coarse aggregate particles thus resulting in a “pessimun effect” of the expansion. Overall, the differences in ASR kinetics and magnitude between reactive coarse and fine aggregates could thus likely be explained by the following two phenomena:

- *Aggregates crushing*: The aggregates’ crushing plays a significant role on ASR expansion. This procedure “generally” increases their reactivity by increasing the specific surface of the reactive aggregate minerals;
- *Concrete alkali leaching*: It is clear that alkali leaching from concrete test specimens can decrease ASR expansion over the concrete prism test [45-48]. This leaching effect could partially explain why coarse aggregates presented less expansion than fine aggregates, as the available alkalis take more time to reach and react with the reactive silica inside the coarse aggregate particles and thus an important amount of alkalis can be leached due to diffusion effects outside the concrete specimens. Otherwise, this phenomenon is less seen for smaller particles since the reactive silica is reached faster and ASR gel is formed before alkali leaching takes place in a significant manner.

Regarding the effects of concrete strength on AAR kinetics, it is interesting to note, when comparing the various graphs in Figure 11, that no significant differences were observed in the AAR kinetics for the range of strengths used in this project (from 25 up to 45 MPa, reactive aggregates NM and Tx). Those results are interesting but somewhat surprising. The total alkali content in the concretes ranged from 3.9 (25 MPa) to 5.3 (45 MPa) kg/m³, which could have induced some differences in the reaction kinetics and/or the magnitude of expansion; however, the various mixes were designed with the same volume of aggregates and pastes and the water-to-cement ratio varied from 0.37 to 0.61. This suggests that not only the total concrete alkali content but also the concrete mix characteristics impact on the reaction/expansion kinetics. Further work is required to evaluate the combined effects of the above parameters on ASR expansion, especially on the potential effects of the above mixture characteristics on the alkali hydroxides concentration in the pore solution, the composition and diffusion potential of alkali-silica gel, etc.

Considering the development of AAR distress features in the concrete specimens, it is important to mention that the *AAR expansion level* reached in an affected concrete specimen is not necessarily a direct measure of the *degree of damage* attained by the AAR-distressed concrete material. Expansion is indeed a feature commonly used and easily measured in laboratory investigations to evaluate/classify the potential alkali-reactivity of concrete aggregates and can allow comparing, at specific/ selected levels, the presence/development of

different features of deterioration in concrete. Interestingly, the various graphs in Figure 14 however show that the DRI values generally increase steadily and fairly similarly, with only a few exceptions, with increasing expansion in the various concrete mixtures investigated. Sanchez et al. [4] showed that this good correlation actually results from a strong increasing trend in the development of *Opened cracks (with and without reaction products)* both in the reactive aggregate particles (first) and in the cement paste (resulting from the reaction/expansion within the reactive aggregate particles) as a function of increasing expansion in the concrete specimens investigated. Moreover, Sanchez et al. [4] showed that a fair proportion of the opened cracks in the aggregate particles actually results from the presence of a large number of *Closed cracks* within the coarse aggregate particles, most likely created, in good part, through aggregate processing operations or weathering; such cracks are then used by the pore solution as “fast track” zones to access the inner parts of the particles, thus generating alkali-silica reaction products that induce excessive internal expansion forces and cracking extending into the cement paste with increasing expansion.

10.7.2 Micromechanical coupling

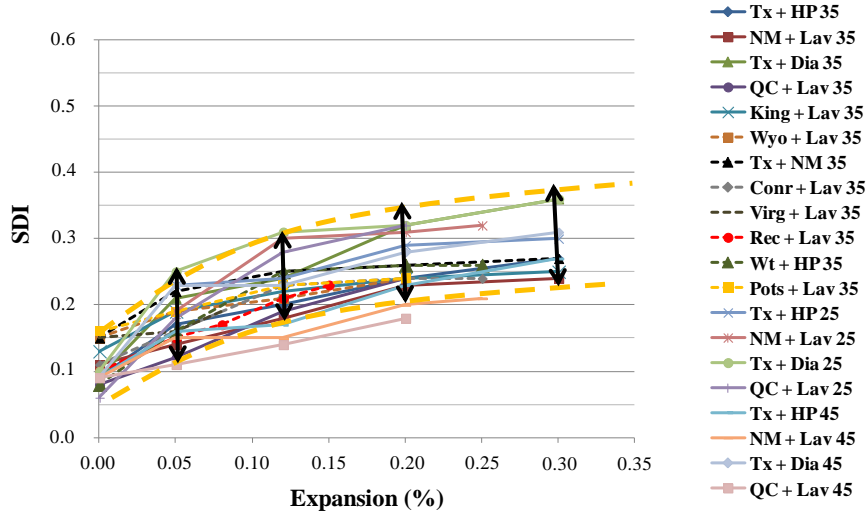
10.7.2.1 Understanding and measuring AAR distress in concrete as a function of increasing expansion

As stated by Sanchez et al. [6, 7], the use of an "extended" DRI determination, using the semi-quantitative petrographic number in combination with complementary observations, such as the measurements of the cracks' length and density and the complete analysis of the counts of distress features, can reliably assess the development and progress of distress in concrete due to AAR. Moreover, this tool confirmed its efficiency for analyzing the condition in concretes of different strengths (25, 35 and 45 MPa) and incorporating various aggregate types (i.e. fine vs. coarse aggregates) and nature (i.e. ≠ lithotypes).

Based on the analysis of the data from the "extended DRI determination" mentioned above and of the development of ASR cracking within individual reactive aggregate particles of different types, Sanchez et al. [6, 7] suggested that the development of ASR cracking within concrete incorporating “quartz-bearing” reactive aggregates (e.g. greywacke, siliceous limestone, gneiss, schist, argillite, etc.) can likely be explained by the following two-step process: a), the formation of "new" cracks within the reactive aggregate particles in the early stages of the chemical reaction (including ASR “activation” of (pre-existing) closed cracks

formed through aggregate processing operations), and b), the extension of the above cracks into the cement paste to form a cracking network with increasing expansion. Following the minimum energy law, it would indeed be easier for the expanding system to propagate the cracks produced through step (a) described above, instead of creating a significant number of new cracks. In other words, new cracks will always be generated as the alkali reaction keeps developing, but the amount of “new” cracks will be overcome by the increase in length and width of the cracks already formed, thus making the counts of distress features to keep increasing, but at a lower rate, with increasing expansion in the system. This proposed mechanism is supported by the analysis of the *Stiffness Damage Index* (SDI) and *Plastic deformation Index* (PDI) indices described in section 6.2.2. Figure 19 illustrates the progress of the above indices as a function of expansion in all concrete specimens investigated in this study. One notices that, on an average, the SDI generally displays an increasing trend with increasing expansion in all test specimens (i.e. a similar trend for concretes of different strengths (25, 35 and 45 MPa) and incorporating various aggregate types (i.e. fine vs. coarse aggregates) and nature (i.e. \neq lithotypes)), which typically tends to level off at higher expansion levels (Figure 19A). This suggests, as confirmed by petrographic analysis (carried out at the magnification used for DRI determination), that a fair amount of “new” ASR cracking is formed at low/moderate levels of expansion (e.g. 0.05 – 0.12%), mostly inside the aggregate particles, thus resulting in significant energy spent in the system (i.e. resulting in steadily increasing SDI and PDI values) to close those cracks. As the expansion progresses (0.20% or greater), the development of new cracks within the aggregate particles stabilizes or increases at a lower rate (at least cracks visible at the magnification used for DRI determination), while existing cracks extend into the cement paste to form a network connecting cracks progressing through reactive aggregate particles with each other. Those cracks also increase in length and width and become filled by significant amounts of alkali-silica reaction products with progressive expansion. This phenomenon would result in the increasing trend of the SDI to progressively level off, since the energy required for closing cracks at a given damage degree is proportional to the *cracks’ number \times the cracks’ width* of an affected concrete specimen, and is also reduced by the presence of increasing amounts of gel in those cracks, thus showing a concave tendency “SDI vs. expansion level” and agreeing with the microscopic results. The same behavior is also seen for the PDI parameter (Figure 19B).

A – SDI vs. Expansion



B – PDI vs. Expansion

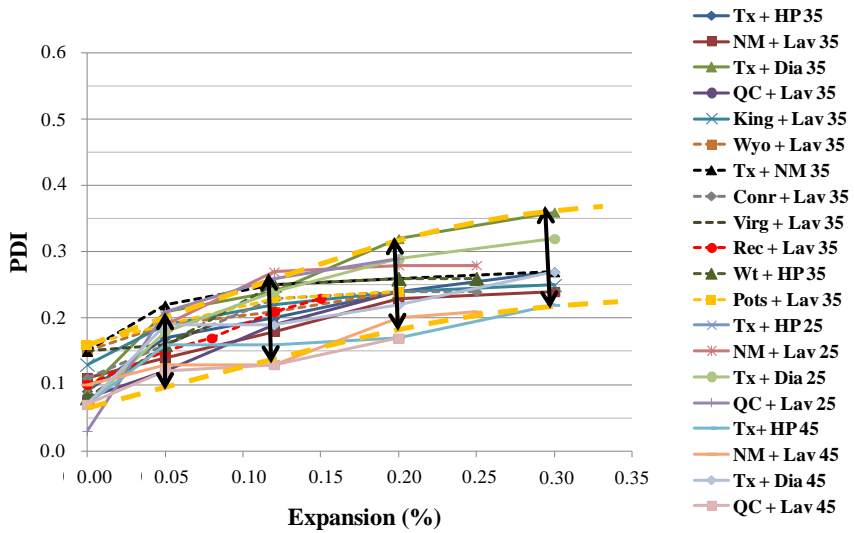


Figure 19: SDT envelopes using, as output parameters, the indices proposed in this project: A) SDI and; B) PDI.

10.7.2.2 Understanding how the development of AAR features of deterioration influence the mechanical properties of concretes

The extensive testing carried out in this study allowed to observe, despite some variability related to the materials characteristics (concrete strengths, aggregate types and natures (fine and coarse aggregates), etc.), a strong correlation between the development of microscopic features of deterioration (visible on polished concrete sections at 15-16x magnification under the stereomicroscope – described in details by Sanchez [6, 7]) and changes in the mechanical properties of the concrete specimens as a function of expansion due to ASR; this is illustrated in Figure 20 and summarized in Table 4 as a classification of damage degree in concrete due

to ASR. The next few subsections present a global analysis of test data obtained in this study on concretes of different strengths and incorporating a range of alkali-reactive quartz-bearing rocks (category 2 of reactive rock types according to the Appendix B of CSA A23.1-2009); these would somewhat correspond to the reaction model proposed by Dunant & Scrivener [49], as a review of the microstructural condition and resulting mechanical properties of concrete with progressive expansion due to ASR. The results obtained in this study suggests that the "scenario" described hereafter could apply to a conventional concretes (25 to 45 MPa) incorporating reactive quartz-bearing coarse aggregates as well as some reactive sands.

It is important to keep in mind that the coupling presented hereafter, i.e. between the development of physical distress features of ASR (e.g. cracking) and the resulting impact on the mechanical performance of the concrete, is based on test data obtained on aging concrete materials (different concrete mix designs and a variety of reactive rock types and forms) in a "free and accelerated expansion environment". Although such an approach allowed a valid comparative performance analysis considering the strict conditions under which the specimens were cured and tested, one should realize that the features described and the resulting analyses/conclusions would not necessarily apply directly to the condition assessment of concrete cores extracted from ASR-affected structural concrete members in service, which are largely influenced by the presence of different stress fields (bi/triaxial stresses, restraints, etc.). It is believed, however, that the analyses presented hereafter could serve as a reference (and perhaps as worst case scenario) in the process of quantifying the progress of damage in concrete undergoing deleterious expansion due to ASR in the field.

Table 4: Classification of the damage degree in concrete due to ASR

Classification of ASR damage degree (%)	Reference expansion level (%) ¹	Assessment of ASR				
		Stiffness reduction (%)	Compressive strength reduction (%)	Tensile strength reduction (%)	SDI	DRI
Negligible	0.00 – 0.03	-	-	-	0.06 – 0.16	100 - 155
Marginal	0.04 ± 0.01	5 – 37	(-)10 – 15	15 – 60	0.11 – 0.25	210 - 400
Moderate	0.11 ± 0.01	20 – 50	0 – 20	40 – 65	0.15 – 0.31	330 - 500
High	0.20 ± 0.01	35 – 60	13 – 25	45 – 80	0.19 – 0.32	500 - 765
Very high	0.30 ± 0.01	40 – 67	20 – 35		0.22 – 0.36	600 – 925

¹ These levels of expansion should not be considered as strict limits between the various classes of damage degree but more as indicators/reference levels for which comparative analysis of petrographic and mechanical data was carried out allowing to highlight significant damage levels in concrete due to the progress of ASR.

Negligible damage (< 0.03%)

The “control” concrete specimens that were examined in this study showed "negligible" to very low levels of expansion, i.e. ranging from 0.00% up to about 0.03%. The petrographic examination of such concrete specimens identified the presence, as the main features of "deterioration", of *Closed cracks within the aggregate particles*, likely originating from aggregate processing operations, as well as initiation of some ASR-related cracking. Very limited (traces), localized microcracks were observed in the cement paste, mostly unrelated to aggregate's cracking and possibly resulting from various phenomena such as shrinkage, improper/excessive consolidation, etc. Overall, those specimens had DRIs ranging from 100 to 155. The stiffness damage index (SDI) obtained from those specimens ranged from 0.06 to 0.16 (Table 4).

Marginal expansion due to ASR (e.g. 0.03 – 0.05%)

In the beginning of “significant” ASR development, which correspond to the marginal/low expansion levels (between 0.03% and about 0.05%) or the *inception period* mentioned by some authors, the major distress features correspond to the development of opened cracks due to ASR within some of the reactive aggregate particles, thus resulting in a strong increase of both the SDI parameter and the DRI number (Table 4). This distress feature, which has in good part developed from pre-existing closed cracks, likely results in a significant drop in the “stiffness” of the reactive aggregate particles and, moreover, of the stiffness of the concrete material as a whole. Mindess et al. [50] indeed suggested that, for ordinary concretes, the modulus of elasticity is largely governed by the modulus of elasticity (ME) of the coarse aggregate. Therefore, this phenomenon is likely responsible for the rapid and significant drop in modulus of elasticity (reaching up to about 40%, depending on the reactive rock type) of the ASR-affected concretes observed at low expansion levels (Figure 20A; Table 4). It is important to mention that no significant microcracking, at least visible at the magnification used for the DRI (about 15x), was observed in the cement paste of the various concrete specimens examined at that level of expansion; however, it is likely that cracking has developed at the submicroscopic level in the immediate vicinity of some reacting aggregate particles, thus contributing to the drop in ME observed already at low expansion levels. Moreover, the above distress features also tend to affect significantly the tensile strength of

the affected materials at this stage of ASR expansion/reaction process, with reductions ranging from about 15 to 60% being observed, depending on the reactive rock type (Table 4); the concrete fracture mechanism in tension is indeed a direct and brittle mechanism caused by the “stress concentration” in the presence of micro defects/pores, which are generated/enhanced by ASR, although the features of deterioration at this reaction step appear to largely remain within the aggregate particles (Figure 20B). On the other hand, the development of such cracking within the aggregate particles does not seem to affect significantly the compressive strength of the concretes (-10 to 15%, depending on the reactive rock type), which failure mode is more progressive by nature (Figure 20C; Table 4).

It is interesting to mention that Sanchez et al. [6] showed that 45 MPA concretes incorporating a highly reactive sand (Tx) or a highly reactive gravel (NM) both showed higher internal damage (DRI values) at this low expansion level than 25 and 35 MPA concretes incorporating the same aggregates (Figure 14B). The difference was related to the larger frequency of both closed and opened cracks within the reactive aggregate particles, with or without reaction products. This resulted in slightly higher Hysteresis area and lower Modulus of Elasticity values for the 45 MPa concretes at that expansion level; however, the difference was not apparent using the SDI parameter (See Figure 13).

Moderate expansion due to ASR (e.g. about 0.10 – 0.12%)

When the expansion progresses to moderate levels ($\approx 0.12\%$), the number/proportion of “Opened cracks within the aggregate particles”, with and without reaction products, keep increasing and some “new cracks” are generated; however, the main feature characterizing this second stage of the ASR reaction/expansion process is that some of the above cracks actually extend into the cement paste, affecting both the bulk cement paste in the close vicinity of the aggregate particles (with still a limited extent at this stage) and some areas of the interfacial transition zone (ITZ). This results in significant increase in the SDI (about 0.15-0.31) and DRI (about 330 – 500) values, which likely explains why the affected material’s “stiffness” keeps dropping (20 to 50% reduction in modulus of elasticity depending on the reactive rock type), but at a slightly lower rate, as the stiffness’ loss is relatively more important when the aggregates are damaged than the cement paste itself (Figure 20A; Table 4). At such moderate expansion levels, the tensile strength attained its largest reduction for the vast majority of the concrete mixtures (40 to 65% depending on the reactive rock type) (Figure 20B; Table 4). This suggests that some cracks have already reached their critical

lengths at this expansion level, thus causing unstable crack growth in the system that would lead to the full concrete fracture in tension with the application of higher stress level. Since some cracks formed within the aggregate particles reach the cement paste at this stage, the fracture in tension is likely facilitated in the affected concrete specimens. In terms of compressive strength loss, moderate reductions are found at this stage (0 to 20% depending on the reactive rock type), as some cracks reach the cement paste, likely damaging the bulk paste itself and the ITZ. Therefore, when concretes in that condition are loaded in compression, some ASR cracks that are near the ITZ could be used as “fast tracks” to initiate and propagate fracture, as they are even less stiff than the ITZ itself (Figure 20C). The compressive strength loss at this expansion level might still be acceptable from a structural reliability point of view.

Regarding the effect of the concrete mix design on damage development at this stage, similar behaviors were once again observed for 25 and 35 MPa concretes, with the progress of damage described above resulting in a steady increase in SDI and DRI values against increasing ASR expansion; on the other hand, the development of damage progressed only slightly between 0.05 and 0.12% expansion in the case of the 45 MPa concretes (Sanchez et al. [4, 6]) (Figures 13 and 14).

High expansion due to ASR (e.g. about 0.20%)

For high expansion levels (about 0.20%), the generation of “new” cracks within the aggregate particles and the cement paste seems to be overcome by an increase in length and width of the existing cracks. Also, at this stage, the vast majority of the cracks generated within the aggregate particles reach the cement paste where they link into a dense network of cracking, resulting in continuing increase in DRI values (500-765; Table 4). The modulus of elasticity of the majority of the affected concrete mixtures keeps dropping, reaching 35 to about 60% loss depending on the reactive rock type; however, the reduction rate slowed down significantly and even levelled off for some concretes between 0.12 and 0.20% (Figure 20A; Table 4). This suggests that the extension into a cracking network within the concrete matrix observed at high expansion levels (0.20 – 0.30%) does not result in an increased rate of stiffness loss of the concrete, which is also highlighted by stabilized SDI values (0.19-0.32), Table 4), perhaps partly due to the increasing presence of alkali-silica reaction products in those cracks. Likewise, this cracking extension process does not seem to affect further the tensile strength of the concrete since these cracks have already reached their *critical length* to

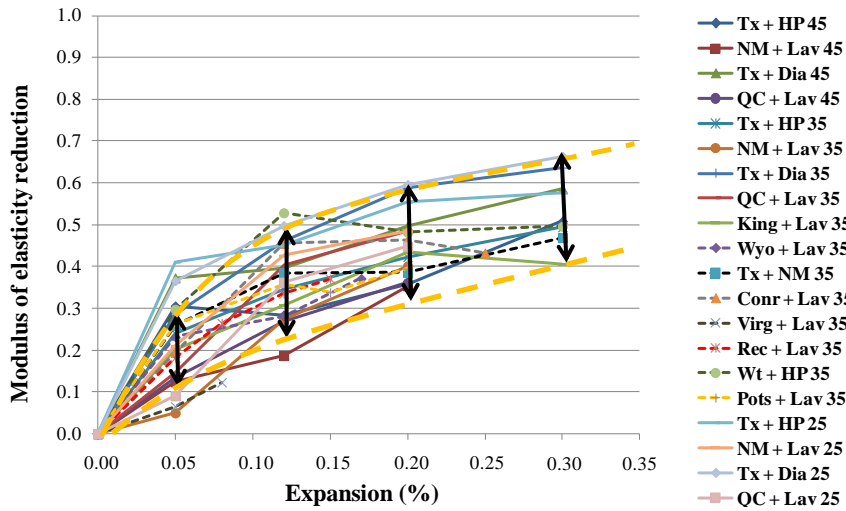
cause tensile failure at the moderate levels of expansion for all concrete mixtures studied, at least determined through the test procedure used in this project – gas pressure test (Figure 20B). On the other hand, a continuing/progressive loss in compressive strength, now ranging from 10 to 35%, is observed at this expansion stage in the affected concretes (Figure 20C). As the mechanism of fracture in compression is more ductile than the mechanism in tension, the development of cracking networks creates instability in the system, thus resulting in progressive losses in compressive strength. This assumption agrees with the work of Kubo and Nakata [12], where important compressive strength losses were found only for concretes damaged due to ASR at expansion levels $\geq 0.30\%$.

It might be interesting to mention that expansion levels of about 0.20% could lead to the “steel yielding”, whether one considers that the concrete/steel bonding would not suffer at such expansion, phenomenon already found on several stirrups used for shear reinforcement in bridge columns in Japan [51]. Also, such a cracking network could significantly impact on the performance in durability of the affected material (e.g. risk of steel corrosion, freezing and thawing distress, chloride/sulfate ions penetration, carbonation, etc.).

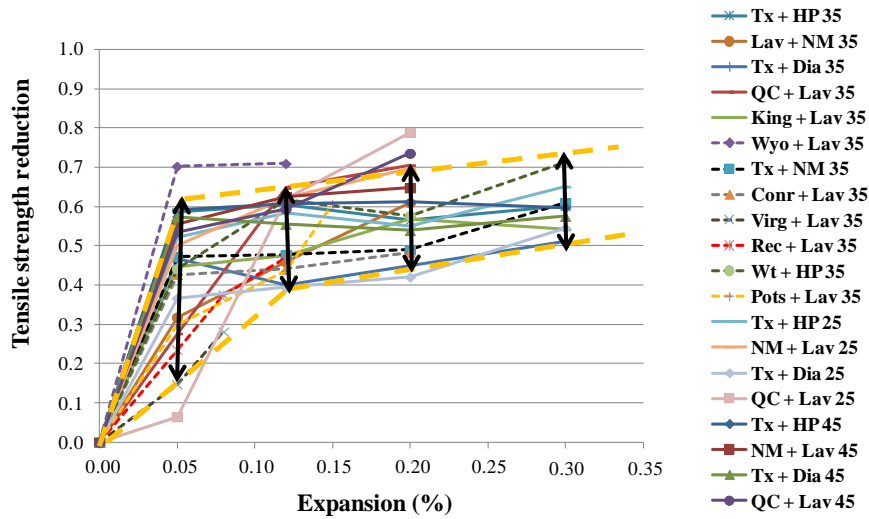
Very high expansion due to ASR (e.g. $\approx 0.30\%$; this is the maximum expansion level investigated in this study)

At this expansion level, extensive cracking is found into the cement paste with cracks largely connecting reactive aggregate particles with one another. Consequently, DRI values kept increasing up to this level, mainly from the spreading of cracking into the cement paste and the aggregate particles. Losses in modulus of elasticity and tensile strength have largely leveled off, reaching values of about 70% and 80%, respectively. On the other hand, compressive strength losses continue to progress with losses of 35% or greater being observed. Therefore, from this expansion level, ASR cannot be considered anymore “only” a serviceability/durability related problem since the loss in the mechanical properties of the affected materials reach important values at this reaction point, which might possibly induce structural capacity concerns, mainly when the distress of concrete elements with poor reinforcement and/or unsuitable detailing. However, the results presented here possibly represent the “worst scenario”, since they were obtained from specimens undergoing a free expansion process that could probably not represent the behavior of ASR-affected concrete elements in the field that are under biaxial/triaxial states of stresses/restraints.

A – Modulus of elasticity



B – Tensile strength



C – Compressive strength

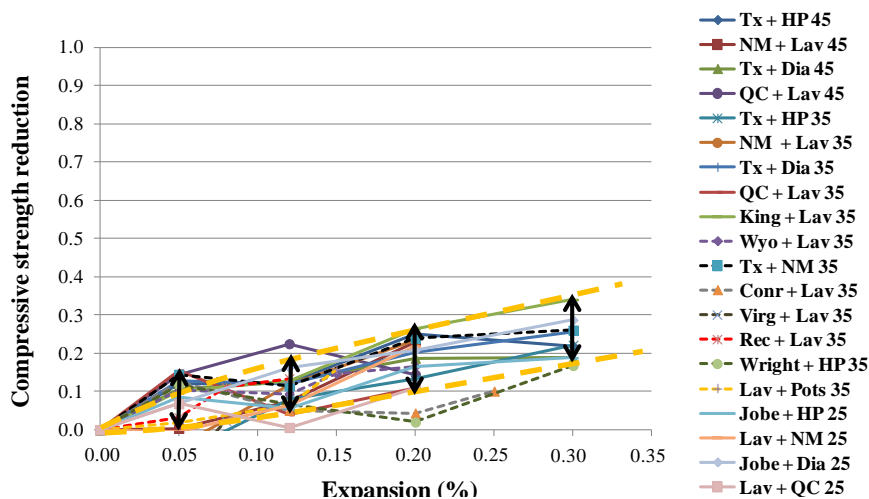


Figure 20: Mechanical properties losses (i.e. compared to a sound concrete presenting the same maturity) as a function of concrete expansions: A) Modulus of elasticity; B) Tensile strength and; C) Compressive strength.

Globally, the above data indicate that both compressive strength and tensile strength measurements show limited usefulness for assessing the “state of AAR development”, at least up to the 0.30% expansion level used in this study. Therefore, both procedures should be essentially used for the “determination of concrete properties” at a given time of analysis as their capacity for quantifying the extent of ASR-related damage is limited (and sometime misleading) considering their progress as a function of expansion. However, the ME parameter showed to have the potential for assessing both the AAR development and the stiffness reduction as a function of the AAR expansion levels.

In addition, it is interesting to mention that the phenomena observed on AAR affected concretes (mainly for the modulus of elasticity, tensile strength and SDI parameters) seems similar to the fracture/failure behavior usually found for “sound” concrete specimens subjected to compression/tension cycles (and fatigue), where the formation/progression of “new cracks” is rapidly generated in the beginning of the “cyclic effects” up to a point after which a level off trend takes place. This last behavior happens due to the “balance” between the cracks formation/propagation and the “stabilization mechanism” provided by the aggregate particles present in the concrete matrix, which tends to redistribute uniformly the stresses in the bulk cement paste. Finally, if the effects/distresses keep increasing, the energy spent in the system eventually extends some of the cracks generated, leading to the material’s failure [52].

10.7.3 Global analysis and definition of AAR damage degrees

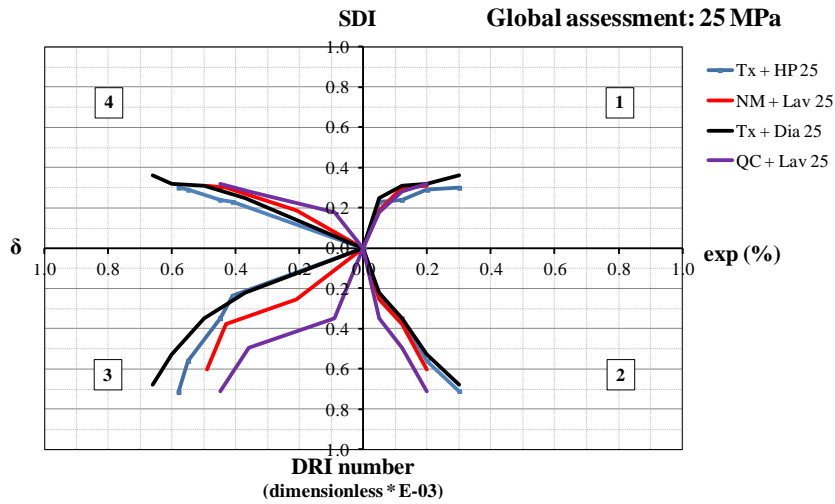
As part of this study, the reliability of various tools for the damage assessment in concretes incorporating various types of alkali-reactive aggregates was investigated. Ideally, such tools should take into account the progress of the physical effect of this deleterious mechanism on the concrete material’s properties through the quantification of damage features, such as cracking at the micro and macro levels in the affected materials, with the resulting impact these features may have on either the stiffness or the mechanical properties (compressive and tensile strengths) of the materials affected. The extensive testing carried out in this study on concretes of different strengths (25, 35 and 45 MPa) and incorporating various aggregate types (i.e. fine vs. coarse aggregates) and nature (i.e. \neq lithotypes) showed that the Damage Rating Index (DRI) and the Stiffness Damage Test (SDT) can indeed reliably assess condition in aging concrete affected by ASR through a selected number of critical output parameters.

Moreover, the link between the micromechanical tools can thus facilitate the understanding of the global ASR distress process.

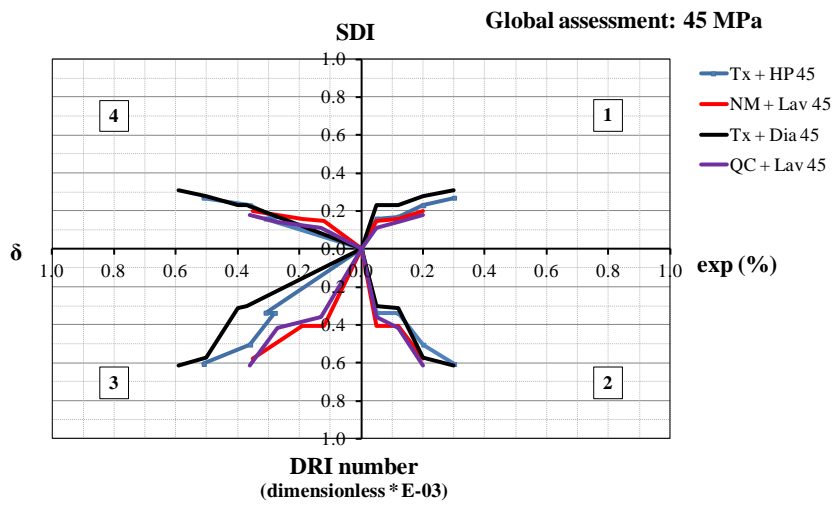
In this work, a four-quadrant chart is proposed (Figure 21), which correlates the expansion attained by AAR-affected specimens (right wing x-axis) with the micromechanical data derived from both stiffness damage testing and semi-quantitative petrographic examinations. In addition to the expansion, the variables presented in this graph are the following: a) the SDI parameter, which are indicative of the extent of internal cracking in the overall concrete material (top y-axis); b) DRI number (divided by 1000), which assesses the microscopic damage degree in the AAR affected concrete (bottom y-axis) and; c) the damage variable “ δ ”, which represents in this case the modulus of elasticity reduction of damaged/aging concretes (left wing x-axis).

The below figures show strong correlations between the micro mechanical and microstructural data obtained for all the concrete mixtures (i.e. \neq strengths and aggregate types/natures) investigated in this study. Similar “damage patterns”, which are represented by the presence of “strong data envelopes”, were indeed found in each of the four quadrants forming those graphs. Exceptions are found for two mixtures discussed previously: King + Lav and Pots + Lav. Interestingly, the latter showed similar mechanical trends than the other alkali-silica reactive aggregates, but located just outside of the data grouping in two out of four quadrants, likely due to differences found on the DRI analysis. The identification of cracks in the Pots reactive aggregate particles was particularly a challenge considering the petrographic characteristics of that medium-grained siliceous sandstone, which might have distorted the results achieved in the DRI. Actually, under accelerated testing conditions in the laboratory, the siliceous cement binding the well-rounded quartz grains of the sandstone tends to dissolve readily under the effect of the concrete pore solution, which results in the disaggregation of the reactive particles, thus masking the presence of cracks within these particles and lower DRI values against increasing expansion. In the case of the alkali-carbonate reactive King aggregate, which is susceptible to alkali-carbonate reaction (ACR) in concrete, largely different microscopic features of deterioration characterized by large amount of cracking within the cement paste and somewhat limited cracking in the aggregate particles were obtained, resulting in greater DRI values against increasing expansion than typical alkali-silica reactive aggregates. This reaction still needs to be further studied in terms of either chemical or distress development.

A



B



C

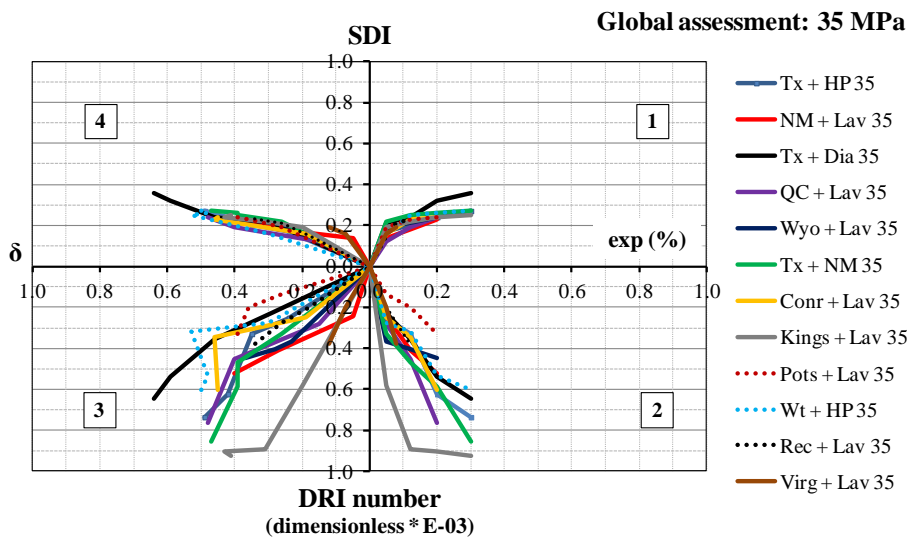


Figure 21: Global analysis charts for: A) 25 MPa mixtures. B) 45 MPa mixtures. C) 35 MPa mixtures. δ is the module of elasticity reduction, calculated as the module of a distressed concrete at a given time (E_i), divided by the module of a “sound” concrete with the same mix design and maturity (E_0).

Finally, considering the plots results, strong correlations can generally be observed in quadrants 1 (SDI vs. expansion), 2 (Exp vs. DRI) and 4 (δ vs. SDI). More scatter in the data is obtained in the Quadrant 3 (d vs. DRI); this might be related to the fact that the attribution of the weighing factors used in the DRI calculations is likely not be optimized to result in the best possible correlation with the stiffness loss in the concrete material.

10.7.4 Data analysis of variance (ANOVA)

10.7.4.1 Significance of concrete properties' changes as a function of AAR development

In order to assess the statistical validity and significance of the database generated as part of this study, analyses of variance (two-variable ANOVA), taking into account both the individual specimens and the various concrete mixtures, were carried out.

First, two-variable ANOVA was performed on the SDT results obtained through the 35 MPa mixtures' analysis, in order to verify the significance of the test output parameters (with a significant level of 5%) as a function of AAR development. The results indicated that the two indices proposed in this work (SDI and PDI) are statistically significant for all the concrete mixtures, aggregate types/natures and expansion levels studied, as all the "F values" were greater than the "F_{critic}" and the "p values" were less than 0.05 for each case (Table 5). Therefore, both indices are able to provide "diagnostic" assessment of AAR distress in concrete. It is important to mention that the same analysis for the 25 and 45 MPa mixtures was already performed and fully presented in Sanchez et al. [4].

Table 5: Two-variable ANOVA on the SDT results for the 35 MPa concrete mixtures incorporating different aggregate types/natures.

ANOVA analysis				SDI						PDI					
Aggregate type	Strength (MPa)	Load (%)	Expansion (%)	SDL_F	SDI_Fcritic	F>Fcritic	SDI_P value	α	P< α	PDI_F	PDI_Fcritic	F>Fcritic	PDI_P value	α	P< α
Tx + HP	35	40	0.05% - 0.30%	98.43	4.75	X	0.00002	0.05	X	21.88	4.75	X	0.00124	0.05	X
NM + Lav	35	40	0.05% - 0.25%	20.53	4.75	X	0.00148	0.05	X	10.04	4.75	X	0.00936	0.05	X
Tx + Dia	35	40	0.05% - 0.30%	122.37	4.75	X	0.00001	0.05	X	187.67	4.75	X	0.00000	0.05	X
QC + Lav	35	40	0.05% - 0.20%	9.68	6.94	X	0.02928	0.05	X	35.60	6.94	X	0.00283	0.05	X
Wyo + Lav	35	40	0.05% - 0.20%	7.96	6.94	X	0.04026	0.05	X	14.00	6.94	X	0.01563	0.05	X
Tx + NM	35	40	0.05% - 0.30%	6.89	4.75	X	0.02269	0.05	X	273.00	4.75	X	0.00000	0.05	X
Conr + Lav	35	40	0.05% - 0.25%	140.00	4.75	X	0.00001	0.05	X	436.75	4.75	X	0.00002	0.05	X
King + Lav	35	40	0.05% - 0.30%	12.66	4.75	X	0.00526	0.05	X	32.97	4.75	X	0.00040	0.05	X
Pots + Lav	35	40	0.05% - 0.20%	9.50	6.94	X	0.03025	0.05	X	10.69	6.94	X	0.02483	0.05	X
Wt + HP	35	40	0.05% - 0.25%	31.32	4.75	X	0.00046	0.05	X	10.06	4.75	X	0.00933	0.05	X
Rec + Lav	35	40	0.05% - 0.15%	36.75	6.94	X	0.00266	0.05	X	43.78	6.94	X	0.02500	0.05	X
Virg + Lav	35	40	0.05% - 0.08%	36.00	18.50	X	0.02667	0.05	X	196.00	18.50	X	0.00506	0.05	X

Second, the same analysis (two-variable ANOVA) was carried out on the mechanical properties of the affected 35 MPa concretes (i.e. modulus of elasticity, tensile strength and compressive strength) in order to verify, once again, the significance of the results obtained as a function of AAR development. In other words, this study aimed to verify/discuss statistically the influence of AAR on each of the mechanical properties of the concrete. The results of the above analysis showed that the modulus of elasticity is a mechanical property that is statistically significantly affected by the development of AAR, as, once again, all the “F values” were greater than the “F_{critic}” and the “p values” were less than 0.05 for each case (Table 6). However, both the tensile strength and the compressive strength were not considered statistically significant towards AAR development.

Table 6: Two-variable ANOVA analysis on the mechanical properties results for the 35 MPa concrete mixtures incorporating different aggregate types/natures.

ANOVA analysis			Modulus of elasticity loss						Tensile strength loss						Compressive strength loss					
Aggregate type	Strength (MPa)	Expansion (%)	SDI_F	SDI_Fcritic	F>Fcritic	SDI_P value	α	P<α	PDI_F	PDI_Fcritic	F>Fcritic	PDI_P value	α	P<α	PDI_F	PDI_Fcritic	F>Fcritic	PDI_P value	α	P<α
Tx + HP	35	0.05% - 0.30%	24.49	4.75	X	0.00091	0.05	X	0.25	9.27	-	0.85708	0.05	-	16.31	9.27	X	0.02315	0.05	X
NM + Lav	35	0.05% - 0.25%	46.22	4.75	X	0.00015	0.05	X	3.54	9.27	-	0.16331	0.05	-	10.17	9.27	X	0.04424	0.05	X
Tx + Dia	35	0.05% - 0.30%	45.61	4.75	X	0.00016	0.05	X	1.00	9.27	-	0.50000	0.05	-	2.51	9.27	-	0.23448	0.05	-
QC + Lav	35	0.05% - 0.20%	74.59	6.94	X	0.00068	0.05	X	25.16	19	X	0.03822	0.05	X	1.78	19	-	0.36127	0.05	-
Wyo + Lav	35	0.05% - 0.20%	18.78	6.94	X	0.00926	0.05	X	3.00	19	-	0.25000	0.05	-	4.36	19	-	0.18646	0.05	-
Tx + NM	35	0.05% - 0.30%	22.3	4.75	X	0.00118	0.05	X	1.19	9.27	-	0.44451	0.05	-	3.17	9.27	-	0.18433	0.05	-
Conr + Lav	35	0.05% - 0.25%	78.16	4.75	X	0.00062	0.05	X	1.00	19	-	0.50000	0.05	-	15.64	19	-	0.06009	0.05	-
King + Lav	35	0.05% - 0.30%	8.95	4.75	X	0.01235	0.05	X	35.66	9.27	X	0.00758	0.05	X	2.54	9.27	-	0.23154	0.05	-
Pots + Lav	35	0.05% - 0.20%	11.62	6.94	X	0.02153	0.05	X	6.60	19	-	0.13152	0.05	-	0.004	19	-	0.99514	0.05	-
Wt + HP	35	0.05% - 0.25%	40.95	4.75	X	0.00022	0.05	X	53.57	9.27	X	0.00419	0.05	X	1.02	9.27	-	0.49128	0.05	-
Rec + Lav	35	0.05% - 0.15%	120.55	6.94	X	0.00027	0.05	X	3.59	19	-	0.21750	0.05	-	3.66	19	-	0.21456	0.05	-
Virg + Lav	35	0.05% - 0.08%	23.55	18.5	X	0.03992	0.05	X	2.77	161	-	0.34404	0.05	-	173.76	166	X	0.04820	0.05	X

In the case of tensile strength, the results from only three concrete mixtures over twelve were considered statistically significant (i.e. the values from 0.05% up to 0.20% or 0.30%, depending on the maximum expansion level attained), which means that only 25% of the AAR-affected specimens presented a tensile loss statistically significant against increasing AAR expansion. However, considering the results of tensile strength testing illustrated in Figure 16 and the discussions presented in section 6.4.2., it appears that the vast majority of the concrete mixtures attained their “peak loss” for low and moderate expansion levels (from 0.05 to 0.12%), showing a leveling off trend after this maximum point; this might partly explain why the results were not found to be “significant”. Therefore, a complementary “t test” were carried out to verify the significance of Tensile strength losses between the 0.05% and 0.12% values (Table 7). The results show that half of the 35 MPa mixes are different from one mix to another in the 0.05% - 0.12% expansion range, which means that the tensile strength “peak loss” was reached for half of the mixtures at the 0.05% expansion level and at

0.12% for the other half of the mixtures. After those low/moderate expansion levels, the values did not change significantly.

For the compressive strength analysis (as for the tensile strength), three mixes over twelve (25%) were considered statistically significant (i.e. the values from 0.05% up to 0.20% or 0.30%, depending on the mix). However, differently from the tensile strength, the compressive strength losses presented an increase trend towards AAR expansion, which was discussed in section 6.4.3 and illustrated in Figure 17. Therefore, these results mean that the compressive strength values obtained for different expansion levels could not be “distinguished” from one another as a function of AAR development. Thus, a complementary “t test” was performed to determine whether the compressive strength values measured at each of the expansion levels studied were “significantly” affected by ASR, when those results were compared to the results of sound concrete samples with the same maturity (Table 7). The results of the statistical analysis showed that the compressive strength of the various concretes is indeed affected by the development of AAR. Three mixtures over twelve (25%) already presented significance at 0.05%, other three concretes over twelve (25%) showed significance at 0.12% and the others mixes showed significance for higher expansion levels (i.e. greater than 0.20%). These results somewhat agree with the results found in the literature [12, 13] when significant compressive losses are found for high degree of expansion due to ASR.

Table 7: Test analysis on the 35 MPa mixtures regarding both the tensile and the compressive strengths’ behaviors.

t test analysis - Tensile strength loss						t test analysis - Compressive strength loss						Expansion level (%)
Aggregate type	Strength (MPa)	Expansion (%)	PDI_P value	α	P< α	Aggregate type	Strength (MPa)	Expansion (%)	PDI_P value	α	P< α	
Tx + HP	35	0.05% - 0.30%	0.42285	0.05	-	Tx + HP	35	0.05% - 0.30%	-	0.05	X	0.05
NM + Lav	35	0.05% - 0.25%	0.04434	0.05	X	NM + Lav	35	0.05% - 0.25%	-	0.05	X	0.05
Tx + Dia	35	0.05% - 0.30%	0.15588	0.05	-	Tx + Dia	35	0.05% - 0.30%	0.01818	0.05	X	0.12
QC + Lav	35	0.05% - 0.20%	0.02290	0.05	X	QC + Lav	35	0.05% - 0.20%	0.00127	0.05	X	0.20
Wyo + Lav	35	0.05% - 0.20%	0.41548	0.05	-	Wyo + Lav	35	0.05% - 0.20%	0.00008	0.05	X	0.20
Tx + NM	35	0.05% - 0.30%	0.36637	0.05	-	Tx + NM	35	0.05% - 0.30%	0.00004	0.05	X	0.05
Conr + Lav	35	0.05% - 0.25%	0.38529	0.05	-	Conr + Lav	35	0.05% - 0.25%	0.00024	0.05	X	0.20
King + Lav	35	0.05% - 0.30%	0.04773	0.05	X	King + Lav	35	0.05% - 0.30%	0.00150	0.05	X	0.12
Pots + Lav	35	0.05% - 0.20%	0.44228	0.05	-	Pots + Lav	35	0.05% - 0.20%	0.02699	0.05	X	0.20
Wt + HP	35	0.05% - 0.25%	0.01887	0.05	X	Wt + HP	35	0.05% - 0.25%	0.00027	0.05	X	0.30
Rec + Lav	35	0.05% - 0.15%	0.02032	0.05	X	Rec + Lav	35	0.05% - 0.15%	0.00606	0.05	X	0.12
Virg + Lav	35	0.05% - 0.08%	0.02566	0.05	X	Virg + Lav	35	0.05% - 0.08%	0.06077	0.05	-	-

10.7.4.2 Significance of the envelopes results, considering different aggregate types/natures as a function of AAR development

In order to assess the statistical validity and significance of the envelopes generated as part of this study for concretes incorporating different aggregate types/natures (e.g. Figures 19, 20), two-variable ANOVA analyses, taking into account the various micro-mechanical parameters analyzed and the expansion levels studied, were carried out on the 35 MPa mixtures incorporating different aggregate types/natures. The results, presented in Table 9 that can be found in the Supplementary materials section in annex of this paper, show that, with the exception of the compressive strength loss of concrete mixtures that generated low degrees of expansion ($\leq 0.12\%$), all the data were considered different from one another, which means that although a strong “envelope of results” was found over this work, which represented a contribution to the understanding on how AAR influences the properties of the affected materials and enables fair prediction/correlation between AAR expansion and selected concrete properties, different behaviors were still obtained as a function of the aggregate type/nature used, for the same expansion level. These results illustrate the importance of further/deeper analyzing the impact of aggregate’s physical characteristics on the fracture process (i.e. toughness, hardness, etc.) in concrete undergoing expansion due to AAR, as suggested by Reinhard & Mielich [20].

10.7.4.3 Significance of the envelopes results, considering different concrete strengths, as a function of ASR development

In order to assess the statistical validity and significance of the envelopes generated as part of this study for concretes of different strengths, two-variable ANOVA analyses, taking into account the various microscopic and micro-mechanical parameters analyzed, were carried out on the 25, 35 and 45 MPa mixtures. The results, presented in Table 10 that can be found in the Supplementary materials section in annex of this paper, show that, with the exception of the DRI number, which presented similar results disregarding the concrete strength, all the mechanical data (SDT, modulus of elasticity, compressive and tensile strengths) indicated that the distress due to AAR relies on the characteristics of the affected materials (i.e. strength, stiffness, stress/strain behavior, etc.), which agrees with the results obtained in this study (i.e. presence of “envelopes” of results). These results mean that AAR actually affects differently materials presenting different characteristics, for the same expansion level. Therefore, an in depth study on the “composite” material behavior (i.e. ductile/brittle properties, interaction

among the components, etc.) over the fracture process with increasing AAR expansion is still needed, so that one could fully understand the exact roles of materials properties in concrete undergoing AAR damage.

10.8 CONCLUSIONS

The main objective of the test program carried out in this study was to perform the global analysis of concrete damaged due to ASR based on microscopic and mechanical procedures. The main conclusions of the above investigations are:

- *AAR kinetics*
 - Concrete mixtures containing the highly reactive natural Tx and manufactured NM sands presented faster reactivity than those containing highly reactive coarse aggregates. This behavior might be linked to either a higher aggregate's reactivity level or even to the aggregate's size effect. Moreover, similar behaviors were found for the mass gain plots against time (i.e. the faster ASR kinetics, the greater the mass gain over time). Exception was found for the King + Lav mixture, susceptible to the so-called alkali-carbonate reaction (ACR), which presented the "fastest" AAR expansion kinetics of all aggregates investigated but a mass gain that was overcome by several ASR affected mixtures with less final expansion. Therefore, an in depth study is still necessary to allow a better understanding of the ACR chemical/physical mechanisms as a function of its expansion;
 - Singular behavior was observed for the concrete mixture incorporating both fine and coarse highly reactive aggregates together. Those mixtures showed a slower reaction kinetics and sometimes lower ultimate expansion than the concrete mixtures containing just one of those reactive aggregates, fine or coarse. This means that a "competition" develops between both highly reactive aggregate (fine vs. coarse), thus resulting in a "pessimun effect" of the expansion obtained in the test specimens;
 - No significant differences were observed in the AAR kinetics for the range of strengths used in this project (from 25 up to 45 MPa, reactive aggregates NM and Tx). Those results are interesting but somewhat surprising. This suggests that not only the total concrete alkali content but the concrete mix characteristics impact on the reaction/expansion kinetics. Further work is required to evaluate the combined effects of the above parameters on ASR expansion.

- *AAR distress development*
 - Microscopic and mechanical investigations carried out in this study showed that the development of AAR distress features is actually not linear as a function of concrete expansion due to AAR. This phenomenon can likely be explained by the following two-step process: a), the formation of new cracks in the early stages of the chemical reaction, and b), the extension of the above cracks into the cement paste; from this point, it is easier for the expanding system to propagate those cracks instead of creating new ones. Thus, the rate of new cracks' generation decreases or keeps increasing but at a lower rate.
- *ASR influence on the mechanical properties of affected concrete*
 - In the beginning of ASR development (i.e. between 0.0% and about 0.05%), opened cracks are generated by ASR within the aggregate particles, a proportion of which originates from closed cracks resulting from aggregate processing operations. These distress features are likely to cause a significant drop in the “stiffness” of the reactive aggregate particles, as well as of the stiffness and the tensile strength of the affected materials. On the other hand, the development of such cracking within the aggregate particles does not seem to affect significantly the compressive strength of the concretes;
 - For moderate expansion levels ($\approx 0.12\%$), some “new cracks” are generated within the reactive aggregate particles and some of the above cracks actually extend into the ITZ and cement paste with continuing losses in “stiffness” of the affected concrete. At such moderate expansion levels, the tensile strength attained its maximum loss since cracks have already reached their critical lengths causing unstable crack growth in the system. On the other hand, while only mild reductions in compressive strengths are observed as only limited cracking has extended into the bulk cement paste and the ITZ, which could be used as “fast tracks” to initiate and propagate fracture.
 - For higher expansion levels (between $\approx 0.20\%$ and 0.30%), the generation of “new” cracks within the aggregate particles and the cement paste seems to be overcome by an increase in length and width of the existing cracks. Also, at this stage, the vast majority of the cracks generated within the aggregate particles reach the cement paste where they link into a dense network of cracking. Thus, the stiffness of the majority of the affected concrete mixtures keeps dropping at about the same rate. This cracking extension process does not seem to affect further the tensile strength of the concrete while a continuing/progressive loss in compressive strength is observed. Since the mechanism of fracture in compression is more ductile than the mechanism in tension, the

development of cracking networks creates instability in the system, thus resulting in progressive losses in compressive strength;

- *Global AAR analysis*
 - A four-quadrant chart that correlates the expansion attained by ASR-affected samples is proposed, according to the following micro mechanical properties: 1) SDI (a mechanical measure of the amount of internal cracking of affected concretes); b) DRI (semi-quantitative rating of microscopic damage/ cracking) and; c) damage variable “ δ ” (stiffness loss of the ASR-affected concretes);
 - These charts show that the micro mechanical data correlated well for all the concrete mixtures (i.e. \neq strengths and aggregate types/natures) studied in this work since similar “damage patterns”, were found in each quadrant of the charts;
 - Regarding the analysis of ASR development and distress classification, one notices that according to the expansion level and materials characteristics, AAR might come from a serviceability/durability related problem to stress withstand capacity issues. Therefore, care should be taken on the appraisal of AAR damage structures/structural elements;
- *Tools for assessing damage in concrete due to AAR*
 - Overall, the Stiffness Damage Test (SDT) and the Damage Rating Index (DRI) are both reliable and complementary tools for condition assessment of concrete affected by ASR;
 - Analysis of variance (ANOVA) confirmed the significance of the results obtained through this work and the reliability of both SDT and DRI output parameters;
 - The efficacy of the SDT and the DRI was proven on test specimens made and cured under well-controlled laboratory conditions; however, their efficacy needs to be proven by analyzing condition of cores extracted from ASR-affected structural elements in service;
 - The SDT and DRI seem to have the potential of being universal tools for damage assessment in concrete. Therefore, their suitability for evaluating distress mechanisms other than AAR is the next step of those tools development.

10.9 ACKNOWLEDGEMENTS

The funding of this project was provided by a grant from the Quebec Department of Transportation, under the supervision of Mr. Alain Hovington and Mrs. Nadia Pouliot. The authors would like to thank Mr. René Malo and Mr. Mathieu Thomassin from “le Centre de recherche sur les infrastructures en béton (CRIB)” at Laval University, as well as the undergraduate research assistants who helped with the manufacturing and testing of the test

specimens used in this project. L. Sanchez benefits from a Vanier scholarship financed by NSERC (Natural Sciences and Engineering Research Council of Canada).

10.10 REFERENCES

- [1] Fournier, B.; Bérubé, M. A. 2000. Alkali–aggregate reaction in concrete: a review of basic concepts and engineering implications. *Canadian Journal of Civil Engineering*, 27 (2): 167-191.
- [2] Bérubé, M.A.; Smaoui, N.; Bissonnette, B.; Fournier, B. 2005. Outil d'évaluation et de gestion des ouvrages d'art affectés de réactions alcalis-silice (RAS). *Études et Recherches en Transport*, Ministère des Transports du Québec, Septembre, 140 p.
- [3] Fournier, B.; Bérubé, M. A; Folliard, K.; Thomas, M. 2010. Report on the diagnosis, prognosis, and mitigation of alkali-silica reaction (ASR) in transportation structures. US Department of Transportation, Federal Highway Administration, Publication FHWA-HIF-09-004.
- [4] Sanchez, L. F. M.; Fournier, B.; Jolin, M.; Bastien, J. 2014. Evaluation of the Stiffness Damage Test (SDT) as a tool for assessing damage in concrete due to ASR: test loading and output responses for concretes incorporating fine and coarse reactive aggregates. *Cement and Concrete Research*, 56: 213-229.
- [5] Sanchez, L. F. M.; Fournier, B.; Jolin, M.; Bastien, J. 2014. Evaluation of the Stiffness Damage Test (SDT) as a tool for assessing damage in concrete due to ASR: input parameters and test procedure. *Cement and Concrete Composites*, submitted paper, January 2014.
- [6] Sanchez, L. F. M.; Fournier, B.; Jolin, M.; Bedoya, M.A.B.; Bastien, J.; Duchesne, J. 2014 Use of the Damage Rating Index (DRI) to quantify damage due to alkali-silica reaction in concrete incorporating reactive fine and coarse aggregates. *Cement and Concrete Composites*, submitted paper, January 2014.
- [7] Sanchez, L. F. M.; Fournier, B.; Jolin, M.; Duchesne, J. 2014. Assessment of microscopic damage features of alkali-aggregate reaction (AAR) through the Damage Rating Index (DRI). *Cement and Concrete Research*, submitted paper, January 2014.
- [8] Smaoui, N., Bérubé, M.A., Fournier, B., Bissonnette, B. & Durand, B. (2004). Evaluation of the Expansion Attained to Date by Concrete Affected by ASR – Part I: Experimental Study. *Canadian Journal of Civil Engineering*, 31: 826-845.
- [9] Smaoui, N., Fournier, B., Bérubé, M.A., Bissonnette, B. & Durand, B. (2004). Evaluation of the Expansion Attained to Date by Concrete Affected by ASR - Part II : Application to Non-reinforced Concrete Specimens Exposed Outside. *Canadian Journal of Civil Engineering*, 31: 997-1011.
- [10] Bérubé, M.A., Smaoui, N., Fournier, B., Bissonnette, B. & Durand, B. (2005). Evaluation of the Expansion Attained to Date by Concrete Affected by ASR - Part III: Application to Existing Structures. *Canadian Journal of Civil Engineering*, 32: 463-479.
- [11] Crouch, R. S.; Wood, J. G. M. 1990. Damage evolution in ASR affected concretes. *Engineering fracture mechanics*, 35 : 211- 218.
- [12] Kubo, Y.; Nakata, M. 2012. Effect of reactive aggregate on mechanical properties of concrete affected by alkali-silica reaction. *Proceedings of the 14th International Conference on Alkali–Aggregate Reaction in Concrete*, May 20–25th 2012, Austin (Texas), electronic, 2012.
- [13] Nixon, P. J.; Bollinghaus, R. 1985. The effect of alkali aggregate reaction on the tensile strength of concrete. *Durability of Building Materials*, 2 (3): 243-248.
- [14] Smaoui, N.; Bissonnette, B.; Bérubé, M. A.; Fournier, B.; Durant, B. 2006. Mechanical Properties of ASR-Affected Concrete Containing Fine or Coarse Reactive Aggregates. *Journal of ASTM International*, 3 (3) : 01-16.
- [15] ISE 1992. Structural effects of alkali-aggregate reaction: technical guidance on the appraisal of existing structures. The Institution of Structural Engineers (ISE), London, UK.
- [16] Wood, G. M.; Johnson, R. A. 1993. The appraisal and maintenance of structures with alkali-silica reaction. Paper, Institution of Structural Engineers.

- [17] Wood, G. M.; Norris, P.; Leek, D. 1989. Physical Behavior of AAR Damaged Concrete in Structures and in Test Conditions. 8th ICAAR - International Conference on Alkali-Aggregate Reaction in Concrete, July 17-20, Kyoto (Japan).
- [18] Naar, R. 2010. Modelisation du comportement mécanique du béton par approche multi-physique (couplage chimie-mécanique) : application à la réaction alcali-silice. Thèse de doctorat. École Nationale Supérieure des Mines de Paris (France).
- [19] Giaccio G.; Zerbino, R.; Ponce, J. M.; Batic, R. 2008. Mechanical behavior of concretes damage due to ASR. *Cement and Concrete Research*. 38: 993-1004.
- [20] Reinhard, H. W.; Mielich, O. 2011. A fracture mechanics approach to the crack formation in alkali sensitive grains. *Cement and Concrete Research*, 41 : 255- 262.
- [21] Aitcin, P. C.; Mehta P. K. 1990. Effect of Coarse-Aggregate Characteristics on Mechanical Properties of High-Strength Concrete. *ACI Materials Journal*, 87: 103-107.
- [22] Özkan, S.; Canan, T.; Mehmet Ali, T. 2002. Influence of Aggregate Type on Mechanical Behavior of Normal- and High-Strength Concretes. *ACI Materials Journal*, 99 : 528-533.
- [23] Alexander, M. G.; Milne, T. I. 1995. Influence of Cement Blend and Aggregate Type on Stress-Strain Behavior and Elastic Modulus of Concrete. *ACI Materials Journal*, 92 : 227-325.
- [24] Crisp, T. M.; Waldron. P.; Wood. 1989. J. G. M. Development of a non destructive test to quantity damage in deteriorated concrete. *Magazine of Concrete Research*, 45 (165): 247-256.
- [25] Crisp, T. M.; Wood, J. G. M.; Norris, P. 1993. Towards Quantification of Microstructural Damage in AAR Deteriorated Concrete. International Conference on Recent Developments on the Fracture of Concrete and Rock. September.
- [26] Walsh. J. B. 1965. The effects of cracks on the uniaxial elastic compression of rocks.. *Journal of Geophysical Research*, 70: 339-411.
- [27] Crouch. R. S. 1987. Specification for the determination of stiffness damage parameters from the low cyclic uniaxial compression of plain concrete cores. Revision A. Mott. Hay & Anderson. Special services division. Internal technical note.
- [28] Villeneuve, V.; Fournier, B. 2012. Determination of the damage in concrete affected by ASR – the damage rating index (DRI). Proceedings of the 14th International Conference on Alkali-Aggregate Reaction in Concrete, May 20–25th 2012, Austin (Texas), electronic, 2012.
- [29] Shrimmer, F.H. 2006. Development of the Damage Rating Index Method as a tool in the assessment of alkali-aggregate reaction in concrete: a critical review. Proc. Marc-André Bérubé symposium on AAR in concrete, CANMET/ACI Advances in concrete technology seminar, Montréal, Canada, 391-411.
- [30] Grattan-Bellew, P.E.; Danay, A. 1992. Comparison of laboratory and field evaluation of AAR in large dams. Proc. of the International Conference on Concrete AAR in Hydroelectric Plants and Dams, Canadian Electrical Association & Canadian National Committee of the Int. Commission on Large Dams.
- [31] Transtec Group. 2009. Field Site and Petrographic Evaluation - ASR Development and Deployment Program - Field Trials and Demonstration Projects.
- [32] Saint-Pierre, F.; Rivard, P.; Sauriol, B.; Ballivy, G. 2004. Étude de l'évolution de la réaction alcalis-silice par méthodes ultrasoniques. 11e Colloque sur la progression de la recherche québécoise portant sur les ouvrages d'art, Université Laval, Québec, 12 p.
- [33] ASTM C597. 2009. Standard Test Method for Pulse Velocity through Concrete. ASTM International, West Conshohocken (USA).
- [34] Moradi-Marani, F.; Kodjo, S. A.; Rivard, P.; Lamarche, 2014. C. P. Nonlinear acoustic technique of time shift for evaluation of alkali-silica reaction damage in concrete structures. *ACI Materials Journal*, 111 : 1-6.
- [35] Komar, A.; Hartell J.; Boyd, A. J. 2013. Pressure tension test: reliability for assessing concrete deterioration. Proceedings of the Seventh International Conference on Concrete under Severe Conditions - Environment and Loading. Nanjing (China), September.
- [36] Fournier, B.; Bilodeau, A.; Thomas, M.D.A.; Folliard, K. (2007). Uses of Class C fly ash in Ternary Blends for Mitigation of Alkali-Silica Reactivity. EPRI, Palo Alto, Ca: 1014271.
- [37] Tremblay, S. 2011. Étude de l'efficacité d'adjuvants à base de lithium afin de contrôler la réaction alcalis-silice dans le béton frais et dans les structures existantes incorporant cet adjuvant. Mémoire de maîtrise, Géologie et Génie Géologique. Université Laval, Québec.

- [38] Lu, D.; Fournier, B.; Grattan-Bellew, P.E.; Lu, Y.; Xu, Z.; Tang, M. 2008. Expansion behaviour of Spratt and Pittsburg limestones in different test procedures. 13th Int. Conf. of Alkali-Aggregate Reaction in Concrete, Trondheim, Norway, June 16-20.
- [39] Sanchez, L. F. M.; Kuperman, S, C; Helene, P; Kihara, Y. 2008. Trials to correlate the accelerated mortar bar test, the standard and the accelerated concrete prism tests. 13th ICAAR - International Conference on Alkali-Aggregate Reaction in Concrete. June 16-20, Trondheim, Norway.
- [40] Lu, D.; Fournier, B.; Grattan-Bellew, P.E. (2006). Effect of Aggregate Particle Size on Determining Alkali-Silica Reactivity by Accelerated Tests. *Journal of ASTM International*, 3 (9).
- [41] ASTM C1293. 2008. Standard Test Method for Determination of Length Change of Concrete Due to Alkali-Silica Reaction. ASTM International, West Conshohocken (USA).
- [42] A23.2-14C. 2009. Obtaining and Testing Drilled Cores For Compressive Strength Testing. Canadian Standards Association, Mississauga, Ontario (Canada).
- [43] ASTM C 39. 2012. Standard Test Method for Compressive Strength of Cylindrical Concrete Specimens. ASTM International, West Conshohocken (USA).
- [44] ASTM C 1074. 2011. Standard Practice for Estimating Concrete Strength by the Maturity Method. ASTM International, West Conshohocken (USA).
- [45] Lindgård, J. 2013. Alkali-silica reaction (ASR) – Performance testing. PhD Thesis. NTNU (Norwegian University of Science and Technology), Norway.
- [46] Lindgård, J.; Thomas, M.D.A.; Sellevold, E.J.; Pedersen, B.; Andiç-Çakır, O.; Justnes, H.; Rønning, T.J. 2013. Alkali-silica reaction (ASR)—performance testing: Influence of specimen pre-treatment, exposure conditions and prism size on alkali leaching and prism expansion, *Cement and Concrete Research*, 53: 68–90.
- [47] Fournier, B.; Nkinamubanzi, P.C.; Lu, D.; Thomas, M. D. A.; Folliard, K. J.; Ideker, J. 2006. Evaluating potential alkali-reactivity of concrete aggregates – How reliable are the current and new test methods? II Symposium on alkali-aggregate reaction in concrete structures. Brazilian Concrete Institute-Ibracon and Brazilian Committee on Dams-CBDB, Rio de Janeiro, Brazil, September.
- [48] Fournier, B.; Bérubé, A. 2000. Alkali-aggregate reaction in concrete: a review of basic concepts and engineering implications. *Canadian Journal of Civil Engineering*, 27 (2): 167-191.
- [49] Dunant, C. F.; Scrivener, K. L. 2009. Micro mechanical modeling of alkali-silica reaction induced degradation using the AMIE framework. *Cement and Concrete Research*, 40: 517-525.
- [50] Mindess, S.; Young, J. F.; Darwin, D. Concrete. 2003. Book. Pearson Education Ltda, second edition.
- [51] Inoue, S.; Mikata, Y.; Takahashi, Y.; Inamasu, K. 2012. Residual shear capacity of ASR damaged reinforced concrete beams with ruptured stirrups. Proceedings of the 14th International Conference on Alkali-Aggregate Reaction in Concrete, May 20–25th 2012, Austin (Texas), electronic, 2012.
- [52] Neville, A. M. Properties of Concrete. 1997. Book. Pearson Education Ltda, second edition.

ANNEX – Supplementary information

Table 8: Compressive strengths (28-day values) of all concrete mixtures *.

Concrete Mixtures	Compressive strength (MPa) 28-day value	Expansion measurement (%) After being stored at 12°C
Tx + HP 25	27	-
Tx + HP 35	32	-0.010
Tx + HP 45	42	-0.020
NM + Lav 25	27	-
NM + Lav 35	35	-0.030
NM + Lav 45	45	-
Tx + Dia 25	29	-
Tx + Dia 35	36	-
Tx + Dia 45	43	-
QC + Lav 25	28	-
QC + Lav 35	37	-
QC + Lav 45	42	-
Wyo + Lav 35	37	-0.020
Tx + NM 35	37	-0.030
Conr + Lav 35	38	-
King + Lav 35	33	-
Virg + Lav 35	40	-0.020
Rec + Lav 35	39	-0.020
Wt + HP 35	33	-
Lav + Pots 35	37	-0.030

*Stored wrapped at 12°C for 47 days then rewetted for 48h in the moist curing room at 23°C prior to testing..

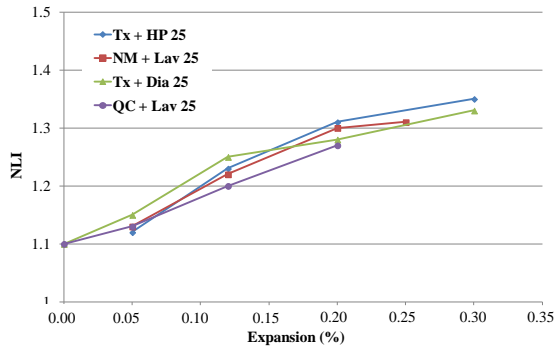
Table 9: Two-variable ANOVA analysis on all the micro mechanical data obtained through the 35 MPa concrete mixtures analyses, incorporating different aggregate types/natures.

ANOVA analysis			Parameter	ANOVA output values					
Aggregate type	Strength (MPa)	Expansion (%)		F	F _{critic}	F>F _{critic}	P value	α	P< α
allmixtures	35	0.05% - 0.30%	SDI	23.36	3.28	X	0.00001	0.05	X
		0.05% - 0.20%	SDI	9.96	4.10	X	0.00416	0.05	X
		0.05% - 0.30%	PDI	14.67	3.28	X	0.00010	0.05	X
		0.05% - 0.20%	PDI	27.64	4.10	X	0.00008	0.05	X
		0.05% - 0.30%	Compressive strength	8.85	3.50	X	0.00228	0.05	X
		0.05% - 0.20%	Compressive strength	2.54	3.88	-	0.12069	0.05	-
		0.05% - 0.30%	Tensile strength	3.98	3.50	X	0.03502	0.05	X
		0.05% - 0.20%	Tensile strength	4.79	3.88	X	0.00058	0.05	X
		0.05% - 0.30%	Modulus of elasticity	34.18	3.28	X	0.00000	0.05	X
		0.05% - 0.20%	Modulus of elasticity	22.30	4.10	X	0.00021	0.05	X
		0.05% - 0.30%	DRI number	45.02	3.28	X	0.00000	0.05	X
		0.05% - 0.20%	DRI number	14.10	4.10	X	0.00105	0.05	X

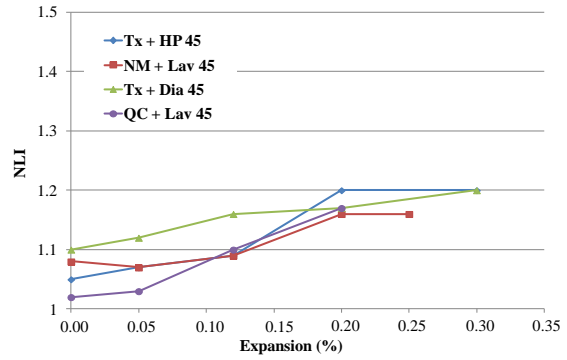
Table 10: Two-variable ANOVA analysis on all the micro mechanical data obtained through 25, 35 and 45 MPa concretes mixtures analyses.

ANOVA analysis				SDI					
Aggregate type	Strength (MPa)	Load (%)	Expansion (%)	SDI_F	SDI_Fcritic	F>Fcritic	SDI_P value	α	P < α
Tx + HP	25, 35 and 45 MPa	40	0.05% - 0.30%	32.12	5.14	X	0.00062	0.05	X
NM + Lav	25, 35 and 45 MPa	40	0.05% - 0.20%	22.94	5.14	X	0.00155	0.05	X
Tx + Dia	25, 35 and 45 MPa	40	0.05% - 0.25%	4.90	5.14	-	0.05468	0.05	-
QC + Lav	25, 35 and 45 MPa	40	0.05% - 0.25%	24.65	6.94	X	0.00563	0.05	X
ANOVA analysis				PDI					
Aggregate type	Strength (MPa)	Load (%)	Expansion (%)	PDI_F	PDI_Fcritic	F>Fcritic	PDI_P value	α	P < α
Tx + HP	25, 35 and 45 MPa	40	0.05% - 0.30%	8.38	5.14	X	0.01832	0.05	X
NM + Lav	25, 35 and 45 MPa	40	0.05% - 0.20%	37.75	5.14	X	0.00093	0.05	X
Tx + Dia	25, 35 and 45 MPa	40	0.05% - 0.25%	3.60	5.14	-	0.09346	0.05	-
QC + Lav	25, 35 and 45 MPa	40	0.05% - 0.25%	24.65	6.94	X	0.00563	0.05	X
ANOVA analysis				Module of elasticity (ME)					
Aggregate type	Strength (MPa)	Load (%)	Expansion (%)	ME_F	PDI_Fcritic	F>Fcritic	ME_P value	α	P < α
Tx + HP	25, 35 and 45 MPa	40	0.05% - 0.30%	15.07	5.14	X	0.00457	0.05	X
NM + Lav	25, 35 and 45 MPa	40	0.05% - 0.20%	16.37	5.14	X	0.00372	0.05	X
Tx + Dia	25, 35 and 45 MPa	40	0.05% - 0.25%	2.79	5.14	X	0.13867	0.05	X
QC + Lav	25, 35 and 45 MPa	40	0.05% - 0.25%	3.31	6.94	-	0.14154	0.05	-
ANOVA analysis				DRI number					
Aggregate type	Strength (MPa)	Load (%)	Expansion (%)	DRI_F	DRI_Fcritic	F>Fcritic	DRI_P value	α	P < α
Tx + HP	25, 35 and 45 MPa	40	0.05% - 0.30%	0.63	5.14	-	0.63876	0.05	-
NM + Lav	25, 35 and 45 MPa	40	0.05% - 0.20%	1.48	5.14	-	0.29996	0.05	-
Tx + Dia	25, 35 and 45 MPa	40	0.05% - 0.25%	0.15	5.14	-	0.86350	0.05	-
QC + Lav	25, 35 and 45 MPa	40	0.05% - 0.25%	0.70	6.94	-	0.54729	0.05	-

A – 25 MPa mixtures: NLI vs. expansion



B – 45 MPa mixtures: NLI vs. expansion



C – 35 MPa mixtures: NLI vs. expansion

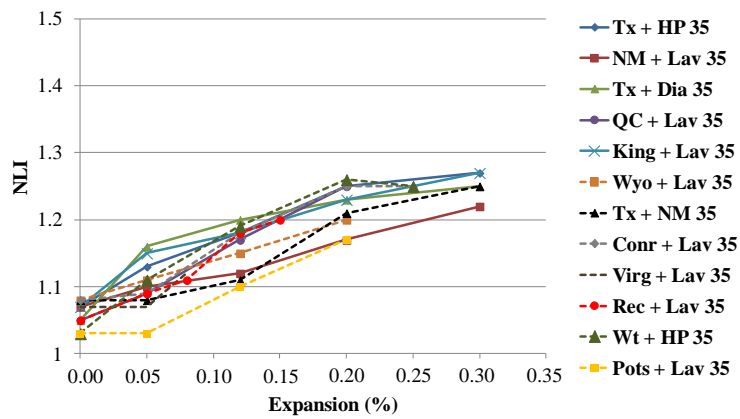


Figure 22: Non linearity index (NLI) (first cycle) for all the mixtures used in this study: A) 25 MPa mixtures; B) 45 MPa mixtures; C) 35 MPa mixtures.

11. PAPER VI: COMPARATIVE STUDY OF A CHEMO-MECHANICAL MODELING FOR ALKALI SILICA REACTION WITH EXPERIMENTAL EVIDENCES

Sanchez. L.F.M.^a; Multon. S.^b; Sellier A. ^c Cyr, M^d; Fournier. B.^e.; Jolin. M.^f

(a) MSc. – Laval University – PhD candidate.

1065, avenue de la Médecine, Pavillon Adrien-Pouliot, local 3755 Tel.: 1 (418) 704-2435

leandrofms@gmail.com / le.sanchez@uol.com.br

(b) Dr - LMDC (Laboratoire des Matériaux et Durabilité des Constructions). INSA, Toulouse, France

stephane.multon@insa-toulouse.fr

(c) Prof. Dr - LMDC (Laboratoire des Matériaux et Durabilité des Constructions). INSA, Toulouse, France

alain.sellier@insa-toulouse.fr

(d) Prof. Dr - LMDC (Laboratoire des Matériaux et Durabilité des Constructions). INSA, Toulouse, France

martin.cyr@insa-toulouse.fr

(e) Prof. Dr. – Laval University. Quebec. QC. Canada

benoit.fournier@ggl.ulaval.ca

(f) Prof. Dr. – Laval University. Quebec. QC. Canada

marc.jolin@gci.ulaval.ca

ABSTRACT

Modeling ASR and the resulting expansions is necessary to obtain relevant predictions of the structural responses of distressed concrete elements. Thus, to be efficient and reliable, models should take into account both chemical and physical ASR aspects. The LMDC developed a chemo-mechanical micromodel which predicts concrete expansion and damage over time. However, the output results of this model were only compared to damaged mortars but never to damaged concrete cast and measured in laboratory. This paper presents and analyzes the LMDC chemo-mechanical micromodel in regard to experimental evidences. Analyses were carried out on three types of concrete (25, 35 and 45 MPa) incorporating two different highly-reactive aggregates (New Mexico gravel and Texas sand). Both the assumptions and the input/output parameters used/obtained in/from the model are discussed. The results showed that the LMDC modeling is reliable and effective in the ASR expansion/damage predictions.

Keywords: alkali-silica reaction (ASR), chemo-mechanical modeling, ASR expansion and damage prediction

RÉSUMÉ

La modélisation de l'avancement de la RAS est nécessaire pour obtenir des prédictions pertinentes des réponses structurales des éléments de béton affectés par ce mécanisme délétère. Ainsi, pour être efficaces et fiables, les modèles doivent tenir compte des aspects physicochimiques de la réaction. Le LMDC a développé un micromodèle physicochimique dont le but est de prédire l'expansion et l'endommagement du béton atteint de RAS. Cependant, les résultats de prédiction de ce modèle n'ont jusqu'ici été comparés qu'au comportement de barres de mortiers affectées par la RAS, mais jamais à des bétons fabriqués et testés en laboratoire. Cet article présente et analyse le micromodèle physicochimique développé au LMDC par une comparaison avec des résultats expérimentaux. Les analyses ont été effectuées sur trois types de béton (25, 35 et 45 MPa) incorporant deux granulats réactifs différents (gravier du Nouveau-Mexique et sable du Texas). Les hypothèses et les paramètres d'entrée/sortie utilisés/obtenus pour le modèle LMDC sont discutés. Les résultats ont montré que le modèle LMDC peut prédire de façon généralement efficace l'expansion et le développement de l'endommagement de bétons par la RAS.

Mots clés: alkali-silica reaction (ASR), chemo-mechanical modeling, ASR expansion and damage prediction

11.1 INTRODUCTION – ASR MODELS

Alkali Silica Reaction (ASR) is a chemical reaction between the alkali hydroxides from the concrete pore solution and the reactive silica from the aggregates used in concrete. This chemical reaction generates a product (alkali-silica gel) that swells in the presence of water, thus inducing stresses and hence causing cracking in the concrete material. It has been found over the years that modeling ASR and the resulting expansions can be very useful to obtain relevant predictions of the structural responses of distressed concrete elements. Thus, to be efficient and reliable, models should take into account both chemical and physical ASR aspects [1].

Several ASR models were developed over the years to predict expansion and damage on both ASR affected materials (microscopic models) [1 to 9] and ASR affected structures/structural elements (macroscopic models) [10 to 14]. The first group has a goal of modeling both the chemical reactions and the mechanical distresses caused by ASR or even the coupling of the two phenomena. The second group aims at understanding the overall distress of structures/structural concrete elements in a real context, simulating their likely in situ behavior [15]. The *Laboratoire des Matériaux et Durabilité des Constructions* (LMDC) developed a micro chemo-mechanical model based on the works of Furusawa et al. [6]; Nielsen et al. [5]; Suwito et al. [8] and Poyet et al. [7] whose final aim was to predict the expansion of concrete structures in service.

11.2 LMDC CHEMO-MECHANICAL MODELING

Multon et al. [1] developed a microscopic ASR model at the LMDC (*Laboratoire des Matériaux et Durabilité des Constructions*), whose main input parameters are the alkali and reactive silica contents, the aggregate’s grading and the mechanical properties of the considered materials (aggregates, mortar/concrete). The model output results are both the determination of concrete expansion and damage due to ASR, taking into account the physicochemical reaction mechanisms (chemo-mechanical modeling) [1]. The LMDC micro-model approach for assessing damage/expansion of concretes is based on the definition of a representative elementary volume of concrete (REV) that contains both a mixture of aggregate particles (reactive or not, and of different sizes) and a cement paste enveloping those particles (Figure 1). The REV is considered to represent the behavior of the bulk concrete volume [1].

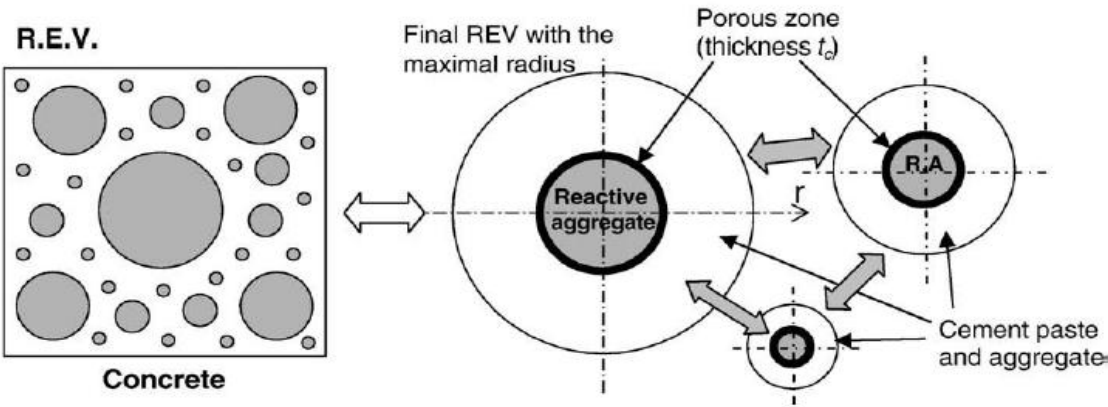


Figure 1: Definition of the Relative Elementary Volume (REV) for several reactive aggregate sizes [1].

In the micromodel, some chemical mechanisms are considered: 1) the alkali diffusion into the aggregate particles; 2) the production of ASR gel with the increase of alkali concentration in the aggregate particles; 3) the decrease of the alkali concentration in the cement paste as a function of their consumption by ASR gel; 4) the displacement of a part of the ASR gels into the cement paste porous zone surrounding the reactive aggregate particles (Figure 1). When that porous zone of thickness t_c is filled by ASR gel, the continuous gel generation provides significant pressure on the surrounding cement paste, leading to the material swelling [1].

In terms of mechanical effects, it is known that ASR expansions occur over long time periods. During this process, ASR affected concretes are subjected to a progressive stress built up that is very likely to cause creep on the distressed materials. LMDC model takes into account creep effects on ASR expansion/distress, by assuming that the modulus of elasticity of the concretes is one third of their instantaneous modulus at 28 days. This assumption is the typical approach used in the French design code for reinforced concrete structures.

If the stresses provided by ASR gel, once all the cement paste porosity is filled, become greater than the tensile strength of the concrete material represented by the REV, cracks and damage¹ are generated in the surrounding cement paste “ring” (Figure 2) [1]. If ASR progresses, which depends on the amount of silica available in the reactive aggregates, the thickness of the distressed concrete “ring” increases up to a point that all the REV is affected/damaged by the deleterious chemical reaction.

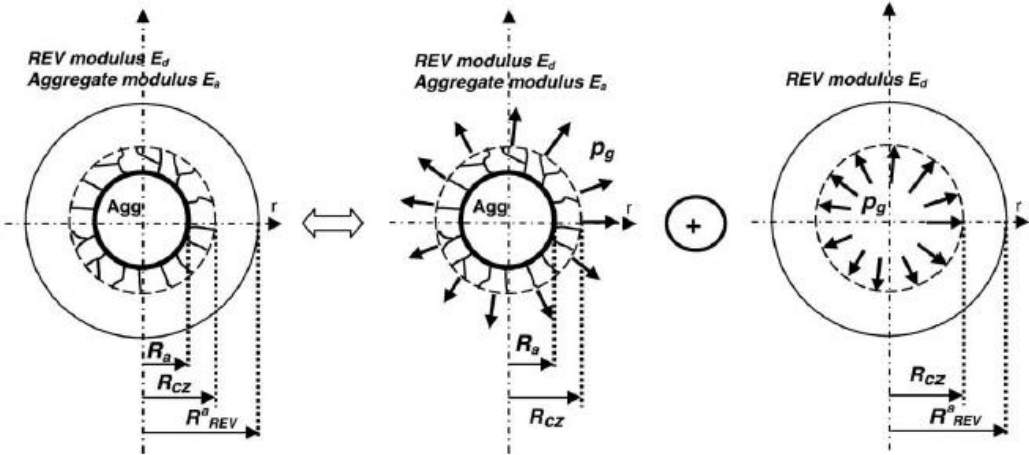


Figure 2: Mechanical equilibrium of the damaged REV [1].

¹ The word damage is defined in this model as being the modulus of elasticity decrease due to the crack formation in tension.

11.3 SCOPE OF WORK

The main goals of the chemo-mechanical ASR micromodel proposed by LMDC were to predict both the expansion and the mechanical damage in affected concrete specimens over time. The LMDC model has already been used for the assessment/ prediction of mortars behavior containing highly reactive aggregates [1, 16]. Although very promising, this model has never been applied so far to concrete specimens cast and cured in the laboratory, which makes its validation difficult since differences between the behavior of ASR-affected mortar and concrete specimens have been widely reported [17 to 22]. Moreover, ASR prediction for concrete with different strengths was never studied using this model.

This paper presents the LMDC chemo-mechanical micromodel assessment aiming at validating its predictive character through the comparison with experimental data recorded for concrete samples of different strengths and incorporating different aggregate types that were cast, cured and tested in the laboratory. The main model variables are “fit” as a function of the behavior observed through laboratory testing and a full discussion about the result’s validation and reliability is provided.

11.4 MATERIALS AND METHODS

11.4.1 Materials and mixture proportions

The analyses were carried out in two main parts:

- *Part I:* With the aim of verifying the influence of the aggregates size and grading on the expansion kinetics due to ASR and to test this parameter through the model, three 35 MPa concrete mixtures were designed using the highly reactive New Mexico gravel (NM). In the first mixture, the NM gravel was used as coarse aggregate (≈ 5 mm to 20 mm in size) with a natural non-reactive sand of granitic composition (Lav). In the second mix, NM was crushed and used as sand (NMs, ≈ 150 μ m to 4.8 mm) in combination with a non-reactive coarse limestone aggregate (HP). In the third and last mix, NM gravel was used both as sand and coarse aggregate. Table 1 gives the aggregate grading and the fineness modulus of the sands used.
- *Part II:* Three types of concrete with different compressive strengths (25 MPa, 35 MPa and 45 MPa) were made incorporating two highly-reactive aggregates (New Mexico gravel - NM and Texas sand - Tx). The main reactive material in the Tx sand is chert present in the coarser fractions of the aggregate material (~ 1.25 –5 mm fractions), while it is chert and

volcanic rock (rhyolite/andesite) particles in the case of the NM gravel. The reactive sand (Tx) and gravel (NM) were used in combination with non-reactive coarse and fine aggregates, respectively. In the case of the mixtures containing the reactive Tx sand, two non-reactive coarse aggregates (a high-purity limestone (HP) and a diabase (Dia)) were used for each of the concrete strengths tested. Table 2 gives the main characteristics of the aggregates selected.

All the concrete mixtures were designed to contain the same amount of paste and aggregates in volume (i.e. from one mix to another), so one can compare similar systems (Tables 3 and 4). All concretes were made with the same conventional (CSA Type GU (equivalent to ASTM type I) high-alkali (0.90% Na₂O_{eq}) Portland cement. Reagent grade NaOH was used to raise the total alkali content of the mixtures to 1.25% Na₂O_{eq}, by cement mass, for accelerating the expansion process due to ASR.

Table 1: Aggregate grading and fineness modulus of the sands used in the part I.

Sand size fractions (mm)	Percentage (%) of aggregates of the fractions used in the concrete mix designs (<i>in volume</i>)		Fineness modulus of the sand used in the mix designs	
	NMs + HP	NMs + NM	NM + HP	NM + NM
4.8 – 2.4	10	10	2.7	2.7
2.4 – 1.2	25	25		
1.2 – 0.6	25	25		
0.6 – 0.3	25	25		
0.3 - 0.15	15	15		

Table 2: Aggregates used in the study.

Aggregate		Location	Rock Type	Specific gravity	Absorption (%)	AMBT 14d exp,%
Coarse	NM	New Mexico (USA)	Polymictic Gravel (mixed volcanics, quartzite, chert)	2.53	1.59	1.114
	HP	Newfoundland (Canada)	High-purity limestone	2.68	0.44	0.001
	Dia	Quebec (Canada)	Diabase (plutonic rock)	3.00	0.51	0.065
Fine	Tx	Corpus Christi (USA)	Polymictic sand (granitic, mixed volcanics, quartzite, chert, quartz)	2.60	0.55	0.995
	Lav	Quebec (Canada)	Natural derived from granite	2.71	0.54	0.032

Table 3: Concrete mix designs used in the part I.

Ingredients	35 MPa - Materials (kg/m ³)	
	NMs (sand) and HP (coarse aggregate)	NMs (sand) and NM (coarse aggregates)
Cement	370 (118) ¹	370 (118)
Sand	738 (292)	714 (264)
Coarse aggregate	1061 (396)	1073 (424)
Water	174 (174)	174 (174)

¹ The number in brackets correspond to the volume occupied by the materials (in L/m³)

Table 4: Concrete mix designs used in the part II.

Ingredients	25 MPa - Materials (kg/m ³)			35 MPa - Materials (kg/m ³)			45 MPa - Materials (kg/m ³)		
	Tx + HP	NM + Lav	Tx + Dia	Tx + HP	NM + Lav	Tx + Dia	Tx + HP	NM + Lav	Tx + Dia
Cement	314 (101) ¹	314 (101)	314 (101)	370 (118)	370 (118)	370 (118)	424 (136)	424 (136)	424 (136)
Sand	790 (304)	714 (264)	896 (344)	790 (304)	714 (264)	896 (344)	790 (304)	714 (264)	896 (344)
Coarse aggregate	1029 (384)	1073 (424)	1029 (343)	1029 (384)	1073 (424)	1029 (343)	1029 (384)	1073 (424)	1029 (343)
Water	192 (192)	192 (192)	192 (192)	174 (174)	174 (174)	174 (174)	157 (157)	157 (157)	157 (157)

¹ The number in brackets correspond to the volume occupied by the materials (in L/m³)

11.4.2 Fabrication and curing of test specimens

For the part I study, 12 specimens, 100 by 200 mm in size, were cast from each of the three concrete mixtures manufactured in the laboratory (NM + Lav, HP + NMs and NM + NMs – 35 MPa) (Table 3). For the part II study, a total of 36 cylinders, 100 by 200 mm in size, were cast from each of the nine concrete mixtures manufactured in the laboratory (Tx + HP, Tx + Dia, NM + Lav – 25, 35 and 45 MPa) (Table 3). After casting, the specimens were placed for 48h in the moist curing room (i.e. after the first 24h in the moist curing room, the specimens were demolded and left in this room for a further 24h). Small holes, 5 mm in diameter by 15 mm long, were then drilled in both ends of each test cylinders and stainless steel gauge studs were glued in place, with a fast-setting cement slurry, for longitudinal expansion measurements. The cylinders were left to harden for 48h prior to performing the “0” length reading, after what they were placed in sealed plastic (22 liters) buckets lined with damp cloth (4 cylinders per bucket). All buckets were then stored at 38°C and 100% R.H. and the test cylinders monitored for length changes regularly. As per ASTM C 1293, the buckets were

cooled to 23 °C for 16 ± 4 h prior to periodic axial expansion measurements. In the study part I, just the expansion kinetics was assessed so there was no mechanical nor microscopic procedures carried out on the specimens.

The test cylinders were monitored for length changes regularly until they reached the expansion levels chosen for this research, i.e. 0.05%, 0.12%, 0.20% and 0.30%. As per ASTM C 1293, the buckets were cooled to 23°C for 16 ± 4 h prior to periodic axial expansion measurements. When the above expansion levels were reached, the specimens were wrapped in plastic film and stored at 12°C until testing (because of testing capacity issues). Prior to mechanical testing, the concrete specimens were measured and weighed in order to confirm that they had not suffered from significant length or mass changes. When the concrete specimens were submitted to petrographic analysis, the samples were cut in two axially and then one of the surfaces thus obtained was polished. A portable hand-polishing device, which uses diamond-impregnated rubber disks, was found most suitable as it does not use loose abrasive powders that can fill up cracks/voids in the concrete and quality polishing is obtained with minimal water supply. Table 5 gives the testing matrix carried out on the concrete specimens of part II.

Table 5: Testing matrix of part II.

Concrete mix designs	Tests	Number of samples for each expansion level			
		0.05%	0.12%	0.20%	0.30%
25, 35 and 45 MPa	• Stiffness damage test / modulus of elasticity;	3	3	3	3
	• Compressive strength;	2	2	2	2
	• Tensile strength.	2	2	2	2
	• Damage Rating Index	2	2	2	2
Total number of samples: 36 for each sub-set x 9 mixtures = <u>324 samples</u>					

11.4.3 Methods for assessment and analysis

The experimental program carried out on the concrete cylinders at various expansion levels includes mechanical testing (*Stiffness Damage Testing* and modulus of elasticity, compressive and tensile strength determinations), and semi-quantitative petrographic analysis through the *Damage Rating Index (DRI)* method.

11.4.3.1 Stiffness Damage Test (SDT) and modulus of elasticity

Three cylinders of each concrete mixture (i.e. concrete strength and reactive aggregate type) at each expansion level chosen for this research were subjected to five cycles of loading/unloading at a controlled loading rate of 0.10 MPa/s. Through this mechanical assessment, the hysteresis area (HA) and the plastic deformation (PD) over the five cycles were measured according to [23]. Moreover, the modulus of elasticity was also obtained, being the average value of the secant modulus of the second and third cycles. All the results presented hereafter are the average values of three samples for each set of samples assessed (i.e. aggregate type, concrete strength and expansion level). Figure 3 illustrates the set-up used for the SDT/modulus of elasticity method.



Figure 3: Set-up used for the Stiffness Damage Test.

11.4.3.2 Damage Rating Index (DRI)

Semi-quantitative petrographic analysis, using the DRI method proposed by Grattan-Bellew & Danay [24] and recently modified by researchers from Laval University [25], was carried out on the concrete specimens of this study. The method consists in a count, under the stereomicroscope ($\approx 16\times$ magnification), of the number of petrographic features of deterioration (commonly associated to ASR) on polished concrete sections on which a grid is first drawn (minimum 200 grid squares to be examined, one by one cm in size). The DRI thus represents the normalized sum (to 100 cm²) of the frequency of these features after their count, over the surface examined and multiplied by weighing factors representing their

relative importance in the overall deterioration process (Figure 4). As the SDT/modulus of elasticity method, the DRI examination was carried out on concrete specimens (100 x 200 cm in size) from all mixtures (i.e. ≠ concrete strengths and reactive aggregate types) and expansion levels chosen for this research.

A

Petrographic features	Abbreviation	Weighing factor
Closed cracks in coarse aggregate	CCA	0.25
Opened cracks in coarse aggregates	OCA	2
Opened crack with reaction product in coarse aggregate	OCAG	2
Coarse aggregate debonded	CAD	3
Disaggregate/corroded aggregate particle	DAP	2
Cracks in cement paste	CCP	3
Cracks with reaction product in cement paste	CCPG	3

B

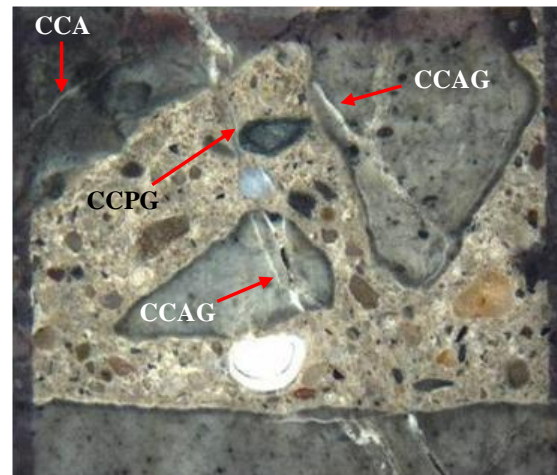


Figure 4: Damage Rating Index method. Micrograph B shows a 1cm² section where most of the petrographic features to be noted in the DRI (as listed in A) can be observed and identified. The distance between the two vertical lines is 1 cm [25].

11.4.3.3 Compressive strength test

Compressive strength of the samples was measured in two ways. First, tests were carried out on two cylinders of each concrete mix to determine their 28-day strength. For this part of the study, as the samples contained highly-reactive aggregates (fine and coarse), the ASTM C 39 [26] procedure could not be strictly followed, as the specimens could already present ASR under the very first 28 days in the moist curing room. Therefore, the samples were wrapped in plastic film and placed at 12°C over a 47-day period (which represents the same 28-day period according to the maturity concepts presented in ASTM C 1074 [27]). Second, the compressive strength test was determined on two of the three cylinders that were stiffness damage tested, with the aim of verifying the results at each ASR expansion level studied.

11.4.3.4 Tensile strength test

Tensile strength was measured according to the pressure tension test [28], on two samples of each concrete mixture and at each ASR expansion level. The pressure tension test, also known as the indirect tension test, was first developed by *The Building Research Council of*

Waterford (UK) as a means of investigating anisotropic behavior in materials. The pressure tension test uses compressed gas to apply an uniformly distributed pressure to the curved surface of standard (100 mm by 200 mm) concrete cylinders or cores. The apparatus consists of a hollow cylindrical test chamber that envelops the curved surface of the test cylinder. At either end of the testing chamber, rubber “O-rings” are used to seal the compressed gas so that it only acts upon the curved surface of the specimen (Figure 5). Both ends are left open to atmospheric pressure, resulting in a biaxial loading configuration. Gas pressure is monotonically increased until the test cylinder fails in a plane transverse to the axis of the testing chamber [28].

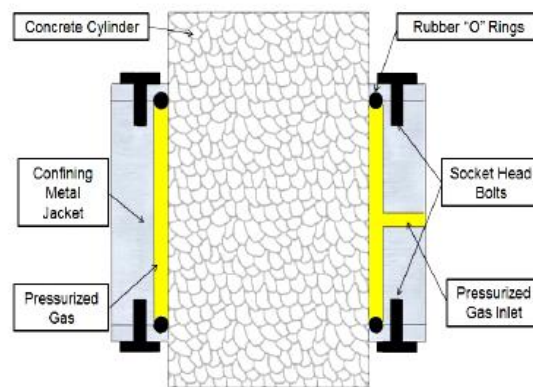


Figure 5: Cross section of pressure chamber [28].

The gas pressure applied to the curved surface is a biaxial loading condition but the reaction forces within the diphasic model differ. In particular, the pore water reacts hydrostatically whereas the solid phase reacts biaxially, resulting in a net internal tensile force driven by the pore fluid. The resultant internal tension force is the primary reason why the pressure tension method is thought to be well suited for detecting durability issues that affect the integrity of the cementitious microstructure [28].

11.4.4 ASR chemo-mechanical modelling

LMDC chemo-mechanical model runs in a *FORTTRAN* basis. In the beginning, a full description and characterization of both reactive and non-reactive aggregates used in the mixtures and of the cement paste itself is required. Therefore, aggregate parameters, such as their reactivity level (presence and amount of available silica), particle size distribution, content and mechanical properties (modulus of elasticity and tensile strength), as well as the

cement paste characteristics, such as water cement ratio, cement alkali content, porosity, and mechanical properties (modulus of elasticity and tensile strength) were registered for all the mixtures used in this work.

The total amount of alkalis for the mixes was obtained through the use of the Na_2O_e addition concept. All the mixes were alkali boosted to achieve 1.25% of Na_2O_e , so that the amount of alkalis adopted depended on the concrete characteristics (i.e. cement content). The amount of soluble silica was measured through the silica dissolution in HF, according to [29]. The values found for the Tx sand and the NM gravel were respectively 2000 mol/m^3 and 2180 mol/m^3 .

The mechanical properties of the aggregates, cement paste as well as the cement paste porosity are parameters that can be determined through experiments carried out in the laboratory. Table 6 presents the mechanical properties of the materials used in the model. The modulus of elasticity values for the different aggregates used were not measured but were rather obtained from the literature for similar rock types [30]. The values of both the modulus of elasticity and the tensile strength of the different concretes were measured in the laboratory using the same procedure of the compressive strength analysis (i.e. 47 days at 12°C , which represents the same 28-day period according to the maturity concepts presented in ASTM C 1074 [27]).

At this point of the work, five parameters were still unknown: 1) the cement paste porosity; 2) the thickness of the connected porosity surrounding the aggregate particles (which enables the gel flowing without causing pressure - t_c); 3-4) the diffusion (D_{agg}) and fixation (F) coefficients for alkalis in the aggregate particles and; 5) the molar volume of ASR gel (V_{gel}^m). The molar volume of ASR gel, the alkalis diffusion/fixation coefficients in the aggregate particles and the thickness of the aggregates connected porosity are parameters that are very important for the modeling procedure, but difficult to assess experimentally. Prior to the “setting phase”, a full comprehension/understanding of their concept and influence on ASR kinetics or amplitude is necessary.

- ASR kinetics: the alkalis diffusion (D_{agg}) and fixation (F) in the aggregate particles are very important for ASR kinetics. These two parameters are quite related to the aggregate characteristics and nature. In general, identical/similar values should be attributed to aggregates with the same nature/lithotype and characteristics, unless there are some chemical/physical explanations indicating that they can be different even for a same aggregate nature;
- ASR amplitude: the molar volume of ASR gel (V_{gel}^m) (i.e. representing ASR gel chemical composition – the LMDC model assumed that *1 mol of Na_2O_{eq} reacts with 5 mol of SiO_2 to*

give 1 mol of ASR gel which gives a Na_2O/SiO_2 of 0.2 [1]), the cement paste porosity and the thickness of the connected porosity surrounding the aggregate particles in the REV (t_c) influence ASR amplitude. The first parameter depends on the environment where ASR is developed (particularly the moisture conditions but likely also the cement and aggregate types, which are the most important source of alkalis in the system), while the second and the third parameters depend on the materials characteristics (aggregate nature, water/cement ratio and concrete strengths).

In order to obtain reliable values for the above five parameters, experimental data involving several aggregate sizes and contents would be necessary so that one could distinguish from “diffusion effects” to “silica dissolution effects” [1]. Unfortunately, in this experimental program, such results were not available. Therefore, some assumptions were adopted for the above parameters:

Table 6: Mechanical parameters adopted in the model for the different materials simulated.

Aggregate		Modulus of elasticity (MPa) ¹	Tensile strength (MPa)
Coarse	NM	77000	-
	HP	70000	-
	Dia	105000	-
Concrete mixture		Modulus of elasticity (MPa)	Tensile strength (MPa)
NM + Lav (25 MPa)		9333.5	3.0
NM + Lav (35 MPa)		10333.5	4.2
NM + Lav (45 MPa)		10666.5	5.0
Tx + HP (25 MPa)		11333.5	3.4
Tx + HP (35 MPa)		12333.5	4.6
Tx + HP (45 MPa)		13000.0	5.0
Tx + Dia (25 MPa)		14000.0	3.2
Tx + Dia (35 MPa)		14000.0	4.1
Tx + Dia (45 MPa)		14333.5	4.7
NMs + HP (35MPa)		12333.5	4.6
NMs + NM (35MPa)		10333.5	4.2

¹ The modulus of elasticity values used in the model were the values measured in the laboratory divided by 3 in order to consider the coupling ASR/creep effects.

11.4.4.1 Cement paste porosity and porous zone of thickness t_c

The cement paste porosity is likely to change as a function of the concrete strength. Higher strength concretes are supposed to present less porosity [31]. Likewise, one could think that it is logical to assume that t_c would change as a function of the bulk concrete porosity, as well as of the aggregate types (sizes, shape, texture, surface hardness, etc.). Therefore, these two unknown variables are linked and two assumptions for their choice are possible:

- The use of different (and realistic) concrete porosities as a function of the concrete strength (i.e. 14%, 15% and 16% for 45, 35 and 25 MPa mixes, respectively [31]), and the t_c adoption through expansion curves fitting;
- The use of a unique porosity value for all mixtures (i.e. 15%), with the possibility of choosing t_c through expansion curves fitting. This choice would very likely contribute at overestimating/underestimating t_c values, but at least the final analysis would be simplified and the results would be a function of only one unknown variable.

In this work, the second assumption was adopted (cement paste porosity for all concrete mixtures as being 15% and t_c ranging as a function of the expansion curves fitting).

11.4.4.2 Alkalis diffusion (D_{agg}) and fixation (F) in the aggregate particles

The diffusion (D_{agg}) and fixation (F) coefficients are difficult to obtain in the laboratory, specially the second parameter, which can represent the aggregate reactivity. They are supposed to change depending on the aggregate type (i.e. mineral components, contents and porosity, etc.). In this work, neither of the above two parameters were measured in the laboratory. However, the diffusion coefficient (D_{agg}) was chosen to present realistic values according to data presented in the literature [32]. Therefore, the D_{agg} value of $4.0 \text{ E-}13 \text{ m}^2/\text{s}$ was adopted for all the aggregates, leaving the fitting being necessary dependent on F values. As for t_c approach, this choice would very likely overestimating/underestimating F values, but the final analysis would be simplified, being a function of just one unknown parameter (F).

11.4.4.3 The molar volume of ASR gel (V_{mgel}^m)

All the concrete mixtures were cast and stored in the same environment which makes logical to select the same molar volume of alkali silica gel (V_{mgel}^m) for all the concrete mixtures. Thus, knowing that V_{mgel}^m plays an important role in the amplitude of ASR, an initial parametric

study was carried out in order to find out the V_{gel}^m value able to allow the fitting of all the measures made in the laboratory [1]. Thereby, the value of $0.49E-4 \text{ m}^3/\text{mol}$ was considered realistic to meet all the mixtures behavior in the laboratory [1].

Once the full description of each concrete mixture was made and regarding the assumptions made over the three previous points, the micromodel was run to obtain the two last parameters, which were not “measurable” in the laboratory (“F” – controlling ASR kinetics and “ t_c ” – controlling ASR amplitude) throughout the analysis of the measured “expansion vs. time” curves of the mixes.

11.5 RESULTS

11.5.1 Expansion vs. time plots: part I – for different NM aggregate sizes and combinations

The aim of the first part of the study was to analyze the capability of the model to reproduce the expansion of concrete containing the NM reactive sand only, NM reactive coarse aggregate or the two aggregates together. Figure 6 presents the expansion against time plots measured in the laboratory for the different NM aggregate size fractions and combinations used in this work. The figure clearly highlights three different ASR kinetics when NM reactive aggregate material is used as: 1) coarse aggregate (square symbol); 2) manufactured fine aggregate (triangle symbol); and 3) both fine and coarse aggregates (circle symbol). The lines represent the fitted curves obtained by the model. The above data shows that using NM as coarse or fine aggregate completely changed both ASR kinetics and the amplitude of the expansion. When NM is used just as coarse aggregate, ASR kinetics is slower and the final amplitude is lower than the mixtures incorporating fine NM particles (i.e. sand particles). When NM is used as both fine and coarse aggregates, the expansion kinetics lies in between the two other behaviors. As a consequence, the expansion measured on the concrete containing the two sizes of reactive aggregates was not the “sum” of the two individual expansions measured on concretes containing only one reactive aggregate size. This phenomenon can likely be explained by the competition in the alkali consumption by the aggregates or, in other words, the dilution effect where alkalis are spread over a much larger number of reactive sites when both coarse and fine NM aggregate particles are used.

Regarding Figure 6, the model is able to reproduce the expansion curves reached by NM mixtures, with only one set of t_c and F parameters ($t_c = 8 \text{ } \mu\text{m}$ and $F = 2.2e-7 \text{ m}^3/\text{m}^3/\text{s}$).

Moreover, the value chosen for t_c was considered realistic as higher porosity zones have already been identified in the first 20 μm around aggregate particles [33].

For ASR amplitude, it is important to notice that the differences observed on the expansions measured between reactive sands and reactive coarse aggregates are obtained using the calculations with the empirical relationship determined in Gao's analysis [21]. In this previous work, it has been shown that ASR expansion amplitudes were modified by the ratio aggregates/specimens' size. Therefore, the authors found that the largest aggregate sizes showed the lowest expansions when the specimen sizes are too small [21]. This effect was modified by the silica content of the reactive aggregates. In the present paper, this relation has been rewritten according to the *reactive aggregate's fractions* rather than according to the *reactive silica content* to obtain a dimensionless relation in the exponential function. The same relation between the volume of gel produced by the reaction and the effective volume of gel necessary to generate pressure can thus be read:

$$V_a^{eff} = \langle V_a^{gel} - V_a^{poro} \rangle^+ \times \left[\exp \left(-c \frac{2R_a}{L} (\phi_s)^x \right) \right]$$

with:

V_a^{poro} : the volume of the connected porosity which accommodates a part of the ASR gel;

ϕ_s : the reactive fraction of aggregate in mass percent, χ , is equal to 0.75 as explained in [21], and c is equal to 113. The difference in the c value, compared to [21], is only due to the modification of the relation form previously stated; however, it corresponds to the value determined in Gao's experiments [21].

If the model was able to obtain an interesting assessment of the final expansion and thus of the competition between aggregate sizes, the kinetics of expansion was quite rapid for the two concretes containing coarse aggregates, i.e. NM + Lav and NM + NMs (Figure 6). However, the difference between model and experiment is highlighted only at the beginning of ASR expansion.

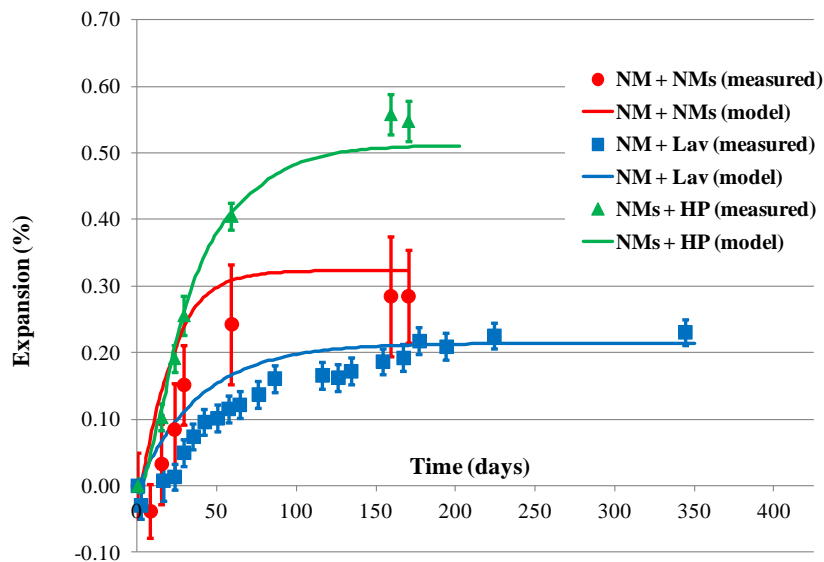


Figure 6: Expansion vs. time plots measured in the laboratory for different concrete mixes incorporating NM gravel as coarse aggregate, manufactured sand, or even both coarse and sand together.

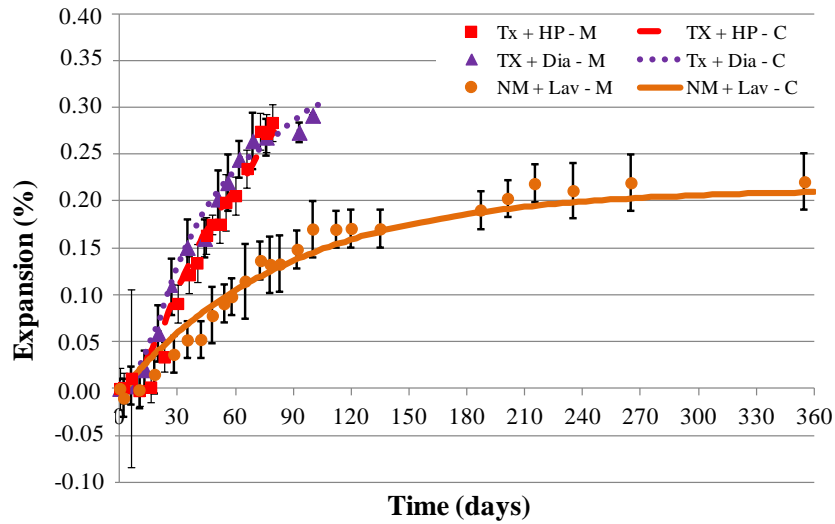
11.5.2 Expansion vs. time plots: part II – for different concrete strengths and reactive aggregates

Figure 7 presents the expansion plotted against time for all nine concrete mixtures with different reactive aggregates and strengths. The plots were divided according to the three different concrete types (i.e. different strengths) studied and the mixtures acronyms are as follows: Mixture name "M" (which means data measured in the laboratory and represented by points with error bars – one standard deviation on each point side of the data points) and Mixture name "C" (which means data calculated from the model and represented by the plain curves).

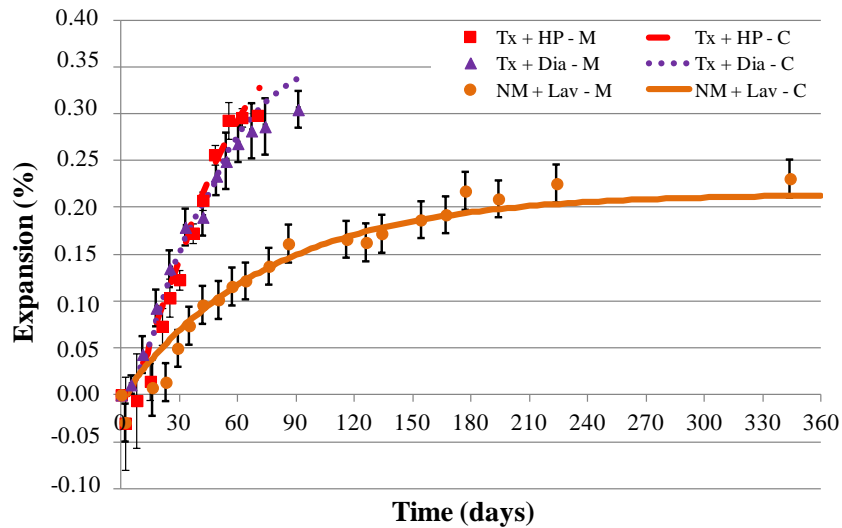
Two different ASR kinetics can be seen in the above graphs, i.e. 1) ASR generated from Tx reactive sand, which is faster and presents a more “linear” expansion curve to reach the maximum expansion value selected as a function of time (this phenomenon likely happened because ASR expansion was stopped at 0.30%; probably the curve shape would be different – i.e. concave shape - whether higher expansion levels were chosen for analysis and thus all (or most) of the silica content of the reactive aggregates was used); and 2) ASR coming from a reactive NM coarse aggregate, which is slower and presents a more concave expansion curve. These results were found for the three concrete strength types assessed.

Regarding ASR coming from the reactive Tx sand, one verifies that it is quite difficult to distinguish the curves for the mixtures incorporating the coarse aggregate HP from those incorporating the coarse aggregate Dia; this means that the expansion behavior over time for those two mixes did not change depending on the nonreactive coarse aggregate characteristics. Considering the differences in concrete strength, normally the greater is the concrete strength (and thus the alkalis content per m³ of concrete due to the higher cement dosage) the faster would likely be the ASR kinetics. However, this was not observed for the concrete mixtures studied, where quite close results were found for all mixes. All the nine concrete mixtures were very well “fitted” by the model in terms of both ASR kinetics and amplitude, except maybe NM + Lav 45 MPa mixture for the middle part of the expansion curve. As discussed previously, ASR kinetics and amplitude fitting was mostly made by the description of two parameters: t_c and F. The F parameter was adopted according to the aggregate type and t_c was determined according to the aggregate type and the quality of the cement paste. In this part of the work, the objective was to obtain the *best fitting* for each expansion curve in order to discuss the efficiency of the mechanical part of the model to obtain a good assessment of distressed concrete from expansion curve fitting. With this objective, the parameters t_c and F were adjusted to obtain an interesting fitting for concretes containing NM coarse aggregate disregarding the concretes containing NM sand, as it was performed in the previous part. This explains the differences in the selected parameters, which will be discussed in the Section 6. Table 7 demonstrates the values chosen for each concrete mixture and strength.

A- 25 MPa mixtures



B- 35 MPa mixtures



C- 45 MPa mixtures

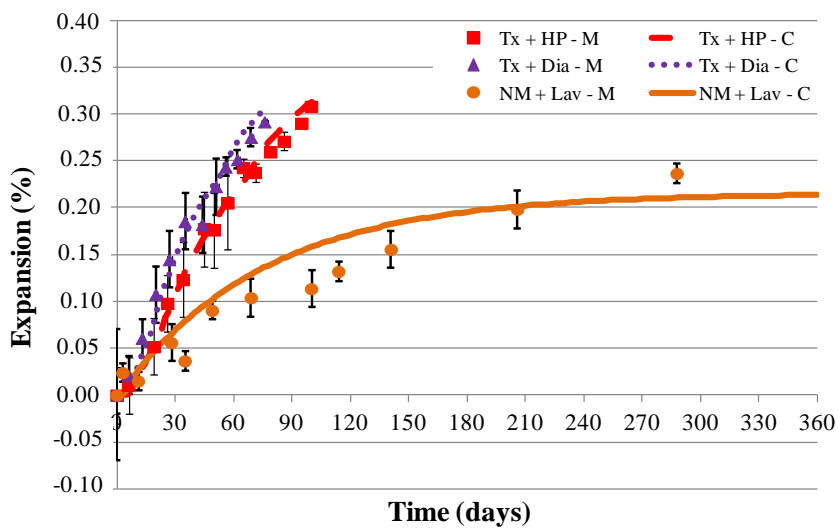


Figure 7: Expansion vs. time plots for all the concrete strengths and aggregates combinations.

Table 7: Physical parameters chosen for the concrete mixtures and strengths.

Concrete mixture	F (m ³ /m ³ /s)	t _c (meters)
Tx + HP, 25 MPa	1.4E-7	0.0120E-3
Tx + HP, 35 MPa	1.4E-7	0.0100E-3
Tx + HP, 45 MPa	1.4E-7	0.0100E-3
Tx + Dia, 25 MPa	1.4E-7	0.0120E-3
Tx + Dia, 35 MPa	1.4E-7	0.0100E-3
Tx + Dia, 45 MPa	1.4E-7	0.0100E-3
NM + Lav, 25 MPa	0.8E-7	0.0080E-3
NM + Lav, 35 MPa	0.8E-7	0.0080E-3
NM + Lav, 45 MPa	0.8E-7	0.0080E-3

11.5.3 Damage vs. expansion plots: part II - different concrete strengths and reactive aggregates

Figure 8 illustrates the results of the damage factor “d” against expansion plots obtained through both laboratory measurements and LMDC model predictions for all the eight concrete mixtures made for the study part II. The damage factor is defined as follows:

$$d_i = 1 - (E_i / E_o)$$

where:

E_i: a mechanical property of the affected concrete, for example the modulus of elasticity (E), at a given time i;

E₀: the same mechanical property of the sound concrete (i.e. at 28 days).

First of all, it is interesting to review the damage process over the model proposed. In the model, it is supposed that cracks are generated when the tensile stresses overcome the tensile strength of the concrete material, thus causing the concrete damage, which means its modulus of elasticity reduction. However, even though the damage is calculated in terms of the stiffness loss, as the model is adopted as being a concrete hollow sphere (reactive aggregate) that applies an internal amount of pressure on a surrounding undamaged concrete (Figure 2), it appears that the damage factor (d) would still be better represented by the modulus of elasticity loss “in tension” or even the tensile strength loss of the distressed material. However, it has been found that the modulus of elasticity in compression is similar to the modulus of elasticity of sound concretes in tension [34]. Therefore, even though this behavior would not possibly be the same for damaged concretes, it was decided to verify the model’s

damage factor (d) with both parameters, even if the crack opening due to ASR expansion could have greater consequences in tension than in compression.

The graphs in Figure 8 suggest that over the expansion levels studied, the tensile strength losses measured in the laboratory reached values of $\approx 70\%$, whereas the modulus of elasticity reached losses of $\approx 65\%$ for the different mixes. Actually, the damaged values for both the modulus of elasticity in compression and the tensile strength presented fairly close results for the majority of the mixes, depending on the concrete characteristics (i.e. concrete strength and aggregate type). On the other hand, the modulus of elasticity distress seems to demonstrate an increasing trend as a function of increasing expansion, while the tensile strength loss seems to be more important for low expansion levels than for higher levels.

The model damage factor (d) also presented an increasing trend with increasing expansion for all concrete mixtures, as expected. The values found ranged between 70% up to 80% for the mixes. Overall, the model predicted quite well the losses of both modulus of elasticity and the tensile strength for low expansion levels (i.e. up to 0.12%). For higher expansions, the model damage factor against expansion curve kept showing and increasing trend while the laboratory test results presented either a lower increasing trend or a stagnation distress pattern for both properties.

Figure 9 presents the results of the plots of the compression damage factor (d_c) against expansion for all the concrete mixtures and strengths. It is known that concrete damage mechanisms in tension and compression are quite different. Thus, the model damage factor (d) cannot be directly converted into compression damage factor. However, Sellier and Bary [35] have proposed an equation to calculate the compression damage factor (d_c) from the tension damage (d_t) [35]:

$$d_c = 1 - (1 - d_t)^{0.15}$$

This relation has been used in this study to evaluate the damage in compression from the damage in tension. Based on the above relationship, the experimental data showed compression damage ranging between 10 and 20%. Likewise, the LMDC model results predicted compressive strength losses of about 20% for all mixtures, which can be considered to agree with the experimental results.

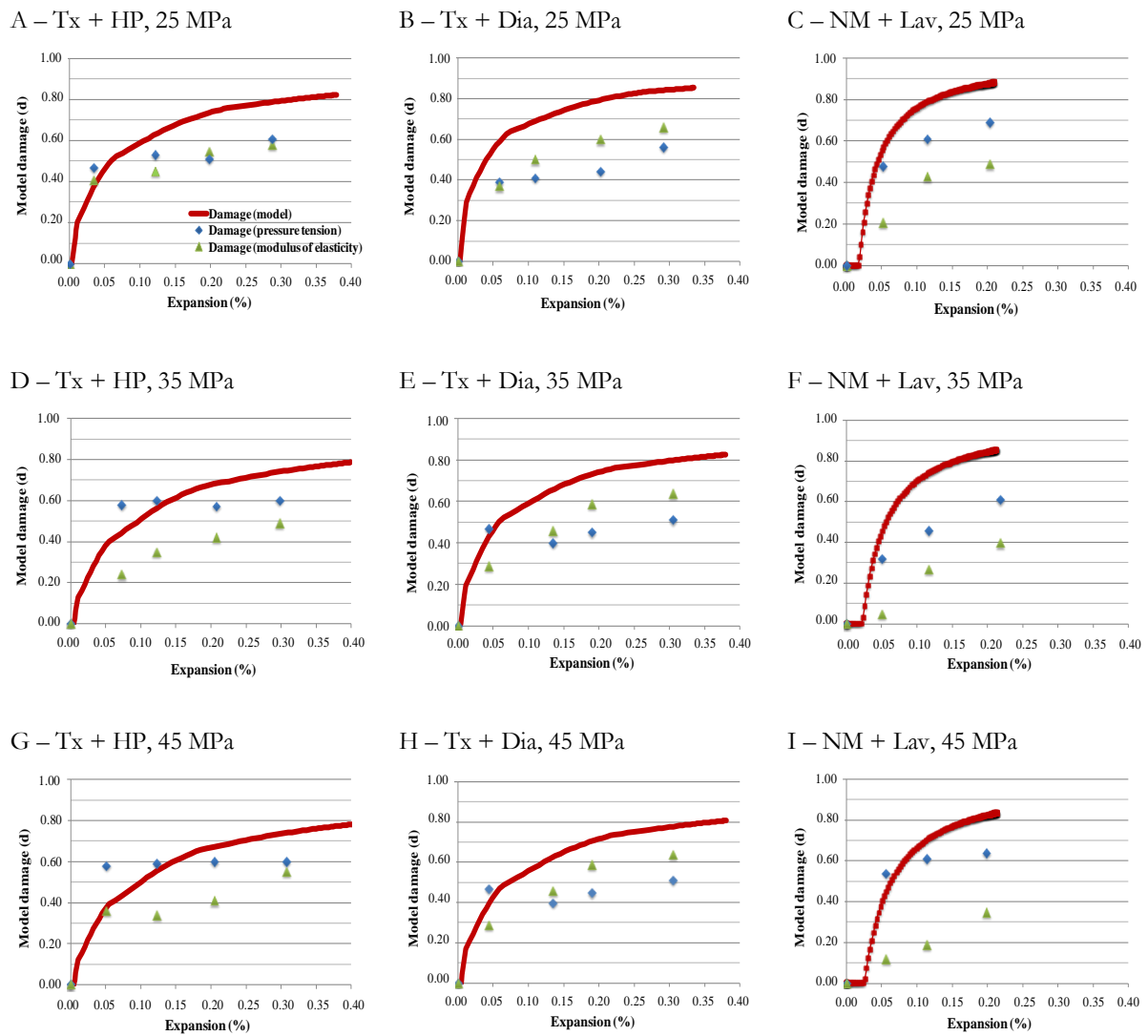
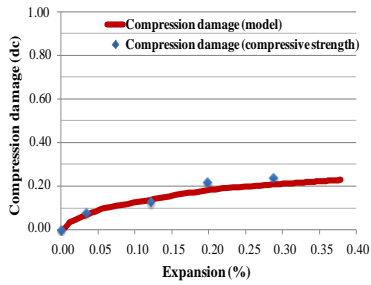
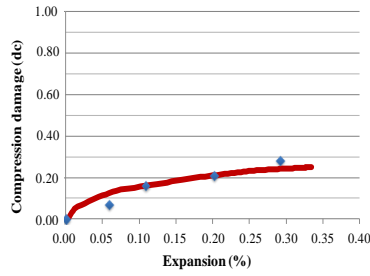


Figure 8: Model damage (modulus of elasticity and tensile strength losses) vs. expansion plots for all the concrete mixtures and aggregates.

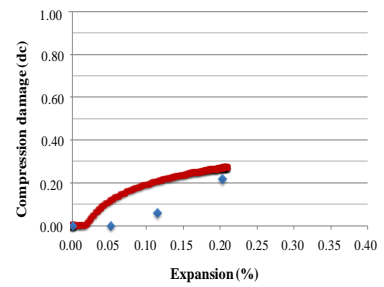
A – Tx + HP, 25 MPa



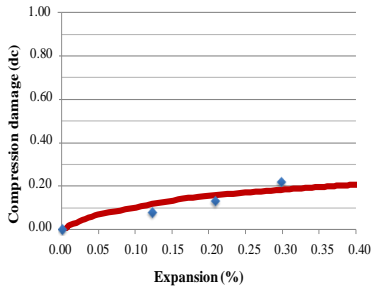
B – Tx + Dia, 25 MPa



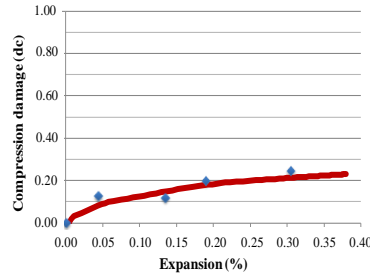
C – NM + Lav, 25 MPa



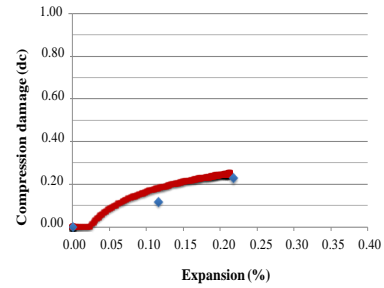
D – Tx + HP, 35 MPa



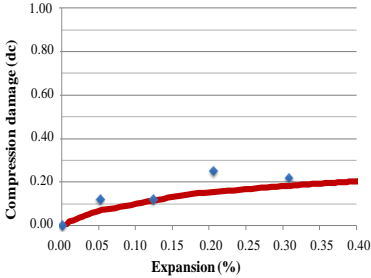
E – Tx + Dia, 35 MPa



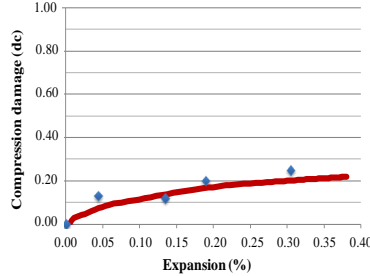
F – NM + Lav, 35 MPa



G – Tx + HP, 45 MPa



H – Tx + Dia, 45 MPa



I – NM + Lav, 45 MPa

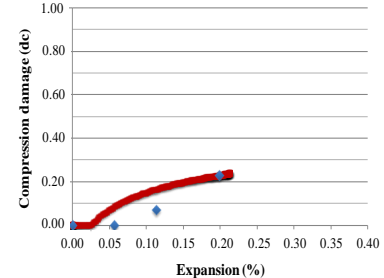


Figure 9: Compression damage factor (dc) vs. expansion plots for all the concrete mixtures and aggregates.

11.6 DISCUSSION

In this study, the LMDC (*Laboratoire des Matériaux et Durabilité des Constructions*) chemo-mechanical model was used to assess and predict expansion and damage due to ASR in test specimens cast from eleven concrete mixtures of different strengths and incorporating different reactive aggregates.

Overall, the results obtained for the part II study for both damage and expansion levels were considered fairly satisfactory, yet further results discussion is made in this section. Likewise, part I study shows that the model is able to reproduce/simulate the expansion amplitude for concrete containing reactive sand and/or coarse aggregate with the same set of parameters; however the differences of initial kinetics between the measurements and the calculations

suggest that it could be interesting to use different input parameters of the chemo-mechanical model (particularly t_c and F) to obtain a better representation of all the expansion kinetics.

11.6.1 ASR development and expansion predictions

In the LMDC model, the alkali concentration is assumed to be uniform in the cement paste. In addition, the aggregates are taken as spherical and of uniform pore structure characteristics over their entire volume. Thus, the concentration of the ionic species and their distribution within the aggregate particle are considered to depend only on time and on the radius r from the center of the reactive aggregate particle (Figure 10). Moreover, the LMDC model assumes that the rate of gel formation is proportional to the alkali concentration in the aggregate particles. In the model, ASR development rate represents the following concepts at the same time: 1) the reactive silica attack; 2) the gel formation rate and; 3) the alkalis consumption by ASR gel. Thus, both ASR kinetics and gel formation (amplitude) are believed to be controlled by the reactive silica destruction due to the alkali diffusion. It is of course understood that the silica attack is mainly achieved by the hydroxyl ions, with the alkalis associated to the process. Also, this model does not consider the role of calcium in the gel formation [1].

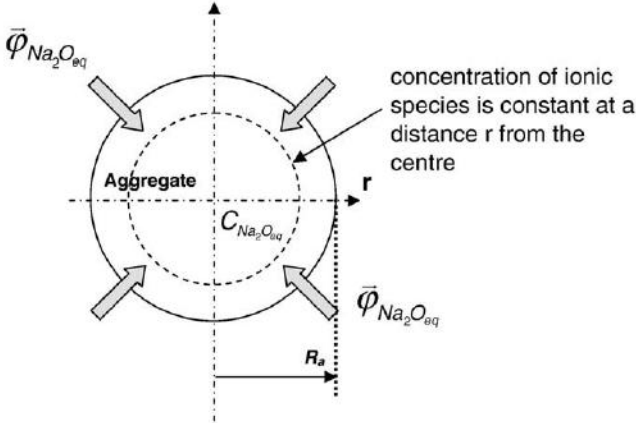


Figure 10: Diffusion of alkali ions in the aggregate particles [1].

In terms of kinetics, the LMDC model is led by the alkali diffusion into the aggregate particles and the dissolution of the reactive silica. In terms of amplitude, the model takes into account the gel composition (which Na_2O/SiO_2 ratio varies mainly from 0.1 up to 0.4; the average value of 0.2 is adopted in this study), the gel volume produced (which is the sum of

the gel volume produced by each of the REV aggregate particles [1]. After formation, ASR gel can either penetrate into the pore volume of the cementitious matrix surrounding the aggregate particle or remain in the aggregate cracks. The connected porosity is modeled as a porosity volume completely filled by ASR gel with an equivalent thickness “ t_c ”, which is assumed not to change as a function of the relative size of the aggregate. Thus, the larger is the aggregate size, the smaller is the "connected pore volume/ aggregate volume" ratio. Therefore, larger aggregates present ultimate major expansion levels [1].

In this work, as discussed previously, the model “fitting” depended on some parameters, mainly F and t_c , which set ASR kinetics and amplitude, respectively. These parameters were adopted according to both the expansions measured in the laboratory and assumptions made before running the model (section 4.4).

Fairly realistic behavior was also found for the part I study (Figure 6), where the three concrete mixtures incorporating the reactive NM as manufactured sand (NM + HP), coarse aggregate (NM + Lav), and both together (NM + NM) were assessed. Figure 6 showed that the three concrete mixtures are quite well fitted using the same set of F and t_c values. Overall, the results of this study part showed that the smaller the NM aggregate particle size, the larger and faster was ASR expansion. Moreover, when NM was used as both coarse and fine aggregates, the results were in between those obtained when NM was used just as a manufactured sand (the fastest and highest reactive behavior) or coarse aggregate (the slowest and lowest reactive behavior), showing the likely presence of a “competition” between ASR coming from the fine and coarse aggregate particles. Therefore, the model was able to reproduce the differences in amplitude and thus the competition between aggregates of different sizes but the initial kinetics was not well-described. The differences in kinetics can likely be explained by the following two topics:

- *Aggregates crushing/grinding*: The aggregates crushing/grinding may play a significant role on ASR expansion. This procedure generally increases their reactivity and can actually change the aggregate’s composition, thus potentially increasing/ decreasing their reactivity [36]. This phenomenon is logic to happen, especially in the case of heterogeneous aggregates such as the NM aggregate. Beyond that, the silica content measurement that is used as an input model parameter (in mol/m³ of aggregate), is made throughout the aggregates crushing/grinding operations, which could distort the “real” amount of silica one finds for coarse aggregates of similar nature, yet misleading the model results [17-22];
- *Concrete alkali leaching*: It is clear that alkali leaching from concrete specimens can decrease ASR expansion over the concrete prism test [18, 19, 37 and 38]. However, this

phenomenon is not taken into account in the LMDC model, which does not consider the movement of alkalis towards the external environment of the REV (future works could consider this effect by coupling this model with finite elements analysis). This leaching effect could partially explain why coarse aggregates presented less expansion than fine aggregates, as the available alkalis take more time to reach and react with the reactive silica inside the coarse aggregate particles and thus an important amount of alkalis can be leached due to diffusion effects outside the concrete specimens. Otherwise, this phenomenon is less important for smaller particles when the reactive silica is reached faster and ASR gel is formed before alkalis leaching takes place in a significant manner.

These two previous phenomena can be taken into account with a modification of F and t_c in order to obtain a better fitting of the expansion curves for the concrete mixtures containing only the reactive sand or only the reactive coarse aggregate used in the study part I. Figure 11 shows the curves fitting and Table 8 illustrates the parameters chosen. It appears from the above data that when NM is used as a fine aggregate (Figure 11), the alkali fixation F is higher, which means that the reaction is faster, which can also explain the kinetics differences for the mixtures and supports the increase of reactivity due to crushing. Moreover, the F value necessary to fit the expansion curve was about 2 times greater than the F value used for NM as a reactive coarse aggregate (Figure 11). On the other hand, the modification in t_c value for NM as a reactive coarse aggregate was small. The little modification can be partly linked to the improvement of the quality of the aggregate texture achieved after crushing process (as NM is a gravel) and by the modification of “wall effects” that happens between the aggregate and cement particles due to their smaller size [31].

The simulation of the expansion kinetics and amplitude of the concrete specimens incorporating NM as coarse and fine aggregates was then obtained, *without supplementary fitting*, when the same parameters discussed previously were chosen for respectively the fine and coarse aggregates in the mixture (taking into account their amounts at each size - Figure 11). It can be observed by comparing Figures 6 and 11 that a better fitting of the expansion of concretes containing only the reactive sand and only the reactive coarse aggregate does not allow a better prediction of concretes containing the two reactive aggregates together. This problem of prediction can be explained by the difficulty to obtain a good assessment of the “scale effect” in the case of concretes incorporating different reactive aggregate types (i.e. fine and coarse aggregates). The relation proposed by Gao et al. [21] to assess this effect was obtained on mortars containing just one reactive aggregate size. The “scale effect” over the expansions due to each aggregate’s size is thus considered separately for each reactive

aggregate type. This is a physical effect that has not been tested yet and for such cases, interactions between the aggregate types (i.e. interactions between the different aggregate sizes) are expected. Therefore, these interactions could maybe cause smaller expansions for concretes incorporating both reactive aggregate types (sand and coarse) instead of just a reactive sand. Therefore, this is one of the main points for which micro chemo mechanical modeling must be improved: the consideration of the scale effect due to the ratio ‘specimen size / aggregate size’ and particularly when interactions between aggregates of different sizes occurs. With this objective, new experimental works should be performed to obtain a better understanding of this phenomenon.

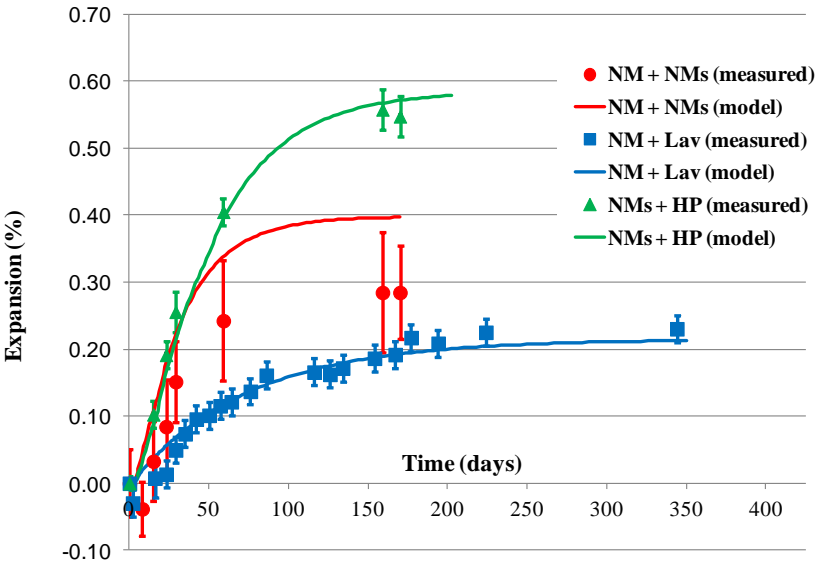


Figure 11: Parametric study for the part I study fitting. NM as sand; NM as coarse aggregate and NM as both sand and coarse aggregate mixed together.

Table 8: Physical parameters chosen for the different NM mixtures.

Concrete mixture	F (m ³ /m ³ /s)	t _c (meters)
NM + HP 35 MPa	1.5E-7	0.006E-3
NM + Lav 35 MPa	0.8E-7	0.008E-3
NM + NM 35 MPa	1.5E-7 / 0.8E-7	0.006E-3 / 0.008E-3

For the part II of the study, F parameters were adopted according to the aggregate type and t_c parameters were determined as a function of both the aggregate types and the cement paste quality (Table 7). Through the results of the nine concrete mixtures, all the expansions plots were well simulated by LMDC model (Figure 7). The values of F lie between 0.8E-7 and 1.4E-7 m³/m³/s, which is a narrow interval and present few differences for all the mixes

studied in this paper (Table 6). The values of t_c lie between 8 and 12 μm for all the concretes (Table 7). It is interesting to notice that the differences found were small. Moreover, the concrete with the smallest strength (and thus probably the greater porosity) presented always the greatest t_c , which was expected.

11.6.2 Model assumptions vs. microscopic observations

The models proposed by Furusawa et al. [6]; Nielsen et al. [5]; Suwito et al. [8] and Poyet et al. [7], as well as the LMDC model proposed by Multon et al. 2009 [1], all consider that the main cause of distress due to ASR is a consequence of ASR gel pressure generated once it fills a porous zone surrounding reactive aggregate particles, thus applying stresses on the cement paste (Figure 12). However, the above authors did not consider, at least in their model calculus, the development/consequences of cracking in the aggregate particles, although [1] have cited that some cracks “are likely to be found in the aggregates” as part of ASR development.

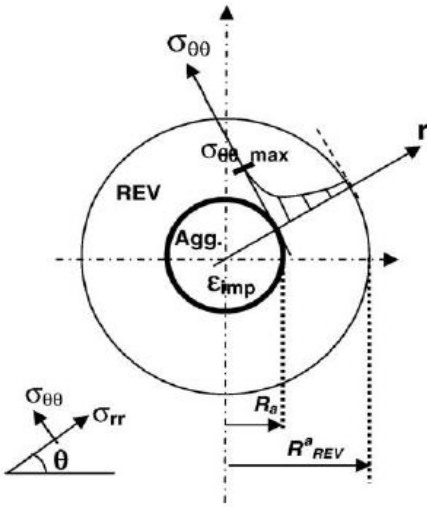


Figure 12: Major stress found in R.E.V. due to ASR expansion [1].

On the other hand, Dunant and Scrivener [4] and Ben Haha et al. [39] observed the presence of a huge amount of cracks inside the aggregates particles according to microscopic and macroscopic observations. They support the hypothesis that damage begins with a gel pocket formation inside the aggregates, before causing cement paste cracking. This statement confronts the LMDC model assumption. Sanchez [40] and Pleau et al. [41] found that either the macroscopic expansion or the “damage” in concrete affected by ASR are strongly related to the microstructural location of cracks. Thus, predicting the expansion and progress of this

harmful chemical reaction is only possible for models whose prediction takes into account the damage consequences at microstructural levels [4, 39]. Figure 13 illustrates three damage mechanisms already adopted in the literature to characterize ASR distress.

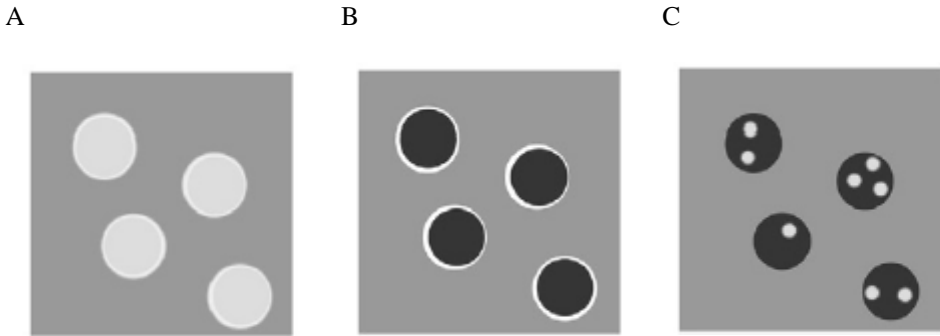
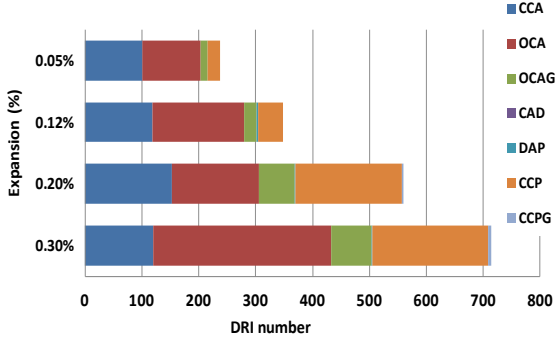


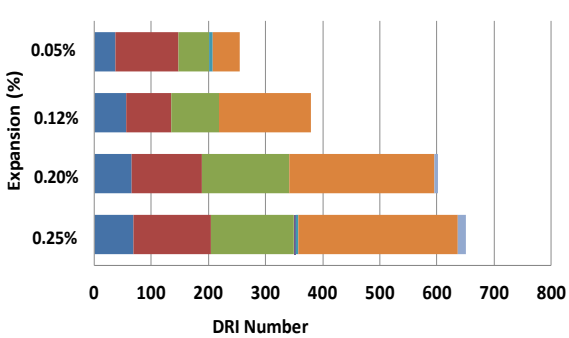
Figure 13: Models used to develop the damage by the RAG: A. expansion of the aggregate particles, B. expansion of the reaction rims and C. expansion of the gel-filled pockets in aggregate particles [4].

Sanchez [40], dealing with the same concrete used in the model over this research, highlighted the presence of a large number of cracks (closed (CCA) and opened (OCA and OCAG) with and without gel, respectively – Figures 4 and 14) inside the aggregate particles for ASR generated either from a reactive sand (i.e. Tx sand) or a reactive coarse aggregate (i.e. NM gravel) and for two compressive strength types (25 and 35 MPa mixtures). The authors performed the *Damage Rating Index (DRI)* method over a wide range of expansion levels and the results are illustrated in Figure 14.

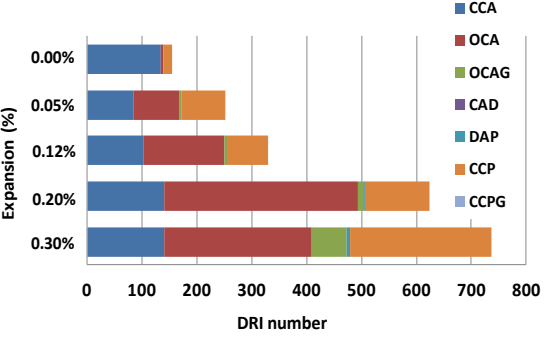
A. DRI, Tx + HP, 25 MPa



B. DRI, NM + Lav, 25 MPa



C. DRI, Tx + HP, 35 MPa



D. DRI, NM + Lav, 35 MPa

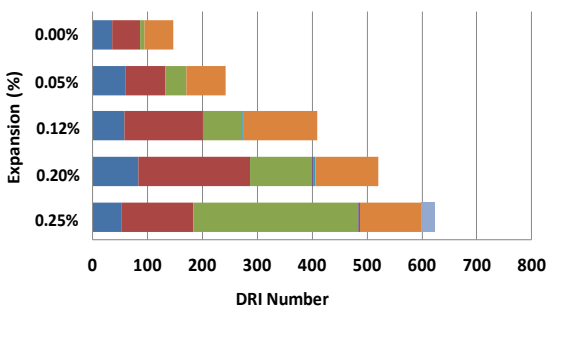


Figure 14: DRI values for 25 and 35 MPa concrete specimens incorporating the Tx sand (A & C) and NM gravel (B & D) [40].

According to Figure 14, the counts for *opened cracks* (with (OCAG) and without (OCA) gel) increases with increasing expansion level for all the specimens and concrete mixtures. Sanchez [40] observed that those cracks generally appear inside the reactive aggregate particles (sand or coarse aggregate) already at low expansion levels (i.e. 0.05%); and when the expansion increases ($\approx 0.12\%$), the cracks also increase in length and width and some of them extend into cement paste [40]. As the expansion level increases further again ($\approx 0.20\%$ or larger), most of the cracks formed inside the aggregate particles already extended into the cement paste, which increased the overall crack density (units/cm²) of the distressed specimens. Afterwards, by about 0.30% of expansion, the cement paste cracks are linked together, thus forming an extended network of cracking. Further analyses on the polished concrete specimens provided the distinction of two main general crack patterns due to ASR, whatever the chemical reaction comes from the sand or the coarse aggregate (Figure 15).

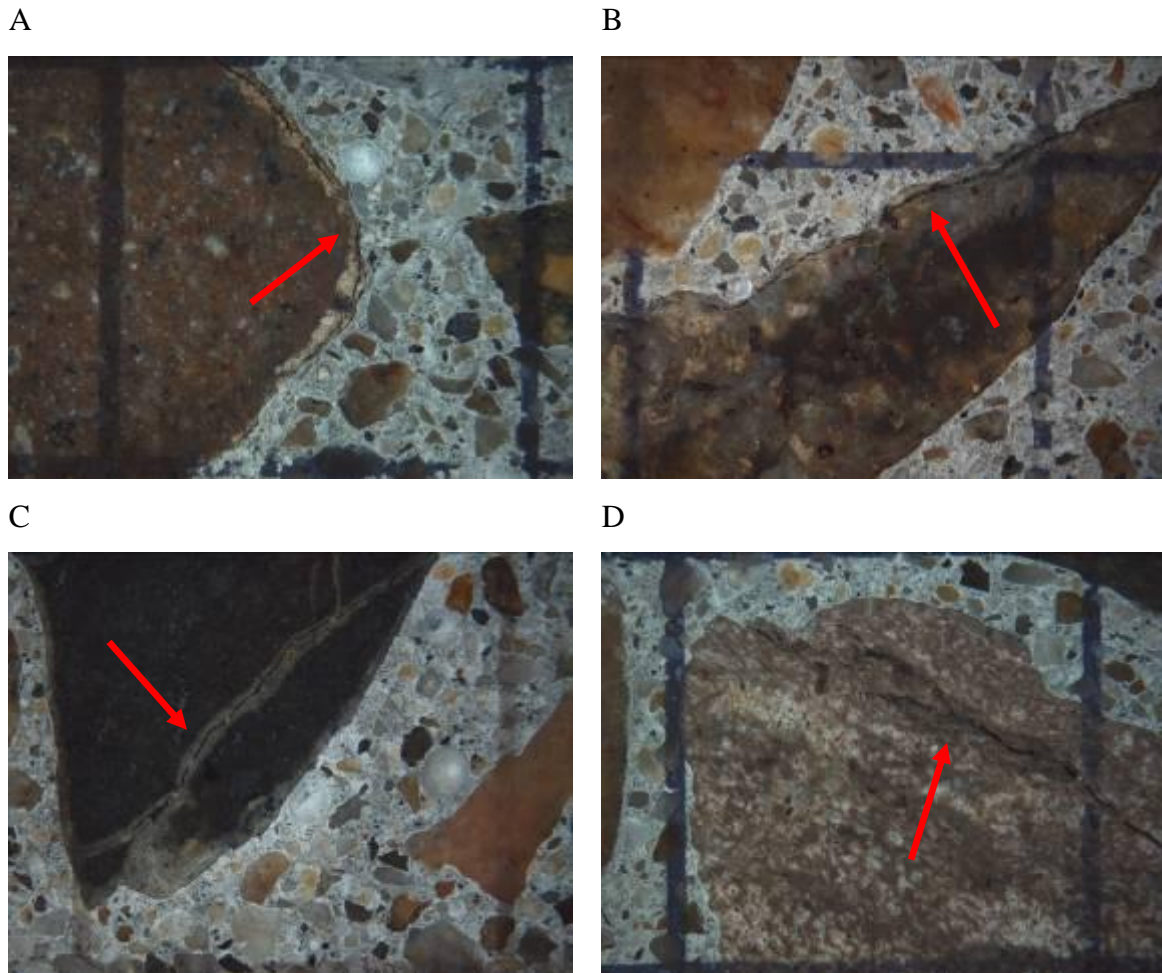


Figure 15: DRI damage features for 25 MPa concrete mixtures cast with NM aggregate for 0.20% and 0.25% expansions. A, B. onion skin cracks in the aggregates; C, D. sharp cracks inside the aggregates [40]. The distance between the vertical lines is equal to 1 cm.

The cracks that developed in the outer portions of the aggregate particles, or the “onion skin” cracks, (Figure 15A and 15B) are likely developing within aggregate particles which do not present preexisting cracked/weak zones (or even pores/defects) that facilitates the penetration of alkalis from the concrete pore solution. Thus, the alkali diffusion would be quite homogeneous towards the internal part of the aggregate particles, thus preferentially forming an almost peripheral cracking pattern (i.e. parallel to the aggregate boundary). On the other hand, the “sharp” cracks present inside the aggregate particles (Figure 15 C and D), can often be caused by the existence of weak/cracked/more porous zones in the aggregate particles, or layering/bedding in the case of sedimentary rocks, that would either facilitate the alkalis diffusion or even be damaged earlier when ASR occurs. It has been found that both crack types will reach the cement paste at a given expansion level; however, “sharp” cracks generally reach the cement paste earlier than “onion skin cracks” [40].

In fact, the assumptions made by the LMDC model could likely well explain the “onion skin” cracks (even though the model considers that ASR cracks are formed in the interfacial transition zone – ITZ – and does not take into account the effects of aggregate cracking) by the progressive alkali diffusion and thus by the progressive silica attack from the aggregate boundary down to the aggregate core. However, even though the model does not consider the crack formation inside the aggregate particles as a primary consequence of the ASR process, if one considers that all the cracks types in the aggregate particles would reach and cause damage in the bulk cement paste after a given expansion level, one verifies that the physical parameters of the model (alkali’s diffusion and fixation in the aggregate particles, cement and aggregates porosity and t_c of the cement paste) could be set in order to consider this phenomenon in an *indirect* way, which was confirmed through Figures 7, 8 and 9. Finally, it is good to mention that Sanchez [40] indicated the presence of minor cracks in the cement paste at the early stages of ASR expansion that were likely not linked to the cracks coming from the aggregate particles. According to [40], these cracks were possibly created due to shrinkage or creep mechanisms, but could even be indirect effects caused by ASR, i.e. zones in the cement paste which achieved important stresses concentration due to the bulk ASR pressure.

11.6.3 Damage results

11.6.3.1 Overall LMDC model data

Globally, the LMDC model was fairly effective in predicting ASR damage in nine different concrete mixtures presenting different strengths (25, 35 and 45 MPa) and reactive aggregate types (fine vs. coarse aggregate). In terms of tension damage responses, comparing the results obtained by the model (i.e. d factor) with the results measured in laboratory (through the gas pressure procedure), one verifies that the model predicted well the tensile losses for low and average expansion levels (up to $\approx 0.10\%$). For larger expansion levels (from $\approx 0.10\%$ up to 0.30%), the results obtained in the laboratory almost stabilized while the model distress kept increasing. This phenomenon could be explained by two possible causes:

- Experimental failures/bias in the laboratory data (i.e. results over the gas pressure test) or the difficulty of the above method of measuring realistic values for tensile strengths of concretes especially for concrete damaged by ASR with the presence of connected or unconnected cracks due to expansion;

- Or because in reality, concretes (cement paste, ITZ and aggregates) are rapidly affected (i.e. mechanically) by ASR in the early stages of the chemical reaction and the rate of increasing damage slows down at higher expansion levels (which can be found in the literature for the modulus of elasticity or even the splitting or direct tension tests [42-43]). Thereby, for larger expansions, the cracks already opened in the beginning of ASR would keep growing (in length and width) instead of having the formation of new cracks, which would result in a reduction in the rate of mechanical properties losses due to fracture mechanic issues; on the other hand, the LMDC model is based on the increase of the cracks number as a function of ASR development. Moreover, the model does not take into consideration the cracks length and width (i.e. assuming a continuous diffuse distress). However, according to microscopic observations [40], it was found that both the number of cracks and their length and width increase as ASR develops. Therefore, this phenomenon could likely have an effect on the model tension damage prediction.

For the compression damage factor d_c , a different behavior is observed: i.e. a quite good relationship with the laboratory results for higher expansions and a slightly weaker correlation for low expansions. This can be explained since, in the beginning of ASR, cracks are mainly formed within the aggregate particles (Figure 14) and just a few distress features are found in the cement paste [40]. This confirms why ASR-distressed concrete material largely maintains its total capacity in compression. On the other hand, for higher expansion levels, the cracks in the aggregate particles reach the bulk cement paste, causing the compressive strength loss.

11.6.3.2 Effect of the concrete mixture design

The data presented in the Figure 8 indicate that, despite some inherent variability in the test results, the greater is the design compressive strength of a distressed material, the earlier it gets distressed in tension due to ASR. On the other hand, the behavior of the modulus of elasticity loss is the opposite (i.e. the greater the design compressive strength, the longer the time for the material to get distressed). Moreover, it seems that the final distress results for both the tension damage and the modulus of elasticity loss are not influenced by the concrete strength, as all the concrete mixtures lost at the highest expansion level between $\approx 55\%$ and 70% for these two different mechanical properties.

Another interesting behavior showed in Figure 8 can be found when the character of the non-reactive coarse aggregate is analyzed for ASR coming from the Tx sand. The results indicate that for the Tx + HP mixtures, i.e. when a non-reactive limestone is used as a coarse

aggregate, the tensile strength losses are more important than the modulus of elasticity losses. On the other hand, for Tx + Dia mixtures, the losses in the modulus of elasticity are greater than the tensile strength losses. These results can possibly be explained by toughness differences in the rock material used for aggregates (K_c), where HP limestone displays lower toughness characteristics than Dia diabase (i.e. HP theoretical average toughness (K_c) – 2.23 MN/m^{1.5}; Dia theoretical average toughness (K_c) – .49 MN/m^{1.5}) [30].

Regarding the model results, the damage factor d shows a progressively increasing behavior vs. time as discussed in 6.3.1, while the measured test values tend to present a sharper loss behavior in the beginning of ASR, being overestimated by the predicted model values for higher expansions levels.

11.6.3.3 Effect of the type of reaction - fine vs. coarse reactive aggregates

The data presented in Figure 8 also illustrate the different damage behaviors between ASR coming from the fine reactive aggregates or the coarse reactive aggregates. The results suggest that, in terms of tensile strength loss, there are almost no differences for ASR coming from Tx vs. NM, neither in the beginning nor in the final loss value. However, the modulus of elasticity of the Tx mixtures decreases earlier than for the NM mixtures. These results can likely be explained by the faster kinetics when ASR is developing in the reactive sand. However, for higher expansion levels, NM and Tx values of modulus of elasticity damage are somewhat comparable. In all cases, the model is able to assess the compressive damage if expansion curves were first well obtained.

11.7 CONCLUSIONS

The main objective of the test program carried out in this study was to verify, discuss and validate the ASR chemo-mechanical model proposed by the LMDC (Laboratoire des Matériaux et Durabilité des Constructions), comparing the results obtained through the model with the results of various tests (expansion, compressive and tensile strength determination, semi-quantitative petrography), carried out in the laboratory, using reactive coarse and fine aggregates and different concrete mix designs (25, 35 and 45 MPa). The main conclusions of the above investigations are:

- Two different ASR kinetics were identified in this study: 1) when ASR comes from the reactive Tx sand (which is faster and presented a “linear” shape up to the highest

expansion chosen for this study, as a function of time) and; 2) ASR coming from the reactive NM gravel (which is slower and presented a more concave shape as a function of time). In general, the greater was the concrete strength and the alkalis content per m^3 of concrete, the faster was the development of ASR expansion for both Tx and NM mixtures;

- The most important physical parameters adopted in the model are the concrete porosity, the thickness of the porous zone surrounding the aggregate particles (t_c), the alkali diffusion (D_{agg}) and fixation (F) coefficients, as well as the molar volume of ASR gel (V_{gel}^m) produced through the reaction. These parameters have an important influence on both ASR kinetics and amplitude and need to be chosen carefully. In this research, V_{gel}^m , D_{agg} and the concrete porosity t_c were chosen to each have a unique value. Therefore, the setting of the expansion plots was carried out as a function of two parameters: F and t_c ;
- It has been found throughout microscopic analyses that the damage assumptions made by the LMDC model does not represent completely the distress features found under the microscope towards the different expansion levels assessed. The microscopic observations suggest that for low expansion levels (i.e. up to 0.05%), it is quite unusual to identify the presence of opened cracks in the cement paste and, when they are present, they are likely generated by other mechanisms of distress than ASR such as shrinkage, creep, etc. When the expansion level increases (i.e. up to $\approx 0.12\%$), the opened cracks formed inside the aggregate particles keep increasing in length and width and some of them reach the cement paste. For higher expansion levels (i.e. $\geq 0.20\%$), most of the opened cracks already extend into the cement paste, which largely increases the crack density (units/ cm^2) in the concrete matrix. Finally, at very high expansion levels ($\approx 0.30\%$), the cement paste cracks are likely to link to each other, thus forming an extended cracking network;
- Even though some assumptions in the LMDC model are different from the microscopic observations found, the results from the model could clearly fit the expansion behaviors and predict reasonably well the damage (compressive and tensile results) of the concrete mixtures studied. As a consequence, this model, which had been only used on mortars with small reactive aggregate particles, is effective to analyze expansion and damage of concrete with a large range of aggregate sizes. These results were achieved through the correct selection of some physical parameters in the model, some of them being difficult to measure in the laboratory. The F parameter changed as a function of the aggregate type (the values ranged from 0.8 and $2.2\text{E}-7$). The t_c changed according to the cement paste

quality and appears to be slightly affected by the aggregate particle size distribution. The values assumed in this paper could be used to estimate the expansion potential of concrete using the same aggregate in other mix design in same environmental conditions.

- The LMDC model could well distinguish the different ASR kinetics happened due to the aggregate sizes found in the three NM mixtures containing the NM as coarse aggregate, manufactured fine aggregate or both together. The amplitude of the expansion can be obtained with only one set of parameters but different parameters have to be adopted to obtain the initial expansion kinetics. This situation can be explained by the effect of three potential factors: the aggregates crushing procedure, the leaching of the concrete over the concrete prism test, and the differences in ITZ (or the interface connected porosity) according to aggregate size. At last, the model is able to evaluate fairly well the competition between aggregates of different sizes with only one set of parameters.
- The model predicts well the development of tensile damage for low and average expansion levels (i.e. up to $\approx 0.10\%$). For larger expansion levels (i.e. from $\approx 0.10\%$ up to 0.30%), the results obtained in the laboratory almost stabilized while the distress according to modeling kept increasing. These results can be explained through two possible assumptions: 1) limitation of the test method used (gas pressure testing) in properly highlighting differences in tensile properties of ASR-affected concrete and; 2) the model disregard to the length and opening of cracks with increasing ASR expansion (assuming a continuous diffuse distress).
- For the compressive damage, the modeling results are in good accordance with the laboratory test results for high expansion levels, while a slightly lower correlation for low expansions was found for concrete containing reactive coarse aggregate. This can likely be explained by the presence of cracks inside the aggregate particles for ASR low expansions (that are not taken into account in the model) which do not change the compressive capacity of the distressed material at low expansion levels.

11.8 ACKNOWLEDGEMENTS

The funding of this project was provided by a grant from the Quebec Department of Transportation, under the supervision of Mr. Alain Hovington and Mrs. Nadia Pouliot. The authors would like to thank Mr. René Malo and Mr. Mathieu Thomassin from “le Centre de recherche sur les infrastructures en béton (CRIB)” at Laval University, as well as the undergraduate research assistants who helped with the manufacturing and testing of the test

specimens used in this project. L. Sanchez benefits from a Vanier scholarship financed by NSERC (Natural Sciences and Engineering Research Council of Canada).

11.9 REFERENCES

- [1] Multon, S.; Sellier, A.; Cyr, M. 2009. Chemo–mechanical modeling for prediction of alkali silica reaction (ASR) expansion. *Cement and concrete research*, 39: 490-500.
- [2] Bazant, Z.P.; Steffens, A. 2000. Mathematical model for kinetics of alkali-silica reaction in concrete, *Cement and Concrete Research*, 30: 419–428.
- [3] Comby-Perot, I.; Bernard, F.; Bouchard, P.O.; Bay, F.; Garcia-Diaz, E. 2009. Development and validation of a 3D computational tool to describe concrete behaviour at mesoscale. Application to the alkali-silica reaction, *Computational Material Science*, 46 (4): 1163-1177.
- [4] Dunant, C.F.; Scrivener, K.L. 2010. Micro-mechanical modelling of alkali–silica-reaction induced degradation using the AMIE framework, *Cement and Concrete Research* 40 (4): 517–525.
- [5] Nielsen, A.; Gottfredsen, F.; Thogersen, F. 1993. Development of stresses in concrete structures with alkali-silica reactions, *Material and Structures*, 26: 152-158.
- [6] Furusawa, Y.; Ohga, H.; Uomoto, T. 1994. An analytical study concerning prediction of concrete expansion due to alkali-silica reaction, in Malhotra (ed.), 3rd International Conference on Durability of Concrete, Nice, France, 1994, 757–780.
- [7] Poyet, S.; Sellier, A.; Capra, B.; Foray, G.; Torrenti, J.-M.; Cognon, H.; Bourdarot, E. 2007. Chemical modelling of Alkali Silica reaction: Influence of the reactive aggregate size distribution, *Materials and Structures*, 40 (: 229–239.
- [8] Suwito, A.; Jin, W.; Xi, Y.; Meyer, C. 2002. A mathematical model for the pessimum effect of ASR in concrete, *Concrete Science and Engineering*, 4: 23-34.
- [9] Charpin, L.; Ehrlacher, A. 2012. A computational linear elastic fracture mechanics-based model for alkali–silica reaction, *Cement and Concrete Research*, 42 (4): 613-625.
- [10] Ulm, F.-J.; Coussy, O.; Li, K.; Larive, C. 2000. Thermo-chemo-mechanics of ASR expansion in concrete structures, *J. Eng. Mech.* 126 (3): 233– 242.
- [11] Li, K.; Coussy, O. 2002. Concrete ASR degradation: from material modeling to structure assessment, *Concrete Science Engineering*, 4: 35-46.
- [12] Saouma, V.; Perotti, L. 2006. Constitutive model for alkali-aggregate reactions, *ACI Materials Journal*, 103 (3): 194-202.
- [13] Grimal, E.; Sellier, A.; Le Pape, Y.; Bourdarot, E. 2008. Creep shrinkage and anisotropic damage in AAR swelling mechanism, part I: a constitutive model, *ACI Materials Journal*, 105: 227-235.
- [14] Comi, C.; Fedele, R.; Perego, U. 2009. A chemo-thermo-damage model for the analysis of concrete dams affected by alkali-silica reaction, *Mechanics of Materials*, 41: 210-230.
- [15] Naar, R. 2009. Modelisation du comportement mécanique du béton par approche multi-physique (couplage chimie-mécanique) : application à la réaction alcali-silice. PhD Thesis. École Nationale Supérieure des Mines de Paris.
- [16] Gao, X. 2010. Contribution to the requalification of Alkali Silica Reaction (ASR) damaged structures: Assessment of the ASR advancement in aggregates. PhD Thesis. Institut National des Sciences Appliquées de Toulouse (INSA Toulouse).
- [17] Lu, D.; Fournier, B.; Grattan-Bellew, P.E. 2006. Evaluation of accelerated test methods for determining alkali-silica reactivity of concrete aggregates. *Cement and concrete composites*, 28 : 546-554.
- [18] Fournier, B.; Nkinamubanzi, P.C.; Lu, D.; Thomas, M. D. A.; Folliard, K. J.; Ideker, J. 2006. Evaluating potential alkali-reactivity of concrete aggregates – How reliable are the current and new test methods? II Symposium on alkali-aggregate reaction in concrete structures. Brazilian Concrete Institute-Ibracon and Brazilian Committee on Dams-CBDB, Rio de Janeiro, Brazil, September.

- [19] Fournier, B.; Bérubé, A. 2000. Alkali-aggregate reaction in concrete: a review of basic concepts and engineering implications. *Canadian journal of civil engineering*, 27 (2): 167-191.
- [20] Sanchez, L. F. M.; Kuperman, S, C; Helene, P; Kihara, Y. 2008. Trials to correlate the accelerated mortar bar test, the standard and the accelerated concrete prism tests. 13th ICAAR - International Conference on Alkali-Aggregate Reaction in Concrete. Trondheim, Norway.
- [21] Gao XX.; Multon S.; Cyr M.; Sellier A. 2013. Alkali-silica reaction (ASR) expansion: Pessimun effect versus scale effect, *Cement and Concrete Research*, 44: 25-33.
- [22] Multon, S.; Cyr, M.; Sellier, A.; Leklou, N.; Petit, L.2008. Coupled effects of aggregate size and alkali content on ASR expansion. *Cement and concrete research*, *Cement and Concrete research*, 38 (3) 350-359.
- [23] Sanchez, L.; Fournier, B.; Jolin, M.; Bastien, J. Evaluation of the Stiffness Damage Test (SDT) as a tool for concrete's assessment damaged due to ASR – test loading and output responses for concretes incorporating fine or coarse reactive aggregates. *Cement and concrete research*, 56: 213-229.
- [24] Grattan-Bellew, P.E.; Danay, A. 1992. Comparison of laboratory and field evaluation of AAR in large dams. Proc. of the International Conference on Concrete AAR in Hydroelectric Plants and Dams, Canadian Electrical Association & Canadian National Committee of the Int. Commission on Large Dams, September 28 – October 2 1992, Fredericton, New Brunswick, (Canada).
- [25] Villeneuve, V.; Fournier, B.; Duchesne, J. 2012. Determination of the damage in concrete affected by ASR – the Damage rating Index (DRI). Proceedings of the 14th International Conference on Alkali-Aggregate Reaction in Concrete, May 20-25th, Austin (Texas), electronic.
- [26] ASTM C 39. 2012. Standard Test Method for Compressive Strength of Cylindrical Concrete Specimens. ASTM International, West Conshohocken (USA), 2012.
- [27] ASTM C 1074. 2011. Standard Practice for Estimating Concrete Strength by the Maturity Method. ASTM International, West Conshohocken (USA), 2011.
- [28] Komar, A.; Hartell J.; Boyd, A. J. 2013. Pressure tension test: reliability for assessing concrete deterioration. Proceedings of the Seventh International Conference on Concrete under Severe Conditions - Environment and Loading. Nanjing, China, September.
- [29] Gao, X,X.; Cyr, M.; Multon, S.; Sellier, A. 2013. Comparative study of chemical methods for the measurement of potentially reactive silica in aggregates. *Cement and Concrete Composites*, 37: 82–94.
- [30] Alexander, M.; Mindess, S. 2005. *Aggregates in concrete*. Book. Taylor & Francis, New York. USA.
- [31] Mindess, S.; Young, J. F.; Darwin, D. 2003. *Concrete*. Book. Pearson Education Ltda. second edition.
- [32] Goto, S.; Roy, D. M. 1981. Diffusion of ions through hardened cement pastes. *Cement and concrete research*, 11: 757-757.
- [33] Scrivener, K.; Crumbie, A.; Laugesen, P. 2004. The Interfacial Transition Zone (ITZ) Between Cement Paste and Aggregate in Concrete. *Interface science*, 12 :411–421.
- [34] Gopalaratnam, V. S.; Shah, S. P. 1985. Softening response of plain concrete in direct tension. *ACI Materials Journal*, 82 (3): 310-323.
- [35] Sellier, A.; Bary, B. 2002. Coupled damage tensors and weakest link theory for the description of crack induced anisotropy in concrete. *Engineering fracture mechanics*, 69: 1925-1939.
- [36] Lu, D.; Fournier, B.; Grattan-Bellew, P.E. 2006. Effect of aggregate particle size on determining alkali-silica reactivity by accelerated tests. *Journal of ASTM International*, 3 (9).
- [37] Lindgard, J. 2013. Alkali-silica reaction (ASR) – Performance testing. PhD Thesis. NTNU (Norwegian University of Science and Technology), Norway.
- [38] Lindgård, J.; Thomas, M.D.A.; Sellevold, E.J.; Pedersen, B.; Andiç-Çakır, O.; Justnes, H.; Rønning, T.J. 2013. Alkali-silica reaction (ASR)—performance testing: Influence of specimen pre-treatment, exposure conditions and prism size on alkali leaching and prism expansion, *Cement and Concrete Research*, 53: 68–90.
- [39] Ben Haha, M.; Gallucci E.; Scrivener, K. L. 2007. Relation of expansion due to alkali silica reaction to the degree of reaction measured by SEM image analysis. *Cement and concrete research* 37 : 1206- 1214.

- [40] Sanchez, L. F. M. Contribution to the assessment of damage in aging concrete infrastructures affected by alkali-aggregate reaction. PhD thesis, Laval University, department of geology and geological engineering (to be published in 2014).
- [41] Pleau, R.; Bérubé, M. A.; Pigeon, M.; Fournier, B.; Raphael, S. 1989, Mechanical Behavior of Concrete Affected by AAR. 8th ICAAR - International Conference on Alkali-Aggregate Reaction in Concrete. Kyoto, Japan, 1989.
- [42] Nixon, P.J.; Bollinghaus, R. 1985. The effect of alkali aggregate reaction on the tensile strength of concrete. *Durability of Building Materials*, 2: 243-248.
- [43] Smaoui. N.; Bérubé. M.A.; Fournier. B.; Bissonnette. B.; Durand. B. 2004. Evaluation of the Expansion Attained to Date by Concrete Affected by ASR - Part I: Experimental Study. *Canadian Journal of Civil Engineering*, 31, 826-845.

12. SCIENTIFIC CONTRIBUTIONS OF THE PHD THESIS

As discussed in previous sections, this PhD work aims at better understanding both the microstructural and mechanical effects of alkali-aggregate reaction (AAR) on aging concrete structures, as a function of its development and for different materials' characteristics (i.e. \neq concrete strengths and aggregate types/natures). Many specific findings of this research can be cited as being either scientific or engineering contributions, as presented hereafter:

Scientific contributions

- Understanding of the development of AAR microscopic features of deterioration in aging concrete as a function of the specimens' expansion levels;
- Proposal of a qualitative microscopic damage model for concretes affected by alkali-silica reaction (ASR);
- Understanding on how the microscopic distress features of AAR influence the mechanical behavior of affected concretes;
- Evaluating the development damage features of the so-called alkali-carbonate reaction (ACR) as a function of concrete expansion, and comparing them to features observed in concretes caused by conventional ASR;
- Proposal and implementation of the microscopic/mechanical coupling as a tool for measuring "overall damage" due to AAR;
- Proposal of a global quantitative damage chart based on AAR micro-mechanical coupling.

Engineering contributions

- Improvement of the *Stiffness Damage Test (SDT)* procedure used for quantifying damage in concrete due to AAR;
- Validation and improvement of the *Damage Rating Index (DRI)* procedure used for quantifying (semi-quantitative tool) damage in concrete due to AAR;
- Proposal of the use of the above microscopic and mechanical tools in a revised management protocol for aging concrete infrastructures (for MTQ - Quebec Ministry of Transportation);
- Discussion/validation of an ASR physico-chemical model developed by the LMDC (Laboratory of Materials and Durability of Constructions Toulouse – INSA Toulouse) research group, through the comparison of experimental data (i.e. chemical, microscopic and mechanical) vs. ASR modeling predictions, based on data obtained in this study for several concrete mixtures (i.e. \neq concrete strengths, mix designs, etc.) and aggregate's nature (i.e. \neq lithotypes) and types (i.e. fine vs.coarse aggregate).

13. CONCLUSIONS AND RECOMMENDATIONS

The main findings of this PhD study, whose detailed results were presented and analyzed in the six scientific papers forming the core of this thesis, are presented hereafter, as a function of the main objectives of the research identified in Section 3.

13.1 Summary of the experimental program

In this work, concrete cylinders, 100 by 200 mm in size, were cast from three types of non-air entrained concrete mix designs (25, 35 and 45 MPa mix design strengths) and incorporating ten moderately to highly-reactive aggregates (fine and coarse aggregates) in order to evaluate the efficacy of various laboratory test procedures for quantifying damage with the progress of expansion due to alkali-aggregate reaction (AAR). Moreover, some concrete cores were extracted from different zones of two structural elements of the Robert Bourassa/Charest viaduct, an aging concrete structure, constructed in the 1960's and suffering from significant visual damage due to ASR (i.e. exposed, not exposed), which enabled the use/treatment of "real" data (from existing structures/structural elements in service), enriching the analyses constructed in the project.

Once cast, all the manufactured concrete specimens were placed in sealed plastic containers lined with damp cloth (4 cylinders per bucket), which were then stored at 38°C and 100% R.H. All the test cylinders were monitored regularly and removed, by sets of three, from the high-temperature storage conditions for microscopic and mechanical testing when they reached the following expansion levels: 0.05% ± 0.01%, 0.12% ± 0.01%, 0.20% ± 0.01% and 0.30% ± 0.01%. Prior to mechanical testing (i.e. SDT, modulus of elasticity, compressive and tensile strength), both ends of each cylinder were carefully mechanically ground and then ultrasonic pulse velocity measurements were performed over all concrete samples. In the case of the petrographic assessment, when the above expansion levels were reached, the concrete specimens were cut, polished, rewrapped (i.e. plastic film) and restored at 23 ± 2 °C until subjected to the examination.

13.2 Development of AAR expansion and distress features in concrete

In terms of AAR kinetics, concrete mixtures containing highly reactive sands generally presented faster reactivity (onset of expansion and expansion rates) than those containing highly reactive coarse aggregates. This behavior was found to be linked to the aggregate' size effect; i.e. greater surface area which accelerates the attack by the alkali hydroxides from the pore solution for the same amount of reactive silica in the particles.

Interesting behaviors were also found for the mass gain plots. In the majority of cases, the mass gain and expansion behaviors were similar. An exception was observed for the King + Lav mixture, susceptible to *alkali-carbonate reaction* (ACR), and which presented the “fastest” AAR expansion kinetics of all aggregates investigated. However, its mass gain was exceeded by many other mixtures that did not present either fast reaction kinetics or comparable final expansion levels. Therefore, an in depth study is necessary to allow a better understanding of the ACR chemical/physical mechanisms as a function of expansion.

An interesting behavior was also observed for the concrete mixture incorporating both fine and coarse highly reactive aggregates together, i.e. Tx sand + NM gravel and NM manufactured sand + NM gravel; those mixtures showed a *slower reaction kinetics* and sometimes lower ultimate expansion than the concrete mixtures containing just one of those reactive aggregates, fine or coarse. This means that a “competition” develops between both highly reactive aggregate (fine vs. coarse) and, although the system presents a greater amount of available silica, this competition strongly impacts on both the AAR reaction kinetics and its magnitude for the same amount of available alkalis (or cement content), thus resulting in a “pessimun effect” of the expansion obtained in the test specimens.

Regarding the effects of concrete strength on AAR kinetics, no significant differences were observed in the AAR kinetics and magnitude for the range of strengths used in this project (from 25 up to 45 MPa, reactive aggregates NM and Tx). Those results are interesting, but somewhat surprising. The total alkali content in the concretes ranged from 3.9 to 5.3 kg/m³, which could have induced some differences in the reaction kinetics and/or the magnitude of expansion; however, the various mixes were designed with the same volume of aggregates and pastes and the water-to-cement ratio varied from 0.37 to 0.61. This suggests that not only the total concrete alkali content but the concrete mix characteristics impact on the

reaction/expansion kinetics and magnitude. Further work is required to evaluate the combined effects of the above parameters on ASR expansion.

Considering AAR distress development, first of all, it is good to mention that the AAR expansion levels of affected concretes do not mean directly the “damage degree” attained by the AAR-distressed materials. Expansion is a feature commonly used and easily measured in laboratory investigations to evaluate/classify the potential alkali-reactivity of concrete aggregates and can allow comparing, at specific/selected levels, the presence/development of different features of deterioration in concrete. Disregarding the characteristics of the damaged concretes used in this work (i.e. different concrete strengths and aggregate types/natures, etc.), which introduced the differences found among different mixtures and made the correlation “expansion level vs. damage degree” not linear, it has been found that the concrete “damage features” generally increase with increasing expansion in the test specimens.

Overall a strong pattern of increasing of the *Opened cracks* (with and without gel) both in the reactive aggregate particles and in the cement paste was observed as a function of the expansion levels increase of the affected specimens. These are thus considered as strongly indicative features of the development of AAR in concrete. Moreover, over this work, the presence of a large number of *Closed cracks* within the coarse aggregate particles was observed, which are most likely created, in good part, through aggregate processing operations. In addition, it was proposed that in concretes where ASR expansion is generated either in the coarse or the fine aggregate particles, the pore solution “uses” at least some of these “fast track” zones to access the inner parts of the particles, generating alkali-silica gel and inducing excessive expansion forces that will in turn cause those cracks to open and extend into the cement paste with increasing expansion. For higher expansion values (0.25%, 0.30% and further), an increase in the number of *Closed cracks* in the reactive sand particles is observed, which could be linked to the important pressures caused by ASR within the concrete matrix. On the other hand, the number of *Closed cracks* within the non-reactive coarse aggregate particles increases with increasing expansion, and can even become opened, which means that ASR pressure in the concrete matrix influences the development of new cracks even in those non-reactive particles, more or less depending on the mechanical characteristics of the non-reactive material.

13.3 Proposal of a qualitative microscopic model of distress for ASR-affected concretes

The petrographic examination of numerous polished concrete sections incorporating a range of reactive rock types allowed to develop a qualitative microscopic model of ASR damage development, which can be described as follows (see Figure 16 of Paper IV, in Section 9, for micrographs) :

- in the early stages of the reaction/ expansion process (e.g. low expansion levels of $\leq 0.05\%$), the main microscopic feature is the presence of closed cracks within the aggregate particles and some of these cracks start to open resulting from the internal pressure generated by alkali-silica gel formation. At that stage, only a few cracks are visible in the cement paste and they are generally very thin and tight; it is unusual to observe opened cracks in the cement paste at this level, at least at the magnification used for the DRI.
- With the progress of ASR, some of the opened cracks that were formed inside the aggregate particles with the onset of expansion increases in length and width, and some of them extend into the bulk cement paste; this is readily visible in the test specimens showing 0.12% expansion. At that point, only a small amount of silica gel can be undoubtedly identified in the cracks in the cement paste, at the magnification used for the DRI.
- In the test specimens with higher expansion levels (i.e. 0.20%), most of the opened cracks formed inside the aggregate particles already reached the cement paste. Therefore, the “*crack density values (counts/m²)*”, calculated by the sum of the counts of both opened cracks in the aggregate particles and in the cement paste (with or without reaction products) divided by the overall area examined (in cm²), are noticeably greater than before. Likewise, the presence of alkali-silica gel can be easily found at that level, mainly inside the aggregate particles.
- Finally, at very high expansion levels (0.25-0.30%), the cracks in the cement paste are often found to link to other cracks thus generating an important cracking network. Exceptions were found for concretes incorporating an alkali-carbonate reactive limestone (King) and a reactive siliceous sandstone (orthoquartzite - Pots), where either a largely different damage pattern was observed or much lower distress features were obtained compared to the other mixtures, respectively, mainly due to different reaction mechanisms.

The above observations can globally be described using a qualitative model partly defined based on two cracking types that were commonly found in the aggregate particles of the

concrete specimens examined. *Sharp* (Type A) and/or *Onion skin* (Type B) cracks were found to form within the aggregates particles in the early stages of the reaction, then extending into the cement paste with increasing expansion to eventually connect reactive aggregate particles in an extensive cracking network (see Figure 17 of Paper IV, in Section 9, for qualitative model). Type A and Type B cracks are not necessarily present at the same time in the affected aggregate particles. Their presence will be a function of rock type characteristics. On the other hand, a different pattern of damage generation was observed with the alkali-carbonate reactive aggregate *King*. In that case, extensive cracking in the cement paste develops in the early stages of the reaction/expansion process, with cracking also developing, but to a lesser extent, within the reactive aggregate particles.

13.4 Tools for the condition assessment of ASR-affected concrete

Ultrasonic pulse velocity (UPV)

The results obtained in this study confirmed that the UPV was generally unable to efficiently differentiate the levels of damage observed as a function of the expansion levels of the test specimens for the various series of ASR-affected concretes used in this study. Likewise, the dynamic modulus of elasticity output parameter, although presenting better results than the UPV, did not allow reliable/useful damage assessments between the various concrete specimens affected by ASR used in this study. Similar conclusions are also reported already in the literature.

Stiffness Damage Test (SDT)

The extensive testing carried out in this study strongly indicate that the Stiffness Damage Test (SDT) is able to provide a reliable assessment of the ASR expansion effects on damage generation (i.e. physical integrity loss) for different concrete types (\neq concrete strengths, \neq aggregate types/natures, etc.). In order to do so, the results obtained in this study have clearly showed that the SDT loading level should be selected on the basis of a percentage of the concrete mix design strength instead of a fixed loading value of 5.5 or 10 MPa, as previously suggested in the literature. Therefore, carrying out the SDT with percentages of loading of more than 30%, and preferably 40% of the concrete mix design strength, is required for the SDT to be a diagnostic tool for assessing the degree of expansion attained by ASR-affected concretes. The statistical analysis (ANOVA) of the test data obtained in this study indeed confirmed that loading at 30% of the concrete mix design strength could sometimes

distinguish the development of ASR damage between specimens of different expansion levels; however, the use of 40% loading level is a preferable scenario for all the cases studied.

The hysteresis area (HA) and the plastic deformation (PD) over the complete five loading/unloading cycles, as well as the average value of the modulus of elasticity obtained in the second and third cycles, were found to be the best parameters to use as output responses of the test. The use of the dissipated energy (HA parameter) obtained over five cycles was found to be a statistically superior output parameter than that proposed by Smaoui et al. (2004b), who proposed the use of the HA values for the 1st cycle only. In addition, results showed that even when using 40% of the concrete strength, SDT seems to maintain its “non-destructive” character, at least up to the expansion levels used in this project (0.30%). This assumption was confirmed by the examination of the test specimens through the Damage Rating Index (DRI), as well as from the statistical analysis of the results of either compressive or tensile strength determinations after the cyclic procedure. Therefore, although the examination under the SEM of polished concrete sections after completion of the SDT would likely indicate the progression of some microcracks after stiffness damage testing in ASR-affected concrete specimens having reached higher expansion levels, it was demonstrated that performing the SDT at the 40% loading level provides a more reliable assessment of the current condition of concrete affected by ASR without inducing significant additional damage that could jeopardize the reliability of the assessment. Also, concrete specimens could be used for mechanical testing (compressive and tensile strengths) determination, petrographic examination or chemical (e.g. water soluble alkali content) assessments after completion of the SDT without jeopardizing the quality/reliability of the test results.

However, the ultimate goal of the stiffness damage test is to enable the condition assessment of aging infrastructures affected by AAR in service, or even from other distress mechanisms. Considering that for the vast majority of the cases one does not know the 28-day compressive strength of the concretes used and, moreover, the strength of concrete increases or decreases over time compared to the 28-day value, depending on either the type of deleterious mechanism causing concrete distress or even the type of structural element and exposure conditions, the use of the 40% of the 28-day mix design strength becomes a difficult approach for practical engineering situations. Consequently, the most important question when an aging concrete infrastructure needs to be assessed through the SDT would be: what load level should be used for testing ? In general, the greater the concrete mix design strength is, the

greater the output parameters of the test (hysteresis area and plastic deformation values) will be, with the first parameter being much more sensitive to the loading level used.

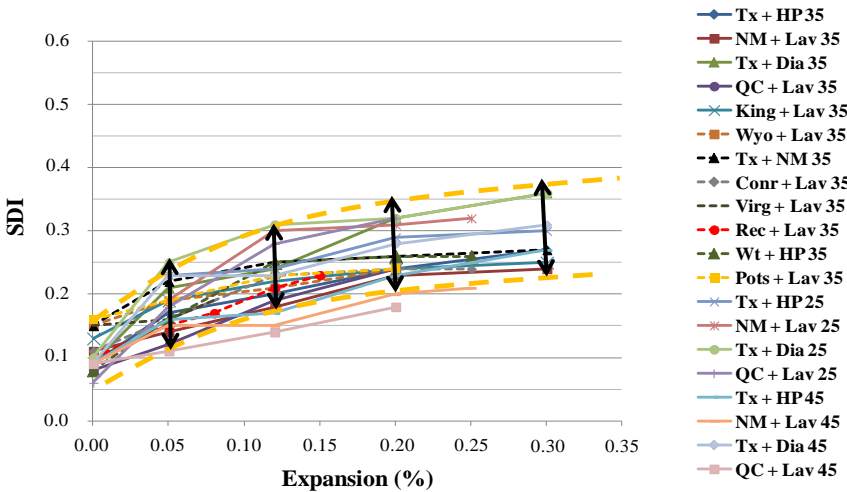
The data obtained in this study confirmed that using absolute SDT output values for characterizing concrete damage can result in misleading conclusions, as the test is very sensitive to the concrete design strength and characteristics (i.e. aggregate's type, contents, etc). Beyond that, the use of absolute SDT values limits the understanding of what really happens in terms of damage generation and development, as the hysteresis area and plastic deformation are linked to the amount of energy implemented in the system, which will be always greater for concretes of greater design strengths or even stiffnesses.

As part of this research, a new approach was proposed for the analysis of the SDT results, involving the determination of the *Stiffness Damage Index* (SDI) and the *Plastic deformation Index* (PDI). The above Indices take into account not just the total amount of dissipated energy, but rather the ratio “dissipated energy/total energy” implemented in the system during stiffness damage testing, which better represents/explains AAR “distress” as a function of expansion in the test specimens. The first parameter (SDI) can be easily linked to the physical integrity of a material as it represents the “real” percentage of energy used for the crack's closure process under compressive loading. The second parameter (PDI) represents almost the same phenomenon (i.e. sliding across surfaces over crack's closure), but it could still be linked to the material's performance in the field, as it represents the amount of plastic deformation of an affected material under compressive loading. Our results showed that, on an average, and disregarding the material's strength, the SDI displays an increasing trend with increasing expansion in the test specimens, which tends to level off at higher expansion levels. This suggests that a large amount of “new” ASR cracking is formed at low/moderate levels of expansion (e.g. 0.05 – 0.12%), mostly inside the aggregate particles, as confirmed by petrographic (DRI) analysis. As the expansion progresses (0.20% or greater), the number of cracks keeps partially increasing, but some existing cracks keep increasing in length and width. This phenomenon would contribute at slowing down the increasing trend of SDI, since the energy required for closing cracks at a given damage degree is proportional to the *cracks' number x the cracks' width* of an affected concrete specimen, thus showing a concave tendency “SDI vs. expansion level” and agreeing with the microscopic results. Moreover, the concave shape could even be enhanced by the difficulty for the cracks to fully close under

loading because of the presence of ASR gel. The same behavior is also seen for the PDI parameter (Figure 13.1).

Finally, according to the extensive stiffness damage testing carried out on test cylinders cast from a wide range of concrete mixtures (25 to 45 MPa), incorporating a variety of reactive rock types (coarse aggregates and sands) and tested at different expansion levels due to ASR, the SDI, PDI, NLI and ME parameters should be used as diagnostic “output responses” of the cyclic test. Moreover, the reliability of the above parameters was confirmed through ANOVA analysis and this proposed approach allows the generation of an “envelope of AAR distress values” using the SDI (Figure 13.1A) or PDI (Figure 13.1B) indices which enables the use of the SDT for quantitative damage assessment in concrete due to ASR.

A – SDI vs. Expansion



B – PDI vs. Expansion

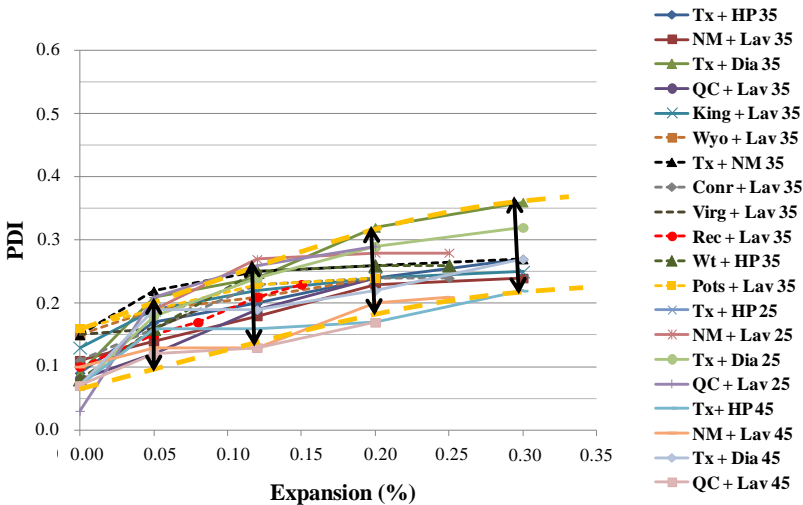


Figure 13.1: SDT envelopes using, as output parameters, the indices proposed in this project: A) SDI and B) PDI.

In addition, the extensive testing carried out in this study on ASR-affected laboratory and field specimens confirmed that several factors influence the reliability and reproducibility of the SDT results. For instance, when a damage assessment is carried out on sampled concrete from AAR-affected structures/elements in service, one should take into account, for the interpretation of the test results, the location and environmental characteristics of the specimens (cores) extracted, as significant variations in SDT results can be obtained at different depths in the concrete element(s), as a function of the exposure condition (notably the availability of moisture) of the element investigated. Moreover, using cores with a length/diameter of 2.0 ± 0.10 and for which a close control on the conditioning history (i.e. moisture condition following coring up to the time of testing) has been applied is critical for obtaining reliable results. Figure 13.2 illustrates the practical SDT procedure proposed as an outcome of this project, in view of avoiding any misinterpretation of the test results.

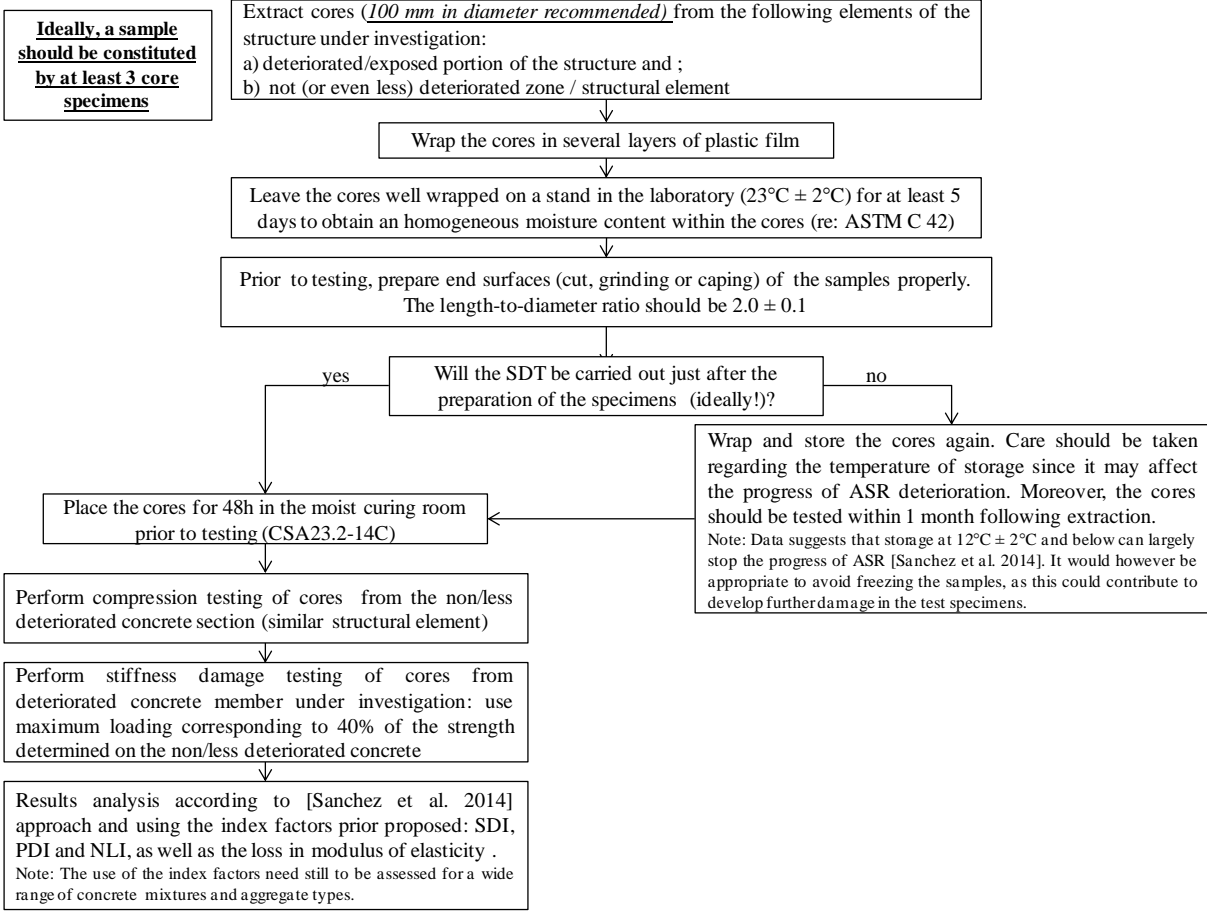


Figure 13.2: SDT standard and practical procedure.

Damage Rating Index (DRI)

The DRI, using the new procedure proposed by Villeneuve et al. 2012, can reliably assess the expansion levels in ASR-affected specimens incorporating either reactive sands or reactive coarse aggregates/gravels. However, the use of just the semi-quantitative DRI number does not provide in-depth information, neither on the petrographic features of deterioration in the test specimens, nor on the deleterious mechanism(s) involved. Interesting and important information is indeed obtained through the analysis of the detailed DRI counts (number and %) as a function of the expansion level of the affected specimens.

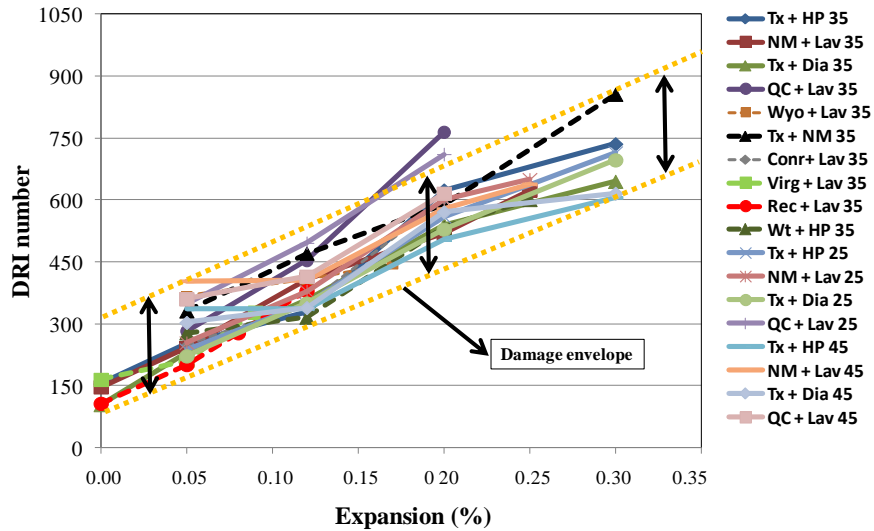
In comparing different ASR mechanisms, no significant differences in the DRI numbers were obtained between 25 and 35 MPa concretes, at similar expansion level, whether the expansion is generated by a reactive sand (Tx) or a reactive coarse aggregate (NM). This suggests that a similar distress process happens for both mixtures and the slight differences could likely be linked to the heterogeneity of either the material studied (concrete and aggregates) or the ASR damage process. However, the pattern seems slightly different for the 45 MPa concretes. The latter indeed present a greater amount of cracking (mainly closed, sometimes opened cracks) inside the aggregate particles with a greater presence of reaction products at the early stage of the reaction ($\approx 0.05\%$), similar DRI values between 0.05 and 0.12% expansion and, finally, rates of increasing DRI values (as a function of increasing expansion) similar to that obtained for 25 and 35 MPa concretes at higher expansions (0.20% and 0.30%). Moreover, the presence of gel in cracks of the aggregate particles and of the cement paste is significantly greater for 45 MPa concrete specimens, for all expansion levels. On the other hand, in general, cracking in the cement paste was significantly more difficult to identify in the 45 MPa concretes than in the 25 and 35 MPa concretes, at least at the magnification used for the DRI procedure ($\approx 15x$ to $16x$); this was particularly true for the polished sections incorporating reactive sands (Tx and Wt). Finally, in a qualitative way, the cracks from ASR coming from reactive sands are a very thin and sparsely distributed within the concrete matrix, while for ASR coming from coarse aggregates, the cracks are slightly wider (on average) and more localized/concentrated being associated to a lower number of reactive (coarse) aggregate particles.

The testing carried out in this study showed that similar trends/rates for increasing DRI numbers are obtained as a function of expansion for a variety of concrete mixtures (25 to 45 MPa) and reactive rock types (Figure 13.3A). Therefore, a strong envelope of “microscopic

damage results” is proposed that correlates DRI numbers and the expansion level of the affected samples, which begins (in average) at 150 for 0.0% of expansion and reaches between 650 and 850 at 0.30% of expansion, depending on the aggregate type. However, exceptions were observed for the two reactive King and Pots aggregates mentioned before, which respectively presented much higher (from 350 at 0.0% up to 965 at 0.30%) and much lower (from 150 at 0.0% up to 300 at 0.16%) DRI values. Concretes incorporating the alkali-carbonate reactive King aggregate are characterized by a much higher frequency of cracking in the cement paste for low and moderate expansion levels, which significantly differed from the other mixes and made the DRI results higher and outside the envelope for all the expansion levels studied. This so-called *alkali-carbonate reaction*, which is the source of debates in the scientific community, showed in this work to be largely different from the ordinary ASR. On the other hand, in the case of concretes incorporating the reactive Pots aggregate, it was extremely difficult to identify cracks in both the aggregate particles and in the cement paste over the expansion levels. Therefore, the features of deterioration, although somewhat similar to those identified in ASR-affected concretes, showed much lower frequencies at all expansion levels, thus falling below the general envelope.

The measurements of crack density (CD) (counts/cm²), provides interesting and complementary information about AAR distress. This parameter was found to increase steadily with increasing expansion in affected concrete specimens. Overall, similar rates of increasing CD values as a function of increasing expansion were obtained, despite some small differences, between concretes of different strengths and incorporating different reactive rock types, thus allowing proposing an envelope of expected CD values as a function of increasing expansion due to ASR in the test specimens (Figure 13.3B). However, this common pattern cannot be applied to the alkali-carbonate King limestone aggregate, which showed greater cracking densities for all the expansion levels studied (mainly for low and average expansion levels).

A – DRI number vs. Expansion



B – Crack density vs. Expansion

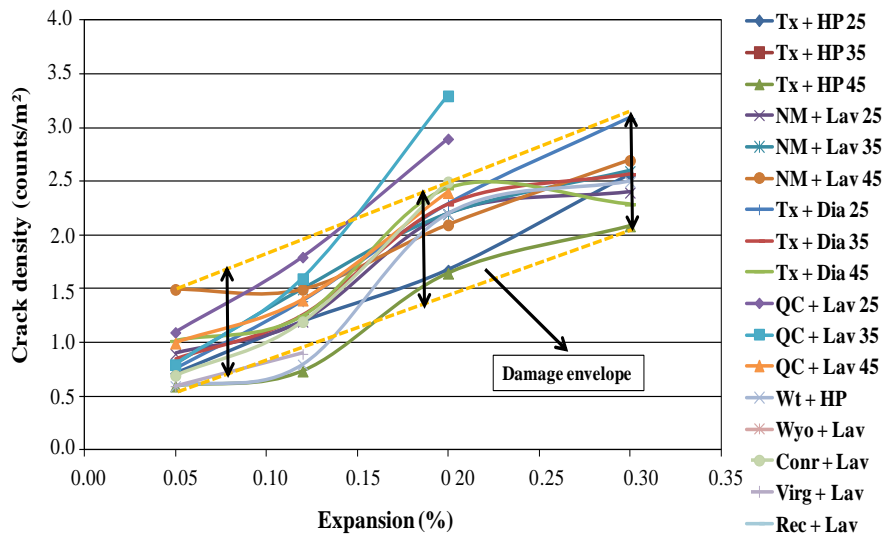


Figure 13.3: DRI envelopes using: A) DRI numbers (following the test procedure proposed by Villeneuve et al. (2012), and B) Crack density (counts/cm²).

13.5 Coupling between the development of the physical (microstructural) features of AAR and the mechanical behavior of the affected concretes

Interesting information was obtained through the coupling of microscopic features of deterioration and the mechanical behavior of the AAR affected concrete specimens.

Petrographic investigations carried out in this study suggest that the development of cracking within individual alkali-silica reactive aggregate particles does not follow a linear pattern as a function of expansion in concrete. It was observed through crack counting within individual

reactive aggregate particles that a significant number of new ("Opened") cracks will form in the early stages of the chemical reaction until some of them reach given critical lengths and widths. Following the minimum energy law, it will then be easier for the expanding system to extend those "critical" cracks instead of creating new ones. Thus, the rate of crack generation within the aggregate particles will start slowing down. In other words, new cracks will likely be generated as the alkali reaction keeps progressing, but the amount of "new" cracks will be overcome by the increase in length and width of the cracks already formed, thus making the counts of distress features to keep increasing but at a lower rate. On the other hand, the behavior of the *Closed cracks* within the aggregate particles as a function of expansion in the affected concretes was quite different. Looking at the reactive particles behavior, it seems that for low/moderate expansion levels (i.e. $\leq 0.12\%$), the counts/proportions of closed cracks generally decrease with increasing ASR expansion, while the counts of *Opened cracks* increase. This phenomenon likely means that some closed cracks in the reactive aggregate particles are used for the development of ASR opened cracks, due to the fragile character of those zones. This trend keeps happening up to the point at which new closed cracks are likely to be formed in the reactive particles and even in non-reactive coarse aggregate particles, when ASR is generated by the reactive sand, in response to the increasing ASR pressure generated within the concrete matrix due to ASR. The extent to which closed cracks will develop within the aggregate particles will depend on the mechanical properties of the rock types involved, especially their *toughness*, as cracking will develop/progress at the easiest location (e.g. within aggregate particle of lower toughness, interfacial transition zone, etc.). It also likely depends on the mechanical characteristics of the concrete matrix.

The extensive testing carried out in this study allowed to observe, despite some variability related to the material characteristics (concrete strengths, aggregate types and natures, etc.), a strong correlation between the development of microscopic features of deterioration (visible on polished concrete sections at 15-16x magnification under the stereomicroscope) and changes in the mechanical properties of the concrete specimens as a function of expansion due to ASR. The conclusions to be drawn from the global analysis of test data obtained on concretes of different strengths incorporating alkali-reactive quartz-bearing rocks (category 2 of reactive rock types according to the Appendix B of CSA A23.1-2009; these would somewhat correspond to the reaction Model C illustrated in Figure 2.14 and proposed by Dunant and Scrivener 2009).

It is important to keep in mind that the coupling presented hereafter, i.e. between the development of physical distress features of ASR (e.g. cracking) and the resulting impact on the mechanical performance of the concrete, is based on test data obtained on aging concrete materials (different concrete mix designs and a variety of reactive rock types and natures) in a "free and accelerated expansion environment". Although such an approach allowed a solid comparative performance analysis considering the strict conditions under which the specimens were cured and tested, one should realize that the features described and the resulting analyses/conclusions would not necessarily apply to the condition assessment of concrete cores extracted from ASR-affected structural concrete members in service, which are likely largely influenced by the presence of different stress fields (bi/triaxial stresses, restraints, etc.). It is believed, however, that the analyses presented hereafter could serve as a reference (and perhaps as worst case scenario) in the process of quantifying the progress of damage in concrete undergoing deleterious expansion due to ASR in the field.

Table 13.1: Classification of the damage degree in concrete due to ASR

Classification of ASR damage degree (%)	Reference expansion level (%) ¹	Assessment of ASR				
		Stiffness loss (%)	Compressive strength loss (%)	Tensile strength loss (%)	SDI	DRI
Negligible	0.00 – 0.04	-	-	-	0.06 – 0.16	100 - 155
Marginal	0.05 ± 0.01	5 – 37	(-)10 – 15	15 – 60	0.11 – 0.25	210 - 400
Moderate	0.12 ± 0.01	20 – 50	0 – 20	40 – 65	0.15 – 0.31	330 - 500
High	0.20 ± 0.01	35 – 60	13 – 25	45 – 80	0.19 – 0.32	500 - 765
Very high	0.30 ± 0.01	40 – 67	20 – 35		0.22 – 0.36	600 – 925

¹ These levels of expansion should not be considered as strict limits between the various classes of damage degree but more as indicators/reference levels for which comparative analysis of petrographic and mechanical data was carried out and that allow highlighting significant damage levels in concrete due to the progress of ASR.

Negligible damage (< 0.03%)

The “control” concrete specimens that were examined in this study showed "negligible" to very low levels of expansion, i.e. ranging from 0.00% up to about 0.03%. The petrographic examination of such concrete specimens identified the presence, as the main features of "deterioration", of *Closed cracks in the aggregate particles*, likely originating from aggregate processing operations, as well as initiation of some ASR-related cracking. Very limited (traces), localized microcracks were observed in the cement paste, generally unrelated to aggregate’s cracking and possibly resulting from various phenomena such as shrinkage, improper/excessive consolidation, etc. Overall, those specimens had DRIs ranging from 100

to 155. The stiffness damage index (SDI) obtained from those specimens ranged from 0.06 to 0.16 (Table 13.1).

Marginal expansion due to ASR (e.g. 0.03 – 0.05%)

In the beginning of “significant” ASR development, which correspond to the marginal/low expansion levels (between 0.03% and about 0.05%) or the *inception period* mentioned by some authors, the major distress features correspond to the development of opened cracks due to ASR within the aggregate particles, thus resulting in a strong increase of both the SDI parameter and the DRI number (Table 13.1). This distress feature, which has in good part developed from pre-existing (closed cracks) originating from aggregate processing operations, likely results in a significant drop in the “stiffness” of the reactive aggregate particles and, moreover, of the stiffness of the concrete material as a whole. Mindess et al. (2003) indeed suggested that, for ordinary concretes, the modulus of elasticity is largely governed by the modulus of elasticity (ME) of the coarse aggregate. Therefore, this phenomenon is likely responsible for the rapid and significant drop in modulus of elasticity (reaching $\approx 40\%$, depending on the reactive rock type) of the ASR-affected concretes observed at low expansion levels (Figure 13.4A; Table 13.1). It is important to mention that no significant microcracking, at least visible at the magnification used for the DRI (about 15x), was observed in the cement paste of the various concrete specimens examined at that level of expansion; however, it is likely that cracking may have developed at the submicroscopic level in the immediate vicinity of the reacting aggregate particles and that may contribute to the drop in ME observed already at low expansion levels. Moreover, the above distress features also tend to affect significantly the tensile strength of the affected materials at this stage of ASR expansion/reaction process, with reductions ranging from about 15 to 60% being observed, depending on the reactive rock type (Table 13.1); the concrete fracture mechanism in tension is indeed a direct and not ductile mechanism caused by the “stress intensity factors” formation in the presence of micro defects/pores, which are generated/enhanced by ASR, although the features of deterioration at this reaction step appear to largely remain within the aggregate particles (Figure 13.4B). On the other hand, the development of such cracking within the aggregate particles does not seem to affect significantly the compressive strength of the concretes (-10 to 15%, depending on the reactive rock type) (Figure 13.4C; Table 13.1).

Moderate expansion due to ASR (e.g. about 0.10 – 0.12%)

When the expansion progresses to moderate levels ($\approx 0.12\%$), the number/proportion of “Opened cracks within the aggregate particles”, with and without reaction products, keep increasing and some “new cracks” are generated; however, the main feature characterizing this second stage of the ASR reaction/expansion process is that some of the above cracks actually extend into the cement paste, affecting both the bulk cement paste in the close vicinity of the aggregate particles (with still a limited extent at this stage) and some areas of the interfacial transition zone (ITZ). This results in significant increase in the SDI (about 0.15-0.31) and DRI (about 330 – 500) values, which likely explains why the affected material’s “stiffness” keeps dropping (20 to 50% reduction in modulus of elasticity depending on the reactive rock type), but at a slightly lower rate, as the stiffness’ reduction is relatively more important when the aggregates are damaged than the cement paste itself (Figure 13.4A; Table 13.1). At such moderate expansion levels, the tensile strength attained its maximum loss for the vast majority of the concrete mixtures (40 to 65% depending on the reactive rock type) (Figure 13.4B; Table 13.1). This suggests that some cracks have already reached their critical lengths at this expansion level, thus causing unstable crack growth in the system that would lead to the full concrete fracture in tension with the application of higher stress level. Since some cracks formed within the aggregate particles reach the cement paste at this stage, the fracture in tension is likely facilitated in the affected concrete specimens. In terms of compressive strength reduction, moderate reductions are found at this stage (0 to 20% depending on the reactive rock type), as some cracks reach the cement paste, likely damaging the bulk paste itself and the ITZ. Therefore, when concretes in that condition are loaded in compression, some ASR cracks that are near the ITZ could be used as “fast tracks” to initiate and propagate fracture, as they are even less stiff than the ITZ itself (Figure 13.4C). The compressive strength loss at this expansion level might still be considered quite tolerable, since the reduced values likely remain in the “safety zone” commonly used when concrete materials are designed.

High expansion due to ASR (e.g. about 0.20%)

For high expansion levels (about 0.20%), the generation of “new” cracks within the aggregate particles and the cement paste seems to be overcome by an increase in length and width of the existing cracks. Also, at this stage, the vast majority of the cracks generated within the aggregate particles reach the cement paste where they link into a dense network of cracking, resulting in continuing increase in DRI values (500-765; Table 13.1). The modulus of

elasticity of the majority of the affected concrete mixtures keeps dropping, reaching 35 to about 60% loss depending on the reactive rock type; however, the reduction rate slowed down significantly and even levelled off for some concretes between 0.12 and 0.20% (Figure 13.4A; Table 13.1). This suggests that the extension into a cracking network within the concrete matrix observed at high expansion levels (0.20 – 0.30%) does not result in an increased rate of stiffness reduction of the concrete, which is also highlighted by stabilized SDI values (0.19-0.32), Table 13.1), perhaps also because of the increasing presence of alkali-silica reaction products in those cracks. Likewise, this cracking extension process does not seem to affect further the tensile strength of the concrete since these cracks have already reached their *critical length* to cause tensile failure at the moderate levels of expansion for all concrete mixtures studied, at least determined through the test procedure used in this project – gas pressure test (Figure 13.1B). On the other hand, a continuing/progressive loss in compressive strength, now ranging from 10 to 35%, is observed at this expansion stage in the affected concretes (Figure 13.1C). As the mechanism of fracture in compression is more ductile than the mechanism in tension, the development of cracking networks creates instability in the system, thus resulting in progressive reductions in compressive strength. This assumption agrees with the work of Kubo and Nakata (2012), where important compressive strength losses were found only for concretes damaged due to ASR at expansion levels $\geq 0.30\%$.

It might be interesting to mention that expansion levels of about 0.20% could lead to the “steel yielding”, whether one considers that the concrete/steel bonding would not suffer at such expansion, phenomenon already found on several stirrups used for shear reinforcement in bridge columns in Japan (Inoue et al. 2012). Also, such a cracking network could significant impact on the performance in durability of the affected material (e.g. risk of steel corrosion, freezing and thawing distress, chloride/sulphate ions penetration, carbonation, etc.).

Very high expansion due to ASR (e.g. $\approx 0.30\%$; this is the maximum expansion level investigated in this study)

At this expansion level, extensive cracking is found into the cement paste with cracks largely connecting reactive aggregate particles with one another. Consequently, DRI values kept increasing up to this level, mainly from the spreading of cracking into the cement paste and the aggregate particles. Reductions in modulus of elasticity and tensile strength have largely levelled off, reaching values of about 70% and 80%, respectively. On the other hand, compressive strength reductions continue to progress with losses of 35% or greater being observed. Therefore, from this expansion level, ASR cannot be considered anymore just a

serviceability/durability related problem since the reduction in the mechanical properties of the affected materials reach important values at this reaction point.

Globally, the above data indicate that both the compressive strength and the tensile strength procedures show limited usefulness for assessing the “state of AAR development, at least up to the 0.30% expansion level used in this study. Therefore, both procedures need to be essentially used for the “determination of concrete properties” at a given time of analysis as their capacity for quantifying the extent of ASR-related damage is limited considering their progress as a function of expansion. However, the ME parameter showed to have the potential for assessing both the AAR development and the stiffness reduction as a function of the AAR expansion levels.

Concluding remarks

Analyzing the data illustrated in Figures 13.1 and 13.4 and the statistical analysis of variance (ANOVA) performed in the sections 10.7.4.2/10.7.4.3 of the Thesis on the data obtained in the “envelope of results” of each mechanical property studied, the results were found to be different from one to another, which means that although a strong “data envelope” was obtained over this work (which represented a contribution to the understanding on how AAR influences the properties of the affected materials and enables fair prediction/correlation between AAR expansion and selected concrete properties), different behaviors were still obtained as a function of either the aggregate type/nature used or the strength of the material in question, for the same expansion level.

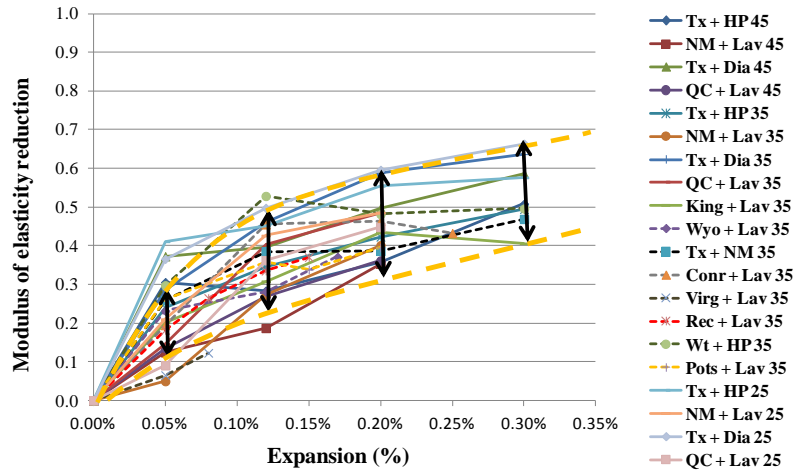
Considering the differences according to the use of different aggregate types and natures, no easy/direct evidences were found to distinguish the results behavior according to the aggregates nature or mineralogy. However, it has been found that concrete mixtures incorporating reactive sands seem to show earlier important mechanical properties reductions than distressed materials incorporating reactive coarse aggregates. These results illustrate the importance of further/deeper analyzing the impact of aggregate`s physical characteristics on the fracture process (i.e. toughness, hardness, etc.) in concrete undergoing expansion due to AAR, as suggested by Reinhard & Mielich (2011).

Considering the differences among different concrete strengths, generally, the greater in the concrete strength, the slower is the mechanical properties reductions over time. Moreover, the final reductions were found to be a slightly lower for concretes with greater compressive mechanical strengths.

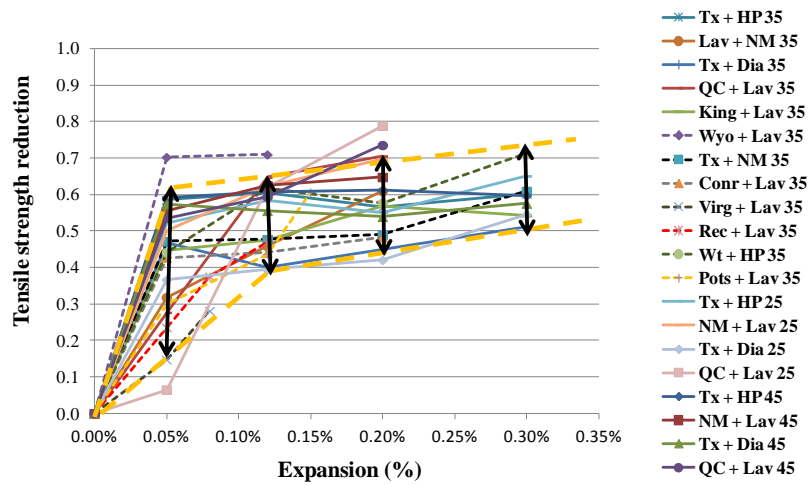
Figures 13.1 and 13.4 indicate that the mechanical properties of the various concretes investigated in this study are similarly affected by the progress of AAR, which is highlighted by the presence of somewhat parallel curves regrouped into distinct “data envelopes” for each of the properties evaluated. The analysis (ANOVA) of the data further indicated that the behaviors observed for the various reactive rocks/sands and mix designs (25 to 45 MPa) are statistically different. Actually, it was found that the mechanical properties of the concrete mixtures incorporating reactive sands are generally more rapidly affected by the progress of AAR. On the other hand, the extent by which the mechanical properties of concretes incorporating different reactive coarse aggregates was found to vary significantly from rock type to another, and no simple “grouping” of performance could be achieved on the basis of generic rock types. These results stress the importance of deeper analyzing the impact of aggregate`s physical (i.e. grain size, toughness, hardness, etc.) and mineralogical (size, nature and distribution of reactive minerals) characteristics on the fracture process in concrete undergoing expansion due to AAR, as suggested by Reinhard & Mielich (2011).

Considering the mix designs investigated, it was generally found that the greater is the concrete strength, the slower is the mechanical properties reductions over time. Moreover, the final reductions were found to be slightly lower for concretes with greater compressive mechanical strengths.

A – Modulus of elasticity



B – Tensile strength



C – Compressive strength

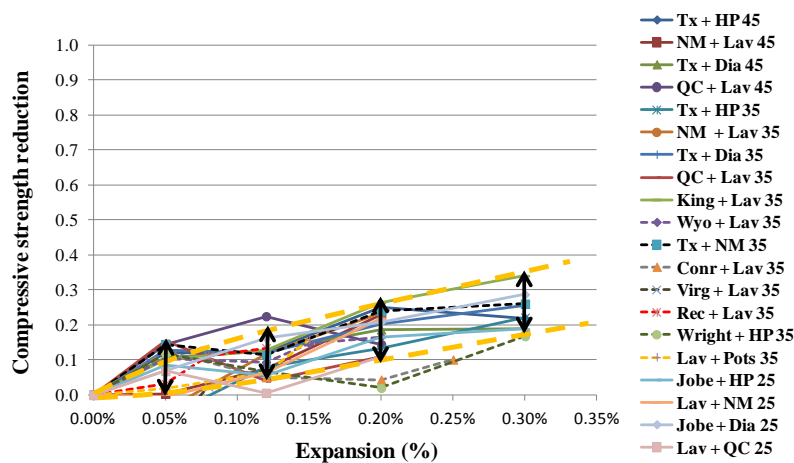


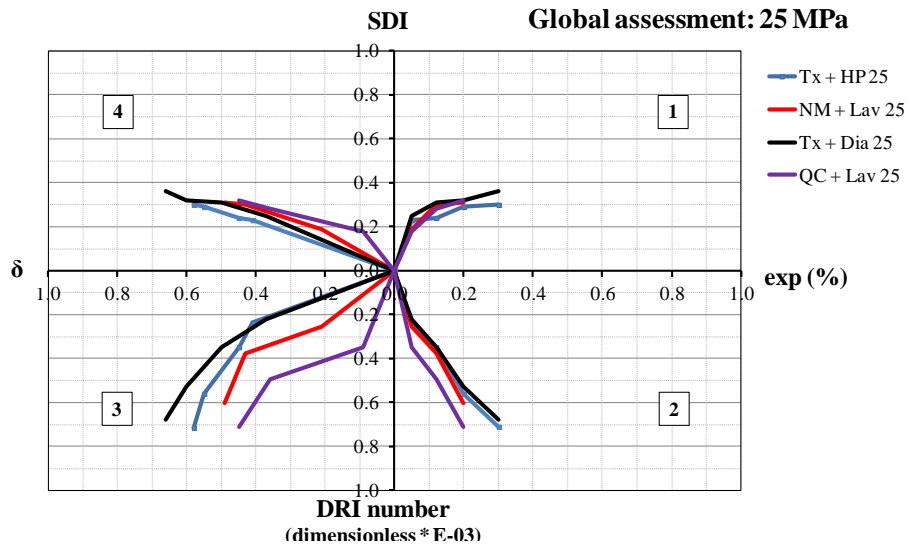
Figure 13.4: Mechanical properties reduction (i.e. compared to a sound concrete presenting the same maturity) as a function of concrete expansions: A) Modulus of elasticity. B) Tensile Strength. C) Compressive strength.

13.6 Quantitative damage chart/plot based on AAR micro-mechanical coupling

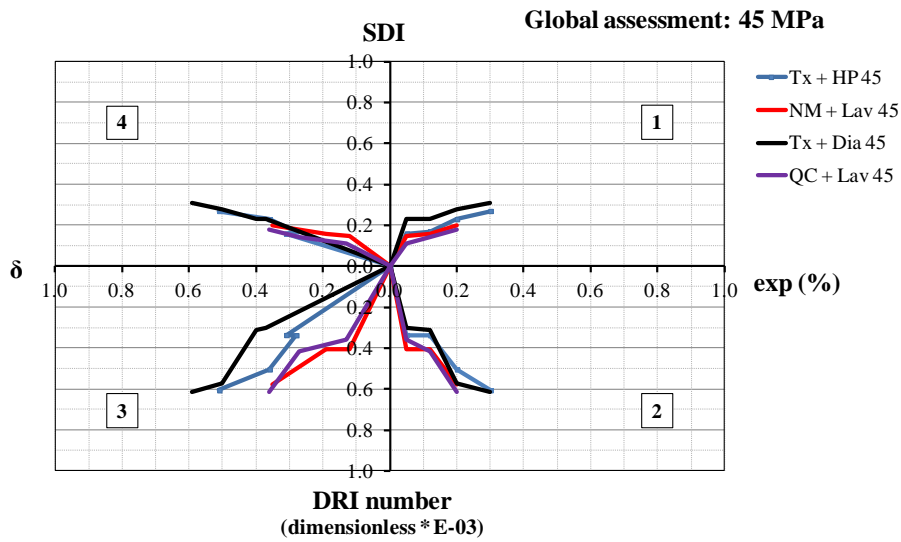
Through the data obtained in the microscopic and mechanical testing presented earlier and considering the envelopes presented above, it is possible to draw a “global assessment chart” of concrete distressed due to AAR, based on the “damage’s definition” illustrated in Figure 2.7, i.e. linking the expansion attained by affected concrete (right wing x-axis) with both the microscopic features (DRI number - bottom y-axis) and the mechanical behavior of affected materials (SDI - top y-axis and δ – left wing x-axis, which means the modulus of elasticity reduction in (%)) (Figure 13.5).

The below figures show strong correlations between the micro mechanical and microstructural data obtained for all the concrete mixtures (i.e. \neq strengths and aggregate types/natures) investigated in this study. Similar “damage patterns”, which are represented by the presence of “strong data envelopes”, were indeed found in each of the four quadrants forming those graphs. Exceptions are found for two mixtures discussed previously: King + Lav and Pots + Lav. Interestingly, the latter showed similar trends than the other alkali-silica reactive aggregates which located just outside of the data grouping in two out of four quadrants. The identification of cracks in the reactive aggregate particles was particularly a challenge considering the petrographic characteristics of that medium-grained siliceous sandstone, which might have distorted the results achieved in the DRI. Actually, under accelerated testing conditions in the laboratory, the siliceous cement binding the well-rounded quartz grains of the sandstone tends to dissolve readily under the effect of the concrete pore solution, which results in the disaggregation of the reactive particles, thus masking the presence of cracks within these particles and lower DRI values against increasing expansion. In the case of the alkali-carbonate reactive King aggregate, which is susceptible to alkali-carbonate reaction (ACR) in concrete, largely different microscopic features of deterioration characterized by large amount of cracking within the cement paste and somewhat limited cracking in the aggregate particles were obtained, this resulted in greater DRI values against increasing expansion than typical alkali-silica reactive aggregates. This reaction still needs to be further studied in terms of either chemical or distress development.

A



B



C

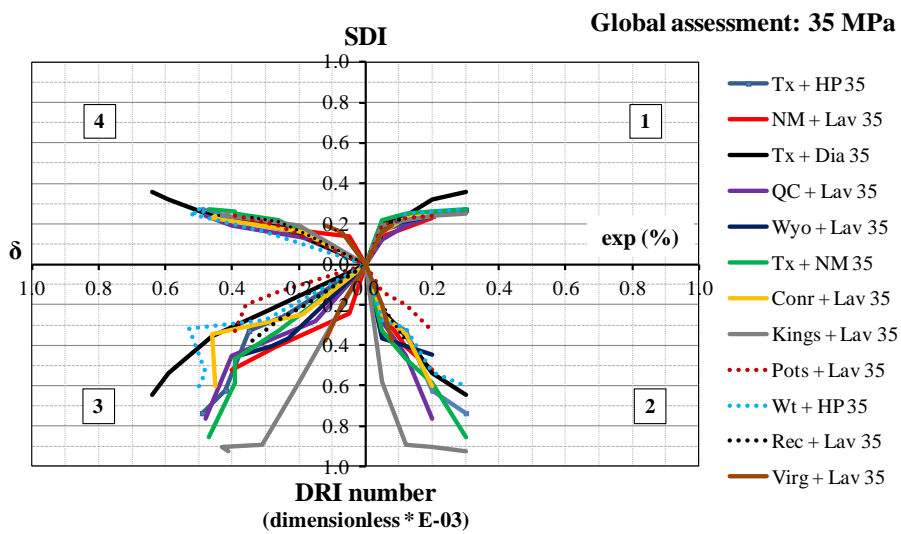


Figure 13.5: Global analysis charts for: A) 25 MPa mixtures. B) 45 MPa mixtures. C) 35 MPa mixtures.

These global plots enable the linkage/correlation between the critical output parameters from SDT and DRI testing and the development of micro-mechanical distress features within the AAR-affected materials, thus contributing to better understand the global ASR distress process. Strong correlations can generally be observed in quadrants 1 (SDI vs. expansion), 2 (Exp vs. DRI) and 4 (δ vs. SDI). More scatter in the data is obtained in the Quadrant 3 (d vs. DRI); this might be related to the fact that the attribution of the weighing factors used in the DRI calculations is likely not be optimized to produce the best possible correlation with the stiffness loss in the concrete material.

13.7 Validation of an ASR physico-chemical model for ASR

The Laboratoire des Matériaux et Durabilité des Constructions (LMDC) model (INSA, Toulouse, France), was tested through this project for predicting expansion and damage in concrete affected by ASR. It was the first time this model was applied for the condition assessment/prediction of laboratory-made concrete specimens, as the last studies dealt with the assessment of ASR affected mortar specimens.

The results showed that, since some variables of the model were set to better represent the expansion phenomenon measured in the laboratory, the LMDC model was clearly able to well predict (without supplementary fitting) the “damage” in terms of compressive and tensile strength reductions in the concrete specimens studied.

In terms of the prediction of the tensile strength losses, the LMDC model predicted quite well the damage values up to moderate expansion levels (i.e. up to $\approx 0.10\%$). On the other hand, while the model predicted continuous reductions in the tensile strength beyond the 0.12% expansion level, laboratory investigations showed that the tensile strength reductions were actually stabilizing beyond the above expansion stage. The above discrepancy could be explained through two possible assumptions:

- 1) problems in the experimental data (i.e. difficulty of measuring reliably the tensile strength of concretes in the laboratory using the gas pressure test) and;
- 2) the model does not consider the increase in cracking as a function of ASR expansion, which disables the damage to stabilize when the critical crack length is reached, as found for the experimental data.

For the compressive strength losses, the modeling results are in fairly good agreement with the laboratory results for all the expansion levels studied.

Finally, it has been found, through the petrographic analyses carried out on the specimens tested in this PhD project, that some “damage assumptions” made by the LMDC model do not fully/adequately represent the distress features identified under the microscope at the different expansion levels assessed in this work. This is mainly the case for the progressive development of opened cracks within the reactive aggregate particles, a typical feature of ASR in the concrete specimens incorporating a variety of reactive rock types selected in this study. Therefore, some variables should be adopted, taken into account these common ASR distress features (at least indirectly), in order to reliably assess both the expansion levels and the damage values measured/found in the laboratory.

13.8 Comprehensive management approach for assessing aging concrete infrastructure affected by AAR – a brief discussion

First, it is good to mention again that this PhD project aimed at understanding, through a micromechanical perspective, the development of concrete distress due to AAR. Therefore, microscopic and mechanical tools/test procedures that showed potential for ASR condition assessment in the past were studied in-depth, in order to optimize their diagnostic potential/character. Since this work aimed at providing a more fundamental evaluation of the efficacy of the above tools, it was considered more appropriate to work through laboratory specimens made and cured under very well-controlled conditions, and undergoing free-expansion (i.e. in a non restrained mode). Therefore, once our understanding of the link between the AAR distress development and the mechanical response of the "material" was improved, and since both test procedures (i.e. microscopic - DRI and mechanical - SDT) proved to be efficient for detecting/analyzing AAR distress, the next step would be to apply the laboratory-chosen approach in the assessment of “aging concrete structures/structural elements, reinforced or not”, which takes part of the “Recommendations for future work” section of the Thesis. However, this sections aims at briefly discussing the potential use of the micromechanical data obtained through this research for the condition assessment of concrete infrastructure.

- As previously discussed, the responses of the concrete "material" to AAR development are related to both the material's characteristics and field conditions, i.e. concrete mix design

(concrete strength, aggregate nature/type, etc.), concrete element type (column, beam, slab, wall, etc., reinforced/non reinforced/prestressed, presenting uni/bi/tri-axial stress states, etc.), zone of the concrete element (exposed/non-exposed to moisture), sample's location/characteristics (distance from the element surface, very likely the coring direction, samples size/geometry etc.), and test pre-conditioning (drying/wetting effect). Therefore, one should admit that the test results obtained from a "single location" within the structure/structural element in question just represent a punctual assessment of the damage degree and cannot be used do "fully describe" the condition of the other parts of the structure/structural element. Moreover, this situation forces to plan condition assessments of aging concrete infrastructure from two different point of views or objectives: 1) a full-scale analysis of several different elements/zones and directions, enabling the detailed "damage mapping" of a structure/structural elements, which allows the understanding of the damage variation throughout the structure/structural element in question (which could allow a more focused application of different repair strategies/procedures according to the distress degree found at different locations) or; 2) focusing on the condition assessment of a potential element/zone/direction that represents the "worst" case scenario, enabling the assessment of the structure focusing at safety issues;

- The research program carried out in the laboratory identified a number of critical mechanical parameters (SDI, PDI, modulus of elasticity, compressive and tensile strength) and microstructural parameters (DRI number, Crack density (CD), cracks number/width) with strong potential for appraising condition of aging concrete infrastructure. Considering the structure safety and its "Ultimate limit state (ULS)" and "Serviceability limit state (SLS)", the values of modulus of elasticity, compressive strength (somewhat the tensile strength, depending on the structure type), and cracks number/width could be directly used for re-calculating the "actual safety" and verifying the need of retrofitting of the structure/structural element in question. Otherwise, the SDI and PDI values, which represent the amount of internal cracking within the concrete material, is likely to correlate with the durability-related issues of the damaged material. The higher is the SDI (or PDI) value, the easier is the penetration of chloride/sulfate ions as well as water within the affected element, which accelerates the distress process or even causes harmful secondary effects such as corrosion of the steel reinforcement. In addition, the DRI and CD data, which indicates AAR development degree/severity, could be used to understand/identify AAR progression, and thus simulate possible further distress due to the chemical reaction. Although the above data obtained on cores extracted at specific locations of a structural

element provide most valuable/interesting information, and quite often represent the only data available in condition assessment investigations, cannot be directly correlated with the amount of “actual distress” found in that element, since other aspects critically influence the material’s response towards AAR development, such as the concrete element types, zones, reinforcements detailing, restrains or reinforcements, stress states, etc. Therefore, all the data coming from the micromechanical laboratory assessments should be used with care when carrying out the condition assessment of an aging infrastructure.

- Finally, these micromechanical testing data obtained in the laboratory might be used as “input data” for analyzing AAR diagnosis/prognosis through AAR micro/macro models, since several of those mathematical/physicochemical models consider either the mechanical damage or the expansion results over time as their “output results”. Thus, the experimental data could give an idea not only about the actual distress degree of an aging infrastructure, but also about the potential for further distress due to AAR when combined with information obtained from other experimental procedures such as residual expansion testing, soluble alkalis determination, etc.

13.9 Recommendations for future work

After carrying out an extensive experimental work on the assessment of AAR damage in concretes, and taking into account the study conclusions stated in the previous sections, some recommendations and suggestions for future works can be proposed, as follows:

- Since the SDT and DRI have proven their efficiency for the evaluation of either the mechanical or the microscopic damage levels of AAR affected laboratory-made specimens, it is now possible to improve/validate the scale of analysis of distressed concrete in service using both tools. Therefore, one needs to verify the procedures and new approaches proposed over this work for condition assessment of concrete elements or structures in service, which usually present different conditions from those of laboratory made specimens;
- Based on the data obtained in this study regarding the different factors affecting the variability of the SDT and DRI, efforts should be made to standardize those tests with the objective of reducing variations related to the use of different procedures from one lab/person to another;
- In addition, both tools have presented great potential of being “global damage assessment procedures” and in depth studies could be carried out to evaluate their efficacy for

quantifying damage in concrete affected by other deleterious mechanisms such as freeze-thaw action, delayed ettringite formation, etc.;

- Overall, all the concrete mixtures investigated were found to present the same trend through the different mechanical and microscopic analyses carried out, which enabled the generation of some strong “envelopes of distress”. However, to better understand why those differences occurred among the different concrete mixtures used in this project, further work is still needed on the “rock mechanics” subject. This would allow a better understanding of the effect of parameters (i.e. hardness, toughness, etc.) that likely play a significant role on AAR distress development and how they influence the bulk concrete matrix damage generation;
- An exception, in terms of performance towards the various tests carried out in this study, was found for the concrete mixture incorporating the King limestone, which is supposed to generate a different chemical and harmful reaction, i.e. the so-called *alkali-carbonate reaction* (ACR). Further work is still needed in order to enable a better understanding of this issue in both microscopic and mechanical scales;
- This work generated a large database for the coupling of microscopic features of deterioration and the corresponding mechanical behavior of the AAR affected concretes. However, more data is required in order to confirm the above coupling in the case of ASR concrete elements in service;
- Finally, once the questions about how and how much AAR generated “damage” as a function of progressive expansion are at least partially answered/explained, which was the main objective of this PhD project, it appears critical to determine how the various tools investigated in this study can be used for evaluating the potential of further distress of aging concrete structures suffering from AAR. Moreover, the development of practices that could mitigate (even in a palliative manner) or even stop the harmful reaction will always be the biggest challenge of this worldwide issue with regards to the durability and serviceability of concrete infrastructure: alkali-aggregate reaction (AAR).

14. REFERENCES

- ASTM C 1293. 2012. Standard test method for determination of length change of concrete due to alkali-silica reaction. ASTM International, West Conshohocken (USA).
- ASTM C 39. 2012. Standard test method for compressive strength of cylindrical concrete specimens. ASTM International, West Conshohocken (USA).
- ASTM C 1074. 2011. Standard practice for estimating concrete strength by the maturity method. ASTM International, West Conshohocken (USA).
- Alexander, M. G.; Milne, T. I. 1995. Influence of cement blend and aggregate type on stress-strain behavior and elastic modulus of concrete. *ACI Materials Journal*, 92: 227-325.
- Aitcin, P. C.; Mehta P. K. 1990. Effect of coarse-aggregate characteristics on mechanical properties of high-strength concrete. *ACI Materials Journal*, 87: 103-107.
- Bazant, Z. P.; Steffens, A. 2000. Mathematical model for kinetics of alkali-silica reaction in concrete, *Cement and Concrete Research*, 30: 419-428.
- Ben Haha, M.; Gallucci E.; Scrivener, K. L. 2007. Relation of expansion due to alkali-silica reaction to the degree of reaction measured by SEM image analysis. *Cement and Concrete Research*, 37: 1206- 1214.
- Bérard, J; Roux, R. 1986. La viabilité des bétons du Québec : le rôle des granulats. *Canadian Journal of Civil Engineering*, 13: 12-24.
- Bérubé, M.A.; Smaoui, N.; Bissonnette, B.; Fournier, B. 2005a. Outil d'évaluation et de gestion des ouvrages d'art affectés de réactions alcalis-silice (RAS). *Études et Recherches en Transport*, Ministère des Transports du Québec, Septembre, 140 p.
- Bérubé, M.A.; Smaoui, N.; Fournier, B.; Bissonnette, B.; Durand, B. 2005b. Evaluation of the expansion attained to date by concrete affected by ASR - Part III: Application to existing structures. *Canadian Journal of Civil Engineering*, 32: 463-479.
- Bérubé, M. A.; Fournier, B.; Côté, T. 2012. Using the damage rating index for assessing the expansion of concrete affected by freeze-thaw, sulphate attack, or ASR. 14th ICAAR - International Conference on Alkali-Aggregate Reaction in Concrete. May 20-25th, Austin (Texas), electronic.
- Blight, G.E.; McIver, J.R.; Schutte, W.K.; Rimmer, R. 1981. The effects of alkali-aggregate reaction on reinforced concrete structures made with Witwatersrand quartzite aggregate. 5th ICAAR - International Conference on Alkali-Aggregate Reaction in Concrete, Cape Town, South Africa, 733-739, 1981.
- British Cement Association (BCA). 1992. The diagnosis of alkali silica reaction – report of a working party. British Cement Association, Crowthorne, England.
- Broekmans, M.A.T.M. 2002. The alkali-silica reaction: mineralogical and geochemical aspects of some Dutch concretes and Norwegian mylonites, PhD. Thesis, Utrecht University, Netherlands, 144 p.
- Charpin, L.; Ehrlacher, A. 2012. A computational linear elastic fracture mechanics-based model for alkali-silica reaction, *Cement and Concrete Research*, 42 (4): 613-625.
- Clemona, G.G.; Lane, S.; Freeman, T.; Lozev, M. 2000. Evaluation of nondestructive evaluation methods for application in early detection of deterioration in concrete pavements. VTRC 00-R13. Virginia Transportation Research Council, Charlottesville, USA, 26p.
- Comby-Perot, I.; Bernard, F.; Bouchard, P-O; Bay, F.; Garcia-Diaz, E. 2009. Development and validation of a 3D computational tool to describe concrete behaviour at mesoscale. Application to the alkali-silica reaction, *Computational Material Science*, 46 (4): 1163-1177.
- Comi, C.; Fedele, F.; Perego, U. 2009. A chemo-thermo-damage model for the analysis of concrete dams affected by alkali-silica reaction, *Mechanics of Materials*. 41: 210-230.
- Crisp, T. M.; Waldron. P.; Wood. J. G. M. 1993. Development of a non destructive test to quantify damage in deteriorated concrete. *Magazine of Concrete Research*. 45 (165): 247-256.
- Crisp, T. M.; Wood, J. G. M.; Norris, P. 1989. Towards Quantification of Microstructural Damage in AAR Deteriorated Concrete. International Conference on Recent Developments on the Fracture of Concrete and Rock. The University of Wales, Cardiff, September 1989, 9p.
- Crouch. R. S. 1987. Specification for the determination of stiffness damage parameters from the low cyclic uniaxial compression of plain concrete cores. Revision A. Mott. Hay & Anderson. Special services division. Internal technical note.

- Crouch, R. S.; Wood, J. G. M. 1990. Damage evolution in ASR affected concretes. *Engineering fracture mechanics*, 35 :211- 218.
- CSA A23.1. Concrete Materials and Methods of Concrete Construction - APPENDIX B. Canadian Standards Association, Mississauga, Ontario (Canada),
- CSA A23.2-14A. Potential Expansivity of Aggregates (Procedure for Length Change due to Alkali-Aggregate Reaction in Concrete Prisms at 38°C). Canadian Standards Association, Mississauga, Ontario (Canada),
- CSA A864. Guide to the Evaluation and Management of Concrete Structures Affected by Alkali-Aggregate Reaction. Canadian Standards Association, Mississauga, Ontario (Canada),
- Dunant, C. F.; Scrivener, K. L. 2009. Micro mechanical modeling of alkali-silica reaction induced degradation using the AMIE framework. *Cement and Concrete Research*, 40 :517- 525.
- Dunant, C.; Bentz, E. 2012. The effect of multi-axial restraint on ASR-affected concrete. 14th ICAAR - International Conference on Alkali-Aggregate Reaction in Concrete. May 20-25th, Austin (Texas), electronic.
- Dunbar, P.A.; Grattan-Bellew, P.E. 1995. Results of damage rating evaluation of condition of concrete from a number of structures affected by ASR. CANMET/ACI International Workshop on Alkali-Aggregate Reactions in Concrete, Dartmouth, Canada, October 1995.
- Fecteau, P. L.; Fournier, B.; Choquette, M.; Duchesne, J. 2012. Contribution to the understanding of the so-called alkali-carbonate reaction (ACR). 14th ICAAR - International Conference on Alkali-Aggregate Reaction in Concrete. May 20-25th, Austin (Texas), electronic.
- Fournier, B.; Bérubé, A. 2000. Alkali-aggregate reaction in concrete: a review of basic concepts and engineering implications. *Canadian Journal of Civil Engineering*, 27 (2): 167-191.
- Fournier, B.; Nkinamubanzi, P.C.; Lu, D.; Thomas, M. D. A.; Folliard, K. J.; Ideker, J. 2006. Evaluating potential alkali-reactivity of concrete aggregates – How reliable are the current and new test methods? II Symposium on alkali-aggregate reaction in concrete structures. Brazilian Concrete Institute-Ibracon and Brazilian Committee on Dams-CBDB, Rio de Janeiro, Brazil, September 2006.
- Fournier, B.; Bérubé, M. A.; Folliard, K.; Thomas, M.D.A. 2010. Report on the diagnosis, prognosis, and mitigation of alkali-silica reaction (ASR) in transportation structures. US Department of Transportation, Federal Highway Administration, Publication FHWA-HIF-09-004, January 2010.
- Furusawa, Y.; Ohga, H.; Uomoto, T. 1994. An analytical study concerning prediction of concrete expansion due to alkali-silica reaction, in Malhotra (ed.), 3rd International CANMET-ACI Conference on Durability of Concrete, Nice, France, 1994, 757–780.
- Gao XX; Multon S.; Cyr M.; Sellier A. 2013. Alkali–silica reaction (ASR) expansion: Pessimun effect versus scale effect, *Cement and Concrete Research*, 44 : 25-33.
- Giaccio G.; Zerbino, R.; Ponce, J. M.; Batic, R. 2008. Mechanical behavior of concretes damage due to ASR. *Cement and Concrete Research*. 38: 993-1004.
- Giannini, E.; Folliard, K. 2012. Stiffness damage and mechanical testing of core specimens for the evaluation of structures affected by ASR 14th ICAAR - International Conference on Alkali-Aggregate Reaction in Concrete, May 20-25th, Austin (Texas), electronic.
- Golterman, P. 1995. Mechanical predictions on concrete deterioration – Part 2: classification on crack patterns. *ACI Materials Journal*. 92: 01-06.
- Grattan-Bellew, P.E.; Danay, A. 1992. Comparison of laboratory and field evaluation of AAR in large dams, International Conference on Concrete AAR in Hydroelectric Plants and Dams, Canadian Electrical Association & Canadian National Committee of the Int. Commission on Large Dams, September 28 – October 2 1992, Fredericton, New Brunswick, (Canada), 23p.
- Grattan-Bellew, P.E.; Mitchell, L.D. 2006. Quantitative petrographic analysis of concrete –The Damage Rating Index (DRI) method, a review. Marc-André Bérubé symposium on AAR in concrete, CANMET/ACI Advances in concrete technology seminar, Montréal, Canada, May 31 & June 1, 2006.
- Grimal, E.; Sellier, A.; Le Pape, Y.; Bourdarot, E. 2008. Creep shrinkage and anisotropic damage in AAR swelling mechanism, part I: a constitutive model, *ACI Materials Journal*, 105 : 227-235.
- Guédon-Dubied, J.S.; Cadoret, G.; Durieux, V.; Martineau, F.; Fasseu, P.; Van Overbecke, V., 2000. Study on Tournai limestone in Antoing Cimescaut quarry – petrological, chemical and alkali-

- reactivity approach. 11th ICAAR - International Conference on Alkali-Aggregate Reaction in Concrete, June 11 – 16th, Quebec, Quebec (Canada), 335-344.
- Inoue, S.; Mikata, Y.; Takahashi, Y.; Inamasu, K. 2012. Residual shear capacity of ASR damaged reinforced concrete beams with ruptured stirrups. 14th International conference on alkali-aggregate reaction (ICAAR). Texas, USA.
- ISE 1992. Structural effects of alkali-aggregate reaction: technical guidance on the appraisal of existing structures. The Institution of Structural Engineers (ISE), Upper Belgrave St., London, UK.
- Katayama, T. 2010. The so-called alkali-carbonate reaction (ACR) — Its mineralogical and geochemical details, with special reference to ASR. *Cement and Concrete Research*, 40: 643-675.
- Katayama, T.; Grattan-Bellew, P. E. 2012. Petrography of Kingston experimental sidewalk at age 22 years. ASR as the cause of deleteriously expansive, so-called alkali-carbonate reaction. 14th ICAAR - International Conference on Alkali-Aggregate Reaction in Concrete. May 20-25th, Austin (Texas), electronic.
- Kubo, Y.; Nakata, M. 2012. Effect of reactive aggregate on mechanical properties of concrete affected by alkali-silica reaction. 14th ICAAR - International Conference on Alkali-Aggregate Reaction in Concrete. May 20-25th, Austin (Texas), electronic.
- Li, K.; Coussy, O. 2002. Concrete ASR degradation: from material modeling to structure assessment, *Concrete Science and Engineering*. 4: 35-46.
- Lindgård, J.; Skjolsvold, O.; Haugen, M.; Hagelia, P.; Wigum, B.J. 2004. Experience from evaluation of degree of damage in fluorescent impregnated plan polished sections of half-cores based on the “Crack Index Method”. 12th ICAAR - International Conference on Alkali-Aggregate Reaction in Concrete, Beijing (China), 939-947.
- Lindgård, J.; Haugen, M.; Castro, N.; Thomas, M.D.A. 2012. Advantages of using plane polished analysis as part of microstructural analyses to describe internal cracking due to Alkali-Silica Reaction. 14th ICAAR - International Conference on Alkali-Aggregate Reaction in Concrete, May 20-25th 2012, Austin (Texas), electronic.
- Lu, D.; Fournier, B.; Grattan-Bellew, P.E. 2006. Evaluation of accelerated test methods for determining alkali-silica reactivity of concrete aggregates. *Cement and Concrete Composites*, 28 : 546-554.
- Multon, S.; Cyr, M.; Sellier, A.; Leklou, N.; Petit, L. 2008. Coupled effects of aggregate size and alkali content on ASR expansion. *Cement and Concrete Research*, 38 (3): 350-359.
- Multon, S.; Sellier, A.; Cyr, M. 2009. Chemo-mechanical modeling for prediction of alkali silica reaction (ASR) expansion. *Cement and Concrete Research*, 39 :490-500.
- Mindess, S.; Young, J. F.; Darwin, D. 2003. *Concrete*. Book. Pearson Education Ltda. second edition.
- Naar, R. 2010. Modelisation du comportement mécanique du béton par approche multi-physique (couplage chimie-mécanique) : application à la réaction alcalis-silice. Thèse de doctorat. École Nationale Supérieure des Mines de Paris.
- Nielsen, A.; Gottfredsen, F.; Thogersen, F. 1993. Development of stresses in concrete structures with alkali-silica reactions, *Material and Structures*, 26: 152-158.
- Nixon, P. J.; Bollinghaus, R. 1985. The effect of alkali aggregate reaction on the tensile strength of concrete. *Durability of Building Materials*, 02: 243-248.
- Özkan, S.; Canan, T.; Mehmet Ali, T. 2002. Influence of Aggregate Type on Mechanical Behavior of Normal- and High-Strength Concretes. *ACI Materials Journal*, 99: 528-533.
- Pleau, R.; Bérubé, M. A.; Pigeon, M.; Fournier, B.; Raphael, S. 1989. Mechanical Behavior of Concrete Affected by AAR. 8th ICAAR - International Conference on Alkali-Aggregate Reaction in Concrete. Kyoto, Japan, 721-726, 1989.
- Portland Cement Association. 2002. Types and Causes of concrete deterioration – Concrete Information. PCA R&D Serial No. 2617, 16p.
- Poyet, S.; Sellier, A.; Capra, B.; Foray, G.; Torrenti, J. M.; Cognon, H.; Bourdarot, E. 2007. Chemical modelling of Alkali Silica reaction: Influence of the reactive aggregate size distribution, *Materials and Structures*, 40: 229–239.
- Powers, T.C.; H.H. Steinour, H.H. 1955. An interpretation of published researches on the alkali-aggregate reaction. *Journal of the American Concrete Institute*, Proceedings Vol. 51, 785-812.

- Powers, L.; Shrimmer, F. H. 2007. Quantification of ASR in Concrete: An Introduction to the Damage-Rating Index Method. 29th International Conference on Cement Microscopy, 20-24 May 2007, Québec, Canada, 527p.
- Reinhard, H. W.; Mielich, O. 2011. A fracture mechanics approach to the crack formation in alkali sensitive grains. *Cement and Concrete Research*, 41 : 255- 262.
- Rivard, P.; Fournier, B.; Ballivy, G. 2000. Quantitative petrographic Technique for Concrete Damage Due to ASR: Experimental and Application. *Cement, Concrete and Aggregates*, 22 (1): 63-72.
- Rivard, P.; Fournier, B.; Ballivy, G. 2002. The DRI method for ASR affected concrete - A Critical review of petrographic features of deterioration and Evaluation Criteria. *Cement, Concrete and Aggregates*, 24(2): 1-10.
- Rivard, P.; Ballivy, G. 2005. Assessment of the expansion related to alkali-silica reaction by the Damage Rating Index method. *Construction and Building Materials*, 19: 83-90.
- Salomon, M., Panetier, J.L. 1994. Quantification du degré d'avancement de l'alcali-réaction dans les bétons et de la néofissuration associée. 3rd CANMET/ACI International Conference on the Durability of Concrete, Nice, France, 383-401, 1994.
- Sanchez, L.; Fournier, B.; Jolin, M.; Bastien, J. Evaluation of the Stiffness Damage Test (SDT) as a tool for concrete's assessment damaged due to ASR – test loading and output responses for concretes incorporating fine or coarse reactive aggregates. *Cement and concrete research*, 56: 213-229.
- Sanchez, L. F. M.; Fournier, B.; Jolin, M.; Bastien, J. 2014. Evaluation of the Stiffness Damage Test (SDT) as a tool for assessing damage in concrete due to ASR: input parameters and test procedure. *Cement and Concrete Composites*, submitted paper, January 2014.
- Sanchez, L. F. M.; Fournier, B.; Jolin, M.; Bedoya, M.A.B.; Bastien, J.; Duchesne, J. 2014 Use of the Damage Rating Index (DRI) to quantify damage due to alkali-silica reaction in concrete incorporating reactive fine and coarse aggregates. *Cement and Concrete Composites*, submitted paper, January 2014.
- Sanchez, L. F. M.; Fournier, B.; Jolin, M.; Duchesne, J. 2014. Assessment of microscopic damage features of alkali-aggregate reaction (AAR) through the Damage Rating Index (DRI). *Cement and Concrete Research*, submitted paper, January 2014
- Sanchez, L. F. M.; Multon, S.; Sellier, A.; Cyr, M.; Fournier, B. Comparative study of a chemo-mechanical modeling for alkali-silica reaction with experimental evidences. *Construction and Building Materials*, submitted paper, January 2014.
- Sanchez, L. F. M.; Kuperman, S, C; Helene, P; Kihara, Y. 2008. Trials to correlate the accelerated mortar bar test, the standard and the accelerated concrete prism tests. 13th ICAAR - International Conference on Alkali-Aggregate Reaction in Concrete. June 16-20 2008, Trondheim, Norway.
- Saouma, V.; Perotti, L. 2006. Constitutive model for alkali-aggregate reactions, *ACI Materials Journal*, 103 (3): 194-202.
- Shrimmer, F.H. 2000. Application and use of Damage Rating Index in assessment of AAR-affected concrete-selected case studies. 11th ICAAR - International conference on alkali-aggregate reaction (ICAAR). June 11 – 16th, Quebec, Quebec (Canada), 899-907.
- Shrimmer, F.H. 2006. Development of the Damage Rating Index Method as a tool in the assessment of alkali-aggregate reaction in concrete: a critical review. Marc-André Bérubé symposium on AAR in concrete, CANMET/ACI Advances in concrete technology seminar, May 31 & June 1, Montréal (Canada), 391-411.
- Sims, I.; Hunt, B.; Miglio, B. 1992. Quantifying microscopical examinations of concrete for AAR and other durability aspects. American Concrete Institute, SP 131-114, 267-287.
- Smaoui, N.; Bérubé, M. A.; Fournier, B.; Bissonnette, B. 2004a. Influence of Specimen Geometry, Orientation of Casting Plane, and Mode of Concrete Consolidation on Expansion Due to ASR. *Cement, Concrete and Aggregates*, 26 (2) : 58-70.
- Smaoui, N.; Bérubé, M.A.; Fournier, B.; Bissonnette, B.; Durand, B. 2004b. Evaluation of the Expansion Attained to Date by Concrete Affected by ASR - Part I: Experimental Study. *Canadian Journal of Civil Engineering*, 31 : 826-845
- Smaoui, N.; Bissonnette, B.; Bérubé, M. A.; Fournier, B.; Durant, B. 2006. Mechanical Properties of ASR-Affected Concrete Containing Fine or Coarse Reactive Aggregates. *Journal of ASTM International*, 3 (3) : 01-16.

- St-John, D.A.; Poole, A.W.; Sims, I. 1998. Concrete Petrography: A handbook of investigative techniques, Arnold, London, 1998.
- Suwito, A.; Jin, W.; Xi, Y.; Meyer, C. 2002. A mathematical model for the pessimum effect of ASR in concrete, *Concrete Science and Engineering*, 4: 23-34.
- Transtec Group. 2009. Field Site and Petrographic Evaluation - ASR Development and Deployment Program - Field Trials and Demonstration Projects. September.
- Tremblay, S. 2011. Étude de l'efficacité d'adjuvants à base de lithium afin de contrôler la réaction alcalis-silice dans le béton frais et dans les structures existantes incorporant cet adjuvant. Mémoire de maîtrise, *Géologie et Génie Géologique*. Université Laval, Québec.
- Ulm, F. J.; Coussy, O.; Li, K.; Larive, C. 2000. Thermo-chemo-mechanics of ASR expansion in concrete structures, *Journal of Engineering Mechanics.*, 126 (3): 233– 242.
- Villeneuve, V. 2011. Détermination de l'endommagement du béton par méthode pétrographique quantitative. Mémoire de maîtrise, *Géologie et Génie Géologique*. Université Laval, Québec.
- Villeneuve, V.; Fournier, B.; Duchesne, J. 2012. Determination of the damage in concrete affected by ASR – The damage rating index (DRI). 14th ICAAR - International Conference on Alkali-Aggregate Reaction in Concrete. May 20-25th, Austin (Texas), electronic.
- Walker, H. N.; Lane, D. S.; Stutzman, P. E. 2006. Petrographic Methods of Examining Hardened Concrete: A Petrographic Manual, FHWA-HRT-04-150, Federal Highway Administration, McLean, VA (USA).
- Walsh. J. B. 1965. The effects of cracks on the uniaxial elastic compression of rocks. *Journal of Geophysical Research*, 70: 339 - 411.
- Wood, G. M.; Johnson, R. A. 1993. The appraisal and maintenance of structures with alkali-silica reaction. Paper, Institution of Structural Engineers.
- Wood, G. M.; Norris, P.; Leek, D. 1989. Physical Behavior of AAR Damaged Concrete in Structures and in Test Conditions. 8th ICAAR - International Conference on Alkali-Aggregate Reaction in Concrete, 765-770, Kyoto, Japan, 1989
- Wood, G. M. J.; Nixon, P. J.; Livesey, P. 1996. Relating ASR structural damage to concrete composition and environment. ICAAR - International Conference on Alkali-Aggregate Reaction in Concrete, Melbourne (Australia), pp 450 – 457, 1996.